

University of Alberta

Growth behavior of surface cracks in pipeline steels exposed to near-neutral pH environments

by

AFOLABI TAIWO EGBEWANDE

A thesis submitted to the Faculty of Graduate Studies and Research
in partial fulfillment of the requirements for the degree of

Doctor of Philosophy

in

Materials Engineering

Chemical and Materials Engineering

©Afolabi Taiwo Egbewande

Fall 2013

Edmonton, Alberta

Permission is hereby granted to the University of Alberta Libraries to reproduce single copies of this thesis and to lend or sell such copies for private, scholarly or scientific research purposes only. Where the thesis is converted to, or otherwise made available in digital form, the University of Alberta will advise potential users of the thesis of these terms.

The author reserves all other publication and other rights in association with the copyright in the thesis and, except as herein before provided, neither the thesis nor any substantial portion thereof may be printed or otherwise reproduced in any material form whatsoever without the author's prior written permission.

Dedicated to

My mum

Eunice Yemisi Egbewande

*In recognition of your immense sacrifice,
Without which 'this' could never have been.*

*For seeing that 'this' could be
When 'this' certainly shouldn't be
And toiling to ensure that 'this' now is
Thank you.*

ABSTRACT

This study is part of a larger study designed to help a consortium of pipeline operators replace current (very expensive) approaches to managing stress corrosion cracking (SCC) concerns in near-neutral pH (NNPH) environments with mathematical models that predict SCC growth rates. This could significantly reduce the cost of pipeline integrity management programs. The goal was to help find ways to improve the accuracy of existing models.

NNPHSCC cracks are surface-type flaws. However, NNPHSCC was typically modelled as through-thickness cracks in previous laboratory studies. This was identified as a major reason why current NNPHSCC models are inaccurate. Therefore, this study was designed to model NNPHSCC cracks as surface-type flaws rather than through-thickness cracks.

Results showed contrary to popular opinion that surface-type flaws propagated less rapidly than through-thickness cracks in NNPHSCC environments. Also, inherent variations in the local environment under a disbondment produce hydrogen concentration gradients that result in very high propagation rates at the open mouth of a disbondment. The propagation rate declines very sharply non-linearly distance away from the open mouth inside the disbondment. It was determined the environmental factor used to account for the contribution of the environment to crack propagation, could be up to ten times higher at the open mouth compared to other locations under the disbondment. Identifying these issues helps to guide NNPHSCC modellers in selecting more appropriate growth rates for SCC programs. A series of propagation rate ranges under various environmental and mechanical loading conditions were determined.

Contrary to popular opinions, increased CO₂ concentration in groundwater decreased crack propagation rates by intensifying (environmental) crack tip blunting. This delayed crack re-initiation from a dormant state. Under benign loading conditions, this helps to reduce/stop

crack growth by driving towards dormancy. Mechanically blunting a crack tip was found to produce the same effect. Hydrogen enhanced localized plasticity (also called hydrogen enhanced low temperature creep) was found to be responsible for this blunting effect. Means of manipulating the mechanical loading factors to produce this effect were identified.

ACKNOWLEDGEMENT

My sincerest appreciations go to Dr Weixing Chen for giving me the opportunity to work on this project. I am very grateful for his most valuable guidance, timely advice and support throughout the duration of this study. I sincerely appreciate Dr. Reginald Eadie for making his research facilities available to me for this work and for sharing his vast insight and knowledge in the field freely with me. I acknowledge Dr. Hao Zhang's valuable contributions and technical support at various stages of this work.

I am grateful to NSERC for the award of PGSD Scholarship, and special thanks are due to TransCanada, Spectra Energy, Department of Transportation, Pipeline Research Council, and Enbridge for financial support for this study. I must also express my profound appreciation to Messieurs Clark Bicknell, Dave Parlin, James Mckinnon, Herb Green, Kevin Heidebrecht, Robert (Bob) Smith and, Walter Boddez, Les Dean, and Richard Cooper for their technical assistance. Mr Clarke Bicknell was amazing in every way possible. I will also like to express my gratitude to my wonderful friends – the Rabiun, the Oladirans, the Idowus, the Obiosa-Maifes, Joy Welke, Janna Olson, Tammy Adante – and colleagues in the group: Majid Eslami, Mohammad Marvasti, Xinwei Cui, Hao Li, Tianfei Wang, Dong Ziquiang, Tinyong Xing, Yonwang Kang, and others.

I am profoundly grateful for the understanding and wonderful support of my dad and siblings – the 'Folas – Folake, Folarin and Folahan (D.Y.), who were put to great inconveniences when I decided to proceed on this study. Words will fail to express my gratitude to Mrs. E.Y. Egbewande (my mum, most prized friend, and supporter); your love, faith and passion has been my best encouragement at every stage of my pursuits. Finally, my unreserved appreciation goes to God, the source of my wisdom and understanding.

Table of Contents

| | | |
|-------|--|----|
| 1.0 | <i>Introduction</i> | 2 |
| | References..... | 5 |
| 2.1 | Important background concepts | 7 |
| 2.1.1 | General description of corrosion..... | 7 |
| 2.1.2 | Galvanic corrosion | 10 |
| 2.1.3 | Pitting corrosion..... | 10 |
| 2.1.4 | Hydrogen embrittlement (hydrogen induced cracking) | 12 |
| 2.1.5 | Pipelines operation and corrosion prevention | 12 |
| 2.2 | Environmentally induced cracking | 13 |
| 2.2.1 | Stress corrosion cracking | 14 |
| 2.2.2 | History of stress corrosion cracking..... | 14 |
| 2.2.3 | SCC in pipelines..... | 16 |
| 2.2.4 | SCC development | 18 |
| 2.3 | Effects of alloy metallurgy – material factors..... | 20 |
| 2.3.1 | Microstructure..... | 22 |
| 2.3.2 | Inclusions | 24 |
| 2.3.3 | Carbon content and alloying additions..... | 26 |
| 2.3.4 | Weld heat affected zones | 28 |
| 2.3.5 | Precipitates | 29 |
| 2.3.6 | Grain size | 30 |
| 2.3.7 | Lattice strain (deformation) | 31 |
| 2.4 | Mechanical factors – stress | 32 |
| 2.4.1 | Forming process and residual stress..... | 35 |
| 2.4.2 | Stress concentration | 37 |

| | | |
|-------|--|----|
| 2.4.3 | Hydrostatic testing | 37 |
| 2.4.3 | Summary of the effect of stress on SCC | 39 |
| 2.4.4 | Cyclic loading | 41 |
| 2.4.5 | Effect of strain rates | 45 |
| 2.5 | Environmental factors | 47 |
| 2.5.1 | Soil | 47 |
| 2.5.2 | Role of hydrogen..... | 49 |
| 2.5.3 | Electrolytes | 51 |
| 2.5.4 | Effect of applied potential..... | 54 |
| 2.5.5 | Effect of the type of coating..... | 57 |
| 2.5.6 | Seasonal variation | 61 |
| 2.6 | Corrosion fatigue | 63 |
| 2.6.1 | Corrosion Fatigue Mechanisms | 65 |
| 2.6.2 | Factors controlling corrosion fatigue | 69 |
| 2.6.3 | Mechanical factors | 69 |
| 2.6.4 | Corrosion fatigue initiation | 72 |
| 2.6.5 | Corrosion fatigue crack propagation..... | 74 |
| 2.7 | SCC propagation mechanisms | 76 |
| 2.7 | Dormancy..... | 82 |
| 2.8 | Mechanisms of hydrogen embrittlement..... | 83 |
| 2.8.1 | Decohesion model..... | 83 |
| 2.8.2 | Adsorption model..... | 86 |
| 2.8.3 | Pressure theory..... | 86 |
| 2.8.4 | Surface energy theory | 87 |
| 2.8.5 | Enhanced plastic flow theory | 87 |
| 2.8.6 | Hydride formation theory..... | 89 |
| 2.8.7 | Hydrogen attack | 89 |

| | | |
|---------|--|-----|
| 2.9 | Predictive modeling of NNPHSCC..... | 89 |
| 2.9.2 | Crack tip strain rate model..... | 95 |
| 2.9.3 | Superposition model..... | 98 |
| 2.9.4 | Corrosion fatigue model..... | 100 |
| 2.10 | Fatigue Cracking details..... | 102 |
| 2.10 | Crack closure..... | 108 |
| 2.11 | SCC in near-neutral pH environment and current models – A discussion..... | 113 |
| 2.12 | Objective..... | 117 |
| | References..... | 118 |
| 3.0 | Introduction..... | 147 |
| 3.1 | Experimental..... | 151 |
| 3.1.1 | Sample preparation..... | 151 |
| 3.1.2 | Mechanical loading..... | 156 |
| 3.1.3 | Post-test Analysis..... | 158 |
| 3.2 | Results..... | 159 |
| 3.2.1 | Characteristics of crack growth monitored by potential drop systems..... | 159 |
| 3.2.2 | Morphological characteristics of cracks on surface..... | 161 |
| 3.2.3 | Morphological characteristics of cracks at the depth direction..... | 166 |
| 3.2.4 | Morphological characteristics of fracture surface..... | 169 |
| 3.2.5 | Determination of crack growth rate..... | 169 |
| 3.3 | Discussion..... | 173 |
| 3.3.1 | Variation in local environment under the disbondment..... | 173 |
| 3.3.1.1 | Variation in CO ₂ concentration in the solution in contact with specimen surface..... | 173 |
| 3.3.1.2 | Effect of hydrogen abundance on dissolution rate..... | 175 |
| 3.3.1.3 | Variation in hydrogen concentration at the crack tip with distance from the open mouth ... | 176 |
| 3.3.2 | General understanding of cracking mechanisms of pipeline steels in near-neutral pH environments..... | 177 |

| | | |
|---------|--|-----|
| 3.3.3 | Crack growth mechanisms under disbonded coating | 179 |
| 3.3.3.1 | Crack growth at the surface tip | 179 |
| 3.3.3.2 | Crack growth at the depth tip | 184 |
| 3.3.4 | Growth rate behavior of surface cracks under disbonded coating | 186 |
| 3.4 | Conclusions | 190 |
| 3.5 | References | 192 |
| 4.0 | Introduction | 197 |
| 4.1 | Experimental | 199 |
| 4.1.1 | Sample preparation | 199 |
| 4.1.2 | Mechanical loading | 206 |
| 4.1.3 | Post-test Analysis | 206 |
| 4.2 | Results | 207 |
| 4.2.1 | Crack growth behavior of sharp crack under propagating loading in 5% CO ₂ (Test 1) | 208 |
| 4.2.2 | Crack growth behavior of sharp crack preceded by non-propagating loading in 5% CO ₂ (Test II) | 211 |
| 4.2.2.1 | Condition for crack initiation | 211 |
| 4.2.2.2 | Characteristics of crack morphologies | 212 |
| 4.2.2.3 | Crack growth rate behavior | 220 |
| 4.2.3 | Crack growth behavior of sharp crack preceded by non-propagating loading in 20% CO ₂ (Test III) | 223 |
| 4.2.3.1 | Condition of crack initiation | 225 |
| 4.2.3.2 | Characteristics of Crack morphology | 225 |
| 4.3 | Discussion | 232 |
| 4.3.1 | Crack growth rate behavior | 232 |
| 4.3.2 | Crack growth mechanisms of dormant cracks | 235 |
| 4.3.3 | Mechanisms of crack dormancy | 243 |
| 4.3.4 | Rate of discontinuous crack propagation | 248 |

| | | |
|---------|--|-----|
| 4.4 | Conclusions..... | 254 |
| | References..... | 257 |
| 5.1 | Introduction..... | 261 |
| 5.2 | Experimental..... | 263 |
| 5.2.1 | Justification of sample geometry and crack size/geometry used | 270 |
| 5.2.2 | Justification of stress level used..... | 271 |
| 5.3 | Results..... | 272 |
| 5.3.1 | Mechanical deformation of crack tip in air (Test P1) | 272 |
| 5.3.2 | Test results in the 20% CO ₂ environment | 274 |
| 5.3.2.1 | Corrosion behavior at sample surface | 274 |
| 5.3.2.2 | Crack re-initiation after hydrostatic testing..... | 274 |
| 5.3.2.3 | Crack tip morphology following reloading after hydrostatic testing | 276 |
| 5.3.2.4 | Crack propagation behavior | 276 |
| 5.3.3 | Test results in the 5% CO ₂ environment (Tests II and III)..... | 284 |
| 5.3.3.1 | Corrosion behavior at sample surface | 284 |
| 5.3.3.2 | Crack re-initiation following loading in the 5% CO ₂ environment after hydrostatic testing 284 | |
| 5.3.3.3 | Crack tip morphology following loading in the 5% environment after hydrostatic testing 285 | |
| 5.3.3.4 | Crack propagation behavior in the 5% CO ₂ environment..... | 289 |
| 5.3.4 | Comparison of fracture face morphologies..... | 294 |
| 5.4 | Discussion..... | 294 |
| 5.4.1 | Current understanding of crack propagation mechanisms | 294 |
| 5.4.2 | Crack re-initiation conditions..... | 298 |
| 5.4.2.1 | Environmentally enhanced mechanical considerations..... | 298 |
| 5.4.2.2 | Crack tip morphology considerations | 303 |
| 5.4.3 | Crack propagation..... | 306 |

| | | |
|---------|---|-----|
| 5.4.3.1 | Environmental effect on crack growth rates | 307 |
| 5.4.3.2 | Effect of loading frequency on growth rates | 308 |
| 5.4.3.3 | General Growth Behaviour at open circuit potential | 309 |
| 5.5 | Conclusions..... | 313 |
| | References..... | 314 |
| 6.1 | Introduction..... | 319 |
| 6.2 | Experimental | 320 |
| 6.2.1 | Sample preparation | 320 |
| 6.2.2 | Mechanical loading..... | 327 |
| 6.2.3 | Post-test Analysis..... | 327 |
| 6.3 | Results..... | 328 |
| 6.3.1 | Crack growth behavior of sharp crack under propagating loading (Test 1)..... | 328 |
| 6.3.2 | Crack growth behavior of sharp crack preceded by non-propagating loading (Test II) | 328 |
| 6.3.3 | Test results in 5% CO ₂ testing environment and applied cathodic potential of 0.9V | 334 |
| 6.3.3.1 | Corrosion behavior..... | 334 |
| 6.3.3.2 | Characteristics of crack morphologies | 334 |
| 6.3.3.3 | Condition of crack re- initiation..... | 339 |
| 6.3.3.4 | Crack growth rate behavior..... | 339 |
| 6.4 | Test IV results | 347 |
| 6.4.1 | Comparison of crack behavior when loaded at 100% SMYS in direct contact with C2 solution, in indirect contact with C2 solution and in air – Test IV | 347 |
| 6.4.2 | Crack growth behavior in test IV | 347 |
| 6.5 | Discussion..... | 350 |
| 6.5.1 | Crack morphology..... | 350 |
| 6.5.2 | Role of crack wall dissolution..... | 350 |
| 6.5.3 | Effect of hydrogen on crack morphology | 352 |
| 6.5.4 | Effect of hydrogen- enhanced localized plastic deformation..... | 357 |

| | | |
|-----------|---|-----|
| 6.5.6 | Crack propagation..... | 359 |
| 6.6 | Conclusions..... | 367 |
| | References..... | 368 |
| 7.0 | Introduction..... | 373 |
| 7.1 | Experimental..... | 375 |
| 7.1.1 | Justification of sample geometry and crack size/geometry used | 381 |
| 7.2 | Results..... | 382 |
| 7.2.1 | Mechanical deformation of crack tip in air (Test P1) | 382 |
| 7.2.2 | Open circuit potential test results..... | 384 |
| 7.2.2.1 | Corrosion behavior at sample surface at OCP | 384 |
| 7.2.2.2 | Crack re-initiation following loading at OCP..... | 384 |
| 7.2.2.3 | Crack propagation behavior at OCP | 387 |
| 7.2.3 | Test results at an applied potential of -0.9V | 387 |
| 7.2.3.1 | Surface features observed at -0.9V | 387 |
| 7.2.3.2 | Crack re-initiation following loading at -0.9V..... | 393 |
| 7.2.3.3 | Crack propagation behavior at -0.9V..... | 393 |
| 7.2.4 | Test results at an applied cathodic potential of -1.2V | 393 |
| 7.2.4.1 | Surface features observed at -1.2V | 393 |
| 7.2.4.2 | Crack re-initiation following loading at -1.2V..... | 394 |
| 7.2.4.3 | Crack propagation behavior at -1.2V..... | 394 |
| 7.3 | Discussion..... | 400 |
| 7.3.1 | Crack growth mechanism at applied cathodic potential of -1.2V | 400 |
| 7.3.2 | Crack growth mechanism at applied cathodic potential of -0.9V | 405 |
| 7.3.3 | Crack growth behaviour..... | 409 |
| 7.3.3.1 | Crack re-initiation | 409 |
| 7.3.3.2 | Crack propagation..... | 410 |
| 7.3.3.2.1 | Crack propagation – Average growth rates..... | 410 |

| | | |
|-----------|--|-----|
| 7.3.3.2.2 | Crack propagation – Corrosion fatigue behaviour | 412 |
| 7.4 | Conclusion | 418 |
| | References..... | 420 |
| | CONCLUSIONS..... | 423 |
| 8.1 | Summary and Conclusions..... | 424 |
| 8.2 | Recommendations for future work | 428 |
| A1.0 | Introduction..... | 431 |
| A2.0 | Experimental method | 432 |
| A3.0 | Results and discussion | 436 |
| A4.0 | Relevance of hydrogen permeation study to crack growth study | 445 |
| A5.0 | Conclusion | 448 |
| | References..... | 449 |
| B.1 | Materials | 454 |
| B.2 | Metallography | 454 |
| B.3 | Sample preparation | 454 |
| B.3.1 | Sample machining..... | 454 |
| B.3.2 | Sample Pre-fatigue cracking | 459 |
| B.3.3 | Wire attachment | 459 |
| B.4 | Test solution..... | 459 |
| B.5 | Chemical analysis of test solution..... | 459 |
| B.6 | Test Cell | 462 |
| B.7 | Test assembly | 462 |
| B.8 | Cathodic protection..... | 464 |
| B.9 | Crack growth measurement | 465 |
| B.10 | Post-test Sample analysis | 465 |
| B.11 | Potential Drop Data analysis..... | 467 |
| B.11 | Hydrogen permeation testing | 470 |

List of Tables

| | |
|--|-----|
| Table 2.1: Composition of simulation NNPHSCC soil solutions. Concentrations are in g/litre. pH measure after solution was sparged with 5% CO ₂ bal N ₂ | 55 |
| Table 3-1: Alloy (X65) composition..... | 152 |
| Table 3-2: Initial and final stress intensities calculated for the crack at the open mouth | 157 |
| Table 4-1: Alloy (X65) composition..... | 200 |
| Table 4-2: Test conditions | 205 |
| Table 4-3: Characteristics of crack growth for cracks on the specimen surface..... | 213 |
| Table 4-4: Characteristics of crack growth for cracks in the depth direction | 221 |
| Table 4-5: Width of crack opening at the bottom of pit after correction for hinge effect in test I | 245 |
| Table 4-6: Width of crack opening at the bottom of pit in test III..... | 247 |
| Table 5-1: Alloy (X65) composition..... | 264 |
| Table 5-2: Details of test conditions | 269 |
| Table 5-3: Characteristics of crack growth for cracks on the specimen surface | 283 |
| Table 5-4: Characteristics of crack growth for cracks in the depth direction..... | 283 |
| Table 5-5: Critical combined factor for surface crack initiation at the open mouth. All units in [(MPa√m) ³ Hz ^{-0.1}] | 300 |
| Table 5-6: Critical combined factor for depth crack initiation at the open mouth. All units in [(MPa√m) ³ Hz ^{-0.1}] | 300 |
| Table 6-1: Alloy (X65) composition..... | 323 |
| Table 6-2: Test conditions | 326 |
| Table 6-3: Characteristics of crack growth for cracks on the specimen surface | 340 |
| Table 6-3: Characteristics of crack growth for cracks in the depth direction..... | 341 |

| | |
|---|-----|
| Table 6-5: Width of crack crevice at the pre-fatigue crack tip (measured at the edge of the EDM slot) after correction for hinge effect at the open mouth | 356 |
| Table 7-1: Alloy (X65) composition..... | 378 |
| Table 7-2: Summary of test conditions | 380 |
| Table 7-3: Characteristics of crack growth for cracks on the specimen surface | 389 |
| Table 7-4: Characteristics of crack growth for cracks in the depth direction | 390 |
| Table A-1: Test Matrix | 435 |
| Table A-2: Summary of diffusion coefficients | 440 |
| Table B- 1: Alloy (X65) composition | 455 |
| Table B- 2: C2 solution composition (pH=6.29) | 461 |

List of Figures

| | |
|---|-----|
| Figure 2.1: Illustration of the electrochemical nature of corrosion [1]. | 9 |
| Figure 2.2: Showing SCC cracks and pitting corrosion on a pipeline | 11 |
| Figure 2.3: Factors required for SCC to occur | 21 |
| Figure 2.4:(a) Preferential corrosion attack in pearlite region , (b) Showing corrosion along banded structure [15]. | 23 |
| Figure 2.5: Stresses in pipelines [4] | 34 |
| Figure 2.6: Modes of loading a) mode I, b) mod II, c) mode III [63] | 43 |
| Figure 2.7: Variation of elongation to failure with applied cathodic potential [79] | 50 |
| Figure 2.8: Potential ranges where SCC is likely to occur [1] | 56 |
| Figure 2.9: showing a pipeline in which severe de-bonding of the polyethylene coating has occurred. | 59 |
| Figure 2.10: Tape tenting around a tape overlap [45] | 59 |
| Figure 2.11: Illustration of fatigue life reduction due to load cycling in aggressive environment [100] | 64 |
| Figure 2.12: Schematic illustration of (a) slip dissolution mechanism (b) hydrogen embrittlement in aqueous media [101] | 67 |
| Figure 2.13: Schematic representations of possible combinations of mechanical fatigue and environmentally enhanced crack growth (a) fatigue crack growth in inert environment (b) stress corrosion cracking under sustained loading (c) True corrosion fatigue (d) superposition of (a) and (b), (e) superposition of (b) and (d) [101] | 75 |
| Figure 2.14: Crack propagation by film rupture model showing corrosion tunnel mechanism with grooved fracture face [34] | 78 |
| Figure 2.15: Crack propagation mechanism by tunnel mechanism (a) by formation of tunnel at slip steps and ductile deformation and fracture of remaining ligament (b) schematic representation of tunnel mechanism of SCC and flat slot formation [34] | 79 |
| Figure 2.16: Stages of NNPHSCC crack propagation [46] | 91 |
| 2.9.1 Dissolution controlled model | 92 |
| Figure 2.17: Dependence of fatigue (a) threshold stress (b) threshold stress intensity on crack length [203] | 106 |
| Figure 2.18: Comparison of experimental and predicted value of fatigue threshold [203] | 107 |

| | |
|---|-----|
| Figure 2.19: Illustration of short crack growth deceleration [202] | 109 |
| Figure 2.20: Crack closure mechanisms [208]..... | 111 |
| Figure 2.21: Classification of cracks..... | 114 |
| Figure 2.22: Progression of a typical NNPHSCC crack | 115 |
| Figure 3-1: Typical microstructure of the alloy X65 used in this study | 153 |
| Figure 3-2: Test sample designed for this study | 154 |
| Figure 3-3: Schematic drawing of the corrosion test cell used for study | 155 |
| Figure 3-4: Potential drop data showing crack propagation during test | 160 |
| Figure 3-5: Corrosion products on sample surface | 162 |
| Figure 3-6: Low magnification image of crack tip (a) open mouth (b) 75 mm from the open mouth (c) 150 mm from the open mouth..... | 163 |
| Figure 3-7: Pre-crack tips in the 5% CO ₂ environment (a) open mouth, (b) 75 mm from open mouth and (c) 150 mm from open mouth | 164 |
| Figure 3-8: High magnification image of the crack tip at the sample surface (a) open mouth, (b) 75 mm from open mouth, (c) 150 mm from open mouth..... | 165 |
| Figure 3-9: Low magnification image of crack tip in the depth (a) open mouth, (b) 75 mm from open mouth, (c) 150 mm from open mouth | 167 |
| Figure 3-10: High magnification image of the crack tip in the depth direction (a) open mouth, (b) 75 mm from open mouth, (c) 150 mm from open mouth | 168 |
| Figure 3-11: Fracture face (half section) of cracks at (a) open mouth (b) 150 mm from OM..... | 170 |
| Figure 3-12: (a) Pre- and post-crack sizes at sample surface (b) Pre- and post-crack sizes in depth direction | 171 |
| Figure 3-13: Variation of average growth rates with distance from the open mouth | 172 |
| Figure 3-14: Variations in crack aspect ratio with distance from the open mouth of the disbondment.... | 174 |
| Figure 3-15: Comparison of the corrosion fatigue behavior of crack growth data at the open mouth to that of a through-thickness crack. | 187 |
| Figure 4-1: Typical microstructure of the alloy X65 used in this study | 201 |
| FIGURE 4-2: Test sample designed for this study | 202 |
| Figure 4-3: Schematic drawing of the corrosion test cell used for study..... | 204 |

| | |
|--|-----|
| Figure 4-4: Low magnification image of pre-crack tip and crack tip (a) open mouth (b) 75 mm from the open mouth (c) 150 mm from the open mouth | 209 |
| Figure 4-5: High magnification image of the crack tip width measured at sample surface (a) open mouth, (b) 75 mm from open mouth, (c) 150 mm from open mouth..... | 210 |
| Figure 4-6: Potential drop data for test II..... | 214 |
| Figure 4-7: Post-test crack lengths measured at the sample surface after test II at (a) open mouth, (b) 75 mm from OM, (c) 150 mm from OM | 215 |
| Figure 4-8: Crack tip Morphology at the sample surface in Test II (a) OM (b) 75 mm from OM, (c) 150 mm from OM | 216 |
| Figure 4-9: Crack morphology in the depth direction for test II (a) Open mouth, (b) 75 mm from OM, (c) 150 mm from OM | 218 |
| Figure 4-10: Crack tip morphology in depth direction at higher magnification for test II (a) Open mouth, (b) 75 mm from OM, (c) 150 mm from OM (d) higher magnification of (c) | 219 |
| Figure 4-11: Initial aspect ratios | 222 |
| Figure 4-12: Average crack growth rates measured at sample surface..... | 224 |
| Figure 4-13: Pre-fatigue crack and post-test crack tips in the 20% CO ₂ environment - test III (a) open mouth, (b) 75 mm from open mouth and (c) 150 mm from open mouth..... | 226 |
| Figure 4-14: High magnification image of the crack tip width at sample surface for test III (a) open mouth, (b) 75 mm from open mouth, (c) 150 mm from open mouth..... | 227 |
| Figure 4-15: Low magnification image of crack tip in the depth direction for test III (a) open mouth, (b) 75 mm from open mouth, (c) 150 mm from open mouth | 229 |
| Figure 4-16: High magnification image of the crack tip in the depth direction for test III (a) open mouth, (b) 75 mm from open mouth, (c) 150 mm from open mouth..... | 230 |
| Figure 4-17: Aspect ratios of cracks in Test III | 231 |
| Figure 4-18: Crack growth rate of Test III..... | 231 |
| Figure 4-19: Combined corrosion fatigue analysis for tests II and III..... | 233 |
| Figure 4-20: Comparison of the corrosion fatigue behavior of crack growth data at the open mouth in test 1 to that of a through-thickness crack | 236 |
| Figure 4-21: (a) Stress distribution ahead of a crack tip (b) triaxial stress state in the hydrogen process zone (c) profile of a crack that experienced periodic dormancy during crack propagation..... | 238 |
| Figure 4-22: Comparison of crack growth rate (a) at sample surface (b) in the depth direction | 249 |

| | |
|---|-----|
| Figure 4-23: Crack morphology in the depth direction of the crack located at MP of Test III..... | 252 |
| Figure 5-1: Typical microstructure of the alloy X65 used in this study | 265 |
| FIGURE 5-2: Test sample designed for this study | 266 |
| Figure 5-3: Schematic drawing of the corrosion test cell used for study..... | 268 |
| Figure 5-4: Pre-fatigue crack morphology of verification test (a) before, and (b) after 1min hold at 100% SMYS..... | 273 |
| Figure 5-5: Post-test surface features before cleaning (a) test I, (b) Test II and III. Insets are higher magnification images (at 400X)..... | 275 |
| Figure 5-6: Crack tip morphology at sample surface in test I (a) at 75 mm from OM, (b) at 150 mm from OM..... | 277 |
| Figure 5-7: Secondary cracks at the pre-fatigue crack tip in test I (a) at low magnification, (b high magnification | 278 |
| Figure 5-8: Surface crack profile for test I at (a) 75 mm from OM, (b) 150 mm from OM | 279 |
| Figure 5-9: Crack morphology in the depth direction in test I (a) at 75 mm from OM, (b) at 150 mm from OM..... | 280 |
| Figure 5-10: Crack tip morphology in the depth direction in test I (a) at 75 mm from OM, (b) at 150 mm from OM | 281 |
| Figure 5-11: Fractured surface for test I showing half of crack section (a) open mouth (b) 75 mm from OM, (c) 150 mm from OM | 282 |
| Figure 5-12: Post-test pre-fatigue crack tip morphology (a) 75 mm from OM in test II, (b) 150 mm from OM in test II, (c) 75 mm from OM in test III, (d) 150 mm from OM in test III..... | 286 |
| Figure 5-13 : Surface profiles of cracks at 75 mm from OM in (a) Test II and (b) Test III | 287 |
| Figure 5-14 : Surface profiles of cracks at 150 mm from OM in (i) Test II and (iii) Test III..... | 288 |
| Figure 5-15: Depth profiles of cracks at 75 mm in(a) Test II and (b) Test III..... | 290 |
| Figure 5-16: Depth profiles of cracks at 150 mm in (a) Test II and (b) Test III..... | 291 |
| Figure 5-17: Crack tips at higher magnification at 75 mm from OM in depth direction (a) Test II, (b) Test III | 292 |
| Figure 5-18: Crack tips at higher magnification at 150 mm from OM in depth direction (a) Test II, (b) Test III..... | 293 |
| Figure 5-19: Fractured surface of test II showing just half of crack cross section (a) open mouth (b) 75 mm from OM, (c) 150 mm from OM | 295 |

| | |
|--|-----|
| Figure 5-20: Fractured surface for test III showing half of crack section (a) open mouth (b) 75 mm from OM, (c) 150 mm from OM | 296 |
| Figure 5-21: Growth rate data for all tests reported; showing Chen and Sutherby’s combined factor. Data for the long crack was obtained in the same environment as the other tests results presented in the figure. | 304 |
| Figure 5-22: Comparison of growth at 100% SMYS max stress and 75% max stress. Test Prev was done at 75% SMYS, and subjected to low temperature creep prior to crack re-initiation in 5% CO ₂ environment [18]...... | 311 |
| FIGURE 6-1: Test sample designed for this study. All units in mm. | 322 |
| Figure 6-2: Typical microstructure of the alloy X65 used in this study | 324 |
| Figure 6-3: Schematic drawing of the corrosion test cell used for study..... | 325 |
| Figure 6-4: Pre-crack tips in Test I (a) open mouth, (b) 75 mm from open mouth and (c) 150 mm from open mouth..... | 329 |
| Figure 6-5 High magnification image of the crack tip in test I (a) open mouth, (b) 75 mm from open mouth, (c) 150 mm from open mouth..... | 330 |
| Figure 6-6: Post-test crack lengths measured at the sample surface after test II | 332 |
| Figure 6-7: Crack tip Morphology in Test II (a) OM (b) 75 mm from OM, (c) 150 mm from OM..... | 333 |
| Figure 6-8: Corrosion behavior at the sample surface (a) at the open mouth (b) 75 mm from the open mouth, (c) 150 mm from the open mouth. | 335 |
| Figure 6-9: Post test crack lengths at the sample surface in test III (a) at the open mouth (b) at 75 mm from open mouth (c) at 150 mm from open mouth..... | 336 |
| Figure 6-10: Crack tip morphology in test III (a) at the open mouth (b) 75 mm from open mouth (c) at 150 mm from open mouth..... | 338 |
| Figure 6-11: Fracture surface morphology of the test sample in test III at the (a) OM, (b) 75 mm from OM and (c) 150 mm from OM. The images clearly show that while there was significant growth at the open mouth in both the surface and depth directions, there was very little growth at 75 mm from the OM and no growth at 150 mm from the OM. | 342 |
| Figure 6-12: Crack growth behavior in tests I and III..... | 343 |
| Figure 6-13: Initial aspect ratios | 344 |
| Figure 6-14: Final aspect ratios..... | 345 |
| Figure 6-15: Ratio of initial to final aspect ratios | 346 |

| | |
|--|-----|
| Figure 6-16: Crack morphology when cyclically loaded in (a) air, (b) indirect contact of crack tip with C2 solution, (c) direct contact of crack tip with C2 solution | 348 |
| Figure 6-17: Crack outlines: in air, indirect contact with solution, direct contact with solution. Crack outline at sample surface (horizontal), crack outline in depth direction (vertical)..... | 349 |
| Figure 6-18: Variation of cathodic potential with distance from the open mouth, at different applied potentials. Legend shows the cathodic potential applied at the open mouth of the disbondment..... | 351 |
| Figure 6-19: Comparison of crack crevice width in (a) Tests II (red) and (b) Test III (blue). Outline shows both the precrack and in-test crack growth combined | 356 |
| Figure 6-20: Fracture face morphology at the open mouth in (a) test III and (b) test II | 362 |
| Figure 6-21: Combined crack growth factor plot for tests I and III..... | 364 |
| Figure 6-22: Comparison of the growth rates in test III with those of a through-thickness crack..... | 366 |
| FIGURE 7-1: Test sample designed for this study. All units in mm. | 377 |
| Figure 7-2: Typical microstructure of the alloy X65 used in this study | 379 |
| Figure 7-3: Schematic Drawing of the corrosion test cell used for the study | 380 |
| Figure 7-4: Pre-crack morphology of verification test..... | 383 |
| Figure 7-5: Crack tip morphology after 1min hold at 100% SMYS..... | 383 |
| Figure 7-6: Post-test surface features before cleaning in test I | 385 |
| Figure 7-7: Corroded surface at (a) open mouth (b) 75 mm and (c) 150 mm from the open mouth (d) Higher magnification image of 150 mm from OM..... | 386 |
| Figure 7-8: Average growth rates; growth initiated at R=0.58 in test I, but at R=0.6 in tests II and III... | 388 |
| Figure 7-9: (a) Initial aspect ratio (b) Final aspect ratio | 391 |
| Figure 7-10: Corroded surface of the test sample at (a) open mouth (b) 75 mm from open mouth (c) 150 mm from open mouth (d)150 mm from open mouth after sample has been rotated at 45° relative to secondary detector to confirm the features seen are pits not deposits on sample surface. Sample was tested at -0.9V cathodic potential..... | 392 |
| Figure 7-11: Corroded surface of the test sample at (a) open mouth (b) 75 mm from open mouth (c) 150 mm from open mouth. Sample was tested at -1.2V cathodic potential..... | 395 |
| Figure 7-12: Half section of ruptured sample. Sample ruptured during test and was manually held together for photo. Micro-crack colony was found oriented along a 45° line from shear lip. | 396 |
| Figure 7-13: a) Array of tiny secondary cracks at crack tip next to shear lip, b) higher magnification image of crack array..... | 397 |

| | |
|---|-----|
| Figure 7-14: Cluster of pits at crack tip (75 mm from open mouth). Highlighted area shows dense pit clusters around the final crack tip | 398 |
| Figure 7-15: Variation of potential with distance from the open mouth of a disbondment | 399 |
| Figure 7-16: Schematic depiction of hydrogen distribution within disbondment at an applied potential of -1.2V..... | 401 |
| Figure 7-17: Schematic depiction of hydrogen ion distribution inside a disbondment at an applied potential of -0.9V | 408 |
| Figure 7-18: Growth curves in test III | 413 |
| Figure 7-19: Ratio of initial aspect ratio to final aspect ratio | 415 |
| Figure 7-20: Growth curves in tests at OCP and -1.2V | 417 |
| Figure A-1: Test setup | 433 |
| Figure A-2: Variation in permeation behavior with distance from open mouth at OCP in test I | 437 |
| Figure A-3: Variation in permeation behavior with distance from open mouth at -1.2V (Test II)..... | 439 |
| Figure A-4: Repeat test of permeation behavior at -1.2V | 440 |
| Figure A-5: Variation in permeation behavior with distance from open mouth at -0.9V (test II) | 442 |
| Figure A-6: Variation of permeation behavior with distance from the open mouth at OCP in 20% CO ₂ environment. | 443 |
| Figure B-1: Typical microstructure of the alloy X65 used in this study..... | 456 |
| Figure B-2: Test sample designed for this stud..... | 457 |
| Figure B-3: Test sample orientation on pipe section | 458 |
| Figure B-4: Wire connections for test setup | 460 |
| Figure B-5: Corrosion test cell used for this study | 463 |
| Figure B-6: Typical potential drop data..... | 468 |
| Figure B-7: Stress intensity factor equation for a semi-elliptical crack..... | 471 |
| Figure B- 8: Test setup..... | 472 |

CHAPTER ONE

INTRODUCTION

1.0

Introduction

It is estimated that the oil and gas pipeline network in Canada alone is almost long enough to stretch all the way from earth to the moon and back [1]. Although, pipelines are buried seemingly harmlessly all around us, they present an ever present risk of danger capable of unleashing immense horror and destruction in the event of an accidental pipeline rupture followed by an explosion. Such accidental rupture of pipelines often results from the compromise of pipeline integrity by the formation of in-service cracks on pipelines. It is instructive to note that there is hardly any single pipeline network in Canada, or elsewhere around the world, that does not have these cracks at various stages of growth.

Since near-neutral pH stress corrosion cracking (NNPHSCC) was discovered on Canadian pipelines in 1985, several pipeline ruptures have been attributed to NNPHSCC in Canada and the US. This form of corrosion often occurs even where otherwise effective corrosion prevention measures are put in place. NNPHSCC usually initiates on pipeline surface at sites of coating imperfection, disbondment or mechanical damage. At such sites groundwater containing CO₂ and specific chemical species could set up a potent environment with pH in the 5.5-7.5 range which activates NNPHSCC development. Popular opinion among NNPHSCC researchers is that NNPHSCC develops through a combination of anodic dissolution and hydrogen embrittlement. Anodic hydrogen embrittlement is thought to be responsible for the quasi-cleavage nature of crack propagation in rather ductile materials while anodic dissolution is assumed to be responsible for the often noticed corrosion and widening of the crack walls.

There are two aspects to the NNPHSCC problem – initiation and propagation. A lot of studies have been conducted on the initiation aspect of the problem and our understanding of the initiation mechanism has significantly improved over the years. Although a lot of studies have

also been carried out on the propagation aspect of the problem, current understanding of the propagation of these cracks could still be quite surprisingly inadequate. NNPHSCC is currently managed by in-line inspection for oil pipelines or by hydrostatic testing for gas pipelines. These expensive procedures need to be repeated at predetermined intervals and involve digging up the pipe in order to carry out tests and inspection for crack growth. Re-inspection intervals are currently determined using empirical models that have proven to rather underestimate crack growth rates [2]. This increases the risk of accidental pipeline rupture. To reduce this risk, a few more inspections than necessary are usually carried out, further increasing the cost of pipeline integrity management schemes. Further, it is not possible to dig up just every pipe. Hence, there is a significant interest among pipeline operators in replacing the current industry approach with accurate mathematical models that can predict the initiation and growth rate of NNPHSCC cracks.

Careful examination of currently available literature on the growth of NNPHSCC cracks revealed that currently existing models were developed using samples and/or crack geometries that do not properly represent those of NNPHSCC cracks typically observed in the field. For instance, whereas NNPHSCC cracks are typically shallow non-through-thickness cracks, existing models were developed using samples that simulate through-thickness cracks. Results from contemporary research in fatigue crack growth suggest that shallow cracks tend to grow at significantly higher rates than through-thickness cracks [3]. Shallow cracks may even grow under loading conditions where through-thickness cracks are typically dormant. This difference in the behaviour of shallow and through-thickness cracks may be responsible for the underestimation of the growth rate of NNPHSCC cracks.

Therefore, this study was conducted to produce a model that more accurately predicts the growth behaviour of NNPHSCC cracks on steel pipelines, by simulating the growth of shallow cracks rather than through-thickness cracks, in a near-neutral pH environment. In order to achieve this objective, a unique sample and corrosion cell that have never been used in any reported NNPHSCC study have been designed for this study. The design removes several experimental constraints that have hitherto precluded a thorough investigation of the growth rate of NNPHSCC cracks using shallow flaws. The new design also allows the study of several NNPHSCC rate parameters simultaneously.

This thesis reports the findings of recent studies conducted by the author as part of a bigger project on the stress corrosion cracking of pipeline steels in near neutral pH environments. The thesis is presented with a detailed literature review of the problem (Chapter 2), results and discussions are presented in chapters 3-7 and Appendix A.

In Chapter 3, the crack growth behavior of a sharp crack at open circuit potential, representative of an actively growing crack, was examined along with the influence of spatial separation from the open mouth of a disbondment on crack tip morphology and on variations in growth rates.

In Chapter 4, the influence of environmental blunting of the crack tip under conditions where environmentally enhanced creep deformation is possible was examined. This revealed vital information on the effect of crack tip/wall dissolution as well as the effect of low temperature creep and hydrogen enhanced plasticity. Conditions for crack re-initiation at the tip of an environmentally blunted crack were also examined.

In Chapter 5, the role of mechanical deformation, under conditions where environmentally enhanced creep deformation could occur, was examined. Variations in the effect

of spatial separation from the open mouth of the disbondment, and its attendant gradient of environmental effects, on crack tip morphology were examined. Conditions for crack re-initiation under these conditions, which are representative of crack behavior after hydrostatic testing, were determined.

In Chapter 6, the role of hydrogen enhanced room temperature creep, under conditions where crack tip/wall dissolution was eliminated, was examined.

In Chapter 7, the effect of applied cathodic potentials on the nature of the environment under the disbondment, and its effect on crack growth rates, was determined. This study also revealed vital information on possible stress corrosion cracking initiation mechanism.

A summary of findings and suggestions for future work is provided in Chapter 8.

Appendix A presents hydrogen permeation data – a qualitative measure of the amount of hydrogen present in the system. This provides a qualitative measure of the variation in hydrogen flux through the system with distance from the open mouth.

The methodology of study is attached as Appendix B.

References

- 1) National Energy Board, (1996) "Public Enquiry Concerning Stress Corrosion Cracking on Canadian Oil and Gas Pipelines," Report #MH-2-95.
- 2) Chen, W., and Sutherby, R. L., (2007) *J. Metallurgical and Materials Transactions*, 38A: 1260-1268.
- 3) McClung, R. C., and Sehitoglu, H., (1992) *ASME J. of Engr. Matls. Tech.*, 114: 1-7.

CHAPTER TWO

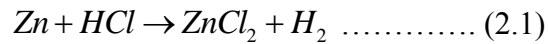
LITERATURE REVIEW

2.1 Important background concepts

This section is intended to briefly introduce important concepts that are relevant to subsequent development of the discussion on near-neutral pH stress corrosion cracking (NNPHSCC) of oil and gas steel pipelines. The contents of section 2.1 are only intended as brief introductions and more detailed information is provided on each concept as necessary later in this chapter.

2.1.1 General description of corrosion

Corrosion is usually defined as the destructive result of chemical reaction between a metal or a metal alloy and its environment. Corrosion returns a piece of metal to its original combined (often oxide) form. Aqueous corrosion is one of the most often encountered types of corrosion. NNPHSCC involves aqueous corrosion. Aqueous corrosion involves the transfer of electronic charge in aqueous solutions, such as water, seawater, atmospheric moisture, ground water *etc.*, basically water in which various salts and gases are dissolved [1, 2]. Thus, aqueous corrosion is electrochemical in nature, with the aqueous solution acting as the electrolyte through which electronic charge(s) are transferred. As in all electrochemical reactions, some form of anodic and cathodic reaction must occur concurrently within the solution. A typical corrosion reaction is the attack of zinc by hydrochloric acid [1],



in which the anodic and cathodic reactions are:



This type of half reactions is typical of most corrosion processes i.e., the corroding metal (anode) is oxidized to provide electrons for the reduction of another ionic specie. This is illustrated in figure 2.1. It must be pointed out that a sequence of half-cell reactions might sometimes be involved in forming the final corrosion product. It is important to stress that the corroding metal is always the anode in corrosion processes. The cathode in this type of reaction may often be difficult to identify. Sometimes it is another metal to which the corroding metal is coupled, but often it is not the entire metal piece; it might just be a localized region of the same piece of metal that becomes cathodic relative to other regions because of metallurgical differences, differential aeration, differences in concentration of the solution to which the parts of the same piece of metal is exposed, *etc.* For steel corrosion, iron always acts as the anode while the cathode may be any of those aforementioned.

There are different forms of corrosion, but galvanic and pitting corrosion are of particular importance to the rest of this dissertation and are the only ones briefly discussed here. Also, several mechanisms are known to operate in most corrosion processes, but hydrogen induced cracking is of special relevance to subsequent discussion in this dissertation and it is the only one discussed in this section on background concepts.

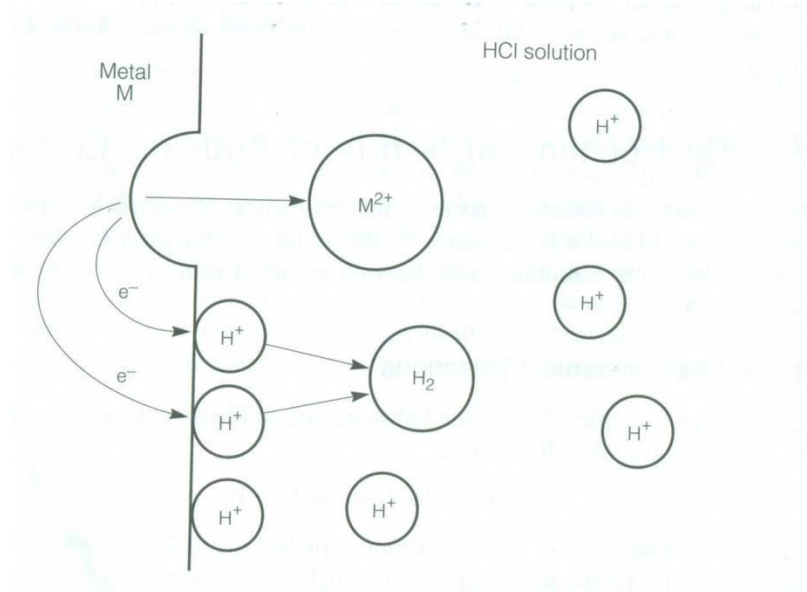


Figure 2.1: Illustration of the electrochemical nature of corrosion [1].

2.1.2 Galvanic corrosion

This type of corrosion, which occurs when two dissimilar metals are coupled in the presence of an electrolyte, causes one of the metals to be preferentially attacked while the other is protected from corrosion attack. Which metal gets attacked and which is not is mainly determined by the position of the two metals on the galvanic series (or electrochemical series). Generally, the more anodic material (the one with the more negative potential) gets attacked while the more cathodic one (the one with the more positive electrochemical potential) is seemingly immune to attack. However, as already mentioned localized metallurgical (or environmental) variations within the same piece of metal can cause one part to be anodic relative to the other, resulting in galvanic corrosion.

2.1.3 Pitting corrosion

A pitted pipeline surface is shown in Figure 2.2. Pitting corrosion occurs as a result of localized attack of an otherwise resistant metal surface that results in the formation of holes (pits) on the metal surface [1, 3]. It usually occurs as a result of localized/non-uniform dissolution at the metal surface, possibly because of differences between the rate of dissolution of precipitates/inclusions and the adjacent matrix. Pitting corrosion is a very insidious form of corrosion as it may cause a material to fail as a result of perforation with an otherwise little loss of mass. Pits may be widely spaced or may occur very close together, in which case neighbouring pits may coalesce to form a bigger one. Pits are sites for stress concentration, hence cracks may initiate from such sites at applied stress levels below the yield strength of the alloy. This is of particular significance in SCC of pipeline steels as will be discussed later.

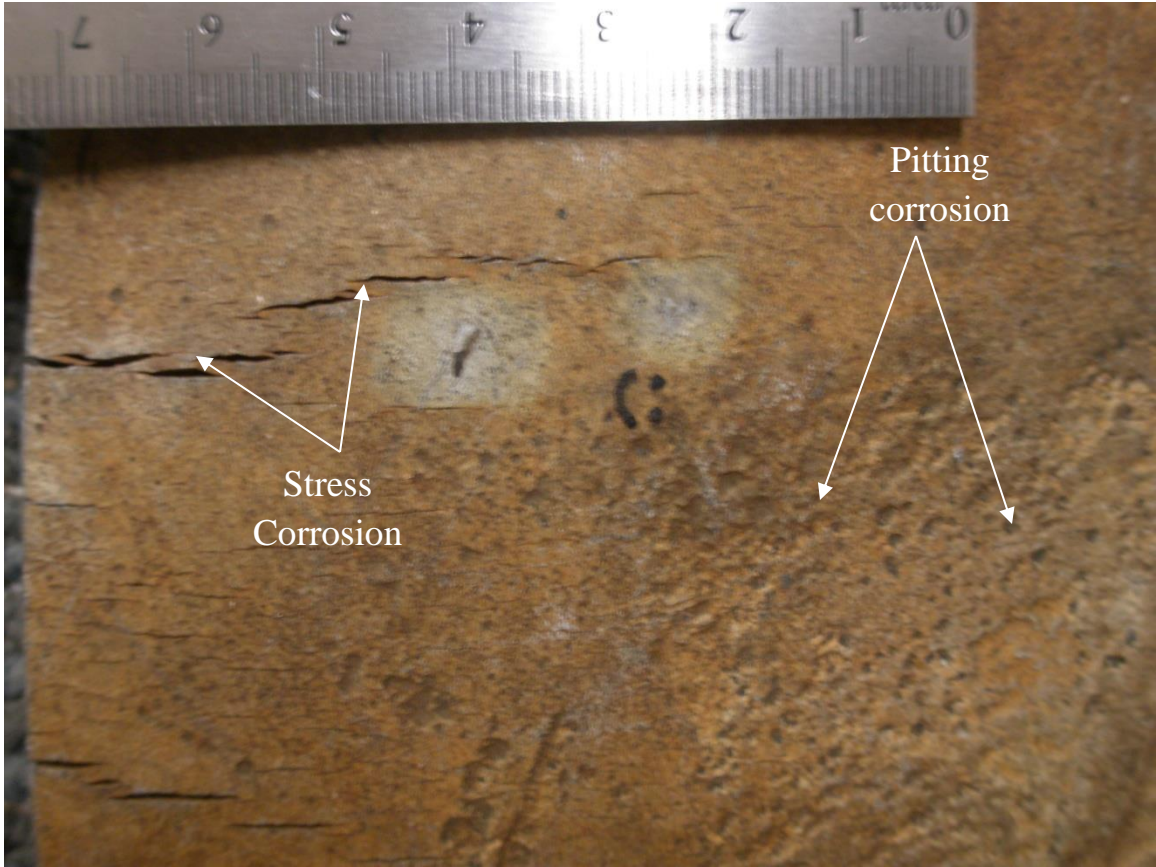


Figure 2.2: Showing SCC cracks and pitting corrosion on a pipeline

2.1.4 Hydrogen embrittlement (hydrogen induced cracking)

Hydrogen assisted cracking is a well-known metallurgical phenomenon. This effect is caused by the entrapment of atomic hydrogen within the crystal lattice of a metal. Hydrogen has only one proton in its nucleus and is so small that it can easily migrate through the crystal structure of metals and alloys [1]. Its entry into metals is known to result in a loss of ductility, which could assist brittle cracking. Also, atomic hydrogen may recombine within the crystal lattice, forming hydrogen gas, which may form internal voids from which cracks may nucleate due to high (local) gas pressure [1]. It is also generally accepted that hydrogen inside a metal lattice may act to weaken interatomic bonds between metal atoms especially around crack tips where plane strain stress conditions exist. Furthermore, at high temperatures, hydrogen is also capable of reacting with carbon in steel causing degradation in mechanical properties. NNPHSCC is known to involve hydrogen assisted cracking. Several mechanisms are known to contribute to hydrogen assisted cracking. More substantial information is provided on this subject in later sections.

2.1.5 Pipelines operation and corrosion prevention

Oil and gas pipelines are an important part of the energy industry. To satisfy the enormous daily demand for energy, copious amounts of oil and gas products have to be conveyed from various production facilities to the final consumer in an economic, safe and energy efficient manner. A network of steel pipelines has proven to be adequate for this purpose. Oil and gas pipelines either bear compressed or pressurized petroleum products; hence, they operate at intensely high pressures. For example, natural gas is compressed to as high as 8700 kPa [4]. Thus, to prevent disastrous failures great care must be taken to ensure that there is no sudden release of the enormous pressures stored in these pipelines. As earlier suggested, corrosion can compromise the safe operation of these pipelines; hence, several measures have been developed over the years to forestall the occurrence of accidental leakages and/or rupture of operating pipelines.

To prevent most forms of corrosion, several methods have been devised to isolate the pipe surface from the environment, in a bid to prevent moisture and ions that induce the electrochemical processes that cause corrosion from reaching the pipe surface. A major way of achieving this is by applying different types of coatings to the pipe surface. Corrosion protection techniques such as cathodic or anodic protection, in which an applied potential is used to prevent corrosion of pipelines, may also be used alone or in combination with surface coatings. Common examples of coating materials include: asphalt, coal tar and polyethylene tape. However, in the presence of holidays, breaks, or localized de-bonding of the coating material, isolated portions of the pipe surface may be exposed to the environment. This sort of localized exposure of the pipe surface to the environment has been found to be a major recipe for environmentally assisted cracking – a broad group of corrosion phenomena to which stress corrosion cracking belongs.

2.2 Environmentally induced cracking

Environmentally induced cracking refers to brittle material failures that result from the interaction between a tensile stress and a corrosive environment. Corrosion rates are typically quite low and EIC often results in component failure at operating stresses well below the yield strength of the material in question [1]. EIC is further subdivided into:

1. Stress Corrosion Cracking (SCC)
2. Corrosion Fatigue (CF)
3. Hydrogen Embrittlement (HE)***

***Pure HE of steels is more appropriately classified as part of hydrogen damage rather than as part of EIC. However, it is included here because some of the mechanisms involved in HE are similar to those typically associated with EIC

2.2.1 Stress corrosion cracking

Stress corrosion cracking (SCC) is customarily defined as the delayed failure of alloys by cracking when exposed to certain environments in the presence of static tensile stress [2]. SCC is distinguished from other forms of corrosion cracking failures by the fact that *‘the stress level at which such failures occur is typically well below the stress required for mechanical failure in the absence of corrosion, and the threshold stress level below which stress corrosion cracking cannot occur may be as low as 10% of the yield strength of the alloy’* [2]. The tensile stress leading to SCC failure may result from service loads (hoop stress for a pipeline), residual stresses from the fabrication process, mismatch in fit-up, soil movement, heat treatment or by wedging action of corrosion products.

2.2.2 History of stress corrosion cracking

Stress corrosion cracking (SCC) was first observed in the last half of the 19th century as the so called season cracking of cold drawn brass cartridge shells in ammonium fumes. It became a very important problem in the explosion of firearm ammunition during the world wars. With the rapidly expanding power industry during the industrial revolution, SCC quickly acquired a certain notoriety which earned it its deserved attention with the frequent cracking of brass condenser tubing (but not unalloyed copper) and the caustic cracking of carbon steel engine boilers. It was during this era that the problem became important enough to acquire its own name “season cracking”. SCC was also observed on mild steels in nitrate environment and aluminum alloys in moist atmosphere in the early 20th century. Early in the same century it became obvious very quickly that the problem was more widespread than originally thought as SCC was detected on magnesium alloys in moist atmospheres; with the advent of the aerospace industry it was found on titanium in nitrates, hot salts, methanol and N₂O₄, on martensitic steels in the aerospace

industry; stainless steels in chlorides in the paper, chemical and petroleum industries; pipeline steels under cathodic protection; and nickel alloys in nuclear-purity water [5, 6]. Soon, SCC was observed in almost all metals and alloys, even pure metals, in certain environments and under certain service conditions.

With the notoriety SCC was gaining in the late 19th century, early work quickly identified ammonia environments with SCC. It soon became obvious that certain material-environment interaction were necessary for the development of the phenomenon. However, with the list of known material-environment interactions growing by the day, exception to the known rule(s) quickly multiplied and it became known early that there may not be any specificity to the environment/material combinations required for SCC to develop. With further understanding of the problem, it was realized that regardless of the environment in which it occurs, the specific causative species do not need to be present in large quantities or at a high concentration before SCC develops.

The development of the electron microscope, transmission electron microscope and particularly the carbon replica technique led to significant advancement in the understanding of the SCC phenomena. With carbon replicas of fracture surfaces, it was discovered that SCC fracture faces contained macroscopically brittle failure features and electron microscopy led to the differentiation of the features involved in SCC from those of other failures. For instance it was quickly realized that even when SCC occurred in very ductile materials, SCC cracks are always macroscopically brittle. Finally, the development of fracture mechanics has had a tremendous impact on current understanding of SCC. The ability to analyze the stress fields and stress distribution around cracks coupled with increases in the understanding of material behavior under fatigue situations opened new vistas in the study of SCC.

Although there has been a lot of improvement in our understanding of SCC, and clearly there has been a lot of progress made over the years, there still remains a lot of uncertainty about the phenomenon. For instance, there is yet a lot of uncertainty about its initiation and propagation mechanism. Although there are lots of theories about how SCC initiates and develops over time, there is not a single theory that fully explains (by itself) all that is involved in the initiation or propagation of SCC either individually or as whole. Worse still, there is not a single theory that is universally accepted by experts in this field on the initiation and propagation of SCC. Perhaps, more than anything else, the best testimonial to the incompleteness of our understanding of SCC is the fact that despite the huge resources devoted yearly to researching and managing SCC, there are still quite a few failure/rupture incidences, often with grave consequences, attributed to SCC around the world. Among what is known for certain right now are: certain materials with high strength and ductility fail catastrophically in certain environments; SCC is able to develop well below nominal fracture stress in purely mechanical failures; the fact that a material is inert to SCC in one environment does not mean it won't perform woefully in other environments; SCC is still discovered frequently in new material/environment combinations. And oh lest we forget, SCC can be either transgranular or intergranular. Besides these, many things still reside in the realm of speculations.

2.2.3 SCC in pipelines

SCC is a major problem plaguing oil and gas pipelines around the world. From Canada to Australia, Europe, Middle East to the United States, SCC induced pipeline failures have been reported. Generally, innocuous looking, very fine and shallow cracks develop on the surface of

the pipe; they deepen, elongate and/or coalesce over time to form decent size cracks that ultimately lead to leakage or outright rupture of segment(s) of the pipe.

At first, SCC in pipelines was thought to be exclusively intergranular in nature, but some of the more recent failures have been shown to be transgranular [7]. This difference in the nature of fracture has been the subject of much research and it is now recognized that two unique forms of SCC are possible in buried pipelines. Further, it has also been established that the operational type of SCC is dependent on the nature of the environment in which the corrosion occurs, particularly its pH – intergranular SCC (IGSCC) occurs in environments having pH values of about 9.0-10.5 while transgranular SCC occurs in environments having pH values of about 5.5-8.5 (TGSCC). Consequently, intergranular SCC is sometimes referred to as high pH SCC while transgranular SCC is referred to as near-neutral pH SCC. Apart from the mode of crack propagation, IGSS can be distinguished from TGSCC by the following features [8]:

1. **Temperature dependence:** IGSCC displays a temperature sensitivity not shown by TGSCC in field and laboratory tests. IGSCC is known to typically develop at service temperatures above 100°F whereas no correlation has been found between temperature and TGSCC. Hence most IGSCC failures occurred in the vicinity of compressor stations and though failures do occur as far as 20km downstream from a compressor station, the frequency of occurrence of IGSCC colonies decreases exponentially with distance from compressor stations [4]. However TGSCC does seem to occur more frequently in colder climates where CO₂ concentration in groundwater is higher [4].
2. **Nature of corrosion products at corrosion site:** TGSCC is associated with relatively large amounts of white iron carbonate trapped between the coating and the pipe surface

whereas very little carbonate is present in IGSCC and any carbonate present is usually incorporated into the magnetite film that almost inevitably forms in IGSCC. The open mouth of IGSCC is usually coated with dark oxidized material while the remote end of the wall is shiny silver in color.

3. **Crack width:** IGSCC cracks are usually very fine due to the effectiveness of the tenacious magnetite film in preventing the dissolution of the crack walls. TGSCC cracks on the other hand, are usually wide, due to significant lateral dissolution of the crack walls.
4. **Crack density:** TGSCC are characterized by high densities of cracks in localized regions whereas IGSCC are more widely spaced.
5. **Potential ranges:** TGSCC typically occurs at the open circuit potential, usually between -760 to 790 mV (Cu/CuSO₄), or close to the free corrosion potential. This suggests that TGSCC occurs where the pipe surface is shielded from the applied cathodic protection. IGSCC usually occurs at more anodic potentials, -650 to -750 mV (Cu/CuSO₄), suggesting it develops where the applied cathodic potential does not effectively reach the pipe surface.

2.2.4 SCC development

From the general picture of SCC that has emerged from both laboratory and field investigations, the occurrence of SCC begins with the appearance of corrosion pits. Often the role of corrosion pits in the initiation of SCC is only considered from its mechanical point of view – stress amplification around pits. However, equally important to SCC development is the presence of the corrosion products, often formed as a porous cap, on top of the pits. The presence

of this cap modifies the ion exchange process between the electrolyte within the pit and that in the surrounding bulk solution, while selectively permitting the ingress of anions such as chlorides. This effectively alters the solution chemistry, generating the right kind of environment for SCC, and developing concentration gradients as well as pH differences between the pit electrolyte and the surrounding electrolyte.

With the right pit morphology and stress-environment combination, tiny SCC cracks may initiate from the bottom of pits or from jagged edges. If the right level of stress or stress cycles is sustained, progressive crack propagation could occur until the crack is long enough to initiate unstable crack propagation leading to the rupture of the final ligament of material [4]. Typical SCC cracks were shown in Figure 2.2. Stress corrosion cracking on buried pipelines starts with the development of small cracks on the outside surface of the pipe. Generally, these cracks which form in colonies of cracks positioned in the same direction, are initially not visible to the eyes but must be revealed by magnetic particle inspection. These cracks, which are usually oriented along the same direction, can grow over a long period of time and deepen, or cracks within a colony may join together to form longer cracks, that may cause the pipe to leak [9]. Under favourable conditions, such cracks may propagate and reach a critical size at which they become unstable, resulting in fast fracture behaviour. However, it must be emphasized that it has been observed in a few cases that neither the presence of a pre-existing flaw nor the formation of corrosion pits is necessary for the initiation of SCC cracks. The combined effect of the right environment and a susceptible material may sometimes be sufficient for SCC initiation from a smooth surface. Although no instance of SCC initiation from a smooth surface in pipeline steels, without the presence of a notch or corrosion pits, was found in literature in the course of this review, instances of such have been reported in other systems. In a systematic study, Smialowska

and Gust [10] found that when stainless steels are in their passive state and conditions favoured pitting then pits formed first. But when conditions favour the formation of a protective layer with limited protective ability, stress corrosion cracks nucleated on the apparently smooth metal surface. It has also been reported that in the absence of pre-existing flaws titanium alloys may not develop SCC in a salt water environment, however, they readily develop SCC from a smooth surface in methanol [11]. In another study, it was found that SCC may not initiate on 13-8Mo in salt water unless a corrosion pit is first formed, but in acidified salt water (with HCl), SCC easily initiates on a smooth surface [11].

It has been shown that three conditions must be simultaneously met for SCC to occur in pipelines [4, 12]: a specific potent crack-initiating environment must be present at the pipe surface, the metallurgy of the alloy must be susceptible to SCC, and tensile stresses above the threshold required for SCC in the particular environment-material combination must be present (Figure 2.3).

The factors that have been identified as contributing to the development of SCC are individually discussed in the following sections.

2.3 Effects of alloy metallurgy – material factors

Experimental studies and critical examination of previous failures have suggested that pure metals are more resistant to SCC cracking than alloys of the same metal but are not immune to SCC [1]. It has also been observed that transgranular cracks preferentially propagate on specific planes, especially the low index planes such as {100}, {110} and {210} [13]. These and other observations suggested early in the quest to understand the SCC phenomenon that SCC kinetics may be strongly influenced by the metallurgy of the alloy in question. The influence of the alloy's metallurgy on SCC is discussed in the following sections.

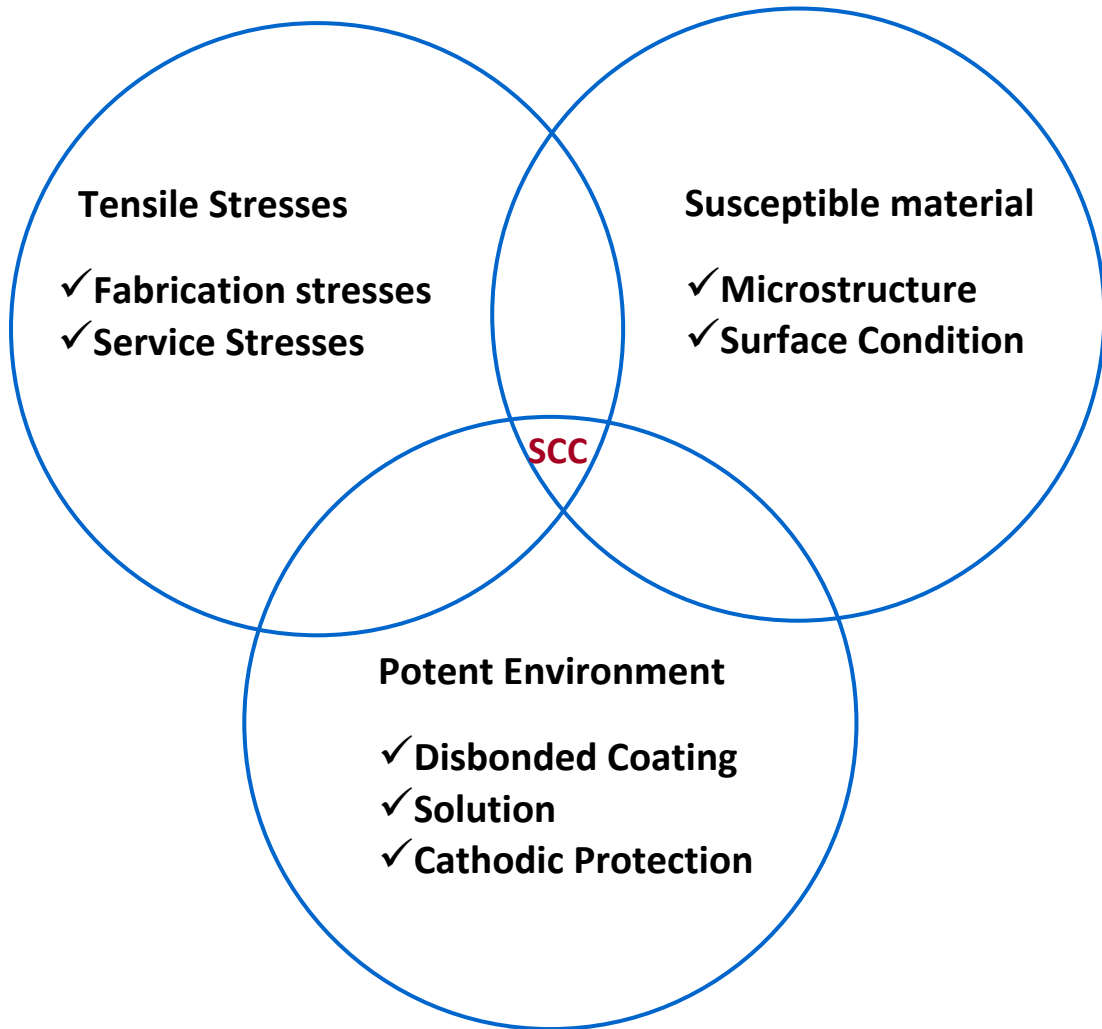
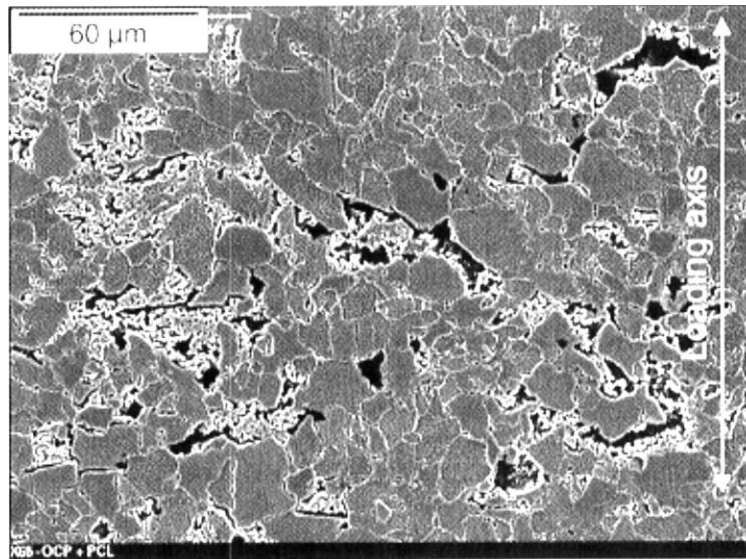


Figure 2.3: Factors required for SCC to occur

2.3.1 Microstructure

Bulger *et al.* [14] have analyzed available data and concluded that differences in microstructure can have a significant effect on susceptibility to SCC. It was found that resistance to SCC decreases with yield strength for alloys that have the same microstructure. However, the relationship between SCC resistance and yield strength was found to be dependent on the alloy's microstructure. For alloys with the same yield strength, it was found that uniform bainitic structures or polygonal ferrite structures are less susceptible to SCC than ferrite-pearlite structures. For example, X70 which has a bainitic microstructure in the water quenched condition was found to be more resistant to SCC than X65 which has a ferrite-pearlite structure although they have similar yield strengths. Chu *et al.* [15] and Chen *et al.* [16] observed that pearlitic colonies and banded phases in X65 are more susceptible to pitting corrosion and crack initiation and propagation than adjacent ferrite grains (Figure 2.4a). Cracks were observed to propagate preferentially along the banded planes irrespective of direction of the externally applied stress (Figure 2.4b). Torres-Islas [17] *et al.* found that martensitic structures are more susceptible to SCC than other structures and attributed this to the highly stressed microstructure of martensitic structures which results from the excess carbon trapped interstitially. Kushida *et al.* [18] opined that non uniform structures such as ferrite-pearlite increased susceptibility of pipeline steels to SCC.

(a)



(b)

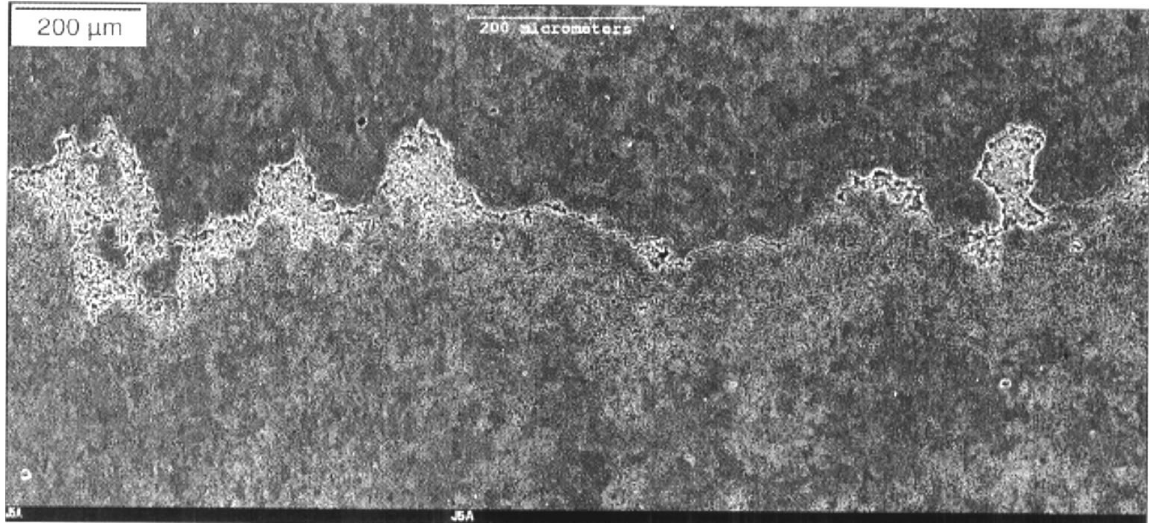


Figure 2.4:(a)Preferential corrosion attack in pearlite region , (b) Showing corrosion along banded structure [15].

The high susceptibility of pearlitic steels to SCC is related to the influence of metallurgical discontinuities on the alloy's susceptibility to galvanic corrosion [15]. Localized corrosion and microcrack development can be expected to occur at metallurgical discontinuities such as grain boundaries, pearlite colonies and banded structures because of the galvanic effect set up between the discontinuity and adjacent ferrite matrix. The galvanic effect can persist even after crack initiation; in a situation where pearlite colonies intersecting the specimen surface extend deep into the material or forms a continuous interconnected network with other colonies, the interface between the pearlite and adjacent ferrite provides a favourable path for crack propagation [15]. This leads to an extensive distribution of closely spaced SCC cracks, which can then coalesce with other cracks, leading to rapid crack propagation through the material. This may ultimately lead to a complete failure of the pipeline in service. It has been suggested that the presence of martensitic colonies can similarly aid SCC [19]. Bulk alloy composition can also affect the stability of passive films as well as phase distribution within the alloy system, for example the amount of/distribution of chromium in stainless steels.

2.3.2 Inclusions

A few published results suggest that inclusions may play an important role in the initiation and propagation of SCC cracks. For example, *Fang et al.* [20] found that iron carbonate deposits and deposits enriched in Mn and Si were formed around pits in NNPHSCC tests on X80 steel. The composition of these deposits was found to vary with the composition of adjacent inclusions. In particular the morphology of pits was found to be closely associated with inclusion chemistry. The study also detailed the presence of Mn and Fe oxide inclusions around corrosion pits. Asher and Singh [21] have also suggested that the dissolution of MnS inclusions might aid pit formation in slow strain rate test simulation of NNPHSCC in X65 steel.

It is probably conceivable that inclusions can increase an alloy's susceptibility to SCC cracking. Since the composition of inclusions and the adjacent matrix is expected to be different, then it is possible that there might be a significant difference in their galvanic potentials. Thus, depending on the relative potentials, the inclusion might be anodic or cathodic to the surrounding matrix. This will set up localized micro galvanic couples within the material, causing localized galvanic corrosion at the precipitate/matrix interface. If the inclusion is cathodic, corrosion at this interface can ultimately cause the inclusion to detach from the matrix, leaving a pit where the inclusion once occupied. This pit can then become a crack initiation site within the matrix, if sufficient stress concentration develops around it. An anodic inclusion will also produce a similar effect, though the inclusion itself is preferentially attacked in this case. Besides the galvanic effect, differences in dissolution rate between the inclusion and the adjacent matrix can also lead to pit formation. Cracks might also form by inclusion/matrix decohesion at the interface under sufficient loading conditions.

The above discussion points to the fact that production process for pipeline steels can significantly influence its susceptibility to SCC. Inclusions are generally formed during the steel making and casting processes, either due to inadequate cleanliness of the casting environment or inadequate removal of impurities (including slag materials) prior to pouring. Often inclusions are oxides that form due to inadequate shielding of the melt, or inadequate de-oxidation of melt prior to pouring. Inclusions may also form when tramp elements such as sulphur, phosphorus *etc.* are present in the charge. Hence, adequate care must be taken during the casting operation to prevent/reduce the formation of inclusions during the casting process.

2.3.3 Carbon content and alloying additions

It has been found that decarburized steel has a high resistance to caustic SCC and that susceptibility to SCC increases with increasing carbon content [22, 23]. Hence, steels with high carbon content are more prone to SCC than those with lower carbon content [22] and this behaviour is noticeable even at very low carbon contents. However, with increasing carbon content, the susceptibility to SCC peaks and resistance to SCC improves with additional carbon content. For example, Kowaka and Kitamura [24] found that irons with 0.009 and 0.05% carbon were more sensitive to SCC than annealed 0.12% carbon steel. Even higher carbon contents were found to retard SCC [25].

This behaviour has been attributed to the segregation pattern of carbon and its influence on the electrochemical properties of steels. Atrens *et al.* [26] found that in X70 pipeline steel, carbon concentration at grain boundaries reached up to 10at% even when the nominal carbon concentration is about 0.06at%.

Generally, it has been found that alloyed steels show improved resistance to SCC compared to unalloyed steels. In the absence of alloying additions, intergranular and intragranular precipitates and segregates are mainly composed of carbon. However, in the presence of alloying additions like Ti, carbide particles are precipitated and carbon is tied up (probably in proportion to the amount of Ti present in microalloyed steels). This removal of carbon from solid solution was thought to improve resistance to SCC [27].

The presence of carbon in solid solution induces lattice distortion, causing plastic strains that might aid the rupture of oxide layers [28]. Points at which oxide films rupture will be suitable sites for pit nucleation, which are fertile areas for SCC crack initiation. Carbon is also

known to have a strong influence on the anodic oxidation of iron. It has been shown that carbon decreases the ability of iron to passivate and also promotes the accumulation of magnetite on corroding surfaces, in caustic solutions [29], and in dilute alkaline solutions [30]. Studies have shown that anodic oxidation of iron increases with carbon content up to about 0.4-0.6% but decreases with higher carbon content [31, 32]. Flis and Moroz [33] explained the effect of carbon on passivation thus:

“Solid solutions of iron and carbon are more reactive than pure iron for thermodynamic reasons; therefore its active dissolution is enhanced. However, the hindrance in passivation can be rather associated with an effect of carbon on the formation of passive films. Due to the dissolution of iron, carbon accumulates on the corroding surface in the form of particles such as atom clusters and/or fine carbide precipitates. These particles can disturb the growth of the protective oxide film by introducing inhomogeneity on the substrate surface and into the structure of the film. It can be supposed that the accumulated particles will make the film growth directly on iron by electrochemical oxidation difficult. Instead, a film will grow largely by the precipitation mode and therefore it will be less protective”.

Considering the fact that the carbon content of pipeline steels falls in the range where susceptibility has been found very high, it is conceivable that pipeline steels will be fairly susceptible to SCC.

Finally, minor alloying elements can cause local changes in passive film-forming elements (carbon causes sensitization in stainless steels), impurity elements can segregate to grain boundaries and cause local differences in the corrosion rate (phosphorus in nickel and

nickel based alloys), and inclusions can cause local crack tip chemistry changes as the crack intersects them (for example manganese sulphides in steels) [34].

2.3.4 Weld heat affected zones

It has been observed that NNPHSCC cracks in pipelines are often seen at or near the toe of the longitudinal weld seam [1]. Bulger *et al.* [14] reported a 30% increase in crack propagation rates in the HAZ of a welded pipe. Consistent with this, many of the SCC induced pipeline ruptures have been found to have occurred in this area. There might be several reasons for this behaviour. First, the weld seam is usually not flush with the pipe surface; rather, a weld crown is usually formed. When the surface coating, especially polyethylene coatings, are applied, tenting, a situation in which there is no adhesion or partial adhesion, may occur in this region. Holidays in the coating may therefore form in this region which allows groundwater to gain access to the weld seam region of the pipe, the pool being essentially formed in the HAZ area. This generates an environment that is suitable for SCC in this region (more on the environment in section 2.5). This is often aided by a large stress magnification near the toe of the weld.

Perhaps a more important effect of HAZ is its influence on the metallurgy of the weld region. This becomes more important when one considers that even in several laboratory studies that simulated SCC without surface coatings, the HAZ was found to be more susceptible to SCC than the base metal [4, 35]. This effect might be due to stress at the toe of the weld. Another reason might be the formation of non-equilibrium structures in this region, which may act as metallurgical discontinuities that aid pitting, from which SCC cracks can subsequently initiate. This may also point to the influence of ductility on crack initiation, as the HAZ is known to be

more brittle than the base metal. Finally expansion and contraction of the weld pool and the area immediately next to it may also lead to the generation of residual stresses in this region, a factor that is known to enhance SCC cracking.

2.3.5 Precipitates

The effect of precipitates in pipeline steels mainly depends on the nature of the precipitates – intergranular precipitates or intragranular precipitates. Intergranular precipitates such as carbides in stainless steels and nickel base alloys can cause a depletion of protective film formers such as chromium adjacent to the grain boundary leading to a greater susceptibility to SCC cracking [34]. In most pipeline materials, the alloy composition and/or alloy processing procedures are designed to prevent the formation of significant intergranular precipitates. However, manganese is usually added to remove sulphur from solid solution. The resulting MnS precipitates are often preferentially attacked in a corrosive environment leading to pitting which can then act as initiation sites for SCC cracks.

Another significant influence of the nature/type of precipitates on susceptibility to SCC is its influence on hydrogen permeability of the metal lattice. This effect depends on the strength of the precipitate in question. If the precipitate has a higher strength than the matrix then the bulk of the deformation is concentrated in the surrounding matrix, filling the precipitate/matrix interface with dislocations. Hence hydrogen segregates to the interface; if sufficient embrittlement occurs, a crack may be initiated here which then propagates through the matrix. On the other hand if the precipitate is softer, then the precipitate is more easily deformed and more stress will be deflected to the particle which may cause it to rupture initiating a rupture induced crack in this region. If this occurs in the vicinity of the crack tip, hydrogen embrittlement may strongly influence the size of the plastic zone ahead of the crack tip [36]; the more the hydrogen

concentration the smaller the size of the plastic zone and the more susceptible the alloy is to cracking. It is also reasonable to assume that there must be a critical hydrogen concentration required to induce cracking. Thus the presence of precipitate can modify the ease with which hydrogen can permeate the lattice [36].

Alloying additions, especially Ti, V and Nb, *etc.* which are major constituents of pipeline steels, as well as the size of their respective precipitates, have been found to influence the hydrogen permeability of steels. Grabke *et al.* [37] found that both TiC and NbC can significantly increase the amount of hydrogen trapped within a microalloyed steel lattice. They suggested that this effect is probably due to the high amount of finely dispersed carbide particles, and the associated lattice strains. Generally, hydrogen is known to concentrate in regions of high lattice strains [1]. Hence, the presence of a large number of lattice distortion sites, due to fine carbides can increase hydrogen uptake. They found that VC and VN tend to have a strong influence on the amount of hydrogen trapped within the lattice, and attributed this to the tendency of VC and VN to stabilize high dislocation densities and cause internal strains in their surroundings. Dislocations are efficient trap sites for hydrogen since they are usually associated with fairly large lattice distortions. Thus pipeline steels with VC, VN, TiC and NbC tend to have a high density of hydrogen trap sites, resulting in an increased susceptibility to SCC. In a detailed study of the effect of MnS and other second phases on hydrogen occlusivity, Mardrid *et al.* [38] determined that the amount of hydrogen occluded into steel and the risk of hydrogen damage is a function of the volume fraction of inclusions.

2.3.6 Grain size

Grain boundaries play an important role in adjusting the mismatched strain among deformed grains under loading [39]. It has been suggested that fine grained ferrous alloys have a

lower susceptibility to hydrogen embrittlement than coarse grained ferrous alloys [40]. A decrease in hydrogen content was found for fine grained materials compared to those with grains larger than 70 μm [38]; although fine grained materials had greater total grain boundary areas, they seemed to trap relatively little hydrogen. This behavior was related to lower lattice mismatch with progressively smaller grain sizes. It was also shown that alloys with larger grain sizes suffered more severe loss of ductility after hydrogen charging compared to those with smaller grain sizes. This was attributed to the lower hydrogen concentration at grain boundaries in the fine grained alloys. For hydrogen charged specimens, coarse grain size alloys were found to be more susceptible to intergranular fracture than fine grained alloys. Hence, coarse grained pipeline steels are more liable to SCC than fine grained alloys.

2.3.7 Lattice strain (deformation)

Plastic deformation increases the amount of lattice defects and imperfections formed within the lattice of any material. These defects and imperfections, dislocations, vacancies *etc.*, are associated with energies and strain fields which can interact with the lattice to increase the amount of internal stress in the lattice. Moreover, plastic deformation reduces the ductility of the alloy and reduces the size of the plastic zone ahead of any advancing crack, reducing the lattice resistance to crack propagation. All these are factors that can significantly influence the lattice resistance to SCC, by increasing the number of sites at which hydrogen can be trapped. Thus, plastic deformation can be expected to increase an alloy's susceptibility to SCC.

Expectedly, it has been shown that plastic deformation increases the susceptibility of microalloyed steels to SCC [41]. It was found that the corrosion current density (a measure of the rate of corrosion) increased monotonically with plastic deformation prior to laboratory test. For

alloy X52, it was found that for a 10% strain, corrosion current density increased by about 17% [41].

2.4 Mechanical factors – stress

Considerable research has been carried out to investigate the role played by applied stress in the SCC phenomena. Results of such studies almost unanimously conclude that the presence of tensile stresses is necessary for the propagation of SCC cracks. In laboratory studies, tensile stresses have also been found to play a vital role in crack initiation as SCC is precluded below some specific threshold stress level unique to each material [12].

The stress experienced by a buried pipeline stems from different sources. As would be generally expected, the largest stress experienced by the pipeline is that due to the pressurization of the pipe contents. Other sources of stress include those imposed bending or axial tension, those imposed by the pipeline installation process, by soil movement, and residual stresses generated by the pipe fabrication process [4]. Heavy rains or periodic flooding of pipeline sites may result in soil slides or washouts which may undermine the stability of the soil on which pipeline supports are mounted. This may cause bending due to pipe sagging in areas where the soil support has been compromised.

The orientation of SCC cracks has been found to be dependent on the direction of the stress producing it [4]. Stresses can either be in the circumferential or longitudinal direction (figure 2.5). The direction of crack propagation is usually perpendicular to the direction of the stress producing it. Hence, longitudinal cracks are caused by circumferential stresses while circumferential cracks are caused by longitudinal stresses. It has been suggested that 73% of failures in Canadian pipelines have involved axial cracks, which suggests that circumferential

stresses controlled most of the failures experienced in service [4]. Circumferential stresses originate from [4]:

1. Hoop stress due to the operating pressure
2. Residual stress created during pipe fabrication.
3. Bending stresses result from subjecting out-of-round pipes to internal pressure
4. Localized stresses around the weld seam, mechanical gouges, corrosion pits and other areas of stress concentration
5. Secondary stresses resulting from soil settlement or land slides
6. Temperature differences through the pipe wall thickness.

Longitudinal stresses originate from [4]:

1. Internal operating pressure with a resolved component in the longitudinal direction, usually about half to one-third of the hoop stress
2. Stresses that can bend the pipeline such as soil settlement and landslides
3. Stresses due to temperature changes along the axis of the pipe

Other crucial factors that determine the influence of stress on SCC include:

1. Load cycling
2. Strain rates
3. Hydrostatic testing
4. Stress concentration

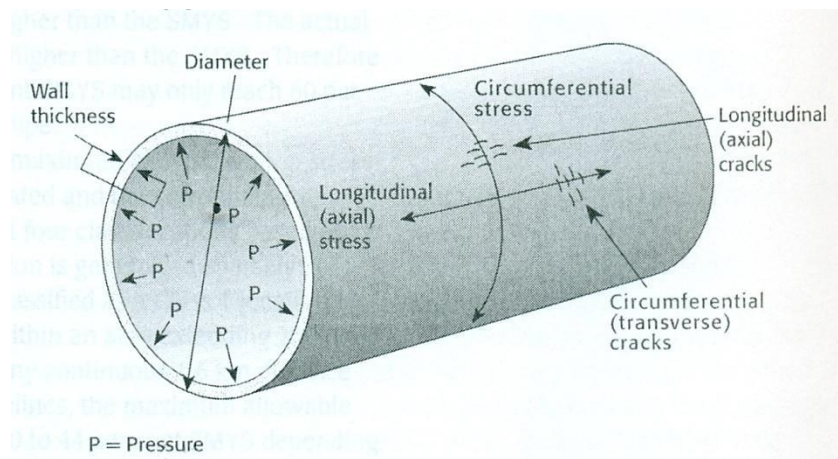


Figure 2.5: Stresses in pipelines [4]

2.4.1 Forming process and residual stress

Considering the method by which pipes are formed, residual stresses can be developed during the formation of plate materials and/or during the pipe fabrication process. The production process for the plates from which pipelines are produced involves several stages of rolling. This might be especially significant when one considers the fact that the final rolling stage (finish rolling) involves a large amount of strain (up to 70%). This has the potential to lead to the formation of intensely high residual stresses unless a stress relief heat treatment is carefully carried out after the finish rolling process.

Common methods by which line pipes are produced include by double submerged arc welding (DSAW), electrical resistance welding (ERW) or by seamless methods. In the DSAW process, the pipe is rolled into a tube, welded longitudinally and typically (although not always) expanded to final round shape by pressurizing it with water [4]. ERW pipes are cold formed into cylindrical shapes and then welded longitudinally. Seamless pipes are not commonly used because they are expensive and production time, hence delivery time, is usually rather too long. Both the ERW and the DSAW processes have the potential to induce residual stresses in the finished pipe. The residual stresses resulting from sheet material bending during pipe production are often tensile in nature and have been shown to be between 0% and 20% of the alloy yield strength [42].

It has been shown that there is a correlation between residual stresses and locations of linepipe SCC [43]. Beavers *et al.* [44] determined that residual stresses in areas where SCC colonies were formed were twice as high as those in unaffected areas, 216 MPa and 108 MPa respectively. Van Bowen *et al.* [45] have also determined that the formation of micropits and microcracks could occur preferentially in areas where tensile residual stress were about 200 MPa

while only little pitting or general corrosion or microcracking occurred on the pipeline surfaces with compressive residual stress.

Many of the pipes currently used in the oil and gas transportation welds have long seams where the the two ends of the bent plate are welded together to form a closed tube. Often, NNP-HSCC cracks are found concentrated around these weld seams [4]. This is often attributed to the residual stresses induced by the welding process and the associated stress concentration. Also the coating tends to form a tent in this region, providing easy access of groundwater to the weld toe area. Welding of pipe seam during the fabrication process can create high weld-cooling induced stresses in the weld area and in the HAZ regions adjacent to it. Rapid cooling of the weld also produces a microstructure that is different from that of the base material. It is known that that residual stresses may vary from compressive stress up to 77% of the alloy yield strength and tensile stresses up to 20% of the yield strength [4, 42]. Baker [46] found that the resultant residual stress produced at girth welds in pipes may increase the probability of circumferential SCC.

There are a few ways the effects of residual stresses can be reduced. One of such ways is to introduce compressive stresses at the pipe surface to counter the effect of tensile residual stresses. This can be done by shot peening or by grit blasting. Beavers *et al.* [47] have shown that grit blasted surfaces are more resistant to high pH SCC by inducing compressive stresses at the pipe surface.

2.4.2 Stress concentration

Stress concentration is known to occur around geometric discontinuities and defects in engineering materials. Stress concentration can modify/amplify the local stress in engineering structures to levels well beyond the nominal design stress. This effect can be much more crucial when combined with an aggressive environment as is often associated with NNPHSCC and high pH SCC. The National Energy Board reported that all the ruptures reviewed in their report on SCC were associated with a stress raiser [4]. Of the eleven ruptures reviewed, five occurred near the long seam weld of the pipe, five were associated with general corrosion (reduced wall thickness) and one rupture initiated from a gouge on the pipe surface.

The operating pressures of pipelines are strictly regulated and are chosen such that the service stress is well below the specified minimum yield strength of the material. These stresses are usually carefully regulated to within 72 to 85% of the specified minimum yield strength [4, 48, 49]. Attempts to simulate SCC initiation in the laboratory at benign/service stress ranges have been largely unsuccessful. Often SCC initiation and propagation in laboratory studies have only been obtained at stress levels well in excess of the normal pipeline operating ranges [50, 51]. Therefore, many researchers believe that stress raisers probably play a very significant role in the initiation and propagation of SCC.

2.4.3 Hydrostatic testing

Hydrostatic testing is used to determine the structural integrity of pipelines and to establish a safe operating pressure [4]. Before a new pipeline is issued an operating permit, regulatory authorities require the pipeline be made to undergo a hydrostatic pressure test successfully. This procedure involves pressurizing the pipeline/pipe segment to pressures in excess of its intended operating pressures. Hydrostatic testing may also be periodically redone to

detect cracks on operating pipelines or rather to determine a safe operating limit for serviceable pipelines. The goal is to determine how safe it is to operate the pipeline until the next designated retesting period given its current condition. During hydrostatic testing, a section of the pipeline is filled with a low-compressibility liquid, usually water, the pressure is then raised above the level at which the pipeline is designed to operate [4]. Next, the pressure is held at a prescribed amount, usually lower than the initial loading phase, for the amount of time recommended by the regulatory authority. Usually the test involves initially loading the pipeline to 110% of its SMYS for 1hr followed by a load shed to 90% SMYS for 24 hours [52]. The initial loading phase is designed to cause the rupture of critical sized flaws while the second (prolonged) loading regime is designed to test for leaks. Periodic retesting of pipelines is often necessary for pipelines that have defects that propagate over time such as SCC. Any successful test is only an indication that the pipe is safe for operation for a certain period of time – that is until the cracks grow to a critical size that could cause rupture. Thus it is often necessary to conduct re-tests periodically over the service life of the pipeline or pipe segment.

Besides causing critical size flaws to rupture, hydrostatic testing has been found to inhibit crack propagation by blunting the crack tip, making it harder for such cracks to re-initiate in service [35]. Thus even though crack propagation might occur during the test itself, there is no reduction in the overall life because the associated crack tip blunting ensures that growth rates are depressed for some time after the test. It has been shown that hydrostatic testing is no more harmful to pipelines than depressurization as the load-unload transients during depressurization occur at strain rates that can accelerate or re-initiate cracks in such a way that depressurization may be more detrimental to the predicted life of a pipe than hydrostatic stress [53-56].

2.4.3 Summary of the effect of stress on SCC

Results of laboratory tests with notched and smooth samples have shown that TGSCC initiates in areas of high stress concentration [21]. In a slow strain rate test, Asher and Singh [21] showed that for X65 steel, preferential dissolution commences around inclusion sites (particularly large inclusions) and scratches in less than 27 hours, when a load of about 35% yield strength is applied. In fact at this stress level, some inclusions were found to have already fallen out of the specimen surface, producing pits which showed crack-like features. Chemical analysis showed that MnS inclusions were particularly susceptible to this type of behaviour. When samples were loaded to about 65% of the yield strength for the same period of time, they found even more intense localized dissolution, including dissolution around very fine inclusions, resulting in the formation of very fine pits on the specimen surface. Samples loaded to just under the yield strength of the alloy showed numerous larger pits, and even more extensive localized dissolution around inclusions. When specimen samples were loaded to a little above the yield strength of the material, pits became larger, deeper and increased in number. This was attributed to a more intense galvanic corrosion of MnS inclusions at this stress level.

The above shows that stress levels can strongly influence the onset and extent of pitting by aggravating localized dissolution and/or breaking up of particles. Since such pits act as regions of stress concentrations, if the radius of curvature of such pits is small enough, localized plastic deformation may occur at the bottom or even on the edges of such pits (since pits are often irregularly shaped and sharp edges do occur), causing cracks to initiate in such regions. Cracks were found to have initiated in X65 at stresses as low as 65% of the yield strength.

Another influence of stress on SCC is its apparent ability to worsen hydrogen embrittlement. Stress concentration has been shown to facilitate the ingress of hydrogen and its

subsequent localized accumulation, causing hydrogen embrittlement of steel. It has been reported in several studies involving slow strain rate tests [21] that SCC cracks were concentrated in regions of high stress concentrations such as at the transition point for necking or directly next to the fracture surface. This points to the fact that plastic deformation was necessary for TGSCC of pipeline steels in near-neutral pH environments [21]. It has been suggested that such isolation of cracking to regions of high plasticity and stress triaxiality might be a strong indication that stress concentration facilitates hydrogen diffusion and aids the TGSCC process. It also appears that there is a strong correlation between hydrogen solubility in pipeline steels, lattice strain and microstructure [33]. The role of stress concentration on SCC becomes even more obvious when one considers previous studies have shown that smooth slow strain rate test samples showed no significant deterioration in properties when held in air at stress levels up to 85% of the yield strength [57, 57, 58].

There is a bit of controversy on the nature of stress required for the initiation and propagation of SCC cracks. Results of laboratory experiments, where no SCC cracks could be initiated under constant loading conditions, but in which cyclic loadings were used to generate cracks similar to field observed SCC, have suggested that stress fluctuations is a necessary requirement for the occurrence of SCC [4, 53, 59, 60]. The result of full scale tests carried out by CANMET has also suggested that pressure fluctuations inside operating pipelines is a necessary ingredient in NNPHSCC [61]. In this study static loading, up to 80% of the yield strength, produced no SCC cracks, but it is known that SCC cracking occurs at stress levels much lower than 80% yield strength. Judging by this, it might be concluded as has already been suggested in some quarters that some level of cyclic loading, no matter how low the frequency, might be a necessary condition for SCC.

2.4.4 Cyclic loading

Attempts at producing stress-corrosion cracking in laboratories have involved subjecting pipeline materials to cyclic loading or other non-static loading as in the case of slow strain rate tests. There have been a few reports of high pH SCC being produced under static loading [50, 56, 62, 63] but initiating near-neutral pH SCC in the laboratory under stressing conditions that are representative of those on an operating gas pipeline has proven very difficult. For instance researchers at CANMET produced clusters of transgranular cracks that appeared very similar to near-neutral pH stress-corrosion cracks that occurred under field conditions but these cracks only initiated in tests that involved thousands of high-amplitude (low-stress ratio) stress cycles [51]. While such high cycles may be experienced on oil pipelines, this situation is quite unrepresentative of gas pipelines.

Experimental data suggests that quite a few cyclic loading parameters can have a significant effect on the initiation and propagation of SCC cracks. Among such are, the maximum stress (σ_{max}) to which the material is loaded, stress amplitude (difference between the maximum and minimum stresses in the cyclic pattern), stress intensity factor, strain rate, and loading frequency. Usually, the maximum/minimum stress applied is stated in terms of the percentage of the specified minimum yield strength (SMYS) rather than the actual yield strength of the alloy. It should be noted that the SMYS can be significantly lower than the actual yield strength; up to 30% lower than the actual yield strength [4].

More often than not, the stress amplitude is described in terms of the stress ratio, R-value, as the ratio of the minimum stress to the maximum stress in the cyclic pattern:

$$R = \frac{\sigma_{min}}{\sigma_{max}} \dots \dots \dots (2.4)$$

The stress intensity factor is defined by the laws of fracture mechanics. This parameter describes the stress state near the tip of a crack by an applied load or residual stress. It is commonly applied to cracks in a homogenous material in the linear elastic loading regime and is most useful for determining the fracture criteria for brittle materials. Among other things the stress intensity depends on the sample geometry, crack shape, crack size and crack location as well as the mode of loading. There are three distinct modes of loading in fracture mechanics: crack opening mode, crack shearing mode, and crack tearing mode. These three modes are illustrated in Figure 2.6. For mode I loading, the stress intensity factor is expressed in its general form as:

$$K_I = \sigma\sqrt{\pi a} \cdot f\left(\frac{a}{w}\right) \dots\dots\dots (2.5)$$

where σ is the applied stress, a is the crack length, and $f(a/w)$ is a geometric factor.

When materials are subjected to a fluctuating stress, they fail at a stress level much lower than would have caused failure under static load. The fatigue life, defined as the number of cycles to failure, increases with reducing maximum stress until the endurance limit or the fatigue limit is reached. The endurance limit is the stress at/below which the material is able to survive an infinite number of cycles without failure. Generally, for engineering alloys, the fatigue limit only refers to the stress level below which the material does not fail within a specified number of cycles, usually between 10^7 or 10^8 cycles.

In a bid to establish realistic in-service cyclic loading parameters for SCC research, CEPA found that there is a clear distinction between in-service cyclic loading experienced by oil pipelines compared to gas pipelines [64]. Oil (liquid) pipelines were found to experience an average of 2500 low R cycles annually while gas pipelines undergo fewer than 10 low R cycles per year. In this study, low R cycles was defined as $R < 0.5$. They also found that pressure changes on liquid lines occur more rapidly than on gas lines. Whereas, during a shutdown, a

liquid line can be brought from highest operating pressure down to minimum operating pressure in just 15minutes, it takes up to 24hours to shut down a gas line. This disparity is due to the incompressibility of liquids compared to the high compressibility of gases. Therefore, oil pipelines experience much higher strain rates than gas pipelines.

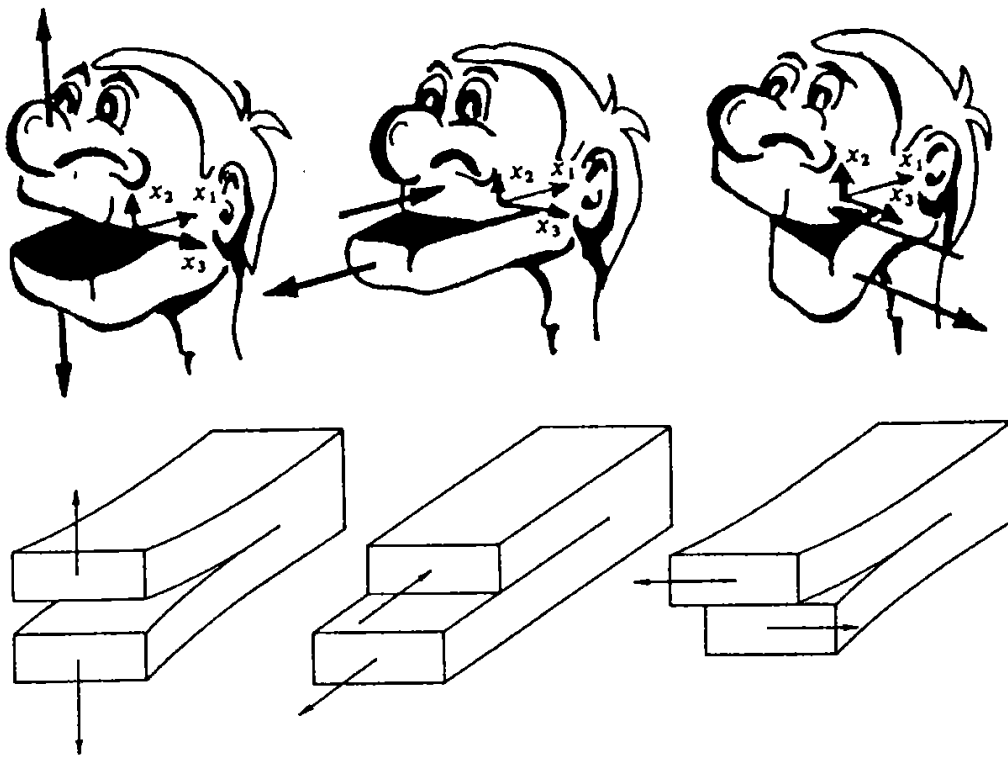


Figure 2.6: Modes of loading a) mode I, b) mod II, c) mode III [63]

Whereas gas lines only experienced high R stress ratio above R=0.9 90% of the pressure cycle, liquid lines experience R=0.7 stress ratios 90% of the time. This difference in stress ratio is quite important as it significantly impacts the change in stress intensity (ΔK). ΔK is often employed as a means of characterizing crack propagation. Hence care must be taken to select realistic stress ratios for SCC experiments. ΔK is related to stress amplitude by

$$\Delta K = K_{max}(1 - R) \dots\dots\dots (2.6)$$

where K_{max} is the stress intensity factor at maximum stress.

In addition to the above, it is a generally known fact that a pipeline that is exposed to cyclic pressure fluctuations may experience cyclic softening. Cyclic softening is a phenomenon in which the application of stress cycles at maximum stress levels below the yield strength causes the steel to exhibit local micro-plastic deformation after a period of load cycles. This phenomenon manifests itself as a loss of yield strength and can significantly reduce the threshold stress. The stress ratio and stress state at the crack tip can have a significant effect on the extent of cyclic softening that occurs in a given material. These two effects, the relationship between ΔK and R and the influence of R on cyclic softening can have a significant effect on the initiation and propagation of SCC cracks. For instance, Beavers and Hagerdorn [55, 56] found that changing R ratios from 0.9 to 0.6 while keeping all other test conditions constant caused crack propagation rates to increase by a factor of two. Chen and Sutherby [65] found that crack tips subjected to low ΔK values showed significantly higher crack tip dissolution than those subjected to high ΔK values. Hence cracks subjected to low R cyclic loads tend to have sharper crack tips than those subjected to high R cyclic loads. Hence cracks subject to high ΔK values are more prone to purely mechanical advancement or corrosion fatigue than those subjected to lower ΔK .

Recently there have been reports of SCC initiation under static loading in near neutral pH environments [66-68]. It must be noted however, that in the work by Fang *et al.* [68], SCC initiation only occurred at very high applied stresses, above the SMYS of the pipeline material used, and it is unclear whether these cracks would propagate or remain dormant under normal pipeline operating conditions. Also, the test samples used in the work by Jia *et al.* [67] have very thin walls that are unrepresentative of actual pipelines, hence it is not known if the reported SCC initiation and crack propagation is a side effect of the stress state. It is also pertinent to note that Jia *et al.* could not produce any cracks perpendicular to the loading direction or any SCC features when the applied stress was below 95.6% SMYS.

2.4.5 Effect of strain rates

Another factor that has been shown to have a significant effect on the rate of propagation of stress corrosion cracks is the strain rate at the crack tip. It has been established that many material-environment combinations where NNPHSCC are found are sensitive to the strain rates associated with the applied stress [50, 54, 69]. It has been suggested that for high pressure pipelines, both dissolution and hydrogen ingress into the steel are involved in crack propagation [8]. Parkins and Beavers [57] opined that the mechanistic implications of strain rate are more obvious in material-environment combinations where SCC is dissolution controlled. In such systems, SCC occurs by repeated film formation and film rupture at the crack tip, and the repetition of filming and dissolution and film rupture is sustained by film dissolution in the metal beyond the crack tip [69]. Even where the mechanism of crack propagation is associated with hydrogen ingress, indications seem to have emerged that the prevailing strain rate might still significantly influence crack propagation [69]. Generally, crack propagation rates increase with

increased strain rates. Beavers [43] determined that there is a strong correlation between the rate of SCC crack propagation and crack tip strain rates. Strain rate effects were found to be most pronounced at intermediate values as too high strain rates causes rapid ductile rupture before any significant crack tip dissolution/film formation or hydrogen permeation can occur [70]. This finding should not be surprising as decreasing the frequency of cyclic loading allows more interaction time between the material and the environment, hence more time for hydrogen to diffuse into the material [71]. Lichter *et al.* [72] showed that even in the absence of hydrogen, increasing strain may accelerate corrosion rates by an order of magnitude, which implies that localized microplasticity or some other hydrogen independent strain effect contributes to SCC propagation. However, one needs to be careful when applying laboratory generated data to actual pipelines. Oil and gas pipelines, especially gas pipelines, are only subjected to very few cycles per day. The cumulative effect of dissolution and repassivation reactions between these load cycling events would probably have a pronounced effect on crack tip sharpness, hence the rate of crack propagation. Chen and Sutherby [65] have found that crack tip blunting may occur at low frequency cyclic loading at or below 0.0025 Hz and suggested that this phenomenon is produced by low temperature creep. It is generally known that steels exhibit higher strengths at high strain rates than at lower strain rates. Wang and Chen [73,2] have also shown that high strain rates cause larger room temperature creep deformation during static loading following a load ramping-up event. Eadie *et al.* [71] opined that room temperature creep might contribute to near-neutral pH SCC. It is not unimaginable then that the relationship between strain rates and low temperature creep may in fact be the reason why higher strain rates produce higher SCC propagation rates.

2.5 Environmental factors

Environment refers to the condition at the pipe surface [4]. The environment might or might not be exactly the same as that of the surroundings on a macro scale. For example, the environment at a buried pipeline surface may not be exactly the same as that of the surrounding soil as the SCC environment might be isolated from the (larger) surrounding environment [4]. Almost all studies agree that the environment required for NNPHSCC is one with a low concentration of carbonic acid and bicarbonate ions in the presence of ionic species such as chloride, sulphate and nitrate ions. This essentially means that the environment must be such that some amount of CO_2 is dissolved in a suitable medium, usually dilute ground water for buried pipelines.

Another important component of the SCC environment is that cathodic protection current is unable to effectively reach the pipe either because of coatings such as polyethylene tapes, high resistance soils, or a poor cathodic protection system design [12]. This is necessary to enable the formation of a dilute carbonic acid solution with a pH in the range 5.5-7.5. The carbonic acid is required to furnish hydrogen which is usually an active agent in SCC.

Several environmental factors might influence the occurrence of or the kinetics of SCC. These factors are discussed next.

2.5.1 Soil

Some of the soil characteristics that may influence the tendency of SCC occurrence include: soil type, soil drainage, topography, CO_2 levels, temperature, electrical conductivity or its inverse – resistivity, and the presence of inhibitors. However it must be said that no correlation has ever been found between soil chemistry and SCC – high or low pH. It has

however been observed that soil type could have a significant effect on the performance of coatings especially polyethylene tape coatings. Bluish-coloured clays tend to hold a lot of moisture and create soil stresses which have been found to aid SCC development [4, 74]. These soils tend to drain poorly, hence retain more of the aggressive environment that is required for the development of SCC. It has also been said that SCC may be more prevalent in clays and silts (lacustrine soils) than in sands and gravel (glaciofluvial soils). Generally, imperfectly drained or poorly drained soils, which tend to provide a steady supply of moisture and tend to support anaerobic and seasonally reducing environmental conditions, tend to be more conducive for NNPHSCC occurrence [75]. However, areas that are constantly at high moisture level have been said to be less likely to develop NNPHSCC than areas where moisture level constantly varies. Areas with anaerobic soils are also believed to be more conducive to the development of NNPHSCC because of the presence of sulphate reducing bacteria, which aggravate hydrogen embrittlement of steels, by producing sulphides that act as hydrogen recombination poisons [76].

Soil resistivity can also determine whether or not cathodic potential is able to permeate through to the pipe surface. High soil resistivity can prevent the delivery of sufficient cathodic potential to holiday sites. Groundwater conductivity also determines how effectively cathodic protection reaches holidays and disbondments. Often, NNPHSCC is only found on asphalt coated lines in dry soils where soil resistivity is so high that cathodic protection cannot reach the pipe surface [75]. Soils with lower corrosion currents and lower corrosion potentials have also been found to support higher crack propagation in laboratory tested X65 steel samples [77].

2.5.2 Role of hydrogen

There are possibly several ways by which hydrogen can influence an alloy's susceptibility to SCC. Hydrogen is known to have an affinity for highly stressed areas (tensile only) and highly deformed areas in metals [78]. Crack tips and porosities are some of such regions with localized stress concentrations. Hydrogen embrittlement at such sites could result in a loss of ductility, making it easier for cracks to propagate by lowering the stress required for plastic deformation. It has been established in several studies, in which steel specimen samples were pre-charged with hydrogen, that hydrogen aids crack propagation. For example, in an SEM examination of fractured sample surfaces, Gu *et al.* [70] found that pre-charging with hydrogen increases the fraction of surface area over which brittle type crack propagation occurred. Delafosse and Magnin [79] showed that steel samples fail at decreasing elongation with increasing cathodic potentials in slow strain rate tests (Figure 2.7), due to increased hydrogen ingress into the material. Parkins [80] found that the hydrogen induced reduction of ductility of pipeline steels requires a continued supply of hydrogen during the deformation process. He found that when precharged specimens were subjected to SSRT tests in air, the elongation to failure was similar to samples that had not been precharged while those tested in solution showed marked reduction in ductility.

Hydrogen is also known to induce/enhance the anodic dissolution of iron [81, 82] by the reaction $Fe + 2H^+ \rightarrow 2H_{ad} + Fe^{2+}$ (where the subscript 'ad' refers to adsorbed hydrogen). This reaction, could result in the sharpening of otherwise blunt (hence, dormant) cracks, increasing the probability of crack propagation at low stress levels.

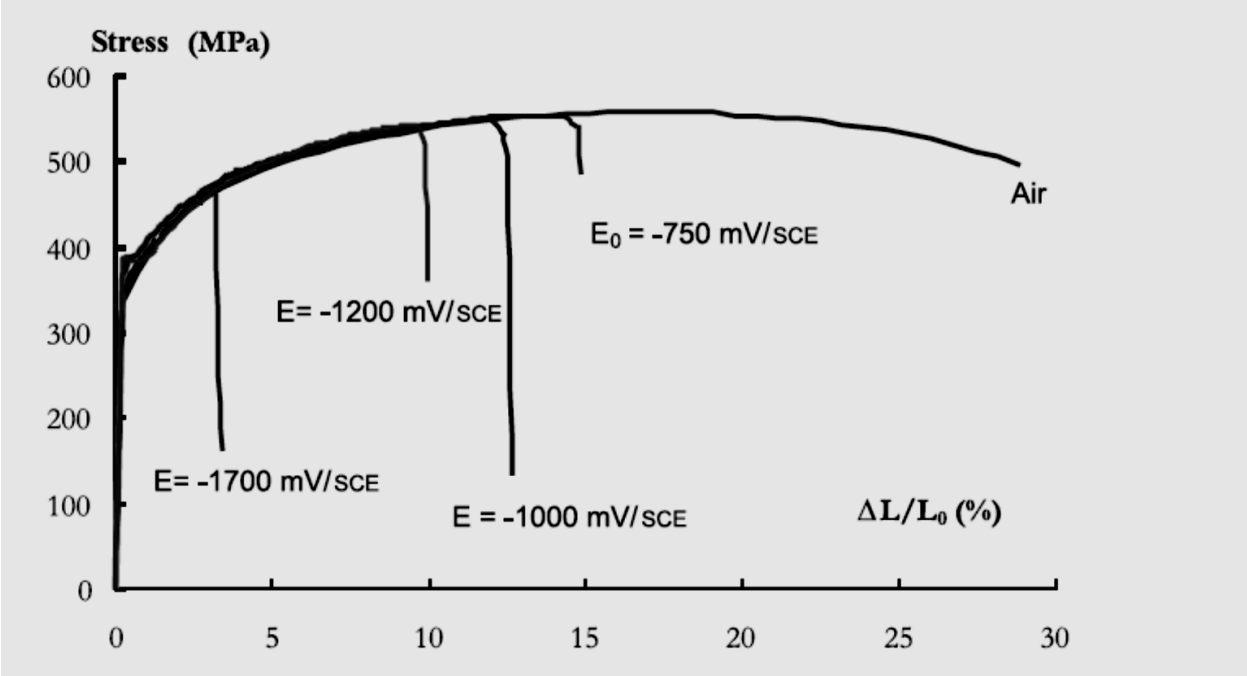


Figure 2.7: Variation of elongation to failure with applied cathodic potential [79]

It has been shown that the effect of hydrogen embrittlement is more pronounced at low pH values than at higher pH values [70, 83-85]. Also, the application of a cathodic potential has been shown to increase the hydrogen concentration around crack tips [70], possibly by increasing the rate of hydrogen adsorption. Both factors – a low pH environment and some level of cathodic protection – are present in operating pipelines. Furthermore, there is no shortage of atomic hydrogen from microbial activities, cathodic reduction of hydrogen or from the dissociation of ground water. Hence, pipelines might be very susceptible to hydrogen assisted NNPHSCC.

Jack *et al.* [86] also found that increasing hydrogen concentrations correlated more with increasing bicarbonate levels than with lower pH, implying that hydrogen for SCC cracking results from the electrolysis of the bicarbonate species in solution rather than the H⁺ directly generated from water.

2.5.3 Electrolytes

The concentration and composition of the groundwater in contact with the pipe surface where a coating disbands or holidays exists has a significant effect on the probability of SCC occurring and/or the severity of SCC if it occurs. As already mentioned, NNPHSCC develops in a carbonate-bicarbonate environment. This kind of environment is developed when CO₂ dissolves in ground water.

CO₂ plays a major role in maintaining the pH of the solution at the pipeline surface in the near neutral range. Ordinarily, when water dissociates by the reaction $2H_2O + 2e \rightarrow H_2 + 2OH^-$ or $O_2 + 2H_2O + 4e \rightarrow 4OH^-$, the generation of hydroxyl ions causes the pH of the solution to increase. In the absence of CO₂, the pH may increase to about 11-12 [87]. However, when CO₂ is

present, CO_2 dissolves in groundwater to form carbonic acid by the reaction $\text{CO}_2 + \text{H}_2\text{O} \rightarrow \text{H}_2\text{CO}_3$ which can further react with water to produce a hydronium ion and a bicarbonate ion by $\text{H}_2\text{CO}_3 + \text{H}_2\text{O} \rightarrow \text{H}_3\text{O}^+ + \text{HCO}_3^-$ [12, 88]. The bicarbonate ion is weakly basic while the hydronium ion is an acid radical. The formation of this pair of ions lowers the pH of the solution to the near neutral range, if CO_2 is present at a sufficiently high partial pressure. Apart from its influence on the pH of the solution, hydronium ions can be reduced to furnish hydrogen gas at the pipe surface. This reduction reaction is another major source of hydrogen in NNPHSCC.

In the field, the CO_2 involved in the development of the SCC environment comes from the decay of organic matter in the soil [4, 89]. It is widely believed that crack propagation rates increase with increasing concentration of CO_2 [77, 90-92]. However it has been noted that CO_2 concentration may have the opposite trend on crack initiation. Cracks are usually initiated from the bottom of corrosion pits. Increasing CO_2 tends to increase the rate of general corrosion preventing the development of pits and probably blunting the tips of shallow cracks or obliterating shallow cracks altogether where the dissolution rate is high enough [61].

Since Parkins [8] found that CO_2 is necessary for the development of the NNPHSCC environment, laboratory studies of SCC usually involve sparging simulated ground water with CO_2 . The sparging gas is typically 5% CO_2 balance N_2 in keeping with the original finding, but sparging gas containing as high as 20% CO_2 has been used. Increasing concentrations of CO_2 in the sparging gas usually results in lower pH and increase in the hydrogen permeation rates [93, 94]. Thus higher concentrations of CO_2 in the sparging gas produce a more aggressive

environment. Increasing concentration of CO₂ has been found to increase the anodic reaction – steel dissolution – by destabilizing the protective oxide film formed at the surface of the material [95].

The concentration of hydrogen recombination poisons, especially sulphur, in the electrolyte can also have a significant effect on the severity of SCC. It is well documented that sulphur promotes the ingress of hydrogen into metal lattices [80]. The presence of sulphide reducing bacteria in the surrounding soil and media can lead to the reduction of sulphates in the surrounding soils as well as the reduction of manganese sulphide inclusions present in the steel. Another source of sulphur is the presence of H₂S either in the surrounding soil or as part of the pipe contents. It is well known that the presence of as little as 1% H₂S in the near-neutral pH environment can remarkably increase the cracking susceptibility of steels by as high as a factor of 6 for pipeline steels.

Other species that may influence the tendency of a soil solution to support SCC include Ca²⁺, CO₃²⁻, SO₄²⁻, K⁺ and Mg. It is well documented that iron carbonate, calcium carbonate, and iron sulphides are typically present in the corrosion products found at NNPHSCC sites (Jack *et al.* in [96]. He *et al.* [97] found that the addition of dilute amounts of Ca²⁺ and CO₃⁻ ions to simulated soil solution (NS4) increased the production of hydrogen at open circuit potential and that increasing calcium concentration reduces the effectiveness of cathodic protection. It has also been found that the formation of CaCO₃ on the specimen surface lowers the pH of the solution counterbalancing the pH increase resulting from the discharge of hydrogen by the applied cathodic potential [97, 98]. Beavers and Worthingham [89] also discovered that the ratio of [Na + K]/[Mg + Ca] seems higher for high pH SCC than for NNPHSCC, and that the ratio was always higher at sites where SCC is found compared to those devoid of SCC.

There have been different types of simulated soil solutions developed for use in the laboratory study of NNPHSCC. These solutions have been developed by mimicking the

composition/concentration of electrochemical species found in analysis of solutions taken from various sites where SCC had been detected. The compositions of the more commonly used solutions are shown in Table 2.1.

2.5.4 Effect of applied potential

It has been established that steels are generally not susceptible to NNPHSCC at open circuit potential (i.e. where no cathodic potential is applied) [94]. The effect of applied potential on SCC is shown in Figure 2.8 [1]. As can be seen from the hatched area in this figure, the presence of some passive film is necessary for SCC to occur [1]. It can be seen from the Figure 2.8 that in zone 1, SCC is closely associated with potentials at which pitting is likely to occur, while in zone 2, the passive film is relatively weak at potentials barely adequate to form a passive film [1]. By critically examining the potential ranges over which SCC occurs, it seems that an unstable passive oxide film must be present before SCC cracking can occur. NNPHSCC is known to be typically associated with locations where there is little general corrosion which is indicative of either surface passivation or transpassive behaviour. Also, in keeping with the usually observed wide walls of NNPHSCC, potentiodynamic polarization tests suggest that active corrosion occurs in NNPHSCC systems [53].

Field observations have shown that 87% of SCC occurs in pipelines with polyethylene coatings [8]. Chen *et al.* [94] explained that polyethylene tapes can form long disbondments trapping water against the pipe and reducing the amount of cathodic protection current reaching the pipe surface. This is likely to reduce the effective cathodic potential at the pipe surface to the active-passive region where pitting readily occurs, ultimately leading to SCC.

Table 2.1: Composition of simulation NNPHSCC soil solutions. Concentrations are in g/litre. pH measure after solution was sparged with 5% CO₂ bal N₂

| | KCl | NaHCO ₃ | CaCl ₂ .2H ₂ O | MgSO ₄ .7H ₂ O | CaCO ₃ | pH |
|-----|--------|--------------------|--------------------------------------|--------------------------------------|-------------------|------|
| NS4 | 0.122 | 0.486 | 0.181 | 0.131 | 0 | 6.3 |
| C1 | 0.0035 | 0.0195 | 0.0255 | 0.0274 | 0.0061 | 5.89 |
| C2 | 0.0035 | 0.0195 | 0.0255 | 0.0274 | 0.0606 | 6.29 |
| C3 | 0.0035 | 0.0195 | 0.0255 | 0.0274 | 0.2422 | 6.83 |
| C4 | 0.0035 | 0.0195 | 0.0255 | 0.0274 | 0.4845 | 7.19 |

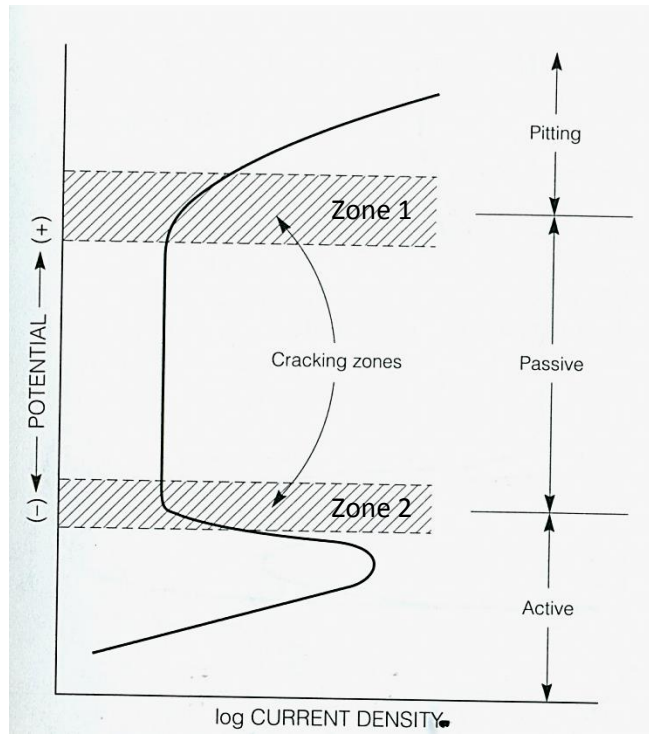


Figure 2.8: Potential ranges where SCC is likely to occur [1]

It has been shown that more anodic potentials tend to inhibit the occurrence of NNPHSCC. Such anodic currents will increase the general corrosion rates, which tends to prevent/reduce SCC incidences. Beavers *et al.* [89] found that applying a cathodic potential of just 100mV to pipeline steels in NS4 solution, while sparging with 5% CO₂ gas, increases the hydrogen permeation rate by a factor of two. Since increased hydrogen ingress into steels is known to increase SCC propagation, it follows that cathodic protection could enhance NNPHSCC.

Finally, the amount of CO₂ within the system may affect the amount of cathodic polarization needed to effectively protect pipeline materials. Johnson *et al.* [93] found that at low concentrations of CO₂, between 0 and 0.5% CO₂, the pH of simulated soil solutions increase with cathodic polarization while the pH decreased with increasing cathodic potentials at higher CO₂ concentrations (10-100% CO₂). This suggests that at high concentrations of CO₂, higher cathodic potentials are needed to maintain cathodic protection of pipeline surfaces.

2.5.5 Effect of the type of coating

It has been severally determined in laboratory studies and field observations that the type of coating applied to the pipeline surface may have an influence on whether a pipeline ultimately experiences NNPHSCC or not or the extent to which it does. Some coatings are known to be more permissive of SCC than others.

Several types of coatings are used to protect the surface of pipelines from the environment. These include: over-the-ditch type polyethylene tape, asphalt and coal tar coating, fusion bonded epoxy coating, extruded polyethylene coating, *etc.* [4]. Field observations have shown that 87% of SCC occurs in pipelines with polyethylene coatings [8]. A study has also

found that “single wrapped polyethylene coated pipe had five times as many SCC colonies per metre as asphalt/coal tar coated pipe, while double- wrapped polyethylene tape coated pipe had nine times as many colonies per meter as asphalt/coal tar coated pipe” [76].

Polyethylene tape is a wraparound-the-pipe type of coating. It may be applied right at the mill or on the go in the field and was the most widely used coating on Canadian pipelines from the early 1960s up to the early 1980s. The national board of enquiry report details that most of the NNPHSCC crack failures on Canadian pipelines occurred on polyethylene wrapped pipelines that were installed between 1968 and 1973 [93]. Generally, SCC cracks form where there are holidays, breaks, or localized de-bonding of the coating material, at which points the pipe is directly exposed to the environment. Since polyethylene coatings are usually spirally wrapped round the pipe, there is a high tendency for the coating to de-bond from the pipe surface when the adhesive holding the tape to the pipe surface fails or is otherwise compromised and unable to stick to the pipe surface as anticipated. Figure 2.9 shows a polyethylene coated pipeline with significant de-bonding of the coating. Most of the susceptible pipes are seam welded and the welded seam is often not flush with the rest of the pipe surface. Hence, tape tenting tends to occur around these welded seams. Tenting may also occur in the contact area between the helix of the spirally wound tape. Tape tenting is illustrated in Figure 2.10. If ground water gains access to such de-bonded sites, SCC may readily occur. The possibility of several de-bonded sites being exposed to the environment is perhaps the main reason why polyethylene coated pipelines are more susceptible to SCC. Also, the disbonded tape shields the pipe surface from the applied cathodic protection, preventing sufficient cathodic potential from reaching the pipe surface and rendering the CP ineffective in preventing NNPHSCC.



Figure 2.9: showing a pipeline in which severe de-bonding of the polyethylene coating has occurred.

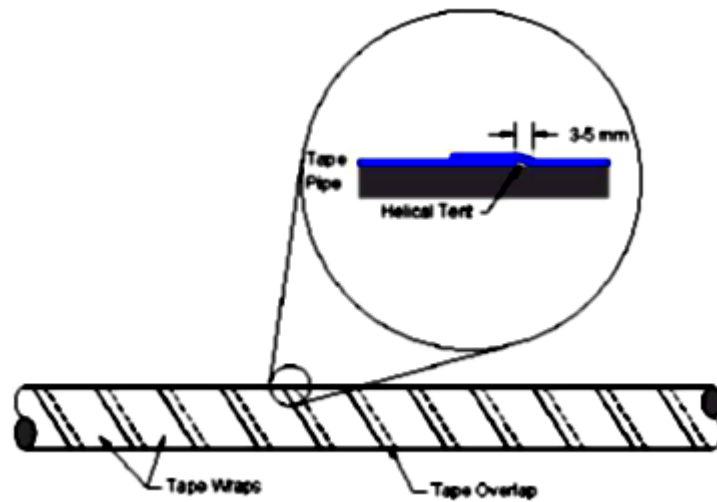


Figure 2.10: Tape tenting around a tape overlap [45]

Fortunately, there has been quite some improvement in polyethylene tape coating technology, such that modern vintage tapes are less likely to disbond from the pipe surface. In the event of a disbondment of the more modern tapes, the tape itself separates from the adhesive such that the adhesive continues to protect the pipe surface [4].

Prior to the wide acceptance of the polyethylene tape, coal tar and asphalt coatings were mainly used, up until the early 1960s. They were commonly applied to the pipe over the ditch (on the right of way) with minimal surface preparation. Asphalt and coal tar coatings are relatively brittle and are usually applied in thicknesses of 2-4mm. Unless the pipe surface is carefully prepared, these coatings are particularly prone to poor adhesion to the pipe surface. Also because they are brittle, soil stresses tend to easily make them to disbond from the pipe surface. Asphalt and coal tar coatings may also disbond, especially due to poor surface preparation. However when they disbond, they tend to become saturated with moisture such that they still retain a good measure of conductivity, hence they let the cathodic potential through to the pipe surface. Also, because they are brittle, they tend to break into pieces, so that CP current is still able to reach the pipe surface in the disbonded area. Nonetheless, SCC might still occur where the soil resistivity is so high that the CP current cannot reach the pipeline [46]. However, these coatings are less susceptible to SCC than polyethylene tapes [75]. In fact it has been found that polyethylene tapes are ten times more susceptible to NNPHSCC than either asphalt or coal tar coated pipelines [75].

Fusion bonded epoxy coatings came on the market much later than polyethylene or asphalt or coal tar coatings and are the most widely used coating on newer generation lines. It has been recognized that fusion-bonded epoxy (FBE) coatings are an effective protection against SCC since no SCC has been found under these coatings [46]. Just like asphalt and coal tar coatings,

when epoxy coatings disbond, they get saturated with moisture and are permeable to the applied cathodic potential effectively preventing the development of SCC. Extruded polyethylene coatings are usually monolithic in structure and, usually thick and tough, such that even punctures from mechanical damage are likely. They have also not been associated with SCC. It must be stressed that these newer coatings have only been in service for a relatively short time; so it is perhaps premature to irreproachably talk about their excellent SCC prevention qualities.

It must be mentioned however, that all coatings are susceptible to developing holidays or disbondment/holes due to mechanical damage, improper handling, improper applications, rock chips *etc.* However, it is crucial that cathodic potential be able to reach such regions of disbondment or imperfection at sufficient levels to prevent the development of SCC, barring which SCC will likely develop on any pipeline irrespective of the type of coating applied.

2.5.6 Seasonal variation

There are a few electrochemical and environmental factors that change across seasons on a pipeline with ongoing SCC issues. Some of these factors include: solution concentration, CO₂ levels, bacteria activity level, temperature, oxygen levels, soil resistivity, soilwater pH *etc.* Laboratory research results suggest these changes may have noticeable influence on SCC initiation and propagation.

Delanty and O'Beirne [75] found that CO₂ concentration in the bulk soil solution adjacent on the pipe surface varies significantly with the seasons. For instance soil CO₂ level was 4% in winter but could be up to 23% in spring. Since carbonic acid concentration is directly related to CO₂ concentrations in the surround soil, carbonic acid concentrations can also be expected to vary with the seasons. Indeed Delanty and O'Beirne's measurements revealed that

carbonic concentration in the soil water was 20 times higher in winter. This means that pipelines with disbonded coatings are exposed to higher levels of acidity and lower pH, in winter. Therefore, dissolution rates should be more intense in winter and pipelines may experience more localized type of corrosion, e.g. pitting, under this condition. Increased dissolution may also increase crack tip blunting and may lead to crack dormancy. Beavers and Harle [53] have proposed that crack growth may occur only during the fall and winter months when soil acidity is higher and trapped solutions are more concentrated and crack dormancy or near dormancy may occur during spring and summer months.

Another issue that may have significant effect on crack propagation/initiation is the level of dissolved oxygen in ground water. As previously mentioned, NNPHSCC occurs in anaerobic conditions when insufficient cathodic protection is supplied to the pipe surface. It is inconceivable that no oxygen reaches the surface of pipelines that are buried in shallow grounds. It is also reasonable to assume that more oxygen will be dissolved in ground water at the high temperatures of the spring and summer months than the winter months. It is known that the presence of oxygen introduces an alternative reduction reaction path to the hydrogen reduction reaction, $O_2 + 2H_2O + 4e^- \rightarrow 4OH^-$. This reaction increases the corrosion potential and reduces the kinetics of the hydrogen generation reaction. Also, the reaction products formed in the presence of oxygen tend to prevent/reduce the assimilation of hydrogen in the metal lattice. Johnson *et al.* [93] found that the presence of oxygen in low concentrations, up to 1%, reduces crack propagation while higher concentrations, 10% or more, in the sparging gas increases the crack propagation rate. Gu *et al.* [99] found that oxygen reduces the ductility to failure of pipeline steels in groundwater.

It can also be expected that there will be less microbial activity in the winter months compared to summer/spring, hence sulphide reduction may occur to a lesser extent in winter. There is a lot of speculation on the exact manner by which seasonal variations impacts SCC of pipelines, hence it is generally understood that more research is required to further understand its influence on SCC initiation and propagation.

2.6 Corrosion fatigue

Corrosion fatigue (CF) consists of the sequential stages of metal damage that evolve with accumulated load cycling, in an aggressive environment compared to inert or benign ones, and resulting from the interaction of irreversible cyclic plastic deformation with localized chemical or electrochemical reactions [100]. Similar to SCC, CF involves the use of a susceptible material in an aggressive environment, with suitable chemical and electrochemical parameters, and mechanical loading [101]. Corrosion fatigue is sometimes referred to as ‘enhanced fatigue failure due to corrosion’. This is perhaps due to the fact that the effect of corrosion fatigue is almost always greater than the added effects of corrosion damage and fatigue. In the presence of an aggressive environment capable of supporting CF, both the fatigue limit and the fatigue life can be markedly reduced and in a lot of cases, the endurance limit is no longer observed [101]. An example of fatigue life reduction and the elimination of the fatigue limit of high –strength steel is shown in Figure 2.11. CF involves these processes – 1) corrosion damage, 2) anodic metal dissolution and cathodic reactions (usually hydrogen reduction), 3) mechanical fatigue [101]. CF leads to a reduction in the fatigue resistance of the susceptible materials due to the synergistic enhancements of fatigue caused by the above processes [101]. The exact nature of CF is

dependent on the particular environment and can be either transgranular to intergranular or a combination of both.

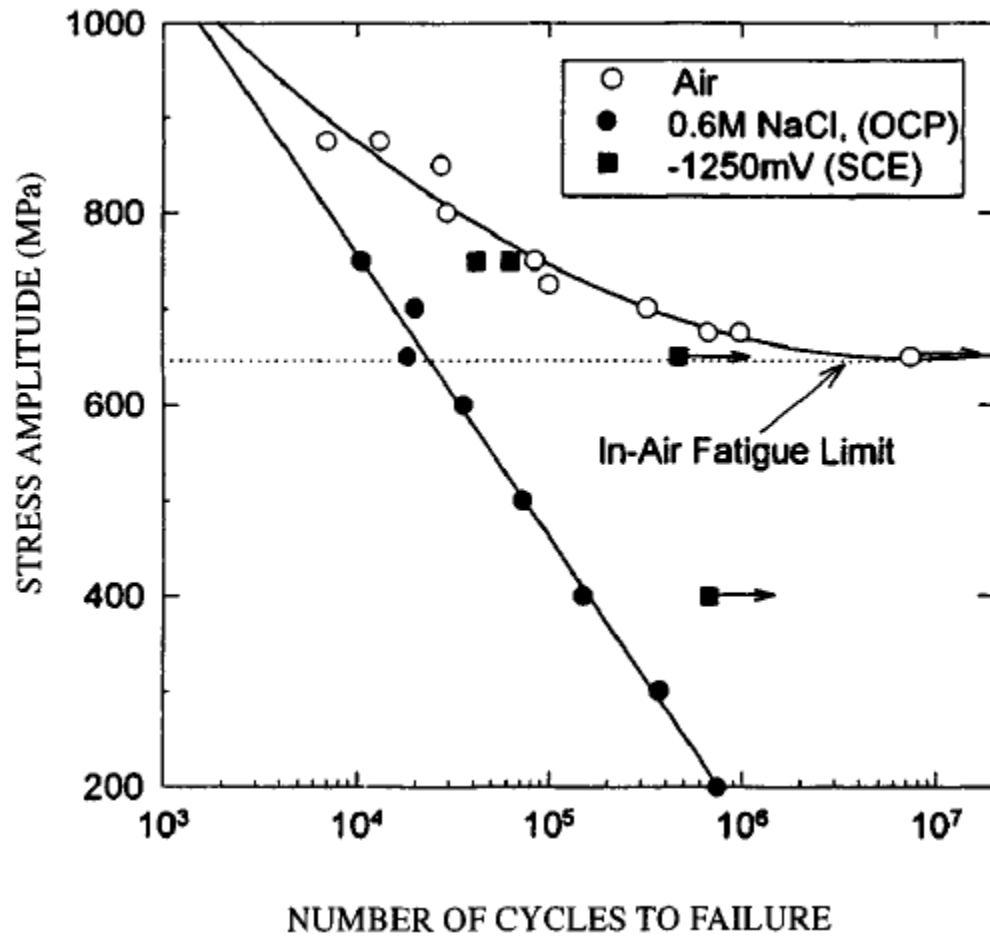


Figure 2.11: Illustration of fatigue life reduction due to load cycling in aggressive environment [100]

A corrosive environment almost always compromises the fatigue properties of an engineering alloy; hence, it is often assumed that CF is not material-environment specific. Localized corrosion, pitting for example, generates favorable sites for CF crack initiation, but pitting is not a necessary pre-requisite for failure as pits are not the only sites where CF has been found to initiate.

2.6.1 Corrosion Fatigue Mechanisms

Gangloff [100] in his exhaustive review of corrosion fatigue explained that CF damage accumulates with increasing load cycle count (N) in four stages: i) cyclic plastic deformation, ii) microcrack initiation, iii) growth of small crack and linkup (coalescence), iv) macrocrack propagation. For materials that possess a measure of ductility, like pipeline materials, CF involves plastic deformation and it is the localization of plastic deformation during cyclic loading that causes fatigue failure at a stress level far below the nominal yield strength of the material [101]. Like SCC, CF may also involve i) hydrogen embrittlement ii) enhanced localized plasticity, iii) interaction of dislocations with surface dissolution, iv) films or adsorbed atoms, v) and combinations of these processes [100, 102-106]. There is yet no consensus on the contribution of each of the above mechanisms to CF. Existing mechanism based models only provide an insight into the phenomenon, but are not able to accurately predict CF as observed from field generated data.

Figure 2.12 shows a schematic illustration of the process by which CF initiates and propagates [101]. Figure 2.12a shows that cracks propagate by slip dissolution resulting from the diffusion of active species such as water molecules and halides to the crack tip followed by the rupture of the protective oxide film at a slip step or in the immediate wake of a crack tip by

strain concentration or fretting contact between the crack faces; dissolution of the exposed surface; and, nucleation and growth of oxide on the bare surface. This mechanism is often referred to as the passive film rupture. Transient anodic dissolution mechanism is often applied to CF propagation in carbon and stainless steels in high temperature pure water and is sometimes applied to titanium and aluminum alloys in aqueous chloride solutions. Localized plastic straining ruptures the protective film at the crack tip so that the crack propagates by transient anodic dissolution of metal at the breached film. The crack propagates at a decreasing rate while the surface re-passivates pending the repetition of the sequence. Since this model is based on dissolution/passivation of crack tips, CF is expected to depend Faradaically on the anodic charge per load cycle and should be governed by surface repassivation reaction kinetics in the occluded crack solution and by the time between ruptures determined from the local strain rate and film ductility. It must be stressed that the film rupture model is complex and there is no general consensus as to its validity as confirming data exist but the model has been found untenable for several specific alloy-environment combinations.

Hydrogen embrittlement (Figure 2.12b) is a popular alternative mechanism for CF, especially in ferritic and martensitic steels, aluminum, titanium and nickel based alloys exposed to gaseous and liquid media within 100°C of ambient temperature [100, 102, 104, 107-110]. It must be pointed out that this hypothesis is only supported by circumstantial but extensive evidence. Here the proposition is as follows [100, 101]:

1. mass transport of specific species occurs within the pit or crevice solution, crack tip dissolution and hydrolysis of cations for local acidification

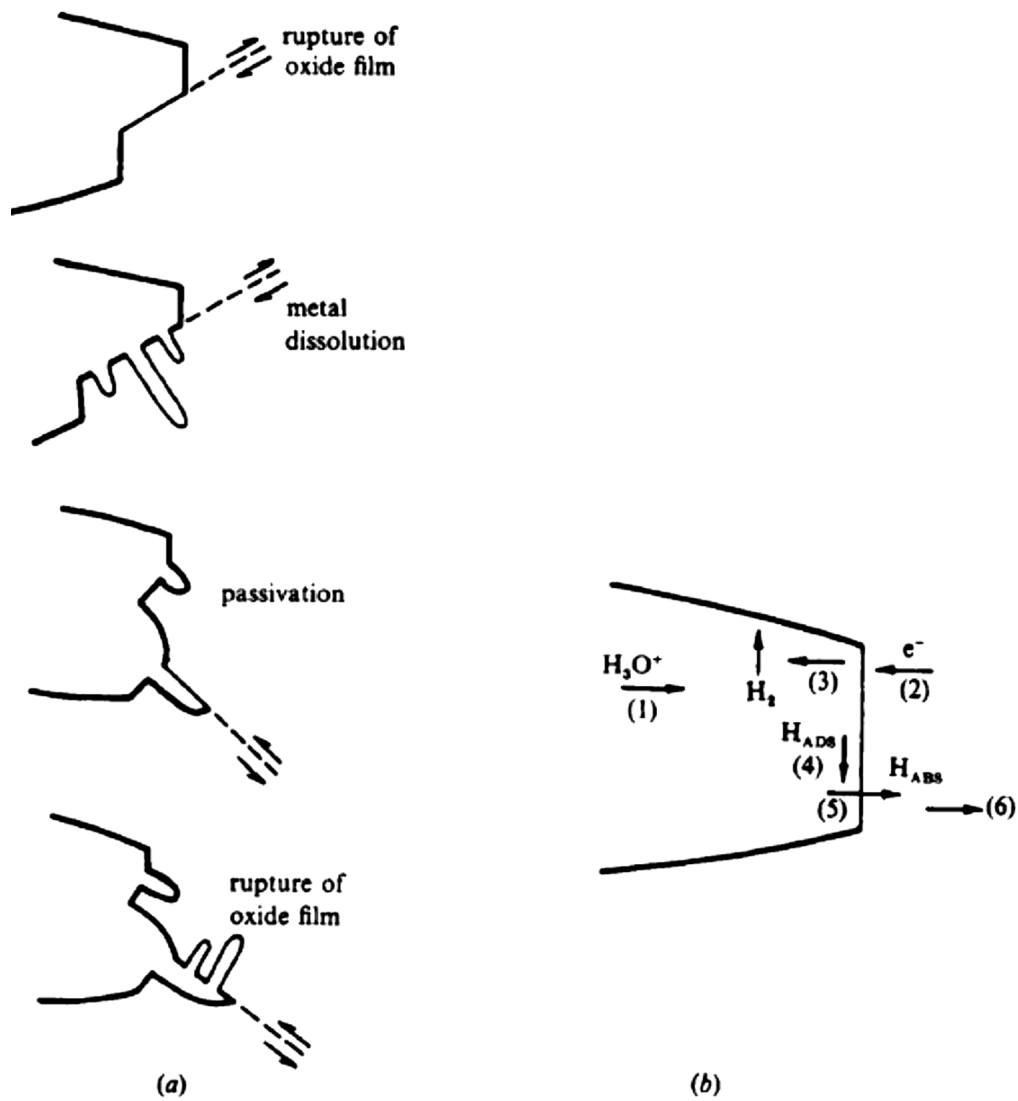


Figure 2.12: Schematic illustration of (a) slip dissolution mechanism (b)hydrogen embrittlement in aqueous media[101]

2. Hydrogen is produced by the electrochemical reduction of hydrogen ions or water. Adsorbed hydrogen may also be furnished by the reactions/ electrolysis of H_2O , C_2H_2 , H_2S or CO_2 at the metal surfaces.
3. Hydrogen is chemically adsorbed on strained but clean initiation sites or crack surfaces
4. The adsorbed hydrogen then diffuses by lattice, interface or dislocation mechanisms in the initiation-volume or crack tip plastic zone.
5. Segregation of lattice hydrogen to high energy sites such as grain boundaries, internal interfaces, and regions of high triaxiality ahead of the crack tip or void.

CF damage is enhanced by hydrogen-affected lattice bond decohesion, grain or dislocation cell boundary decohesion, enhanced localized plasticity or metal hydride formation.

In addition to the above, other mechanisms have been proposed based on the interaction between dislocations and environment-based processes at initiation sites or crack tip surfaces. Dislocation modeling and in-situ TEM microscopy have shown that adsorbed hydrogen localizes plastic deformation in several pure metals and alloys [111]. It has also been shown that reaction-product films are not capable of sustaining extensive plastic deformation compared to the base metal. This behavior has led to the hypothesis that CF may be caused by any of 1) interference with the reversibility of slip, 2) localization of persistent slip bands, 3) reduction of near-surface plasticity leading to reduced or enhanced CF depending on the cracking mechanism, 4) localization of near-surface dislocation structure and voids, or 5) film-induced cleavage [104, 112, 113]. It has also been suggested that adsorbed cations could affect fatigue in a similar way. It has also been

proposed that anodic dissolution at sample surface or at the crack tip may eliminate near-surface work hardening, enhancing fatigue damage.

2.6.2 Factors controlling corrosion fatigue

Some of the main issues that are central to understanding the influence of material, environmental and mechanical factors on CF can be summarized thus:

- 1) Mass transport and electrochemical reaction/kinetics are central and critical to the CF phenomenon. For example: [100]
 - a. The effect of electrolyte composition, electrode potential, pH, temperature, viscosity, conductivity, biological activity, *etc.* are governed by mass transport.
 - b. Electrochemical reactions within pits, crevices, and cracks – including the role of strain in exposing fresh surfaces to sustain these processes – are very crucial to the CF phenomenon.
- 2) Corrosion fatigue is time dependent [100]. The rate at which CF progresses is determined by one or more of the slow steps in the mass transport and crack surface reaction sequence. For instance, it has been determined that slow loading rates accelerate CF damage.

2.6.3 Mechanical factors

Since CF is essentially an environment enhanced version of fatigue, it can be reasonably expected that the same mechanical factors that affect fatigue failure also exert a significant influence on CF. However, most of these effects are exacerbated by the aggressive environment

involved in CF. Under cyclic loading, crack closure – fretting contact between the mating surfaces at low stress levels above zero load during unloading; pumping of the aggressive solution to the crack tip by the crack walls; and progressive blunting and re-sharpening of the crack tip by the reversing load; can significantly influence the rate of dissolution [114]. Therefore, cyclic frequency and loading waveform can strongly influence the progression of CF, to a greater extent than in ordinary fatigue.

There has been a lot of work done on characterizing and modeling the effect of frequency on the propagation of CF based on the film rupture and hydrogen environment embrittlement mechanisms. These studies have given rise to the following conclusions [107, 110, 115-117]:

1. Fatigue crack propagation is independent of frequency for alloys in inert gases, moist air and vacuum at low temperatures
2. Under the influence of an aggressive environment (CF), the frequency response can be any of the following
 - a. Pure time dependence: Here da/dN is proportional to $(1/\alpha f)$
 - b. Cycle-time dependence: here da/dN is proportional to $(1/\alpha f)^\beta$, β is on the order of 0.5
 - c. Cycle dependence: here da/dN is enhanced by the environment but frequency – independent.

where α represents the proportion of the load-cycle time that produces CF damage and is usually taken as 2 for symmetrical loading cycles since unloading is usually assumed to have no significant contribution to environmentally enhanced crack propagation [102].

Generally, time dependent cracking occurs in high strength SCC susceptible alloys at K_{\max} above K_{ISCC} or at very high da/dt while cycle time dependence occurs at ΔK levels below K_{ISCC} or at very low da/dt . Cycle dependence/frequency independent, otherwise referred to as true corrosion fatigue, occurs at very low ΔK , at high loading frequencies or for alloys that resist environmental cracking [100].

Four stages are involved in the development of fatigue damage [101]:

1. Pre-crack cyclic deformation: here plastic strain is accumulated in local regions; dislocation and other substructures develop; persistent slip bands appear - slip bands that develop on the surface of a deformed material during cyclic deformation and that re-appear at the same locations during further cyclic deformation after polishing the surface; extrusions and intrusions develop
2. Crack initiation and stage I growth: Cracks, rather microcracks, form due to the deepening of intrusions. At this stage, crack growth is within the planes of high shear stress
3. Stage II crack propagation: microcracks develop into well-defined cracks on the planes of high tensile stress in a direction that is perpendicular to the maximum tensile stress.
4. Rupture (otherwise referred to as ductile fracture): occurs when the crack reaches a critical size and the remaining cross section of material cannot support the applied load.

A corrosive environment usually intensifies all stages except the ductile rupture phase.

2.6.4 Corrosion fatigue initiation

A little background information on corrosion fatigue initiation is relevant because for low-stress high-cycle fatigue, such as in many SCC cases, crack initiation comprises a fairly large portion of the total component life. It is a general knowledge that fatigue failures initiate in alloys on the surface or subsurface of the component and are often associated with surface defects, usually non-metallic inclusions. Such inclusions must meet two criteria [118]:

- 2a.** The inclusion must be of a critical size or greater
- 2b.** The inclusion must have a low deformability

In steels the main culprits are alumina, spinels, and calcium aluminates larger than 10 μ m in diameter. MnS inclusions, which are far more common in steels, and often have an elongated structure, are much less frequently the source of fatigue crack initiation. This is because even though these elongated inclusions can act as stress raisers, it is their ability to enhance the localization of plastic deformation around themselves that is more critical to the fatigue properties of a material.

In the presence of an aggressive environment, localized attack around inclusions may provide favourable sites for the initiation of CF cracks. It has been shown that in the presence of an aggressive environment, inclusions may show a significant difference in their susceptibility to crack initiation than in air. For instance, calcium-aluminates, which were found to contribute significantly to fatigue crack initiation in air, did not have any significant contribution to cracking in a sodium chloride environment, whereas sulfide inclusions which were less

susceptible to cracking in air significantly raise susceptibility to fatigue cracking in sodium chloride solutions [119-121]. This behavior is due to the significantly higher electrochemical activity of sulfides compared to aluminates in steels. Sulphide inclusions and the areas immediately surrounding them have been shown to be anodic to steel [122, 123]. Dissolution of sulphide particles can also lead to the formation of hydrogen sulfide and HS^- ions which are known to enhance the development of pits and may catalyze anodic dissolution of iron and enhance the absorption of hydrogen. The application of cyclic loading is known to increase the corrosion rate at an inclusion-matrix interface relative to the stress-free or static loading condition, enhancing the formation of micropits from which fatigue cracks can subsequently initiate [122].

Cathodic polarization can influence both the initiation and propagation of CF in steels. Opposing trends have been reported, depending on whether the steel specimen was initially smooth or notched. For smooth (un-cracked) steel specimens, fatigue life was only reduced when the dissolution rate exceeds a critical value; hence, cathodic polarization reduces or eliminates CF initiation in smooth samples by suppressing anodic dissolution and preventing the formation of pits making crack initiation more difficult [124-126]. These same studies also reported that CF was accelerated by cathodic polarization due to enhanced hydrogen effects. Dissolution and pitting strongly influence the initiation of an environment-enhanced fatigue crack [124, 126, 127], while hydrogen plays a less significant role at high loading frequencies, near-threshold stress intensities, and uniaxial stress states typical of smooth specimens. Low frequency and hydrostatic stress states at crack tips enhance the hydrogen effect through crack tip acidification at free corrosion potentials and water reduction at cathodic potentials. This trend is reversed when aluminum is subjected to anodic/cathodic polarization. It has been reported that in aluminum, CF is accelerated by anodic polarization or extreme cathodic polarization and is arrested by moderate cathodic polarization [128-130].

2.6.5 Corrosion fatigue crack propagation

Similar to pure fatigue, CF is usually characterized using fracture mechanics laws by relating the average rate of crack advancement per load cycle (da/dN) to the applied stress intensity factor range (ΔK). In the presence of an aggressive environment, CF can propagate at maximum stress intensities (K_{max}) well below the threshold stress intensity for SCC or pure fatigue, at a rate that is significantly higher than ordinarily expected.

As already mentioned, CF can be cycle dependent, time dependent, or purely cycle-time dependent. To understand this categorization, it is important to consider the effect of the aggressive environment on the growth of CF by separately considering the crack growth under pure mechanical fatigue and under SCC conditions. Figure 2.13a shows a typical sigmoidal variation of crack growth rates with stress intensity factor under pure fatigue conditions while figure 2.13b plots a typical data as crack velocity vs stress intensity factor. This figure shows a unique stress intensity (K_{ISCC}), called the stress intensity threshold, below which the environment has no effect and no crack propagation will occur. Just above this stress is region I, in which crack propagation rapidly increases with stress intensity. In region II, steady crack growth occurs and crack propagation is relatively independent of stress intensity. When the maximum stress intensity approaches the fracture toughness of the material, crack propagation increases rapidly in region III. Figure 2.13c depicts true corrosion fatigue, where cyclic plastic deformation and the environment interact synergistically to produce a cycle and time dependent crack propagation. Time dependent fatigue crack propagation is depicted in figure 2.13d, showing a simple superposition of mechanical fatigue and the effect of the environment. Here stress corrosion fatigue only occurs when $K_{max} > K_{ISCC}$. In this form of CF, the cyclic waveform is unimportant. Figure 2.13e depicts cycle-time dependent corrosion fatigue which involves complete cycle-time dependent crack propagation over the entire life cycle of the crack. This behavior is the most general form of corrosion fatigue.

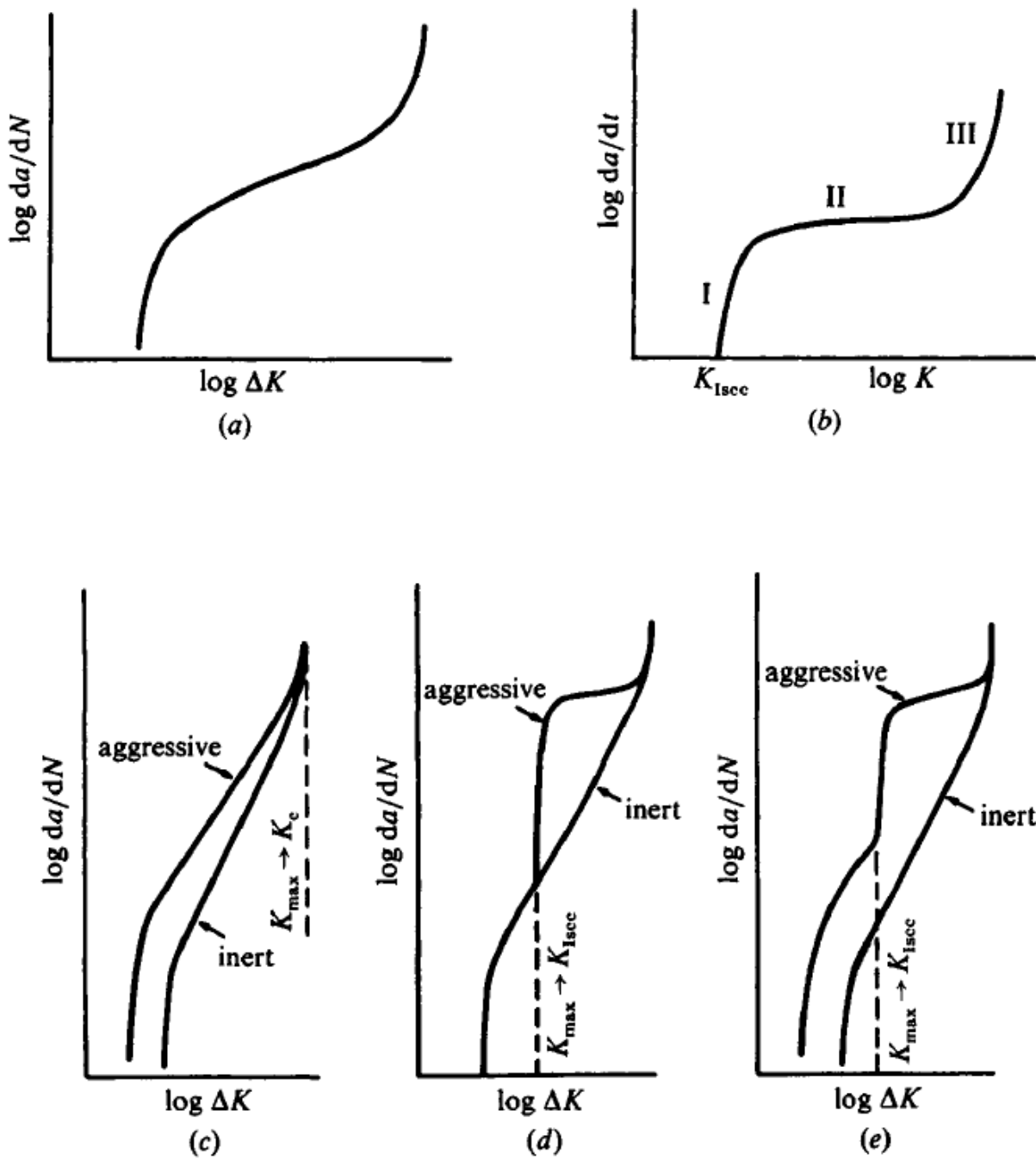


Figure 2.13: Schematic representations of possible combinations of mechanical fatigue and environmentally enhanced crack growth (a) fatigue crack growth in inert environment (b) stress corrosion cracking under sustained loading (c) True corrosion fatigue (d) superposition of (a) and (b), (e) superposition of (b) and (d) [101]

2.7 SCC propagation mechanisms

It is impractical to provide a full list of the mechanisms that have been proposed for the propagation of stress corrosion cracking. Several mechanisms have been proposed and they are as diverse as they are many. Among the most prominent mechanisms are [34]:

- 1. Dissolution mechanisms:** Proponents of this mechanism ascribe the observed SCC propagation to the repeated rupture of protective passive films, repassivation of the exposed underlying surface, and a continued repetition of the whole cycle. After a rupture of the protective film at the crack tip, there is a burst of anodic dissolution, advancing the crack. Since a free surface cannot support stress, the protective layer on the crack wall preserves the shape of the crack and concentrates plastic deformation at the crack tip. Although the fact that anodic dissolution is involved in the NNPHSCC process is incontrovertible, it has been well documented that a dissolution mechanism alone cannot account for NNPHSCC as crack propagation rates are significantly higher than only dissolution mechanisms can properly account for. Among the mechanisms in this category are the film rupture and the active path mechanisms. The active path mechanism supposes there are preferentially corroded paths in metals and alloys on which crack propagation by SCC is localized. Among such paths are grain boundaries, dislocation pile ups and second phase boundaries. This mechanism may be reasonable for intergranular SCC but it does not explain NNPHSCC.
- 2. Mechanical fracture mechanisms:** here it is assumed that stress concentration at the base of corrosion pits increases over time until ductile rupture occurs [131]. Early

versions of this mechanism assumed that localized crack propagation occurred by localized dissolution until the remaining ligament between adjacent cracks failed by ductile rupture. There have been several revisions of this mechanism among which are:

2a. corrosion tunnel mechanism: Here, the proposal is that fine arrays of small corrosion tunnels form at emerging slip steps and grow in diameter and length until the remaining ligament is unable to sustain the stress, causing ductile rupture. Hence crack propagation occurs by repeated dissolution tunneling and ductile rupture. A crack that propagates by this mechanism should present clearly defined grooving on the fracture surface coupled with ductile rupture indicators such as microvoid coalescence as illustrated in Figure 2.14. Such slots are typically not observed in SCC. It has been suggested that stress application modifies the tunnels to thin flat slots as depicted in Figure 2.15. Features similar to those depicted in Figure 2.15 have been observed in some transgranular SCC.

2b. adsorption-enhanced plasticity: the proposal here is that the chemisorption of environmental species enhances the nucleation and motion of dislocations at the crack tip and promotes the shear processes that give rise to brittle cleavage-like features. The adsorption mechanism is assumed to be dependent on the applied potential and the competitive adsorption between aggressive and inhibitor species is assumed to account for the role of inhibitors in slowing down cracking. However, there has been no evidence of preferential adsorption sites involved in SCC [1].

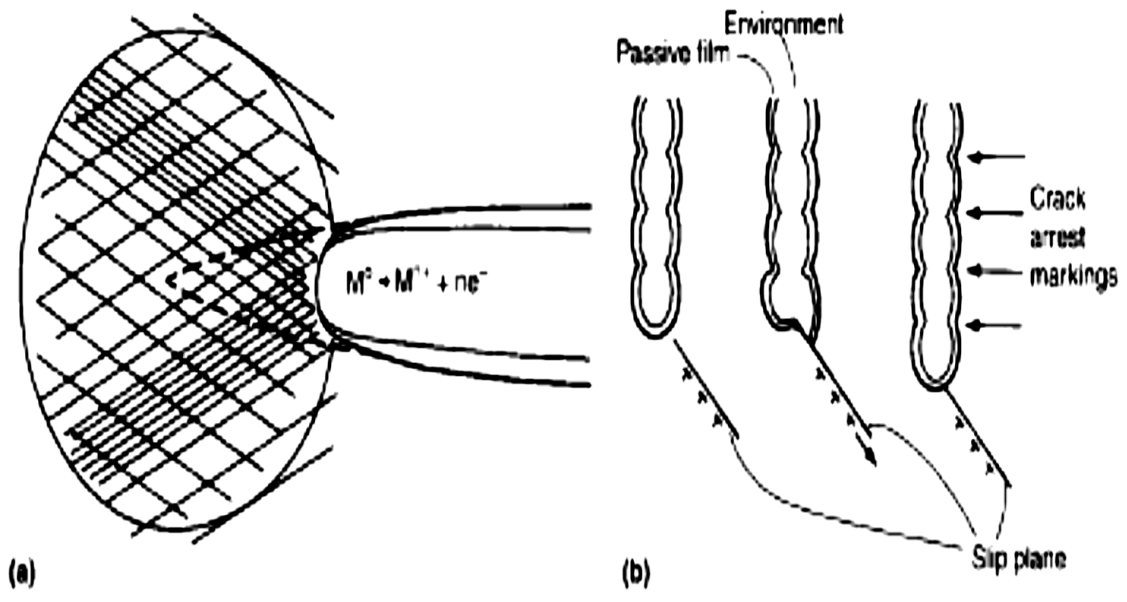


Figure 2.14: Crack propagation by film rupture model showing corrosion tunnel mechanism with grooved fracture face [34]

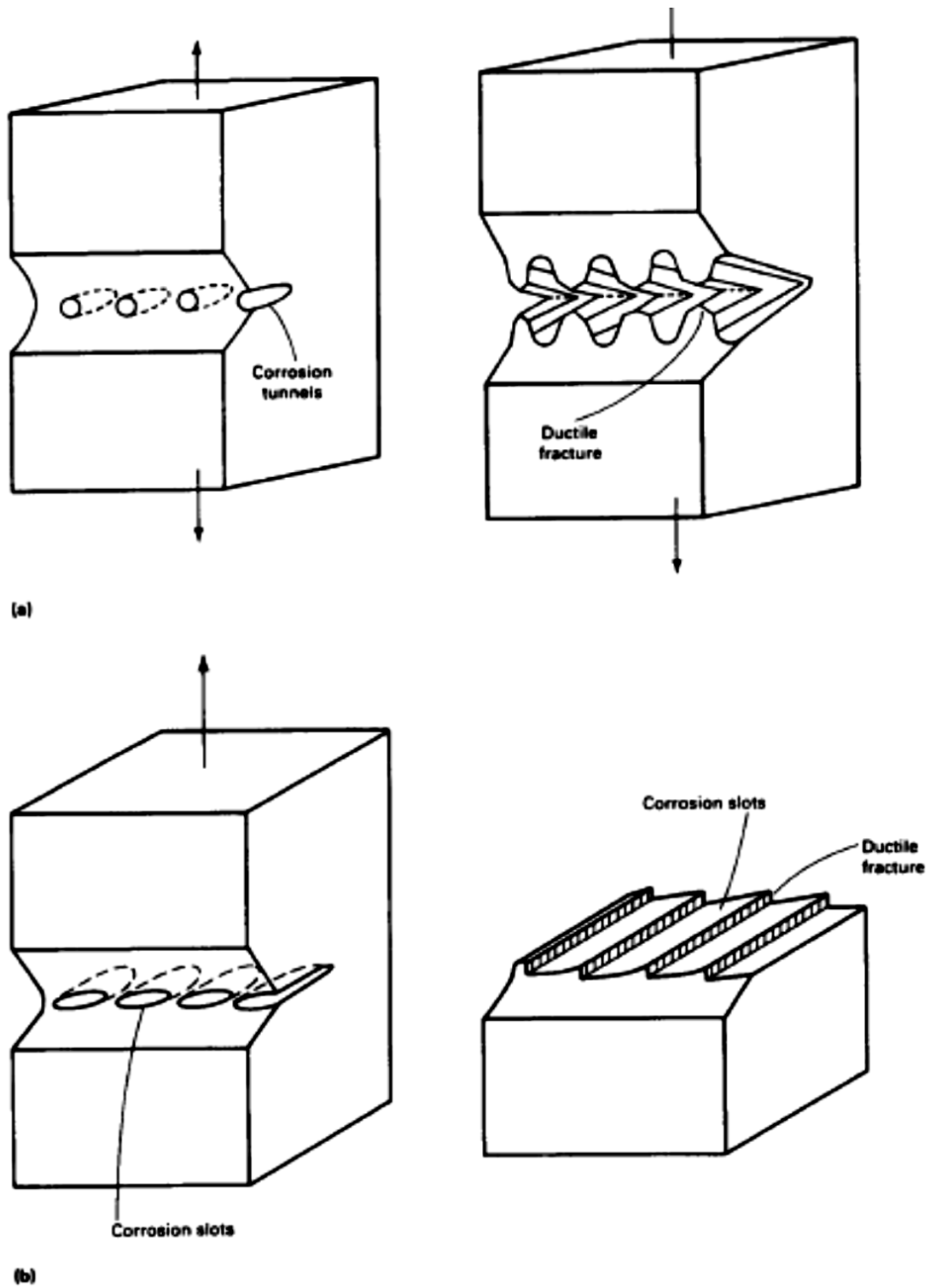


Figure 2.15: Crack propagation mechanism by tunnel mechanism (a) by formation of tunnel at slip steps and ductile deformation and fracture of remaining ligament (b) schematic representation of tunnel mechanism of SCC and flat slot formation [34]

This mechanism also does not explain the measurable but limited plasticity ahead of a sharp crack tip in a ductile material and the discontinuous nature of crack propagation.

2c. film induced cleavage: This mechanism was originally proposed in 1959. It explained that vacancy injection and de-alloying could generate brittle fracture. More contemporary versions of this model propose that [132]: i) In a corrosive environment, a thin film forms on the surface of the metal/alloy ii) brittle cracks initiate in this thin layer of film iii) some of the brittle cracks propagate through the film/matrix interface with sufficient velocity to keep propagating in the ductile matrix iv) the crack continues to propagate in the ductile matrix and will eventually be arrested until the process is repeated all over again. Anodic dissolution and corrosion are not required to cause crack propagation but only to form the required brittle surface film. However, there is no evidence to suggest that surface films are sufficiently brittle to sustain crack propagation into the ductile matrix since most of the films involved in SCC are hydrated and are not likely to be that brittle. However there are computer simulation results that have suggested that surface layers can indeed initiate brittle fracture even if the layer is ductile depending on lattice mismatch [133].

2d. atomic surface mobility: This mechanism assumes that crack growth occurs by the capture of surface vacancies at the crack tip and counter current surface diffusion of atoms away from the crack tip [134, 135]. It predicts that SCC involves surface mobility maximization at the expense of bulk diffusion in a metal crystal and should be prevalent at temperatures below half the melting point of the metal in question. It proposes that SCC is produced by low melting compounds that enhance surface mobility. Parkins [136]

refuted this mechanism by noting that although SCC in carbon steels occurs in the presence of low melting compounds in nitrates, it also occurs in the presence of high melting point compounds like Fe_3O_4 . Oriani [137] also suggested that there are obvious demerits to this proposal since the flow of surface atoms in a stressed piece of metal should be towards the crack tip not away from it.

2e. localized surface plasticity: Here, film rupture is assumed to initiate large anodic currents at the site of rupture by a galvanic coupling of the underlying metal and passivated surface. SCC initiation is known to involve both mechanical creep and anodic dissolution. It has also been suggested that anodic currents can aid creep occurrence [138]. At the crack tip, if a high creep rate is produced by the anodic current, then softening could occur by a surface defect structure reducing the strain hardening by primary creep. The softening structure even though it is able to deform plastically ahead of the surrounding metal is unable to do so because it is constrained by the surrounding material. Microstrain within the softened volume then produces a triaxial state of stress which hinders plastic slip. Continued straining of this volume can only produce a brittle crack. Jones [138] likened the crack tip under this condition to the soft solder joining the ends of two pieces of steel bars, wherein loading normal to the solder joint produces a brittle fracture of the solder due to the triaxial stress state which prevents plastic deformation of the normally ductile solder. This mechanism is able to explain several aspects of SCC propagation like the resistance of pure metals to SCC (no second phases, more uniform deformation) and discontinuous crack propagation (the softened crack tip must reform at an arrested crack tip before a new brittle crack burst can occur).

2f. hydrogen embrittlement: It is often noted that some of the features found in SCC are similar to those found in hydrogen induced cracking. Therefore, it is widely assumed that hydrogen plays some, albeit uncertain, role in SCC propagation. It has been noted that the effects of factors such as yield strength, impurity segregation and temperature on crack propagation in ferritic alloys in aqueous media follow the same pattern as in hydrogen induced cracking. Also it is assumed that since anodic dissolution must have a corresponding cathodic reaction, and hydrogen reduction is often the cathodic reaction and hydrogen is known to easily migrate into metal lattice, it is highly likely that hydrogen plays some role in SCC propagation. Several mechanisms have been proposed to account for the role of hydrogen in enhancing crack propagation. These mechanisms will be briefly discussed in section 2.8.

2.7 Dormancy

A cursory look at macrographs of SCC colonies suggests that most of the cracks within the colony are dormant (not propagating). In fact it has been found that 95% of cracks within a colony in field studies are dormant, with a blunt tip, and are very shallow in nature (under 1mm in depth) [139]. Generally crack dormancy refers to a state in which a crack experiencing cyclic or non-cyclic loading either does not grow at all or is growing at a very small rate (typically less than 10^{-9} mm/s). In this way, dormancy does not necessarily mean there are no long term safety concerns as far as pipelines are concerned. Chen [140] argued that a crack growing at 5×10^{-9} mm/s could still reach a third of its wall thickness in 20 years.

Generally, dormant cracks in the field present with blunted crack tips and corroded walls. Although crack propagation may not be occurring, continued corrosion of crack walls may

occur, causing further crack blunting and decreasing the probability of growth re-activation [54]. This is because several cycles of severe mechanical loading might be required to re-sharpen the tip of a dormant crack prior to growth reactivation. It is generally believed that high strain rate events such as the complete unloading and reloading of pipelines during shutdowns may be required to reactivate dormant cracks.

Several factors may influence the tendency for a given crack to attain dormancy. Among these are environmental factors, crack tip strain rates, stress transients *etc.* There is no general consensus on the environment-material-stress interactions required for SCC crack dormancy nor are there any concrete explanation as to why some cracks grow in the field while others are dormant.

Laboratory studies often have to be carried out under very severe mechanical loading conditions that are not representative of normal pipeline operating conditions because it has been almost impossible to grow cracks under benign conditions which are more representative of normal pipeline operating conditions in the lab. Under normal operating conditions, laboratories are usually only able to generate short cracks that soon become dormant and impossible to reinitiate under benign conditions [51, 141].

2.8 Mechanisms of hydrogen embrittlement

2.8.1 Decohesion model

The pioneer work on the embrittlement effect of hydrogen on steels was done by Troiano *et al.* [142] and Slaughter *et al.* [143]. They provided the initial framework for what is now known as the decohesion model of hydrogen embrittlement. They opined that the dissolution of hydrogen in steels leads to the concentration of hydrogen in regions of positive hydrostatic

component, θ , of elastic stress and that such concentrated hydrogen weakens the lattice so that a crack nucleates under the applied stress. Li *et al.* [144] further developed this concept by developing expressions for the variation of chemical potential of an interstitial solute with stress state of the metal matrix and making relevant deductions from it. They found that the local stress needed to separate atoms from each other on a hydrogen coated surface, in order to generate free surfaces, has to rise to very large values in order to overcome the interatomic forces. Contrary to the original proposition by Troiano *et al.*, Li *et al.* found that the large stresses at crack tips can concentrate interstitial hydrogen by several orders of magnitude above the stress-free solubility. They also proposed that as hydrogen concentration is increased, the attractive force between metal atoms is decreased as well as the maximum cohesive force, F_m , developable by the atomic bond. This provided a framework for later assertion by Oriani [144] that the condition for hydrogen-induced crack propagation is that the local tensile stress σ_z' at the crack tip in mode I loading just equals to the hydrogen-concentration-reduced local maximum cohesive force, F_m per unit area (the hydrogen concentration at the crack tip being much larger than the concentration in the absence of the stress state of which σ_z' is one component). It was therefore proposed that

$$\sigma_z' = nF_m(c_H) \dots\dots\dots (2.7)$$

where n is the number of metal atoms per unit area of crack plane and c_H is hydrogen concentration. The exact value of σ_z' relative to the externally applied stress is dependent on the macroscopic characteristic of the crack through the radius of curvature of the crack tip and the crack length. Realizing that the radius of curvature of the crack tip reflects the microscopic plastic properties of the material at the location in question, e.g. matrix, grain boundary, *etc.*,

Oriani [144] adapted Gilman's modification of the Inglis relation for the stress at the tip of a crack blunted by plastic deformation

$$\sigma_z' = k' \sigma (L/\rho)^{0.5} = k'' K/\rho^{0.5} \dots\dots\dots (2.8)$$

where σ is the externally applied stress, k' and k'' are numerical parameters and K is the stress intensity parameter, ρ is the radius of curvature of the crack tip, and L is the crack length.

Combining the two equations above,

$$K = k\rho^{0.5} F_m(c_H) \dots\dots\dots (2.9)$$

Since F_m is a decreasing function of c_H , and c_H increases with tensile stress state, equation 3 therefore suggests that for a perfectly homogenous steel there must exist a value of chemical potential of hydrogen for a given value of K below which a crack will not propagate, and also that for a given value of chemical potential there must exist a value of K below which a crack remains immobile. These thresholds have been demonstrated in several studies and some researchers accept that crack propagation can be switched on and off by changing the hydrogen pressure.

Although the core principle of the decohesion theory is that hydrogen reduces the bond strength between atoms and lowers the stress requires to initiate a crack, it was explained that the manner in which the local stress is generated and the specific expression to be used for the $F_m(c_H)$ and other functions will vary from material to material. For example, many low strength steels fail with similar dimple-rupture appearance irrespective of whether failure occurred with or without hydrogen, making it difficult to determine whether hydrogen induced decohesion played any role in such failures [145]. However, Oriani and Josephic [146], using load

relaxation at constant crack length constraint approach, showed that a threshold value of hydrogen fugacity exists beyond which hydrogen-assisted crack propagation occurs, through enhanced decohesive nucleation and immediate subsequent growth of microvoids. It was therefore theorized that the effect of hydrogen in such steels is to increase the number and mean size of microvoids at a given value of plastic strain over what would have occurred in the absence of hydrogen, by a decohesion mechanism. This ensures that the critical conditions for final ductile rupture such as critical area fraction of voids is attained at smaller values of plastic deformation with hydrogen than without it.

2.8.2 Adsorption model

The original adsorption energy model was proposed by Petch and Stables [147], and the various forms of this model developed since the original work have been dubbed the Petch-Stables model. In simple terms, this model holds that due to the fact that the surface energy, γ , of a metal surface is lowered by a finite amount, $\Delta\gamma$, by the adsorption thereon of hydrogen, the energy required from a stress field to grow a crack is lower in the presence of hydrogen than in its absence. Li *et al.* suggested that while the adsorption model is thermodynamically correct, it possibly only describes the final separated state of crack and may not necessarily describe the intervening stages in the development/formation of a crack.

2.8.3 Pressure theory

This theory is premised on the fact that hydrogen diffuses to internal voids, fissures and interfaces where it forms molecular hydrogen causing a buildup of hydrogen pressure which aids void growth and crack propagation [148]. When atomic hydrogen recombines at free surfaces inside the material, it expands and the pressure increases as the hydrogen concentration increases until the local yield strength is exceeded causing plastic deformation and void creation in such

areas. Griffith proposed that for a crack to grow, the system must undergo a decrease in local energy content. The energy released by the expanding molecular hydrogen inside steels can facilitate crack growth by supplying the portion of strain needed to cause cracks to advance [149].

2.8.4 Surface energy theory

The original proposition of what has now come to be known as surface energy theory of hydrogen degradation is attributed to Petch and Stables [147] who opined that hydrogen enhances crack propagation by adsorbing on the free surface created by cracking and decreasing the work of fracture. Although there have been a few criticisms of this model on the grounds that: it cannot account for the reversibility of degradation, underestimates the work of fracture, does not account for discontinuous crack growth, and that it cannot explain why oxygen which has a greater heat of adsorption than hydrogen suppresses the effect of hydrogen on crack propagation, this theory still subsists in contemporary literature. Some researchers believe that oxygen preferentially adsorbs at the crack tip thereby preventing the ingress of hydrogen, but because of its atomic size, it might be thermodynamically more favourable for oxygen atoms to reside at atomic sites unfavourable for crack propagation [150, 151]. Other researchers have shown that the occurrence of plastic flow may screen a sharp crack tip from extreme stress concentration while allowing some elastic stress concentration, may account for the underestimation of the work of crack propagation and discontinuous crack growth [152, 153].

2.8.5 Enhanced plastic flow theory

Beacham [154] proposed that hydrogen enhances crack propagation by enhancing dislocation motion. Subsequent work on this proposition has led to the expansion of this definition to include the fact that hydrogen could also lead to the creation of dislocations at

surface and/or crack tips, leading to localized softening within the alloy [155]. The model is based on hydrogen-deformation interactions that occur on a microscopic scale, hence usually not observed in tests that probe material behaviour on a macroscopic scale. Typically when this mechanism is in operation, it is observed that within a certain range of temperatures and strain rates, the introduction of hydrogen into solid solution decreases the barriers to dislocation motion, increasing the amount of deformation that occurs in a localized region adjacent to the crack tip [156-160]. Birnbaum [156] using an in-situ TEM analysis observed that dislocation motion increased at the crack tip when hydrogen gas is introduced into the test. Of particular significance is the fact that increase in dislocation mobility occurs at constant stress. It was not only observed that the introduction of hydrogen into the test environment increases dislocation mobility but also that the removal of hydrogen from the test environment results in noticeable decrease in dislocation mobility. The behaviour was observed for both edge and screw dislocations, mixed dislocations and also for dislocation tangles [161]. In bcc metals, enhanced dislocation mobility was observed on {112} and {110} slip planes. The extent of dislocation mobility enhancement was observed to be more intense with increase in interstitial solutes (such as C) concentration for high purity iron. It was also observed that the presence of hydrogen in solid solution localized ductile rupture to regions close to the crack tip in notched specimens. Cracks that had propagated and arrested in vacuum could be re-started in a hydrogen environment without increasing the external load.

It must be mentioned that even though this mechanism has been proven to operate in certain alloys, hydrogen has also been shown to cause a hardening of other materials including some steels. It has been shown however that hydrogen may enhance plastic flow at the crack tip by causing shear localization to the crack tip.

2.8.6 Hydride formation theory

In some alloys especially the transition metals and magnesium, hydrogen is known to enhance cracking by the formation of brittle metal hydrides at the crack tip. This usually occurs spontaneously when sufficient hydrogen pressure builds up. Such hydrides are typically very brittle and can cleave under an applied stress. Such cracks will typically arrest when they propagate into the ductile base metal. However, the triaxial stress state at a crack tip is known to enhance hydride precipitation, hence the crack tip may enhance the tendency to form brittle hydrides. Therefore in a system that supports hydride formation, in the presence of a crack tip (which modifies the stress state), crack propagation could occur by the repeated precipitation and cleavage of hydrides. Hydrides are typically not observed in pipeline steels.

2.8.7 Hydrogen attack

This may occur by surface or internal decarburization of steel, usually at high temperatures. In this case, hydrogen diffuses into steel at high temperature and reacts with carbon to form a hydrocarbon, usually methane. This reaction may also occur at the surface of steel. The loss of carbon then weakens the steel in question. The associated loss of strength enhances crack propagation.

2.9 Predictive modeling of NNPHSCC

Near-neutral pH stress corrosion cracking is a dynamic process that occurs progressively over time. Generally, pipeline operators carry out periodically scheduled inspection in order to ascertain the serviceability/integrity of pipelines. Once an ongoing SCC issue is discovered, such

sites must be carefully monitored in order to prevent catastrophic failures or accidental discharges and the attendant environmental and economic issues.

For ease of modeling NNPHSCC, the pipeline integrity manager often categorizes the lifecycle of an NNPHSCC crack into four stages (Figure 2.16). The stages usually involved are: i) establishment of conditions necessary for NNPHSCC development on pipe surface 2) microcrack initiation 3) growth and coalescence of microcracks leading to development of large cracks 4) coalescence of large cracks leading to failure. The remedial measures introduced are dependent on how mature the SCC site is. Among the usually recommended remedies are: grinding cracks off, putting a sleeve over areas where there is significant thickness loss, hydrotesting, section replacement, *etc.*

Apart from understanding the mechanisms involved in the development of NNPHSCC, the pipeline integrity manager's dilemma also includes being able to predict the rate of progression of ongoing NNPHSCC. Usually, pipeline integrity management involves relying on one crack propagation model or the other in order to determine what remedies may be required to prevent unpalatable eventualities at different stages over the lifetime of the pipeline or sections of it. These models also help the pipeline operator to schedule inspection intervals, hydrotesting intervals *etc.*

Numerous laboratory investigations have been conducted on the subject of stress corrosion cracking. Hence numerous theories and models have been developed on the subject. A discussion has been published in identifying the merits and demerits of these models [9], yet there is no consensus on any model. Perhaps the fact that there is not a consensus on the mechanism responsible for the development of SCC nor is there a single mechanism that

explains all aspects of SCC, significantly undermines the development of an all-encompassing predictive model. Indeed it is very unlikely that a single model will ever fully explain all there is to know about SCC as there are probably a few mechanisms simultaneously involved in the development of the phenomenon. Some of the more popular proposed SCC mechanisms/models are presented in the next section.

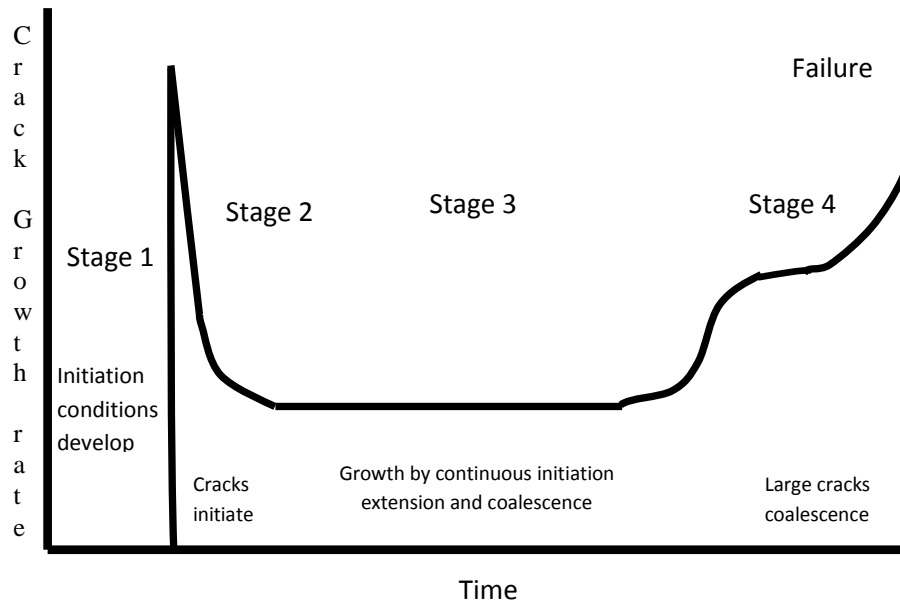


Figure 2.16: Stages of NNPSCC crack propagation [46]

2.9.1 Dissolution controlled model

Initial attempts to model corrosion induced crack growth related growth rates to the dissolution current density. It was found that for systems that display dissolution controlled environment sensitive cracking, the magnitude of crack growth showed a very reasonable correlation with the measured dissolution current density [162]. This led to a crack growth model given as [28]:

$$\frac{da}{dt} = i_a \cdot \frac{M}{zFd} \dots\dots\dots (2.10)$$

where da/dt is the crack velocity, i_a is the anodic current density, M is the atomic weight of the metal, z is the valency of the solvated species and F is the Faraday's constant.

Although it is conceivable that anodic dissolution plays some role in the development of NNPHSCC [91, 163], several laboratory data could not be correlated with this model. Parkins [91, 162] observed that crack growth rates were much higher than predicted by the anodic dissolution mechanism. The data used to generate the above model are typically obtained on pre-cracked specimens loaded above K_{ISCC} or from slow strain rate tests involving very high stresses and strain rates [162]. Such high strains and stresses are not observed in service conditions, except in the later stages of stress corrosion crack growth, and the earlier stages of growth may involve appreciably lower crack growth rates than those predicted by the above equation. Parkins [162] also reported that the crack growth rate reduces markedly with increasing test time under monotonic stress conditions. So this model has very poor correlation with both static and cyclic loading situations.

It was later explained that dissolution controlled model only holds for as long as the crack tip remains bare and un-filmed. This is only likely under severe straining conditions. If a film forms at the crack tip, dissolution ceases, and dissolution rate remains zero until film rupture occurs and reactivates dissolution. Hence, the average stress corrosion rate depends on the processes of metal dissolution, film formation and film rupture. This explanation is the general form of what is now known as the film rupture model. The film rupture model, also known as the slip-dissolution model, proposes that SCC progress by the opening up of the crack by the applied stress and the stress-induced rupture of the protective film formed in aggressive environments. The exposed surface then dissolves leading to crack growth. This mechanism was first postulated by Champion [164] and Logan [165] who proposed that localized plastic deformation at the crack tip could rupture the passivating film.

Although this model is fairly popular, there is no consensus on the manner in which dissolution occurs. Some researchers believe that once the film is ruptured and crack propagation starts, continuous crack growth occurs because the rate of film rupture far exceeds the rate of crack tip passivation. Others believe that it is necessary for the film to be reformed and grow to a sufficient thickness before rupture is repeated. Hence in their estimation, the crack tip must repassivate completely and rupture is only cyclical or discontinuous.

It must be mentioned that there is ample evidence to suggest that SCC propagation can be discontinuous. Among these evidences are the facts that crack arrest markings and discontinuous cracking have been observed in various media. NNPHSCC is often crystallographically orientated, fracture surfaces are flat and opposing faces match precisely suggesting very little crack tip dissolution during crack propagation. Thus, even though the film rupture mechanism is

widely accepted among SCC researchers, most researchers only agree that the mechanism is only viable for high pH SCC but not for NNPHSCC.

There have been lots of other models developed in the dissolution model category. Among these are the preferential crack tip dissolution model, which attributes SCC propagation to the presence of active paths in the material; crack tip stresses, and chemical-mechanical interactions [131, 166, 167]. As it currently stands, only the film rupture model has gained any significant acceptance and all but the film rupture model have been eliminated.

There have been some attempts to modify the dissolution mechanism in modern times to make it applicable to NNPHSCC. For instance, there have been various attempts to couple film rupture with the hydrogen enhancement of film rupture and dissolution, in order to account for the usually observed disparity between actual growth rates and those proposed by the film rupture model. Parkins *et al.* [8] showed that SCC crack propagation involved both hydrogen ingress into steel and anodic dissolution and suggested that hydrogen enhances crack growth (film rupture) by reducing alloy ductility. Mao and Li [168] suggested there is a synergy between hydrogen and stress effect on anodic dissolution of the crack tip during SCC propagation. Cheng *et al.* [169] suggested that the dissolution mechanism could predict SCC propagation rate if the effect of hydrogen on anodic dissolution in the absence of stress, the effect of stress on anodic dissolution in the absence of hydrogen and the synergistic effect of hydrogen and stress on anodic dissolution rate at the crack tip could be separately determined. However, Lu *et al.* [170] recently concluded that the synergistic effect due to hydrogen and local stress field is negligible and anodic dissolution must be contributing to SCC through other mechanisms yet to be satisfactorily explained. This insignificance of the synergism between anodic dissolution and

applied stress is in agreement with previous findings by Qiao *et al.* [171, 172] and Lu *et al.* [173].

2.9.2 Crack tip strain rate model

The film rupture model assumes that under cyclic loading, plastic strain accumulation at the crack tip can rupture the protective film causing crack advancement by a dissolution mechanism till the protective film is formed again. Increased strain at the crack tip increases the anodic dissolution rate and also increases the ingress of hydrogen into the metal. The crack tip strain rate model attempts to relate the crack propagation rate to the periodicity of slip-induced film rupture [174]. This model is widely accepted and is recognized as valid for both types of SCC [174-179].

It has been suggested that the crack tip strain rate is not a measurable parameter [174, 180] as the strain of interest is very local to the crack tip where stress amplification occurs [181]. Hence modeling the crack tip strain rate is assumed to be out of the question, and fundamentally derived crack tip strain rate equations have to be developed. Many attempts have been made at deriving such equations and some of these are discussed next.

Beavers [177] proposed that a critical strain rate is required at the crack tip to cause crack growth. He used the relationship between the crack tip opening displacement (CTOD) and crack growth driving force parameter (J_{IC}) in small yielding situation (which neglects the plastic component of J). Considering the relationship between K_{max} , ΔK and R , ($\Delta K = K_{max} (1-R)$) a model of the following form was proposed:

$$\dot{\epsilon} = 4f(1 - R) \dots\dots\dots (2.11)$$

This model predicts a zero strain rate with static loads ($f=0$ and $R=1$), a fact that correctly predicts that cyclic loading is necessary for crack growth. However, given that the plastic component of J was ignored and analysis only assumed small scale yielding which does not reflect the main role of plasticity in near-neutral pH cracking of pipeline steels, this model might not be useful for crack growth behavior predictions in near-neutral pH environment.

There have been several attempts at incorporating plasticity into the crack tip strain rate model. Rice *et al.* [182], using finite element methods, evaluated crack opening displacement rate near the crack tip for a steady growing crack under plane strain, small-scale yielding conditions in elastic-perfect plastic materials (no strain-hardening) and proposed that:

$$\dot{\delta} = \frac{\alpha \dot{J}}{\sigma_y} + \beta \left(\frac{\sigma_y}{E}\right) \dot{a} \ln\left(\frac{R}{x}\right) \dots\dots\dots (2.12)$$

where $\dot{\delta}$ is the crack tip opening displacement rate, \dot{J} is the rate of change of the J-integral with time, \dot{a} is the crack growth rate, σ_y is the yield strength, E is the Young's modulus, x is the distance from the growing crack tip for evaluation of the crack opening displacement rate, and β, α and R are constants. Equation 2.12 was converted to an approximate expression of the crack tip strain rate by making relevant assumptions for parameter r , into:

$$\dot{\epsilon}_{ct} = \dot{\delta}/x \dots\dots\dots (2.13)$$

This approximation can only give an evaluation based on crack tip opening displacement rate but cannot correlate environmentally assisted cracking quantitatively [178] and cannot be applied to work hardening materials. Shoji *et al.* [183] and Suzuki *et al.* [184] modified a previous work by Gao and Hwang [185] in order to include the effect of work hardening and proposed that:

$$\dot{\epsilon}_{ct} = \frac{\beta \sigma_y n}{E(n-1)} \left(2 \frac{\dot{K}}{K} + \frac{\dot{a}}{r_o} \right) \left\{ \ln \left[\frac{\lambda}{r_o} \left(\frac{K}{\sigma_y} \right)^2 \right] \right\}^{\frac{1}{n}-1} \dots\dots\dots (2.14)$$

Where \dot{a} is the crack propagation rate, \dot{K} the rate of change of K, r_o is the characteristic distance at the crack tip where strain rate should be defined. However, this equation fails to account for the possible effect of creep on the crack tip strain rate and the determination of r_o is necessary but not easy.

Parkins and Beavers [57] and Been and Sutherby [186] applied the above equation to their experimental data and found that there is a linear relationship between the crack propagation rate and crack tip strain rate. Been and Sutherby [186] compared their data with Parkins and Beavers' and found that the crack tip strain rate could be related to frequency and that the crack tip experiences lower strain rates at lower frequencies and crack propagation rates decrease accordingly. One major setback of this model however, is that it yielded a rather poor correlation with field data for NNPHSCC.

Other researchers have attempted a composite dissolution-strain-rate model. Ford and Andersen [187] proposed that:

$$\dot{a} = \frac{M}{z\rho F} \frac{i_o(t_o)^m}{(1-m)(\epsilon_f)^m} (\dot{\epsilon}_{ct})^m \dots\dots\dots (2.15)$$

where t_o is the duration of constant current density i_o , ϵ_f the strain to fracture of the oxide film, m is the slope of the current decay curve (the repassivation rate) and $\dot{\epsilon}_{ct}$ is the crack tip strain rate which accounts for the mechanical contributions.

Peng *et al.* [181] modified the above equation and proposed:

$$\dot{a} = \frac{M}{z\rho F} \frac{i_o(t_o)^m}{(1-m)(\varepsilon_f)^m} \left[\frac{\beta\sigma_y n}{E(n-1)} \left(2 \frac{\dot{K}}{K} + \frac{\dot{a}}{r_o} \right) \left\{ \ln \left[\frac{\lambda}{r_o} \left(\frac{K}{\sigma_y} \right)^2 \right] \right\}^{\frac{1}{n}-1} \right]^m \dots\dots\dots (2.16)$$

However, the estimation of the characteristic distance is a difficult issue in this model too. Even with the best estimate of the critical distance, only a marginal correlation is found with laboratory results and there was no attempt to validate the model with field data. Also there is really no clear evidence that the crack propagation rate is related to the characteristic distance.

In a very broad review of the strain rate model, Chen and Sutherby [9] concluded that the crack tip strain rate model generally yields rather poor correlations with field observations of NNPSCC.

2.9.3 Superposition model

This model assumes that fatigue and SCC are separate processes whose influences add up to the observed rate of SCC crack growth [92]. It was first introduced by Wei and Landes who modeled the growth of cracks undergoing cyclic loading in an aggressive environment as distinctly separate factors – fatigue crack growth (mechanical factor) aided by the environment.

This relationship is usually expressed in the form [188-190]:

$$\left(\frac{da}{dN} \right)_{total} = \left(\frac{da}{dN} \right)_{fatigue} + \frac{1}{f} \left(\frac{da}{dt} \right)_{SCC} \dots\dots\dots (2.17)$$

where a is the crack size, N is the number of cycles, t is time, and f is the frequency of the cyclic loading (cycles/sec). In the above equation, (da/dN)_{total} is the total crack growth rate (mm/cycle),

$(da/dN)_{\text{fatigue}}$ is the cyclic growth rate in air (mm/year), and $(da/dt)_{\text{SCC}}$ is the stress corrosion crack growth rate (mm/s) at **constant load**. Applying this model to NNPHSCC in pipeline steels initially seemed natural, since most of the initial NNPHSCC ravaged pipelines were operated under very mild pressure fluctuations. However, it has been observed that the model is not inherently representative of the NNPHSCC process. Crack growth on pipeline steels exposed to near neutral pH environment has never been observed under monotonic loading [9]. Even if a NNPHSCC crack is initiated under monotonic loading or mild mechanical cycling conditions, the crack soon becomes dormant. This in fact coincides with the fact that the majority of cracks found on high pressure gas pipelines are usually in a dormant state. It has also been pointed out that the contribution of the SCC term in the superposition model is negligible, leaving only the fatigue term. In fact, the crack growth rate in the original superposition model was found to fit an equation of the form [190]

$$(da/dN)_{\text{fatigue}} = C (\Delta K)^m \dots\dots\dots (2.18)$$

which is the familiar Paris law. Chen and Sutherby [9] argued that this equation does not fit their reported NNPHSCC data, and could not be expected to fit such data since it does not include the effect of loading frequency and maximum stress intensity factor. Many researchers have compared their crack growth results with this model. Experimental crack growth data obtained by Plumtree *et al.*, Zhang *et al.*, and Beavers and Jaske could not be fitted to superposition model while the general trend was consistent with the model in some cases [9, 191, 192, 20]. Beavers and Jaske [193] proposed a modified version of the superposition model by replacing the fatigue crack propagation term with a corrosion fatigue term and reported an improved fit to their

experimental data. Others have introduced the stress shielding and crack coalescence effect and have been able to produce a simplified prediction of crack colony behavior [188-190].

A major shortcoming of this model is that it assumes the SCC component of crack advancement is a time-constant value over several years. Using this model for crack growth predictions generally leads to an underestimation of the crack growth rate in near-neutral pH environment. An appropriate growth model should represent the synergistic interaction between environmental factor and mechanical (loading) factor. The above model evidently does not represent such an interaction.

2.9.4 Corrosion fatigue model

Environmentally enhanced cracking can generally be classified into four groups: true stress corrosion cracking, true corrosion fatigue, combination of normal fatigue and SCC and a synergy of the latter two [9]. Pure SCC refers to crack propagation in corrosive environment but under exclusively static loading. Stress corrosion cracking of oil and gas pipelines definitely does not fit this category as the typical gas pipeline experiences a few tens of cycles per year while a typical oil line experiences a few thousand cycles annually. True corrosion fatigue involves corrosive environment-enhanced crack propagation with growth rates similar to those observed in regular fatigue situations. Considering the fact that the growth of SCC cracks in near neutral pH environments involve a synergistic influence of fatigue and corrosion cracking, it seems NNPHSCC belongs in the true corrosion fatigue category and a corrosion fatigue model should be better suited to the modeling of NNPHSCC crack growth rates.

Been *et al.* [191] observed that crack propagation in near-neutral pH environment, crack propagation was higher at lower frequencies and suggested that a corrosion fatigue mechanism is

probably more suited to NNPHSCC. Chen and Sutherby [9] conducted several tests using a pipeline material (X65) in two different simulated near-neutral pH soil solutions, and carried out a pure fatigue analysis on the results and observed that the crack propagation rate could not be account for by ΔK alone as tests carried out at the same ΔK but different K_{max} showed increased growth rate with increasing K_{max} . Also the rate of crack propagation was found to decrease sharply with increasing ΔK in one medium. They concluded that crack propagation rates in near neutral pH environment cannot be characterized by either ΔK or K_{max} alone. They also applied the crack tip strain rate model to their result but could not obtain a good fit. This conclusion is in agreement with that reached by Vasudevan *et al.* [194], who found that both ΔK and K_{max} control the growth of fatigue cracks. They concluded ΔK and K_{max} embody two thresholds that are intrinsic to fatigue crack propagation. K_{max} , they suggested, is a primary driving force needed to quantify crack advancement, while ΔK accounts for the cyclic loading effect. They concluded that there could not be any data correlation to either of these parameters individually as either of them provides an incomplete description of the cracking process.

Based on these conclusions, Chen and Sutherby used a serendipity approach to obtain a true corrosion fatigue model that accounts for the combined effect of K_{max} , ΔK and loading frequency on the crack propagation rate and obtained a good fit with minimal scatter with

$$\left(\frac{da}{dN} \right) \propto (\Delta K)^2 K_{max} / f^\alpha \dots\dots\dots (2.19)$$

where ΔK is the change in stress intensity at the crack tip due to cyclic loading, K_{max} is the maximum stress intensity at the crack tip, and α is a factor that represents the influence of the corrosion environment on the crack growth rate. This relationship consists of two parts,

$(\Delta K)^2 K_{\max}$ and $1/f^\alpha$. The first term, $(\Delta K)^2 K_{\max}$ accounts for the fatigue contribution to crack propagation in agreement with the Paris law while the second factor $1/f^\alpha$ accounts for crack propagation enhancement by the aggressive environment. In addition to giving a much better fit to experimental data than exists hitherto, this model was able to demarcate between the active growth region and the threshold region below which no crack propagation will occur.

Despite the reported success of Chen and Sutherby's model [9], it cannot be described as being all encompassing in its ability to model field observations of NNPHSS. Some factors in the model, ΔK and K_{\max} , are strongly dependent on the geometry of the specimen, while α is dependent on the severity of the corrosion environment. Therefore, the validity of this model needs to be determined using other crack geometries. Also, the appropriate values of α for different environmental conditions need to be determined. With regards to pipelines, when one considers the fact that the data used to generate the model above were obtained using a compact tension specimen which does not adequately represent NNPHSCC cracking in the field as discussed in the next section one realizes that a re-validation of this model must be carried out.

2.10 Fatigue Cracking details

As mentioned earlier, cyclic loading can cause material failure at stresses lower than the nominal yield strength of the material. This failure is often preceded by the formation of cracks which advance under stress reversal until rupture occurs. But one may ask, how exactly does crack initiation occur? Hunter and Fricke [195-198] carefully studied the progressive nature of fatigue damage and found that slip occurred very early in the fatigue life. The amount of slip increases in intensity with increasing number of cycles until a saturation level is reached at which point cracks are initiated. Forsyth [199-201] proposed that crack initiation and crack

propagation develops in two stages, stage I and stage II, as follows. Due to cyclic loading, intrusions and extrusions form in the slip bands of a material. These features act as microscopic notches and provide sites for crack initiation. In stage I, cracks develop as a result of dislocation motion along slip planes. Hence, cracks tend to show a preferential orientation along the slip system with the maximum shear stress since they form on closely aligned planes. These cracks continue to grow along the slip plane but at this stage they are so short, only a few grain diameters in length that the fracture faces are featureless. In stage II, cracks grow on planes which are normal to the principal tensile stress and the fracture faces display fatigue striations. The formation of microcracks can be accentuated by favourable crack initiation sites like second phases and grain boundaries or at the root of notches where a triaxial state of stress exists.

Most models and fatigue relationships were generated from test pieces containing macroscopically long cracks, often in excess of 20mm. However, most defects in engineering materials, including pipelines, are often shorter than this. As pointed out above, cracks progress from very tiny microscopic features into long macroscopic ones. Hence, (especially) for small structures or those that fail from features that are short in comparison to the overall structural dimensions, it is important to model cracks using short crack sizes that are more comparable to those found in real life.

In characterizing the crack tip for analyzing crack propagation, using K_I or J-integral, the concept of similitude is assumed to be valid. This implies that for cracks of different sizes subjected to the same stress intensity in the same material (microstructure) and environment, crack tip plastic zone sizes are equal and the stress and strain distributions along the borders of

these zones (ahead of the crack tip) are identical [202]. There will however be a deviation from the similitude concept when [119, 202]

1. crack size are on the local microstructural scale
2. crack size is comparable to the extent of local plasticity for non-stationary flaws
3. through-thickness out of plane stress is different
4. crack propagation mechanisms are different
5. extensive fatigue crack closure occurs
6. external environment significantly influences crack growth

Most of these reasons for the exclusion of the similitude principle apply to short cracks. Short cracks are cracks that are

1. on the order of the grain size
2. of length comparable to the size of the plastic zone ahead of the crack tip
3. physically small ($\leq 0.5-1$ mm) in length

This is because the above factors influence significantly the crack driving force, K_I , near the crack tip and it is the near tip parameter that determines crack propagation behavior not the global value of the driving force. It has been shown that physically short cracks, i.e. cracks that are only long in terms of continuum mechanics and LEFM analyses, also propagate at a higher rate than long cracks under the same stress intensity [202].

In order to better understand the uniqueness of short cracks it is necessary to separate the unique behavior of small cracks into two categories:

1. threshold stress intensity considerations including the relationship between the smooth bar endurance limit, $\Delta\sigma_e$ and the threshold stress intensity for fatigue crack growth, ΔK_{th}
2. comparison of the kinetics of small crack growth to kinetics of large crack growth.

The application of fracture mechanics to fatigue has resulted in the definition of threshold below which no further crack propagation occurs, ΔK_{th} . For a given stress and frequency in a particular environment, ΔK_{th} is a material property and it follows that as crack sizes become exceedingly small, the allowable stress range should be exceedingly high. However the limiting case where the crack approaches zero length, is the smooth bar endurance limit which is approximately half the tensile strength of the material. For practical purposes, ΔK_{th} is defined as the stress intensity value below which crack propagation rate is $\leq 10^{-10}$ m/cycle [195]. From normal fracture mechanics considerations the threshold stress intensity is defined as

$$\Delta K_{th} = \Delta\sigma_{th} \sqrt{\pi a} \cdot f\left(\frac{a}{w}\right) \dots \dots \dots (2.20)$$

Kitagawa *et al.* [203, 204] analyzed crack growth data for specimens of three different steels containing small surface type flaws and found that all three steels show the same relationship between $\Delta\sigma_{th}$ and crack length, corresponding to the same ΔK_{th} as specimens containing long through-thickness cracks (Figure 2.17a). However, $\Delta\sigma_{th}$ decreases asymptotically with decreasing crack length as the smooth bar endurance limit is approached indicating that ΔK_{th} decreases with decreasing crack sizes. This indicates that small cracks can propagate at ΔK values below those defined by the conventional ΔK_{th} for large cracks.

El-Hadad *et al.* [205, 206] observed that the threshold behavior for small cracks could be more accurately modeled (Figure 2.18) by modifying the stress intensity equation as follows:

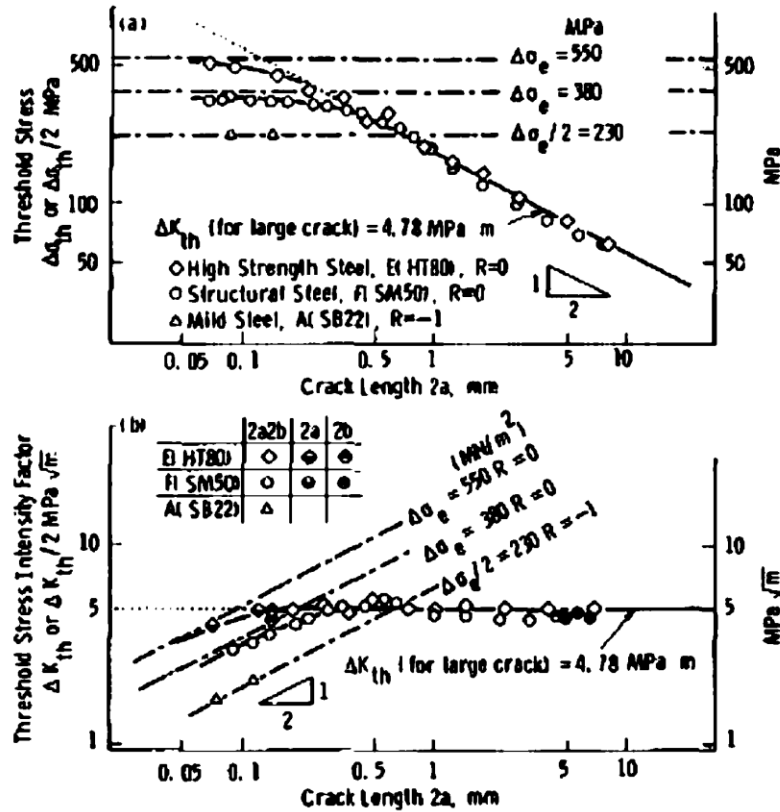


Figure 2.17: Dependence of fatigue (a) threshold stress (b) threshold stress intensity on crack length [203]

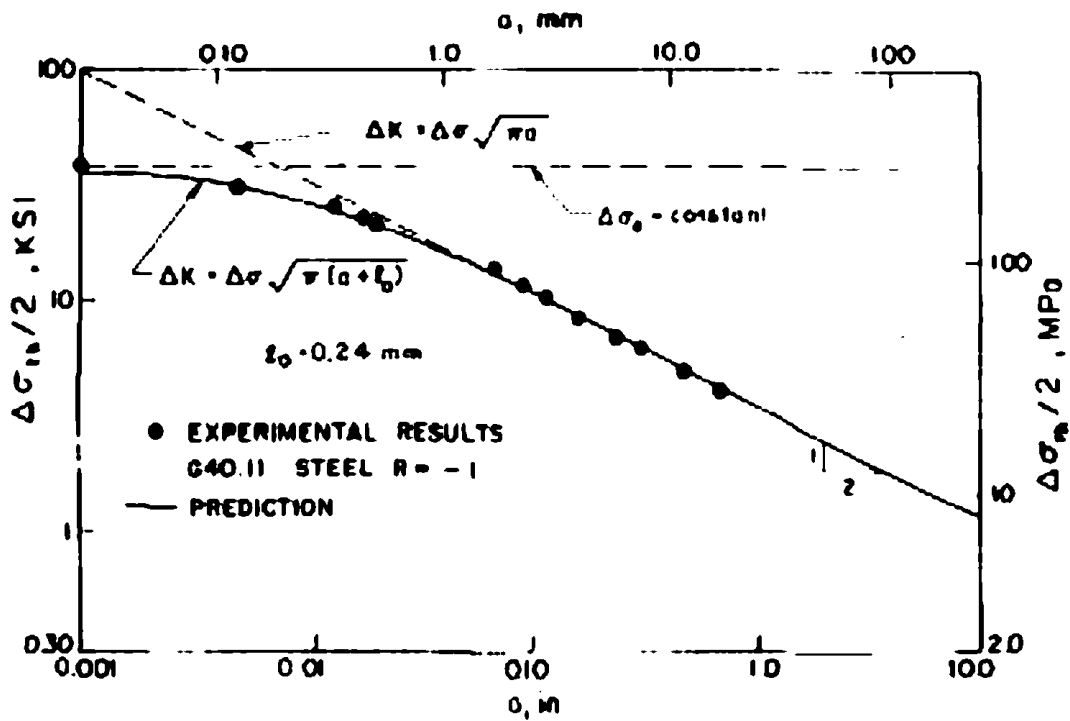


Figure 2.18: Comparison of experimental and predicted value of fatigue threshold [203]

$$\Delta K = \Delta\sigma\sqrt{\pi(a + l_o)} \cdot f\left(\frac{a}{w}\right) \dots\dots\dots (2.21)$$

Where the term $(a+l_o)$ is a so called effective crack length which accounts for the small crack behavior. l_o was suggested to be a constant for a given material and can be calculated by substituting the endurance limit range for the stress range in the above

$$l_o = \frac{1}{\pi} \left(\frac{\Delta K_{th}}{\Delta\sigma_e} \right)^2 \dots\dots\dots (2.22)$$

It is obvious that as a increases, l_o makes a more significant contribution to stress intensity and as crack size approaches zero, l_o provides a finite value for ΔK .

Examination of the results reported by several studies shows that the growth rate of short cracks could be up to two orders of magnitude higher than that of long cracks. Another main feature of short crack growth is the fact that the initially high growth rate of short cracks decelerates progressively and may arrest in some cases, and eventually merges with that of long cracks as depicted in Figure 2.19. This tendency of short cracks to show decreasing growth rates towards the long crack growth threshold has been attributed to crack closure and crack interaction with microstructural features especially grain boundaries [202].

2.10 Crack closure

Crack closure refers to a reduction in the effective stress intensity range at the crack tip during cyclic loading as a result of contact of crack surfaces during the unloading process at positive values of externally applied stress. This phenomenon can reduce the rate of crack propagation during cyclic loading by reducing the driving force for crack propagation at the crack tip.

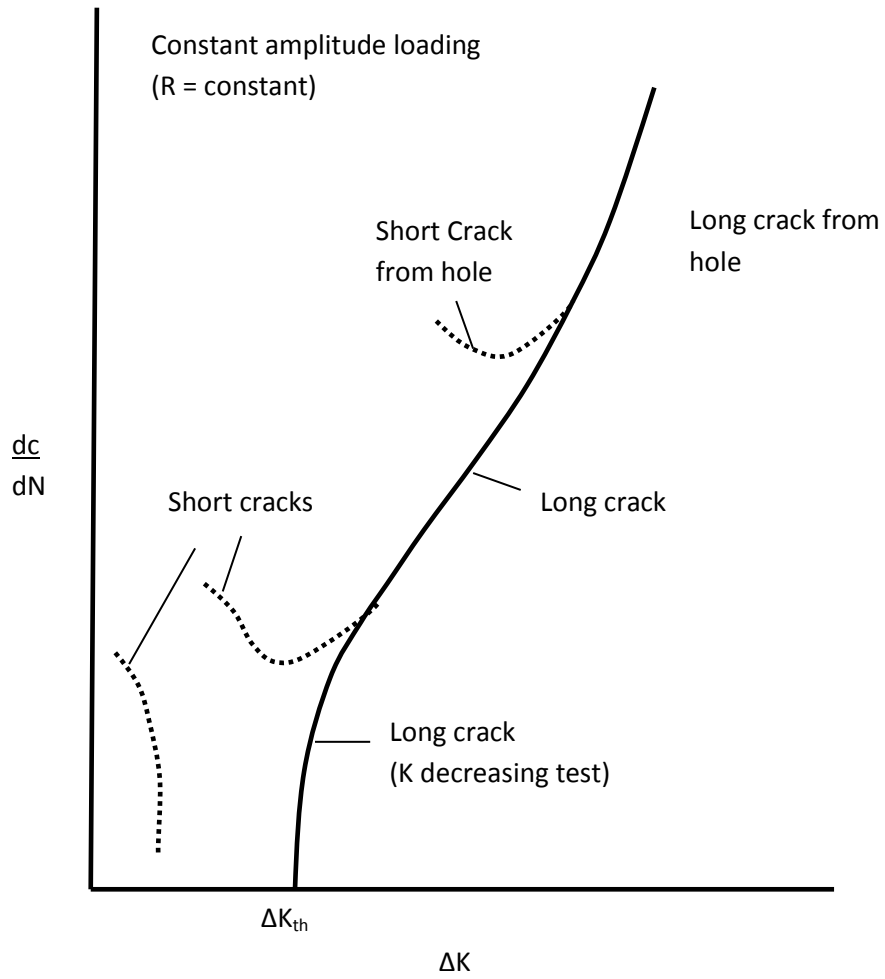
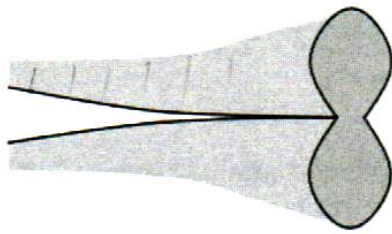


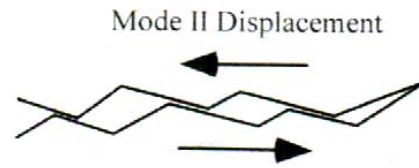
Figure 2.19: Illustration of short crack growth deceleration [202]

Several reasons have been suggested for the crack closure effect. Among them are (Figure 2.20):

1. **Plasticity-induced closure:** As a crack grows a plastic zone forms ahead of the crack, where the material has already been locally deformed. When the crack advances, the material that had previously been permanently deformed forms an envelope of plastic zones in the wake of the crack front. When the restraint is relieved, there is a displacement normal to the crack surfaces. This usually poses no problems as long as the crack is fully open. However, during cyclic unloading, the crack surfaces touch before the minimum load in the waveform is reached. This effect shields the crack from experiencing the effect of the remaining portion of the cyclic unloading. Rather than the crack tip experiencing a tensile stress after crack face contact, compressive stresses are developed in the crack wake during the lower part of the cycle. James and Knott [207] grew a fatigue crack in a standard specimen and then removed a small amount of material from the crack faces up to 0.5mm from the crack tip. When they placed the sample back in the test machine, they observed the crack growth rate increased by an order of magnitude compared to the previous measurement, confirming the role played by the size of the plastic wake behind the advancing crack front.
2. **Oxide induced closure:** The crack closure effect may be generated by the presence of corrosion products in the crack crevice. When oxides or corrosion products are trapped between the crack faces, they can form localized wedges bring the opposite faces into contact at more positive stresses during cyclic unloading. If this occurs to a significant extent, the crack tip may not experience the full stress range being applied and this can slow down crack advance.



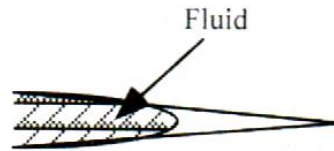
(a)



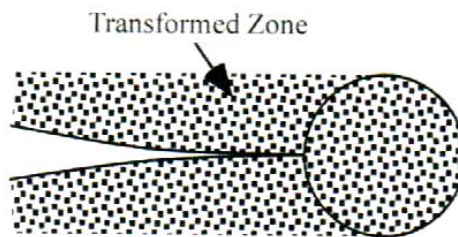
(b)



(c)



(d)



(e)

Figure 2.20: Crack closure mechanisms [208]

3. **Asperity induced closure:** for ductile materials, the crack path is often quite irregular and high points on the fracture surfaces may interlock during unloading, producing the same effect as above. On a global scale, most fatigue cracks propagate in mode I loading. However, because of crack interaction with microstructural features, there could be local crack deflections. This often leads to mixed mode crack propagation. When a crack deviates from its mode I symmetry path, it may experience mode II displacements, which may cause contact between the upper and lower crack faces at a positive load. This can be more severe in coarse grained materials.

This phenomenon has led to the development of the effective stress-intensity range concept. Assuming a cracked specimen is cyclically loaded to stress levels corresponding to K_{max} and K_{min} and that the crack faces come into contact at a positive stress intensity factor (also the stress intensity at which the crack opens on the loading cycle), K_{op} , stresses below K_{op} do not contribute to crack propagation and the effective stress intensity range is defined as

$$\Delta K_{eff} \equiv K_{max} - K_{op} \dots\dots\dots (2.23)$$

Elber [209], who was first to propose the closure concept, proposed a modified Paris-Erdogan equation as

$$\frac{da}{dN} = C \Delta K_{eff}^m \dots\dots\dots (2.24)$$

2.11 SCC in near-neutral pH environment and current models – A discussion

Generally, for the purpose of modelling, engineering cracks can be divided into two categories: long cracks and short/shallow cracks (short in the direction of propagation). Short cracks are further divided into microstructurally short cracks and mechanically short cracks. The former is usually less than 100 μm ; its growth is usually microstructure dependent, and is not governed by rules of fracture mechanics. Mechanically short/small/shallow cracks are usually around 1 mm long, but size may be subject to other factors. The laws of fracture mechanics can be applied to analyze the growth of mechanically short/small/shallow cracks. The distinguishing features of these different kinds of are summarized in Figure 2.21 while the evolution of a typical NNPHSCC is schematically depicted in Figure 2.22.

NNPHSCC cracks are usually initiated from corrosion induced defects such as pits generated from localized dissolution or pits resulting from the removal of inclusions and/or precipitates from solid solution. A NNPHSCC crack spends a very small fraction of its lifetime, shortly after crack initiation, as a microstructurally short crack. The exact amount of time spent in this category can be expected to be strongly influenced by coating type, microstructures, millscapes, and residual stress levels. The crack then progresses with further growth into the mechanically short crack category and remains mechanically short for a significant portion of its lifetime. Growth rate in this region is primarily determined by pipeline operation conditions and residual stresses. This stage is usually the focus of integrity management programs. The cracks eventually morph into long type cracks, typically with very high growth rates that ultimately lead to leakage or failure in a very short time.

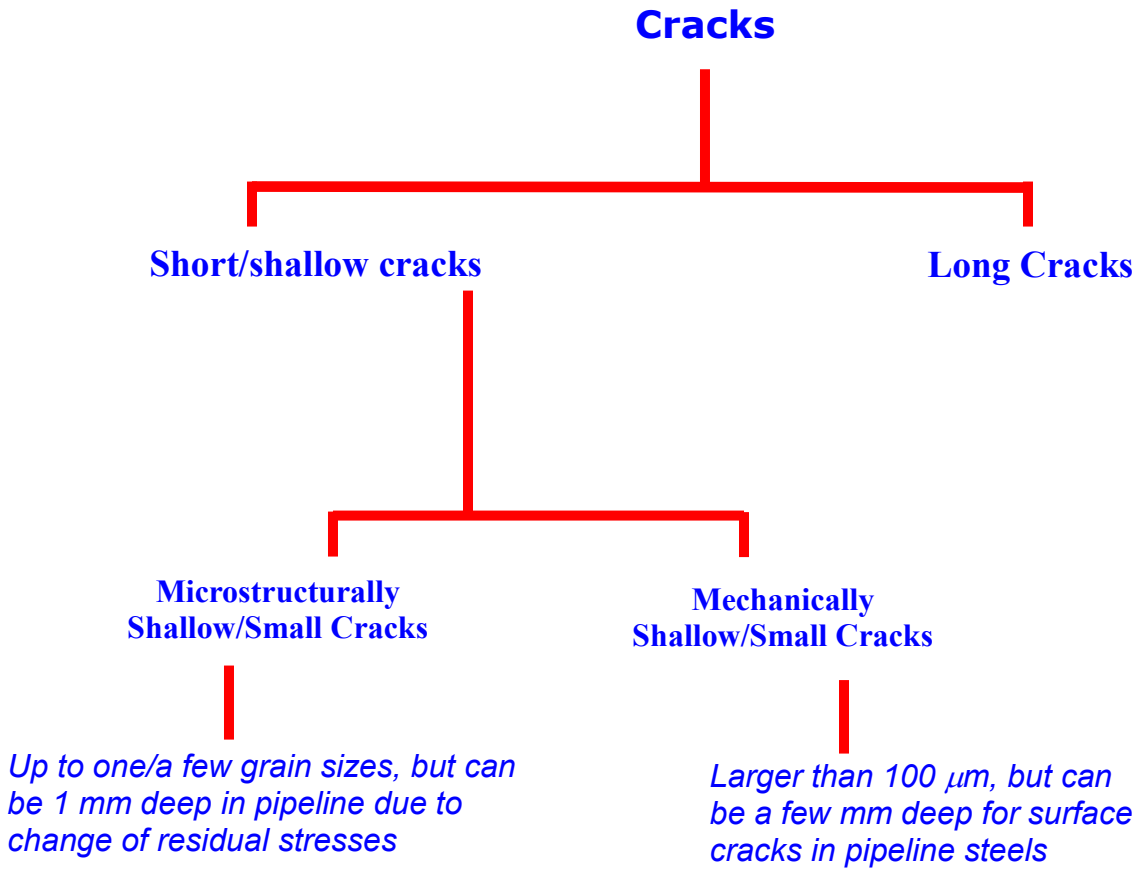


Figure 2.21: Classification of cracks

NNPH CRACK GROWTH BEHAVIOR

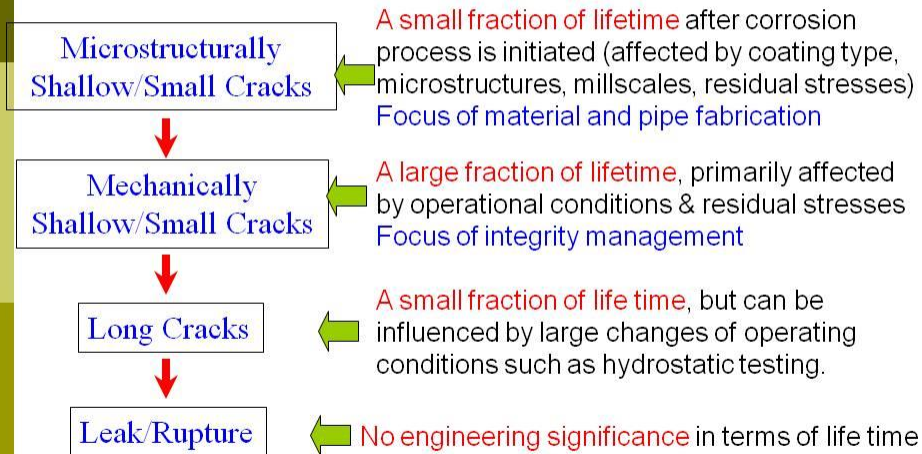


Figure 2.22: Progression of a typical NNPHSCC crack

The main shortcoming of existing models is their tendency to underestimate the growth rate of SCC cracks in near neutral pH environments. To understand the reason behind this, a recourse to some fundamental issues in fracture mechanics is relevant. It is important to recall that most of the common forms of the various expressions of linear elastic fracture mechanics were developed for through-thickness cracks which are more familiar in engineering structures. As discussed earlier, corrections must be applied to these expressions when applied to other crack geometries. However, most of the currently available models were generated with specimens that feature long through-thickness cracks even though a cursory look at NNPHSCC crack images reveals that they are typically “short” surface cracks over much of their lifetime. This perhaps is one of the reasons responsible for the usually poor correlation of these models to field data on NNPHSCC. Existing models also have the shortcoming of assuming that the rate of crack propagation in pipelines is constant and independent of pipeline operating conditions. This is evidently too simplistic.

From the above discussion, it is evident that the challenge of modeling the growth rates of NNPHSCC cracks reduces to that of modeling mechanically short cracks. Hence, if more accurate models are to be developed, such models will have to focus on developing sample geometry and testing conditions that enable a study of the growth rate of mechanically short cracks in a near-neutral pH environment. This is the approach that will be adopted in this study.

2.12 Objective

Chen and Sutherby [9] recently developed a corrosion fatigue model that provided much better fit to NNPHSCC crack growth data than those that previously existed. However, this model needs to be validated with crack growth data obtained with crack geometries, surface cracks, that are more representative of field NNPHSCC. Therefore, the objectives of this research are to *conduct a series of studies aimed at determining empirical growth rates for typical pipeline steel, and to use the result of these studies to validate Chen and Sutherby's model. Particularly, this study will provide better understanding of ways to improve the corrosion fatigue model developed by Chen and Sutherby using short surface type flaws. These studies will also enhance current understanding of the nature of SCC crack growth in near-neutral pH environments as well as the mechanisms involved in NNPHSCC crack growth.*

References

- [1] Jones, D.A., 1992, "Principles and prevention of corrosion," Maxwell Macmillan Canada, Toronto, pp. 568.
- [2] Chatterjee, U.K., Bose, S.K., and Roy, S.k., 2001, "Environmental degradation of metals," Marcel Dekker, Inc., New York, pp. 498.
- [3] Fontana, M.G., 1986, "Corrosion Engineering," McGraw-Hill Book Company, New York, pp. 556.
- [4] National Energy Board, 1996, "Public Enquiry Concerning Stress Corrosion Cracking on Canadian Oil and Gas Pipelines," report #MH-2-95.
- [5] Brown, B.F., 1972, Naval Research Laboratory, U.S. Gov't Printing Office, Washington, pp. 2.
- [6] Kruger, J., 1980, "Stress Corrosion Cracking," Freund Publishing House, Israel, pp. 5-37.
- [7] Justice, J. T., and Mackenzie, J. D., 1988, "Progress in the control of stress corrosion cracking in a 914mm O.D. gas transmission pipeline," NG-18/EPRG Seventh biennial joint technical meeting on line pipe research, pipeline research committee of the American Gas Association, pp. Paper No. 28.
- [8] Parkins, R. N., Blanchard, W. K. J., and Delanty, B. S., 1994, "Transgranular Stress Corrosion Cracking of High-Pressure Pipelines in Contact with Solutions of Near Neutral pH," Corrosion (USA), **50**(5) pp. 394-408.

- [9] Chen, W., and Sutherby, R. L., 2007, "Crack Growth Behavior of Pipeline Steel in Near-Neutral pH Soil Environments," *Metallurgical and Materials Transactions A*, **38A**(6) pp. 1260-1268.
- [10] Szklarska-Smialowska, Z., and Gust, J., 1979, "The Initiation of Stress Corrosion Cracks and Pits in Austenitic Cr-Ni Steel in MgCl₂ Solutions at 40-90 Deg C," *Corrosion Science*, **19**(11) pp. 753-766.
- [11] Brown, B. F., 1972, "A preface to the problem of stress corrosion cracking," *Stress Corrosion Cracking of Metals—A State of the Art*, American Society for Testing and Materials, Baltimore, pp. 8.
- [12] Beavers, J. A., and Harle, B. A., 2001, "Mechanisms of High-pH and Near-Neutral-pH SCC of Underground Pipelines," *Journal of Offshore Mechanics and Arctic Engineering*, **123**pp. 147-151.
- [13] Liu, R., Narita, N., Altstetter, C., 1980, "Studies of the Orientations of Fracture Surfaces Produced in Austenitic Stainless Steels by Stress Corrosion Cracking and Hydrogen Embrittlement," *Metall.Trans.A.*, **11A**(9) pp. 1563-1574.
- [14] Bulger, J. T., Lu, B. T., and Luo, J. L., 2006, "Microstructural Effect on Near-Neutral pH Stress Corrosion Cracking Resistance of Pipeline Steels," *Journal of Materials Science*, **41**(15) pp. 5001-5005.

[15] Chu, R., Chen, W., Wang, S. H., 2004, "Microstructure Dependence of Stress Corrosion Cracking Initiation in X-65 Pipeline Steel Exposed to a Near-Neutral pH Soil Environment," *Corrosion*, **60**(3) pp. 275-283.

[16] Chen, W., Wang, S., Chu, R., 2003, "Effect of Precyclic Loading on Stress-Corrosion-Cracking Initiation in an X-65 Pipeline Steel Exposed to Near-Neutral pH Soil Environment," *Metallurgical and Materials Transactions A. Physical Metallurgy and Materials Science*, **34A**(11) pp. 2601-2608.

[17] Torres-Islas, A., Gonzalez-Rodriguez, J. G., Uruchurtu, J., 2008, "Stress Corrosion Cracking Study of Microalloyed Pipeline Steels in Dilute NaHCO₃ Solutions," *Corrosion Science*, **50**(10) pp. 2831-2839.

[18] Kushida, T., Nose, K., Asahi, H., 2001, "Effects of metallurgical factors and test conditions on near neutral pH SCC of pipeline steels," *Corrosion 2001, NACE*, pp. Paper # 01213.

[19] King, F., 2010, ""Development of Guidelines for Identification of SCC Sites and Estimation of Re-inspection Intervals for SCC Direct Assessment". A report prepared for the US Department of Transportation Pipeline and Hazardous Materials Safety Administration and Pipeline Research Council International, Inc. by Integrity Corrosion Consulting Ltd." DTPH56-06-T-000013, .

[20] Fang, B., Han, E. H., Elboujdaini, M., 2006, "Stress-Corrosion Crack Initiation of High-Strength Pipeline Steel in Near-Neutral pH Environments," *International Journal of ISSI*, **3**(1) pp. 20-25.

[21] Asher, S. L., and Singh, P. M., 2009, "Role of Stress in Transgranular Stress Corrosion Cracking of Transmission Pipelines in Near-Neutral pH Environments," *Corrosion*, **65**(2) pp. 79-87.

[22] BOHNENKAMP, K., 1969, "PAPER FROM PROCEEDINGS OF CONFERENCE FUNDAMENTAL ASPECTS OF STRESS-CORROSION CRACKING," NACE, Houston, TX., pp. 374-383.

[23] BOHNENKAMP, K., 1968, "Stress Corrosion Cracking of Mild Steel in Concentrated Caustic Soda," *ARCH EISENHUTTENW*, **39**(5) pp. 361-368.

[24] Kowaka, M., and Kitamura, M., 1975, "Effect of Heat Treatment on Stress-Corrosion Cracking of Mild Steels, in Boiling Caustic Solution," *Journal of the Japan Institute of Metals*, **39**(4) pp. 381-387.

[25] Champion, F. A., 1957, *Chem. Ind.*, pp. 967.

[26] Atrens, A., Wang, J. Q., Stiller, K., 2006, "Atom Probe Field Ion Microscope Measurements of Carbon Segregation at an Alpha:Alpha Grain Boundary and Service Failures by Intergranular Stress Corrosion Cracking," *Corrosion Science*, **48**(1) pp. 79-92.

[27] Parkins, R. N., Slattery, P. W., and Poulson, B. S., 1981, "The Effects of Alloying Additions to Ferritic Steels upon Stress Corrosion Cracking Resistance," *Corrosion*, **37**(11) pp. 650-664.

[28] Parkins, R. N., 1980, "Predictive Approaches to Stress Corrosion Cracking Failure," *Corrosion Science*, **20**(2) pp. 147-166.

- [29] Flis, J., Dawson, J. L., Gill, J., 1991, "Impedance and Electrochemical Noise Measurements on Iron and Iron--Carbon Alloys in Hot Caustic Soda," *Corrosion Science*, **32**(8) pp. 877-892.
- [30] Flis, J., and Ziomek-Moroz, M., 2008, "Effect of Carbon on Stress Corrosion Cracking and Anodic Oxidation of Iron in NaOH Solutions," *Corrosion Science*., **50**(6) pp. 1726-1733.
- [31] Flis, J., Oranowska, H., and Szklarska-Smialowska, Z., 1990, "An Ellipsometric Study of Surface Films Grown on Iron and Iron--Carbon Alloys in 0.05M KOH," *Corros.Sci.*, **30**(11) pp. 1085-1099.
- [32] ABDUL, A. A. A., ANWAR, M. M., and SANAD, S. H., 1969, "Potentiokinetic Study of the Effect of C on Corrosion of some Steels in Alkaline Solutions," *CORROSION SCI.*, **9**(6) pp. 405-412.
- [33] Asher, S., and Singh, P. M., 2008, "Hydrogen Production and Permeation in Near-Neutral pH Environments," *Corrosion 2008, NACE*, pp. Paper No. 08411.
- [34] Jones, R.H., 2003, "Stress-corrosion cracking," *ASM International, Materials Park, OH*, pp. 346-366.
- [35] Harle, B. A., Beavers, J. A., and Jaske, E., 1995, "Mechanical and metallurgical effects on low-pH stress corrosion cracking of natural gas pipelines," *Corrosion '95, NACE*, pp. Paper #. 646.
- [36] Tsay, L. W., Lu, H. L., and Chen, C., 2008, "The Effect of Grain Size and Aging on Hydrogen Embrittlement of a Maraging Steel," *Corrosion Science*, **50**(9) pp. 2506-2511.

- [37] Grabke, H. J., Gehrmann, F., and Riecke, E., 2001, "Hydrogen in Microalloyed Steels," *Steel Research*, **72**(5-6) pp. 225-235.
- [38] Madrid, M., Chan, S. L. I., and Charles, J. A., 2000, "Effect of Grain Size and Second Phase Particles on the Occlusivity of Iron and Steels," *Material Research Innovations*, **3**pp. 263-270.
- [39] Dieter, G.E., 1988, "Mechanical Metallurgy," McGraw-Hill Book Company, pp. 186-187.
- [40] Madrid, M., Chan, S. L. I., and Charles, J. A., 1985, "Hydrogen Occlusivity and Embrittlement in Iron--Effect of Grain Structure and Cold Work," *Mater.Sci.Technol.*, **1**(6) pp. 454-460.
- [41] Li, X. C., Eadie, R. L., and Luo, J. L., 2008, "Influence of Plasticity on Corrosion and Stress Corrosion Cracking Behaviour in Near Neutral pH Environment," *Corrosion Engineering Science and Technology*, **43**(4) pp. 297-303.
- [42] Roy, G., Kiff, D., and Revie, R.W., 1993, "Residual stress in CANMET/industry SCC consortium Pipe Specimens," *Protected Business Information*, 93-33(TR), .
- [43] Beavers, J.A. and W.V. Harper. 2004. *Stress Corrosion Cracking Prediction Model*. NACE International CORROSION/2004. Paper 04189.
- [44] Beavers, J. A., Johnson, J. T., and Sutherby, R. L., 2000, "Materials factors influencing the initiation of Near-Neutral pH SCC on underground pipelines," *International Pipeline Conference*, ASME, New York, NY, **2**, pp. 979-988.

[45] Boven, G. V., Chen, W., and Rogge, R., 2007, "The Role of Residual Stress in Neutral pH Stress Corrosion Cracking of Pipeline Steels. Part I: Pitting and Cracking Occurrence," *Acta Materialia*, **55**(1) pp. 29-42.

[46] Beavers, J.A., 2005, "Stress Corrosion Cracking Study," Report submitted to Department of Transportation Research and Special Programs Administration, Office of Pipeline Safety by Michael Baker Jr., Inc., OPS TTO8, .

[47] Beavers, J. A., Thompson, N. G., and Coulson, K. E. W., 1993, "Effects of surface preparation and coatings on SCC susceptibility of line pipe: Phase 2 - Field studies," *Corrosion*/1993, pp. Paper number 93597.

[48] Institute of Gas Engineers, 1993, "Steel Pipelines for High Pressure Gas Transmission," pp. Edition 3.

[49] U.S. Department of Transportation, 1994, "Pipeline Safety Regulations," pp. CFR Parts 192 and 195.

[50] Zheng, W., Revie, R. W., Tyson, G. S., 1996, "Pipeline SCC in Near-Neutral pH Environment: Results of full-scale tests," *Corrosion '96*, NACE, pp. Paper # 253.

[51] M. Elboudjaini, YZ. Wang, RW. Revie, RN. Parkins, MT. Shehata, Stress Corrosion Crack Initiation Processes: Pitting and Microcrack Coalescence, In *Proceedings of Corrosion 2000*, Houston, Texas, USA, 2000.

- [52] Brongers, M. P. H., Beavers, J. A., Jaske, C. E., 2000, "Effect of Hydrostatic Testing on Ductile Tearing of X-65 Line Pipe Steel with Stress Corrosion Cracks," *Corrosion (USA)*, **56**(10) pp. 1050-1058.
- [53] Beavers, J. A., and Harle, B. A., 1996, "Mechanisms of High pH and Near-Neutral pH SCC of Underground Pipes," *International Pipeline Conference*, ASME, New York, **1**, pp. 555-564.
- [54] Beavers, J.A., 2004, "Near-Neutral pH SCC: Dormancy and re-initiation of stress corrosion cracks," Report for Gas Research Insitute, Report R1025-01R, Contract GRI-7045, .
- [55] Beavers, J.A., and Hagerdorn, E.L., 1996, "Low-pH SCC: Mechanical Effects on Crack Propagation," *Pipeline Research Council International*, Pipeline Research Committee Report R207-01, .
- [56] Beavers, J. A., and Hagerdorn, E. L., 1996, "Near-Neutral pH SCC: Mechanical effects on Crack Propagation," ninth Symposium on Pipeline Research, A.G.A. Cat no L51746 Paper 24.
- [57] Parkins, R. N., and Beavers, J. A., 2003, "Some Effects of Strain Rate on the Transgranular Stress Corrosion Cracking of Ferritic Steels in Dilute Near-Neutral-pH Solutions," *Corrosion*, **59**(3) pp. 258-273.
- [58] Fang, B., Han, E., Wang, J., 2006, "Hydrogen in Stress Corrosion Cracking of X-70 Pipeline Steels in Near-Neutral pH Solutions," *Journal of Materials Science*, **41**(6) pp. 1797-1803.
- [59] Rebak, R.B., Xia, Z., Safruddin, R. and Szklarska-Smialowska, Z., *Effect of Solution Composition and Electrochemical Potential*

on Stress Corrosion Cracking of X-52 Pipeline Steel. Corrosion, 1996. 52(5): p. 396.

[60] Office of Pipeline Safety, 2005, "Stress corrosion cracking study," TTO Number 8, Integrity Management Program, Moon Township, PA.

[61] Wang, Y. Z., Revie, R. W., and Parkins, R. N., 1999, "Mechanistic aspects of stress corrosion crack initiation and early propagation," Corrosion '99, NACE, NACE, pp. paper # 99143.

[62] Wilmott, M., and Sutherby, R. L., 1998, "The role of pressure and pressure fluctuations in the growth of stress corrosion cracks in linepipe steels," International Pipeline Conference, ASME, **1**, pp. 409-422.

[63] Meyer, M., and Pontremoli, M., 2001, "Comparing of laboratory behaviour of different pipeline steels regarding their near-neutral pH SCC susceptibility," 13th Bienial PRCI-EPRG Joint Technical Meeting on Linepipe Research.

[64] Sutherby, R., Jack, T., VanBoven, G., 2000, "CEPA study on characterization of pipeline pressure fluctuations in terms relevant to stress corrosion cracking," 2000 International Pipeline Conference, ASME, **2**, pp. 989-996.

[65] Chen, W., and Sutherby, R., 2004, "Environmental effect of crack growth rate of pipeline steel in near-neutral pH soil environments," 2004 International Pipeline Conference, pp. Paper IPC04-0449.

[66] Ghosh, S., Rana, V. P. S., Kain, V., 2011, "Role of Residual Stresses Induced by Industrial Fabrication on Stress Corrosion Cracking Susceptibility of Austenitic Stainless Steel," *Materials and Design*, **32**(7) pp. 3823-3831.

[67] Jia, Y. Z., Wang, J. Q., Han, E. H., 2011, "Stress Corrosion Cracking of X80 Pipeline Steel in Near-Neutral pH Environment Under Constant Load Tests with and without Preload," *Journal of Materials Science & Technology*, **27**(11) pp. 1039-1046.

[68] Fang, B. Y., Han, E. H., Wang, J. Q., 2007, "Stress Corrosion Cracking of X-70 Pipeline Steel in Near Neutral pH Solution Subjected to Constant Load and Cyclic Load Testing," *Corrosion Engineering Science and Technology*, **42**(2) pp. 123-129.

[69] Kane, R.D., 1993, "ASTM STP 1210, "Slow strain rate testing for the evaluation of Environmentally Induced Cracking: Research and Engineering applications", " West Conshohocken, PA:ASTM international, .

[70] Gu, B., Luo, J., and Mao, X., 1999, "Hydrogen-Facilitated Anodic Dissolution-Type Stress Corrosion Cracking of Pipeline Steels in Near-Neutral pH Solution," *Corrosion*, **55**(1) pp. 96-106.

[71] Eadie, R. L., Szklarz, K. E., and Sutherby, R. L., 2005, "Corrosion Fatigue and Near-Neutral pH Stress Corrosion Cracking of Pipeline Steel and the Effect of Hydrogen Sulfide," *Corrosion*, **61**(2) pp. 167-173.

- [72] Lichter, B. D., Lu, H., and Flanagan, W. F., 2001, "Strain-enhanced dissolution: a model for transgranular stress-corrosion cracking," Second International Conference on Environment Sensitive and Corrosion Damage, pp. 271-278.
- [73] Wang, S., Zhang, Y., and Chen, W., 2001, "Room Temperature Creep and Strain-Rate-Dependent Stress-Strain Behavior of Pipeline Steels," Journal of Materials Science (USA), **36**(8) pp. 1931-1938.
- [74] Cole, A. T., Newman, R. C., and Sieradzki, K., 1988, "A Comparison and Evaluation of "Bare Surface" Electrochemical Techniques for the Investigation of Stress Corrosion Cracking in Alpha Brass," Corros.Sci., **28**(1) pp. 109-118.
- [75] Delanty, B., and O'beirne, J., 1992, "Major Field Study Compares Pipeline SCC with Coatings," Oil and Gas Journal, **90**(24) pp. 39-44.
- [76] CEPA, 1996, "Submission to the National Energy Board," Proceeding MH-2-95, .
- [77] Beavers, J. A., Durr, C. L., Delanty, B. S., 2001, "Near-neutral pH SCC: crack propagation in susceptible soil environments," CORROSION 2001, NACE, pp. Paper # 01217.
- [78] Brass, A. M., Chene, J., and Boutry-Forveille, A., 1996, "Measurements of Deuterium and Tritium Concentration Enhancement at the Crack Tip of High Strength Steels," Corrosion Science, **38**(4) pp. 569-585.
- [79] Delafosse, D., and Magnin, T., 2001, "Hydrogen Induced Plasticity in Stress Corrosion Cracking of Engineering Systems," Engineering Fracture Mechanics (UK), **68**(6) pp. 693-729.

- [80] Parkins, R. N., 1998, "The influence of hydrogen on crack growth in pipelines," Material for resource recovery and transport, L. Colins, ed. pp. 35-49.
- [81] Dafft, E. G., Bohnenkamp, K., and Engell, H. J., 1979, "Investigations of the Hydrogen Evolution Kinetics and Hydrogen Absorption by Iron Electrodes during Cathodic Polarization," Corrosion Science, **19**(9) pp. 591-612.
- [82] Kato, C., Grabke, H. J., Egert, B., 1984, "Electrochemical and Surface Analytical Studies on Hydrogen Permeation with Fe--Cu Alloys in Sulfuric Acid with and without H Sub 2 S," Corros.Sci., **24**(7) pp. 591-611.
- [83] Gao, H., Cao, W., Fang, C., 1994, "Analysis of Crack Tip Hydrogen Distribution Under I/II Mixed Mode Loads," Fatigue Fract.Eng.Mater.Struct., **17**(10) pp. 1213-1220.
- [84] Qiao, L. J., Hsiao, C. M., and Chu, W. Y., 1988, "The Concentration of Hydrogen at Crack Tip of Austenitic Stainless Steel After Stress Corrosion and Polarization," Scr.Metall., **22**(5) pp. 627-630.
- [85] Sun, S., Shiozawa, K., Gu, J., 1995, "Investigation of Deformation Field and Hydrogen Partition Around Crack Tip in Fcc Single Crystal," Metall.Mater.Trans.A, **26A**(3) pp. 731-739.
- [86] Jack, T. R., Wilmott, M. J., and Chen, W., 1999, "Proc. EPRG/PRCI 12th Biennial Joint Technical Meeting on Line Pipe Research," Evaluation of SCC susceptibility of X-70 steel in contact with various soil solutions at near neutral pH: Comparison of laboratory predictions with field conditions, Netherlands, pp. paper 10.

- [87] Fang, B. Y., Atrens, A., Wang, J. Q., 2003, "Review of Stress Corrosion Cracking of Pipeline Steels in 'Low' and 'High' pH Solutions," *Journal of Materials Science*, **38**(1) pp. 127-132.
- [88] Asher, S., . Singh, P., Colwell, J., 2005, "Crack Initiation of Line Pipe Steels in Near-Neutral pH Environments," 16th International Corrosion Congress, China, .
- [89] Beavers, J. A., and Worthingham, R., 2002, "The influence of soil chemistry on SCC of underground pipelines," 2002 International Pipeline Conference, ASME, pp. Paper no. IPC2002-27146.
- [90] Zheng, W., Revie, R.W., MacLeod, F.A., 1998, "Low pH SCC: Environmental effects on crack propagation," Prepared for PRCI Project PR-230 9413, MTL 98-41, .
- [91] Parkins, R.N., 1999, "A review of stress corrosion cracking of pipelines in contact with near-neutral (low) pH solutions," PRCI, Report for the Line Pipe Research Supervisory Committee of PRC International, .
- [92] Chen, W., and Zheng, W., 2005, "Progress in understanding of pipeline SCC:Initiation and propagation," *Symposium on Pipelines for the 21st century*, W. Chen, ed. pp. 419-416.
- [93] J. T. Johnson, C. L. Durr, and J. A. Beavers, 2000. Effects of O₂ and CO₂ on Near-Neutral-pH Stress Corrosion Crack Propagation, *Corrosion*, p.356.

- [94] Chen, W., King, F., Jack, T. R., 2002, "Environmental Aspects of Near-Neutral pH Stress Corrosion Cracking of Pipeline Steel," Metallurgical and Materials Transactions A, **33A**(5) pp. 1429-1436A.
- [95] Burstein, G. T., and Linter, B. R., 1999, "Reactions of Pipeline Steels in Carbon Dioxide Solutions," Corrosion Science (USA), **41**(1) pp. 117-139.
- [96] Jack T R, Erno B, Krist K, 2000. Generation on near neutral pH and high pH SCC environments on buried pipelines. Corrosion/2000, NACE International, Houston, TX. p.11
- [97] He, D. X., Chen, W., and Luo, J. L., 2004, "Effect of Cathodic Potential on Hydrogen Content in a Pipeline Steel Exposed to NS4 Near-Neutral pH Soil Solution," Corrosion, **60**(8) pp. 778-786.
- [98] Zhang, Z. Y., 2003, "Corrosion and Hydrogen Permeation Characters of Pipeline Steel in Synthetic Near-Neutral pH Environments and Development of Cracking Environments," .
- [99] Gu, B., Yu, W. Z., Luo, J. L., 1999, "Transgranular Stress Corrosion Cracking of X-80 and X-52 Pipeline Steels in Dilute Aqueous Solution with Near-Neutral pH," Corrosion, **55**(3) pp. 312-318.
- [100] Gangloff, R.P., 2005, "Corrosion Tests and Standards: Application and Interpretation," ASTM International, West Conshohocken, pp. 302.
- [101] Wang, Y.Z., 2000, "Corrosion Fatigue," John Wiley & Sons, Inc., .

[102] GANGLOFF, R.P., 1990, "In: Environment Induced cracking of Metals," NACE, Houston, TX, pp. 55-109.

[103] GANGLOFF, R.P., and Ives, M.B., 1990, "Environment induced cracking of metals," NACE, Texas, .

[104] Duquette, D.J., 1981, "Mechanisms of Corrosion Fatigue of Aluminum Alloys," AGARD, AGARD Report No AGARD-CP-316, .

[105] Devereux, O., McEvily, A.J., and Staehle, R.W., 1972, "Corrosion Fatigue, Chemistry, Mechanics and Microstructure," NACE, Houston, TX, .

[106] Moody, N.R., and Thompson, A.W., 1990, "Hydrogen effects on materials behaviour," TMS-AIME, Warrendale, .

[107] Holroyd, N. J. H., and Hardie, D., 1982, "Factors Controlling Crack Velocity in 7000 Series Aluminium Alloys during Fatigue in an Aggressive Environment," Corros.Sci., **23**(6) pp. 527-546.

[108] Griffiths, A. J., Hutchings, R. B., and Turnbull, A., 1993, "Validation of the Role of Bulk Charging of Hydrogen in the Corrosion Fatigue Cracking of Low Alloy Steel," Scr.Metall.Mater., **29**(5) pp. 623-626.

[109] Scott, P. M., Thorpe, T. W., and Silvester, D. R. V., 1982, "Rate-Determining Processes for Corrosion Fatigue Crack Growth in Ferritic Steels in Seawater," Corros.Sci., **23**(6) pp. 559-575.

- [110] BLACKBURN, M. J., and SPEIDEL, M. O., 1972, "INFLUENCE OF MICROSTRUCTURE ON THE STRESS-CORROSION CRACKING OF LIGHT ALLOYS," .
- [111] Birnbaum, H.K., 1990, "Environment Induced Cracking in Metals," NACE, Houston,TX, pp. 21-29.
- [112] Grinberg, N. M., 1982, "The Effect of Vacuum on Fatigue Crack Growth," International Journal of Fatigue, **4**(2) pp. 83-95.
- [113] Sudarshan, T. S., and Louthan, M. R., 1987, "Gaseous Environment Effects on Fatigue Behavior of Metals," International Materials Reviews, **32**(3) pp. 121-151.
- [114] Wang, Y.Z., 2000, "Uhlig's Corosion Handbook,"John Wiley & Sons, pp. 221-232.
- [115] Ford, F. P., 1988, "Status of Research on Environmentally Assisted Cracking in LWR Pressure Vessel Steels," J.Pressure Vessel Technol.(Trans.ASME), **110**(2) pp. 113-128.
- [116] Ford, F. P., 1990, "The Crack Tip System and its Relevance to the Prediction of Cracking in Aqueous Environments," First International Conference on Environmentinduced Cracking of Metals, R. P. Gangloff and M. B. Ives, eds. NACE, Houston, TX, **NACE**, pp. 139-166.
- [117] Hudak, S. J., 1988, "Corrosion Fatigue Crack Growth: The Role of Crack Tip Deformation and Film Formation Kinetics," Transactions of ASME, **28** (103), pp. 26-35.
- [118] Kiessling, R., 1978, "Non-metallic Inclusions in Steel," Metals Society, London, UK, .
- [119] SURESH, S., 1991, "Fatigue of Materials", Cambridge University Press, Cambridge.

[120] Wang, Y., and Akid, R., 1996, "Role of Nonmetallic Inclusions in Fatigue, Pitting, and Corrosion Fatigue," *Corrosion*, **52**(2) pp. 92-102.

[121] Wang, Y., Akid, R., and Miller, K. J., 1995, "The Effect of Cathodic Polarization on Corrosion Fatigue of a High Strength Steel in Salt Water," *Fatigue Fract. Eng. Mater. Struct.* (United Kingdom), **18**(3) pp. 293-303.

[122] Ray, G. P., Jarman, R. A., and Thomas, J. G. N., 1985, "The Influence of Non-Metallic Inclusions on the Corrosion Fatigue of Mild Steel," *Corros.Sci.*, **25**(3) pp. 171-184.

[123] Jones, D.C., 1982, "Corrosion Processes," Applied science publishers, London, UK, pp. 161.

[124] Lee, H., and Uhlig, H., 1972, "Corrosion Fatigue of Type 4140 High-Strength Steel," *Metallurgical Transactions*, **3**(11) pp. 2949-&.

[125] Rajpathak, S.S., and Hartt, W.H., 1990, "Environmentally Assisted Cracking: Science and Engineering, ASTM STP 1049," American Society for Testing Materials, Philadelphia, pp. 425-446.

[126] Duquette, D., and Uhlig, H., 1968, "Effect of Dissolved Oxygen and Nacl on Corrosion Fatigue of 0.18 Percent Carbon Steel," *Asm Transactions Quarterly*, **61**(3) pp. 449-&.

[127] Duquette, D.J., 1990, "Corrosion fatigue crack initiation Processes: A state-of-the-Art review," NACE, Houston, TX, pp. 45-53.

- [128] Piascik, R., and Gangloff, R., 1993, "Environmental Fatigue of an Al-Li-Cu Alloy .2. Microscopic Hydrogen Cracking Processes," *Metallurgical Transactions A-Physical Metallurgy and Materials Science*, **24**(12) pp. 2751-2762.
- [129] Piascik, R., and Gangloff, R., 1991, "Environmental Fatigue of an Al-Li-Cu Alloy .1. Intrinsic Crack-Propagation Kinetics in Hydrogenous Environments," *Metallurgical Transactions A-Physical Metallurgy and Materials Science*, **22**(10) pp. 2415-2428.
- [130] Stoltz, R., and Pelloux, R., 1972, "Mechanisms of Corrosion Fatigue Crack-Propagation in Al-Zn-mg Alloys," *Metallurgical Transactions*, **3**(9) pp. 2433-&.
- [131] Harwood, J.J., 1956, "Stress Corrosion Cracking and Embrittlement," John Willey & Sons, pp. 1.
- [132] Sieradzki, K., and Newman, R., 1985, "Brittle Behavior of Ductile Metals during Stress-Corrosion Cracking," *Philosophical Magazine A-Physics of Condensed Matter Structure Defects and Mechanical Properties*, **51**(1) pp. 95-132.
- [133] Sieradzki, K., Dienes, G., and Paskin, A., 1984, "The Influence of Films on Near Crack Tip Deformation and Fracture," *Journal of Metals*, **36**(12) pp. 30-30.
- [134] Galvele, J., 1987, "A Stress-Corrosion Cracking Mechanism Based on Surface Mobility," *Corrosion Science*, **27**(1) pp. 1-33.

- [135] Duffo, G.S., and Galvele, J.R., 1990, "In: Environment-induced cracking of metals - Proceedings of the First International Conference on Environment-Induced Cracking of Metals. R. P. Gangloff and M. B. Ives (eds)," NACE, Houston, TX, pp. 261.
- [136] Parkins, R.N., 1990, "In: Environment-Induced Cracking of Metals," NACE, Houston, TX, pp. 1.
- [137] Oriani, R.A., 1990, "In: Environment Induced Cracking of Metals," NACE, Houston, TX, pp. 263.
- [138] Revie, R., and Uhlig, H., 1974, "Effect of Applied Potential and Surface Dissolution on Creep-Behavior of Copper," *Acta Metallurgica*, **22**(5) pp. 619-627.
- [139] Fessler, R. R., and Krist, K., 2000, "Research challenges regarding stress-corrosion cracking of pipelines," *Corrosion 2000*; NACE, Houston TX, paper # 00370.
- [140] Chen, W., King, F., and Vokes, E., 2002, "Characteristics of Near-Neutral-pH Stress Corrosion Cracks in an X-65 Pipeline," *Corrosion*, **58**(3) pp. 267-275.
- [141] Boven, G. V., 2003, "The Influence of Residual Stress on the Initiation and Propagation of Transgranular Stress Corrosion Cracking in High Pressure Natural Gas Transmission Pipelines". Masters thesis, University of Alberta, Edmonton
- [142] Frohberg, R. P., Barnett, W. J., and Troiano, A. R., 1955, "Delayed Failure and Hydrogen Embrittlement in Steel," *Trans. ASM*, **47**pp. 892.
- [143] Slaughter, E.R., Fletcher, E.E., Elsea, A.R., 1956, WADC Tech. Report, Report No 56-83 .

- [144] Oriani, R. A., 1972, "Mechanistic Theory of H Embrittlement of Steels," *Ber.Bunsenges.*, **76**(8) pp. 848-857.
- [145] Thompson, A.W., 1976, "Effects of Hydrogen on the Behavior of Materials," *Metallurgical Society/AIME*, New York, .
- [146] Oriani, R. A., and J, P. H., 1979, *Acta Metallurgica*, **27**pp. 997.
- [147] PETCH, N., and STABLES, P., 1952, "Delayed Fracture of Metals Under Static Load," *Nature*, **169**(4307) pp. 842-843.
- [148] Zapffe, C., and Sims, C., 1941, "Hydrogen Embrittlement, Internal Stress and Defects in Steel," *Transactions of the American Institute of Mining and Metallurgical Engineers*, **145**pp. 225-261.
- [149] CHATTORAJ, I., 1995, "The Effect of Hydrogen-Induced Cracking on the Integrity of Steel-Components," *Sadhana-Academy Proceedings in Engineering Sciences*, **20**pp. 199-211.
- [150] SIMMONS, G., PAO, P., and WEI, R., 1978, "Fracture Mechanics and Surface-Chemistry Studies of Subcritical Crack Growth in Aisi 4340 Steel," *Metallurgical Transactions A-Physical Metallurgy and Materials Science*, **9**(8) pp. 1147-1158.
- [151] HIRTH, J., and RICE, J., 1980, "On the Thermodynamics of Adsorption at Interfaces as it Influences Decohesion," *Metallurgical Transactions A-Physical Metallurgy and Materials Science*, **11**(9) pp. 1501-1511.

- [152] MCMAHON, C., and VITEK, V., 1979, "Effects of Segregated Impurities on Intergranular Fracture Energy," *Acta Metallurgica*, **27**(4) pp. 507-513.
- [153] THOMSON, R., 1978, "Brittle-Fracture in a Ductile Material with Application to Hydrogen Embrittlement," *Journal of Materials Science*, **13**(1) pp. 128-142.
- [154] Beacham, C., 1977, "In: Stress corrosion cracking and hydrogen embrittlement of iron base alloys," NACE, Houston, TX, pp. 376.
- [155] Craig, B., 2003, "Hydrogen damage," ASM International, Member/Customer Service Center, Materials Park, OH, 44073-0002, USA, pp. 367-380.
- [156] Tabata, T., and Birnbaum, H. K., 1984, "Direct Observations of Hydrogen-Enhanced Crack Propagation in Iron," *Scr. Metall.*, **18**(3) pp. 231-236.
- [157] Robertson, I. M., and Birnbaum, H. K., 1986, "An HVEM Study of Hydrogen Effects on the Deformation and Fracture of Nickel," *Acta Metall.*, **34**(3) pp. 353-366.
- [158] Bond, G. M., Robertson, I. M., and Birnbaum, H. K., 1988, "Effects of Hydrogen on Deformation and Fracture Processes in High-Purity Aluminum," *Acta Metall.*, **36**(8) pp. 2193-2197.
- [159] Bond, G. M., Robertson, I. M., and Birnbaum, H. K., 1987, "The Influence of Hydrogen on Deformation and Fracture Processes in High-Strength Aluminum Alloys," *Acta Metall.*, **35**(9) pp. 2289-2296.

- [160] Rozenak, P., Robertson, I. M., and Birnbaum, H. K., 1990, "HVEM Studies of the Effects of Hydrogen on the Deformation and Fracture of AISI Type 316 Austenitic Stainless Steel," *Acta Metallurgica Et Materialia*, **38**(11) pp. 2031-2040.
- [161] BIRNBAUM, H., and SOFRONIS, P., 1994, "Hydrogen-Enhanced Localized Plasticity - a Mechanism for Hydrogen-Related Fracture," *Materials Science and Engineering A-Structural Materials Properties Microstructure and Processing*, **176**(1-2) pp. 191-202.
- [162] Parkins, R. N., 1987, "Factors Influencing Stress Corrosion Crack Growth Kinetics," *Corrosion*. Vol.43, **43**(3) pp. 130-139.
- [163] Parkins, R. N., 2000, "A review of stress corrosion cracking of high pressure gas pipelines," *Corrosion 2000*, NACE, Houston, TX Orlando, Paper #. 363.
- [164] Champion, F.A., 1948, "In: Symposium on Internal Stresses in Metals and Alloys," *Institute of Metals*, pp. 468.
- [165] Logan, H. L., 1952, *J. Res. Natl. Bur. Stand.*, **48**pp. 99.
- [166] DIX, E., 1950, "Aluminum-Zinc-Magnesium Alloys their Development and Commercial Production (1949 Campbell, Edward, Demille, Memorial Lecture)," *Transactions of the American Society for Metals*, **42**pp. 1057-1127.
- [167] Dix, E., 1940, "Acceleration of the Rate of Corrosion by High Constant Stresses," *Transactions of the American Institute of Mining and Metallurgical Engineers*, **137**pp. 11-40.

- [168] Mao, S. X., and Li, M., 1998, "Mechanics and Thermodynamics on the Stress and Hydrogen Interaction in Crack Tip Stress Corrosion: Experiment and Theory," *Journal of the Mechanics and Physics of Solids (UK)*, **46**(6) pp. 1125-1137.
- [169] Cheng, Y. F., 2007, "Thermodynamically Modeling the Interactions of Hydrogen, Stress and Anodic Dissolution at Crack-Tip during Near-Neutral pH SCC in Pipelines," *Journal of Materials Science*, **42**(8) pp. 2701-2705.
- [170] Lu, B. T., Luo, J. L., Norton, P., 2009, "Effects of Dissolved Hydrogen and Elastic and Plastic Deformation on Active Dissolution of Pipeline Steel in Anaerobic Groundwater of Near-Neutral pH," *Acta Materialia*, **57**(1) pp. 41-49.
- [171] Qiao, L. J., Luo, J. L., and Mao, X., 1997, "The Role of Hydrogen in the Process of Stress Corrosion Cracking of Pipeline Steels in Dilute Carbonate-Bicarbonate Solution," *Journal of Materials Science Letters (UK)*, **16**(7) pp. 516-520.
- [172] Qiao, L. J., Luo, J. L., and Mao, X., 1998, "Hydrogen Evolution and Enrichment Around Stress Corrosion Crack Tips of Pipeline Steels in Dilute Bicarbonate Solution," *Corrosion (USA)*, **54**(2) pp. 115-120.
- [173] Lu, B. T., Qiao, L. J., and Luo, J. L., 2005, "ROLE OF HYDROGEN IN STRESS CORROSION CRACKING OF TYPE 304 STAINLESS STEEL," *Corrosion 2005, NACE*, pp. Paper # 05471.
- [174] ANDRESEN, P., and FORD, F., 1988, "Life Prediction by Mechanistic Modeling and System Monitoring of Environmental Cracking of Iron and Nickel-Alloys in Aqueous Systems,"

Materials Science and Engineering A-Structural Materials Properties Microstructure and Processing, **103**(1) pp. 167-184.

[175] Ford, F.P., Taylor, D.F., and ANDRESEN, P.L., 1987, "In: EPRI final report RP2006-6," Electric Power Research Insititute, RP2006-6, .

[176] CONGLETON, J., SHOJI, T., and PARKINS, R., 1985, "The Stress-Corrosion Cracking of Reactor Pressure-Vessel Steel in High-Temperature Water," Corrosion Science, **25**(8-9) pp. 633-650.

[177] Parkins, R.N., Marsh, G.P., and Evans, J.T., 1982, NACE, Houston, TX, pp. 249.

[178] Somerday, B., Young, L., and Gangloff, R., 2000, "Crack Tip Mechanics Effects on Environment-Assisted Cracking of Beta-Titanium Alloys in Aqueous NaCl," Fatigue & Fracture of Engineering Materials & Structures, **23**(1) pp. 39-58.

[179] Young, L. M., Andresen, P. L., and Angeliu, T. M., 2001, "CRACK TIP STRAIN RATE: ESTIMATES BASED ON CONTINUUM THEORY AND EXPERIMENTAL MEASUREMENT," Corrosion 2001, **NACE**, pp. Paper # 01131.

[180] ANDRESEN, P.L., 1988, In: Proceeding of the 3rd International Symposium on Environmental Degradation of Materials in Nuclear Power Systems - Water Reactors, Theus, G.J.;Weels, J.R. (eds), NACE, Houston, TX, pp. 301.

[181] Peng, Q. J., Kwon, J., and Shoji, T., 2004, "Development of a Fundamental Crack Tip Strain Rate Equation and its Application to Quantitative Prediction of Stress Corrosion Cracking

of Stainless Steels in High Temperature Oxygenated Water," *Journal of Nuclear Materials*, **324**(1) pp. 52-61.

[182] RICE, J. R., Drugan, W. J., and Sham, T. L., 1980, "ASTM STP 700,ASTM, 1980," pp. 189.

[183] SHOJI, T., Suzuki, S., and Ballinger, R. G., 1995, "Theoretical Prediction of SCC Growth Behavior - Threshold and Plateau Growth Rate," *Proceedings of the 7th International Symposium on Environmental Degradation of Materials in Nuclear Power Systems - Water Reactors*, NACE, Houston, TX, pp. 881.

[184] Suzuki, S., SHOJI, T., and Yi, Y. S., 1997, "Characteristics of the SCC Surface Crack Propagation in the Low K Region inOxygenated High Temperature Water," *Proceedings of the 8th International Symposium on Environmental Degradation of Materials in Nuclear Power Systems - Water Reactors*, NACE, Houston, TX, pp. 695.

[185] Gao, Y. C., and Hwang, K. C., 1982, "In: *Proceedings of the 5th International Conference on Fracture*", Pergamon Press, pp. 669.

[186] Been, J., and Sutherby, R. L., 2006, "Effect of Loading Frequency on Near-Neutral pH Crack Growth on Operating Pipelines," *NACE Northern Area Western Conference*, Calgary, Canada, Feb 7-8, 2006 .

[187] Ford, F. P., and ANDRESEN, P. L., 1992, "In:*Symposium on fundamental Aspects of Stress Corrosin cracking: Proceedings of a symposium Sponsored by TMS-ASM-MSD Corrosion and Environmental Effects Committee*," pp. 43.

[188] Lambert, S. B., Plumtree, A., and Sutherby, R., 2000, "Modeling of environmental crack growth in pipeline steel," Corrosion 2000, **NACE**, pp. Paper 00364.

[189] S.B. Lambert, R. Sutherby, 1998. Fracture Mechanics Modeling of Stress Corrosion Crack Colonies, International Conference of Pipeline Reliability, Montreal, Canada.

[190] Lambert, S. B., Beavers, J. A., Delanty, B., 2000, "Mechanical factors affecting stress corrosion crack growth rates in buried pipelines," International pipelines Conference, **ASME**, pp. 961-966.

[191] Been, J., King, F., and Sutherby, R., 2008, "Environmentally Assisted Cracking of Pipeline Steels in Near-Neutral pH Environments," Proceedings of Conference on Environment-Induced Cracking of Materials, pp. 221-230.

[192] Plumtree, A., Williams, B. W., Lambert, S. B., 2008, "SCC Growth in Pipeline Steel," Environment-Induced Cracking of Materials, pp. 199-210.

[193] Beavers, J. A., and Jaske, C. E., 1999, "SCC of underground pipelines: A history of the development of test techniques," Corrosion '99, **NACE**, pp. Paper#. 142.

[194] Vasudevan, A. K., and Sadananda, K., 1995, "Classification of Fatigue Crack Growth Behavior," Metall. Mater. Trans. A , **26A**(5) pp. 1221-1234.

[195] Hunter, M. S., and Fricke, W. G., Jr., "Cracking of Notch Fatigue Specimens," Proc. ASTM, **57**,1957, pp. 643-652.

- [196] HUNTER, M. S., and FRICKE, W. G. J., 1956, "Fatigue crack propagation in aluminum alloys," ASTM, **56**, pp. 1038-1050.
- [197] HUNTER, M. S., and FRICKE, W. G. J., 1955, "Effect of alloy content on the metallographic changes accompanying fatigue," ASTM, **55**, pp. 942-953.
- [198] HUNTER, M., and FRICKE, W., 1954, "Metallographic Aspects of Fatigue Behavior of Aluminum," Proceedings-American Society for Testing and Materials, **54**pp. 717-736.
- [199] FORSYTH, P. J. E., 1961, "A two stage process of fatigue crack growth," Proc. of the crack propagation symposium, Cranfield, England, **1**, pp. 76-94.
- [200] FORSYTH, P., 1963, "Fatigue Damage and Crack Growth in Aluminium Alloys," Acta Metallurgica, **11**(7) pp. 703-&.
- [201] MCEVILY, A., and BOETTNER, R., 1963, "On Fatigue Crack Propagation in Fcc Metals," Acta Metallurgica, **11**(7) pp. 725-&.
- [202] SURESH, S., and RITCHIE, R. O., 1984, "Propagation of Short Fatigue Cracks," Int.Met.Rev.Vol.29, **29**(6) pp. 445-476.
- [203] Kitagawa, H., Takahashi, S., Suh, S., 1979, "Quantitative Analysis of Fatigue Process- Microcracks and Slip Lines Under Cyclic Loading, ASTM-STP 675," ASTM, pp. 420-449.
- [204] Kitagawa, H., and Takahashi, S., 1976, "Applicability of fracture mechanics to very small cracks or the cracks in the early stage," Proc. 2nd Int. Conf. on Mech. Beh. of Matls. pp. 627-631.

[205] El Haddad, M. H., Dowling, N. E., and Topper, T. H., 1980, "J-Integral Applications for Short Fatigue Cracks at Notches," *Int. J. of Fracture*, **16**(1) pp. 15.

[206] El Haddad, M. H., Smith, K. N., and Topper, T. H., 1979, "Fatigue Crack Propagation of Short Cracks," *ASME Journal of Engineering Materials Technology*, **101**pp. 42.

[207] JAMES, M., and KNOTT, J., 1985, "An Assessment of Crack Closure and the Extent of the Short Crack Regime in Q1n (Hy80) Steel," *Fatigue & Fracture of Engineering Materials & Structures*, **8**(2) pp. 177-191.

[208] Anderson, T.L., 2005, "Fracture Mechanics - Fundamentals and Applications," Taylor & Francis, New York.

[209] ELBER, W., 1970, "FATIGUE-CRACK CLOSURE UNDER CYCLIC TENSION," *ENG FRACTURE MECH*, **2**(1) pp. 37-45.

CHAPTER THREE

**SURFACE CRACK GROWTH BEHAVIOR OF PIPELINE STEEL UNDER
DISBONDED COATING AT FREE CORROSION POTENTIAL IN NEAR-
NEUTRAL PH SOIL ENVIRONMENTS**

3.0 Introduction

Oil and gas pipelines are crucial facilities in the distribution of oil and gas products. Although they are very expensive to install they are yet the most efficient and/or safest way of moving and distributing oil and gas products. It is estimated that the oil and gas pipeline network in Canada alone is long enough to stretch all the way from earth to the moon and back [1]. Because they often convey flammable products, they present a significant level of danger and may cause significant destruction and chaos in the event of an accidental pipeline rupture followed by an explosion. Since it was first reported, near-neutral pH stress corrosion cracking has been responsible for a few accidental rupture/leakages [2] in Canada, some of which involved loss of property and significant environmental damage.

Near-neutral pH SCC continues to be a major pipeline integrity issue mainly because of imprecise understanding of the initiation and propagation mechanisms. Although it is generally accepted that the near-neutral pH environment plays a role in the development and propagation of these cracks, proper understanding of the role played by the environment or the species in it is at best still evolving [3-10].

Eslami *et al.* [11] used a novel test set up to study the combined influence of pressure fluctuation, coating disbonding and environmental parameters on the initiation of cracks in near-neutral pH environments at open circuit potential. The study established that variations in the localized environments under the disbonded coating could result in varying SCC initiation mechanisms. Such variations in the local environment under the disbondment could result in preferential crack initiation from the mouth of large pits, formation from persistent slip bands, initiation at the bottom of deep scratch lines, and from sub-micrometer pits.

NNPHSCC cracks typically start as very fine surface cracks that grow both in the depth and at the pipe surface over time, sometimes until rupture occurs. Pipeline operators are generally aware that several segments of their pipes have cracks developing on them. However, as long as these cracks have not attained critical sizes above which the pipeline cannot be safely operated, such a pipeline is usually not removed from service. Monitoring/mitigation measures often have to be designed and implemented. Among several other steps, it is often important to determine/monitor crack sizes in order to determine the most appropriate measure to be implemented.

Although mathematical models will provide a cheap means of estimating the progression of NNPHSCC crack sizes, pipeline operators still rely on in-line inspection for oil pipelines and/or hydrostatic testing for gas pipelines because of its much better reliability when compared to currently available models [11]. Both hydrostatic testing and inline inspection are expensive procedures which may involve repeated shut downs, and exhumation of pipelines as well as coating removal at pre-determined intervals. Re-inspection intervals are currently determined using empirical models that have proven to rather underestimate crack growth rates [2].

Underestimation of crack growth rates increases the risk of accidental pipeline rupture and the attending oil spillage. To reduce this risk, conducting a few more inspections than necessary often becomes inevitable, further increasing the cost of pipeline integrity management schemes. The economics of pipeline integrity management, with respect to NNPHSCC management, will drastically improve if the existing models are replaced with more accurate and reliable mathematical models that can predict the growth rate of NNPHSCC cracks upon accounting for operating field conditions, material history and local environmental factors. The often reported poor correlation of available models to field observations may be attributed to

several reasons, including but not limited to the assumption of a constant growth rate over the entire lifespan of the crack, failure to account for possible effects of variations in the local environment, and the use of modeling specimens that do not adequately represent NNPHSCC cracks in laboratory studies.

Careful examination of literature on the growth of NNPHSCC cracks reveals that currently existing models were developed using samples and/or crack geometries that do not properly represent those of NNPHSCC cracks typically observed in the field. For instance, whereas NNPHSCC cracks are typically shallow non-through-thickness cracks, existing models were developed using samples that simulate through-thickness cracks especially the compact tension specimen. Results from contemporary research in fatigue crack growth suggest that shallow cracks tend to grow at significantly higher rates than through-thickness cracks and may grow under conditions where through-thickness cracks are typically dormant [12-27]. This difference in the behaviour of shallow and through-thickness cracks may be responsible for the underestimation of the growth rate of NNPHSCC cracks. The current industry approach also has the shortcoming of assuming that the rate of crack propagation in pipelines is constant rather than dependent on pipeline operating conditions, crack size and morphologies. This is evidently simplistic.

Basic fracture mechanics classifies cracks into two categories: long/deep cracks and short/shallow cracks (short in the direction of propagation). Short cracks are further divided into microstructurally short cracks and mechanically short cracks. The typical SCC crack starts as a microcrack, often from the base of a pit, measuring from a fraction of a micrometer to one or two grain sizes in length. Compared to the overall lifespan of a typical crack, the typical NNPHSCC crack spends only a small, probably insignificant portion of its lifespan in the microstructurally

small crack category. The crack then develops into a mechanically short crack, usually at over 100 μm in length. A SCC crack spends the largest fraction of its life cycle in the mechanically short crack category, and will eventually develop into a long crack for a brief period before final rupture occurs. Therefore the mechanically short crack stage is usually the focus of integrity management programs. Hence, in order to generate more accurate mathematical models, there is a need to simulate NNPHSCC using surface type flaws rather than through-thickness flaws as commonly done.

Chen and Sutherby [9] proposed a true corrosion fatigue model that accounts for NNHPSCC as a synergistic effect of fatigue and corrosion. This model assumes that the influence of both corrosion and fatigue on the propagation of NNHPSCC cracks cannot be separated. It successfully fitted NNPHSCC data much better than the existing models. The general form of the model is given as:

$$\left(\frac{da}{dN}\right) \propto (\Delta K)^2 K_{\max} / f^\gamma \quad (3-1)$$

where ΔK is the change in stress intensity at the crack tip due to cyclic loading, K_{\max} is the maximum stress intensity at the crack tip, and γ is found to be around 0.1, a factor representing the influence of the corrosion environment on the crack growth rate. ΔK and K_{\max} are strongly dependent on the geometry of the specimen, while γ is dependent on the severity of the corrosion environment. Therefore, modified forms of this model need to be produced for several crack forms, specimen geometries and environmental conditions.

There has been no study of the effect of variations in the local environment under the disbondment on the rate of crack propagation. This study is aimed at studying the effect of variations in the local environment under the disbondment on the rate of crack propagation in a

near-neutral pH environment. This was achieved by using a novel setup [11, 28] and a novel non-standard specimen designed with surface flaws that allow the study of variations in local environment with distance from the open mouth of a disbondment on the rate of crack propagation.

3.1 Experimental

3.1.1 Sample preparation

Tensile specimens (Figure 3-2) bearing three reduced sections were machined from the longitudinal direction of a X65 pipe section that had failed in service. The alloy composition is shown in Table 3-1, while a typical alloy microstructure is shown in Figure 3-1. Only pipe sections unaffected by NNPHSCC and other forms of corrosion, and external damage were used. Gauge sections were $23 \times 45 \times 9.2$ mm in dimension and identical semi-circular shallow notches, 0.2032mm wide, with dimensions $2c = 5$ mm (surface length) and $a = 2.5$ mm (depth) were made by electrical discharge machining (EDM) in the middle of each gauge section.

A corrosion test cell consisting of two chambers was designed and fabricated from acrylate (Figure 3-3). The inner tube, named the shielding, was designed to simulate coating disbondment at the surface of a pipe. The width of this inner tube was made adjustable so that coating disbondment of various sizes can be studied. The outer tube holds the bulk solution which simulates the surrounding soil around a pipe in the field while the solution contained in the inner shielding simulates the solution trapped between the coating and the pipe surface on an actual pipeline. The bulk solution in the outer tube was purged by a mixture of certified grade 5% CO₂ (nitrogen balance) fed in through openings at the bottom of the cell, so that CO₂ can only diffuse into the simulated disbondment (shielding) from the open mouth.

Table 3-1: Alloy (X65) composition

| Element | Composition (wt %) |
|------------|--------------------|
| Carbon | 0.13 |
| Manganese | 1.55 |
| Copper | 0.05 |
| Niobium | 0.05 |
| Chromium | 0.08 |
| Molybdenum | 0.01 |
| Vanadium | 0.002 |
| Nickel | 0.05 |
| Aluminum | 0.042 |
| Titanium | 0.002 |
| Nitrogen | 0.009 |
| Iron | Balance |

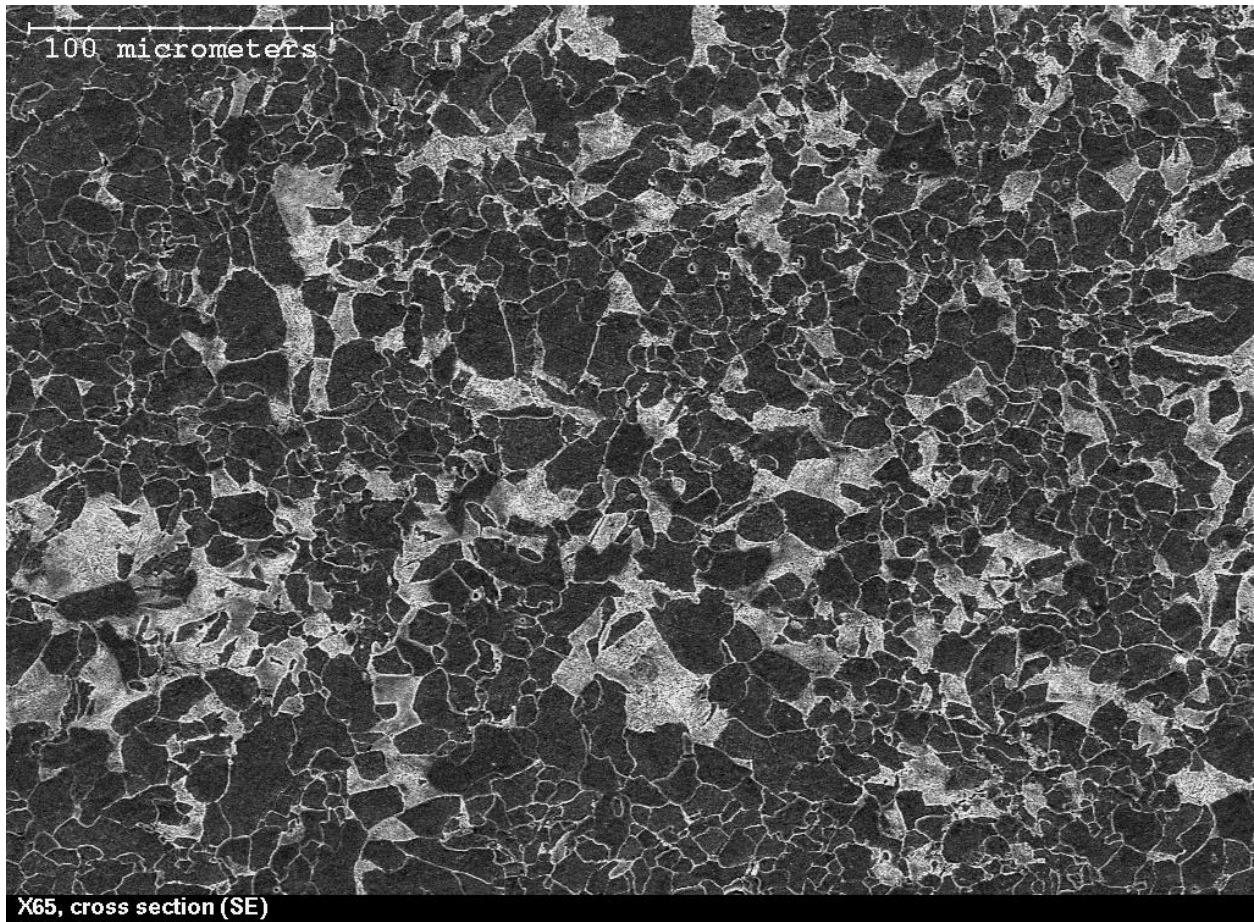


Figure 3-1: Typical microstructure of the alloy X65 used in this study

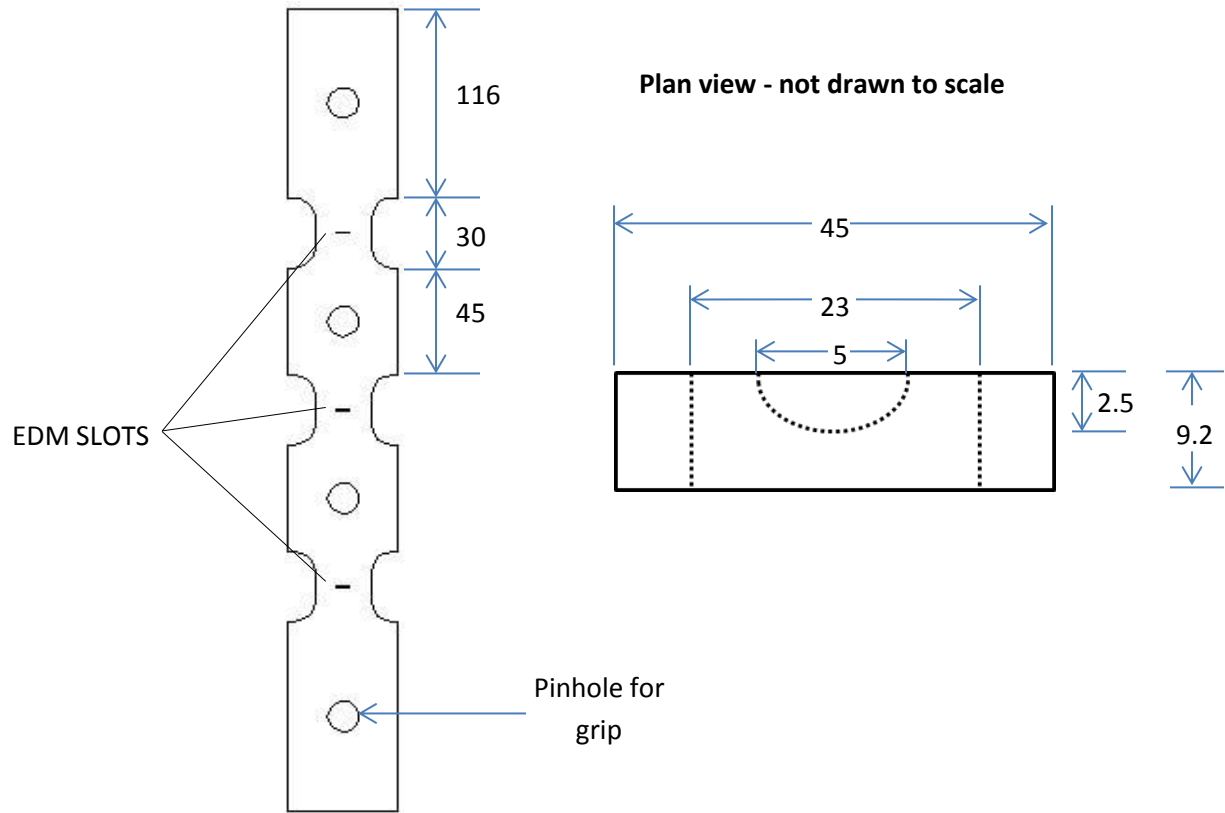


Figure 3-2: Test sample designed for this study

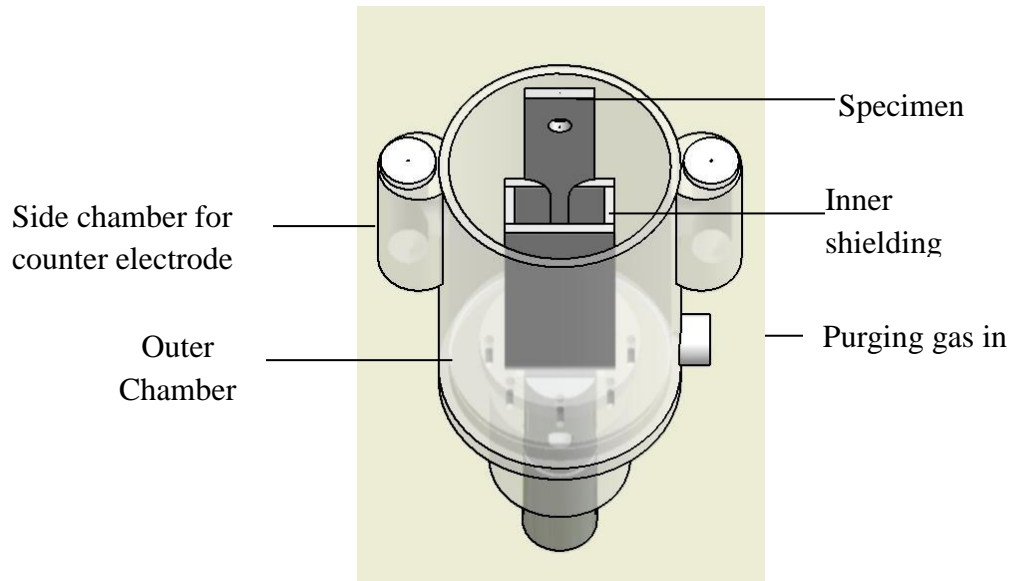


Figure 3-3: Schematic drawing of the corrosion test cell used for study

Preparatory to each test, each gauge section was separately pre-fatigue cracked by tensile cyclic loading in air to produce the required pre-test surface crack length of 3.3 mm. The pre-cracked samples were then exposed to the corrosion media in a sealed test cell and filled with C2 solution (0.0035 KCl, 0.0195 NaHCO₃, 0.0255 CaCl₂.H₂O, 0.0274 MgSO₄.7H₂O, 0.0606 CaCO₃ g/l). The C2 solution was purged with 5% CO₂ + N₂ gas mixture for 48 hours prior to starting the test in order to remove dissolved oxygen and to establish a pH of 6.23. Cyclic stresses with a maximum stress of 75% specified minimum yield strength was applied during the test.

In an attempt to closely simulate real pipeline service conditions, the sides and back surface of each specimen (the one without the surface cracks) were coated with epoxy in order to isolate these surfaces from the corrosion media. Crack growth rates were monitored using a custom made potential drop system through copper wire leads spot welded to the back surface across the EDM slots in each gauge section. A constant current of 20A was applied by the potential drop system in order to measure the potential drop across each crack.

3.1.2 Mechanical loading

Chen and Sutherby analysed the corrosion-fatigue crack growth behavior of X65 pipeline steel using the compact tension specimen geometry in a near-neutral pH environment using the corrosion-fatigue model [9]. This work found that crack growth threshold conditions were below 8500 (MPa·√m)³/Hz^{0.1} in C2 solution. For the current study, a maximum stress of 75% specified minimum yield strength and a cyclic frequency of 0.005 Hz were used. A stress ratio of 0.4 was used and test was purged with 5% CO₂ (N₂ balanced). These conditions would correspond to an initial maximum stress intensity of about 26.8 MPa·m^{0.5} at the sample surface and 24.3 MPa·m^{0.5} in the depth direction (Table 3-2).

Table 3-2: Initial and final stress intensities calculated for the crack at the open mouth

| location | initial | final |
|-------------------|---------|-------|
| K surface (MPa√m) | 26.8 | 34.3 |
| K depth (MPa√m) | 24.3 | 33.9 |

This would yield an initial combined factor of between 11600 to 12100 $(\text{MPa} \cdot \sqrt{\text{m}})^3/\text{Hz}^{0.1}$ at the sample surface and ranging from 8535 to 8917 $(\text{MPa} \cdot \sqrt{\text{m}})^3/\text{Hz}^{0.1}$ in the depth direction at the beginning of corrosion exposure. These ranges arise due to the fact that the initial aspect ratio of the cracks could not be individually controlled during the pre-cracking operation. The relationship for calculating the stress intensity factor for a surface flaw is dependent on the aspect ratio. Since the initial aspect ratios slightly vary, and the growth rate per cycle is a third order function of the ΔK , small changes in the value of ΔK tend to have large effects on the combined factor. On a 9.88 mm thick 36" outside diameter pipeline, the maximum stress intensity factors above correspond to an SCC crack measuring 13.5 mm long at the sample surface with an aspect ratio of 0.1. This translates to a surface crack measuring 1.35 mm deep in X65 plate being subjected to a maximum stress of 75% SMYS. It is typical to operate pipelines at a maximum operating pressure of about 72% SMYS. Aspect ratios of about 0.1 are also typical of SCC cracks in the field [34]. The test was stopped at about 23.2 days because of substantial crack growths at the open mouth of the disbondment (OM).

3.1.3 Post-test Analysis

After each test, the fracture surface was examined and post-test crack lengths determined in order to validate potential drop measurements with actual crack growth measured from the surface of fractured specimens. Potential drop data were converted to crack sizes by block averaging the data and using a mathematical relationship derived by assuming that changes in the resistivity of material with increasing crack propagation is directly related to the changes in the surface area of the crack. Crack growth rates were derived as crack length increase per cycle. Prior to fracture surface examination, iron oxide-type corrosion products were removed using a

rust remover solution composed of water (100ml), HCl (3ml), and cis-2-but-1-4-diol (4ml). Initial fracture face examination was done using an optical microscope. More detailed examination of fracture surfaces was carried out using a Hitachi scanning electron microscope equipped with an energy dispersive x-ray spectrometer for chemical composition analysis.

3.2 Results

3.2.1 Characteristics of crack growth monitored by potential drop systems

The potential drop curves indicating that crack propagation was not preceded by any period of dormancy are shown in Figure 3-4. Only two of the three curves are shown because there were several interruptions in the third recording due to equipment failure. Although the magnitude of potential change in the two curves seems to indicate that crack growths are similar, we have often found that it is impossible to determine the relative amount of growth from the potential drop readings themselves. Hence, a curve fitting technique had to be adopted for individual curves. The serrations in the curves are often indications of processes that interfere with the measured potential, such as static charges, formation of corrosion deposits inside the crack, and little power surges from equipment being turned on and off in the building in the evenings and over the weekends. Although crack growth was indicated by the rising potential curve at 75 mm from the open mouth, the final drop at the end of the curve (which is not replicated at the open mouth) indicates that the crack had stopped growing towards the end of the test.

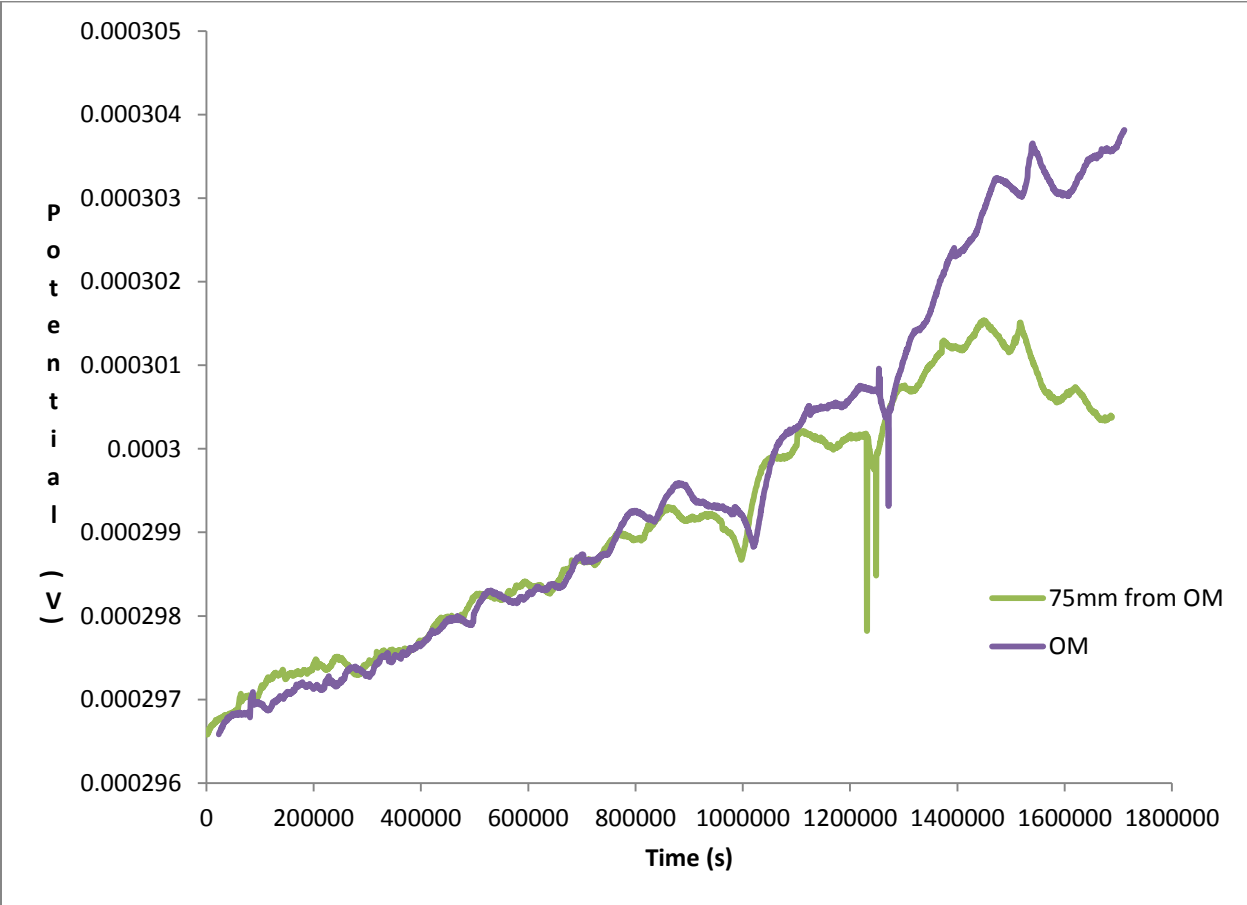


Figure 3-4: Potential drop data showing crack propagation during test

3.2.2 Morphological characteristics of cracks on surface

Post-test low magnification examination of the corroded surfaces reveals the presence of corrosion deposits on the surface of the samples Figure 3-5. These corrosion products were analyzed to be FeCO_3 , Fe_2O_3 and FeOOH by powder mode x-ray diffraction technique.

Despite the low corrosion-fatigue factor in the test design, crack propagation was physically noticed on the sample after the test. Figure 3-6 compares the extent of crack propagation that occurred during the test. It is clear that the largest growth occurred at the open mouth of the disbondment while the least growth occurred at the far end of the disbondment (150 mm from the OM). Generally, the magnitude of change in the measured potential drop follows the same trend as the amount of growth noticed after the test.

At a slightly higher magnification, the behavior of the pre-fatigue crack tip shows that there is significantly higher crack opening at the open mouth of the disbondment while comparable crack opening could be observed at 75 mm and 150 mm from the open mouth. High magnification examination of the post-test crack tip reveals a significant difference in the crack opening size just behind the crack tip (Figures 3-7 and 3-8). At the open mouth, the crack tip was very sharp – much sharper than the crack tip at the other two locations inside the disbondment while the crack tip was bluntest at 150 mm from the open mouth. All cracks are transgranular in nature.

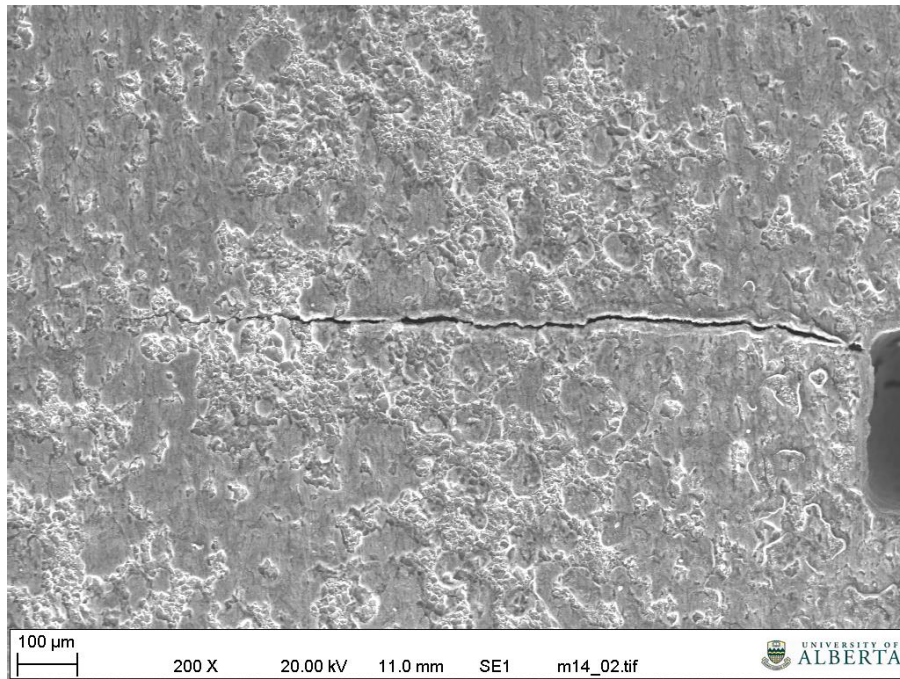


Figure 3-5: Corrosion products on sample surface

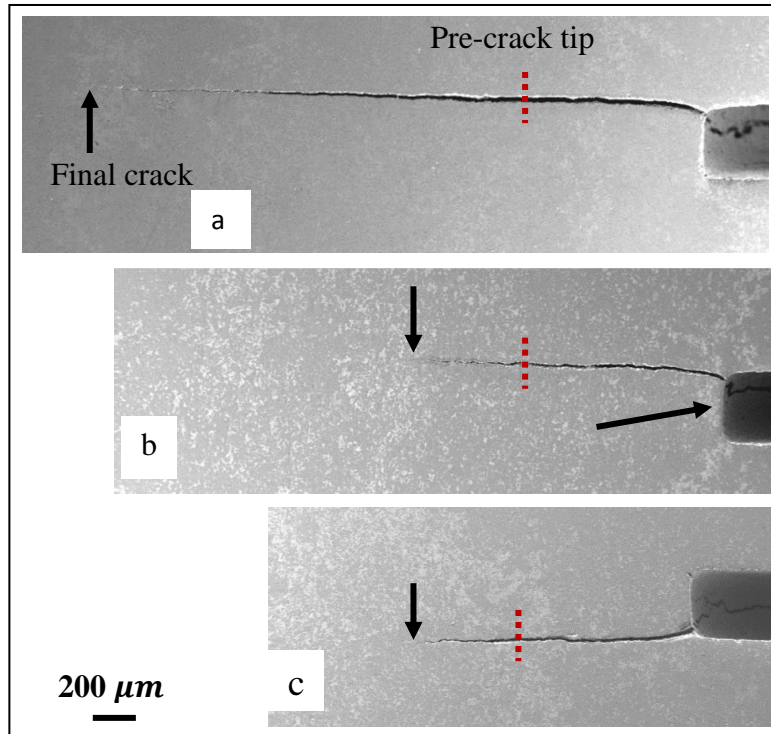


Figure 3-6: Low magnification image of crack tip (a) open mouth (b) 75 mm from the open mouth (c) 150 mm from the open mouth

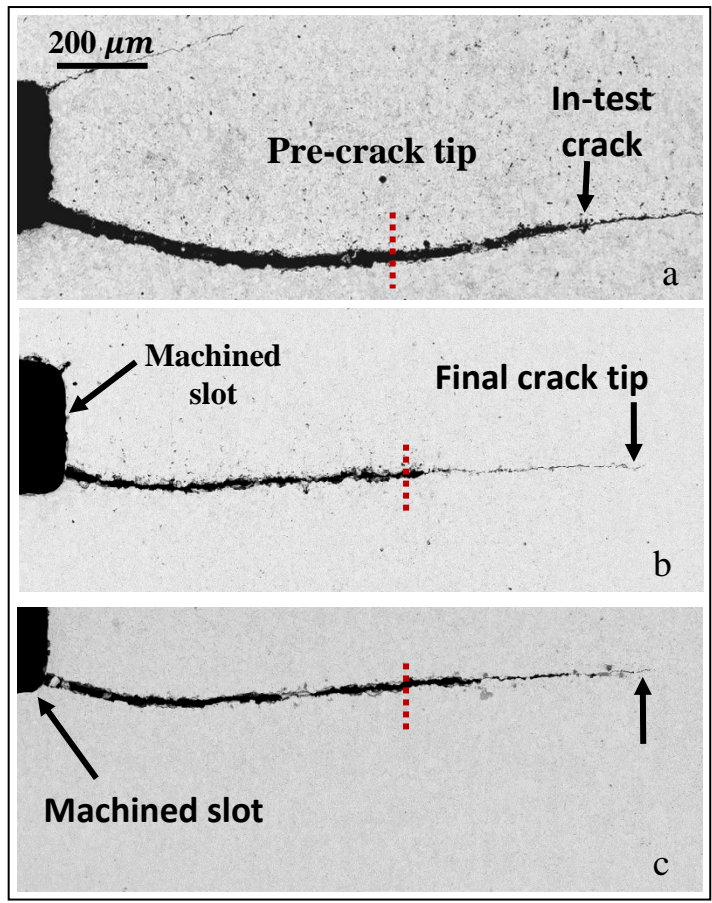


Figure 3-7: Pre-crack tips in the 5% CO₂ environment (a) open mouth, (b) 75 mm from open mouth and (c) 150 mm from open mouth

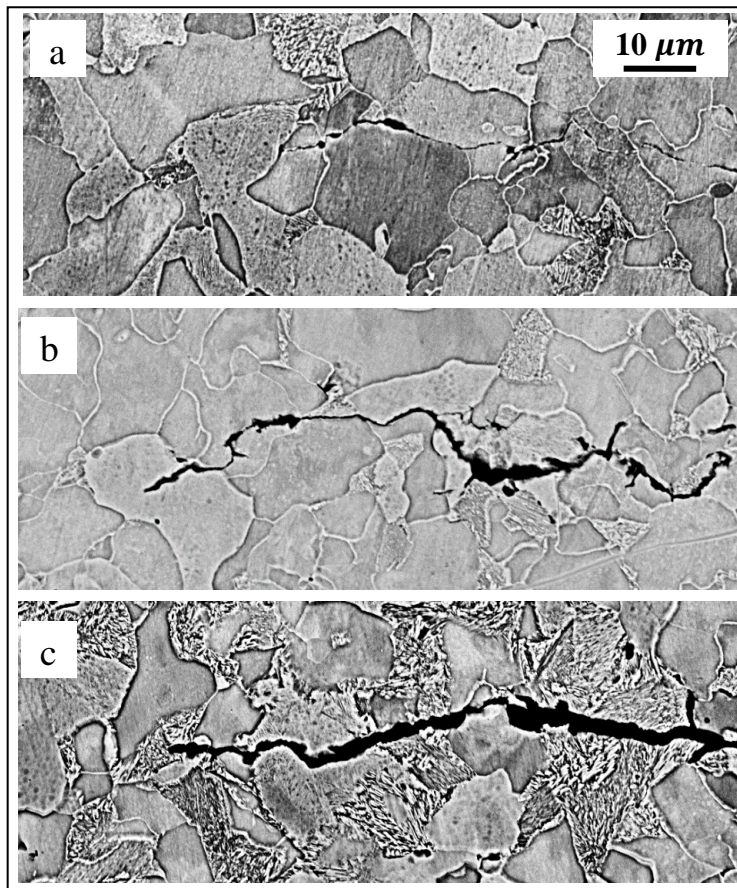


Figure 3-8: High magnification image of the crack tip at the sample surface (a) open mouth, (b) 75 mm from open mouth, (c) 150 mm from open mouth.

3.2.3 Morphological characteristics of cracks at the depth direction

The difference in crack opening size just behind the crack tip is even more pronounced in the depth direction (Figure 3-9). Also, it seems propagating cracks could interact with elongated inclusions in a process that modified their growth path and may affect crack propagation rates. These inclusions were found to be manganese sulphides. Just as previously stated, the magnitudes of the change in potential drop measurements are consistent with the observed increase in crack length during the test.

Comparing the amount of growth in the depth and surface directions shows that more growth occurred along the sample surface than in the depth direction. Lower magnification images reveal that crack openings at the pre-crack root are larger at the sample surface than in the depth direction, making the crack appear to be wider at the surface. The morphology at the crack tip can be better viewed at a higher magnification (Figure 3-10). Again very fine cracks are observed at both the OM and 75 mm from the OM. There is hardly any difference in crack tip width at these two locations. However, there is significant crack tip blunting at 150 mm from the open mouth as evidenced by the significantly wider crack tip. Although it is possible to argue that the increased width might be a result of the interaction between the main crack front and the sulphide inclusion noticed in the micrograph, however, a similar interaction is present in the micrograph at 75 mm from the open mouth but there is no crack tip widening. All cracks seem to be transgranular in the depth direction.

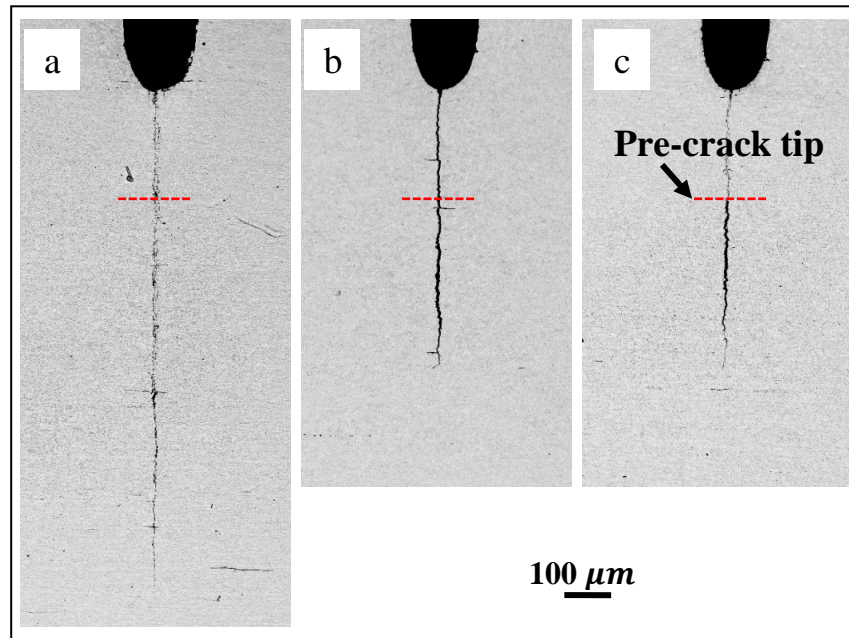


Figure 3-9: Low magnification image of crack tip in the depth (a) open mouth, (b) 75 mm from open mouth, (c) 150 mm from open mouth

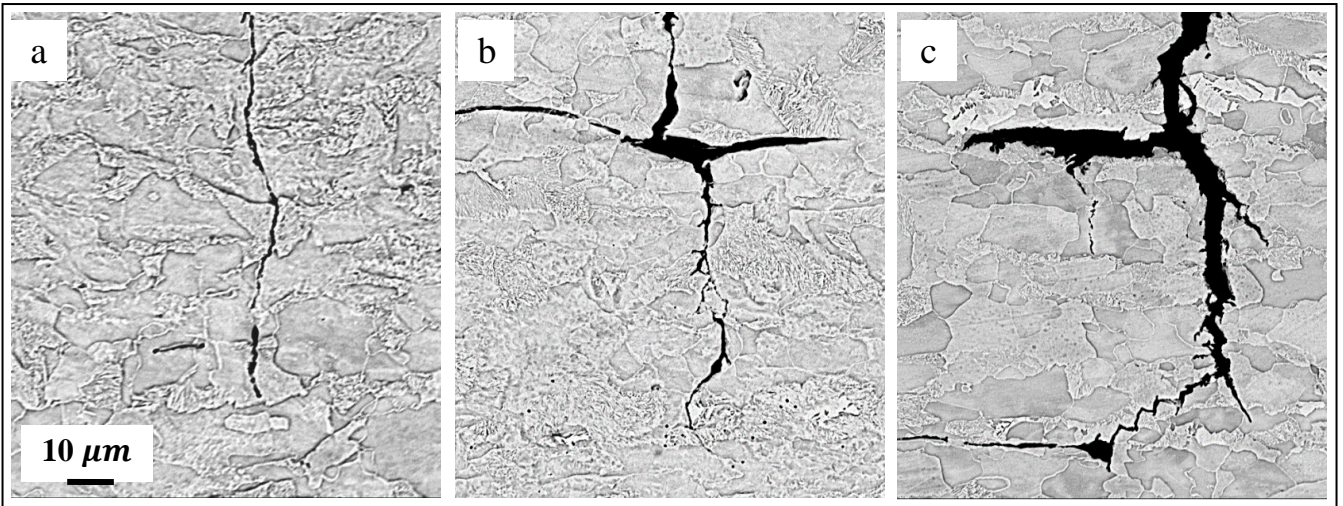


Figure 3-10: High magnification image of the crack tip in the depth direction (a) open mouth, (b) 75 mm from open mouth, (c) 150 mm from open mouth

3.2.4 Morphological characteristics of fracture surface

A typical micrograph of the fracture face, showing the original slot, the pre-crack region, the distinct ledge formed between the pre-fatigue region and the SCC crack propagation region is shown in Figure 3-11. The ledge may have resulted when crack propagation was halted for a while during cyclic loading. Figure 3-11 also shows that shape deviated from its original semi-circular shape during crack propagation in air (during pre-cracking) and in the corrosion media resulting in an elliptical crack shape after the test. Higher magnification examination of the fracture surface showed a quasi-cleavage type of crack propagation.

3.2.5 Determination of crack growth rate

Figure 3-12 shows the initial and final crack sizes at all three locations. This figure indicates the most significant enhancement of crack propagation along the surface and depth directions occurred at the open mouth while much lower enhancement occurs at 75 mm and 150 mm from the open mouth. At the latter locations, the difference in crack growth was very small. Average crack growth rate data (Figure 3-13) indicate a significantly higher growth rate at the open mouth relative to the other locations, while comparable rates were observed at 75 mm and 150 mm from the open mouth.

Analysis of growth at the surface and in the depth directions indicates that growth could be significantly more rapid at the surface compared to the depth direction at the open mouth (Figure 3-12). However, growth rate in the depth direction was found to be lower than at the surface at 75 mm and 150 mm from the open mouth.

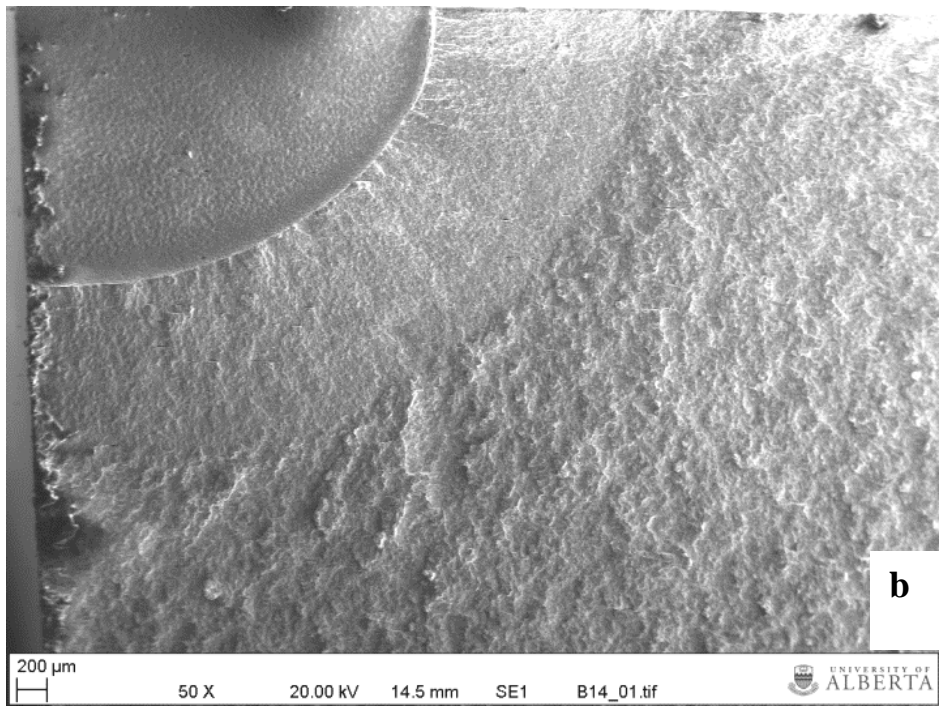
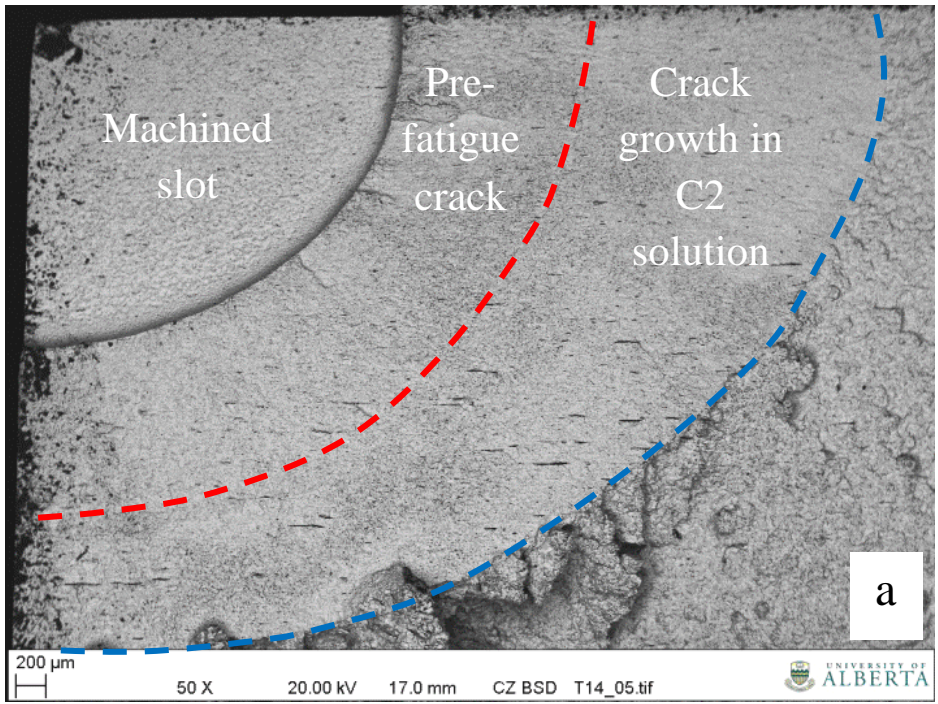


Figure 3-11: Fracture face (half section) of cracks at (a) open mouth (b) 150 mm from OM

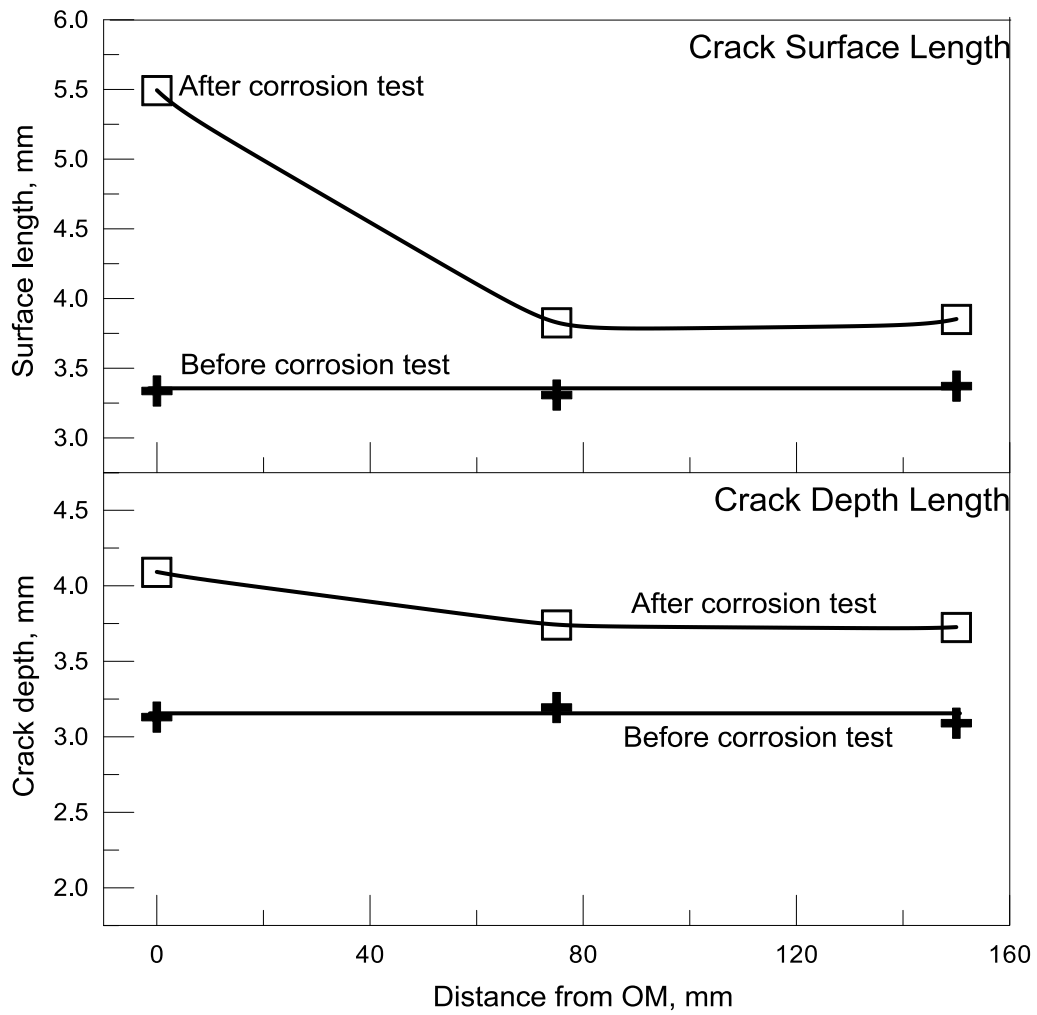


Figure 3-12: (a) Pre- and post-crack sizes at sample surface (b) Pre- and post-crack sizes in depth direction

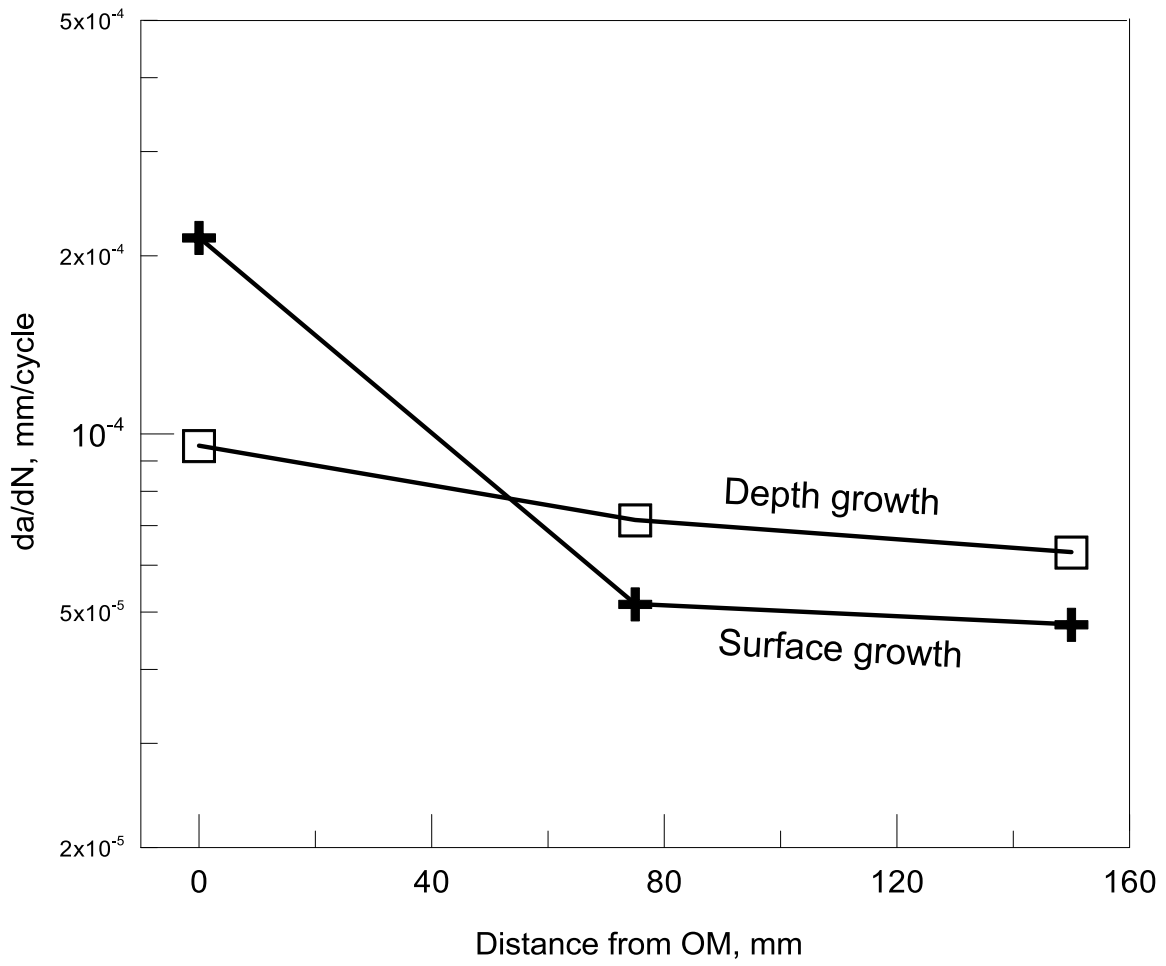


Figure 3-13: Variation of average growth rates with distance from the open mouth

Due to the above different growth scenarios, there were different changes in crack aspect ratios at different locations from the open mouth. As shown in Figure 3-14, the aspect ratios of the pre-fatigued cracks were around 0.94 and varied slightly at different locations. The aspect ratio at the open mouth decreased significantly, indicating much faster growth at the surface than at the depth. However, this trend seemed reversed at 75 and 150 mm from the open mouth and faster growth occurred in the depth than at the surface.

3.3 Discussion

3.3.1 Variation in local environment under the disbondment

3.3.1.1 Variation in CO₂ concentration in the solution in contact with specimen surface

Since the sparging gas was purged in the bulk solution, CO₂ concentration is highest in the bulk solution. The CO₂ concentration in the bulk solution is at equilibrium with the CO₂ concentration in the purging gas. Since the solution at the open mouth is in direct contact with the bulk solution, the concentration of CO₂ at the open mouth is the same as that in the bulk solution. However, inside the disbondment, CO₂ concentration reduces with distance from the open mouth; setting up a CO₂ concentration cell.

It is known that CO₂ is dissolved in water to produce carbonic acid which in turn dissociates to produce hydrogen ions. The amount of CO₂ at locations farther away from the open mouth of disbondment is diffusion controlled. Since diffusion is down a concentration gradient, the concentration of CO₂ decreases with increasing distance from the open mouth, and the concentration of hydrogen ions in contact with the sample surface should also decrease with distance from the open mouth. In another study, Appendix A, it was shown through hydrogen permeation test results that this hydrogen concentration gradient does occur under the simulated disbondment.

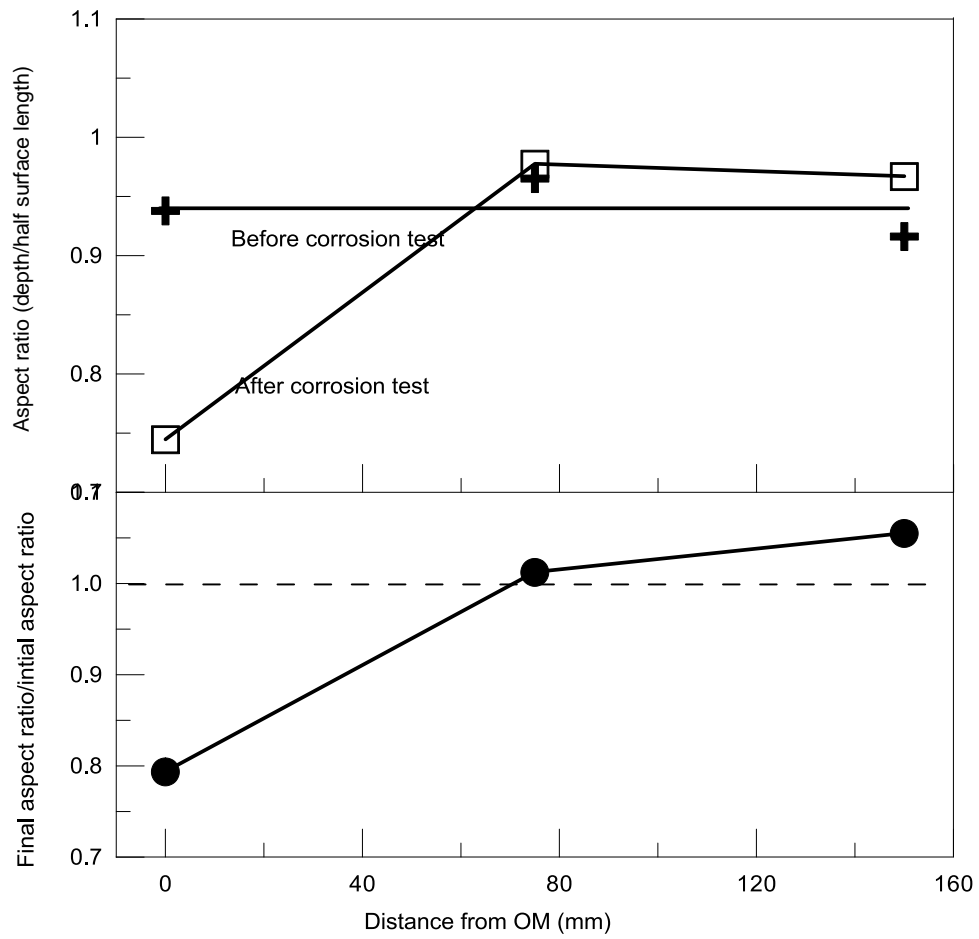
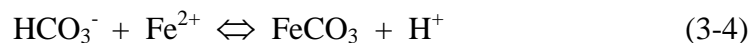


Figure 3-14: Variations in crack aspect ratio with distance from the open mouth of the disbondment

However, this difference in hydrogen concentration is usually not reflected in pH values measured down the disbondment since the solution is buffered because of the equilibrium between the carbonic and carbonate species. This tends to keep the pH uniform at all locations under the disbondment.

3.3.1.2 Effect of hydrogen abundance on dissolution rate

In a near neutral pH solution, carbon dioxide may dissolve in ground water (C2) solution to liberate hydrogen in solution via the reduction reaction proposed by Asher *et al.* [30]:



In the absence of cathodic protection, in order to complete these reactions, the steel sample has to liberate an electron for every hydrogen ion that is reduced. This is achieved through dissolution of iron at the free surfaces. Hence, the more the Fe is dissolved, the more the hydrogen ions are reduced. Chen *et al.* [10] reported that under open circuit potentials, corrosion rate reduces with distance from the open mouth. This is consistent with the CO₂ concentration gradient within the trapped solution as explained above. More dissolution will tend to occur at the open mouth since more hydrogen ions are available to be reduced. Conversely lesser

dissolution will tend to occur farther away from the open mouth since less hydrogen ions are present in the solution in direct contact with the steel surface.

This gradient in the rate of dissolution can have a profound effect on the crack tip morphology and crack growth rate as will be explained in Section 3.3.3.

3.3.1.3 Variation in hydrogen concentration at the crack tip with distance from the open mouth

The final stage in the CO₂ dissolution, Equation 5, above is the production of adsorbable hydrogen. It is a known fact that some of the adsorbable hydrogen migrates into metal lattices, where they tend to cause hydrogen embrittlement which may have a profound effect on cracking [30]. It is also well known that lattice hydrogen tends to segregate to regions with the highest tensile hydrostatic stresses within the metal lattice. For a cracked body, the region with the highest tensile stress corresponds to the plastic zone, otherwise called the process zone [31, 32]. This region may experience a very high level of hydrogen enhanced crack propagation, and the more the amount of hydrogen that segregates here the more intense the rate of hydrogen enhanced crack propagation.

In the absence of a surface film, or where the same amount and type of surface film is formed at all locations inside the disbondment, and where initial mechanical loading is the same, the rate of hydrogen adsorption into the metal lattice at all three crack locations inside the disbondment should be proportional to the concentration of adsorbable hydrogen present at the surface. Hence there should be a higher hydrogen concentration in the lattice at the open mouth. Since initial mechanical conditions at the crack tip are similar at all three locations and more hydrogen is adsorbed into the lattice at the open mouth, a higher lattice concentration at the open

mouth enables the delivery of more hydrogen atoms to the process zone ahead of the crack since hydrogen migration through the lattice is diffusion controlled. This causes more severe hydrogen enhanced crack propagation at the open mouth. This effect should decrease in magnitude with distance from the open mouth.

3.3.2 General understanding of cracking mechanisms of pipeline steels in near-neutral pH environments

The present investigation was conducted primarily to understand 1) how the coating disbondment affects crack growth mechanism 2) the growth rate behavior of surface cracks as compared with that of long through-thickness cracks. In the field, SCC cracking manifests as surface cracks associated with coating disbondment at the pipe surface. Despite this unique crack morphology and its association with coating disbondment, most studies have neglected one or the other component in laboratory simulations of this phenomenon. Also, most studies have employed rather severe loadings rather than the very benign loadings in terms of loading frequency typically experienced in the field. Despite the above uniqueness, it is generally believed that the crack growth mechanisms determined from investigations primarily using compact tension specimens are still applicable.

Crack growth mechanisms of pipeline steels exposed to near neutral pH environments have been traditionally undertaken to understand both the physical process of cracking and the rate behavior of crack growth. The common beliefs are summarized as follows [10]:

- 1) For the physical mechanisms of crack growth, it is generally believed that crack growth proceeds by either or both of the following two processes:

- By dissolution at the crack tip only, which is primarily a process found in the earlier stage of crack growth when the crack is shallow, for example, up to 1 mm, and during the growth of cracks on the pipe surface.
 - By direct cracking of the crack tip through hydrogen embrittlement mechanisms, which is primarily the mechanism of crack growth following the dissolution mechanism in the initial stage.
- 2) When the rate controlling factors are considered, crack growth is believed to be a result of the following competitive processes:
- Crack tip blunting, which results from the dissolution of materials at the crack tip and low temperature creep: The former can cause crack growth but may also cause crack tip blunting because of the non-passivating nature of the corrosion system. The latter occurs when crack grows at a very slow rate or under non-propagating mechanical loading conditions, for example, pressure fluctuating with high R-ratios (minimum stress/maximum stress).
 - Crack tip sharpening, which is caused by fatigue loading and the segregation of hydrogen, a by-product of corrosion, to the crack process zone at and ahead of the crack tip. Crack growth can proceed without a direct exposure of the near neutral pH solution to the crack tip as long as the fatigue component and hydrogen segregation can occur synergistically.

The above two competitive processes have been mathematically synergized through a combined factor in the form of $(\Delta K)^\alpha / K_{\max}^\beta / f^\gamma$, where $\alpha + \beta = 1$ and γ is a factor relevant to corrosiveness of environment or the generation of atomic hydrogen [9, 10]. Based on the above understanding,

the experimental results obtained in this investigation can be rationalized, as discussed in the sections below.

3.3.3 Crack growth mechanisms under disbonded coating

3.3.3.1 Crack growth at the surface tip

Since cathodic protection was not applied, the experiment in this investigation is believed to have simulated the growth of surface cracks exposed to different levels of CO₂. At the open mouth, the aqueous solution was in equilibrium with 5% CO₂ in the gas composition. Down the coating disbondment, the aqueous solution may be considered to be in equilibrium with a CO₂ level progressively lower than 5% CO₂ in the gas mixture except for the initial stage of exposure when the aqueous solution was just introduced into the test cell. In the later situation (early stages), the steel surface within the disbonded coating at all the locations should be exposed to aqueous solution in equilibrium with 5% CO₂+N₂ gas mixture.

With the above consideration, one may try to understand the crack mechanisms at the surface tip, first by taking the growth at the open mouth, where the aqueous solution was always in equilibrium with 5% CO₂ + N₂ gas mixture. The dissolution rate of the X65 pipeline steel in C2 solution in equilibrium with 5% CO₂ + N₂ mixture was measured to be about 1.2×10^{-9} mm/s (~ 0.037 mm/year) [9], which is nearly 3 orders of magnitude lower than the crack growth rate determined at the open mouth, which was $\sim 2 \times 10^{-4}$ mm/cycle or 1.0×10^{-6} mm/s at a loading frequency of 0.005 Hz. The difference may be attributed to the contribution of fatigue loading and hydrogen effects. For the latter effect, the average lattice hydrogen should be the highest at the surface where atomic hydrogen is generated but decreases toward the opposite surface that was isolated from the test solution, as governed by the law of diffusion.

With an increase of distance from the open mouth, crack growth at the surface tip rapidly decreased and stabilized at approximately the same rate at the middle and bottom position. This non-linear profile of growth rate needs further discussion. One could simply relate the growth rate at the surface tip at various positions to the dissolution rate of pipeline steel at those positions. Despite the fact that hydrogen effects on crack growth are predominant, the amount of hydrogen generated should be proportional to the rate of dissolution at the surface. This could rationalize the attempt to correlate the growth rate at the surface tip to the dissolution rate.

It has been observed that the dissolution rate of pipeline steel determined using a setup similar to the one in the present investigation depends on the gap distance between the disbonded coating and the steel surface [33]. When the gap distance was set at about 10 mm, like the one used in the current investigation, a near linear relationship between the rate of dissolution and the distance to the open mouth was found [33]. The abrupt decrease of dissolution rate with increasing distance to the open mouth and an enhancement in dissolution at the open mouth can be found only when the gap is very narrow, for example, 5 mm or less.

The inconsistency between the non-linear crack growth rate at the surface tip and the linear relationship between the dissolution rate at the steel surface and the distance can be bridged by further examining the morphology of the crack tip at various positions. It is clearly shown in Figure 3-8 that the crack tip was so sharp at the open mouth that the crack crevice could hardly be discerned in the microstructure. In contrast, the crack tip at the middle and bottom positions became progressively blunt. In fact, at both locations, the tip is so blunt that it may not be considered to be a “crack” from the definition of fracture mechanics.

Now one may wonder what has caused crack tip blunting at the middle and bottom positions. As briefly discussed in Section 3.3.2, crack tip blunting of pipeline steel in near neutral pH environments is a very common phenomenon that can be caused by:

- 1) Excessive corrosion at the crack tip, particularly in environments with very high CO₂ level, which certainly cannot rationalize the above inconsistency as the CO₂ level is highest at the open mouth but the crack tip is seen to be very sharp instead of blunt;
- 2) Benign fatigue loading, for example, under a near static loading state, which should not be a contributing factor as well since all the cracks were subjected to the same loading scheme and the initial crack dimensions were also almost identical.

It is certain that all the cracks at the beginning of corrosion exposure were sharp as they were fatigue cracked in air by the same scheme. Therefore, there must be a sharp to blunt transition for cracks at the middle and bottom positions of disbonded coating. This suggests that the cracks at the latter positions were growing at least in the initial stage of corrosion exposure. This is also highly possible when environmental conditions were considered. When the fresh solution was added into the cell, the solution was in equilibrium with 5% CO₂ regardless of its position within the disbonded coating. This should lead to a similar situation of growth at all three positions. However, with increasing exposure time, a gradient of CO₂ was gradually formed, which would reduce the environmental driving force at positions farther away from the open mouth.

The above environmental driving force is included in the combined factor, $(\Delta K)^{\alpha}/K_{\max}^{\beta}/f^{\gamma}$, where the term $(1/f^{\gamma})$ is considered to be the environmental factor. In this environmental factor, γ is directly related to the corrosiveness of the environment, which was determined to be

0.1 in C2 solution in equilibrium with 5% CO₂. When the CO₂ level is reduced, the pH of the solution becomes less acidic and the crack growth rate was found to increase linearly with decreasing pH of the solution. Therefore, a lower γ value can be assigned to the middle and the bottom position. For example, the environmental factor $(1/f^\gamma)$ at the open mouth with $\gamma = 0.1$ is calculated to be 1.7 at $f = 0.005$ Hz. When γ is reduced to a third of that at the open mouth, the environmental factor becomes 1.19, which is accompanied with a reduction of the combined factor to $8148 (\text{MPa}\cdot\sqrt{\text{m}})^3/\text{Hz}^{0.033}$ for the crack at the bottom position. The latter is below the threshold value of about $8500 (\text{MPa}\cdot\sqrt{\text{m}})^3/\text{Hz}^{0.1}$ for crack growth. Therefore it is well justified that the surface crack at the middle and the bottom position had been subjected to an environmental driving force transient from a higher value at the beginning of the test to a lower value at the end of the test. This will correspond to a state of crack growth at the beginning of the test and crack dormancy towards the end of the test. This analysis is also consistent with the recorded potential drop data shown in Figure 3-4 for the crack in the middle position. The much blunter tip at the bottom position than the middle position reflects a smaller γ value at the bottom and therefore less driving force for growth.

The transition from a growing state to a non-growing state has been reported previously. A sharp crack produced by pre-fatigue in air was loaded to combined factors below the threshold value and the crack was found to grow in the initial stage of approximately 10 days from the potential drop curves recorded but ceased to grow afterwards [9]. A crack tip morphology very similar to what is seen in Figure 3-8b and 3-8c) was found. In this reported example, the transition from propagating state to non-propagating state was caused by initial sharp state of the crack tip. In the present investigation, the crack tip also experienced a decreasing environmental

driving force due to coating disbondment. The transition from the growing state to non-propagating state could take place even sooner.

Increased blunting of the crack tip with distance from the open mouth of the disbondment cannot be explained by crack tip dissolution as dissolution is highest at the open mouth. The blunting seen at the crack tip in this investigation should be attributed to the occurrence of low temperature creep. When the crack is not propagating, the material at the crack tip will have more time available for time-dependent creep deformation to take place. The much blunter tip at the bottom position than at the middle position indicates that the crack tip at the bottom position must have suffered from more creep deformation, probably because of much shorter propagating period due to much smaller environmental driving force.

The above analysis has finally allowed us to understand the non-linear relationship between the average growth rate at the surface tip and the distance to the open mouth. It is obvious that crack growth at the middle position and the bottom position occurred only in the early stage of the test, for example, approximately 10 days or shorter, especially for the bottom crack. This could increase the average crack growth at the surface tip by at least 2 times, which would make the average crack growth rate curve of the surface tip approach a near linear state and positioned above the average growth rate curve of the crack in the depth direction, as illustrated in Fig. 3-13. The latter conclusion will be further discussed after the crack growth mechanisms in the depth direction are discussed below.

The above discussion has been made based on the crack growth at the bottom position and by assuming a reduced environmental factor with $\gamma = 0.033$, which is only a third of the value used for the open mouth position. One may wonder if the assumption of $\gamma = 0.033$ at the

bottom position is realistic. It is believed that an assumption of $\gamma = 0.033$ is rather conservative. The final combined factor at the surface tip at bottom position was calculated to be 16709 (MPa· $\sqrt{\text{m}}^3/\text{Hz}^{0.1}$) when $\gamma = 0.1$ is used. This would yield a combined factor of about 11737 (MPa· $\sqrt{\text{m}}^3/\text{Hz}^{0.033}$) at end of the test if $\gamma = 0.033$. This suggests that the surface tip at the bottom position was propagating at end of the testing, which is inconsistent with the crack tip morphology observed. Therefore, a γ value lower than 0.033 as assumed must have existed at the location, especially after the CO_2 gradient along the disbonded coating was established during the test.

3.3.3.2 Crack growth at the depth tip

It is interesting that the crack tip morphologies at the depth tip at all three locations were quite similar. The tip was not as sharp as the one seen at the surface tip at the open mouth, but was much sharper than that at the surface tip at the middle and bottom positions. These observations suggest that the growth rate behavior in the depth direction at all three locations was quite similar. As shown in Figure 3-13, the average growth rate was progressively lower but not significantly different with increasing distance to the open mouth. The initial combined factors at the depth tip was at 8725, 8535 and 8918 (MPa· $\sqrt{\text{m}}^3/\text{Hz}^{0.1}$) for the open mouth, middle position and bottom position, respectively. When the environmental driving force was reduced, for example, with $\gamma = 0.033$, the combined factor at the depth tip of the middle crack at the beginning of test should be well below the threshold value of 8500 (MPa· $\sqrt{\text{m}}^3/\text{Hz}^{0.1}$) determined using compact tension specimens. This also suggests the possible occurrence of dormancy during the test, which is also consistent with the blunt appearance of the crack tip in the depth direction.

Again, it should be pointed out that the γ value at the beginning of test should be equal to 0.1 at all locations as discussed previously. The initial growth would also make the combined factor higher. The growth rate should reduce and the crack in the depth direction may cease to grow when the γ value was reduced at the later stage due to the establishment of a CO₂ gradient in the disbanded area. However, the transition to a dormant state should be much less likely at the depth tip of the crack at the open mouth. The substantial growth at the open mouth may have increased the combined factor to or above the threshold value.

There seems one remaining issue to be addressed: why does the surface crack tip grow at relatively higher rate than the depth tip? For example, taking the crack at the open mouth as an example, both the surface crack and the depth crack at this location had been growing all the time. However, the growth rate at the surface tip was much higher than at the depth tip. Although a clear answer to this can be extremely difficult, the following factors can be considered:

First, the lattice surrounding the crack tip at the surface should have much higher diffusible hydrogen than that surrounding the depth tip because of diffusion gradient of hydrogen atoms. This would seem to make the environmental driving force higher at the surface tip. However, the surface tip is under a plane stress state, which could cause much less extent of segregation of atomic hydrogen in the plastic zone at or ahead of the crack tip (crack process zone). It is the amount of segregated hydrogen in the crack process zone that is responsible for the cracking.

Second, the comparison is made under different combined factors. A more justified comparison would be when the initial mechanical driving force, $(\Delta K)^\alpha / K_{\max}^\beta$, was the same both at the surface tip and the depth tip. With such a consideration and because of much higher initial $(\Delta K)^\alpha / K_{\max}^\beta$ value at the surface tip in the current investigation, the crack growth rate at the depth tip, if crack growth can occur, should be higher than what is shown in Figure 3-12.

The less blunt appearance of the depth tip (Figure 3-10) could also be related to its plane strain state as compared with the plane stress state at the surface. Under the same level of applied stress intensity factor, a plane stress state would form a much larger size of (~ 3 times bigger) plastic zone ahead of the crack tip and much higher plastic deformation. Since low temperature creep is a result of motion of existing mobile dislocations, the higher plastic strain at the crack tip would create more mobile dislocations and therefore much higher low temperature creep deformation, which would lead to a blunter crack tip.

The above observation in fact reflects one of the most important characteristics of near-neutral pH cracks found in the field. The aspect ratios of the cracks (depth/surface length) is seen to decrease as the cracks grow, indicating the slower growth at the depth direction, and then to be stabilized at around 0.1 (a/c) at a depth of about 1 mm, which is also the depth at which over 95% of cracks are seen to be dormant [10]. Despite that cracks with such small aspect ratios should have much higher mechanical driving force at the depth tip, the depth tips remain non-propagating until less than 5% of them are subjected to an increased combined factor [9, 10, 34, 35]

3.3.4 Growth rate behavior of surface cracks under disbonded coating

The growth rate behavior is important as it serves as a base for residual life prediction and integrity management in the field. The growth rate behavior of long through-thickness cracks is relatively well established and the growth rate can be correlated to a combined factor with a trend represented by the dashed line in Figure 3-15. In the current investigation, only complete data from the crack at the open mouth are available for analysis, which is also plotted as a

function of the combined factor with $\gamma = 0.1$ in Figure 3-15. In this figure, the crack growth in the depth direction was assumed to occur during the entire period of exposure despite that dormancy at the depth direction at the open mouth may have occurred.

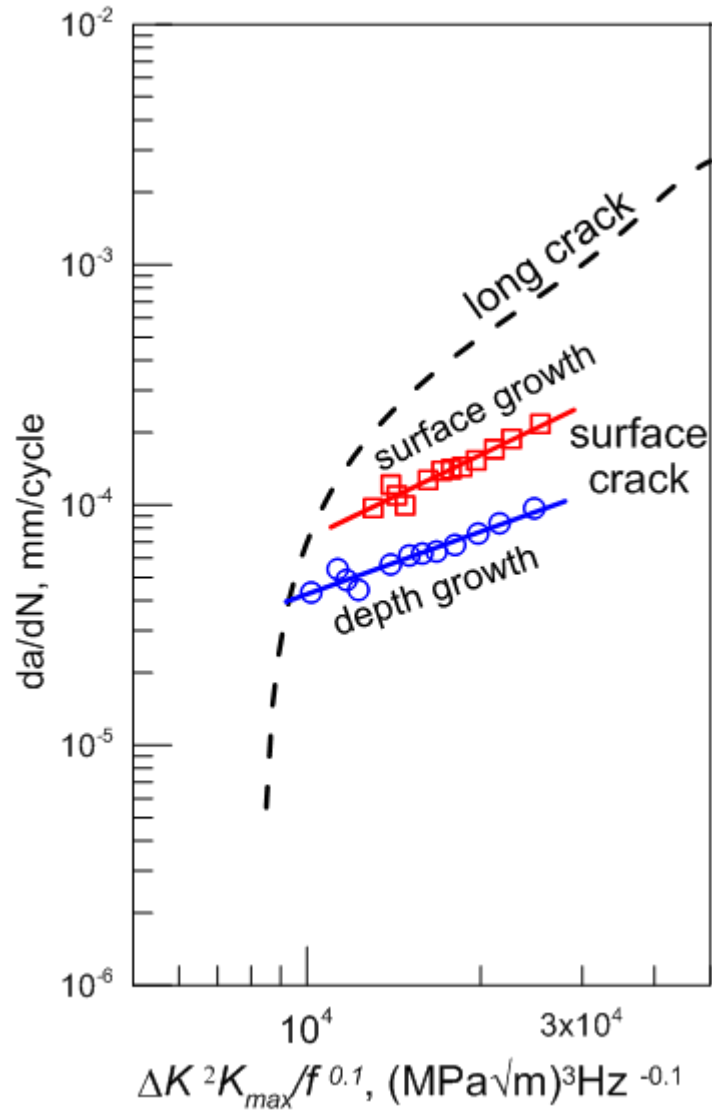


Figure 3-15: Comparison of the corrosion fatigue behavior of crack growth data at the open mouth to that of a through-thickness crack.

The crack growth rate behavior of the surface crack has two distinct features when compared with the growth rate behavior of the long through-thickness cracks exposed to the same environment:

- 1) Surface cracks grow at a lower rate than the long through-thickness crack in the current system when rationalized to the combined factor (Figure 3-15). This is surprisingly different from the general belief that surface cracks can grow at a rate at least the same as long through-thickness cracks if not higher.
- 2) The growth rate of surface cracks is less sensitive to the combined factor compared to long through-thickness cracks.

It is believed that all the above disagreements can be bridged when the environmental specifics of surface cracks and through-thickness cracks, as briefly summarized below, are compared.

- 1) Dissolution is affected by different environmental access paths: the crack tip at the surface can be considered to be exposed to the same environmental conditions as it grows. Surface cracks and through-thickness cracks in CT specimens are no different in this regard. However, for the crack tip away from the surface, the environmental conditions can be very different between the two types of cracks. The different path length will create mini-scale effects of coating disbonding in terms of CO₂ gradient and the environmental driving force for crack growth. Under this situation, the crack crevice will serve as a mini-gap in a way similar to the gap between the surface of the specimen and the disbonded coating being

created in the experimental setup used in this investigation. However, it is hard to determine which type of cracks would be more susceptible to overall crack growth.

- 2) The hydrogen effects are affected by different environmental paths. For a CT specimen, hydrogen is generated on both sides of surface and diffuses to the middle wall of the specimen where lattice hydrogen concentration is the lowest at the beginning but will approach the concentration at the surface with increasing time. The surface crack in the current investigation is designed to simulate the situation in the field and hydrogen is generated only on the surface with the crack and diffuses to the other surface where hydrogen concentration is assumed to be zero. A much weaker hydrogen effect should be expected at the depth crack tip compared to the surface tip.
- 3) Tunneling effects: the crack tip in the middle wall position of CT specimen propagates much faster than the surface tip, as observed in Ref [9] most likely because of factor 2) above and a near plane strain condition. This could increase the crack growth rate at the surface tip of CT specimen because the un-cracked ligament at the surface may bear an increased mechanical driving force when the middle wall tip advances ahead of the surface tip. In contrast, the depth tip of a surface crack is found to grow much slower probably because of hydrogen effects as identified above.

It should be pointed out that the current investigation has not been aimed at determining the threshold of crack growth of surface crack as compared with that determined for the long through-thickness cracks. Cracks in the field frequently and repeatedly become dormant because of the nature of pressure fluctuations. Determining the threshold combined factor above which a

surface crack with sharp tip can start to grow is less meaningful than determining the threshold conditions at which a dormant crack is to be reactivated. The latter is beyond the scope of the current investigation but will be one of our focuses in the future.

3.4 Conclusions

This study examined the effects of variation in the concentration of CO₂ in a near neutral pH environment on the rate of propagation of cracks under a coating disbondment. Among the main findings are:

1. A large disbondment on a pipeline may set up a CO₂ concentration gradient that induces electrochemical processes that significantly affects crack growth behavior.
2. This variation in CO₂ concentration gradient induces a hydrogen concentration gradient from the open mouth to the far end of the disbondment.
3. With 5% CO₂ in the bulk solution surrounding the disbonded site, highest growth rate was obtained at the open mouth while growth rates were similar at 75 mm and 150 mm from the open mouth.
4. The growth rate pattern suggested that hydrogen induced environmental contribution can amplify the mechanical driving force for crack propagation such as at the open mouth
5. Analysis suggests environmental factors could be three times higher at the open mouth than at the locations farther from the open mouth.
6. A combination of low temperature creep and dissolution in the presence of less severe environmental crack propagation enhancement could lead to crack tip blunting. More specifically, while the less severe environmental effects reduce the growth rate, low

temperature creep aids crack tip blunting. Such low temperature induced blunting may delay crack re-initiation when more aggressive loading conditions are introduced.

7. Growth rates were found to be more significantly enhanced at the surface than in the depth direction. The disparity in growth rates was highest at the open mouth where growth was almost two times higher at the surface than in the depth direction
8. Such disparity in growth at the surface compared to that at the depth tip explains why NNPHSCC cracks often have very low aspect ratios (≤ 0.1). Cracks propagate faster at the surface than in the depth direction making them long in the longitudinal direction but shallow in the depth direction.

3.5 References

- [1]. National Energy Board, 1996, "Public Enquiry Concerning Stress Corrosion Cracking on Canadian Oil and Gas Pipelines," Report # MH-2-95.
- [2]. Delanty, B., and O'beirne, J., 1992, "Major Field Study Compares Pipeline SCC with Coatings," Oil and Gas Journal, **90**(24) pp. 39-44.
- [3]. Colwell, J. A., Leis, B. N., and Singh, P. M., 2005, "Recent Developments In Characterizing The Mechanism Of Near Neutral pH SCC," Corrosion/2005; Houston, TX; USA; 3-7 Apr. 2005, paper no. 05161.
- [4]. Parkins, R. N., 2000, "A review of stress corrosion cracking of high pressure gas pipelines," Corrosion 2000, NACE, Orlando, FL.
- [5]. Parkins, R.N., 1999, "A review of stress corrosion cracking of pipelines in contact with near-neutral (low) pH solutions," PRCI, Report for the Line Pipe Research Supervisory Committee of PRC International, .
- [6]. Charles, E. A., and Parkins, R. N., 1995, "Generation of Stress-Corrosion Cracking Environments at Pipeline Surfaces," Corrosion, **51**(7), pp 518-527.
- [7]. Brousseau, R., and Qian, S., 1994, "Distribution of Steady-State Cathodic Currents Underneath a Disbonded Coating," Corrosion, **50**(12) pp. 907-911.
- [8]. Yan, M., Wang, J., Han, E., 2008, "Local Environment Under Simulated Disbonded Coating on Steel Pipelines in Soil Solution," Corrosion Science, **50**(5) pp. 1331-1339.
- [9]. Chen, W., and Sutherby, R. L., 2007, "Crack Growth Behavior of Pipeline Steel in Near-Neutral pH Soil Environments," Metallurgical and Materials Transactions A, **38A**(6) pp. 1260-1268.

- [10]. Chen, W., Kania, R., Worthingham, R., 2009, "Transgranular Crack Growth in the Pipeline Steels Exposed to Near-Neutral pH Soil Aqueous Solutions: The Role of Hydrogen," *Acta Materialia.*, **57**(20) pp. 6200-6214.
- [11]. Eslami, A., Chen, W., Worthingham, R.G., 2011, "Effect of CO₂ on Near-Neutral pH Stress Corrosion Cracking Initiation of Pipeline Steel," *Corrosion Science* , 53, pp. 2318–2327
- [12]. McClung, R. C., and Sehitoglu, H., 1992, "Closure and Growth of Fatigue Cracks at Notches", *ASME Journal of Engineering Materials Technology*, **114**, pp. 1-7.
- [13]. Haddad, M. H. E., Topper, T. H., and Mukherjee, B., 1981, "Review of New Developments in Crack Propagation Studies," *ASTM Journal of Testing and Evaluation*, **9**(2) pp. 65-81.
- [14]. Fine, M.E., and Richie, R.O., 1979, "Fatigue and Microstructure", American Society for Metals, Metals Park, Ohio, pp. 245.
- [15]. Gangloff, R.P., 1983, "Advances in Crack Length Measurement", *Engineering Materials Advisory Ltd.*, Warley, West Midlands, pp. 175.
- [16]. Hudak, S. J., and , J., 1981, "Small Crack Behavior and the Prediction of Fatigue Life," *Journal of Engineering Materials and Technology (Transactions of the ASME)*, **103**(1) pp. 26-35.
- [17]. Schijve, J., 1982, "Fatigue Thresholds" , *Engineering Materials Advisory Ltd.*, Warley, West Midlands, pp. 881.
- [18]. El Haddad, M. H., Smith, K. N., and Topper, T. H., 1979, "A Strain Based Intensity Factor Solution for Short Fatigue Cracks Initiating from Notches," *Fracture Mechanics ASTM STP 677*, pp. 274-289-289.

- [19]. Leis, B. N., and Forte, T. P., 1981, "Fatigue Growth of Initially Physically Short Cracks in Notched Aluminum and Steel Plates," pp. Fracture Mechanics; Philadelphia; Pa.
- [20]. Leis, B.N., and Galliher, R.D., 1982, "Fatigue and Life Prediction, ASTM STP 770," American Society for Testing and Materials, pp. 399-421.
- [21]. Leis, B. N., 1982, "Fatigue Crack Propagation through Inelastic Gradient Fields," International Journal of Pressure Vessels and Piping., **10**(2) pp. 141-158.
- [22]. Shin, C. S., and Smith, R. A., 1988, "Fatigue Crack Growth at Stress Concentrations--the Role of Notch Plasticity and Crack Closure," Eng.Fract.Mech., **29**(3) pp. 301-315.
- [23]. Sun, S., Shiozawa, K., Gu, J., 1995, "Investigation of Deformation Field and Hydrogen Partition Around Crack Tip in Fcc Single Crystal," Metall. Mater. Trans.A, **26A**(3) pp. 731-739.
- [24]. Shin, C. S., and Smith, R. A., 1985, "Fatigue Crack Growth from Sharp Notches," Int.J.Fatigue.Vol.7, **7**(2) pp. 87-93.
- [25]. Tanaka, K., and Nakai, Y., 1983, "Propagation and Nonpropagation of Short Fatigue Cracks at a Sharp Notch," Fatigue Eng. Mater. Struct., **6**(4) pp. 315-327.
- [26]. SEHITOGLU, H., 1983, "Fatigue Life Prediction of Notched Members Based on Local Strain and Elastic--Plastic Fracture Mechanics Concepts," Eng. Fract. Mech., **18**(3) pp. 609-621.
- [27]. Sehitoglu, H., 1985, "Characterization of Crack Closure," Fracture Mechanics: Sixteenth Symposium; Columbus, (868) pp. 361-380.
- [28]. Eslami, A., Fang, B., Kania, R., 2010, "Stress Corrosion Cracking Initiation Under the Disbonded Coating of Pipeline Steel in Near-Neutral pH Environment," Corrosion Science, **52**(11) pp. 3750-3756.

- [29]. S. Asher, P. Singh, J. Colwell, B. Leis. *Crack Initiation of Line Pipe Steels in Near-Neutral pH Environments. 16th International Corrosion Congress*. 2005. Beijing, China
- [30]. Li, J. C. M., Oriani, R. A., and Darken, L. S., 1966, "Thermodynamics of Stressed Solids," *Z. Physik. Chem.*, **49**, pp. 271-290.
- [31]. Gangloff, R. P., 2003, "In: *Comprehensive Structural Integrity*", I. Milne, R.O. Ritchie, and B. Karahaloo, Eds., Elsevier Science, New York, NY, **6**, pp. 31-101.
- [32]. Thomas, R. L. S., Scully, J. R., and Gangloff, R. P., 2003, "Internal Hydrogen Embrittlement of Ultrahigh-Strength AERMET 100 Steel," *Metallurgical and Materials Transactions A*, **34A**(2), pp. 327-344A.
- [33]. Chevil, K., Eslami, A., Chen, W., 2012, "Developing Cathodic Protection Based On Disbondment Geometry", *International Pipeline Conference 2012*,. Paper no. 90675.
- [34]. Chen, W., King, F., and Vokes, E., 2002, "Characteristics of Near-Neutral-pH Stress Corrosion Cracks in an X-65 Pipeline," *Corrosion*, **58**(3) pp. 267-275.
- [35]. Bouaeshi, W., Ironside, S., and Eadie, R., 2007, "Research and Cracking Implications from an Assessment of Two Variants of Near-Neutral pH Crack Colonies in Liquid Pipelines," *Corrosion (Houston)*, **63**(7) pp. 648-660.

CHAPTER FOUR

**SURFACE CRACK INITIATION AND GROWTH OF PIPELINE STEELS
UNDER DISBONDED COATING IN NEAR-NEUTRAL PH SOIL
ENVIRONMENTS AFTER ENVIRONMENTALLY INDUCED CRACK TIP
BLUNTING**

4.0 Introduction

Since it was first identified in the mid '80s, near-neutral pH stress corrosion cracking (NNPHSCC) has remained a virile integrity risk for oil and gas pipelines [1]. Although pipeline integrity groups have developed means of mitigating catastrophic failures, NNPHSCC still remains a major threat to pipeline integrity. This problem often occurs where coatings are disbanded or where there are coating imperfections on the surface of a pipe or where coatings are tented, often along the toe of a seam weld. These cracks are usually trans-granular in nature and are most frequently formed under disbanded polyethylene tape coated pipes [1, 2].

NNPHSCC remains a major problem to oil and gas pipeline integrity managers mainly because of insufficient understanding of the initiation and propagation mechanisms. Although it is generally accepted that the near-neutral pH environment plays a role in the development and propagation of these cracks, proper understanding of the role played by the environment or the species in it are at best still evolving [3-7].

In the field, the CO₂ involved in the development of the SCC environment comes from the decay of organic matter in the soil [2, 8]. Delanty and O'Beirne [1] found that CO₂ concentration in the bulk soil solution adjacent to the pipe surface varies significantly with the seasons. For instance soil CO₂ levels were 4% in winter but could be up to 23% in spring. Since carbonic acid concentration is directly related to CO₂ concentrations, carbonic acid concentrations can also be expected to vary with the seasons. Delanty and O'Beirne's measurements revealed that carbonic concentration in the soil water was 20 times higher in winter. This means that pipelines with disbanded coatings are exposed to higher levels of acidity and lower pH, in winter. Therefore, dissolution rates should be more intense in winter and

pipelines may experience more localized type of corrosion, e.g. pitting, under this condition. Increased dissolution may also increase crack tip blunting and may lead to crack dormancy. Beavers and Harle [9] have proposed that crack growth may occur only during the fall and winter months when soil acidity is higher and trapped solutions are more concentrated and crack dormancy or near dormancy may occur during spring and summer months.

It is known that CO_2 plays a major role in maintaining the pH of the solution at the pipeline surface in the near neutral range when cathodic protection currents are being applied. Ordinarily, when water dissociates by the reaction $2\text{H}_2\text{O} + 2e \rightarrow \text{H}_2 + 2\text{OH}^-$ or $\text{O}_2 + 2\text{H}_2\text{O} + 4e \rightarrow 4\text{OH}^-$, the generation of hydroxyl ions causes the pH of the solution to increase. In the absence of CO_2 , the pH may increase to about 11-12 [10]. However, when CO_2 is present, CO_2 dissolves in groundwater to form carbonic acid by the reaction $\text{CO}_2 + \text{H}_2\text{O} \rightarrow \text{H}_2\text{CO}_3$ which can further react with water to produce a hydronium ion and a bicarbonate ion by $\text{H}_2\text{CO}_3 + \text{H}_2\text{O} \rightarrow \text{H}_3\text{O}^+ + \text{HCO}_3^-$ [8, 11]. The bicarbonate ion is weakly basic while the hydronium ion is an acid radical. The formation of this pair of ions lowers the pH of the solution to the near neutral range, if CO_2 is present at a sufficiently high partial pressure. Apart from its influence on the pH of the solution, hydronium ions can be reduced to furnish hydrogen gas at the pipe surface. This reduction reaction is another major source of hydrogen in NNP HSCC.

It is widely believed that crack propagation rates increase with increasing concentration of CO_2 [12-15]. However it has been noted that CO_2 concentration may have the opposite trend on crack initiation. Cracks are usually initiated from the bottom of corrosion pits. Increasing CO_2

tends to increase the rate of general corrosion preventing the development of pits and probably blunting the tips of shallow cracks or obliterating shallow cracks altogether where the dissolution rate is high enough [16].

There has been no systematic study aimed at determining the effect of CO₂ levels on the growth of surface type NNPHSCC flaws. This study along with the other manuscripts under preparation from this study reports recent findings on the role of CO₂ levels in the propagation of stress corrosion cracks in near-neutral pH environments.

4.1 Experimental

4.1.1 Sample preparation

Tensile specimens (Figure 4-2) bearing three reduced sections were machined from the longitudinal direction of a X65 pipe section that had failed in service. The alloy composition is shown in Table 4-1, while a typical alloy microstructure is shown in Figure 4-1. Only pipe sections unaffected by NNPHSCC and other forms of corrosion, and external damage were used. Gauge sections were 23 mm × 45 mm × 9.2 mm in dimension and identical semi-circular shallow notches, 0.20 mm wide, with dimensions $c = 5$ mm and $a = 2.5$ mm were made by electrical discharge machining (EDM) in the middle of each gauge section.

Table 4-2: Alloy (X65) composition

| Element | Composition (wt %) |
|------------|--------------------|
| Carbon | 0.13 |
| Manganese | 1.55 |
| Copper | 0.05 |
| Niobium | 0.05 |
| Chromium | 0.08 |
| Molybdenum | 0.01 |
| Vanadium | 0.002 |
| Nickel | 0.05 |
| Aluminum | 0.042 |
| Titanium | 0.002 |
| Nitrogen | 0.009 |
| Iron | Balance |

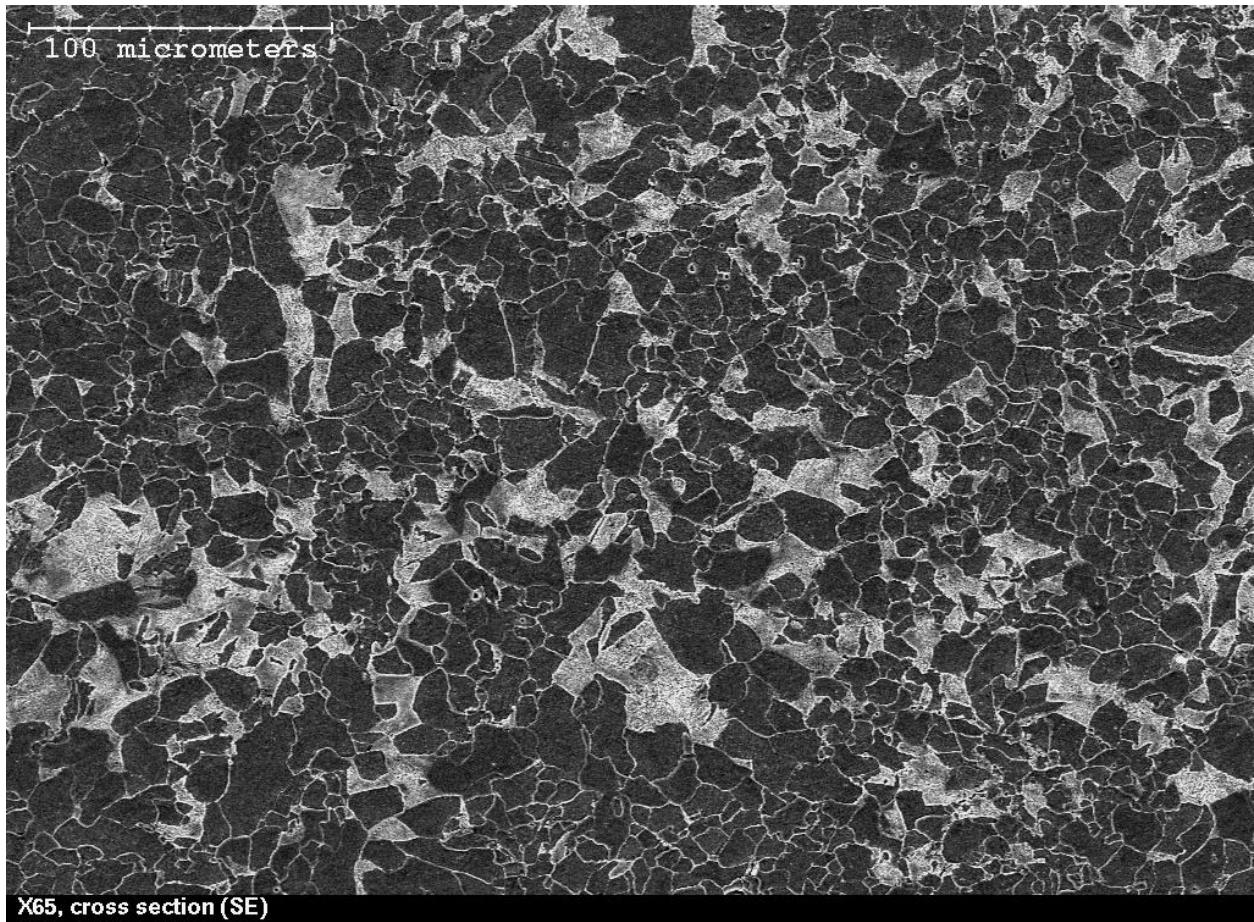


Figure 4-1: Typical microstructure of the alloy X65 used in this study

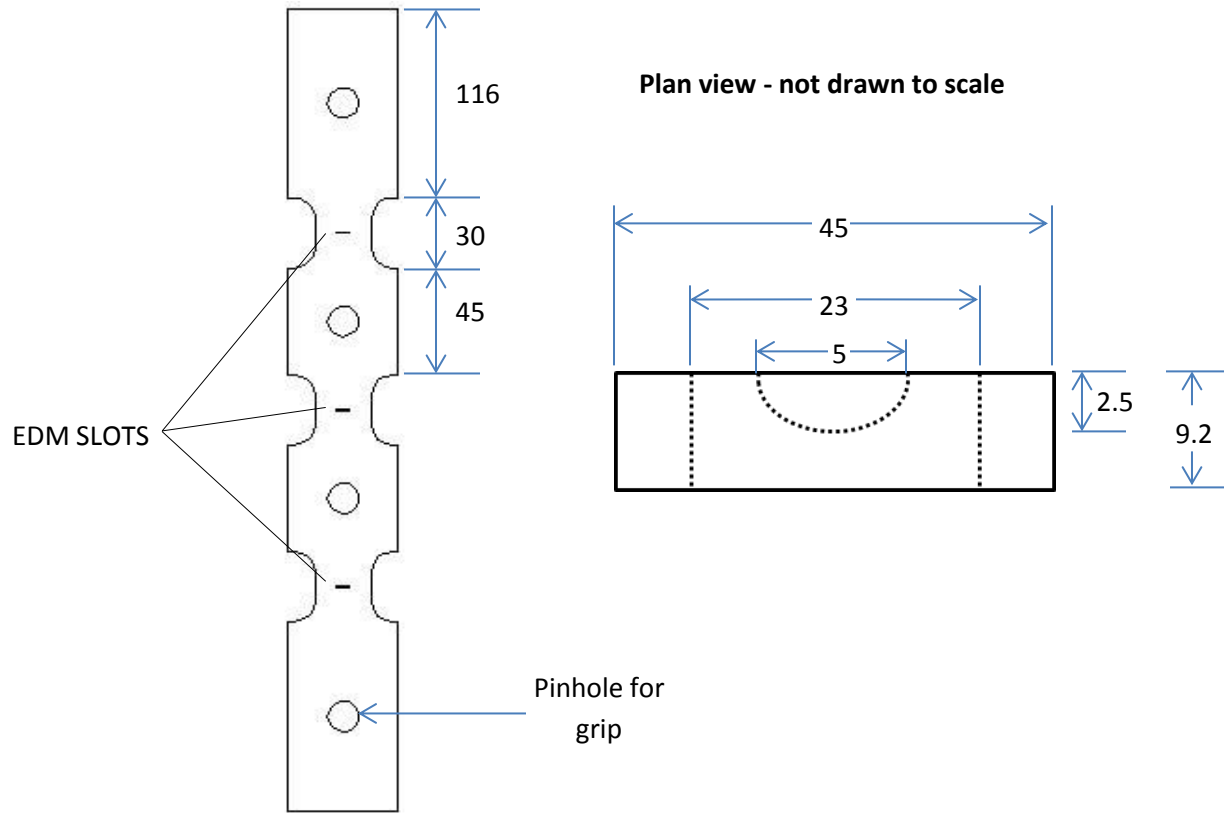


FIGURE 4-2: Test sample designed for this study

A corrosion test cell consisting of two chambers was designed and fabricated from acrylate (Figure 4-3). The inner tube, named the shielding, was designed to simulate coating disbondment at the surface of a pipe. The width of this inner tube was 20 mm and the sample was centered in the simulated disbondment. The outer tube holds the bulk solution which simulates the surrounding soil around a pipe in the field while the solution contained in the inner shielding simulates the solution trapped between the coating and the pipe surface on an actual pipeline.

The corrosion medium used was C2 solution (0.0035 KCl, 0.0195 NaHCO₃, 0.0255 CaCl₂.H₂O, 0.0274 MgSO₄.7H₂O, 0.0606 CaCO₃ g/l), which was purged with either 5% CO₂ + N₂ or 20% CO₂ + N₂ gas mixture for 48 hours prior to starting the test in order to remove dissolved oxygen and to establish a pH of 6.23 and 5.8, respectively. Purging of the test solutions with CO₂ + N₂ gas mixture was also maintained during the corrosion exposure, which was fed in through openings at the bottom of the cell, so that the gas mixture can only diffuse into the simulated disbondment from the open mouth.

For the tests reported in this paper, a maximum stress of 75% specified minimum yield strength and a cyclic frequency of 0.005 Hz were used for both tests. Three tests were performed to investigate the effect of environments on crack growth in near neutral pH conditions under disbonded holidays. A summary of test conditions is given in Table 4-2. Test I was carried out at a single stress ratio of 0.4. A series of stress ratios was used for tests II and III. The rationale behind the tests with different R-ratios is provided in Section 4.2. Tests III and II lasted for about 5 months while test I only lasted for about 23.2 days. Test III was purged with 20% CO₂ while tests I and II were purged with 5% CO₂.

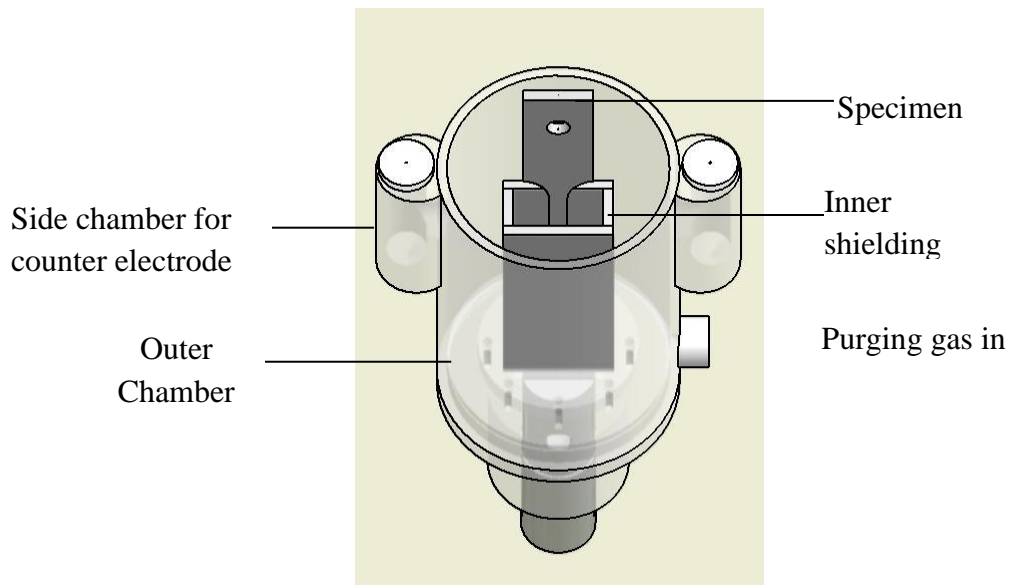


Figure 4-3: Schematic drawing of the corrosion test cell used for study

Table 4-2: Test conditions

| Test conditions | Test 1 | Test II | Test III |
|--|---------------------------------------|---|---|
| Maximum stress | 0.75 SMYS | | |
| Test environments | C2 solution | | |
| Purging gas | 5%CO ₂ +N ₂ Bal | | 20% CO ₂ + N ₂ Bal. |
| Pre-test pH | 6.3 | | 5.6 |
| R-ratio/duration | 0.4/23.2 days | 0.65/14 days 0.6/14 days 0.58/14 days 0.56/14 days 0.53/14 days 0.50/7 days ¹ 0.47/7 days 0.43/7 days 0.40/7 days ² 0.37/7 days 0.33/7 days 0.30/7 days 0.27/7 days | |
| | | 0.22/4.5 days | 0.22/7 days |
| Combined factor at start of test [(MPa√m) ³ Hz ^{-0.1}] | 8770 | 3250 | 3250 |
| Combined factor at the R-ratio at which crack started to grow [(MPa√m) ³ Hz ^{-0.1}] | 8770 | 14330 | 14330 |

¹Approximately the R ratio at which the combined factor at the surface tip of crack reaches the threshold for continuous growth when crack tip is sharp

²Approximately the R ratio at which the combined factor at the tip of crack in the depth direction reaches the threshold for continuous growth when crack tip is sharp

In an attempt to closely simulate real pipeline service conditions, the sides and back surface of each specimen (the one without the surface cracks) were coated with epoxy in order to isolate these surfaces from the corrosion media. Crack growth rates were monitored using a custom made potential drop system through copper wire leads spot welded to the back surface across the EDM slots in each gauge section. A constant current of 20A was applied by the potential drop system in order to measure the potential drop across each crack.

4.1.2 Mechanical loading

Chen and Sutherby [17] developed a corrosion-fatigue model that identified crack growth threshold conditions for X65 pipeline steel to be below $8500 \text{ (MPa}\cdot\text{m)}^3/\text{Hz}^{0.1}$ in C2 solution. For the current study, a combined factor of $4570 \text{ (MPa}\cdot\text{m)}^3/\text{Hz}^{0.1}$ at the sample surface and $3250 \text{ (MPa}\cdot\text{m)}^3/\text{Hz}^{0.1}$ in the depth direction was selected for tests II and III. Other testing conditions are summarized in Table 4-2. Such low combined factors were selected since the aim of this study was to determine the effect of environmentally induced crack tip blunting on crack re-initiation and propagation. The initial testing conditions for test I are as reported in our earlier report and are also summarized in Table 4-2. The goal was to study the effect of dissolution induced crack tip blunting on subsequent crack propagation after crack re-initiation.

4.1.3 Post-test Analysis

After each test, the fracture surface was examined and post-test crack lengths determined in order to validate potential drop measurements with actual crack growth measured from the surface of fractured specimens. Prior to fracture surface examination, iron oxide-type corrosion products were removed using a rust remover solution composed of water (100ml), HCl (3ml),

and cis-2-but-1-4-diol (4ml). Initial fracture face examination was done using an optical microscope. More detailed examination of fracture surfaces was carried out using a Hitachi scanning electron microscope equipped with an energy dispersive x-ray spectrometer for chemical compositional analysis.

4.2 Results

Post-test low magnification examination of the corroded surfaces reveals the presence of corrosion deposits on the surface of the samples. A large amount of corrosion products was found implanted in the cracks in test III while much lesser amount of corrosion products were formed on the surface in tests I and II. These corrosion products were analyzed to be FeCO_3 , Fe_2O_3 and FeOOH by powder mode x-ray diffraction technique. When the corrosion products were removed, only general corrosion was found at all three locations.

In a previous publication (chapter 3) the growth behavior of a sharp surface crack under conditions where crack propagation spontaneously occurs was examined. These test conditions corresponded to test I in this study. A summary of this result is briefly provided in the next subsection. The remaining tests were designed to determine the effect of both the mechanical and environmental factors on the crack growth re-initiation and subsequent propagation mechanisms of the cracks that were loaded initially under non-propagating conditions. The non-propagating conditions were determined based on the threshold value of the combined factor expressed as

$$(\Delta K)^{\alpha}/K_{\max}^{\beta}/f^{\gamma}.$$

4.2.1 Crack growth behavior of sharp crack under propagating loading in 5% CO₂ (Test 1)

Crack propagation started at a stress ratio of 0.4 and was not preceded by any period of dormancy. The extents of crack propagation during the test at the three different locations are compared in Figure 4-4. The most rapid crack propagation occurred at the open mouth of the disbondment while the least growth occurred at the far end of the disbondment (150 mm from the OM). There was a higher crack opening at the pre-crack tip at the open mouth while comparable crack tip opening could be observed at 75 mm and 150 mm from the open mouth. Higher magnification examination of the post-test crack tip reveals a significant difference in the crack opening size just behind the crack tip (Figure 4-5). At the open mouth, the crack tip was very sharp – much sharper than the crack tip at the other two locations inside the disbondment while the crack tip was bluntest at 150 mm from the open mouth. All cracks were transgranular in nature. The same trend was observed in the depth direction.

It was analyzed that the cracks at 75 and 150 mm positions were propagating during the initial stage of exposure but became dormant as they propagated. This was related to the fact that the environments at all the locations within the disbonded coating were the same at the beginning of exposure but had developed a concentration gradient corresponding to the different level of CO₂ in equilibrium with water that decreases with increasing distance from the open mouth. The crack tip became blunter as it moved away from the open mouth, which was caused by the occurrence of low temperature creep rather than the corrosion at the crack tip. The latter should also decrease with increasing distance from the open mouth and therefore would contribute less to the crack tip blunting through dissolution if any dissolution occurred.

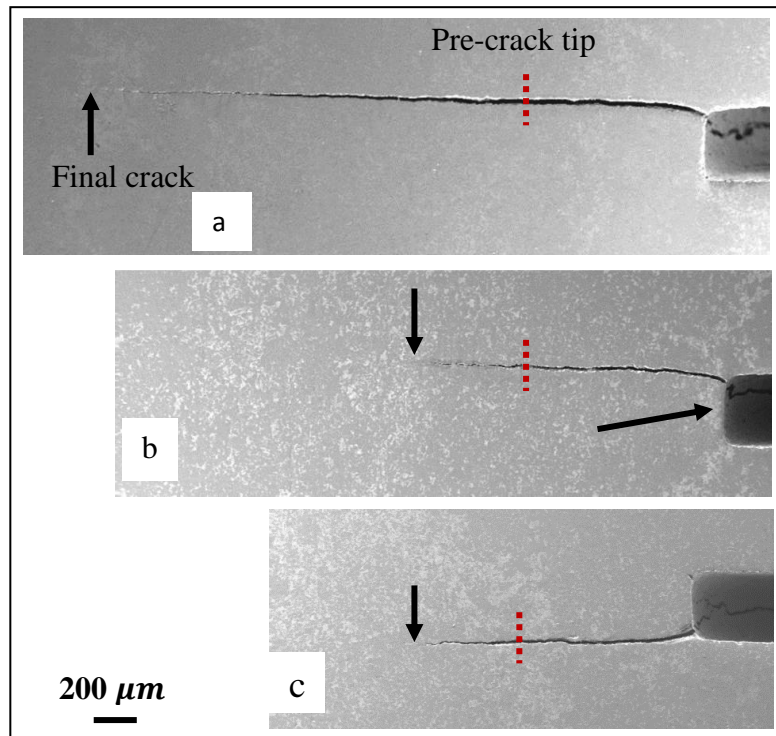


Figure 4-4: Low magnification image of pre-crack tip and crack tip (a) open mouth (b) 75 mm from the open mouth (c) 150 mm from the open mouth

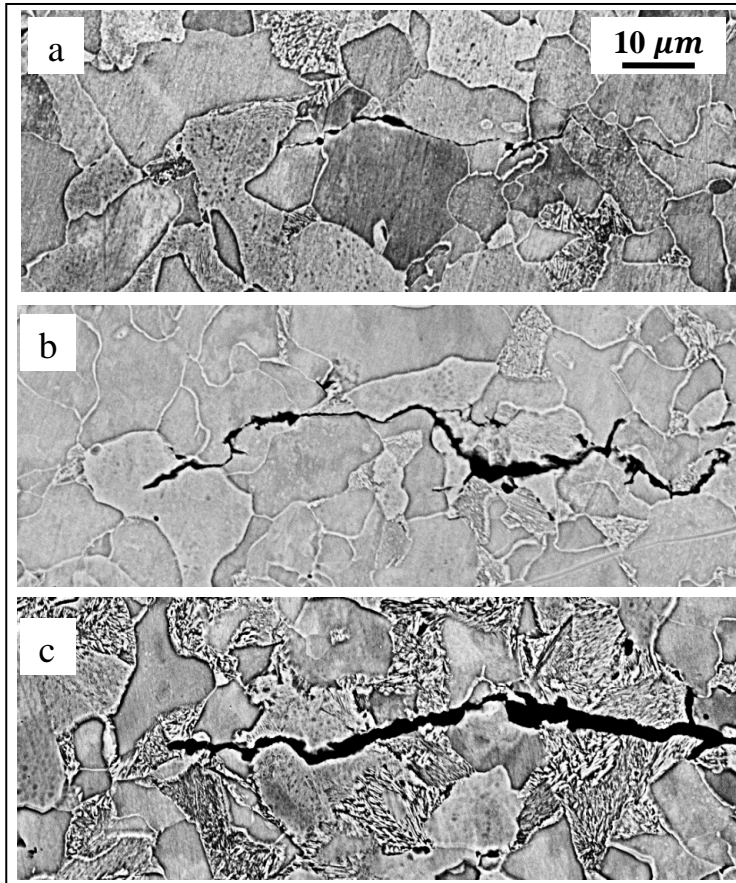


Figure 4-5: High magnification image of the crack tip width measured at sample surface

(a) open mouth, (b) 75 mm from open mouth, (c) 150 mm from open mouth.

4.2.2 Crack growth behavior of sharp crack preceded by non-propagating loading in 5% CO₂ (Test II)

Test I is an idealized situation under which the crack tip from pre-fatigue crack in air prior to corrosion exposure was sharp and the initial mechanical condition measured by a combined factor was also above the threshold such that immediate growth occurred as soon as corrosion exposure started.

Under field operating conditions, pressure fluctuations are often very benign and the combined factor if calculated will be often well below the threshold, even for the oil pipelines that are often under more severe pressure fluctuations than the gas pipelines. This is to say, a growing crack in the field may repeatedly stop growing (crack dormancy). This phenomenon has been extensively discussed by Chen *et al.* [18].

To simulate both mechanical and environmental effects under field situations, Test II was cyclically loaded initially to a R-ratio (0.65) that will not lead to immediate growth, that is, the so-called non-propagating condition. The combined factor corresponding to R=0.65 was calculated to be $2868 (\text{MPa}\sqrt{\text{m}})^2\text{Hz}^{-0.1}$, which is well below the threshold ($\sim 8500 (\text{MPa}\sqrt{\text{m}})^2\text{Hz}^{-0.1}$).

4.2.2.1 Condition for crack initiation

As shown in Table 4-2, crack growth of Test II was not detected until the R ratio was reduced by very small steps, $\sim 0.02 - 0.05$, to about 0.22. At the latter R ratio, the combined factor was determined to be $14330 (\text{MPa}\sqrt{\text{m}})^3\text{Hz}^{-0.1}$, which is well above the threshold value of about $8500 (\text{MPa}\sqrt{\text{m}})^3\text{Hz}^{-0.1}$. According to Test I, crack growth can occur when R is at 0.4 as the

applied stresses and the initial crack dimensions were the same (see Table 4-3). The R-drop process was monitored by a potential drop system. Figure 4-6 compares the change of potential with time under a non-propagating loading and at $R=0.22$ where crack growth was initiated. The potential drop did not detect crack growth at the other two locations possibly because change in crack size was small and the stress applied was not high enough to cause a significantly high enough crack opening.

4.2.2.2 Characteristics of crack morphologies

Crack growth was observed at all the positions as shown in Figure 4-7, despite that it was detected by the potential drop system only at the open mouth for the reasons mentioned above. The crack growth should have occurred primarily at the last R-ratio loading, which is below the threshold R determined based on the threshold of the combined factor. Although crack re-initiation occurred at the same R-ratio at all the positions, the extent of crack growth was found to be quite different, as shown in Figure 4-7. Since the cracks at different positions from the open mouth started at the same time, the fastest growth occurred at the open mouth and slowest growth at the bottom of the disbondment.

At the sample surface, cracks were generally narrow but slightly wider than in Test I. Crack opening just behind the crack tip increased with distance from the open mouth (Figure 4-8). Cracks were generally longer in test II than in test I, which is indicative of more rapid crack propagation in test II. This is even more significant when one considers that the cracks in test II were only subjected to 1945 cycles (4.5 days) during crack propagation while the ones in test I were subjected to 9824 cycles (23.2 days).

Table 4-3: Characteristics of crack growth for cracks on the specimen surface

| | | Initial crack length (mm) | Final Crack length (mm) | Net crack growth (mm) | Average crack growth rate (mm/cycle) |
|----------|-------------------|---------------------------|-------------------------|-----------------------|--------------------------------------|
| Test I | OM ^{***} | 3.34 | 5.4945 | 2.1545 | 2.15E-04 |
| | MP | 3.31 | 3.82875 | 0.51785 | 5.16E-05 |
| | BP | 3.38 | 3.8532 | 0.4782 | 4.77E-05 |
| Test II | OM | 3.32 | 7.36 | 4.05 | 2.08E-03 |
| | MP | 3.30 | 3.73 | 0.44 | 2.24E-04 |
| | BP | 3.31 | 3.53 | 0.23 | 1.16E-04 |
| Test III | OM | 3.42 | 3.82 | 0.40 | 1.55E-04 |
| | MP | 3.44 | 3.86 | 0.42 | 1.60E-04 |
| | BP | 3.40 | 3.71 | 0.31 | 1.21E-04 |

*** OM = open mouth of the disbondment

MP = crack at middle position – 75 mm from the open mouth of the disbondment

BP = crack at bottom position – 150 mm from the open mouth of the disbondment

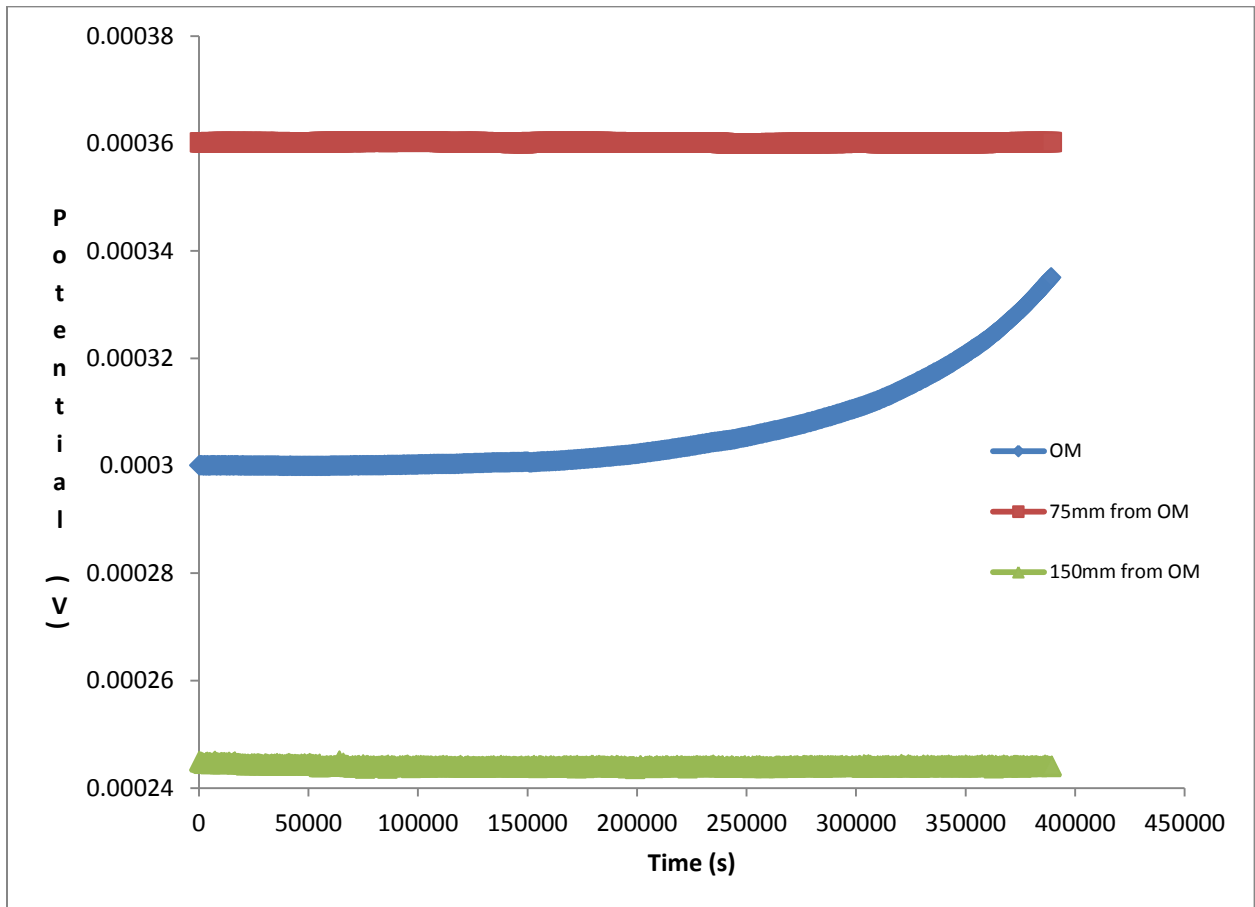


Figure 4-6: Potential drop data for test II

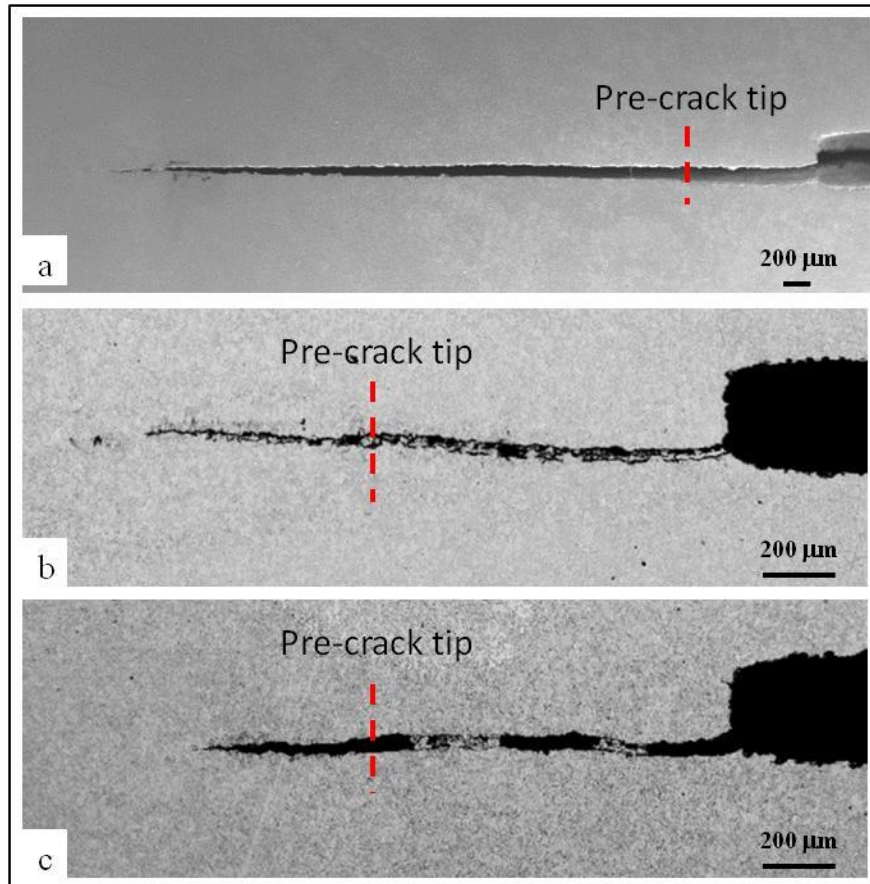


Figure 4-7: Post-test crack lengths measured at the sample surface after test II at (a) open mouth, (b) 75 mm from OM, (c) 150 mm from OM

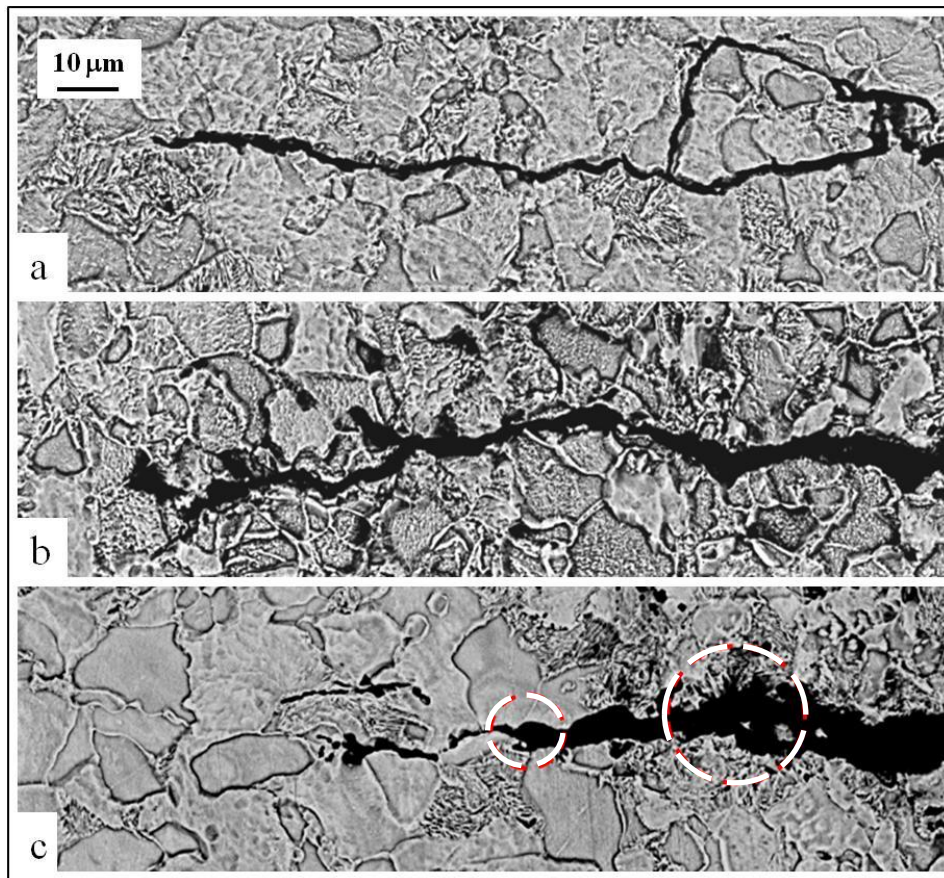


Figure 4-8: Crack tip Morphology at the sample surface in Test II (a) OM (b) 75 mm from OM, (c) 150 mm from OM

The surface crack tip morphologies at different positions to the open mouth were found very similar in Test II. In general, the crack tip is blunt. Despite much faster growth rate at the open mouth in Test II than in Test I, a blunt tip morphology was seen in Test II. Another noticeable morphological feature of the cracks is that there exists a sharp change in crack crevice/width in the vicinity of the crack tip, which is clearly seen in the crack from 150 mm position (see circled areas in Figure 4-8c).

In the depth direction, in test II, the crack was much longer at the open mouth than the other two locations (Figure 4-9). There is a mild wedge-shaped morphology along the crack for the crack from the open mouth, probably because of its long length. The crack crevice along the depth direction was similar for the cracks at the 75 mm and 150 mm positions. The crack tip morphologies are shown in Figure 4-10, which remained generally blunt, especially when compared to the sharp crack tip morphology seen in Figure 4-5a). There is hardly any observable difference in the crack openings behind the crack tip. However there is significant crack branching at 150 mm from the OM. Also, some of the branches at 150 mm from the OM tended to have very sharp crack tips. However, the main crack front itself has a tip comparable to those at the OM and 75 mm from the OM. Crack widths are significantly wider than in test I. The sharp changes in crack width as indicated earlier are also observed in the depth cracks, as marked in Figures 4-9b) and 4-9c).

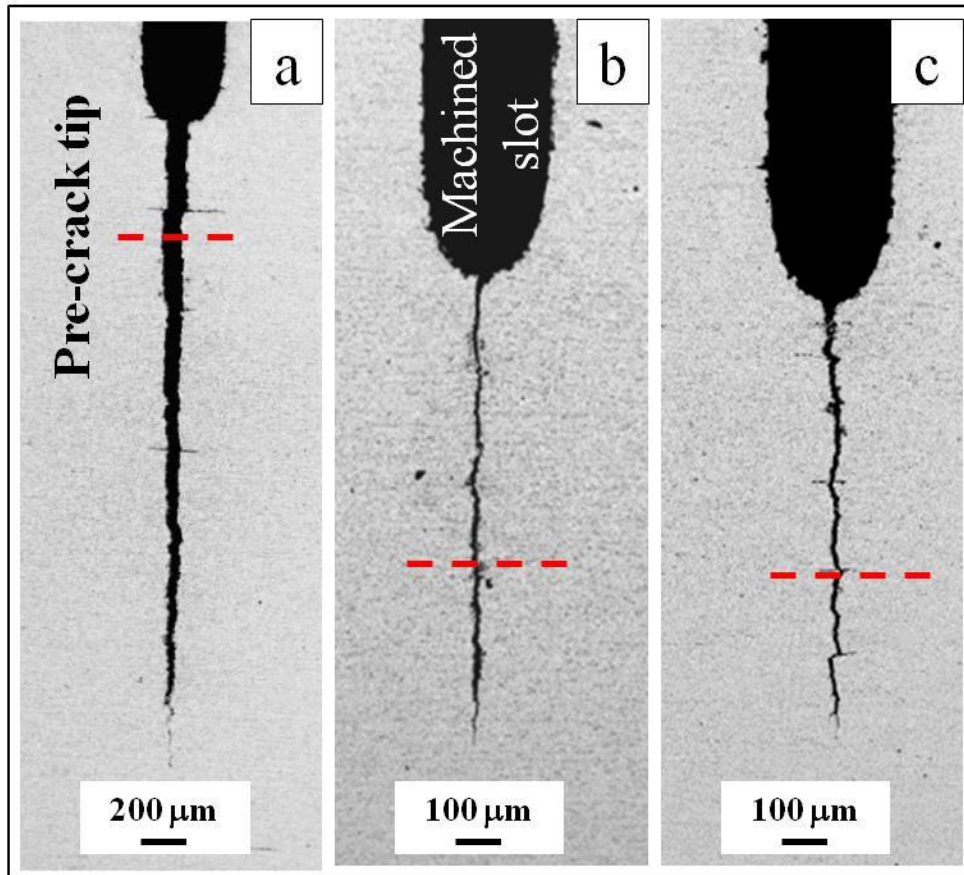


Figure 4-9: Crack morphology in the depth direction for test II (a) Open mouth, (b) 75 mm from OM, (c) 150 mm from OM

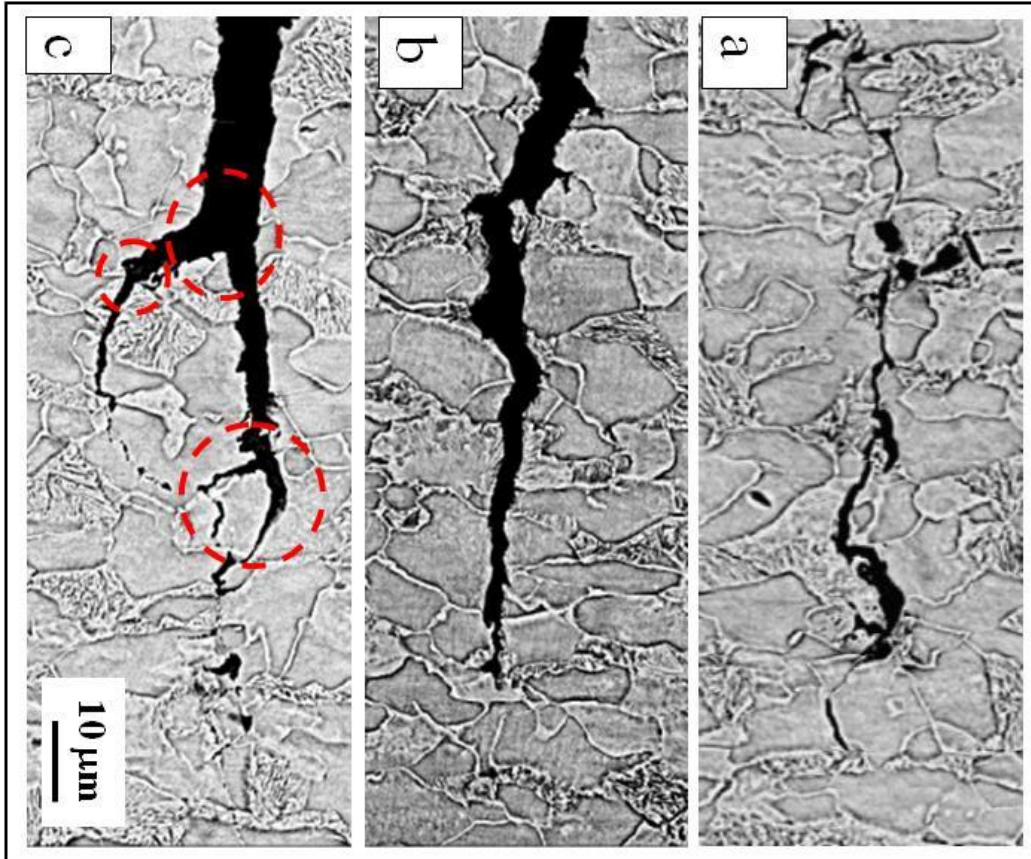


Figure 4-10: Crack tip morphology in depth direction at higher magnification for test II
(a) Open mouth, (b) 75 mm from OM, (c) 150 mm from OM (d) higher magnification of (c)

4.2.2.3 Crack growth rate behavior

Generally crack propagation rates decreased with distance from the open mouth. The initial and final crack sizes are shown in Tables 4-3 and 4-4, while the initial and final aspect ratios are shown in Figures 4-10a). The initial crack aspect ratios at different positions of both specimens can be considered to be similar, despite slight variations that reflect the microstructural heterogeneity in the steel. Figure 4-11b) shows the ratio of aspect ratio after and before the exposure. Aspect ratios decreased at the open mouth but remained about the same at 75 mm and 150 mm positions from the OM. The reduced aspect ratio at the open mouth indicates a faster growth rate at the surface than in the depth. This is consistent with the field findings and was explained to be a result of stronger environmental factor at the crack tip on the surface at the OM (Chapter 3).

The associated average growth rates of Test I and Test II are plotted in Figure 4-12. The average growth rates of Test II were calculated based on the number of cycles during the test at the lowest R-ratio (Table 4-2) at which crack propagation was assumed to have been initiated. Similar trend of growth behavior was found in both specimens. Surface growth rates decreased towards the bottom of the disbondment in test II. It is important to note that crack growth was deferred to much lower stress ratio (0.22) in test II. The crack growth rate at the open mouth is significantly higher than at the other locations while the lowest growth rate was obtained at 150 mm from the open mouth. In fact crack growth rate at the open mouth is about four times higher than at 75 mm from the open mouth. Crack growth rates in test II are obviously significantly higher than in test I.

Table 4-4: Characteristics of crack growth for cracks in the depth direction

| | | Initial crack length (mm) | Final Crack length (mm) | Net crack growth (mm) | Average crack growth rate (mm/cycle) |
|----------|----|---------------------------|-------------------------|-----------------------|--------------------------------------|
| Test I | OM | 3.13 | 4.09 | 0.96 | 9.56E-05 |
| | MP | 3.20 | 3.74 | 0.55 | 7.15E-05 |
| | BP | 3.09 | 3.73 | 0.63 | 6.31E-05 |
| Test II | OM | 3.19 | 5.33 | 2.14 | 1.10E-03 |
| | MP | 3.38 | 3.52 | 0.14 | 7.12E-05 |
| | BP | 3.43 | 3.57 | 0.14 | 7.12E-05 |
| Test III | OM | 3.18 | 3.53 | 0.35 | 1.34E-04 |
| | MP | 3.16 | 3.61 | 0.44 | 1.71E-04 |
| | BP | 3.20 | 3.44 | 0.25 | 9.42E-05 |

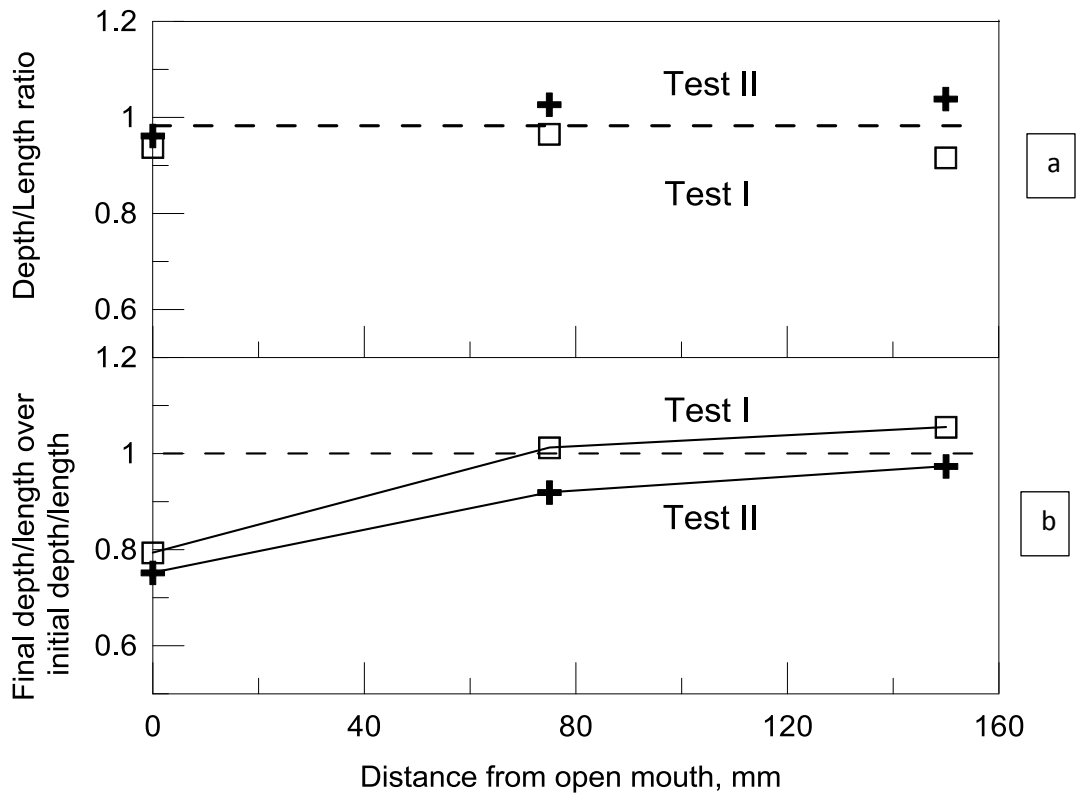


Figure 4-11: Initial aspect ratios

Growth rates in the depth direction are also shown in Figure 4-12. Crack propagation was more rapid at the open mouth than at the other two locations while growth rates at 75 mm and 150 mm are quite similar. The actual depth growth rate at 75 and 150 mm positions in Test II was also much higher than that of cracks at the same positions in Test I, despite similar values shown in Figure 4-12. This was because of much longer growth period and higher growth rate of the longer crack in Test I (also Table 4-2 and Table 4-4).

4.2.3 Crack growth behavior of sharp crack preceded by non-propagating loading in 20% CO₂ (Test III)

Test II simulates the effect of start-stop type crack propagation in the field, and gives a good insight into the effects of cyclic loading history on crack re-initiation and crack propagation. Environmental conditions could modify the crack tip behavior, hence the ability of cracks to re-initiate, as well as the growth rates once crack propagation is resumed.

As mentioned in the introduction, field studies have shown that CO₂ concentrations could vary significantly with the seasons. This variation could influence the ability of cracks to re-initiate and resume propagation. Although there are very few dissenting voices on the effect of increasing CO₂ concentrations on crack re-initiation and subsequent propagation, many researchers believe that higher CO₂ concentrations should give rise to a higher hydrogen concentration hence an increased rate of crack propagation. This section examines the effect of higher CO₂ propagation on crack re-initiation and prevailing growth rates once crack propagation resumes.

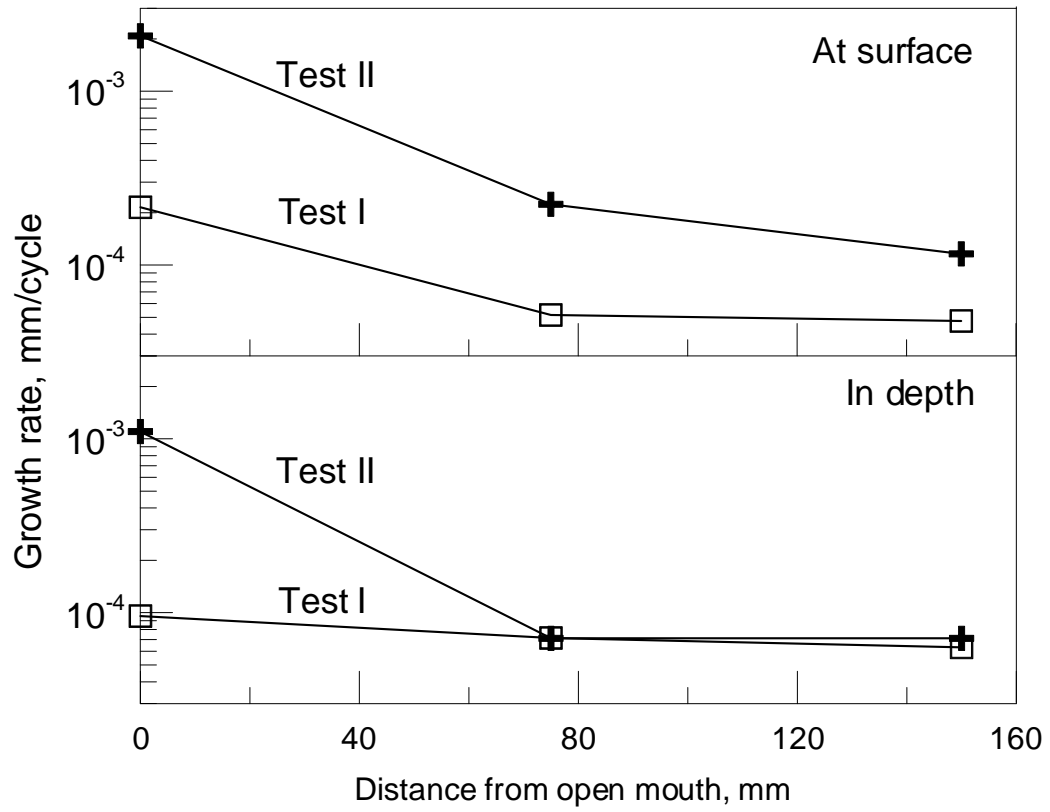


Figure 4-12: Average crack growth rates measured at sample surface

4.2.3.1 Condition of crack initiation

In test III, the potential drop system did not detect crack propagation at any stage, so the test was terminated at the same stress ratio of 0.22 as in test II. The R ratio was reduced by very small steps, ~ 0.02 – 0.05, to about 0.22 as in test II. At the latter R ratio, the combined factor was determined to be $14330 \text{ (MPa}\cdot\sqrt{\text{m}})^3/\text{Hz}^{0.1}$, which is well above the threshold value of about $8500 \text{ (MPa}\cdot\sqrt{\text{m}})^3/\text{Hz}^{0.1}$.

4.2.3.2 Characteristics of Crack morphology

Unlike in test II, crack propagation rates were found to be similar at all three locations in test III. Figure 4-13 compares the crack length on the surface of specimens. Examination of the pre-crack tip in test III indicated that crack tips were significantly blunter (Figures 4-14) than in tests I and II. As in test II, there was no indication of growth at a stress ratio of R=0.4 by the potential drop data.

Wide cracks were observed and despite the prolonged and more severe loading only a little crack propagation occurred during the test. There is not any significantly discernible difference in the crack opening size just behind the crack tip (Figures 4-14) in test III. At the open mouth and 75 mm from the OM, cracks were transgranular in nature. However, examination of the crack path at 150 mm from the open mouth shows that although some mixed mode behavior could be seen, crack propagation was overwhelmingly intergranular along the surface, especially in Figures 4-14c.

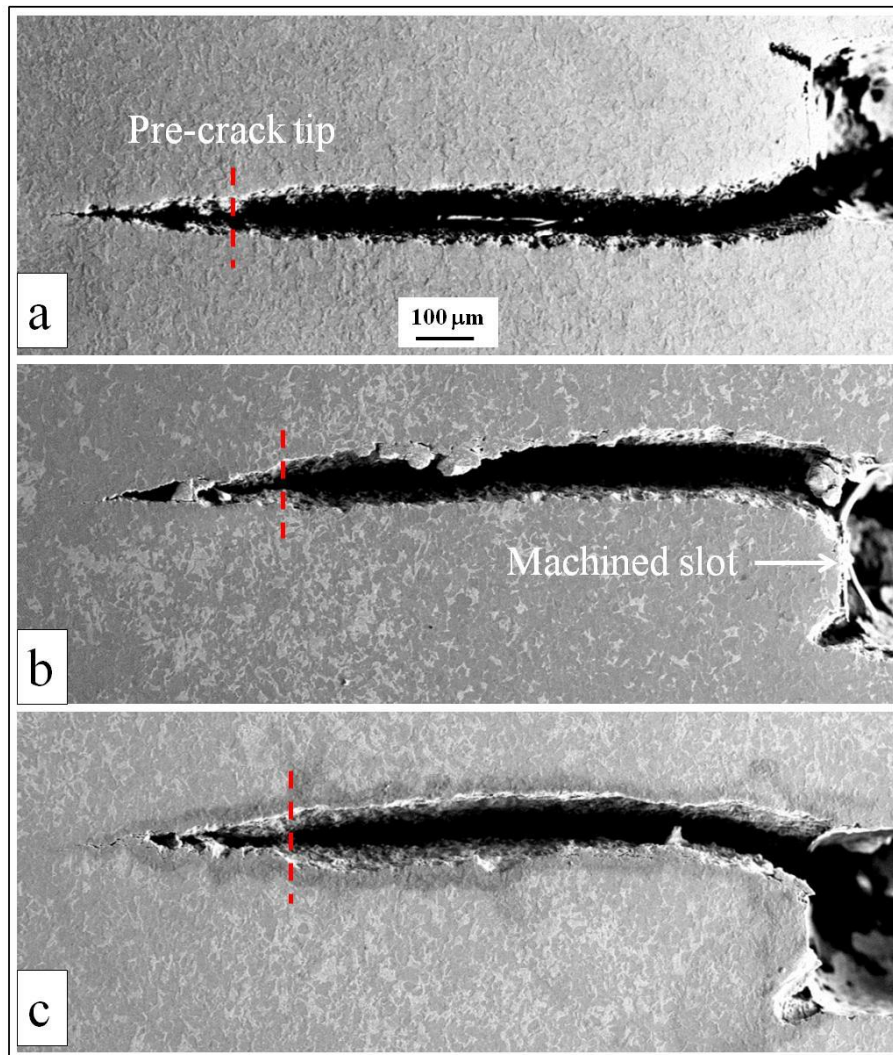


Figure 4-13: Pre-fatigue crack and post-test crack tips in the 20% CO₂ environment - test III (a) open mouth, (b) 75 mm from open mouth and (c) 150 mm from open mouth

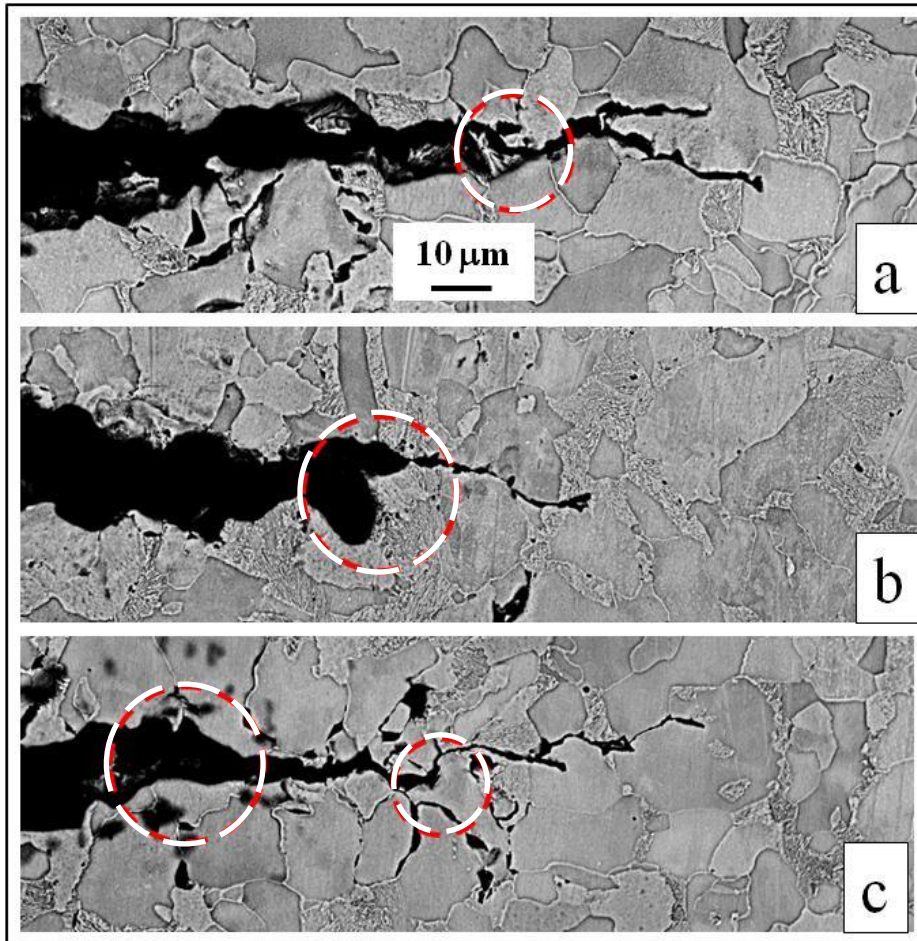


Figure 4-14: High magnification image of the crack tip width at sample surface for test III

(a) open mouth, (b) 75 mm from open mouth, (c) 150 mm from open mouth.

In the depth direction despite the high CO₂ concentration, crack propagation at the open mouth was not as large as in tests I and II, but the extent of crack growth was similar at all three locations (Figures 4-15 and 4-16). Similar to observations at the specimen surface, crack tips were significantly blunted and crack walls are wide. Cracks are generally transgranular at all locations in the depth direction (Figure 4-16), which is different from the intergranular features seen at the surface. Another morphological feature found was the sharp change in crack wall width along the cracks both at the surface and in the depth direction. These sharp changes are circled in Figures 4-14 and 4-16. They were also identified in Test II.

The initial and final crack sizes for all three tests are shown in Tables 4-3 and 4-4 while the initial and final aspect ratios are shown in Figure 4-17. In test III, there is hardly any difference in final crack dimensions at all three locations after the test and no changes in aspect ratios before and after the tests were found. This is quite unlike tests I and II where significant variation in the extent of crack propagation was observed with distance from the open mouth of the disbondment. Crack aspect ratios increased with distance from the open mouth.

The associated surface growth rates are shown in Figure 4-18. Growth rates are very similar at all three locations, suggesting there is hardly any difference in the extent of environmental enhancement with distance from the open mouth in the 20% CO₂ environment. Unlike in tests I and II, a clear indication of the time at which crack growth was initiated in Test III was not found. This makes it very hard to determine an accurate average crack growth rate in Test III.

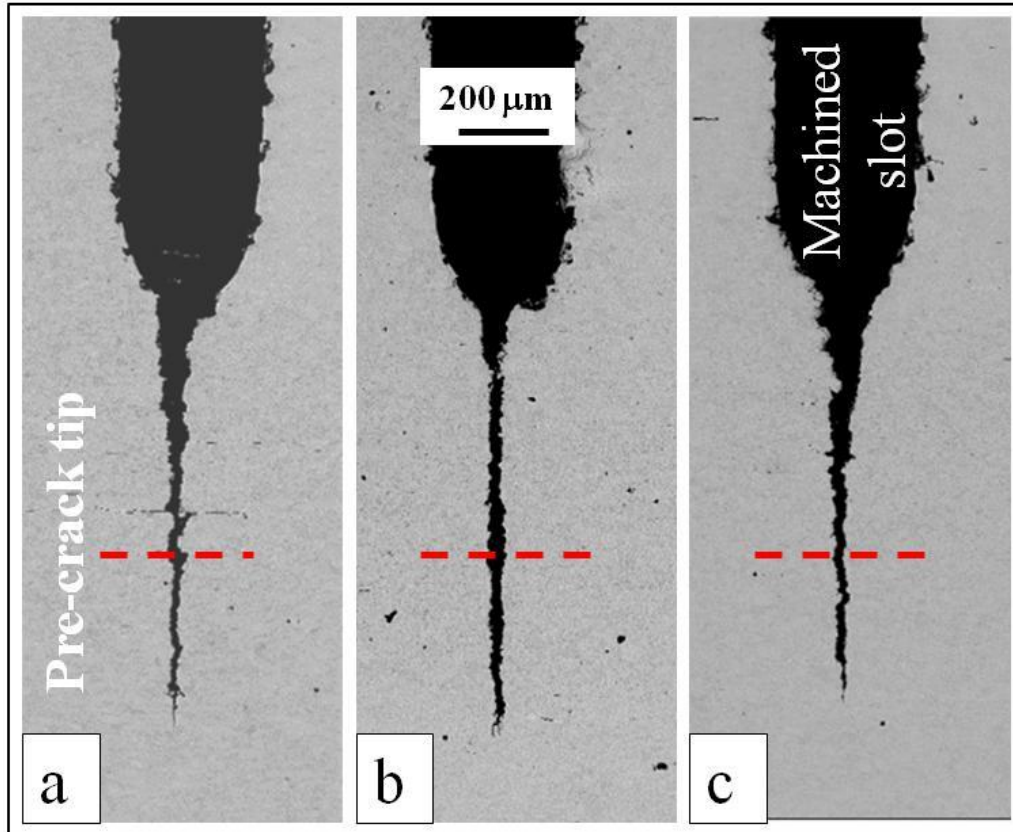


Figure 4-15: Low magnification image of crack tip in the depth direction for test III (a) open mouth, (b) 75 mm from open mouth, (c) 150 mm from open mouth

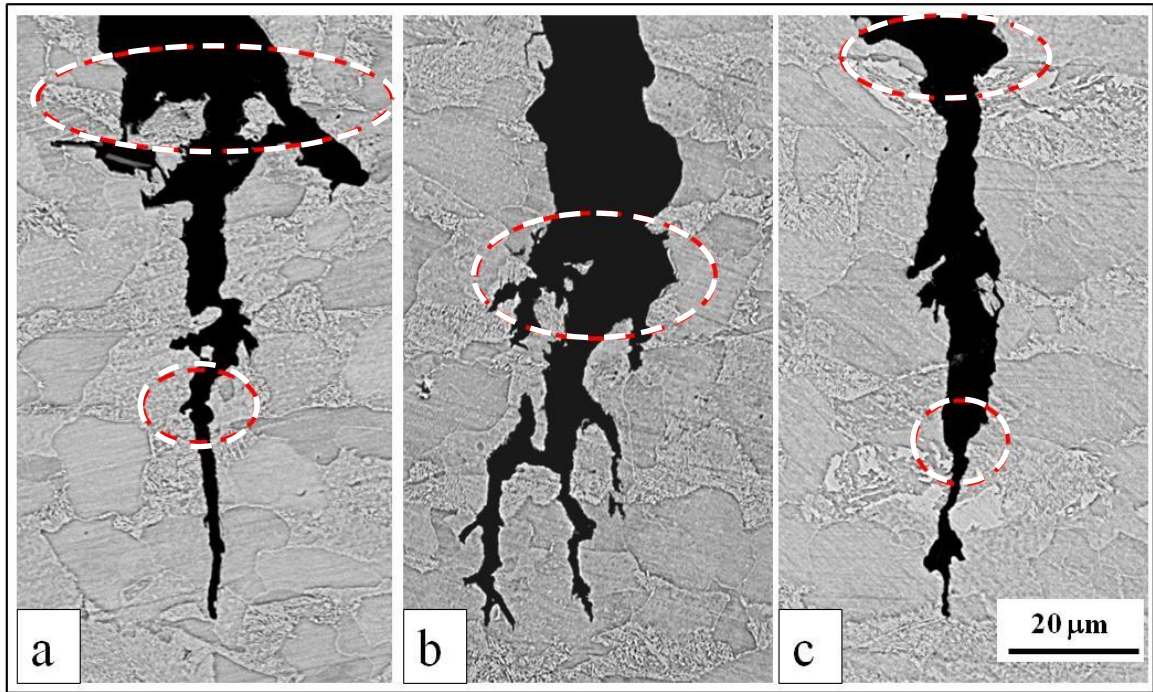


Figure 4-16: High magnification image of the crack tip in the depth direction for test III

(a) open mouth, (b) 75 mm from open mouth, (c) 150 mm from open mouth.



Figure 4-17: Aspect ratios of cracks in Test III

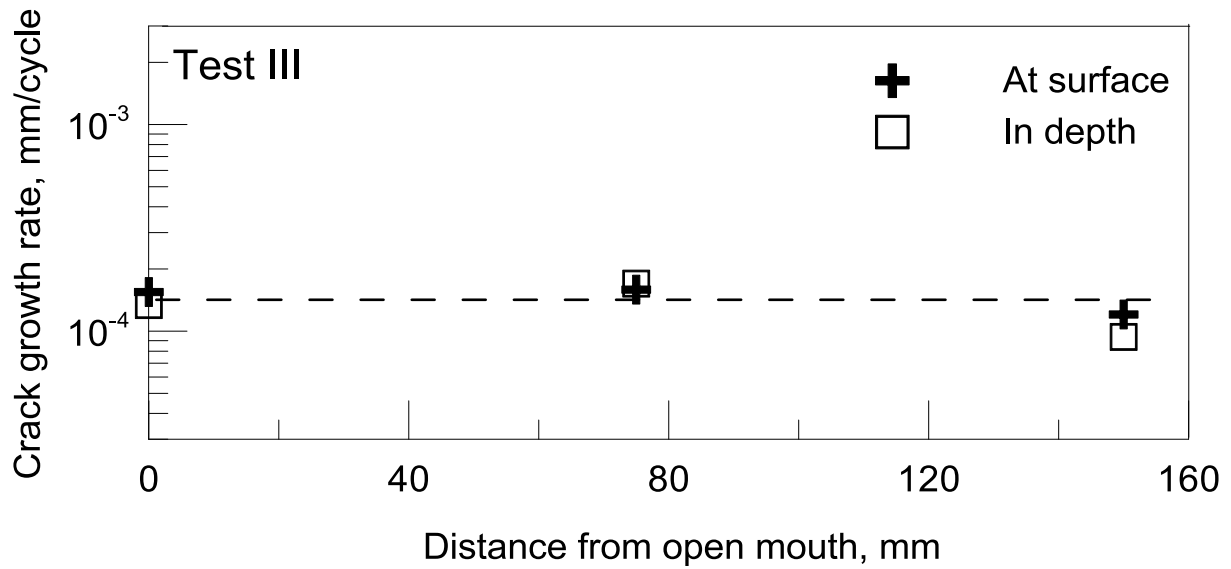


Figure 4-18: Crack growth rate of Test III

When crack growth was assumed to take place during the last R-ratio loading, like in Test II, the average crack growth rates in Test III, as presented in Figure 4-18, were very comparable to those at MP and BP in Test II and I. However, when the entire test period is considered, the average crack growth rates in Test III will be almost 20 times slower than those shown in Figure 4-18.

4.3 Discussion

This investigation is designed to understand the crack growth mechanisms and growth rate behavior of surface cracks in NNpH environments under disbonded coating, especially after a crack has become dormant either because of mechanical or environmental attributes. It seems quite complicated as many factors of testing conditions have been incorporated into the investigation. To rationalize the results obtained, the crack growth rate at the open mouth was analyzed first, from which a clear picture of growth mechanisms and growth rate behavior can be envisioned.

4.3.1 Crack growth rate behavior

Figure 4-19 shows the crack growth rate at the open mouth obtained from Test II, which was calculated based on the potential drop curve recorded and validated using the actual crack growth measured on the fractured surface opened in liquid nitrogen after corrosion exposure. The master crack growth curve obtained from a similar X65 pipeline steel exposed to the same test environment (C2 solution in equilibrium with 5% CO₂ + N₂ Balance) but using compact tension specimen is also comparatively presented. This curve represents the growth behavior of a long crack with a sharp crack tip.

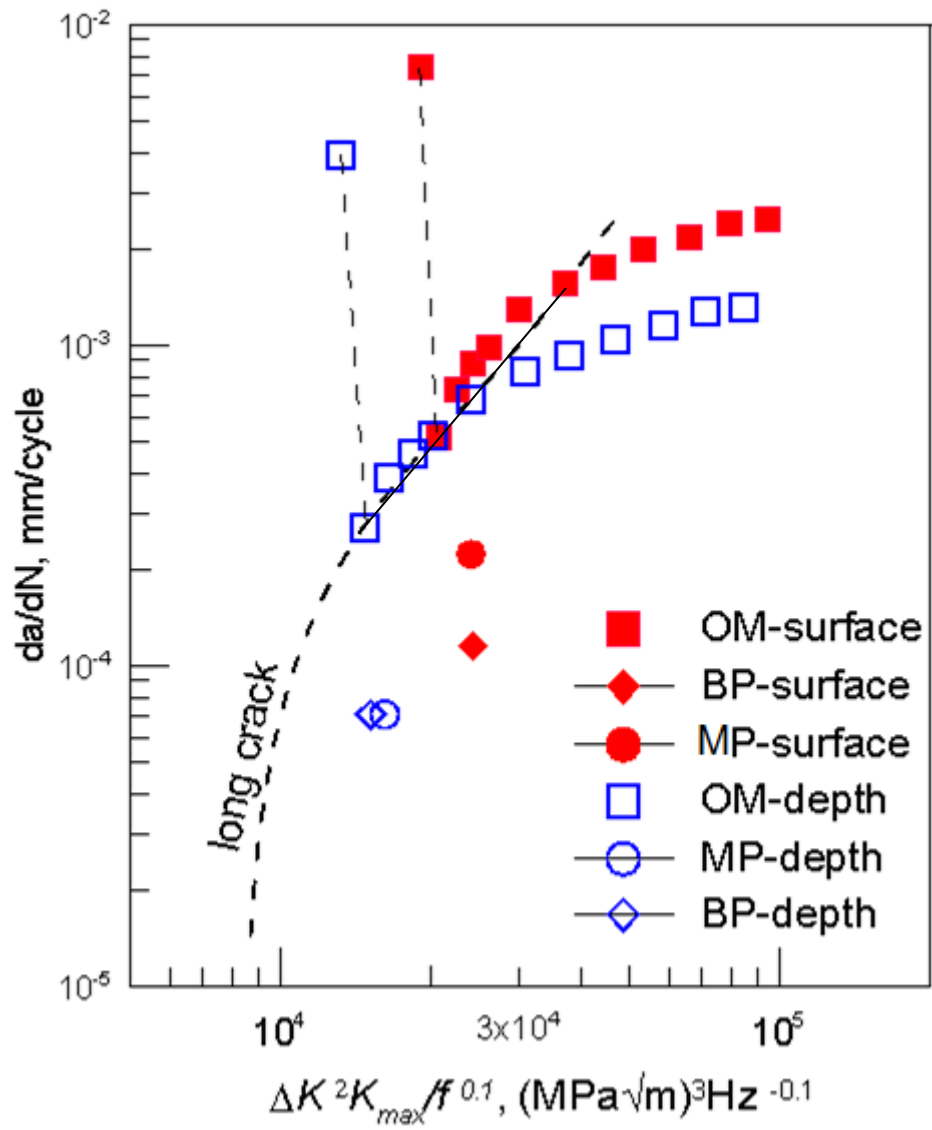


Figure4-19: Combined corrosion fatigue analysis for tests II and III

As shown in Figure 19, crack growth rate at OM is very high at the very beginning of the test. This is followed by a quick drop of crack growth rate with a growth trend quite consistent with the master curve. A deviation from the master curve and different growth rate behavior at the surface and in the depth was observed as the crack propagated.

It is certain that the sharp crack tip obtained from pre-fatigue cracking in air prior to the corrosion exposure had become blunt after a long period of loading under non-propagating conditions (applied combined factor below the threshold). It is well established that stress concentration exists in the material ahead of the blunt tip. When a sharp crack was initiated due to an increase of combined factor (reduction of R-ratio to 0.22 in this case), it would propagate at a much higher rate because of magnified applied stress as a result of stress concentration. Crack growth rate will be reduced after the crack has advanced over the region where stress concentration exists. The different trend in crack growth rate at the later stage of crack growth is usually explained due to the breakdown of linear elastic fracture mechanics assumptions.

The crack growth data at the other two positions (MP and BP) are also presented in Figure 4-19, which were the average growth rates calculated using the time during the last loading period with $R = 0.22$. These growth rates are extremely exaggerated for reasons to be discussed. Although the potential drop systems did not detect any continuous growth at both the MP and BP positions, crack growth was observed (for example, 0.44 mm and 0.23 at surface, respectively, for MP and BP) on the fractured surface after corrosion exposure. This suggests that the thresholds for the occurrence of continuous growth at middle and bottom positions are much higher than that at the open mouth, and crack growth is possible when the combined factor is below the threshold but may occur by a different mechanism.

To activate a dormant crack for continuous growth as the case of the cracks at the open mouth requires a very high driving force (high value of combined factor), which can be rare events in their early stage of crack growth for oil pipelines or for high pressure gas pipelines because of very benign pressure fluctuations and low maximum stress intensity factor. That is, crack growth in the field may proceed primarily by those mechanisms as seen for the cracks at MP and BP positions, which will be the main focus of the discussion in the remaining sections, which have not been investigated so far.

4.3.2 Crack growth mechanisms of dormant cracks

To better understand the crack growth mechanisms of dormant cracks loaded with a combined factor below the threshold for continuous growth, the growth curve in Figure 4-19 was generalized and illustrated in Figure 4-20. In this figure, two threshold positions are identified; one is for the occurrence of continuous growth of the crack with a sharp tip, the other for the crack with a blunt tip, the so-called dormant crack. Crack growth mechanisms can be discussed based on the position of the loading driving force (the combined factor) relative to the position of the two thresholds shown in Figure 4-20.

For the cracks with a sharp tip, fracture mechanics concept such as stress intensity factor can be used to quantify the stress state at the crack tip. When the crack tip is blunt, a stress concentration factor is usually defined and the actual stress in the material ahead of the blunt tip is a function of both the stress concentration factor and the applied nominal stresses through the following expression.

$$\sigma = k_t \sigma_a \quad (4-1)$$

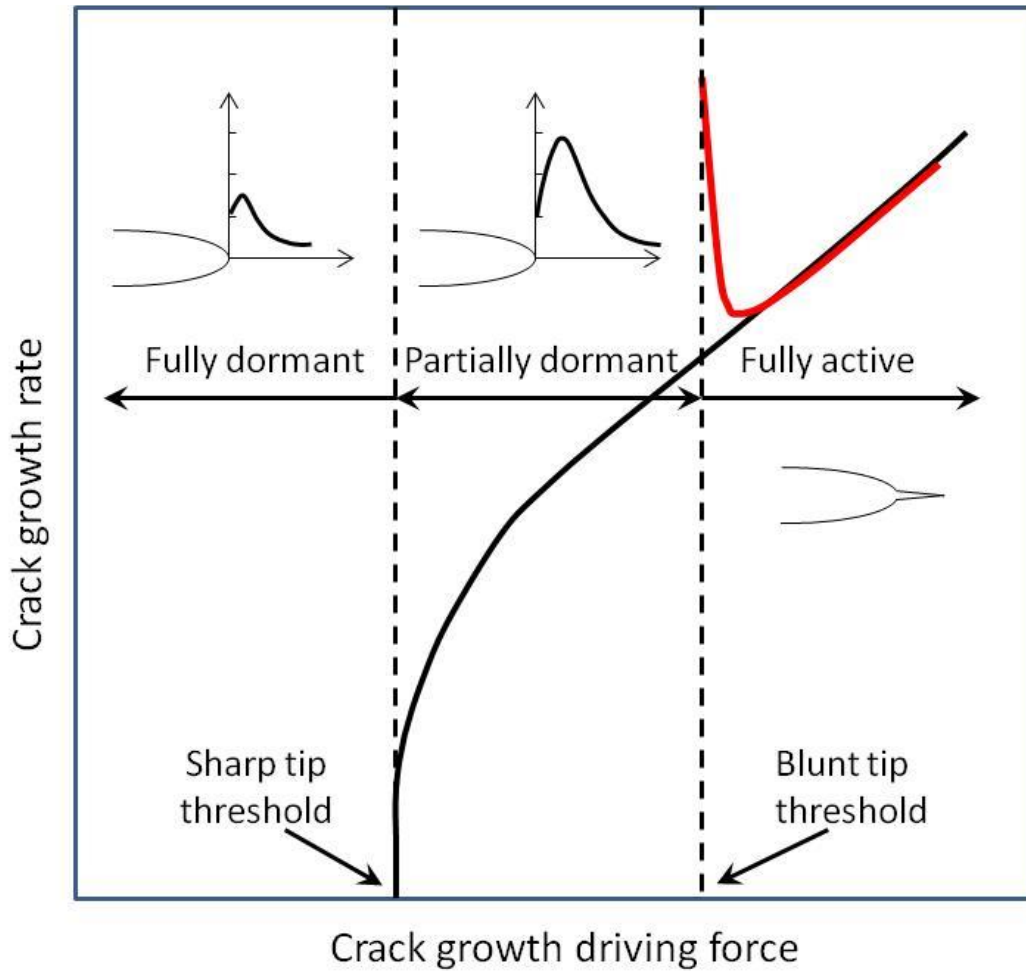


Figure 4-20: Comparison of the corrosion fatigue behavior of crack growth data at the open mouth in test 1 to that of a through-thickness crack

Where, σ_a is the applied stress, k_t is the stress concentration factor, which can be expressed as:

$$k_t = 1 + 2\sqrt{\frac{b}{\rho}} \quad (4-2)$$

When b is the depth of crack with a blunt tip and ρ is the radius at the tip of the blunt crack.

A blunt tip is a common morphological feature of cracks when loaded under the loading conditions at which continuous growth is not possible. Re-activating a dormant crack for active growth is certainly dependent on the magnitude of stress in the material ahead of the crack tip. For a sharp crack the highest stresses exist right at the tip of the crack if yielding at the crack tip has not occurred or has occurred to a very small scale, as determined by linear elastic fracture mechanics equations. For a blunt crack, however, the highest stress is shifted to a region ahead of the crack tip, which is often called the fracture process zone, as shown in Figure 4-21. When the crack is in plane strain loading state, triaxial stresses exist in the fracture process zone. A plane strain loading state is generally assumed for the surface cracks except for the crack tip at the surface.

When steels are exposed to a corrosive environment in which atomic hydrogen, a by-product of corrosion reactions, is generated, the triaxial zone is associated with a segregation of hydrogen as applied stress increases. Under fatigue loading, the segregation can be maximized at the peak fatigue stress. The exact amount of hydrogen segregated depends on the magnitude of the stress in the triaxial zone, the average concentration of hydrogen in the lattice, and the rate of loading and the diffusivity of hydrogen. For the latter factor, a slower loading would yield higher hydrogen segregation at a given diffusivity of hydrogen as governed by the diffusion laws, which is measured by the $(1/f^\gamma)$ term in the combined factor.

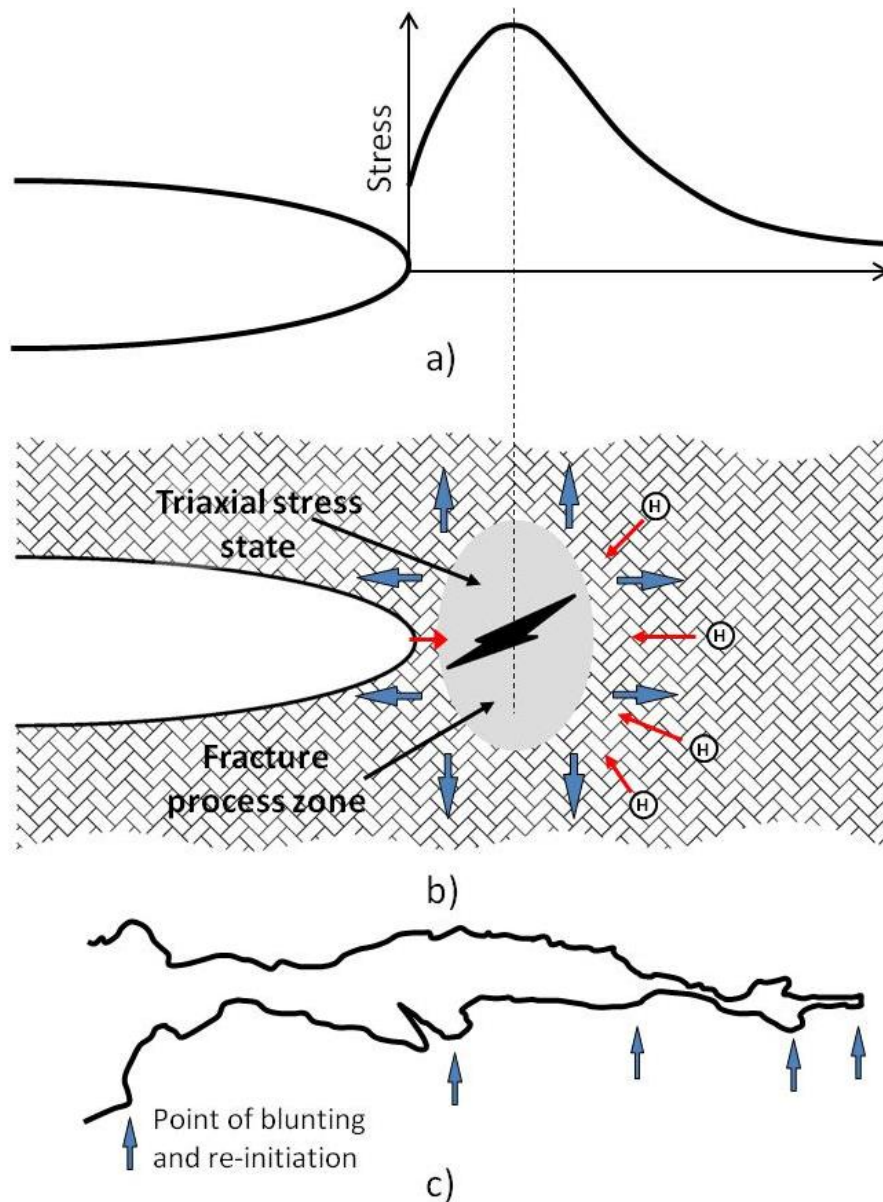


Figure 4-21: (a) Stress distribution ahead of a crack tip (b) triaxial stress state in the hydrogen process zone (c) profile of a crack that experienced periodic dormancy during crack propagation

When a critical level of hydrogen is reached, microcracks may be initiated in the fracture process zone by a hydrogen embrittlement mechanism. This crack can quickly propagate back to join the blunt tip of the main crack and turn the blunt crack into a sharp crack.

When a crack is under fatigue loading, regardless of whether the effects of hydrogen embrittlement are present or not, crack initiation by a fatigue mechanism could also occur in the fracture process zone, although the mutual interaction of hydrogen and fatigue loading would facilitate the crack initiation in the fracture process zone.

Microcracks are usually initiated at the weakest links in the fracture process zone, which are special microstructural features or metallurgical discontinuities in the material, such as inclusions, grain boundaries, secondary phases, or phase interfaces, where diffusible hydrogen in the lattice can be trapped and/or strain incompatibility is present such that initiation of fatigue cracks is facilitated.

Based on the above understanding, crack growth mechanisms occurring when crack growth driving force is below the threshold (for cracks with blunt tip) for continuous growth can be clearly visualized. Since continuous growth is unlikely, all possible mechanisms that may cause discontinuous crack initiation in the fracture process zone should be discussed, which are detailed below:

- a) By hydrogen embrittlement mechanism

It has been determined that the concentration of diffusible hydrogen in the pipeline steels when exposed to NNpH environments was less than 1/10 of the critical hydrogen concentration for forming hydrogen blistering, an instant cracking of steels due to the buildup of hydrogen pressure at hydrogen traps. Although cracking directly by hydrogen blister formation is not

possible, it has been proven that hydrogen assisted cracking is mainly responsible for the cracking of pipeline steels in NNpH environments. This is further discussed below.

b) By static tensile loading

Although near-neutral pH cracking has been termed as stress corrosion cracking due to some historical reasons, cracking of pipeline steels in neutral pH aqueous solutions has never been observed, and a sharp crack will always evolve into a blunt one when loaded with a static tensile stress. Compared to cyclic loading, static tensile loading is most effective in generating time-dependent room temperature creep deformation. Micro-crack formation in the fracture process zone could occur only by hydrogen embrittlement mechanisms by which microcracks form at sites with high hydrogen concentration, except that ductile fracture may occur when high tensile stress causes severe plastic deformation in the material ahead of the crack tip.

As indicated earlier, the concentration of diffusible hydrogen in the pipeline steels when exposed to NNpH environments is less than 1/10 of the critical hydrogen concentration for forming hydrogen blisters, and therefore, an elevation of hydrogen concentration at least by a factor of ten is needed in order to initiate a microcrack in the fracture process zone. This is very unlikely as discussed below:

1) When the crack is shallow, for example in the initial stage of crack growth, the stress in the triaxial zone would be low and therefore would not be able to generate sufficient hydrogen segregation, the amount of which increases with increasing stresses in the triaxial zone.

2) When the crack is long, for example at the latter stage of crack growth, the stress in the fracture process zone is high but the level of diffusible hydrogen in the pipeline steels surrounding the crack tip become much lower because of concentration gradient of hydrogen (highest at the external surface of the pipe and zero at the inner surface).

c) By cyclic loading

Although cyclic loading alone can lead to crack initiation at low stresses, the cyclic loading in the present case is not sufficient to cause crack initiation because of very low loading frequency. The low frequency loading can cause two unfavorable conditions for fatigue crack initiation. First, fatigue crack initiation at a condition near the threshold requires millions of cycles, which is usually determined by cyclic loading at very high frequency (~10 Hz). Such a high number of cycles would require many years to complete at a low loading frequency meaningful to pipeline operation. Second, a low frequency loading leads to the occurrence of low temperature creep and crack tip blunting.

d) By synergistic interaction of hydrogen, static and fatigue loading

The ramping to the peak stress of cyclic loading allows the buildup of hydrogen in the triaxial zone if loading rate matches or is lower than the diffusivity of hydrogen (the effect of K_{max} and $1/f^{\gamma}$), while cyclic stress measured by ΔK can induce cracking directly in the fracture process by a fatigue mechanism. This provides a physical explanation of the combined factor in terms its effect on crack growth.

Despite the above synergistic interaction, this discontinuous crack growth suggested above would be impossible when the crack driving force is lower than the threshold for continuous growth of the crack with a sharp tip. This is simply because of a very low driving force which cannot initiate any crack in the fracture process zone. A typical example of such situation would be the crack growth in the middle and bottom position in Test I, where only the main crack was seen and no crack branching or any other features that are indicative of crack initiation in the fracture process zone ahead of the crack tip are seen to be associated with the main crack.

In contrast to the crack tip morphology at MP and BP in Test I, the discontinuous crack growth seen in Test II and III shows repeated steps of blunting and reactivation, as illustrated in Figure 4-21c), which was made based on the crack image in Figure 4-16c). Similar features are also observed in all cracks under discontinuous growth.

Based on the image in Figure 4-21c), one may wonder what would be the number of cycles needed for each step of discontinuous advance. The average length of each step is measured to be about 10 – 20 μm , as shown in Figure 4-16c), which surprisingly is equivalent to the average size of grains in the materials. The grain size related jumps are quite obvious and generally seen in all the cracks with discontinuous growth shown in this investigation. The time required to generate each jump can be easily calculated to be around 1 to 2 days or 500 to 1000 cycles at a loading frequency of 0.005 Hz.

Since crack initiation at a blunt tip is limited to the size of grain, this localized initiation would not lead to continuous growth of adjacent areas, where their own crack initiations have not occurred due to unfavorable metallurgical conditions. The transition of discontinuous crack growth to continuous growth would occur when crack initiations in the fracture process zones can take place simultaneously at most locations of the crack front.

In operating pipelines, the combined factors calculated from pressure fluctuations and crack dimensions detected are often below the threshold value required for a sharp crack to propagate continuously, especially for high pressure gas pipelines where R ratios are generally higher than 0.9. Discontinuous crack growth involving crack tip blunting (dormant) and crack tip sharpening for growth (active growth) would be a major process of crack advancement. In the early stage of crack growth, only a few events of pressure fluctuations are able to re-activate a

dormant crack for growth, which leads to a very limited growth. This state of crack growth is usually considered to be dormant in the field.

From characterizing the cracks developed in the field, it has been well determined that more than 95% of crack populations remain dormant and only less than 5% of them were found to be able to propagate leading to possible rupture. These latter crack populations are generally located in the region where the tensile residual stresses (for example, up to 110 MPa) and diffusible hydrogen in the steel are very high, raising the combined factor to a level above the threshold for the growth of the crack with a sharp tip. Since these cracks have a blunt tip, crack growth will proceed by the discontinuous mechanism discussed in this investigation. Further discussion will be made to confirm that discontinuous crack growth will take place when the loading combined factor is above the threshold for the growth of the crack with a sharp tip.

4.3.3 Mechanisms of crack dormancy

In pipeline steel-near-neutral pH environment system, crack dormancy is physically related to the crack tip blunting, which is either mechanically or environmentally induced.

a). Mechanically induced

Mechanically induced blunting occurs primarily due to low temperature creep at the crack tip where time-dependent plastic deformation reduces the sharpness of the crack tip such that the stress intensity at the crack tip, a key driving force for crack growth, is reduced to a level below the threshold value necessary for a continuous crack growth. Blunting can start either immediately if the mechanical loading is well below the threshold for crack growth, or gradually when the mechanical loading is below but near the threshold value, under which crack growth was so slow that there is sufficient time for creep to occur. Typical situations of mechanically

induced blunting are demonstrated at the crack tips located at bottom of disbonded coating, as shown in Figures 4-5c), 4-8c) and 4-10c), where the crack tip appears the bluntest or the crack crevice is seen to be the widest. At these locations, corrosion rates should be the lowest because of the lowest CO₂ level in aqueous solution.

To further quantify the mechanically induced blunting, the width of crack crevice at the root of machined slot after exposure was measured and corrected to remove the increase of crack opening due to the hinge effect of different crack length. As is listed in Table 4-5, the highest increase in width was seen at the OM, which is partially caused by corrosion because of the highest CO₂ level at the position (which will be further discussed later). The bottom position should have the least corrosion but has a higher crack width, which should be attributed to mechanically induced blunting (by low temperature creep at the crack tip).

b) Environmentally induced.

Environmentally induced blunting is primarily caused by a direct removal of atoms through dissolution at and around the crack tip. It must be pointed out that the dissolution must occur over a wide area of the cracked surfaces, which is possible only in the corrosion systems in which passivation will not take place, such as the current steel-NNpH environment systems. In the corrosion system where passivating is possible, the crack tip is the only location where corrosion can take place under the assistance of stress and the dissolution of material at the crack tip will lead to a direct advance of the crack tip (crack growth).

Table 4-5: Width of crack opening at the bottom of pit after correction for hinge effect in test I

| Location from open mouth (mm) | Width (μm) |
|-------------------------------|-------------------------|
| 0 | 18.7 |
| 75 | 8.38 |
| 150 | 13.83 |

Environmentally induced blunting is typically seen during the early stage of crack growth and in environments with high levels of CO₂, that is, in more acidic solutions. It is generally believed that the contribution of corrosion to crack advance decreases as a crack propagates in the depth direction because of the reduced CO₂ level, similar to the reduction of CO₂ toward the bottom of a disbanded coating. Because the CO₂ level is highest at the surface, crack growth is faster on the surface and continuous dissolution of the crack crevice at the surface may cause the crack to evolve into a pit.

Typical cases of environmentally induced blunting are demonstrated in Test III, where only limited crack growth had occurred at all positions but a very wide crack crevice had been formed, which to a large extent is caused by a direct removal of materials through dissolution over the cracked surface. Table 4-6 lists the width of crack crevice measured after corrosion exposure and the correction of the hinge effect. For cracks of similar lengths, the crack crevice width should be similar, in the absence of factors that enhance plastic deformation locally. Slight differences in crack lengths should not result in any significant differences in the crack crevice opening (width). Any difference in crack crevice width due to slight differences in crack length could be approximately determined by using the similar triangles approach. This could be used to determine a correction value to be applied to actually measured crevice width in order to eliminate the effect of small differences in crack lengths. After carrying out such a correction, a much wider crack crevice was seen in Test III, compared to that in Test I.

In test I, the crack crevice at BP is about 65% wider than that at MP, despite the fact that the cracks at both positions are very much similar, suggesting similar mechanically induced blunting; environmentally induced blunting should be higher at MP because of a higher rate of corrosion. A similar trend has also been observed in Test II, where the crack crevice at BP is much wider than that at MP, as shown in Figures 4-8 – 4-10. In test III, a larger crack crevice at BP than at MP was also observed. All these suggest the existence of additional factors responsible for crack tip blunting.

Table 4-6: Width of crack opening at the bottom of pit in test III

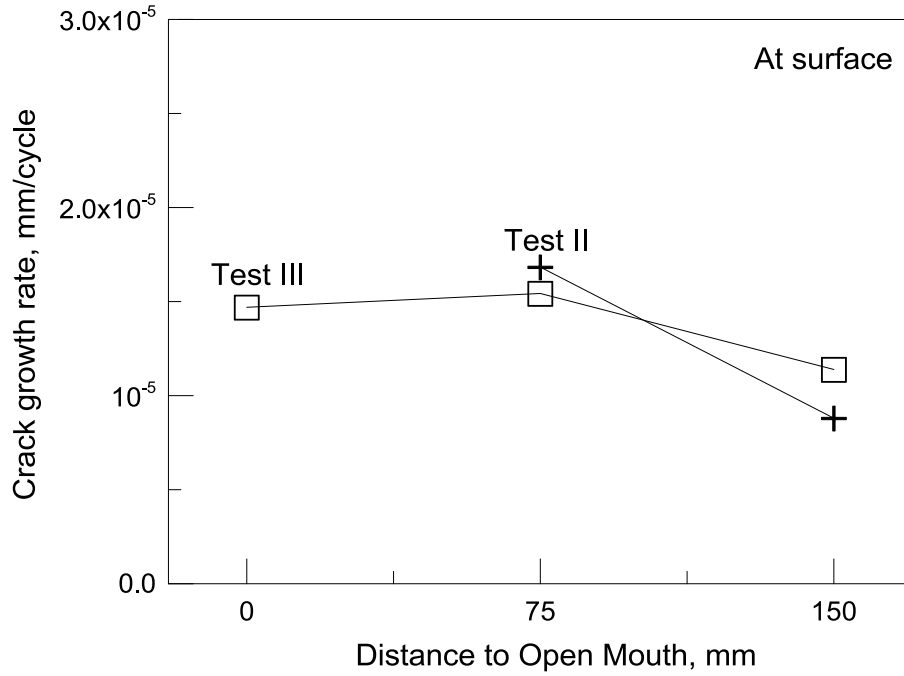
| Distance from open mouth (mm) | Width (mm) |
|-------------------------------|------------|
| 0 | 79.39 |
| 75 | 50.45 |
| 150 | 54.17 |

One possible factor could be hydrogen facilitated plastic deformation, that is, increased low temperature creep in the presence of diffusible hydrogen can cause additional crack tip blunting. This has been proven to be true in the current system. An increase of crack crevice by 33% was observed when the crack tip was segregated with diffusible hydrogen, as compared with the crack crevice loading in air. These results will be published in a future communication.

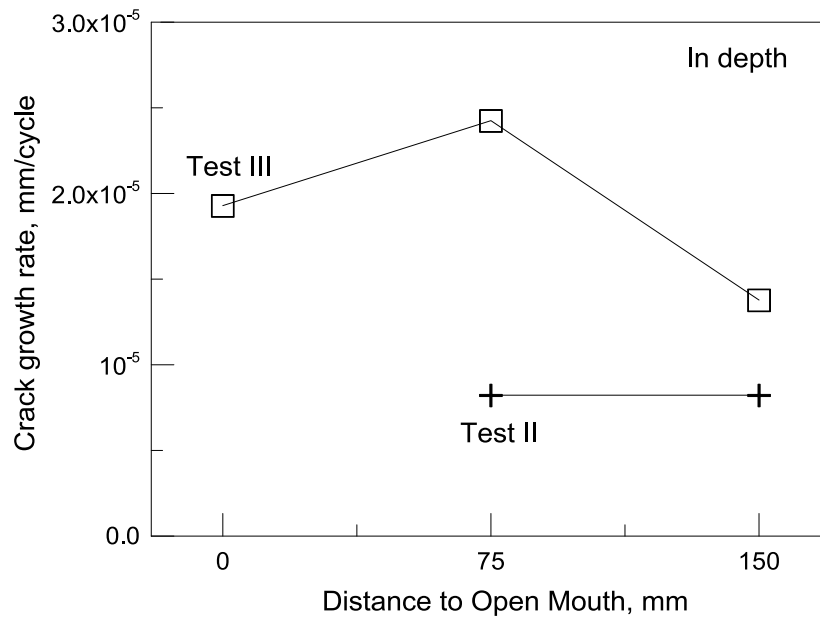
4.3.4 Rate of discontinuous crack propagation

In addition to the understanding of discontinuous crack growth mechanisms, the investigation is also aimed at determining the discontinuous crack growth rate, which is important to remaining life prediction and integrity management. An accurate determination of the discontinuous growth rate can be impossible because of uncertainty of the time at which discontinuous growth starts. However, based on the discussion in previous sections, it is assumed that discontinuous crack started at the threshold for continuous growth of a crack with a sharp tip. This would start when the R ratio in Test II and Test III was reduced to about 0.5 for the crack tip intercepting the surface of the specimen and 0.4 for the crack tip in the depth direction. For the sake of simplicity, the period between $R=0.4$ and $R=0.22$ (end of test) was used.

With the above assumptions, the average discontinuous crack growth rate was calculated and plotted as a function of the position to the open mouth, as shown in Figure 4-22. These growth rates are generally over one order of magnitude lower than those of continuous growth. For Test III, the growth rate was not very much different at various positions, although the middle position appears the highest both at the surface and in the depth direction. For Test II, only the data at MP and BP were used because continuous growth occurred at OM.



a)



b)

Figure 4-22: Comparison of crack growth rate (a) at sample surface (b) in the depth direction

The growth rates in both tests were quite similar at the surface. In the depth direction, the growth rate in Test II was about two times lower.

A discontinuous crack growth rate around 2×10^{-5} mm/cycle was seen in Figure 4-22, which is equivalent to 1×10^{-7} mm/second at a loading frequency of 0.005 Hz. The rate of corrosion of the pipeline steel in C2 solution in equilibrium with 5% CO₂ and 20% CO₂ + N₂ balance was measured to be 1.3×10^{-9} mm/s (or 0.04 mm/year) and 5.1×10^{-9} mm/s (or 0.16 mm/year), respectively, which are generally consistent with the measurements from the field, usually less than 0.2 mm/year. The actual discontinuous growth rate is about 20 to 80 times higher than the rate of dissolution. This simply suggests that discontinuous growth cannot occur through the dissolution of material at the crack tip. Or, in other words, the contribution of dissolution to crack growth can be ignored. A simple calculation can be used to further justify the above considerations. As it was determined that each step of crack advance was about 15 to 20 μm, which takes about 1 to 2 days. Within these periods, the crack advance by dissolution can be about 0.5 to 1 μm and 0.1 to 0.2 μm when exposed to 20% CO₂ and 5% CO₂+N₂ solutions, respectively.

The negligible role of dissolution in crack advance is also consistent with the insensitivity of discontinuous crack growth rate to the environments in terms of their rates of dissolution. It agrees well with our previous findings that crack growth can proceed without a direct exposure of crack tip to the corrosion environment as long as the diffusible hydrogen generated on the steel surface can reach the crack tip.

It is surprising that there is a huge difference in crack crevice between the tests in the environment with 5% CO₂+N₂ (Test I and II) and 20% CO₂ + N₂ gas (Test III). This difference can be bridged now simply by considering the increase of crack crevice by corrosion. In Test III,

the crack crevice at the surface of specimen should have been exposed to the test environment for the entire period of exposure, which is about 133 days. This exposure time should yield a dissolution of crack surface by 58 μm at a dissolution rate of 0.16 mm/year. Because of dissolution on both sides of the cracked surface, a crack crevice of about 116 μm should be measured.

To confirm the above calculations, the crack crevice intercepting the surface of specimen at the middle position in Test III was analyzed. The morphology of the crack crevice traced from Figure 4-13b) is shown in Figure 4-23. There is an obvious transition in the width of crevice between the cracked portion by corrosion and that by fatigue cracking in air prior to the test. The wedge shaped crack crevice could be formed only by an accumulated dissolution of cracked surface for a different length of time depending on the time the cracked surface was created. The measured width of crack crevice for the pre-fatigued crack with a full length of exposure time was about 105 μm , which is very close to 116 μm , the width of crack crevice calculated solely based on the rate of dissolution.

At the site where corrosion cracking by discontinuous crack growth was first initiated, the width of crack crevice was measured to be 51.5 μm . This width can be converted to a time point at which the corrosion will start based on the rate of corrosion. This has been calculated to be 58.7 days. The starting K_{max} at the surface tip of the crack at MP position was 27.95 $\text{MPa}\sqrt{\text{m}}$, which yields a combined factor of about 4544 $(\text{MPa}\sqrt{\text{m}})^3/\text{Hz}^{0.1}$ at the starting R ratio of 0.65. When the R ratio is decreased to 0.52, the combined factor is calculated to be 8547 $(\text{MPa}\sqrt{\text{m}})^3/\text{Hz}^{0.1}$, which is the threshold value for the start of discontinuous crack growth of a blunt crack or continuous growth of a sharp crack as assumed previously.

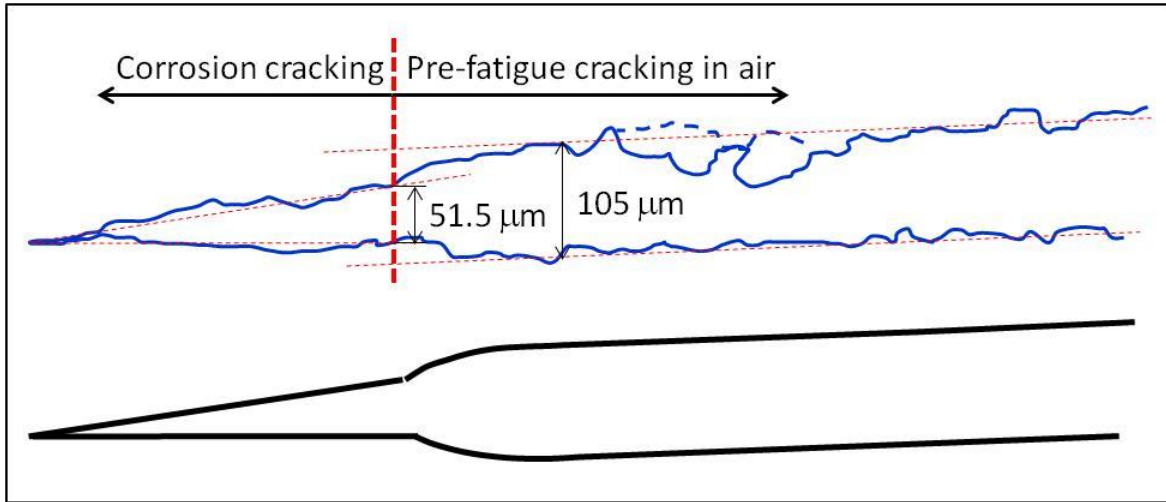


Figure 4-23: Crack morphology in the depth direction of the crack located at MP of Test

III

The time period from the beginning of the discontinuous crack growth (when R was reduced to 0.50 in Table 4-2) to the end of test was 63 days, which agrees well with the time of period (58.7 day) estimated based on the width of crack crevice measured at the location where discontinuous crack growth started (Figure 4-23). This agreement further confirms the assumption that discontinuous crack growth starts at the threshold for the continuous crack growth of the crack with a sharp tip.

Similar calculation could be applied to Test I and Test II. However, the very low dissolution rate in C2 solution in equilibrium with 5% CO₂ will make the estimation inaccurate. For example, a corrosion rate of 0.04 mm/year would yield a maximum dissolution of less than 3 μm for an exposure of 23.5 days in Test I, and less than 15 μm for an exposure of 133 days in Test II, although the width of crack observed generally agrees with the above estimation.

The crack crevice at the root of machined slot in the depth direction was also measured, as shown in Table 4-6. This width is much smaller than that measured at the surface. This is caused by the reduced CO₂ level in the crevice with increasing distance to the crack mouth at the surface of the specimen, a phenomenon similar to the reduced corrosion rate or CO₂ level with increasing the distance from the open mouth of a disbonded coating. This has been well studied in [19].

From the above discussion, one can clearly see the role of corrosion in discontinuous crack growth, which is summarized below:

- 1) Increasing the rate of corrosion directly causes crack tip blunting through the removal of materials from the crack tip, but makes negligible contribution to crack advance. Higher corrosion rate will lead to a larger crack tip radius and in turn a higher threshold for continuous crack growth of the crack with a blunt tip.

- 2) Increasing the rate of corrosion may generate more hydrogen which on one hand would increase the potential of microcrack initiation in the fracture process zone, on the other hand, however, may facilitate plastic deformation further increasing the degree of crack blunting. These two factors may cancel each other in terms of their effect on crack growth.
- 3) Overall, the first factor seems predominant; increasing the threshold for continuous crack growth. The second factor is secondary as the overall discontinuous crack growth rate was not very sensitive to the rate of corrosion. The situation may be very different if the rate of dissolution becomes extremely low, for example, in the case where CO₂ level in the solution is very low such that effects of hydrogen are minimized and microbial corrosion may become predominant.

In Figure 4-22, the growth rate in the depth direction in Test II was lower than that at the surface, while the opposite is observed in Test III. This is believed to be caused by the combined effect of crack tip blunting factor and the hydrogen factor. In Test III, much more hydrogen can be generated and the crack tip in the depth direction has not been blunted to a degree as large as seen at the surface, making the crack growth in the depth direction higher. In Test II, crack tip blunting by corrosion is not very much different between the surface and the depth, leaving hydrogen the dominant factor for crack growth.

4.4 Conclusions

This study examined the dependence of the effect of creep and crack tip dissolution on crack propagation. Major results obtained suggest that:

1. In high CO₂ environments, unless severe mechanical loading is applied, crack propagation may occur by a predominantly dissolution controlled mechanism. However, even with high CO₂ concentrations, the associated growth rates are very low.
2. Under benign loading conditions, determined to be at a combined environmental-fatigue factors below the growth threshold , a sharp crack tip may be blunted by either or both of two factors;
 - a. Environmental crack tip blunting
 - b. Mechanical blunting through low temperature creep.
3. Depending on the operating mechanical loading and/or environmental conditions, crack re-initiation may occur by either
 - a. A dissolution controlled mechanism if mechanical loading is benign and a severe corrosive environment is present
 - b. Purely mechanically driven crack growth if ΔK or R-ratio are severe enough
 - c. By a synergistic effect of environmental and mechanical factors, particularly by hydrogen enhanced crack propagation and mechanical (cyclic) loading. Such synergy results in crack re-initiation at mechanical loading conditions that would have otherwise been below the threshold required for crack propagation.
4. Although increasing CO₂ concentration in the simulated groundwater generates a more acidic solution with more hydrogen ions, it may not necessarily result in a higher crack

propagation rate as the increased hydrogen ion concentration may cause increased crack tip blunting by a dissolution mechanism as well as increased hydrogen enhanced localized plasticity which intensifies crack tip blunting.

5. Generally, on crack re-initiation, a discontinuous type of crack propagation occurs, moving in discontinuous steps that correlate well with the average grain size. Each step in crack propagation required between 500-1000 stress cycles at a stress ratio of 0.22
6. Generally the dissolution mechanism contributes significantly to crack tip blunting but has a negligible effect on actual crack propagation.

References

- [1] Delanty, B., and O'Beirne, J., 1992, "Major Field Study Compares Pipeline SCC with Coatings," *Oil and Gas Journal*, **90**(24) pp. 39-44.
- [2] National Energy Board, 1996, "Public Enquiry Concerning Stress Corrosion Cracking on Canadian Oil and Gas Pipelines," report #MH-2-95.
- [3] Colwell, J. A., Leis, B. N., and Singh, P. M., 2005, "Recent Developments In Characterizing The Mechanism Of Near Neutral pH SCC," *Corrosion/2005*, paper # 05161, .
- [4] Yan, M., Wang, J., Han, E., 2008, "Local Environment Under Simulated Disbonded Coating on Steel Pipelines in Soil Solution," *Corrosion Science*, **50**(5) pp. 1331-1339.
- [5] Zhang, G. A., and Cheng, Y. F., 2009, "Micro-Electrochemical Characterization of Corrosion of Welded X70 Pipeline Steel in Near-Neutral pH Solution," *Corrosion Science*, **51**(8) pp. 1714-1724.
- [6] Chen, X., Du, C., Li, X., 2009, "Effects of Cathodic Potential on the Local Electrochemical Environment Under a Disbonded Coating," *Journal of Applied Electrochemistry*, **39**(5) pp. 697-704.
- [7] Chen, X., Li, X. G., Du, C. W., 2009, "Effect of Cathodic Protection on Corrosion of Pipeline Steel Under Disbonded Coating," *Corrosion Science*, **51**(9) pp. 2242-2245.
- [8] Beavers, J. A., and Worthingham, R., 2002, "The influence of soil chemistry on SCC of underground pipelines," 2002 International Pipeline Conference, ASME, pp. Paper no. IPC2002-27146.
- [9] Beavers, J. A., and Harle, B. A., 1996, "Mechanisms of High pH and Near-Neutral pH SCC of Underground Pipes," International Pipeline Conference, ASME, New York, **1**, pp. 555-564.

- [10] Fang, B. Y., Atrens, A., Wang, J. Q., 2003, "Review of Stress Corrosion Cracking of Pipeline Steels in 'Low' and 'High' pH Solutions," *Journal of Materials Science*, **38**(1) pp. 127-132.
- [11]] S. Asher, P. Singh, J. Colwell, B. Leis. *Crack Initiation of Line Pipe Steels in Near-Neutral pH Environments*. 16th International Corrosion Congress. 2005. Beijing, China.
- [12] Zheng, W., Revie, R.W., MacLeod, F.A., 1998, "Low pH SCC: Environmental effects on crack propagation," Prepared for PRCI Project PR-230 9413, MTL 98-41.
- [13] Parkins, R.N., 1999, "A review of stress corrosion cracking of pipelines in contact with near-neutral (low) pH solutions," PRCI, Report for the Line Pipe Research Supervisory Committee of PRC International.
- [14] Chen, W., and Zheng, W., 2005, "Progress in understanding of pipeline SCC: Initiation and propagation," *Symposium on Pipelines for the 21st century*, W. Chen, ed., Canadian Institute of Mines, Metallurgy and Petroleum, pp. 419-416.
- [15] Beavers, J. A., Durr, C. L., Delanty, B. S., 2001, "Near-neutral pH SCC: crack propagation in susceptible soil environments," *CORROSION/2001*. NACE, Paper No. 01217.
- [16] Wang, Y. Z., Revie, R. W., and Parkins, R. N., 1999, "Mechanistic aspects of stress corrosion crack initiation and early propagation," *Corrosion '99*, NACE, paper no 99143.
- [17] Chen, W., and Sutherby, R. L., 2007, "Crack Growth Behavior of Pipeline Steel in Near-Neutral pH Soil Environments," *Metallurgical and Materials Transactions A*, **38A**(6) pp. 1260-1268.
- [18] Chen, W., Kania, R., Worthingham, R., 2009, "Transgranular Crack Growth in the Pipeline Steels Exposed to Near-Neutral pH Soil Aqueous Solutions: The Role of Hydrogen," *Acta Materialia*, **57**(20) pp. 6200-6214.

[19] Gangloff, R. P., 2003, "*Hydrogen-Assisted Cracking in High-Strength Alloys.*"
Comprehensive Structure Integrity, Volume 6: Environmentally-Assisted Fracture. Elsevier,
Oxford, 2003.

CHAPTER FIVE

GROWTH OF NEAR-NEUTRAL PH STRESS CORROSION CRACKS AT OPEN CIRCUIT POTENTIAL AFTER HYDROSTATIC TESTING

5.1 Introduction

Since its discovery on Canadian oil and gas pipelines in the mid 80's, near-neutral pH stress corrosion cracking has remained a major pipeline integrity concern to pipeline operators. There have been a lot of studies aimed at improving several aspects of the general understanding of this phenomenon. For instance, there have been several studies aimed at determining the influence of ionic species on the initiation and growth of stress corrosion cracks [1-5]. From these studies and others, our understanding of the mechanistic aspects of stress corrosion cracking development has greatly improved. However, there are still a few issues that challenge current understanding of the process. Ideally, mathematical/statistical models would have been more desirable for determining both the most likely sites and corresponding growth rates of stress corrosion cracking. However, up to the present, this has been precluded by insufficient understanding of initiation and growth behavior of the phenomenon. Pipeline integrity management programs still rely on in-line inspection for oil pipelines and/or hydrostatic testing for gas pipelines because of their much better reliability when compared to currently available models [6].

Hydrostatic testing is a qualitative method employed to determine the fitness for service of pressure piping systems. It involves filling the pipe with water and loading to a pressure higher than the design pressure. If the pipe survives without bursting or leaking, then it could be assumed that all existing cracks are below a pre-determined maximum size. This information is then used to determine a safe re-inspection interval, assuming a pre-determined constant crack growth rate. Besides causing critical size flaws to rupture, hydrostatic testing has been found to inhibit crack propagation by blunting the crack tip, making it harder for such cracks to re-initiate in service [7]. However, it has also been contended that although hydrostatic testing itself is a

one-cycle fatigue loading, substantial crack propagation may occur during the process [8-12]. Chen [12] concluded that the extent of crack propagation during hydrostatic testing is environmentally dependent and that hydrostatic testing can reactivate small dormant cracks, reversing any gains in crack growth retardation by crack tip blunting.

Parkins [13-14] determined that CO₂ plays a major role in the development of near-neutral pH stress corrosion cracking. Since crack propagation during hydrostatic testing is environment dependent, CO₂ concentration in the local environment under the disbondment could significantly influence cracking rate during hydrostatic testing. Delanty and O'Beirne [15] found that CO₂ concentration in the bulk soil solution adjacent on the pipe surface varies significantly with the seasons. For instance soil CO₂ levels was 4% in winter but could be up to 23% in spring. Beavers and Harle [16] have proposed that crack growth may occur only during the fall and winter months when soil acidity is higher and trapped solutions are more concentrated and crack dormancy or near dormancy may occur during spring and summer months. Since carbonic acid concentration is directly related to CO₂ concentrations, carbonic acid concentrations can also be expected to vary with the seasons. Indeed Delanty and O'Beirne's measurements revealed that carbonic acid concentration in the soil water was 20 times higher in winter. This means that pipelines with disbonded coatings are exposed to higher levels of acidity and lower pH, in winter. Therefore, dissolution rates should be more intense in winter and pipelines may experience more localized type of corrosion, e.g. pitting, under this condition. Increased dissolution may also increase crack tip blunting and may lead to crack dormancy.

In this communication, variations in crack propagation rates of surface type flaws with CO₂ content in the test environment at open circuit potentials in near-neutral pH range after

hydrostatic testing are presented. These results also detail the variations in growth rates of NNP-HSCC cracks with variation in local environment due to spatial separation from the open mouth of a coating disbondment at open circuit. The effects of varying extremes of CO₂ concentrations are also presented.

5.2 Experimental

This study involved four tests. Test P1 involved pre-fatigue cracking a tensile test sample bearing a single reduced section, width = 23 mm with a semi-circular surface type flaw with depth = 2.5 mm at a maximum stress of 75% of the specified minimum yield strength (SMYS). The crack tip was examined using a scanning electron microscope. This was then followed by rapidly ramping up the load to 100% SMYS in 10 seconds, holding the load at 100% SMYS tensile stress for 1 min followed by very rapid unloading and examining the crack tip after unloading.

For the remaining tests, all samples were made from a section of X-65 pipeline steel removed from service. The alloy composition is shown in Table 5-1, while a typical alloy microstructure is shown in Figure 5-1. Custom made flat tensile specimens (Figure 5-2) having three reduced sections were machined from the longitudinal direction of a sectioned pipe. Gauge sections were 23 mm x 45 mm x 9.2 mm in dimension and identical semi-circular shallow notches, 0.2032mm wide, with dimensions $2c = 5$ mm and $a = 2.5$ mm ('c' and 'a' are the major axis and minor semi-axis dimensions of a semi-elliptical crack) were made by electrical discharge machining (EDM) in the middle of each gauge section.

Table 5-3: Alloy (X65) composition

| Element | Composition (wt %) |
|------------|--------------------|
| Carbon | 0.13 |
| Manganese | 1.55 |
| Copper | 0.05 |
| Niobium | 0.05 |
| Chromium | 0.08 |
| Molybdenum | 0.01 |
| Vanadium | 0.002 |
| Nickel | 0.05 |
| Aluminum | 0.042 |
| Titanium | 0.002 |
| Nitrogen | 0.009 |
| Iron | Balance |

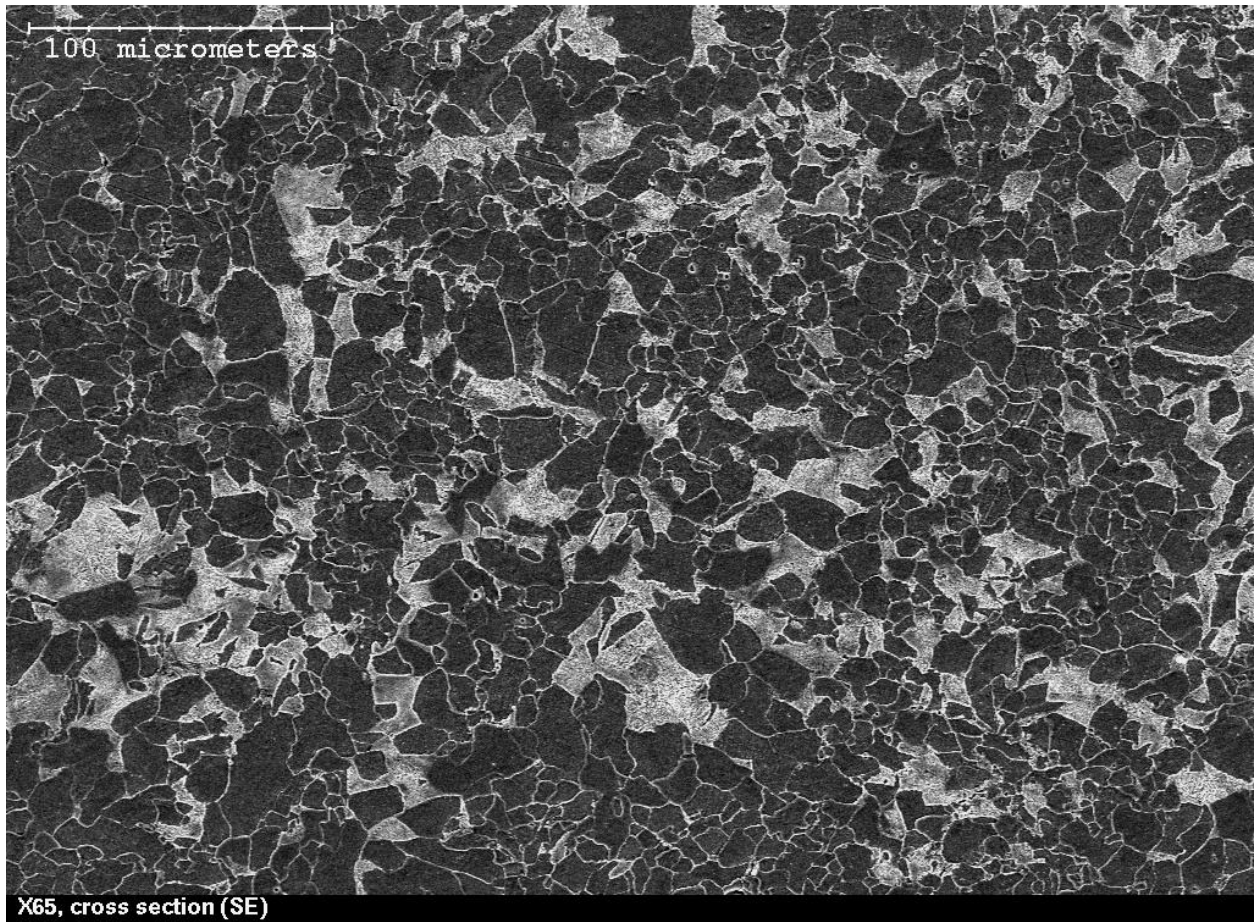


Figure 5-1: Typical microstructure of the alloy X65 used in this study

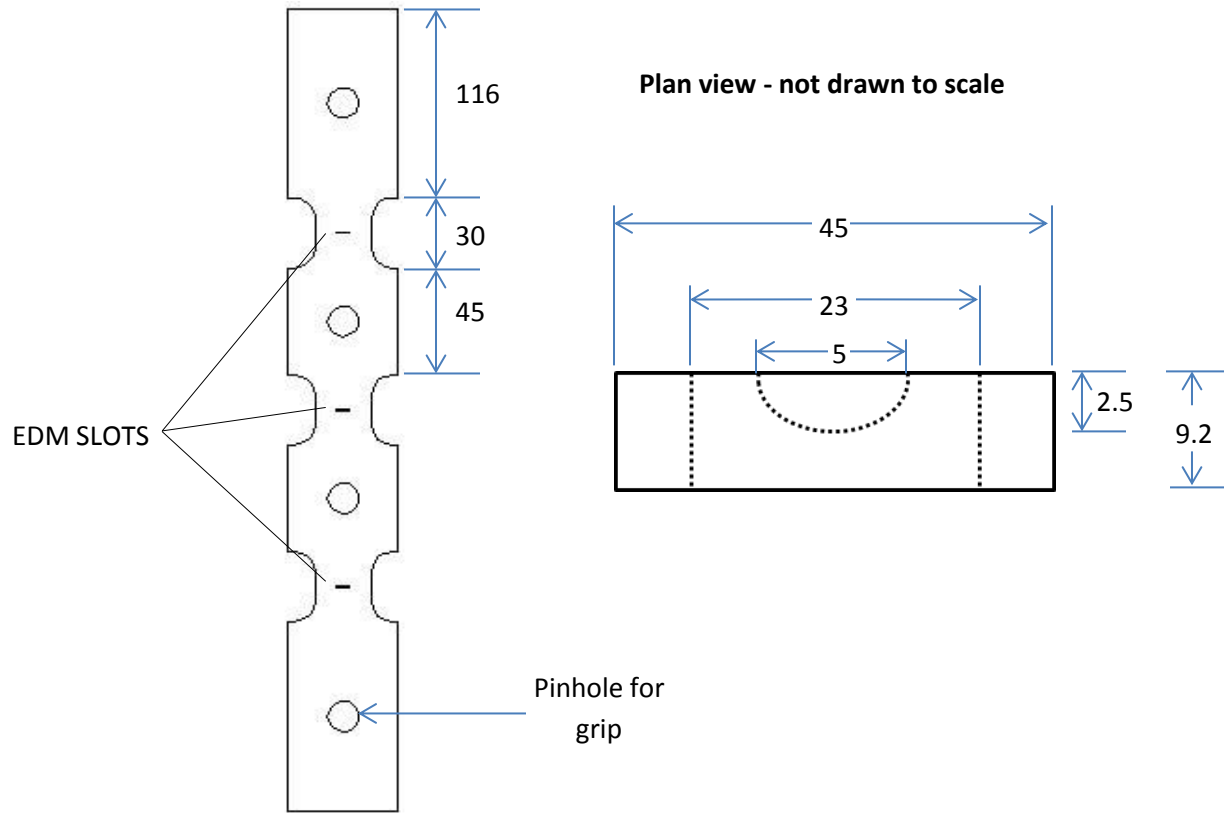


FIGURE 5-2: Test sample designed for this study

A corrosion test cell consisting of two chambers was designed and fabricated from acrylate (Figure 5-3). The inner tube, named the shielding, was designed to simulate coating disbondment at the surface of a pipe. The outer tube holds the bulk solution which simulates the surrounding soil around a pipe in the field while the solution contained in the inner shielding simulates the solution trapped between the coating and the pipe surface on an actual pipeline. The bulk solution in the outer tube was purged by a mixture of certified grade 5% CO₂ (nitrogen balance) fed in through openings at the bottom of the cell, so that CO₂ can only diffuse into the simulated disbondment from the open mouth.

Preparatory to each test, each gauge section was separately pre-fatigue cracked in air to produce the required pre-test half surface crack length of 3.3 mm. The pre-fatigue cracked samples were then exposed to the corrosion media in a sealed test cell and filled with C2 solution (0.0035 KCl, 0.0195 NaHCO₃, 0.0255 CaCl₂.H₂O, 0.0274 MgSO₄.7H₂O, 0.0606 CaCO₃ g/l). Cyclic stresses with a maximum stress of 100% specified minimum yield strength and varying stress ratios was applied during the test. In an attempt to closely simulate real pipeline service conditions, the sides and back surface of each specimen (the one without the surface cracks) were coated with epoxy in order to isolate these surfaces from the corrosion media. Crack growth rates were monitored using a self-assembled potential drop system through copper wire leads soldered across the back of the EDM slots in each gauge section. A constant current of 20A was applied by the potential drop system in order to measure the potential drop across each crack.

For three of the tests reported in this paper, a maximum stress of 100% specified minimum yield strength and a cyclic frequency of 0.005Hz were used for both tests I and II, and 0.0025Hz for test III. All the test conditions are presented in Table 5-2.

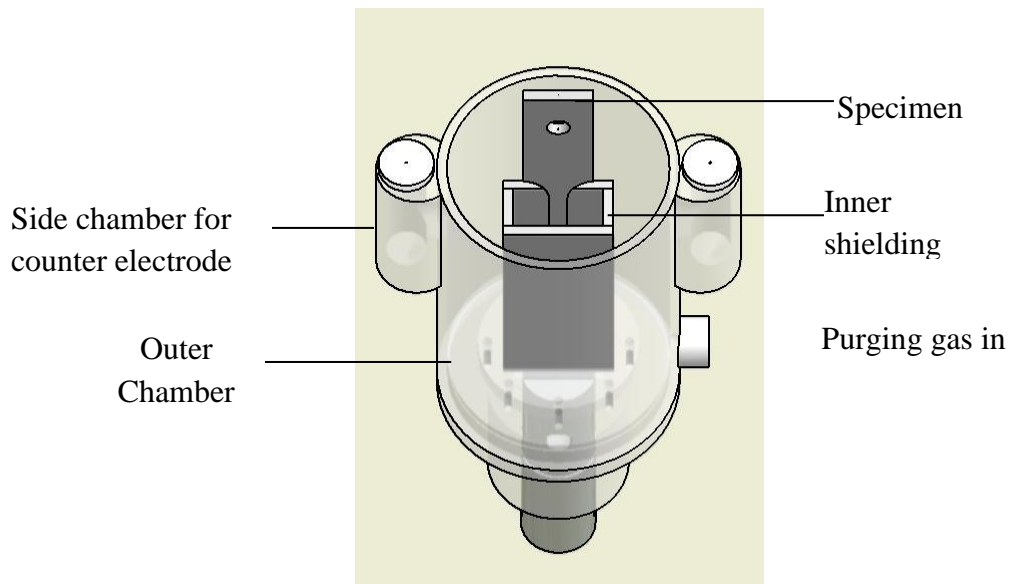


Figure 5-3: Schematic drawing of the corrosion test cell used for study

Table 5-2: Details of test conditions

| | Test P1 | Test I | Test II | Test III |
|---|---|--|---|--|
| Initial stress ratio/duration | Ramp up to 100% SMYS, 10s, hold at 100% SMYS for 1min | 0.65 / 15days 0.60/15days 0.58/15days 0.56 / 3.2 days | 0.65 / 15days 0.60/15days 0.58 / 9.4 days | 0.65/15days 0.60 / 15days 0.58/11.8 days |
| Frequency (Hz) | - | 0.005 | 0.005 | 0.0025 |
| Combined factor at start of test [(MPa√m) ³ Hz ^{-0.1}] | - | 8400 | 9800 | 11000 |
| Combined factor at the R-ratio at which crack started to grow [(MPa√m) ³ Hz ^{-0.1}] | - | 10425 | 11295 | 11088 |
| Maximum stress | 100% SMYS | | | |
| Testing environment | - | C2 solution | | |
| Purging Gas | Air | 20% CO ₂ | 5% CO ₂ | |
| Pre-test pH | - | 5.6 | 6.3 | 6.3 |

Cracks were subjected to a peak stress of 100% SMYS and initially cyclically loaded at a stress ratio of 0.65 which was pre-determined as a condition where no propagation would occur. This was done to allow the material to interact with the environment to simulate a situation where a previously hydrotested crack had been returned into service. The stress ratio was then reduced to 0.6 which is a stress cycle that could be experienced by a liquid line. If growth was not observed at this stress ratio, the stress ratio was gradually reduced in steps of 0.02 till crack propagation was detected by the potential drop system.

After each test, the fracture surface was examined and post-test crack lengths determined in order to validate potential drop measurements with actual crack growth measured from the surface of fractured specimens. Initial fracture-face examination was done using an optical microscope. More detailed examination of fracture surfaces was carried out using a Hitachi scanning electron microscope equipped with an energy dispersive x-ray spectrometer for chemical compositional analysis.

5.2.1 Justification of sample geometry and crack size/geometry used

A cursory look at micrographs of SCC obtained from the field show that these cracks are surface type flaws rather than through-thickness flaws. It is well recognized in fracture mechanics that surface type flaws could propagate differently from through-thickness type flaws; hence, the choice of a surface type flaw for this test. In choosing this type of flaw, care was taken to ensure that the crack size chosen is representative of those in the field and that the mechanical driving forces for crack propagation, maximum stress intensity (K_{max}) and stress intensity ranges (ΔK) are similar to those that could be obtained in the field. For instance for a semicircular flaw that is 3.3 mm deep as chosen in this study, at 100% SMYS, a K_{max} of 31.97 MPa·m^{1/2} and a

stress intensity factor range of $12.79 \text{ MPa}\cdot\text{m}^{1/2}$ is obtained at a stress ratio of 0.6. These mechanical conditions will be similar to those experienced by a field crack measuring 5 mm at the pipe surface having an aspect ratio (a/c) of 0.28. In this case, a K_{max} of $32.09 \text{ MPa}\cdot\text{m}^{1/2}$ and a stress intensity factor range of $12.84 \text{ MPa}\cdot\text{m}^{1/2}$ are obtained at a stress ratio of 0.6. Thus the crack dimensions chosen could be easily obtained in the field, especially on a liquid line. Although it might be argued that individual cracks in the field may never measure 5 mm, pipeline operators typically rely on industry standards for fitness for service assessments. These standards recommend a minimum prescribed spacing between adjacent flaws below which such cracks must not be treated as isolated (or single) flaws. For instance ASME B31G (or BS7910) recommends that cracks that are closer than three times the wall thickness be regarded as interacting flaws. At the lowest level of assessment, these cracks will usually be taken as just one flaw by adding the lengths of all the interacting flaws. However, there are higher levels of analysis that employ a more complex analysis to determine the effective length of cracks. Whichever level of analysis is used, it is typical to have effective cracks lengths that are longer than 5 mm.

5.2.2 Justification of stress level used

In our previous communications [17, 18], crack propagation behavior was examined at stress levels (75% SMYS) that are very close to normal operating conditions. However, some of those tests took a long time to complete. In some instances tests lasted for over 5 months. It is standard practice to conduct accelerated tests to shorten testing times. One of the ways of achieving this is by using higher stress levels for testing. Using such higher stress levels result in

higher maximum stress intensity, K_{max} , leading to more rapid crack re-initiation and higher crack propagation rates. Hence, the choice of a maximum stress of 100% SMYS in this study. Also, although operating stresses are typically kept at <72% SMYS in normal pipeline operations, it is well-known that secondary stresses resulting from residual stress, soil movement and geometric distortions could significantly increase the actual stress experienced by linepipe segments above 72% SMYS.

5.3 Results

5.3.1 Mechanical deformation of crack tip in air (Test P1)

The reasoning behind this experiment design is as follows. Assume a pipeline contains a crack field (colony) which had been hydrotested before without failure. Since hydrotesting involves stresses up to 110% SMYS, the tips of the existing cracks will likely be deformed. The crack tip morphology after pre-fatigue cracking is shown in Figure 5-4a. The figure shows that very fine cracks were initiated at the notch tip during pre-fatigue cracking. The crack morphology after the one minute loading is shown in Figure 5-4b. Figure 5-4b clearly shows how intensely deformed the crack tip region could be after loading to 100% SMYS. This intense deformation resulted in the crack walls moving apart inelastically and causing a severe crack tip blunting. No crack propagation was observed during this test suggesting hydrostatic testing may not necessarily cause crack propagation.

This type of blunting is generally regarded as mechanically induced blunting. It will be shown in one of the companion papers (manuscript under preparation) that environmental factors can also result in a similar blunting. It is instructive to know that in the field, after a hydrostatic testing is complete, if the crack is in contact with groundwater, environmental factors can exert their independent effect until the next scheduled hydrostatic testing and this effect can also influence crack propagation during subsequent hydrostatic testing.

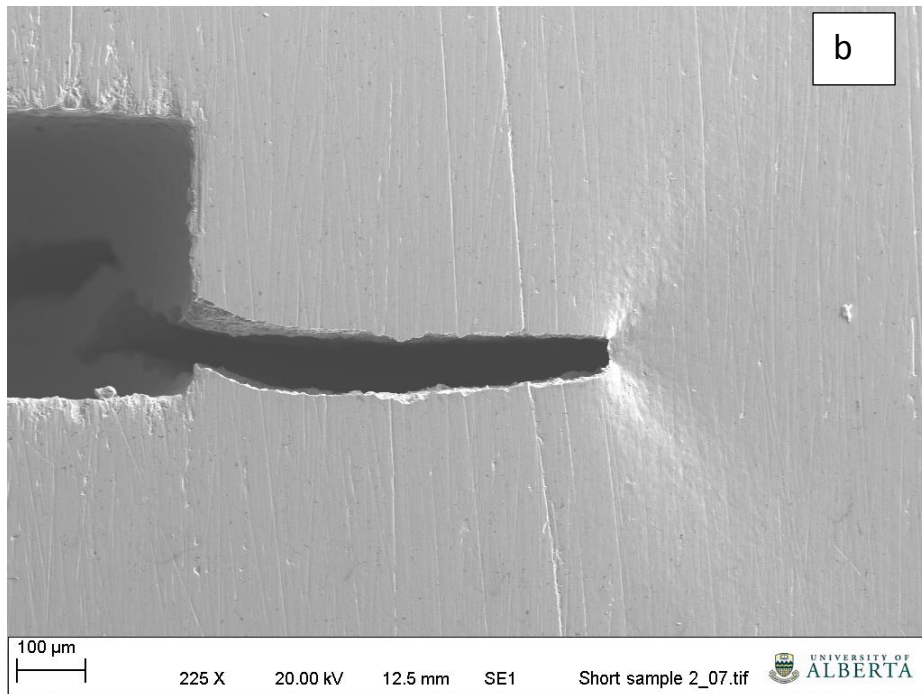
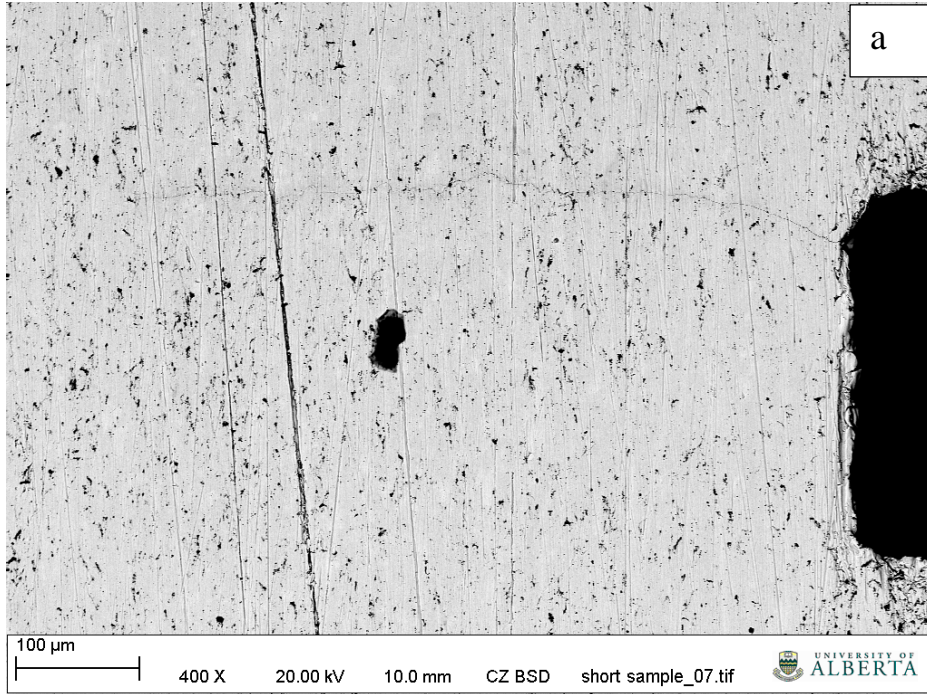


Figure 5-4: Pre-fatigue crack morphology of verification test (a) before, and (b) after 1min hold at 100% SMYS

Based on this verification test, the remaining tests were designed to study the effect of variations in the local environment under the disbondment in combination with the effect of localized crack tip deformation during hydrostatic testing. The rest of this study will examine the combined influence of localized deformation and environmental factor on the rate of crack propagation during hydrostatic testing.

5.3.2 Test results in the 20% CO₂ environment

5.3.2.1 Corrosion behavior at sample surface

Typical sample surface features after testing are shown in Figure 5-5a. Thick loosely adherent deposits of corrosion products were found on the surface of the sample at all three locations. Upon peeling back the corrosion products in test I, only general corrosion was observed at all three locations. The corrosion products were analyzed and found to be FeCO₃, Fe₂O₃ and FeOOH by powder mode x-ray diffraction technique.

5.3.2.2 Crack re-initiation after hydrostatic testing

Crack re-initiation did not occur at a stress ratio of 0.6. No growth was detected at a by the potential drop equipment until the R-ratio was reduced to 0.56. Chen and Sutherby [6] proposed a true corrosion fatigue model $\frac{da}{dN} \propto (\Delta K)^2 \cdot K_{\max}/f^\alpha$ which has been used to clearly identify crack growth thresholds for NNPHSCC (ΔK is the change in stress intensity at the crack tip due to cyclic loading, K_{\max} is the maximum stress intensity at the crack tip, and α is a factor that represents the influence of the corrosion environment on the crack growth rate). Analyzing the current test data using this equation, crack growth reinitiated at a stress ratio of 0.56 which corresponding to a combined factor of approximately 11100 (MPa·√m)³/Hz^{0.1} in the depth direction and 13300(MPa·√m)³/Hz^{0.1} at the sample surface.

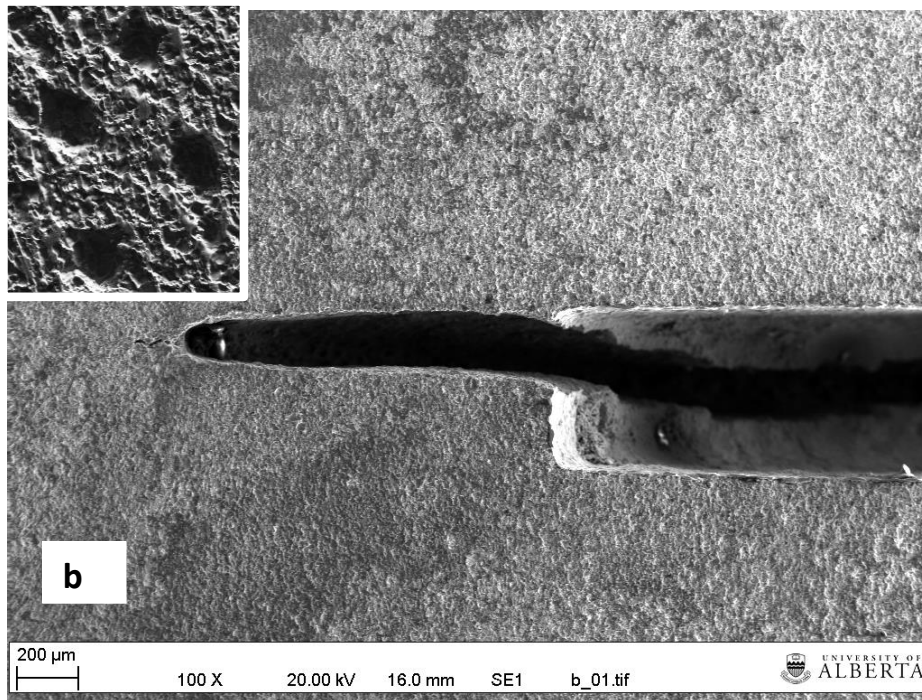
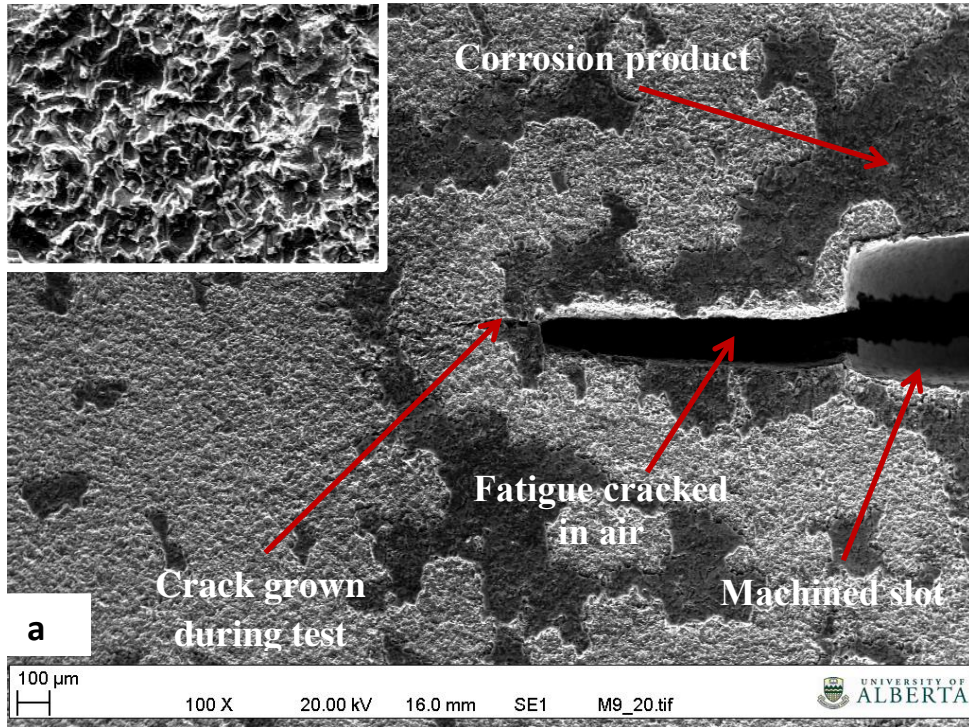


Figure 5-5: Post-test surface features before cleaning (a) test I, (b) Test II and III. Insets are higher magnification images (at 400X)

5.3.2.3 Crack tip morphology following reloading after hydrostatic testing

The test sample ruptured at the open mouth during this test; therefore, crack tip morphologies are available at only 2 locations – 75 mm and 150 mm from the open mouth respectively. This also applies to the rest of the tests presented in subsequent sections.

In test I, scanning electron microscopy reveals intense blunting of the crack tip with 20% CO₂. The pre-fatigue crack tips at the two locations were square in character (Figure 5-6). Secondary cracks were also observed at the tip of the pre-fatigue cracks in test I. High magnification images clearly revealed that secondary cracks preferentially nucleated in the pearlite phase in some instances and at the ferrite-pearlite interface in other instances (Figure 5-7). The final crack tips were very sharp at both locations in (Figures 5-8). Cracks were transgranular in nature.

Examination in the depth direction revealed blunted pre-fatigue crack tips (Figures 5-9 and 5-10). A lot of crack tip branching was observed in the depth direction at 150 mm from the OM, but such branching was not observed at 75 mm from the OM. The branch tips were not as blunted as the main crack front at 150 mm from the OM.

5.3.2.4 Crack propagation behavior

Crack propagation occurred during the test as shown in Figure 5-11. Highest growth rate was observed at the open mouth while growth rates at 75 and 150 mm from the open mouth are quite comparable. The initial and final crack sizes are shown in Tables 5-3 and 5-4 while the initial and final aspect ratios are shown in Table 5-3. The largest reduction in aspect ratios occurred at the open mouth but the reduction in aspect ratios are similar at 75 mm and 150 mm from the open mouth.

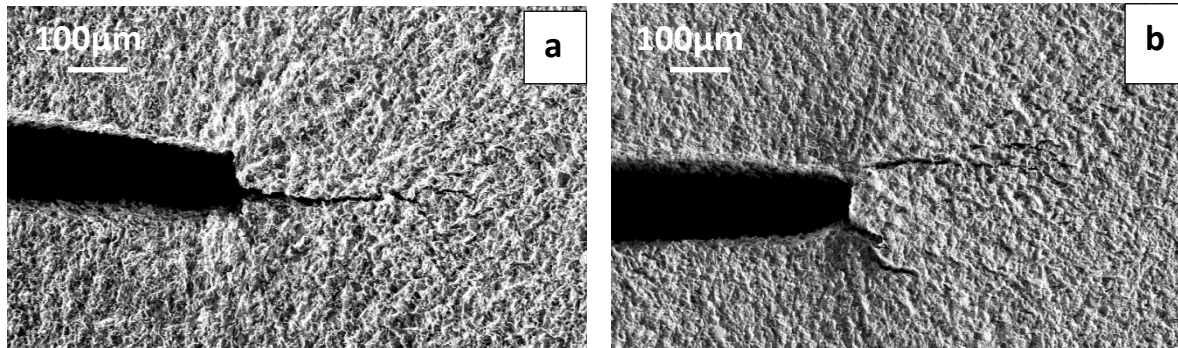


Figure 5-6: Crack tip morphology at sample surface in test I (a) at 75 mm from OM, (b) at 150 mm from OM

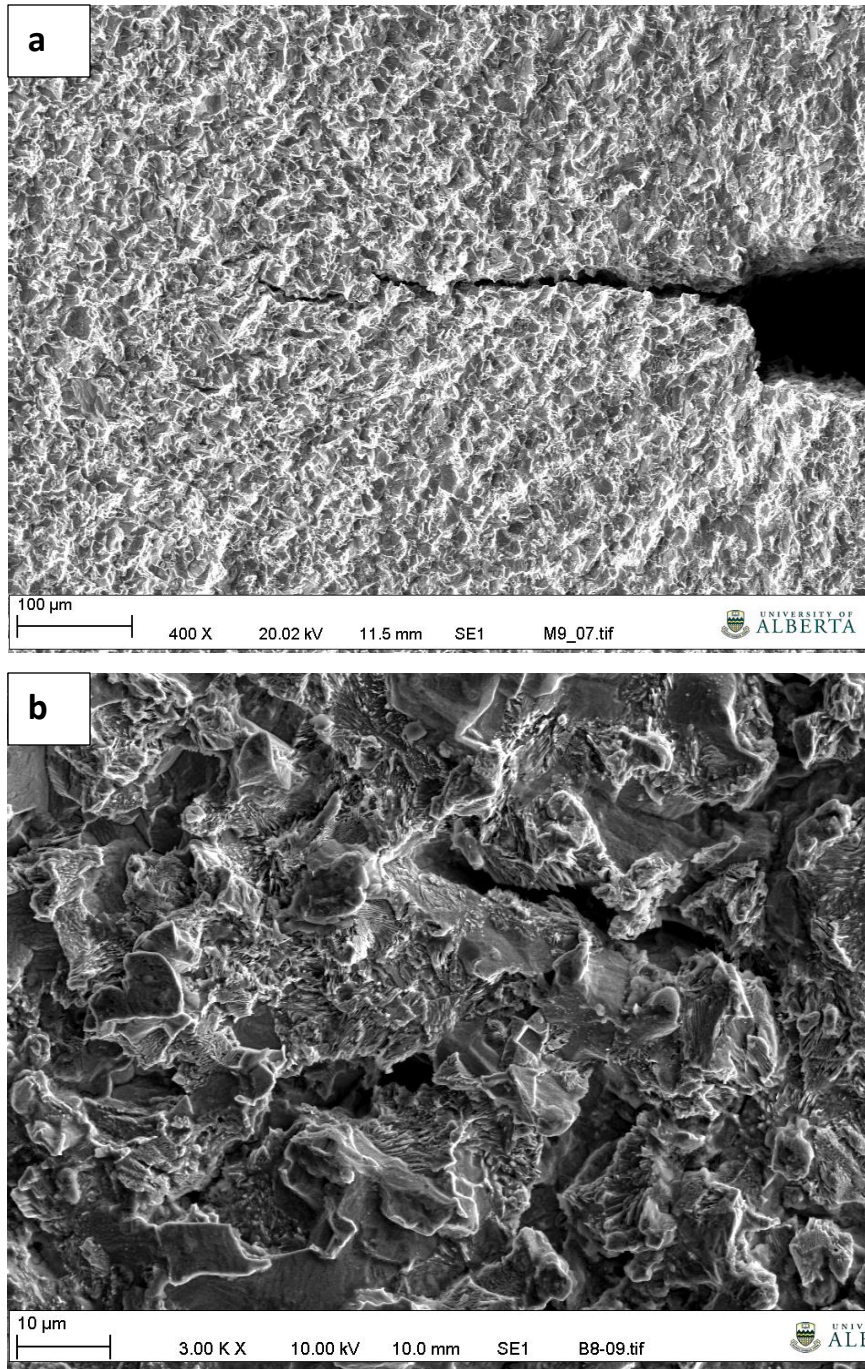


Figure 5-7: Secondary cracks at the pre-fatigue crack tip in test I (a) at low magnification, (b) high magnification

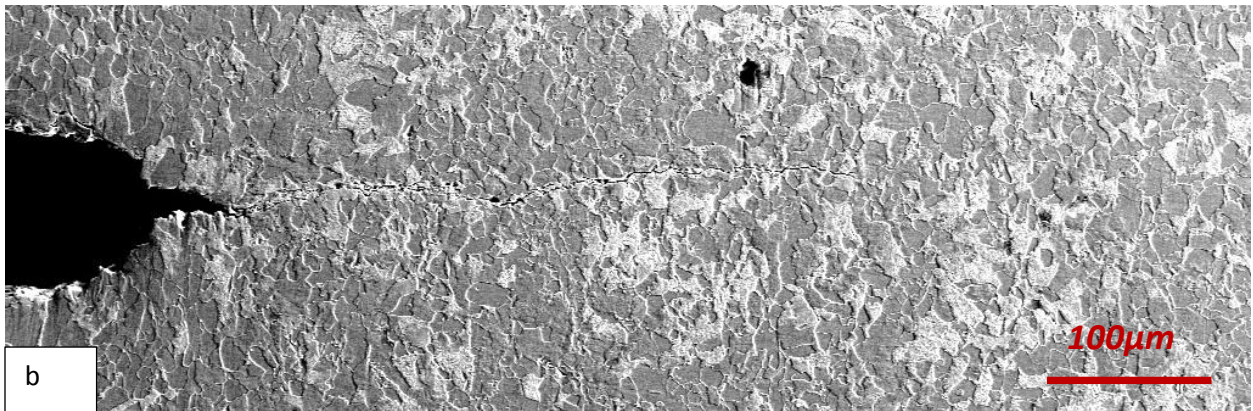
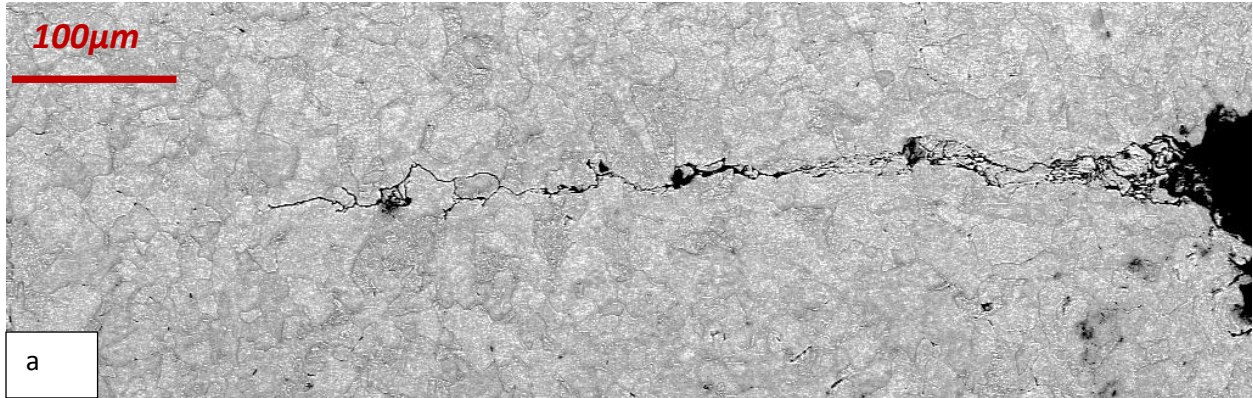


Figure 5-8: Surface crack profile for test I at (a) 75 mm from OM, (b) 150 mm from OM

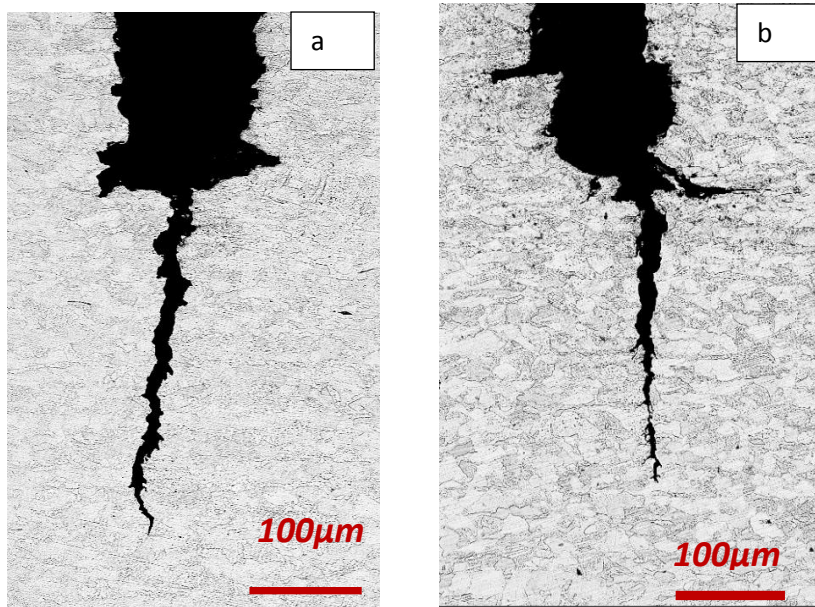


Figure 5-9: Crack morphology in the depth direction in test I (a) at 75 mm from OM, (b) at 150 mm from OM

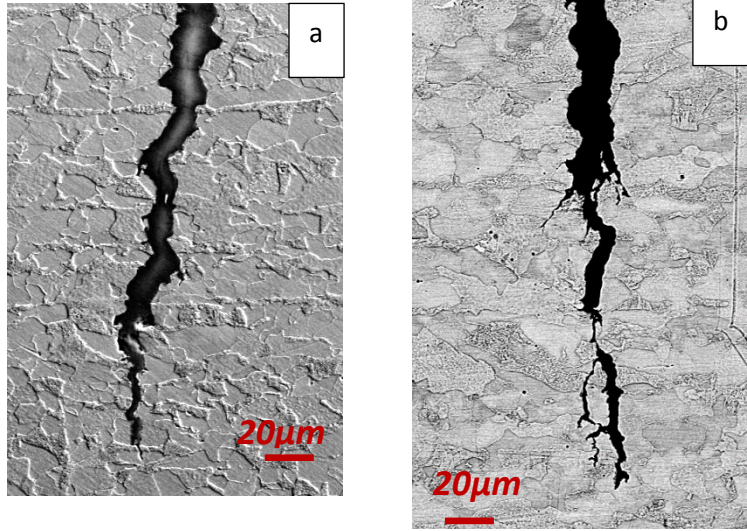


Figure 5-10: Crack tip morphology in the depth direction in test I (a) at 75 mm from OM, (b) at 150 mm from OM

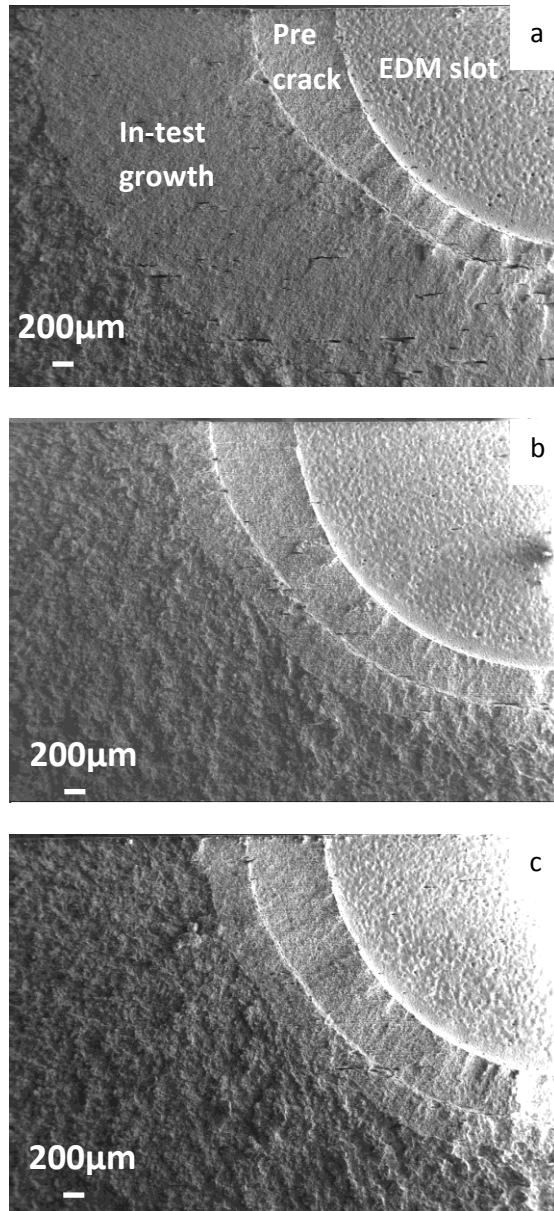


Figure 5-11: Fractured surface for test I showing half of crack section (a) open mouth (b) 75 mm from OM, (c) 150 mm from OM

Table 5-3: Characteristics of crack growth for cracks on the specimen surface

| | | Initial crack length (mm) | Final Crack length (mm) | Net crack growth (mm) | Average crack growth rate (mm/cycle) | Initial/final aspect ratio |
|----------|----|---------------------------|-------------------------|-----------------------|--------------------------------------|----------------------------|
| Test I | OM | 3.42 | 5.21 | 1.79 | 1.30E-03 | 1.08 |
| | MP | 3.30 | 3.76 | 0.46 | 3.37E-04 | 1.03 |
| | BP | 3.41 | 3.85 | 0.44 | 3.22E-04 | 1.04 |
| Test II | OM | 3.54 | 6.25 | 2.71 | 6.68E-04 | 1.17 |
| | MP | 3.52 | 3.97 | 0.45 | 1.11E-04 | 1.03 |
| | BP | 3.55 | 4.26 | 0.71 | 1.75E-04 | 1.01 |
| Test III | OM | 3.37 | 6.25 | 2.88 | 5.66E-04 | 1.14 |
| | MP | 3.45 | 3.89 | 0.44 | 8.57E-05 | 1.05 |
| | BP | 3.34 | 3.74 | 0.41 | 8.02E-05 | 1.07 |

Table 5-4: Characteristics of crack growth for cracks in the depth direction

| | | Initial crack length (mm) | Final Crack length (mm) | Net crack growth (mm) | Average crack growth rate (mm/cycle) |
|----------|----|---------------------------|-------------------------|-----------------------|--------------------------------------|
| Test I | OM | 2.91 | 4.08 | 1.18 | 8.57E-04 |
| | MP | 2.90 | 3.21 | 0.31 | 2.23E-04 |
| | BP | 3.01 | 3.28 | 0.27 | 1.98E-04 |
| Test II | OM | 3.15 | 4.74 | 1.60 | 3.94E-04 |
| | MP | 3.14 | 3.44 | 0.31 | 7.58E-05 |
| | BP | 3.41 | 4.05 | 0.64 | 1.58E-04 |
| Test III | OM | 3.33 | 5.40 | 2.08 | 4.08E-04 |
| | MP | 3.33 | 3.58 | 0.25 | 4.90E-05 |
| | BP | 3.23E+00 | 3.40E+00 | 0.1639 | 3.22E-05 |

5.3.3 Test results in the 5%CO₂ environment (Tests II and III)

5.3.3.1 Corrosion behavior at sample surface

Post-test examination of the corroded sample surfaces revealed that the corrosion behavior was different from that in the 20% environment. Post-test examination of the corroded sample surfaces reveals a thin layer of corrosion products at the sample surface at all three locations in test II (with 5% CO₂) as shown in Figure 5-5b. The corrosion products were analyzed and found to be FeCO₃, Fe₂O₃ and FeOOH by powder mode x-ray diffraction technique. Severe pitting corresponding to intense localized dissolution, coupled with general corrosion was observed at the open mouth (Figure 5-5b inset). Less severe pitting was observed at 75 mm from the open mouth while only general corrosion occurred at the bottom of the disbondment – 150 mm from the open mouth. Corrosion behavior in test III was similar to those in test II, as the same type of testing environment, 5% CO₂ in C2 solution, was used.

5.3.3.2 Crack re-initiation following loading in the 5% CO₂ environment after hydrostatic testing

In test II, no crack propagation was observed at a stress ratio of 0.6. Growth reinitiated at a stress ratio of 0.58 which corresponded to a combined factor of approximately 11300 (MPa·√m)³/Hz^{0.1} in the depth direction and 14100 (MPa·√m)³/Hz^{0.1} at the sample surface. Cracks also re-initiated at a stress ratio of 0.58 in test III (the lower frequency test). However, because of the lower frequency, these conditions correspond to a combined factor of 11100 (MPa·√m)³/Hz^{0.1} in the depth direction and 16300 (MPa·√m)³/Hz^{0.1} at the sample surface.

5.3.3.3 Crack tip morphology following loading in the 5% environment after hydrostatic testing

In both tests II and III, the pre-fatigue crack tips were severely blunted at the two surviving crack locations inside the simulated disbondment (Figure 5-12). Only two locations are shown as the test sample ruptured at the open mouth in tests II and III during the test. There is evidence of significant plastic deformation ahead of the pre-fatigue crack tip. In addition to this, there were several secondary cracks initiated in a colony at the root of the pre-fatigue crack (Figure 5-12). A major distinction between tests II and III is that although the pre-fatigue crack tips in both tests were blunted, the pre-fatigue crack tips in test II were rounded whereas those in test III developed into a squared morphology. A comparison of tests I and II revealed that there is less secondary cracking in the 20% CO₂ environment (Figure 5-6 vs Figure 5-12). It is also evident that the pre-fatigue crack tips in test III developed a squared out morphology similar to the ones in test I. However the pre-fatigue crack tips in test I (20% CO₂ environment) are more squared out than those in test III (5% CO₂ environment). The final post-test crack tips were very fine at 75 mm from OM in both tests II and III. At this location crack openings behind the crack tips were comparable (Figure 5-13). At 150 mm from the open mouth, cracks were blunter than at 75 mm from the open mouth, and the crack opening behind the final post-test crack tips were wider than at 75 mm from the open mouth (Figure 5-14).

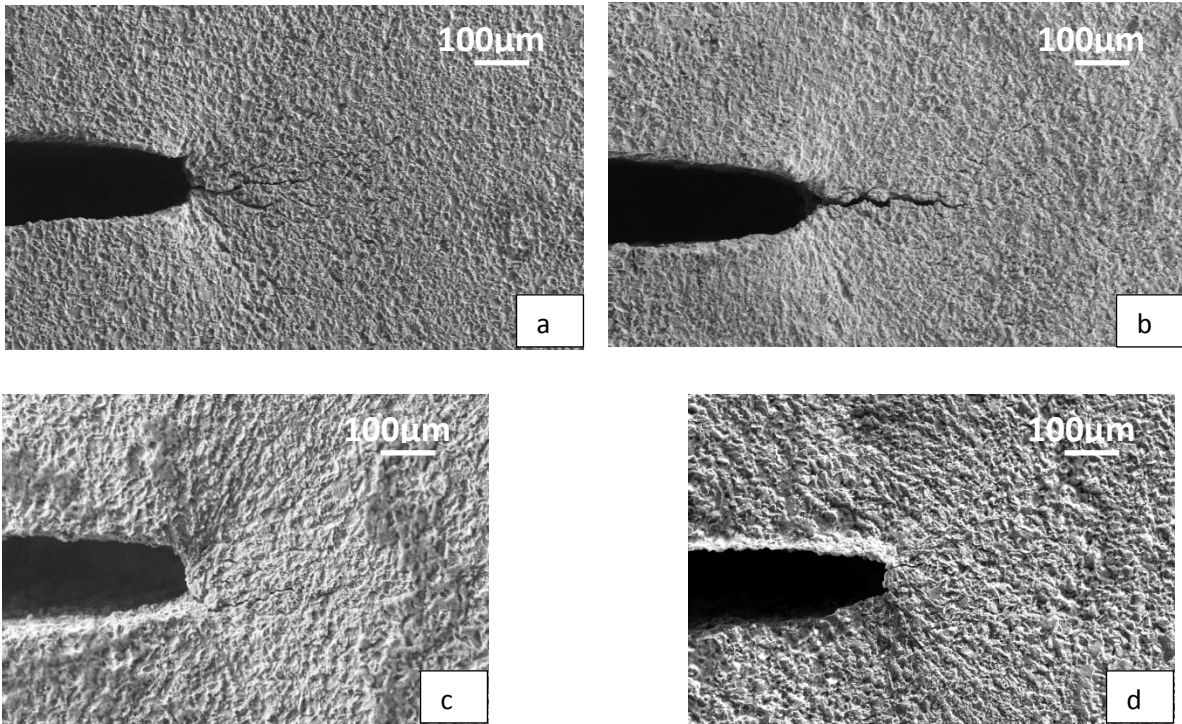


Figure 5-12: Post-test pre-fatigue crack tip morphology (a) 75 mm from OM in test II, (b) 150 mm from OM in test II, (c) 75 mm from OM in test III, (d) 150 mm from OM in test III

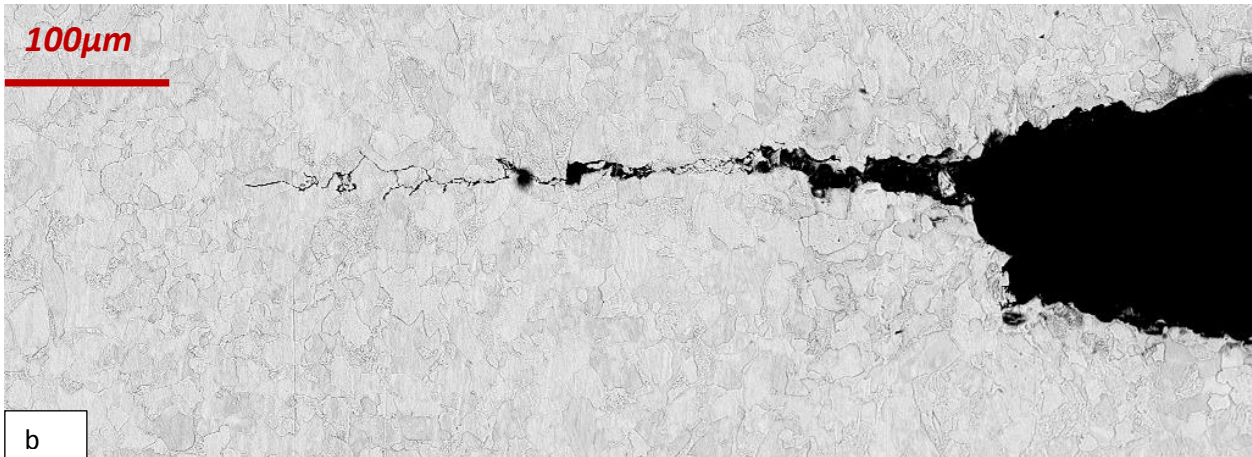
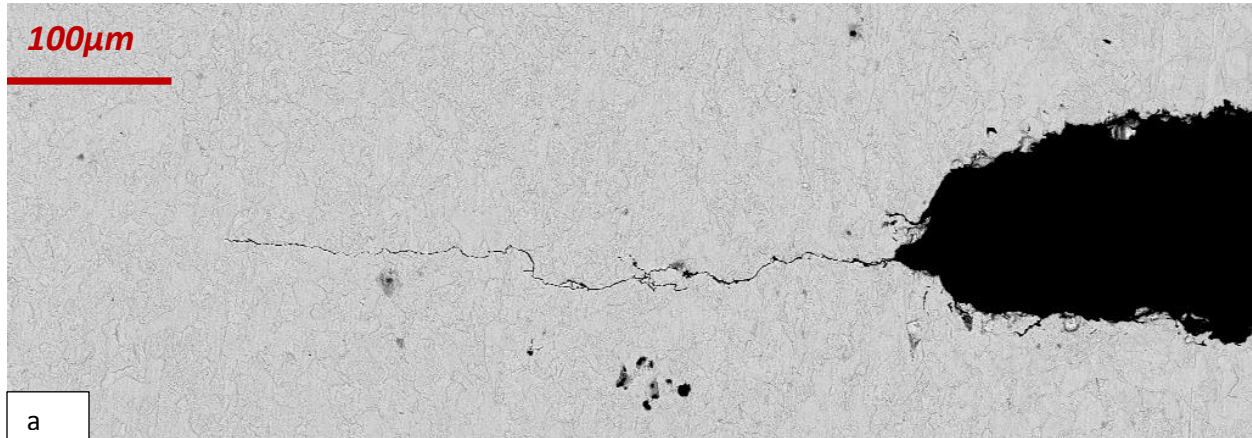


Figure 5-13 : Surface profiles of cracks at 75 mm from OM in (a) Test II and (b) Test III

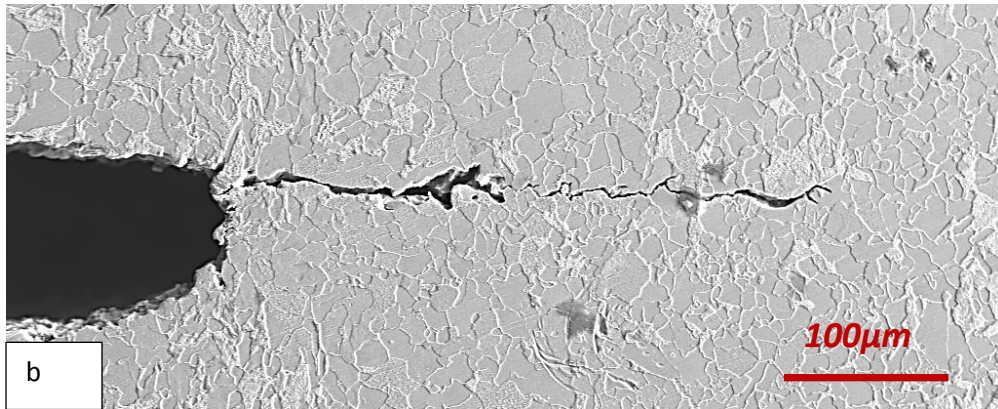
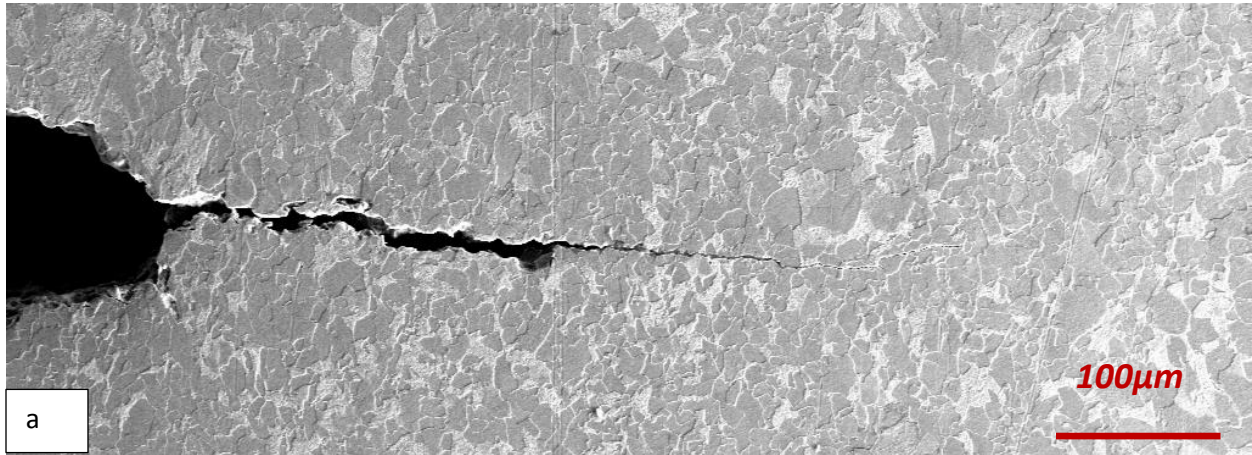


Figure 5-14 : Surface profiles of cracks at 150 mm from OM in (i) Test II and (iii) Test III

Examination in the depth direction also revealed blunted pre-fatigue crack tips (Figures 5-15 and 5-16). Very fine crack tips were also observed at both locations (Figures 5-17 and 5-18). Cracks were transgranular in nature. In test II, it is noticeable that towards the crack tip, cracks that are not connected to the main crack front seem to have initiated inside grains ahead of the main crack front. Some regions where such cracks have not rejoined the main crack front are circled in Figure 5-18. This behavior was not noticed in test III. However, in test III, at 150 mm from the open mouth, significant crack branching seems to have occurred similar to test I. No significant branching was noticed in test II. Generally, cracks were wider in the 20% CO₂ environment than in the 5% CO₂ environment. Also, the final crack tips were noticeably sharper in the 5% CO₂ environment than in the 20% environment despite the fact that crack propagation occurred at more severe mechanical loading in the 20% environment.

5.3.3.4 Crack propagation behavior in the 5% CO₂ environment

The initial and final crack sizes are shown in Tables 5-3 and 5-4. The initial and final aspect ratios are shown in Table 5-3. These tables indicate that while crack propagation occurred at all locations during the test, variations in the local environment with distance from the open mouth could change the extent of growth significantly. In test II, aspect ratios generally decreased at all locations during the test. The largest reduction in aspect ratios occurred at the open mouth while the smallest reduction in aspect ratio occurred at the far end of the disbondment. In test III, aspect ratios generally decreased with distance from the open mouth. However, the lowest decrease in aspect ratios occurred at the open mouth while the largest decrease in aspect ratio occurred at the middle of the disbondment.

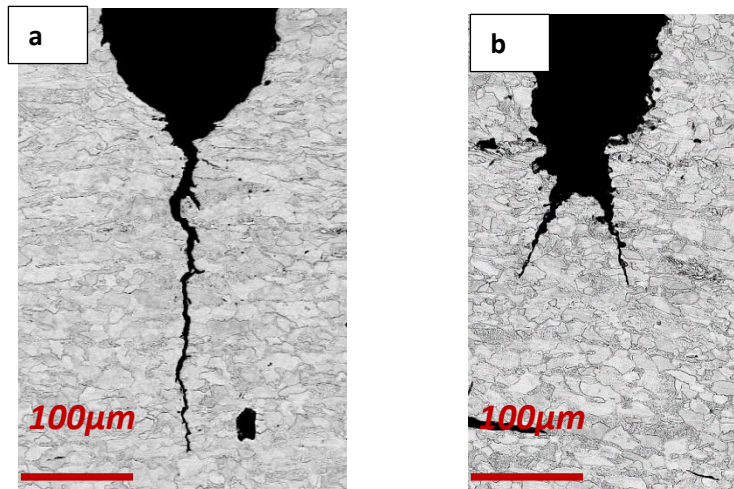


Figure 5-15: Depth profiles of cracks at 75 mm in(a) Test II and (b) Test III

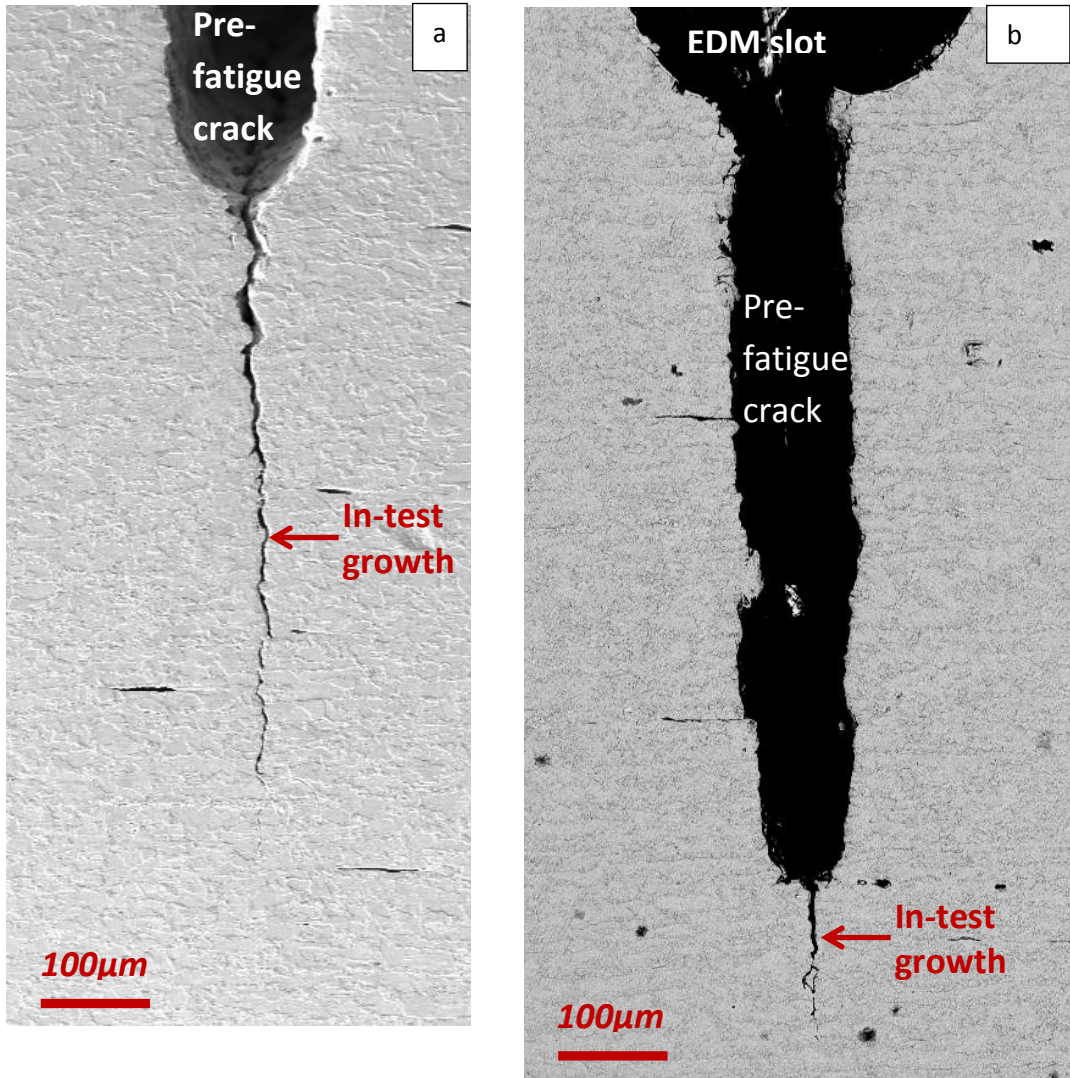


Figure 5-16: Depth profiles of cracks at 150 mm in (a) Test II and (b) Test III

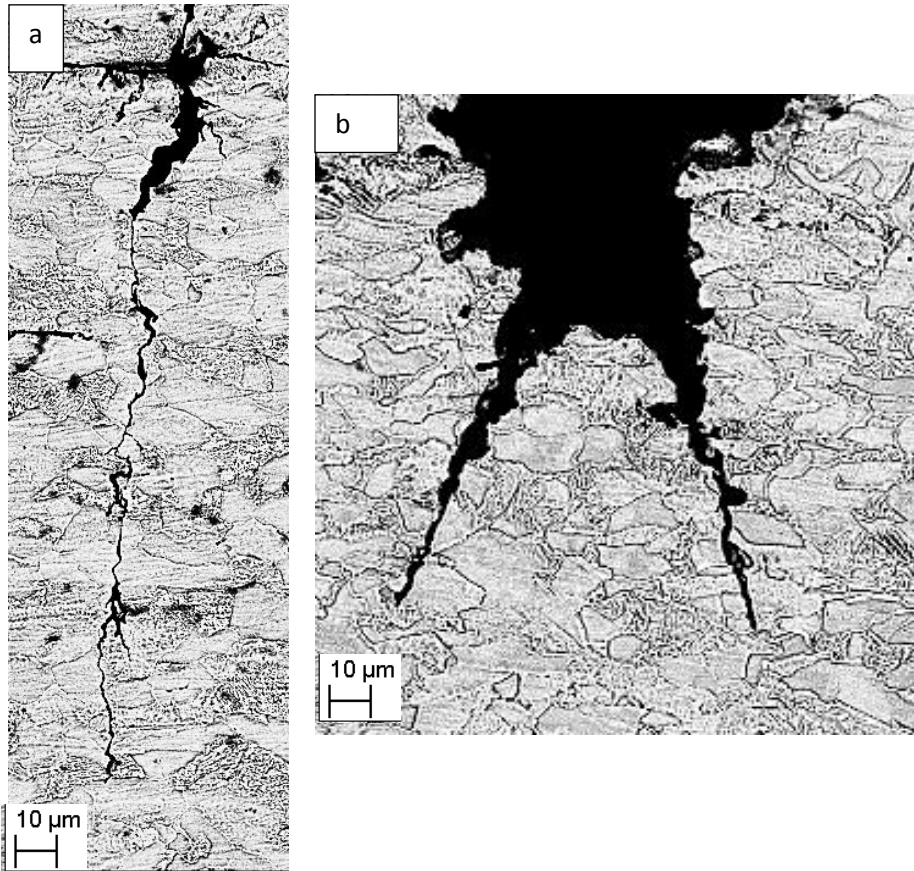


Figure 5-17: Crack tips at higher magnification at 75 mm from OM in depth direction (a) Test II, (b) Test III

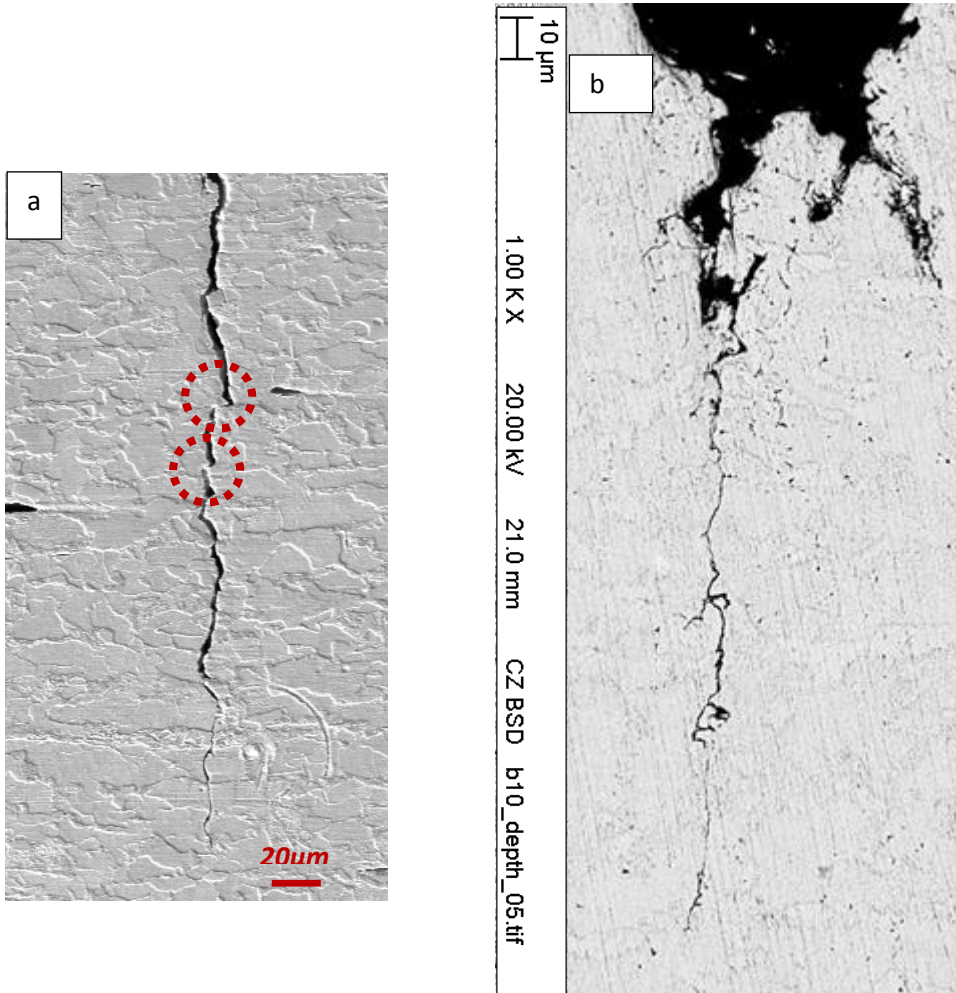


Figure 5-18: Crack tips at higher magnification at 150 mm from OM in depth direction (a) Test II, (b) Test III

Post-test crack propagation rates were determined and a summary is shown in Tables 5-3 and 3. In test II, average crack growth rate was highest at the open mouth and lowest at the far end of the disbondment (150 mm from the open mouth). However, average growth rate at 75 mm and 150 mm from the open mouth are quite comparable. The same trend is observed in test III. However, growth rates are much larger in test II than in test III.

5.3.4 Comparison of fracture face morphologies

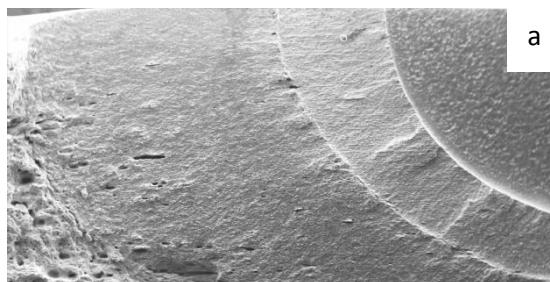
After completing all surface and cross section examination, the samples were broken open in order to examine the actual fracture surfaces. These figures are shown in Figures 5-11, 5-19 and 5-20. The fracture surfaces confirm the observed crack growth trends for all tests. In addition, secondary cracks could be seen on the fracture surface. The density of secondary cracks generally reduced from open mouth to the bottom of the disbondment. Comparison of the density of secondary cracks at the open mouth between the tests in the 5% CO₂ environment and the one in 20% CO₂ environment shows a significantly higher secondary crack population in the 20% CO₂ environment than in the 5% CO₂ environment.

5.4 Discussion

5.4.1 Current understanding of crack propagation mechanisms

In a recent communication, current understanding of the mechanisms involved in NNPHSCC crack propagation were summarized [25]. These were:

1. Pure dissolution mechanism: Believed to be only relevant in the early stages of crack propagation
2. Direct cracking through hydrogen enhanced mechanical mechanisms.



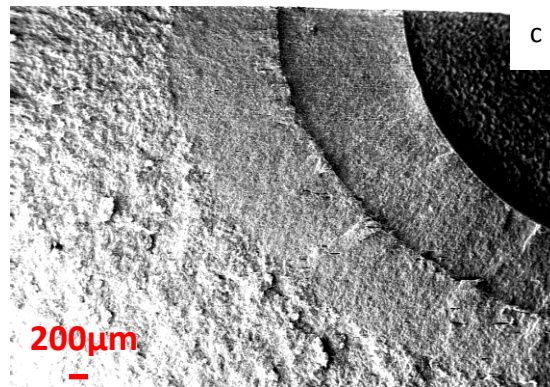
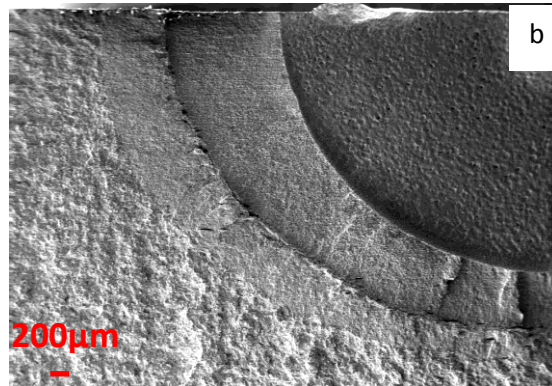


Figure 5-19: Fractured surface of test II showing just half of crack cross section (a) open mouth (b) 75 mm from OM, (c) 150 mm from OM

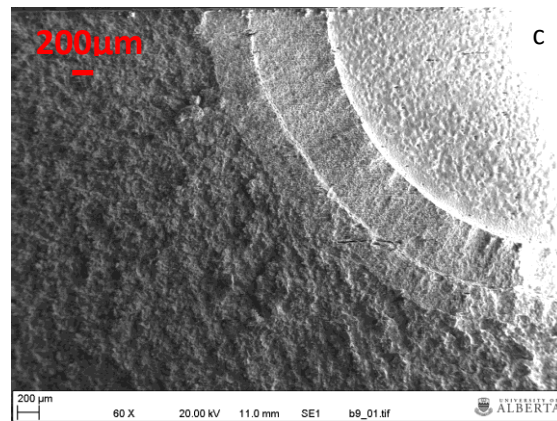
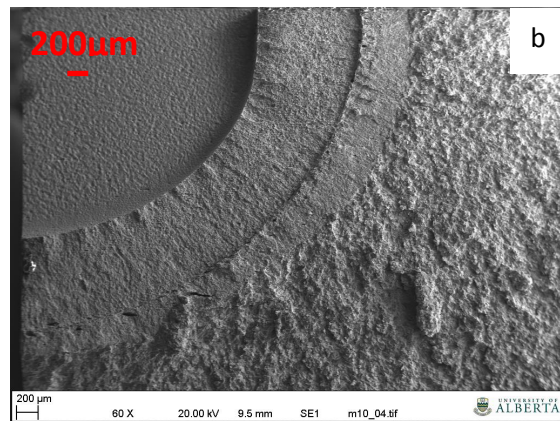
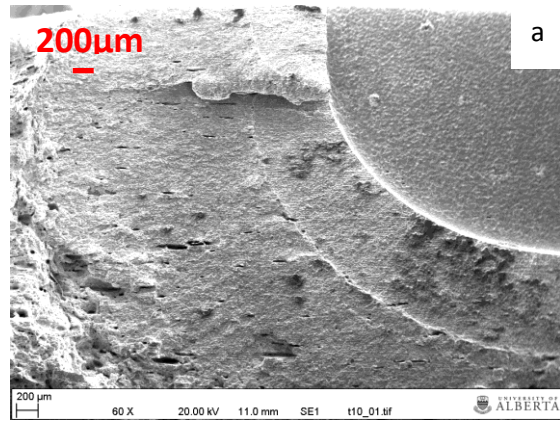


Figure 5-20: Fractured surface for test III showing half of crack section (a) open mouth (b) 75 mm from OM, (c) 150 mm from OM

One of the main conclusions of that study was that growth rates in the environment studied could not be explained by a dissolution controlled mechanism, as growth rates observed were orders of magnitude higher than previously determined dissolution rates. Also it was determined that variations in the CO₂ concentration in the local environment under the disbondment could significantly influence the rate of crack propagation. Specifically, highest growth rate was obtained at the open mouth where CO₂ concentration, hence hydrogen ion concentration at the crack tip, was highest.

It is well recognized that there are two major competing forces as far as growth in CO₂ rich environments are concerned:

1. Crack tip dissolution which tends to blunt the crack tip
2. Crack tip sharpening by hydrogen enhanced mechanical driving forces which tend to accelerate crack propagation.

In a follow-up communication, where crack propagation in the normal pipeline operating pressure range was studied, the following major findings were reported:

1. High CO₂ concentration in the ground water surrounding the pipe may cause very intense dissolution that could blunt the crack tip and could make crack re-initiation difficult and defer crack propagation to very severe mechanical conditions or limit crack propagation to areas with very high residual tensile stresses.
2. Low temperature creep at non-propagating conditions, coupled with hydrogen enhanced localized plasticity, may cause very severe crack tip blunting. The combined effect of these

two mechanisms may drive a propagating crack rapidly towards dormancy and may preclude the re-initiation of cracks at benign mechanical loading conditions.

3. The dissolution mechanism seems to have an insignificant effect on actual crack propagation once cracks are re-initiated.

As mentioned above, other than crack tip dissolution and low temperature creep, crack tip blunting could also be produced by overloading the crack tip as typically occurs during hydrostatic testing.

Some questions then arise:

1. Following the return of a cracked pipe segment to service after hydrostatic testing, the deformation of the crack tip experienced at the maximum stress involved in hydrostatic testing may blunt the crack tip and put the crack in a dormant state. What are the conditions necessary for crack re-initiation?
2. What is the effect of high dissolution rates on crack re-initiation and/or subsequent crack propagation from a mechanically blunted crack tip?
3. What is the effect of loading frequency on low temperature creep and subsequent crack propagation rates?

These questions will be answered in the sections below.

5.4.2 Crack re-initiation conditions

5.4.2.1 Environmentally enhanced mechanical considerations

In two previous communications [17-18], the conditions required for crack re-initiation were examined under two slightly different conditions:

1. When crack propagation occurred at a sharp tip under loading conditions similar to normal pipeline operating pressures
2. When crack re-initiation occurred at a creep and/or dissolution blunted crack tip

In the latter case, crack re-initiation at the open mouth of the simulated disbondment occurred at a combined factor of about $14246 \text{ (MPa}\cdot\sqrt{\text{m}})^3/\text{Hz}^{0.1}$ and a K_{max} of about $27.2 \text{ MPa}\cdot\text{m}^{0.5}$.

In the current study, the aim was to compare the conditions required for re-initiating a mechanically blunted crack with those of a creep/dissolution blunted crack. The combined factors at which crack re-initiation occurred in tests I-III as well as in previously published tests (at 75% SMYS) are shown in Tables 5-5 and 5-6. Although it appears that crack re-initiation was delayed to $R=0.56$ in test I, careful analysis reveals that this condition only corresponded to a combined factor of $13440 \text{ (MPa}\cdot\sqrt{\text{m}})^3/\text{Hz}^{0.1}$ at the sample surface. This unusual disparity in numbers is due to the aspect ratio disparity between the two cracks. Unfortunately, there is no way to control the aspect ratios during precracking. In test III, crack re-initiation occurred at a stress ratio of 0.58 which is the same stress ratio at which re-initiation occurred in test II. The higher combined factor here is due to the fact that test III was conducted at a lower frequency than test I and the combined factor is proportional to $(1/f^\gamma)$. At an applied maximum stress of 75% SMYS [18] crack re-initiation occurred from both a creep blunted crack tip and an environmentally blunted one under very similar combined factors. The same trend was also observed in this study (max applied stress of 100% SMYS) i.e. crack re-initiation occurred at very similar combined factors from a mechanically blunted crack tip (test II) and a mechanically and environmentally blunted crack tip (test I). However, it is important to note that crack re-initiation occurred in the current case at lower combined factors than in the case where the maximum applied stress was 75% SMYS.

Table 5-5: Critical combined factor for surface crack initiation at the open mouth. All units in $[(\text{MPa}\sqrt{\text{m}})^3\text{Hz}^{-0.1}]$

| | 75% | 100% | | |
|---|-------|--------|---------|----------|
| | | Test I | Test II | Test III |
| 20% CO ₂ +N ₂ environment | 21974 | 13440 | - | - |
| 5% CO ₂ +N ₂ environment | 20425 | - | 14154 | 16186 |

Table 5-6: Critical combined factor for depth crack initiation at the open mouth. All units in $[(\text{MPa}\sqrt{\text{m}})^3\text{Hz}^{-0.1}]$

| | 75% | 100% | | |
|---|-------|--------|---------|----------|
| | | Test I | Test II | Test III |
| 20% CO ₂ +N ₂ environment | 14246 | 11711 | - | - |
| 5% CO ₂ +N ₂ environment | 14246 | - | 11350 | 10952 |

It is understandable that crack re-initiation occurred at lower combined factors in the current set of tests compared to those earlier published. Several reasons might be responsible for this:

1. The magnitude of the applied stress:

At the higher K_{max} values at 100% SMYS:

- a. The size of the plastic zone ahead of the crack tip, hence the hydrogen process zone would be larger than at lower K_{max} values, so there is a larger volume over which hydrogen concentration occurs ahead of the crack tip.
- b. The large stress concentration at the crack tip at 100% SMYS causes a more intense plastic deformation of the crack tip region than at 75% SMYS. This results in a higher dislocation density in the plastic zone ahead of the crack tip. Dislocation motion is well known to facilitate hydrogen diffusion into the process zone. Thus a higher dislocation density enhances hydrogen segregation to the process zone. Hydrogen is known to help re-sharpen blunt cracks. Thus, a higher dislocation density increases hydrogen enhanced crack re-initiation.
- c. Assuming there is enough stress concentration ahead of the crack tip under both loading conditions (maximum stress) to cause yielding, then, plastic deformation ahead of the crack tip should result in similar lattice dilations near the crack tip. However, at the higher stress level, 100% SMYS, the plastic zone is larger, resulting from the higher K_{max} . Therefore, hydrogen atoms have a larger volume with lesser obstacle to overcome during diffusion to the process zone. Since hydrogen is known to segregate more to regions of higher tensile stresses within the lattice, higher hydrogen concentration ahead of the crack tip should occur over a larger volume at a maximum applied stress of 100% SMYS than at 75% SMYS.

2. The nature of the crack tip

The nature of the crack tip can have a profound effect on crack re-initiation behavior. For the cracks with a sharp tip, a fracture mechanics concept such as stress intensity factor can be used to quantify the stress state at the crack tip. When the crack tip is blunt, a stress concentration factor is usually defined and the actual stress in the material ahead of the blunt tip is a function of both the stress concentration factor and the applied nominal stresses through the following expression:

$$\sigma = k_t \sigma_a \quad \dots\dots\dots (5.1)$$

where, σ_a is the applied stress, k_t is the stress concentration factor, which can be expressed as:

$$k_t = 1 + 2\sqrt{b/\rho} \quad \dots\dots\dots (5.2)$$

where b is the depth of crack with a blunt tip and ρ is the radius at the tip of the blunt crack.

For very blunt cracks the radius of curvature of the crack tip is large, therefore k_t should be smaller compared to cracks with much sharper tips corresponding to a smaller radius of curvature. Careful consideration of the crack tips under an applied stress of 100% SMYS and 75% SMYS reveals that the radius of curvature is significantly larger in the former case than in the latter. Therefore k_t should be smaller in the former than in the latter case.

However, the stress experienced in the material around the crack tip is actually dependent on the applied stress which is higher in the former than in the latter case. Since there is an inverse square root relationship between k_t and ρ , the higher magnitude of the applied stress in the former case might result in higher stresses in the hydrogen process zone at an applied stress of 100% SMYS than at 75% SMYS. Such higher stresses will result in a larger amount of hydrogen segregating to the crack tip and/or hydrogen process zone in the former case than in the latter. In

such a situation, more hydrogen enhancement of crack re-initiation will occur at 100% SMYS than at 75% SMYS. The combined effect of the discussion above should be that there is more crack tip re-sharpening effect due to better hydrogen-enhanced crack propagation than at 75% SMYS. Thus cracks should be easier to re-initiate at a max stress of 100% SMYS than at 75% SMYS.

It must be mentioned that on actual pipelines, cracks that survive hydrostatic testing are usually not returned to service at such high K_{max} as those in the above analysis. Usually, the line is returned to normal operating pressures, usually between 30-72% SMYS. Under such conditions, the severe crack tip blunting suffered during hydrostatic testing could defer crack propagation to much lower stress ratios as those observed at 75% SMYS. This may explain why a few authors have pointed out that hydrostatic testing may result in a transient cracking retardation after hydrotested lines are returned to service[7-9, 12, 16, 19-22].

5.4.2.2 Crack tip morphology considerations

Careful examination of the growth curves in Figure 5-21 reveals three issues:

1. Why is the pre-fatigue crack tip in test II not squared like the ones in tests I and III?
2. In test II, crack propagation initiated from non-square pre-fatigue crack tips than in test I, but the crack in test II grew slower than the one in test I. Why?
3. Cracks at the open mouth in tests II and III both initiated from very squared pre-fatigue crack tips, but they both displayed very different growth behaviour. Why?

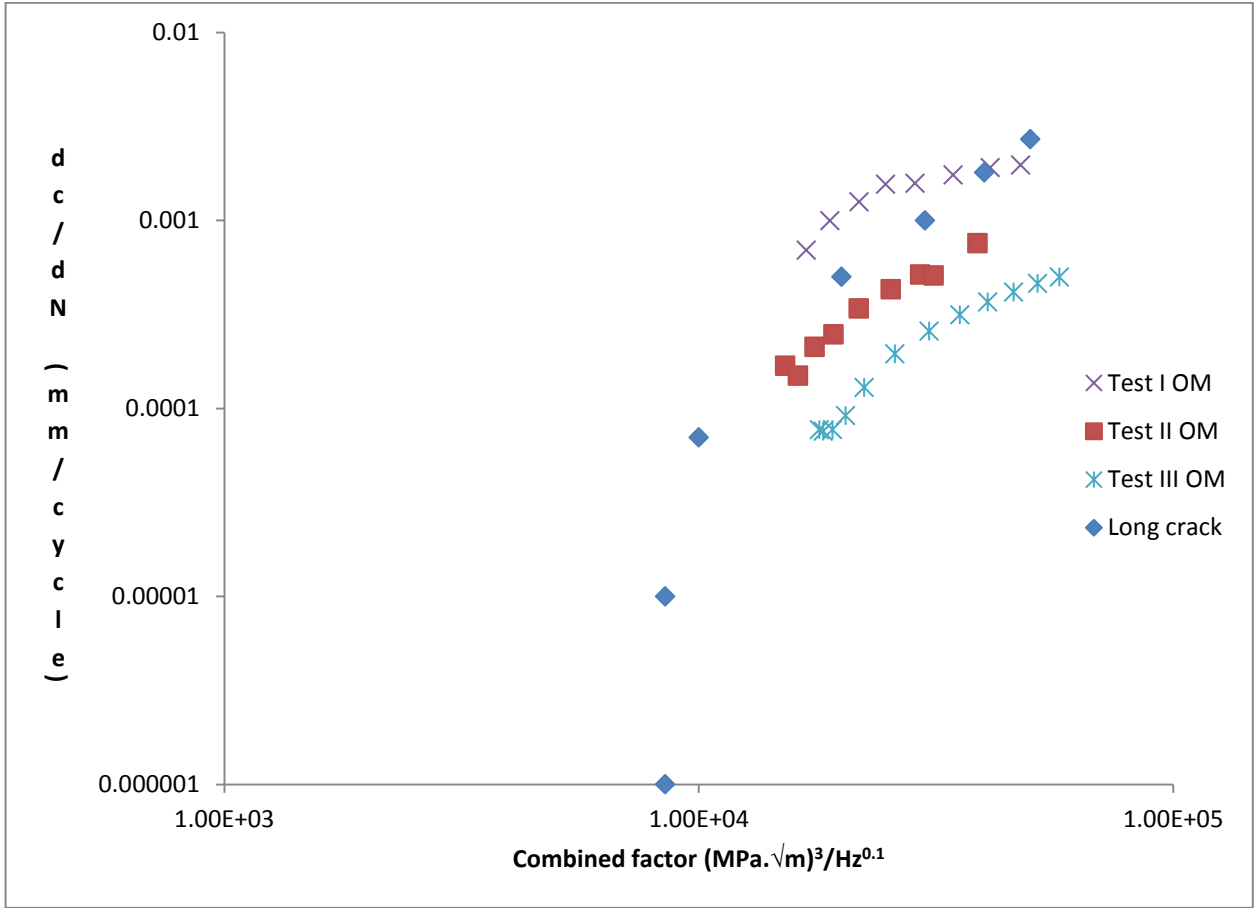


Figure 5-21: Growth rate data for all tests reported; showing Chen and Sutherby's combined factor. Data for the long crack was obtained in the same environment as the other tests results presented in the figure.

The crack tip after pre-fatigue cracking in test P1 is obviously not as square as in tests I and III and not as rounded as in test II. Thus it appears that somehow the pre-fatigue crack tip in test II got rounded while those in tests I and III got more squared during the test. The answer to this puzzle could lie in determining what tests I and III have in common but not with test II.

Tests I and II were conducted under the exact same mechanical loading conditions but different environments while tests II and III were conducted under the same environmental conditions but different frequency. Carefully considering these testing conditions, one realizes that the lower frequency in test III enhances the occurrence of more low temperature creep deformation at the pre-fatigue crack tip. This probably explains the blunted crack tip. The fact that the pre-fatigue crack tip in test III shares the same morphology as that in test I may therefore suggest that somehow the testing condition in test I might have encouraged more severe creep deformation at the crack tip. Since the only difference between tests I and II is the concentration of CO₂ in the sparging gas, it suggests that very high CO₂ concentrations in the testing solution may aid low temperature creep at the pre-fatigue crack tip under severe mechanical loading conditions. It is well documented that one of the mechanisms by which hydrogen embrittlement occurs is hydrogen enhanced localized plastic deformation (HELP) [19-22]. It could then be that the extent of HELP that occurred at the crack tip is dependent on the hydrogen concentration ahead of the crack tip. Since hydrogen concentration is higher in test I than in test II, more HELP assisted creep deformation could occur in test I. More details of the occurrence of HELP assisted creep deformation at room temperature in near-neutral pH SCC will be provided in a future communication (manuscript under preparation).

5.4.3 Crack propagation

A major similarity between tests I and III is the occurrence of crack branching. In test I, environmental crack blunting is more significant than in tests II or III because of the higher CO₂ concentration in the simulated soil solution. Thus, the advancing crack is subjected to more blunting due to the aggressiveness of the environment as the crack propagates. This results in discontinuous crack propagation. Evidence of this was provided in a recent publication by the current authors [18] where start and stop positions of an advancing crack were analyzed and shown to correlate to the grain size of the base metal. Evidence of such discontinuous cracking is obvious along the crack paths in test I. Recesses could be observed along the crack path in Figures 5-9&5-10 corresponding to crack tip positions where the crack becomes stationary and stress assisted dissolution or creep deformation results in a blunt crack tip. Similar to the earlier report, it is fairly obvious that these recesses correspond to the grain size of the alloy. It is very evident in Figure 5-16b that the observed crack branching initiates at points where blunting induced recesses are developed. This indicates that multiple cracks are formed at such recesses in order to re-initiate the temporarily dormant cracks, until a few of them connect with the main crack front, advancing the dormant crack. Such large recesses were not observed in test II possibly because the environment used in test II was not aggressive enough to result in any significant crack tip blunting. However, at such low loading frequencies, creep induced blunting may be sufficient to blunt the tip of a slowly advancing crack long enough to require multiple crack initiations ahead of the crack front for further crack advancement. However, since the crack in test III is more static than that in test II, more time is allowed for hydrogen diffusion to the process zone ahead of the crack tip. Lattice hydrogen is known to be associated with such crack branching. Therefore, lower frequency loadings may allow sufficient environmental interactions with the crack tip over a long

time to produce the same effect as a more aggressive corrosive medium would have produced over a shorter period of time.

5.4.3.1 Environmental effect on crack growth rates

In a previous study, it was determined that at a maximum operating stress of 75% SMYS, very high CO₂ concentration in the surrounding ground water may significantly retard crack propagation close to the open mouth of the disbondment [18]. One of the goals in this study was to determine if this same trend occurs at higher stresses. Comparing the growth rates between tests I and II reveals that the opposite trend occurs following re-initiation at higher stresses. Crack growth rates are significantly higher in the 20% CO₂ environment than in the 5% CO₂ environment although initial combined factors are lower in test I.

It is very interesting to note that crack growth rates in test I are consistently higher than in test II despite the fact that both the initial stress intensities, ΔK and combined factors are lower in test I. This behavior points to the significance of crack propagation enhancement by the hydrogen embrittlement mechanisms. The CO₂ concentration in the trapped solution in test I should be significantly higher than in test II. In the absence of surface films that may impede hydrogen permeation into the specimen, the concentration gradient between the surface concentration of hydrogen and the other surface that was fully protected and isolated from the environment should result in more hydrogen atoms being assimilated into the lattice at all locations in test I than in test II. A higher lattice concentration of hydrogen will aid the diffusion of more hydrogen atoms to the hydrogen process zone ahead of the crack tip, increasing crack propagation rates in test I.

The question then is why is the environmental effect in this study different from that in the earlier study [18] ? First, comparison of the width of the pre-fatigue crack region between tests I and II does not reveal very much difference in pre-fatigue crack widths. This was not the case in

the tests earlier reported. In the earlier report, crack widths were significantly larger in the 20% CO₂ environment. This suggests that more dissolution occurred in the tests reported earlier than in the current one. In the current study, cracks re-initiated much earlier in the 20% CO₂ environment because of the higher maximum stress intensity compared to those in the earlier report. This means the samples spent much less time interacting with the test environment in the current study. It is well known that dissolution is a time-dependent process. Thus, there is probably less dissolution induced crack tip blunting prior to crack re-initiation in the current test than in the previous one. Therefore, crack re-initiation could occur much earlier allowing the cracks to propagate longer than in the previous tests.

Second, at the higher stresses involved in the current tests, crack tips experienced larger strains. These could cause crack tip films to rupture much more frequently than in the previous tests. Crack propagation by crack tip film rupture is a well-documented phenomenon [19, 23, 24]. Under the combined effect of larger crack tip strains and higher film rupture rates, fresh surface for film formation and rupture are exposed much more frequently. In the presence of higher hydrogen-enhanced crack propagation, this could lead to a higher crack propagation rate as observed in this study.

5.4.3.2 Effect of loading frequency on growth rates

It is widely known that the cyclic loading frequency may have a significant effect on crack propagation rates in corrosive environments. Comparing the average growth data in Tables 5-3 and 5-4 reveals that crack growth rates are slightly higher in test II than in test III. Also, the growth data in Figure 5-21 shows that growth rates are higher at the higher frequency. Considering that the environmental contribution to crack propagation in the corrosion-fatigue growth model is correlated with $(1/f^\gamma)$, one would expect higher propagation rates at the lower

frequency. For instance if $\gamma=0.1$ at the open mouth, the environmental contribution in test II is 1.7 while it is 1.82 in test III. Thus, judging by the combined factor alone, the growth rate should be higher in test III than in test II under similar loading conditions as was the case in tests I and II (except for loading frequency). Surprisingly, the growth rates are lower in test III than in test II.

At lower frequencies, the loading rate is lower than at higher frequencies. Since lower frequency cycles are closer to static loading than the higher frequency ones, more creep deformation could occur at the crack tip at lower frequencies. This could reduce the rate of crack propagation when the applied ΔK is increased to levels where crack propagation could occur. This deviation from the expected trend may point to an inherent weakness of the corrosion-fatigue model used here. One would expect, as has been reported by many, that strain rate especially at such high stresses will have some effect on crack propagating rate. Generally it has been observed that crack propagation rate increases with increasing strain rates. For the tests under consideration, crack tip strain rate should be higher at the higher loading frequency (test II). This is perhaps what accounted for the slightly higher growth rate in test II. However, critically examining the combined factor model, one discovers that the model is missing any parameter that accounts for crack tip strain rate. Rather, frequency which could be an indirect representation of loading rate at the crack tip is modeled with an inverse power relationship which does not capture the crack tip strain rate effect. Further work will be carried out to determine ways of accounting for strain rate on the corrosion-fatigue model.

5.4.3.3 General Growth Behaviour at open circuit potential

In their seminal work on the growth behavior of NNPHSCC cracks, Chen and Sutherby [6] were able to fit one single curve to tests carried out at varying K_{\max} , ΔK and frequency ranges. Marvasti *et al.* [25] were similarly able to fit a single curve to growth data obtained under different

loading conditions such as with varying maximum stress intensity factors, varying frequencies and stress intensity ranges. In Figure 5-21, it can be observed that all three growth curves obtained under the same testing conditions seem to bunch together and are such that one can picture that they will eventually merge. However, data obtained with slightly different test conditions, such as those in tests II and III, seem to produce distinctly different data curves. Although the growth curves in Tests II and III seem to be very close they appear to be parallel curves that may never merge. In Figure 5-22, the growth data obtained in an earlier study at a maximum stress of 75% SMYS in a 5% CO₂ environment following crack re-initiation from a state of creep induced dormancy is superimposed on those of the current study. These curves all appear as distinctly different curves unlike those reported by Chen and Sutherby, and Marvasti.

The question then is why does this difference in growth behaviour occur? A major similarity between the studies performed by Chen and Sutherby, and Marvasti is that both studies used CT specimens rather than the surface type flaws used in this study. CT specimens typically have longer flaws than those used in this study. Also CT specimens are designed with through-thickness cracks. Perhaps the difference in crack geometry could explain the observed difference in growth behavior. Looking carefully at the data in Figure 5-22, it appears that the curves in test I and the curve obtained at 75% SMYS appear to share a common curve for the latter part of growth. However the tail portions of these curves, which represent the near threshold conditions, are different. Such behavior where growing cracks have distinctly different growth curves in the near threshold conditions but the same curve after a crack path has been established has been reported by both Marvasti and, Chen and Sutherby.

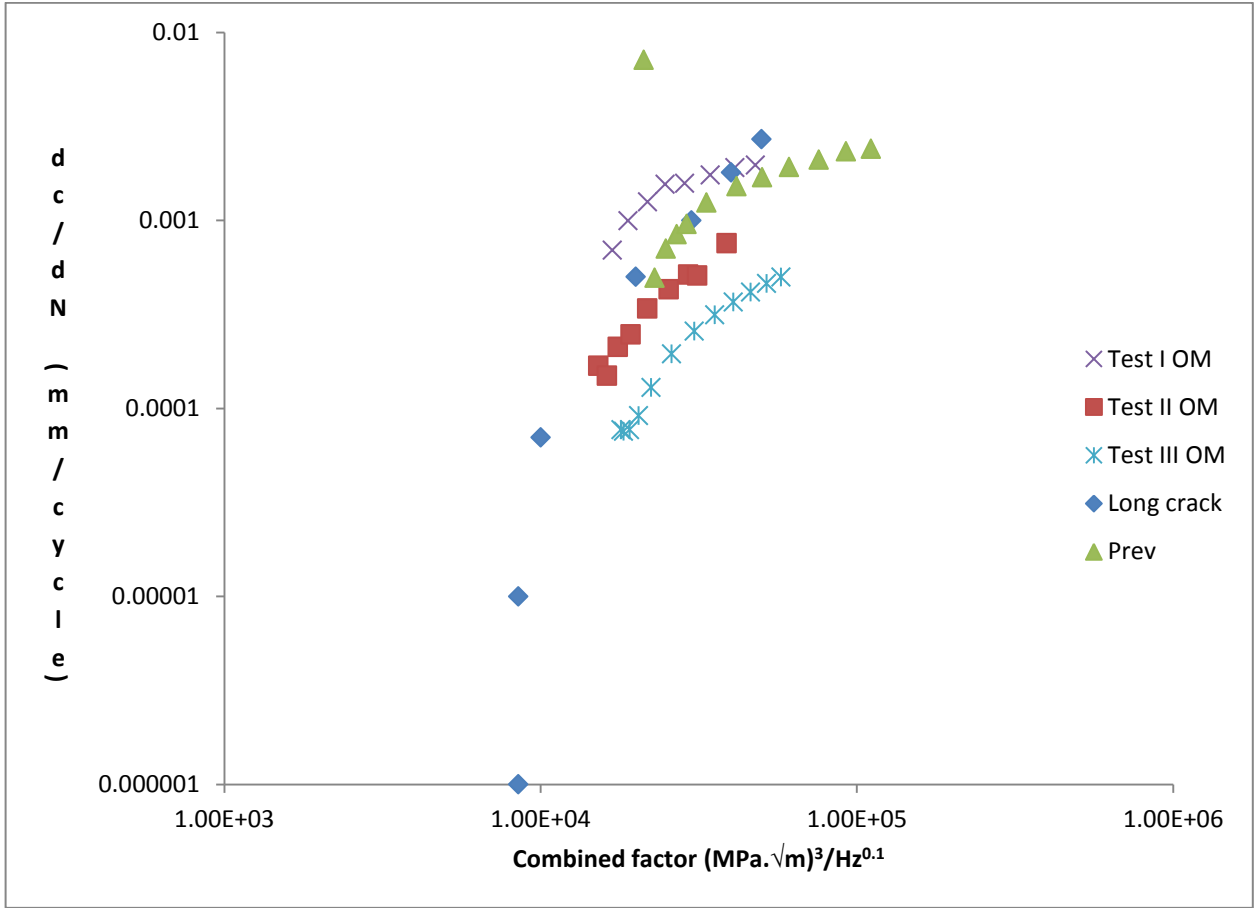


Figure 5-22: Comparison of growth at 100% SMYS max stress and 75% max stress. Test Prev was done at 75% SMYS, and subjected to low temperature creep prior to crack re-initiation in 5% CO₂ environment [18].

The question then is what does test I have in common with the test at 75% SMYS? Careful examination reveals that test I was obtained under a slightly larger stress ratio than both tests II and III. Tests II and III were conducted at the stress intensity ranges where crack re-initiation and propagation was barely possible, whereas test I was conducted under a slightly larger stress intensity range. The test at 75% SMYS was conducted under very severe mechanical loading since crack growth could not be re-initiated at more benign loads following crack tip blunting by low temperature creep. It then appears that these curves might have merged simply because growth under these two conditions was more mechanically driven than in the other tests. Since cracks were barely re-initiated at relatively benign conditions in tests II and III, it is possible that both creep and environmental blunting were still able to exert a large enough effect on crack propagation to cause a noticeable retardation of crack growth. Since mechanical driving forces are larger in test I and the 75% SMYS test, such a retardation effect might be substantially offset by mechanical forces making the retardation effect less noticeable. This suggests that with further propagation of the cracks in tests II and III, an inflexion point may be reached where crack growth curve deviates slightly from its current path to merge with those of tests I and the 75% SMYS curves. Unfortunately, the dimensions of the samples used for this study does not permit the growth of cracks to larger sizes where such an inflexion point may be observed.

This could have a significant effect on hydrostatic testing. The current codes that govern hydrotesting, for example CSA Z662-11 clause 8, mandates that all piping operated at a pressure greater than 700 kPa be hydrotested in two phases – a strength test followed by a leak test. This clause allows for strength tests at pressures of up to 110% SMYS followed by leak test at pressures up to 100% SMYS. The growth rates obtained in this study are similar to what could occur during the leak test. This result therefore indicates that the growth rate during the leak test

may be lower than those observed under operating conditions where crack re-initiation and growth, from a dormant state, typically occur (assuming severe stress ratios as those determined in the previous publication are required to re-initiate stable crack growth).

Finally, comparing the growth rate of the long (through-thickness) crack with those of surface type flaws reveals that contrary to popular opinion that surface flaws could grow at a higher rate or at least the same rate as through-thickness cracks, this study reveals that the growth rate of surface flaws under the testing conditions studied here are lower in every case than that of a through-thickness crack. This is consistent with earlier finding [25]. Reasons why this deviation occurred were adduced in our previous paper and the reader is encouraged to review that paper.

5.5 Conclusions

The results of this study are summarized as follows:

1. The high stresses imposed on a pipeline during hydrostatic testing can cause a severe deformation of the crack tip leading to crack tip blunting.
2. Such severe blunting may prevent the mechanical re-initiation of crack propagation at benign loading conditions. Crack re-initiation may require very severe loading conditions, such as high K_{\max} and moderate ΔK or low K_{\max} and high ΔK , or a high number of stress cycles.
3. Comparison of the combined factors at which crack re-initiation occurred at a maximum stress of 100% SMYS with that at 75% SMYS revealed that crack re-initiation conditions at a blunted tip may be independent of whether blunting was environmentally or mechanically induced.

4. The conditions at which re-initiation occurred were independent of the CO₂ concentration in the groundwater and was also independent of the loading frequency.
5. Contrary to what was observed at benign maximum operating stresses, very high CO₂ concentration in groundwater led to significantly higher crack propagation rates at a maximum operating stress of 100% SMYS.
6. Despite the higher value of the environmental factor in the corrosion-fatigue model, lower loading frequency did not result in a higher crack growth rate. Growth rates were higher at a higher loading frequency. This was related to the higher strain rate at the crack tip which may also result in more rapid crack tip film rupture that may expose fresh surface for crack tip film formation than at the lower frequency.
7. Higher CO₂ concentration in the simulated ground water was found to enhance crack propagation in the depth direction resulting in cracks with higher aspect ratios than in the lower CO₂ concentration environment.
8. Crack growth rates at loading conditions that are slightly higher than that required for crack re-initiation are very comparable both at 100% and 75% SMYS maximum operating stress.

References

- [1] Brousseau, R., and Qian, S., 1994, "Distribution of Steady-State Cathodic Currents Underneath a Disbonded Coating," *Corrosion*, **50**(12) pp. 907-911.

- [2] Brousseau, R., Qian, S., and Gummow, B., 1993, "Investigating the Effect of Pulse Cathodic Protection Underneath a Disbonded Coating," *Materials Performance (USA)*, **32**(6) pp. 21-26.
- [3] Song, F. M., Kirk, D. W., Graydon, J. W., 2002, "Steel Corrosion Under a Disbonded Coating with a Holiday - Part 1: The Model and Validation," *Corrosion*, **58**(12) pp. 1015-1024.
- [4] Song, F. M., Jones, D. A., and Kirk, D. W., 2005, "Predicting Corrosion and Current Flow within a Disc Crevice on Coated Steels," *Corrosion*, **61**(2) pp. 145-154.
- [5] Song, F., and Sridhar, N., 2008, "Predicting Pipeline Corrosion Under Disbonded Coatings with the Influence of Slow Flow Underneath," *Corrosion/2008, NACE*, Paper no. 08145 .
- [6] Chen, W., and Sutherby, R. L., 2007, "Crack Growth Behavior of Pipeline Steel in Near-Neutral pH Soil Environments," *Metallurgical and Materials Transactions A*, **38A**(6) pp. 1260-1268.
- [7] Harle, B. A., Beavers, J. A., and Jaske, E., 1995, "Mechanical and metallurgical effects on low-pH stress corrosion cracking of natural gas pipelines," *Corrosion '95 NACE*, pp. Paper No. 646.
- [8] Brongers, M. P. H., Beavers, J. A., Jaske, C. E., 2000, "Effect of Hydrostatic Testing on Ductile Tearing of X-65 Line Pipe Steel with Stress Corrosion Cracks," *Corrosion (USA)*, **56**(10) pp. 1050-1058.
- [9] Beavers, J. A., and C.E. Jaske. 1998. Near-Neutral-pH SCC In Pipelines: Effects of Pressure Fluctuations on Crack Propagation. *Corrosion/1998*, Paper No. 98257.
- [10] Leis, B. N., and Brust, F. W., 1990, "Hydrotesting Effects. I. Model Predicts Crack Growth and Material Behavior," *Oil Gas J.*, **88**(7) pp. 45-48.
- [11] Leis, B.N., and Brust, F.W., 1992, "Hydrostest strategies for gas transmission pipelines based on ductile-flaw-growth considerations," *NG-18 Report No. 194*, .

- [12] Chen, W., and Sutherby, R.L., 2006, Laboratory simulation of hydrostatic test in near-neutral pH soil environments. In: "International Pipeline Conference 2006, Calgary, Canada,"pp. 25-29.
- [13] Parkins, R.N., 1992, "Environment Sensitive Cracking of High-Pressure Pipelines in Contact with Carbon Dioxide-Containing Solutions," AGA NG-18 Report 205, .
- [14] Chen, X., Du, C., Li, X., 2009, "Effects of Cathodic Potential on the Local Electrochemical Environment Under a Disbonded Coating," Journal of Applied Electrochemistry. **39**(5) pp. 697-704.
- [15] Delanty, B., and O'beirne, J., 1992, "Major Field Study Compares Pipeline SCC with Coatings," Oil and Gas Journal, **90**(24) pp. 39-44.
- [16] Beavers, J. A., and Harle, B. A., 1996, "Mechanisms of High pH and Near-Neutral pH SCC of Underground Pipes," International Pipeline Conference, ASME, New York, **1**, pp. 555-564.
- [17] Egbewande, A. T., Chen, W., Eadie, R., (2013), "Surface Crack Growth Behavior of Pipeline Steel Under Disbonded Coating at Free Corrosion Potential in Near-Neutral pH Soil Environments," Metallurgical and Materials Transactions. Submitted for publication.
- [18] Egbewande, A. T., Chen, W., Eadie, R., (2013), "Transgranular Crack Growth in the Pipeline Steels Exposed to Near-Neutral pH Soil Aqueous Solutions: Discontinuous Crack Growth Mechanism," Acta Materialia. Submitted for publication.
- [19] Beavers, J.A., 2004, "Near-Neutral pH SCC: Dormancy and re-initiation of stress corrosion cracks," Report for Gas Research Institute, Report R1025-01R, Contract GRI-7045.
- [20] Beavers, J.A., and Hagerdorn, E.L., 1996, "Low-pH SCC: Mechanical Effects on Crack Propagation," Pipeline Research Council International, Pipeline Research Committee Report #R207-01.

- [21] Beavers, J. A., and Hagerdorn, E. L., 1996, "Near-Neutral pH SCC: Mechanical effects on Crack Propagation," ninth Symposium on Pipeline Research, A.G.A. Cat no L51746 Paper 24.
- [22] Li, J., Elboujdaini, M., Gao, M., 2008, "Investigation of Plastic Zones Near SCC Tips in a Pipeline After Hydrostatic Testing," Materials Science and Engineering A-Structural Materials Properties Microstructure and Processing, **486**(1-2) pp. 496-502.
- [23] Kane, R.D., 1993, "Slow strain rate testing for the evaluation of Environmentally Induced Cracking: Research and Engineering applications", ASTM international, West Conshohocken, PA, ASTM STP 1210.
- [24] Zheng, W., Revie, R. W., Tyson, W. R., Shen, G., MacLeod, F. A., and Kiff, D., 1996, "Pipeline SCC in Near-Neutral pH Environment: Results of full-scale tests," Corrosion '96, **NACE**, Paper # 253.
- [25] Marvasti, M. H., 2010, "Crack Growth Behavior of Pipeline Steels in Near Neutral pH Soil Environment," MSc. Thesis, Department of Chemical and Materials Engineering, University of Alberta.

CHAPTER SIX

**EFFECT OF HYDROGEN ENHANCED LOCALIZED PLASTICITY ON
STRESS CORROSION CRACKING RE-INITIATION AND PROPAGATION IN
NEAR NEUTRAL PH ENVIRONMENT**

6.1 Introduction

Stress corrosion cracking in near-neutral pH stress corrosion cracking (NNpHSCC) environments remains a potent integrity issue that the oil and gas industry contends with. In many cases, effective monitoring programs have been put in place to detect and mitigate this issue before failure occurs or the general public is put at risk. Improvement in coating and cathodic potential technologies over the years have in some cases reduced the frequency of incidents or delayed SCC onset to later in the life of pipelines and other engineering infrastructures.

General understanding of the factors that promote SCC and the mechanisms involved has improved over the years. Although there is no consensus yet on the mechanism involved, it is generally well accepted that hydrogen furnishing environments generally promote NNPHSCC. Several mechanisms have been proposed: enhanced localized plasticity [1-9], enhanced low temperature creep deformation [10-13], decohesion [14-16], bond weakening[17], film-induced cleavage[18-20], *etc.* Although these mechanisms are sometimes discussed in isolation, it is well understood that several combinations of these mechanisms are involved in NNPHSCC propagation. Often, it is very difficult to separate the effect of each of these mechanisms. Also, many of the effects produced by these mechanisms have only been observed in isolation on the micro-scale in thin film experiments.

Recent studies carried out by the current authors led to the development of an innovative experimental setup that allowed the study of some of these mechanisms in isolation or in selected combinations. This communication reports the role of hydrogen enhanced localized plasticity (HELP) and hydrogen enhanced room temperature creep on crack re-initiation and propagation in near neutral pH SCC environments.

6.2 Experimental

6.2.1 Sample preparation

Tensile specimens (Figure 6-1) bearing three reduced sections were machined from the longitudinal direction of a X65 pipe section that had failed in service. Only pipe sections unaffected by NNPHSCC and other forms of corrosion and external damage were used. The alloy composition is shown in Table 6-1, while a typical alloy microstructure is shown in Figure 6-2. Gauge sections were 23 mm X 30 mm X 9.2 mm in dimension and identical semi-circular shallow notches, 0.2032mm wide, with dimensions $2c=5$ mm and $a=2.5$ mm were made by electrical discharge machining (EDM) in the middle of each gauge section.

A corrosion test cell consisting of two chambers was designed and fabricated from acrylate (Figure 6-3). The inner tube, named the shielding, was designed to simulate coating disbondment at the surface of a pipe. The width of this inner tube was 20 mm and the sample was centered in the simulated disbondment. The outer tube holds the bulk solution which simulates the surrounding soil around a pipe in the field while the solution contained in the inner shielding simulates the solution trapped between the coating and the pipe surface on an actual pipeline. The bulk solution in the outer tube was purged by a mixture of certified grade 5% CO₂, or 20% CO₂ (nitrogen balance) fed in through openings at the bottom of the cell, so that CO₂ can only diffuse into the simulated disbondment from the open mouth.

For tests I, II and III, a maximum stress of 75% specified minimum yield strength and a cyclic frequency of 0.005Hz were used. Three tests were performed to investigate the effect of environmentally enhanced plastic deformation on crack growth in near neutral pH conditions under disbonded coatings. A summary of test conditions is given in Table 6-2. Test I was carried out at a single stress ratio of 0.4. A series of stress ratios was used for tests II, III and IV as shown in Table 6-2. Test I lasted for about 23.2 days, test II for about 5 months, and test III for about 3 months. Tests

I, II and III were purged with 5% CO₂ + N₂. Test IV was conducted at a maximum stress of 100% SMYS. The test was designed to simulate pre-fatigue crack behavior under three different conditions (1) in air; (2) when the crack is in indirect contact with the corrosive media, in which case hydrogen can only reach the crack tip by diffusing through the lattice; (3) when the crack is in direct contact with the corrosive media, the crack tip is well covered with the corrosive media and atomic hydrogen can be directly adsorbed at the crack tip and the hydrogen process zone. To achieve this, the cell was half filled with C2 solution such that the top crack was not in solution at all. The top crack area was masked with a cellophane tape and covered on both the front and the back side with epoxy to prevent pitting corrosion. The side of the specimen bearing the crack in the middle area of the specimen was also masked with cellophane tape and covered with epoxy while the back side was exposed to the solution. Only the backside was in direct contact with the C2 solution and hydrogen could only diffuse to the crack tip through the lattice. The bottom crack was exposed to the solution on the side bearing the crack while the backside was masked with epoxy. The inner shielding was not used in test IV. A stress ratio of 0.65 was applied for 14 days followed by a stress ratio of 0.6 for 11.1 days. The solution was purged with a mixture of 5% CO₂ + N₂.

In an attempt to closely simulate real pipeline service conditions, the sides and back surface of each specimen (the one without the surface cracks) were coated with epoxy in order to isolate these surfaces from the corrosion media. Except for test IV, crack growth rates were monitored using a custom made potential drop system through copper wire leads spot welded across the back of the EDM slots in each gauge section. A constant current of 20A was applied by the potential drop system in order to measure the potential drop across each crack.

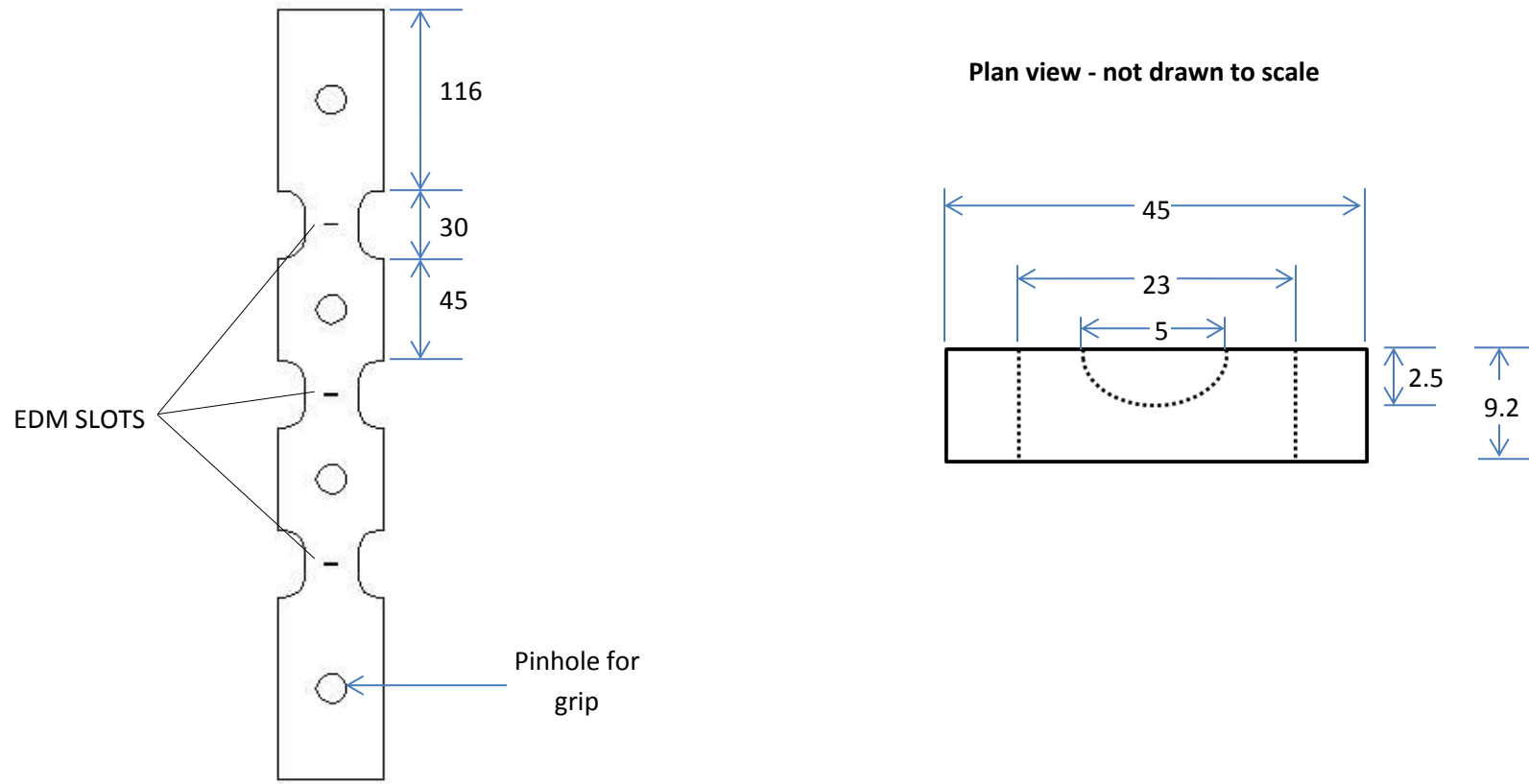


FIGURE 6-1: Test sample designed for this study. All units in mm.

Table 6-4: Alloy (X65) composition

| Element | Composition (wt %) |
|------------|--------------------|
| Carbon | 0.13 |
| Manganese | 1.55 |
| Copper | 0.05 |
| Niobium | 0.05 |
| Chromium | 0.08 |
| Molybdenum | 0.01 |
| Vanadium | 0.002 |
| Nickel | 0.05 |
| Aluminum | 0.042 |
| Titanium | 0.002 |
| Nitrogen | 0.009 |
| Iron | Balance |

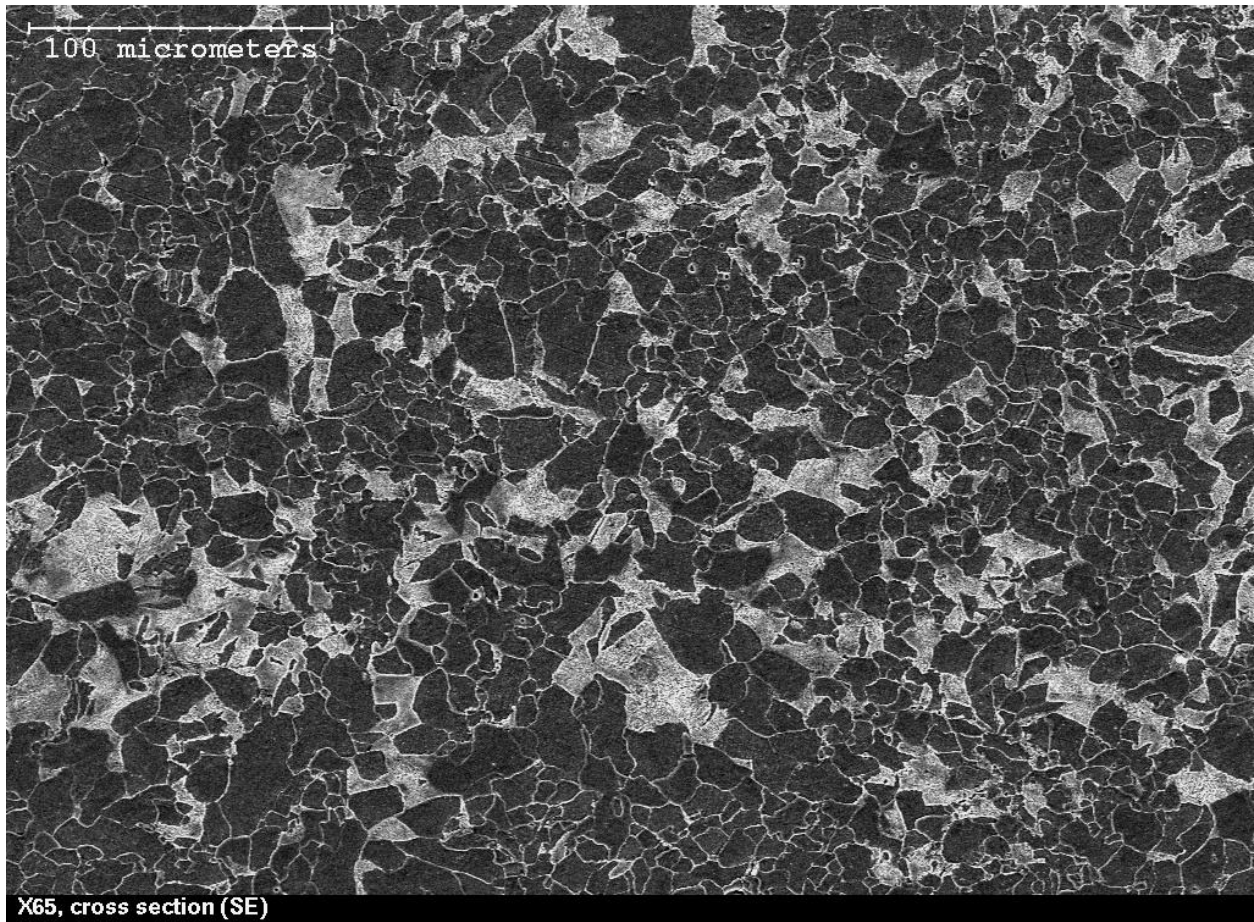


Figure 6-2: Typical microstructure of the alloy X65 used in this study

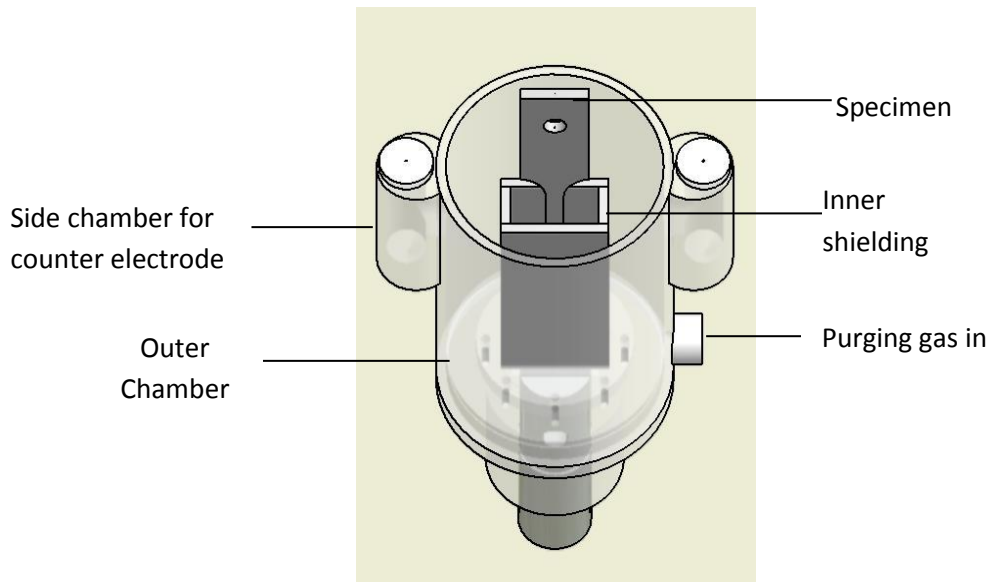


Figure 6-3: Schematic drawing of the corrosion test cell used for study.

Table 6-2: Test conditions

| Test conditions | Test I | Test II | Test III | Test IV |
|---|--|---|---|--|
| Maximum stress | 75% SMYS | | | 100% SMYS |
| Test environments | C2 solution | | | Air, C2 (direct and indirect contact) |
| Purging gas | 5% CO ₂ + N ₂ Bal. | | | |
| Pre-test pH | 6.3 | | | |
| Test potential (SCE) | Open circuit | | -0.9V | Open circuit |
| R-ratio/duration | 0.4/23.2days | 0.65/14 days 0.6/14 days 0.58/14 days 0.56/14 days 0.53/14 days 0.50/7 days 0.47/7 days 0.43/7 days 0.40/7 days 0.37/7 days 0.33/7 days 0.30/7 days 0.27/7 days 0.22/4.5days | 0.65/14 days 0.6/14 days 0.58/14 days 0.56/14 days 0.53/14 days 0.50/7 days 0.47/7 days 0.43/7 days 0.40/7.6 days | 0.65/14days 0.6/11.1days |
| Combined factor at start of test [(MPa√m) ³ Hz ^{-0.1}] | 8770 | 3250 | 3290 | 7250 |
| Combined factor at the R-ratio at which crack started to grow [(MPa√m) ³ Hz ^{-0.1}] | 8770 | 14330 | 9680 | 9470 |

6.2.2 Mechanical loading

Chen and Sutherby [21] developed a corrosion-fatigue model that accounts for NNHPSCC as a synergistic combination of fatigue and corrosion. The general form of the model was given as $\frac{da}{dN} = \frac{\Delta K^2 K_{max}}{f^\gamma}$ where ΔK is the change in stress intensity factor at the crack tip due to cyclic loading, K_{max} is the maximum stress intensity factor at the crack tip, and γ , a factor representing the influence of the corrosion environment on the crack growth rate, is found to be around 0.1. ΔK and K_{max} are strongly dependent on the geometry of the specimen, while γ is dependent on the severity of the corrosion environment. Using this relationship, the threshold condition for X65 pipeline steel was estimated to be below $8500 \text{ (MPa}\cdot\sqrt{\text{m}})^3/\text{Hz}^{0.1}$ in C2 solution. For the current study, an initial combined factor of $3290 \text{ (MPa}\cdot\sqrt{\text{m}})^3/\text{Hz}^{0.1}$ at the sample surface and $7250 \text{ (MPa}\cdot\sqrt{\text{m}})^3/\text{Hz}^{0.1}$ in the depth direction was selected for tests III and IV respectively. Other testing conditions are summarized in Table 6-2. Such low combined factors were selected since the aim of this study was to determine the effect of environmentally assisted creep on crack re-initiation and propagation. The initial testing conditions for test I are as reported in our earlier report and are also summarized in Table 6-2 (chapter 3).

6.2.3 Post-test Analysis

After each test, the fracture surface was examined and post-test crack lengths determined in order to validate potential drop measurements with actual crack growth measured from the surface of fractured specimens. Prior to fracture surface examination, iron oxide-type corrosion products were removed using a rust remover solution composed of water (100ml), HCl (3ml), and cis-2-but-1-4-diol (4ml). Initial fracture face examination was done using an optical microscope. More detailed examination of fracture surfaces was carried out using a Hitachi

scanning electron microscope equipped with an energy dispersive x-ray spectrometer for chemical compositional analysis.

6.3 Results

6.3.1 Crack growth behavior of sharp crack under propagating loading (Test 1)

Crack propagation started at a stress ratio of 0.4 and was not preceded by any period of dormancy. The extents of crack propagation during the test at the three different locations are compared in Table 6-3. The most rapid crack propagation occurred at the open mouth of the disbondment while the least growth occurred at the far end of the disbondment (150 mm from the OM). There was a higher crack opening at the pre-fatigue crack tip at the open mouth while comparable pre-fatigue crack tip opening could be observed at 75 mm and 150 mm from the open mouth. Higher magnification examination of the post-test crack tip reveals a significant difference in the crack opening size just behind the crack tip (Figure 6-5). At the open mouth, the crack tip was very sharp – much sharper than the crack tip at the other two locations inside the disbondment while the crack tip was bluntest at 150 mm from the open mouth. All cracks were transgranular in nature. The same trend was observed in the depth direction.

6.3.2 Crack growth behavior of sharp crack preceded by non-propagating loading (Test II)

To simulate field situations where pipelines typically experience extensive periods of benign R-ratio loading, and to truly simulate the environmental effects in the field, Test II was cyclically loaded initially to a R-ratio (0.65) that will not lead to immediate growth, that is, the so-called non-propagating condition. The combined factor corresponding to R=0.65 was calculated to be 3250, which was well below the threshold (~8500). As shown in Table 6-2, crack growth was not detected until the R ratio was reduced, in small intervals of $\sim 0.03 - 0.05$, to about 0.22, corresponding to a combined factor of 14330, which is well above the threshold value of about 8500.

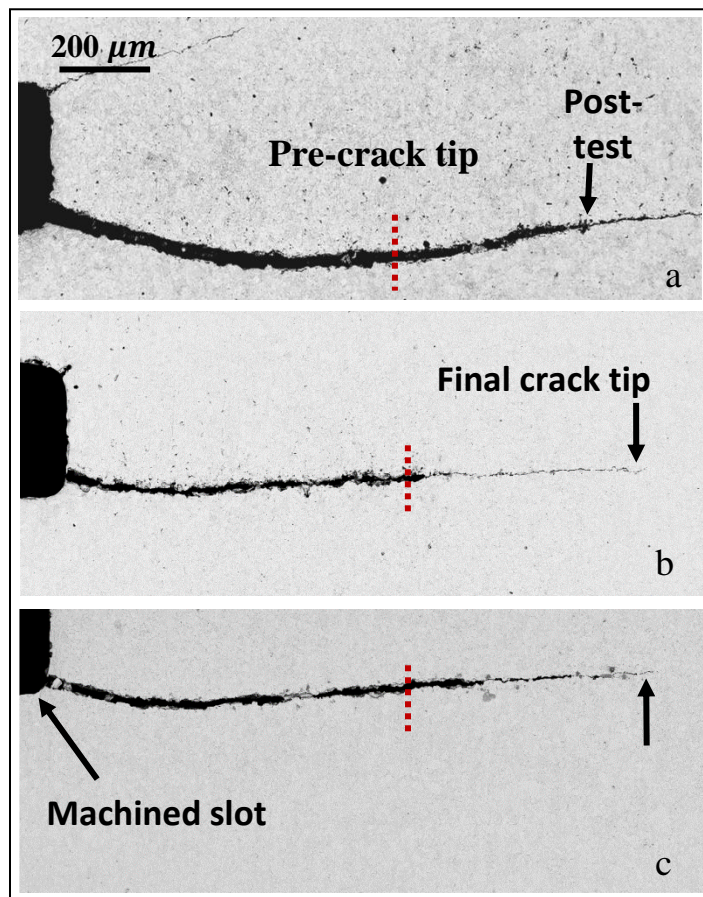


Figure 6-4: Pre-crack tips in Test I (a) open mouth, (b) 75 mm from open mouth and (c) 150 mm from open mouth

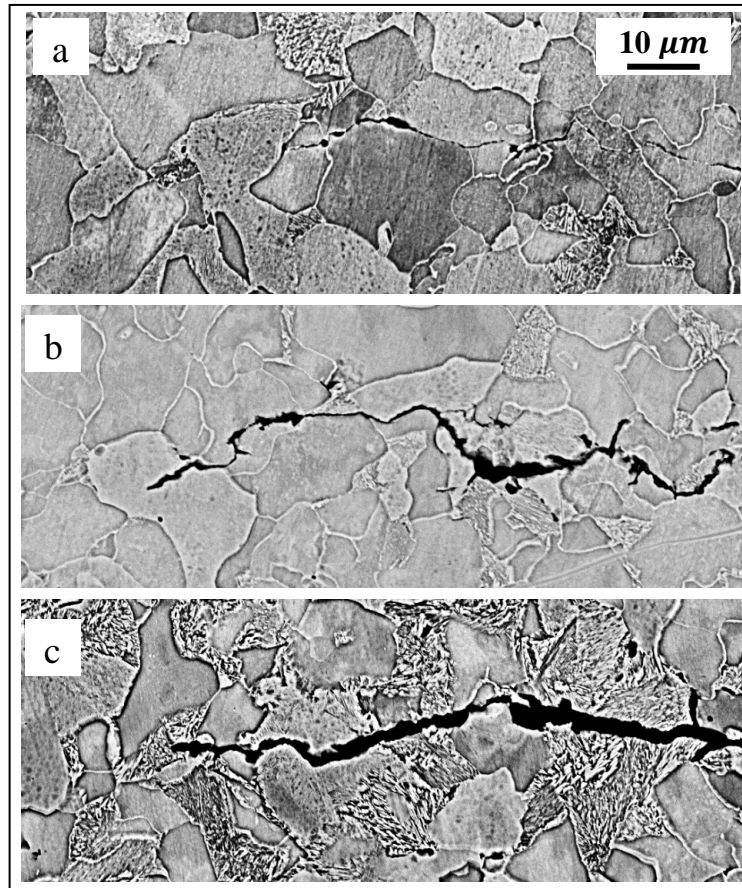


Figure 6-5 High magnification image of the crack tip in test I (a) open mouth, (b) 75 mm from open mouth, (c) 150 mm from open mouth.

At the sample surface, cracks were generally narrow but slightly wider than in Test I. Crack opening just behind the crack tip increased with distance from the open mouth (Figure 6-6). Cracks were generally longer in test II than in test I, which is indicative of more rapid crack propagation in test II. Despite much faster growth rate at the open mouth in Test II than in Test I, final crack tips were not as sharp as in test I (Figure 6-7).

The results of this test were previously published in a recent communication (chapter 4). Careful discussion of the results of the above two studies led to the following conclusions:

1. Contrary to popular belief, a high hydrogen ion concentration in soil water such as that produced by a high concentration of dissolved CO₂, does not necessarily produce a higher crack propagation rate. Such high hydrogen ion concentration may be accompanied by a high dissolution rate, and may effectively blunt the crack tip. In such a situation, unless severe mechanical loading is applied, crack propagation may slowly occur by a predominantly dissolution controlled mechanism. Growth rates under this situation would be well below normally observed SCC rates.
2. Also in environments with a high concentration of dissolved CO₂, severe crack tip blunting may cause the crack tip to be static for a sufficiently long period of time that low temperature creep may become a very significant factor. The combined effect of these two, both crack tip dissolution and low temperature creep, may cause very significant blunting. Under a such condition, crack re-initiation may only occur at very severe mechanical loading conditions.

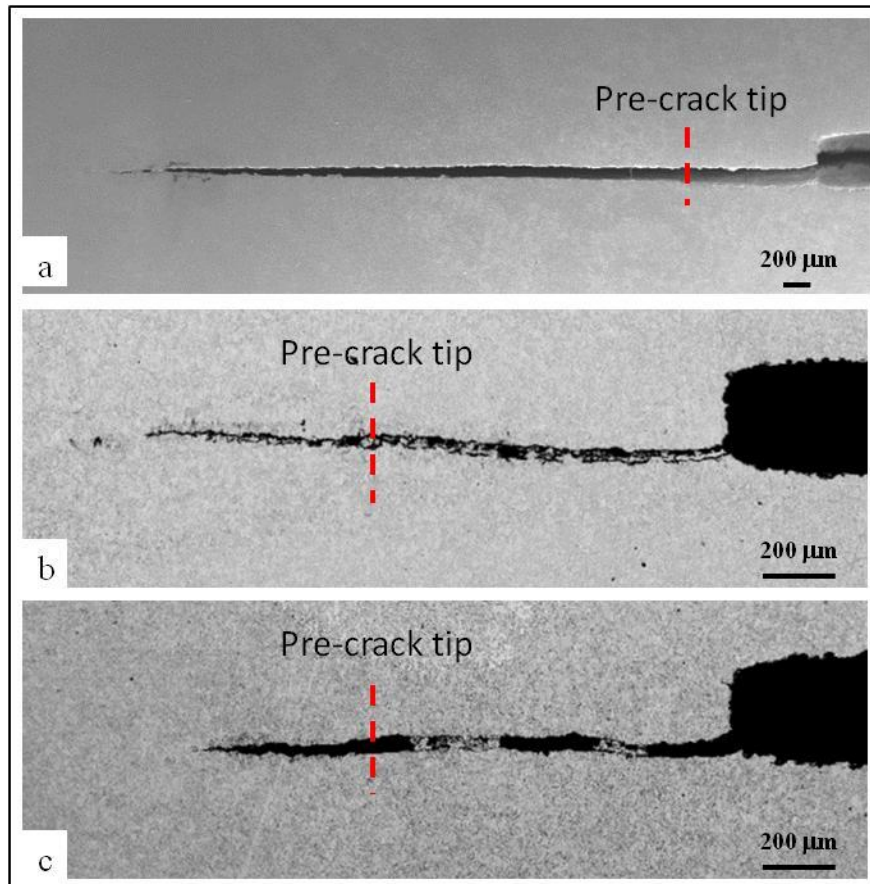


Figure 6-6: Post-test crack lengths measured at the sample surface after test II

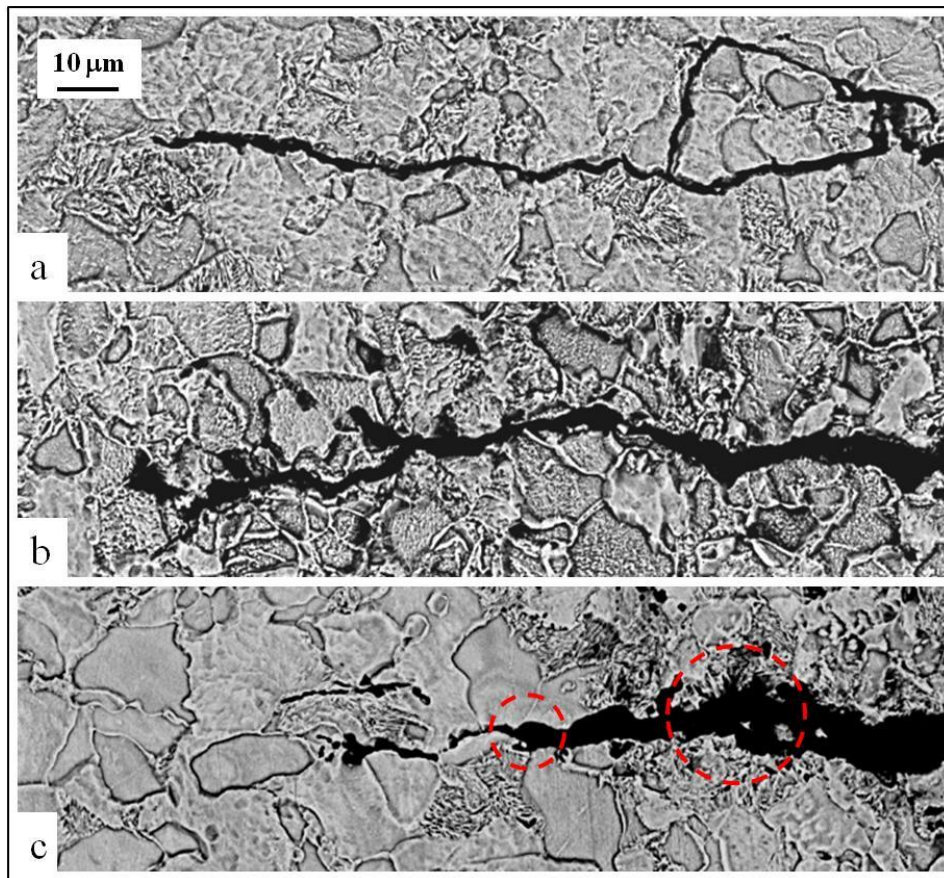


Figure 6-7: Crack tip Morphology in Test II (a) OM (b) 75 mm from OM, (c) 150 mm from OM

Under the testing conditions used for test II, it was impossible to separately study the effect of low temperature creep and crack tip dissolution, as both events occurred simultaneously during the study. In order to separately study the effect of low temperature creep and dissolution on crack re-initiation and subsequent propagation, it was necessary to design a study in which the effect of crack tip dissolution was eliminated so that the effect of low temperature creep, and the influence of other factors on low temperature creep, could be studied. This was achieved by applying a cathodic protection potential at the open mouth in this study. The level of cathodic potential applied was carefully selected so as to prevent complications from water dissociation at the open mouth. The results of this study are presented and discussed below.

6.3.3 Test results in 5% CO₂ testing environment and applied cathodic potential of 0.9V

6.3.3.1 Corrosion behavior

Examination of the sample surface after the test reveals that the metal surface was effectively protected at the open mouth. Pre-test scratches were seen to have been preserved throughout the duration of the test (Figure 6-8a). Slight general corrosion occurred at 75 mm from the open mouth probably due to the cathodic potential drop in the solution away from the open mouth (Figure 6-8b). Severe corrosion occurred at the bottom of the simulated disbondment, at and around 150 mm from the open mouth (Figure 6-8c).

6.3.3.2 Characteristics of crack morphologies

No crack growth was detected by the potential drop measuring system until a stress ratio of 0.4 was reached. Crack re-initiation occurred at the same stress ratio, corresponding to the same initial mechanical conditions, at the three locations. However, different extents of crack propagation were observed at all three locations. Figure 6-9 compares the crack lengths at the surface of the specimens. Since the cracks at different positions to the open mouth started at the same stress ratio, the fastest growth occurred at the open mouth while much smaller rates were determined at both 75 mm and 150 mm from the OM. Growth rates at these two locations were very similar.

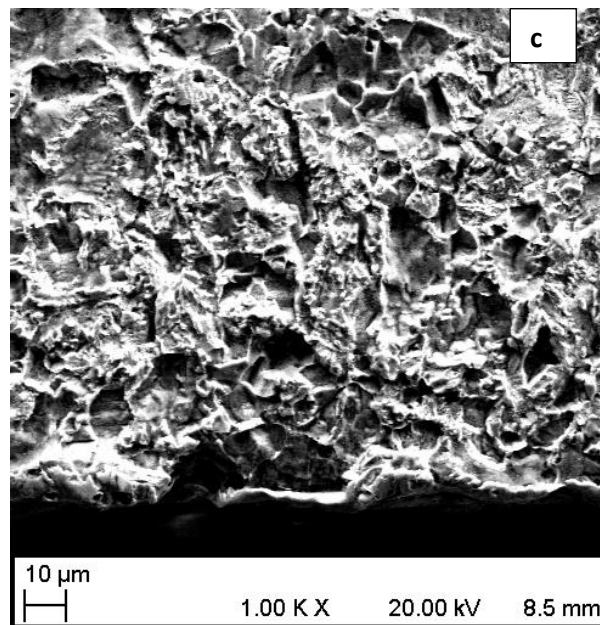
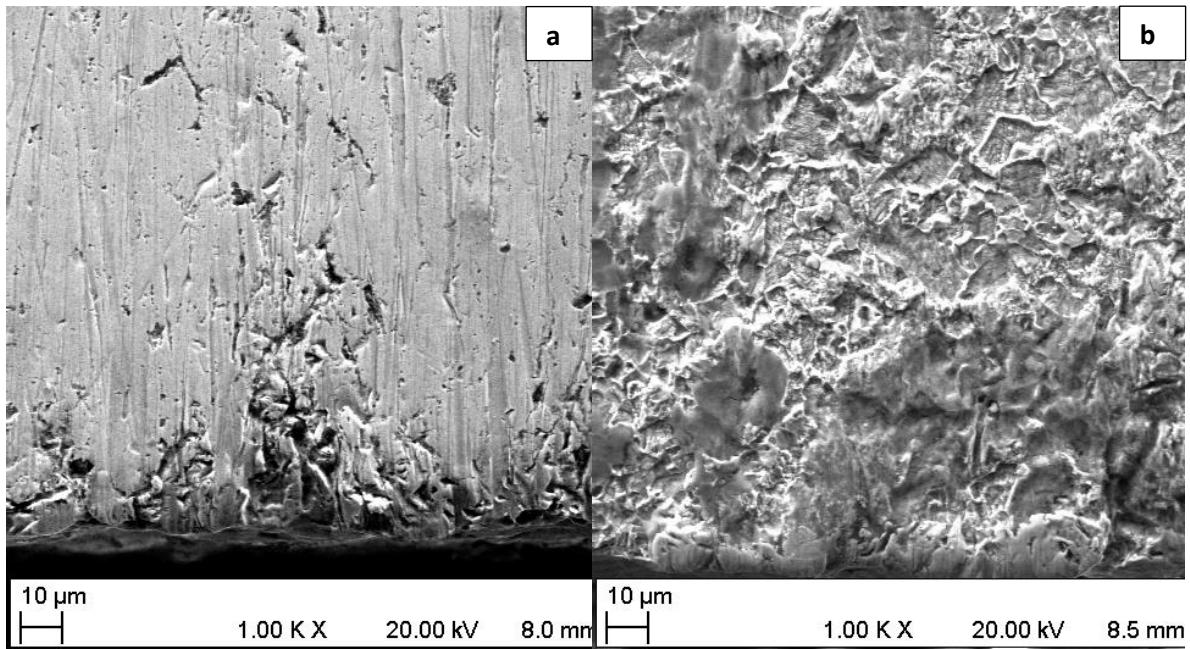


Figure 6-8: Corrosion behavior at the sample surface (a) at the open mouth (b) 75 mm from the open mouth, (c) 150 mm from the open mouth.

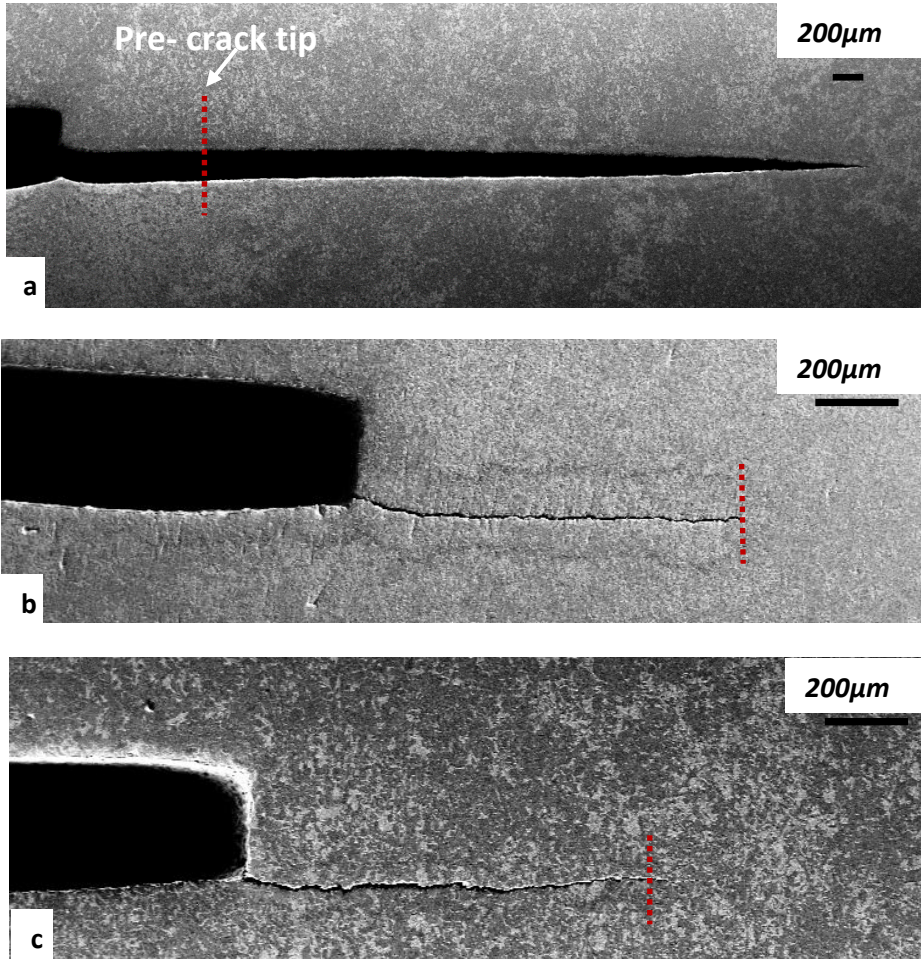


Figure 6-9: Post test crack lengths at the sample surface in test III (a) at the open mouth (b) at 75 mm from open mouth (c) at 150 mm from open mouth

At the sample surface, the crack crevice at the open mouth was significantly wider than at the other locations (Figure 6-9). Very fine crack tips were observed at all three locations in test III (Figure 6-10). Comparison of the crack tips to those in test I suggest that crack tips were sharper at 75 mm and 150 mm from the OM in test III than in test I (Figure 6-10 and Figure 6-4). Comparison of the crack tip at the open mouth in test III and that in test I suggest that the crack tip at the open mouth in test III is blunter than in test I (Figure 6-10a and Figure 6-4a). At 75 mm and 150 mm from the OM, comparisons of crack crevice openings in Figure 6-4 and Figure 6-10 shows that crack crevices are slightly wider in test I than in test III. Crack crevice opening at 75 mm and 150 mm from the open mouth in test II are much wider than those in test III (Figure 6-9 vs Figure 6-6). However, the crevice opening at the open mouth in test III is larger than that in test II. Generally crack tips are much blunter in test II than in either of test I or III.

Cracks were generally longer in test II than in test I, which is indicative of more rapid crack propagation in test II. This is even more significant when one considers that the cracks in test II were only subjected to 1945 cycles while the ones in test I were subjected to 9824 cycles. Cracks in test II are also longer than those in test III except for the open mouth crack. However, cracks in test III were subjected to 3276 cycles indicating a more rapid rate of crack propagation in test II.

In the depth direction, the crack crevice at the open mouth is also very wide; much wider than at the other two locations in test III and also wider than the corresponding open mouth crack in test I. However the crack tip remained very sharp, although the crack opening just a few micrometers behind the crack tip is very wide. The crack opening just behind the crack tips at 75 mm and 150 mm from the open mouth in test III have very comparable widths. However, the crack tips are much blunter than that at the open mouth. Also crack tips are blunter in the depth direction than at the sample surface.

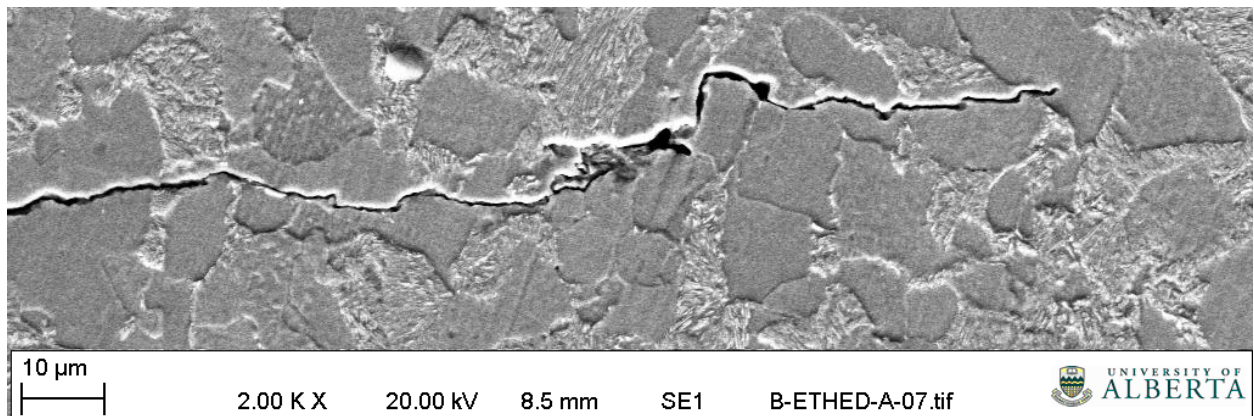
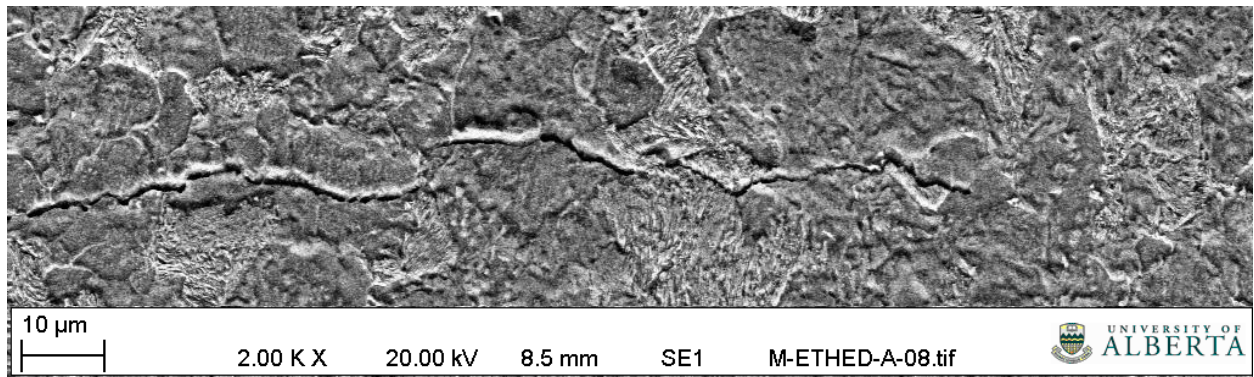
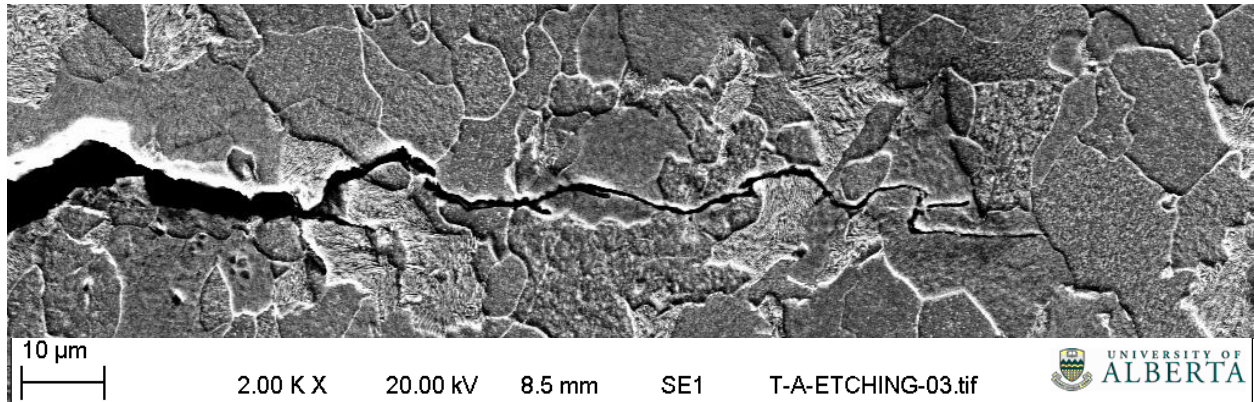


Figure 6-10: Crack tip morphology in test III (a) at the open mouth (b) 75 mm from open mouth (c) at 150 mm from open mouth

Figure 6-11 shows the fracture surface morphology in test III. Figure 6-11(a), shows the presence of a substantial amount of secondary cracks. The fracture surface morphology at 75 mm and 150 mm from the open mouth (Figures 6-11b & 6-11c) do not display this trend. They have very little growth and few secondary cracks as a result of the limited amount of CP reaching these surfaces.

6.3.3.3 Condition of crack re- initiation

As shown in Table 6-2, crack growth was not detected until the R ratio was reduced at very small intervals, ~ 0.02 – 0.03, to 0.4 in test III. At this R ratio, the combined factor was determined to be 9680, which is well above the threshold value of about 8500. The R-drop process was monitored by a potential drop system.

6.3.3.4 Crack growth rate behavior

In test III the highest growth rate was observed at the open mouth where crack growth rate at the sample surface was found to be nearly 7 times higher than at the 75 mm and 150 mm from the open mouth (Figure 6-12). Crack growth rates were very similar at both 75 mm from the OM and 150 mm from the OM. Comparing growth rates at the sample surface and the depth direction shows that growth was more rapid at the sample surface than in the depth direction at the OM. However, zero growth rates in the depth direction at 75 mm and 150 mm from the open mouth suggest that crack propagation only occurred at the sample surface but did not occur at the bottom of the crevice. Crack growth rates in test III are obviously significantly higher than in test I. Growth rates in the depth direction are shown in Figure 6-12.

The initial and final crack sizes are shown in Tables 6-3 and 6-4 while the initial and final aspect ratios are shown in Figures 6-13 and 6-14. The ratio of initial to final aspect ratios are also shown in Figure 6-15. These figures indicate that while crack propagation occurred at all locations during the test, variations in the local environment with distance from the open mouth could change

the character of growth significantly. Aspect ratio decreased at the open mouth but remained about the same at 75 mm and 150 mm from the OM.

Table 6-3: Characteristics of crack growth for cracks on the specimen surface

| | | Initial crack length (mm) | Final Crack length (mm) | Net crack growth (mm) | Average crack growth rate (mm/cycle) |
|----------|--------------|---------------------------|-------------------------|-----------------------|--------------------------------------|
| Test I | OM | 3.34 | 5.49 | 2.15 | 2.15E-04 |
| | MP | 3.31 | 3.83 | 0.52 | 5.16E-05 |
| | BP | 3.38 | 3.85 | 0.48 | 4.77E-05 |
| Test II | OM | 3.32 | 7.36 | 4.05 | 2.08E-03 |
| | MP | 3.30 | 3.73 | 0.44 | 2.24E-04 |
| | BP | 3.31 | 3.53 | 0.23 | 1.16E-04 |
| Test III | OM | 3.54 | 8.12 | 4.58 | 1.40E-03 |
| | MP | 3.50 | 3.66 | 0.16 | 4.90E-05 |
| | BP | 3.62 | 3.62 | 0.00 | 0.00E+00 |
| Test IV | Air | 3.35 | 3.60 | 0.26 | 5.08E-05 |
| | Ind. Contact | 3.37 | 3.60 | 0.25 | 4.64E-05 |
| | Dir. Contact | 3.44 | 3.86 | 0.39 | 8.70E-05 |

Table 6-3: Characteristics of crack growth for cracks in the depth direction

| | | Initial crack length (mm) | Final Crack length (mm) | Net crack growth (mm) | Average crack growth rate (mm/cycle) |
|----------|--------------|---------------------------|-------------------------|-----------------------|--------------------------------------|
| Test I | OM | 3.13 | 4.09 | 0.96 | 9.56E-05 |
| | MP | 3.20 | 3.74 | 0.55 | 7.15E-05 |
| | BP | 3.09 | 3.73 | 0.63 | 6.31E-05 |
| Test II | OM | 3.19 | 5.33 | 2.14 | 1.10E-03 |
| | MP | 3.38 | 3.52 | 0.14 | 7.12E-05 |
| | BP | 3.43 | 3.57 | 0.14 | 7.12E-05 |
| Test III | OM | 3.70 | 6.25 | 2.55 | 7.76E-04 |
| | MP | 3.44 | 3.44 | 0 | 0 |
| | BP | 3.47 | 3.47 | 0 | 0 |
| Test IV | Air | 3.17 | 3.28 | 0.11 | 2.37E-05 |
| | Ind. Contact | 3.05 | 3.21 | 0.16 | 3.43E-05 |
| | Dir. Contact | 3.34 | 3.56 | 0.22 | 4.48E-05 |

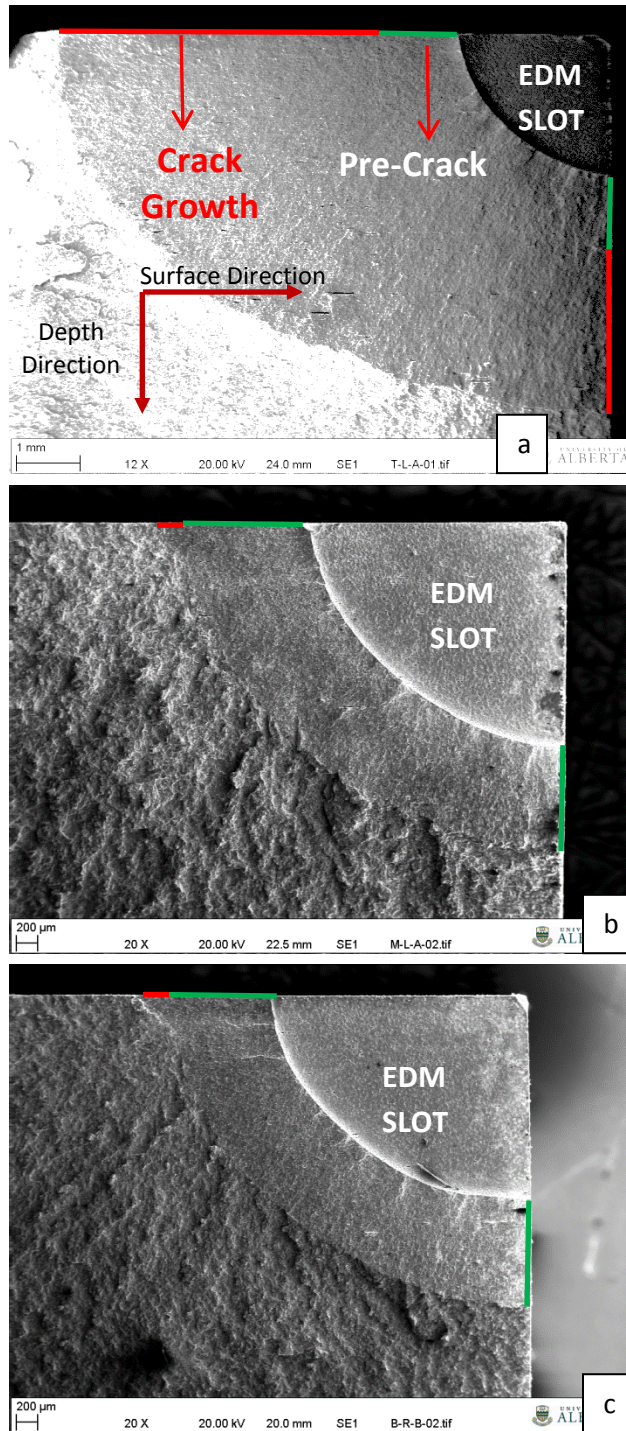


Figure 6-11: Fracture surface morphology of the test sample in test III at the (a) OM, (b) 75 mm from OM and (c) 150 mm from OM. The images clearly show that while there was significant growth at the open mouth in both the surface and depth directions, there was very little growth at 75 mm from the OM and no growth at 150 mm from the OM.

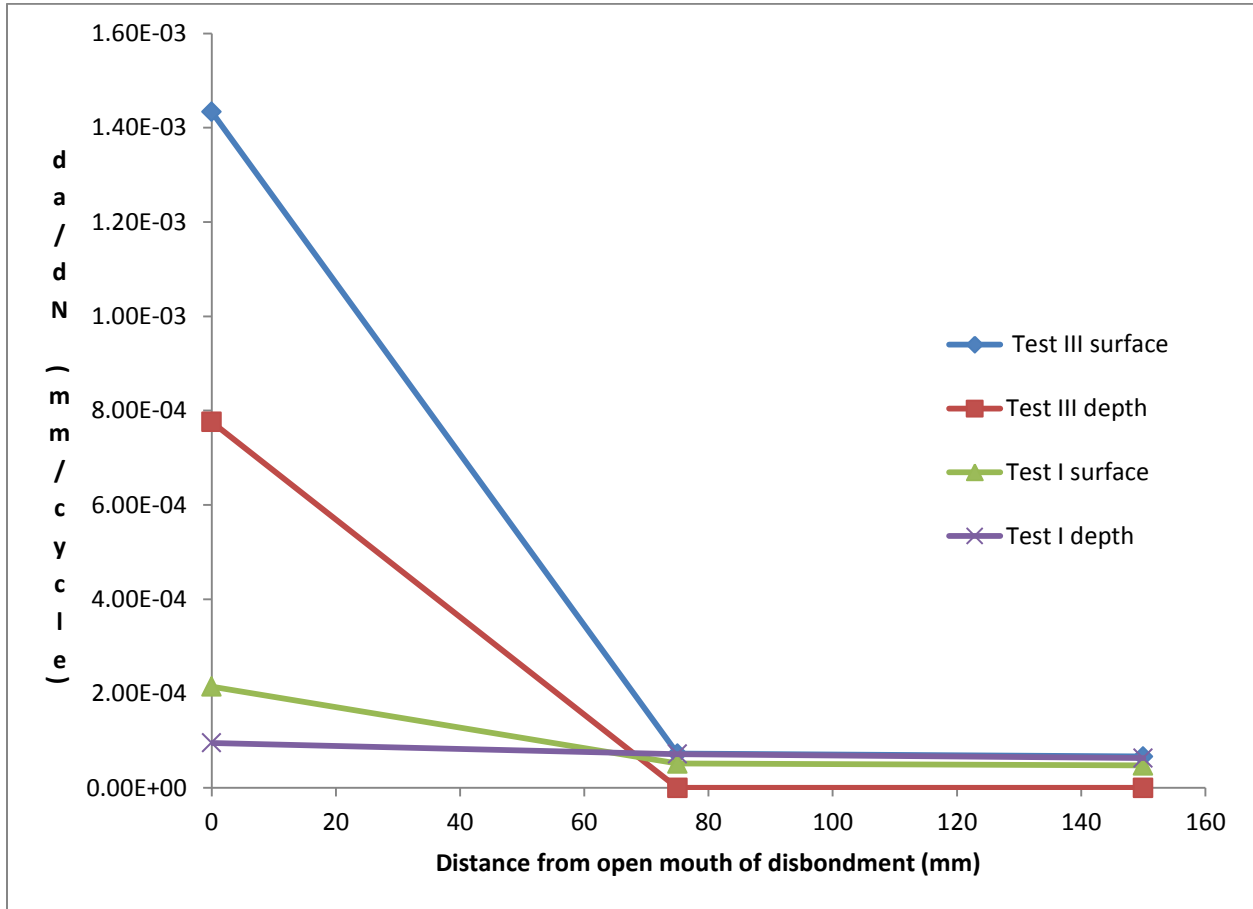


Figure 6-12: Crack growth behavior in tests I and III

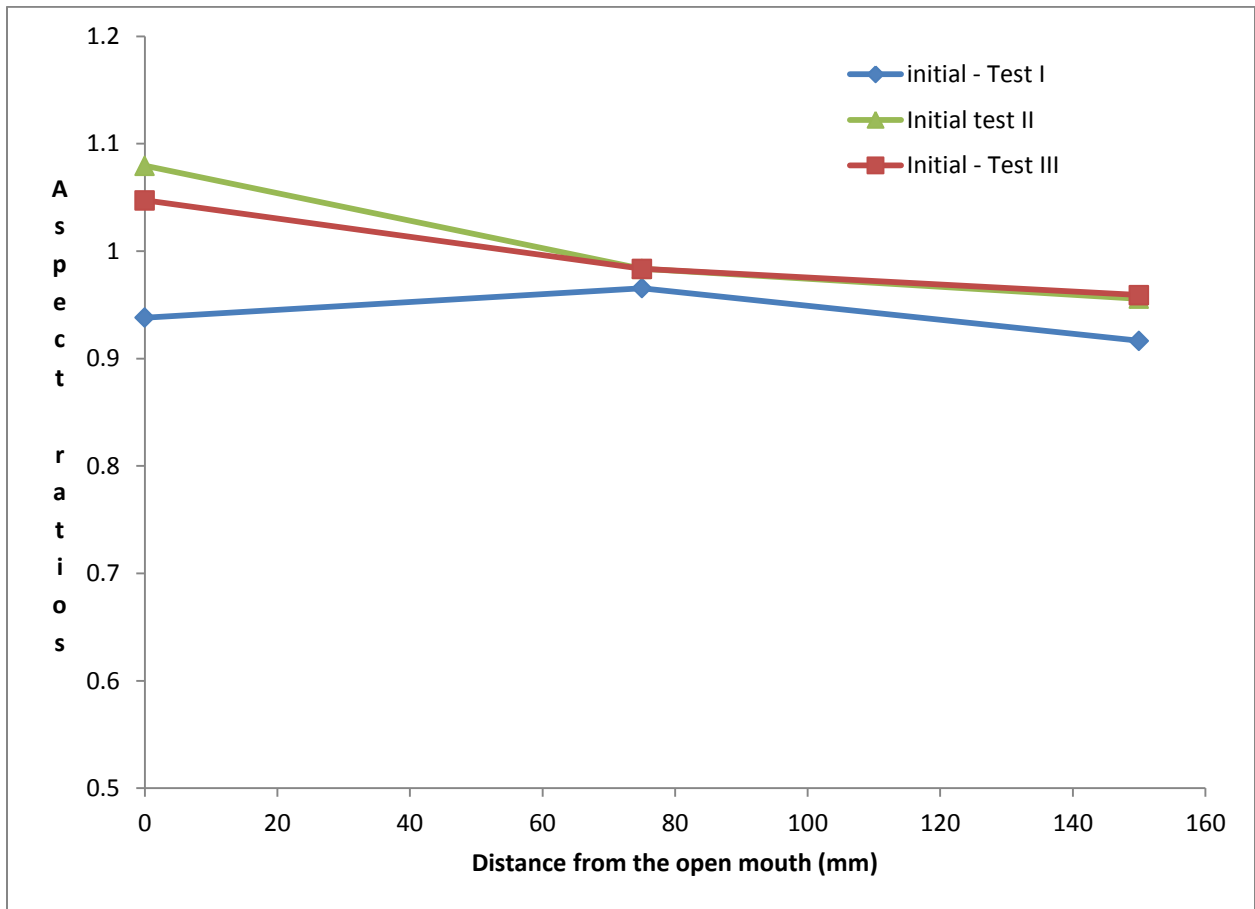


Figure 6-13: Initial aspect ratios

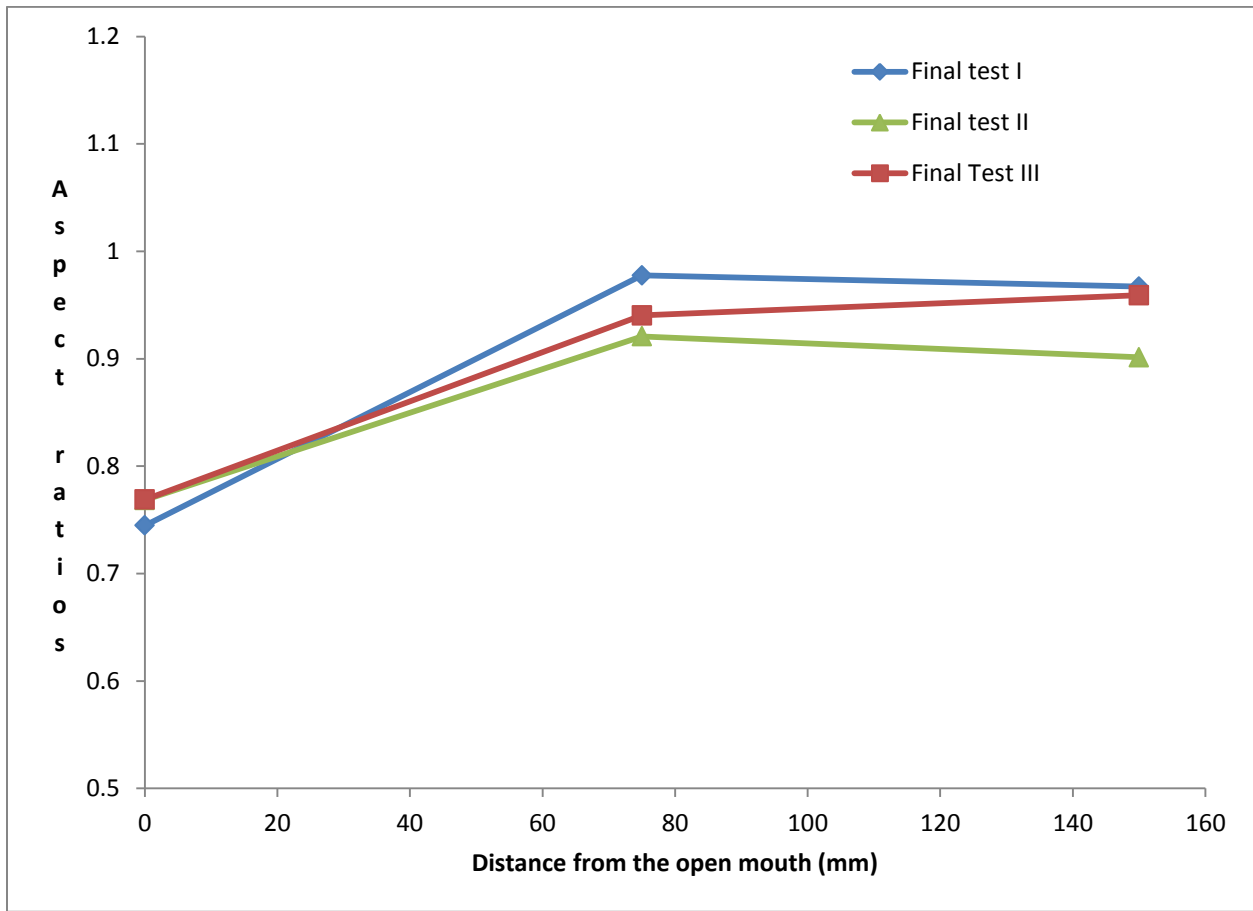


Figure 6-14: Final aspect ratios

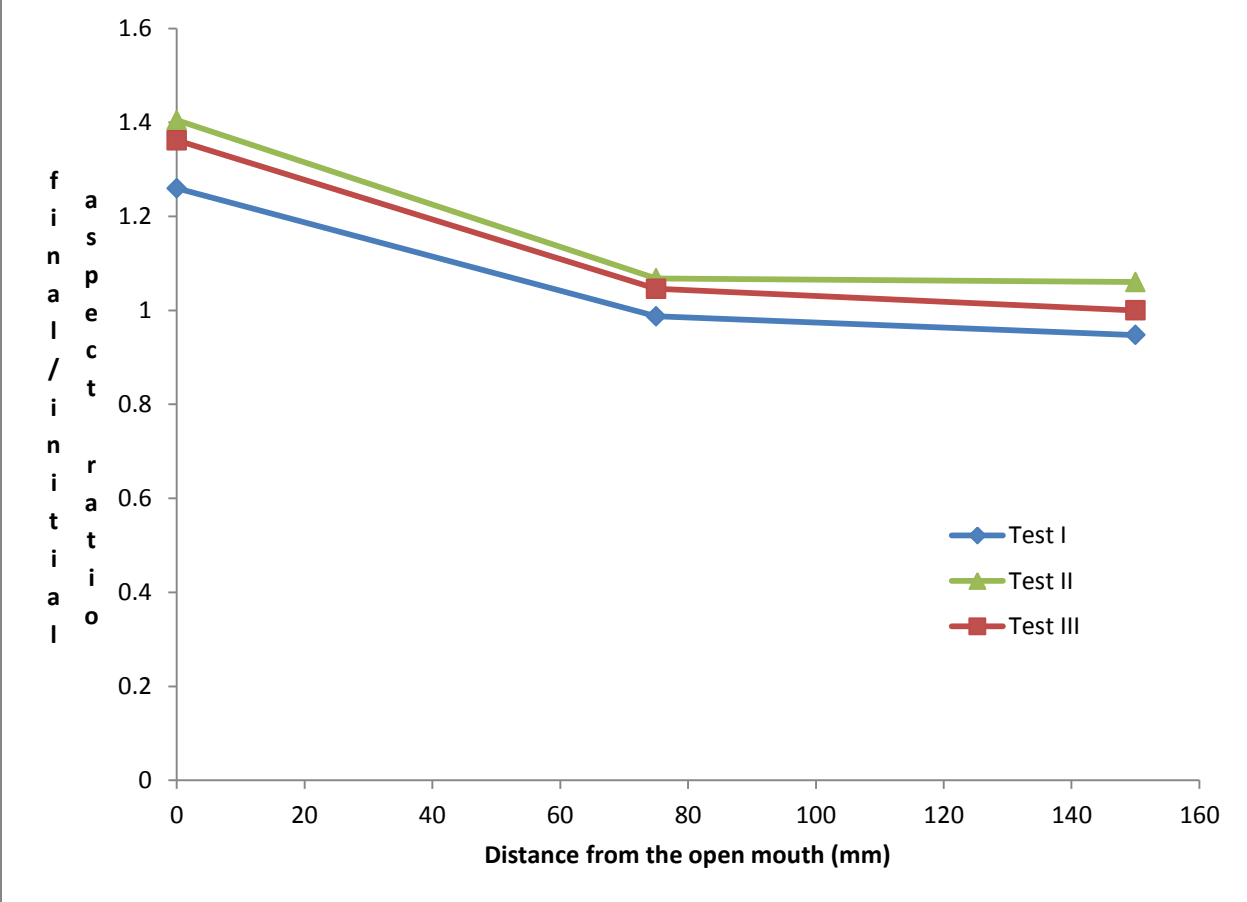


Figure 6-15: Ratio of initial to final aspect ratios

6.4 Test IV results

6.4.1 Comparison of crack behavior when loaded at 100% SMYS in direct contact with C2 solution, in indirect contact with C2 solution and in air – Test IV

This test was conducted to determine the effect of the testing environment on crack behavior in cases where the crack tip is in direct contact with a near neutral pH environment compared to cases where the crack tip is in indirect contact with a near neutral pH environment. The control test was the crack that was cyclically loaded in air.

There was hardly any difference in the morphology of the fatigue pre-crack tip (Figure 6-16). However, when the crack paths are traced out and superimposed as in Figure 6-17, it becomes obvious that at the sample surface, the crack crevice loaded in direct contact with the corrosive media is wider than the one loaded in indirect contact with the C2 solution. Comparing crevice width along the line indicated in Figure 6-17 showed that the crevice is about 30% wider when in direct contact with the solution than when in indirect contact with the solution or in air. Crevice widths are very similar for the cracks loaded in indirect contact with the solution and the one loaded in air. The difference in width is less obvious in the depth direction.

6.4.2 Crack growth behavior in test IV

At the sample surface, very short fine cracks were found to have initiated at the tip of the pre-fatigue cracks in all three cases. Crack lengths are as shown in Tables 6-3 and 6-4. These growth rates are very low and are not included in Figure 6-12 so that they do not overlap the growth rates of Test III. It must also be pointed out that in companion studies (manuscript under preparation) steady growth was not observed at a stress ratio of 0.6 even at a maximum stress of 100% SMYS cyclic loading; even when a much higher number of cyclic loads was applied. It is usual to observe a small transient crack elongation when stress ratios are changed during fatigue loading. It is strongly believed that the growths observed in this test are in fact transient and are not sustained steady growth.

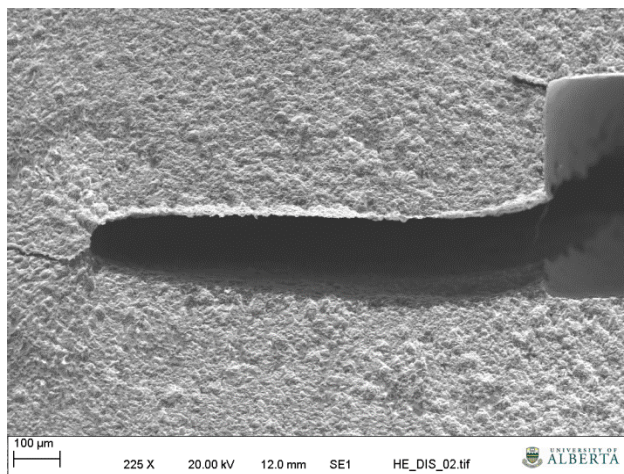
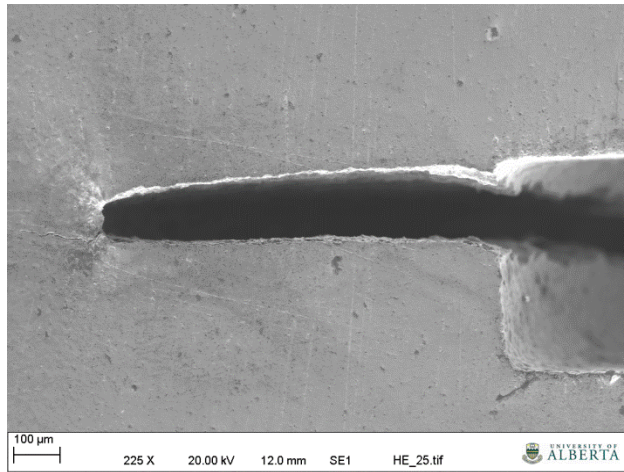
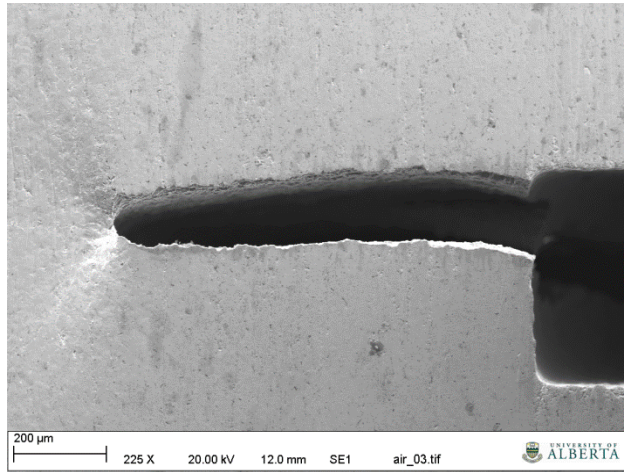


Figure 6-16: Crack morphology when cyclically loaded in (a) air, (b) indirect contact of crack tip with C2 solution, (c) direct contact of crack tip with C2 solution

- air
- front covered
- back covered, front exposed

Crack profile in depth direction

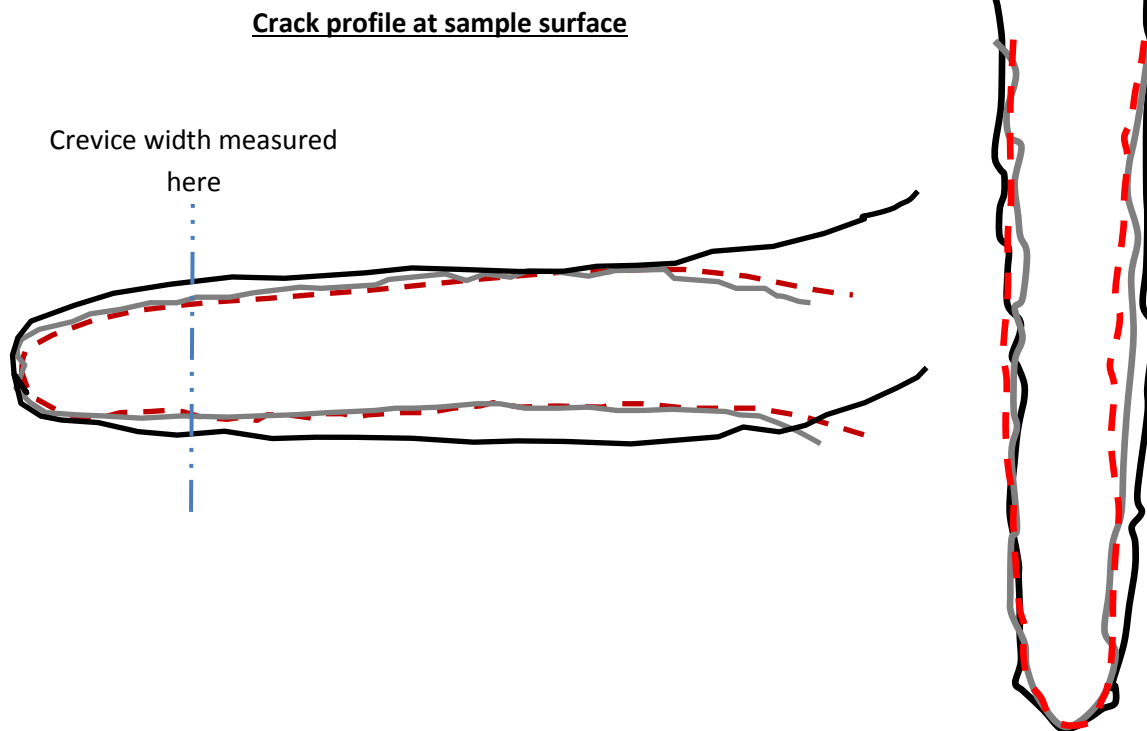


Figure 6-17: Crack outlines: in air, indirect contact with solution, direct contact with solution. Crack outline at sample surface (horizontal), crack outline in depth direction (vertical)

6.5 Discussion

6.5.1 Crack morphology

Besides the difference in crack propagation rates between tests I and III, an equally important observation is the difference in crack crevice width behind the crack tip. The observed difference in crack width may be grouped into two different categories as is the mechanisms responsible for their development:

1. Between tests I and III, a comparison of crevice width at 75 mm and 150 mm from the open mouth reveals the same trend. Crack widths at both locations in each test are quite comparable. However, comparing the crevice width at these locations between the two tests reveals that the crack crevices in test I are slightly wider.
2. Comparison of the crack width at the open mouth in both tests reveals that the OM crack in test III has a much wider crevice than in test I.

To explain these two different scenarios, critical consideration must be given to the different factors that could influence the crevice formation: dissolution, crack tip opening/closure and low temperature creep.

6.5.2 Role of crack wall dissolution

The application of a cathodic potential in test III should suppress any significant crack wall dissolution at the open mouth. This is well supported by the observed full protection of the sample surface at the open mouth as noted in section 6.3.3.1. The variation of cathodic potential under the disbondment with distance from the open mouth is shown in Figure 6-18. This shows that cathodic potential can diminish very significantly with distance from the open mouth, approaching open circuit potentials at the far end of the disbondment. However, a careful examination of the potential variations at the different applied potentials, especially those at the higher applied cathodic potentials, shows that the potential curves never really drop off to the open circuit potential at the far end of the disbondment.

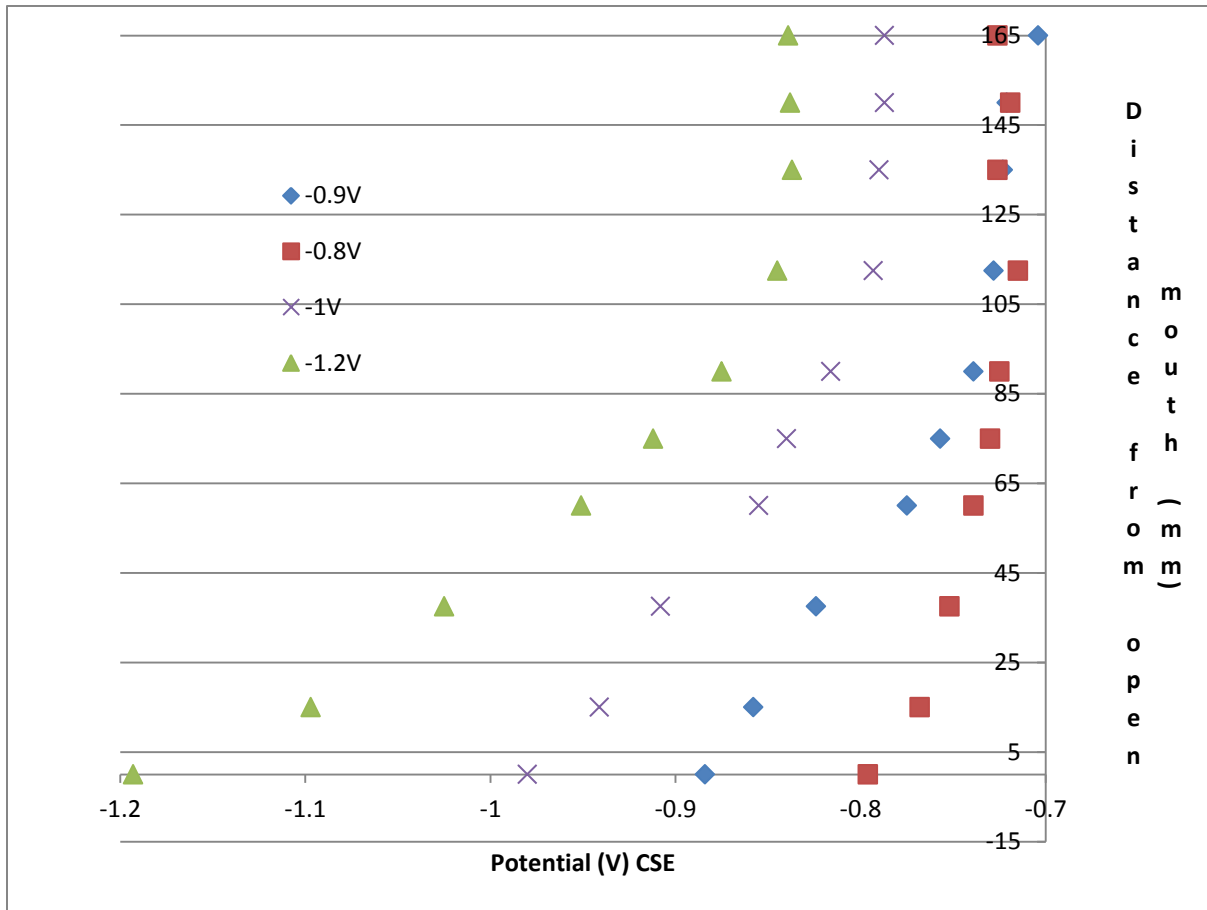


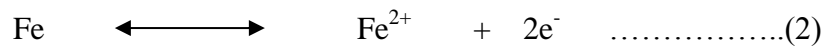
Figure 6-18: Variation of cathodic potential with distance from the open mouth, at different applied potentials. Legend shows the cathodic potential applied at the open mouth of the disbondment

Rather, there is always a residual cathodic potential at the far end of the disbondment. Since a cathodic potential suppresses or slows down anodic dissolution, lesser crevice widening by a dissolution mechanism should occur in test III than in test I. This explains why crack crevices at 75 mm and 150 mm from the OM are wider in test I than in test III. However, a dissolution mechanism does not account for the significantly wider crack crevice at the open mouth in test III, especially given that crack tip dissolution is more intensely suppressed at the OM than at other locations in test III.

6.5.3 Effect of hydrogen on crack morphology

The question then is what is responsible for the wider crack crevice in test III? The answer to this question could probably be traced to the local environment difference at the OM between test I and test III – namely the application of a cathodic potential at the OM in test III and the possible effect of such a cathodic potential. It has been shown elsewhere that when a cathodic potential is applied at the open mouth of a disbondment such as the one used in this study, the following scenario occurs [22]

1. The main source of hydrogen ions within the solution is from the dissolution of CO₂ in the ground water to form carbonic acid and the subsequent dissociation of carbonic acid into hydrogen ions through the reaction



2. Hydrogen ions can only migrate into the disbondment through the open mouth of the disbondment. Hence hydrogen ion concentration in the disbondment is highest at the open mouth.
3. Hydrogen ions being positively charged will prefer to reside at the region of highest cathodic potential. Hence, hydrogen ions should be more reluctant to migrate away from the areas of higher cathodic potential. Therefore, hydrogen ions should preferentially reside at the OM. However, the concentration gradient (chemical driving force) between the open mouth and the far end of the disbondment, still exerts sufficient influence to drive hydrogen diffusion to the farther end of the disbondment. Hydrogen migration to the father end is probably moderated by the reluctance of hydrogen ions to migrate away from the higher cathodic potential areas.
4. In addition to the hydrogen concentration resulting from the dissociation of carbonic acid in solution, more hydrogen could be generated at the OM from the direct dissociation of water into hydrogen and oxygen, if the cathodic potential is high enough.

The implication of the scenario presented above is that hydrogen ion concentration at the surface of the specimen could be significantly higher at the OM than at the other locations under the disbondment in test III. It is known that the majority of hydrogen atoms generated from reduction of hydrogen ions at the surface of a metallic specimen are recombined into hydrogen gas bubbled out of the solution. A small fraction of hydrogen atoms adsorbed on the surface are subsequently able to migrate into the metal lattice. Atomic hydrogen entry into the lattice is driven by the concentration gradient between the atomic hydrogen adsorbed at the exposed metal surface and the opposite surface which was protected or isolated from the corrosive media. It is important to note that the formation of corrosion products on the

surface of the sample is known to reduce the rate of hydrogen entry into the metal lattice. As mentioned earlier, the sample surface was well protected by the applied potential at the OM and this should result in more efficient hydrogen pick up by the lattice at the open mouth than at the other locations in test III. This should also result in more efficient hydrogen pick up at the OM in test III than in test I.

As far as crack behavior is concerned, the amount of atomic hydrogen present in the fracture process zone ahead of the crack tip can significantly influence crack behavior. It is well known that hydrogen will prefer to reside at interstitial lattice positions that are experiencing more tensile loading, such as the plastic zone ahead of the crack tip, where the lattice is more dilated. In this case both the amount of hydrogen adsorbed at the surface in direct contact with the crack tip and the total hydrogen concentration within the overall surrounding metal lattice are important. If a higher concentration of hydrogen atoms is adsorbed on the crack surface around the crack tip, more atomic hydrogen is assimilated directly into the process zone. Also, more atomic hydrogen in the overall metal lattice, means more atomic hydrogen can migrate through the lattice to the fracture process zone until saturation occurs. Therefore, there is a higher tendency that the lattice is more quickly saturated with hydrogen at the open mouth in test III than in test I. The presence of such atomic hydrogen could have a variety of effects, depending on whether crack propagation is occurring or not:

1. Hydrogen enhanced localized plasticity could occur especially under static loading
2. It was shown in earlier publications [23-25] that even at open circuit potential where unconstrained migration of hydrogen ions occurred within the solution, there exists a sufficiently larger atomic hydrogen concentration in the metal lattice at the open mouth to

cause a significantly higher crack advance at the OM than at the other locations. Under crack propagating conditions, the higher concentration of lattice hydrogen at the OM under the applied cathodic potential can significantly modify crack propagation rates.

In a previous study [23], the effect of low temperature creep deformation on crack re-initiation and subsequent crack propagation was discussed. In that study, it was found that load cycling under benign loading conditions where crack propagation could not occur, resulted in low-temperature-creep-induced crack tip blunting. Comparing the open mouth crack crevice width in Figure 6-9 to that in Figure 6-6 it is clear that the crack crevice at the OM in Figure 6-9 is significantly wider, although the final crack length of the crack shown in Table 6-3 and Table 6-4 and that of the OM crack in test III are quite similar. The extent of the difference in crack crevice width was illustrated by tracing out the two crack outlines and superimposing them in Figure 6-19. To quantify the difference in crack crevice width, the width of the crack crevice at the root of the machined slot after exposure was measured and corrected to remove the increase of crack opening due to the hinge effect due to differences in crack length (Table 6-5). Since the difference in crevice width cannot be attributed to crack opening as a result of the difference in crack length, the observed difference in crack length must be attributed to other factors related to the difference in local environment at the OM on account of the applied cathodic potential. A major possibility is hydrogen enhanced creep deformation. The influence of time independent HELP will be discussed in the next section.

Table 6-5: Width of crack crevice at the pre-fatigue crack tip (measured at the edge of the EDM slot) after correction for hinge effect at the open mouth

| | Width (μm) |
|----------|-------------------------|
| Test I | 18.48 |
| Test II | 110.2 |
| Test III | 223.5 |

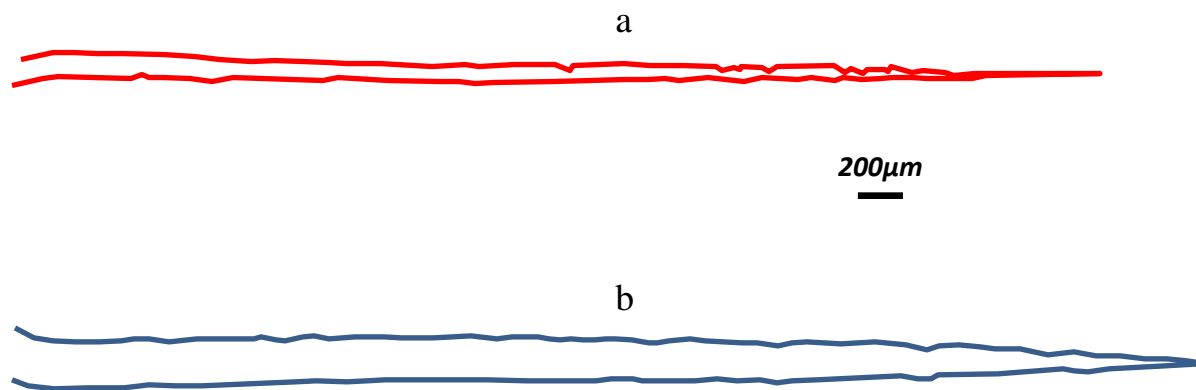


Figure 6-19: Comparison of crack crevice width in (a) Tests II (red) and (b) Test III (blue). Outline shows both the precrack and in-test crack growth combined

6.5.4 Effect of hydrogen- enhanced localized plastic deformation

As mentioned earlier, the wider crack crevice at the OM in test III cannot be attributed to a dissolution process or crack opening on account of crack length compared to the remaining crack ligament. One of the probable reasons for such a wide crack could be enhanced localized plastic deformation. It is well known that hydrogen can either increase or reduce the macroscopic yield strength of metal systems depending on the particular system in question [26]. Hinton and Procter [27] found that at slow strain rates and an applied cathodic potential, between -0.9V – -1.6V (SCE), the ductility of X-65 steel is significantly reduced. The reduced ductility was associated with the formation of transgranular cleavage cracks. Previously, Ulner and Alstetter [28] had observed a decrease of work-hardening rate in stainless steels after hydrogen charging. Neumann [26] opined that such a decrease in work-hardening capability may result in strong strain localization. Such strain localization should then result in localized necking which may occur on a microscopic scale. Such enhanced strain localization upon hydrogen adsorption into steel lattice has been attributed to increased dislocation mobility [8].

Given the intense stress concentration ahead of a crack tip even under non-propagating conditions, there should be a lot more dislocations produced at and near the crack tip in the so called fracture process zone. It has been shown that a high dislocation density develops in the near surface region prior to SCC cracking [30]. The presence of hydrogen in steel lattice could lead to a two prong enhancement of localized plasticity. First, hydrogen aids dislocation motion by weakening long-range barriers to dislocation motion [9]; and second, dislocation motion helps transport more hydrogen if the dislocation velocity is below a critical value [9] causing an autocatalytic effect. By softening the alloy such that permanent deformation occurs more easily at the crack tip than in the absence of hydrogen, increased segregation of hydrogen to the process

zone ahead of the crack tip, such as occurs under an applied cathodic potential, could increase deformation ahead of the crack tip.

Under non-propagating conditions, the resulting localized plasticity would result in an increased crack tip opening due to early onset of permanent deformation of the crack tip region. This could result in a permanent intense deformation of the crack tip area and could result in a wider crack crevice as observed in test III. Such an intense deformation prior to crack propagation could modify the shape (width) of the crevice developed when crack propagation resumes. Evidence of this is shown in the results of test IV. As mentioned in section 3.4, the crack crevice is about 30% wider when there is a direct contact of the simulated soil solution with the crack tip than when the test was done in air or when there is no direct contact of the simulated soil solution with the crack tip. In a case where there is no direct contact of the solution with the crack tip, hydrogen segregation to the crack tip is limited to the amount transported to the hydrogen process zone through the lattice.

The fact that crack crevice width under lattice hydrogen transportation is very similar to that under fatigue in air, suggests that atomic hydrogen is not delivered to the crack tip at a high enough concentration to induce sufficient hydrogen enhanced plastic deformation ahead of the crack tip, to significantly modify the crack shape. However, when there is a direct contact of the simulated soil solution to the crack tip, the crack surface is covered in the hydrogen-bearing solution and hydrogen is directly adsorbed and absorbed on the crack surface, providing a more direct access to the crack tip. This could result in a higher hydrogen concentration ahead of the crack tip, probably resulting in more localized plastic deformation; hence a wider crack crevice. It has been well reported that transgranular SCC propagation is a discontinuous process [30-32].

During such a process it is possible that the crack stays stationary enough under an applied cathodic potential, for the sequence of microscopic activities that result in such intense localized plastic deformation to repeat itself over and over again resulting in a sustained wide crack crevice as observed at the open mouth in test III compared to that in test I.

6.5.6 Crack propagation

It is very interesting to observe that in test III, as in test I, crack propagation occurred at a stress ratio of 0.4. However, in test II, crack propagation was delayed to a stress ratio of 0.22. This points to the importance of localized hydrogen concentration to crack re-initiation.

Comparing the crack growth results in test III with those in test I (Figure 6-12) reveals two very important details:

1. Crack growth rate at the OM in test III is nearly seven times higher than at the same location in test I
2. Crack growth at 75 mm and 150 mm in test III are significantly lower than at the same location in tests I or II.

In test I, crack propagation started from a very sharp pre-fatigue crack tip because loading commenced at a stress ratio that is just severe enough for crack propagation to occur and there was no time allowed for any significant crack tip dissolution or low temperature creep to blunt the crack tip. However, in test II, crack re-initiation was delayed at all locations until a much more severe mechanical loading condition was applied ($R=0.22$) because the crack tip was blunted by a combination of crack tip dissolution and low temperature creep. Although in test III loading started at a benign condition, and gradually increased to more severe conditions until crack re-initiated at a stress ratio of 0.4, the applied cathodic potential protected the crack tip

from blunting by a dissolution mechanism. However, low temperature creep deformation would still occur at these benign conditions and there is no evidence that such creep-induced crack tip blunting did not occur in test III. The fact that very minute crack propagation occurred at 75 mm and 150 mm from the OM indicates that it was impossible to initiate a stable crack growth at these locations, unlike in test I. It should be noted that it is usual to observe a minute transient crack growth each time the stress ratio is changed. However, such growth is usually quickly arrested and the crack attains dormancy. This possibly explains the minute crack growth observed at these two locations. Therefore, it is reasonable to assume that creep induced crack tip blunting indeed occurred during the testing pre $R=0.4$ testing conditions in test III making it impossible for cracks to initiate except at the open mouth in test III. The result is therefore proof that at 75 mm and 150 mm from the OM, the combined environmental-mechanical crack driving forces were unable to overcome the crack tip blunting forces – dissolution and low temperature creep – such that sustained crack propagation could not occur.

The results of test IV suggest that such low temperature creep induced deformation of the crack tip could be more severe under conditions where hydrogen concentration in contact with the surface is higher, as the crack crevice was found to be 30% wider when the cracked surface was directly exposed to the testing solution compared to when the cracked surface was not directly exposed. This suggests that the pre-fatigue crack tip should have experienced more crack tip deformation at the OM than at the other locations.

Despite significant crack tip blunting during the pre- $R=0.4$ cyclic loading, stable crack propagation was able to initiate at the OM in test III and growth rate was almost seven times higher than when testing occurred under the same testing condition except for the application of

a cathodic potential (test I). This suggests that both enhanced deformation and enhanced crack propagation occurred simultaneously under the testing condition in test III. It is well known that hydrogen enhances crack propagation. Although there is no agreement on the mechanism by which this hydrogen enhanced crack propagation occurs, this much is known:

1. The extent of crack propagation enhancement increases with the amount of hydrogen that is able to segregate to the hydrogen process zone ahead of the crack.
2. A critical hydrogen concentration is required to cause crack initiation from a dormant state, and to sustain stable crack propagation
3. At applied stresses below the stress threshold required for direct crack re-initiation from a dormant crack solely by mechanical factors, the amount of hydrogen required to cause crack initiation and stable crack propagation from a dormant crack tip decreases as the level of applied tensile stress increases. The higher the stress applied, the lower the amount of hydrogen required to cause crack re-initiation.

The consequence of the hydrogen distribution provided in section 6.5.3 is that hydrogen concentration at the open mouth in test III should be significantly higher than in both test I and test II. Thus, it is well possible that despite the occurrence of significantly more pre-fatigue crack tip blunting in test III compared to test I, there is a sufficiently high lattice hydrogen concentration at the open mouth to cause an environmentally assisted crack re-initiation and sustained propagation at the open mouth. Hinton and Procter [27] showed that a reduced ductility was associated with the formation of transgranular cleavage cracks. Careful examination of the fracture face at the open mouth in tests I and III reveals a flatter fracture surface, with more cleavage type fracture in test III compared to test I (Figure 6-20). It is well known that hydrogen-enhanced crack propagation could encourage more cleavage type propagation. This confirms a more intense hydrogen enhanced crack propagation at the OM in test III compared to test I.

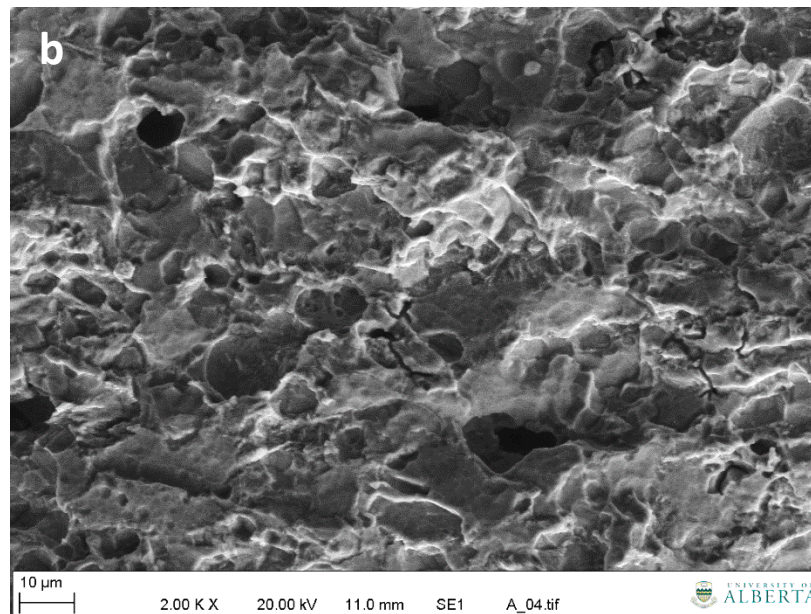
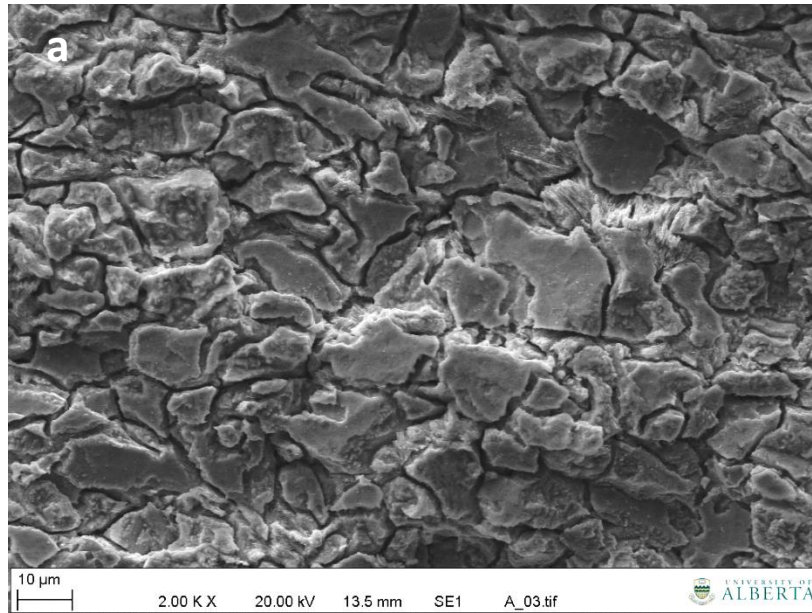


Figure 6-20: Fracture face morphology at the open mouth in (a) test III and (b) test II

In a recent publication [22], the current authors showed that the environmental factor at the OM under open circuit potentials could be three times higher at the open mouth than at 75 mm and 150 mm from the OM. It is therefore reasonable to assume that with a 7 fold increase in crack growth rates under an applied cathodic potential of -0.9V, and the much lower crack propagation rates at other locations, the environmental factor at the OM under an applied cathodic potential of -0.9V might be at least 10 times that at locations within the disbondment. Comparison of the growth curve in tests I and II, Figure 6-21, shows the growth rate at an applied cathodic potential of -0.9V is about an order of magnitude higher in the depth direction than under OCP conditions. Reasons why growth may be enhanced in the depth direction include:

1. A potential difference between the sample surface and the bottom of the pit could create a situation where the bottom of the pit is anodic with respect to the sample surface. Under this situation, the bottom of the pit may become less protected and anodic dissolution could expose fresh metal surface for film formation and subsequent rupture leading to enhanced growth in the depth direction.
2. Increased hydrogen concentration at the open mouth will necessitate the migration of more Cl^- ions to the open mouth to balance out the positive charges of the hydrogen ions. Chlorides are known to cause an acidification effect inside pits which results in increased corrosivity inside pits. Such localized acidification could enhance dissolution and tends to break down passive films that may form at the bottom of the pit. This in combination with the applied stress could ensure that a cycle of film formation and rupture occurs more frequently at the bottom of the pit leading to enhancement of crack propagation in the depth direction.

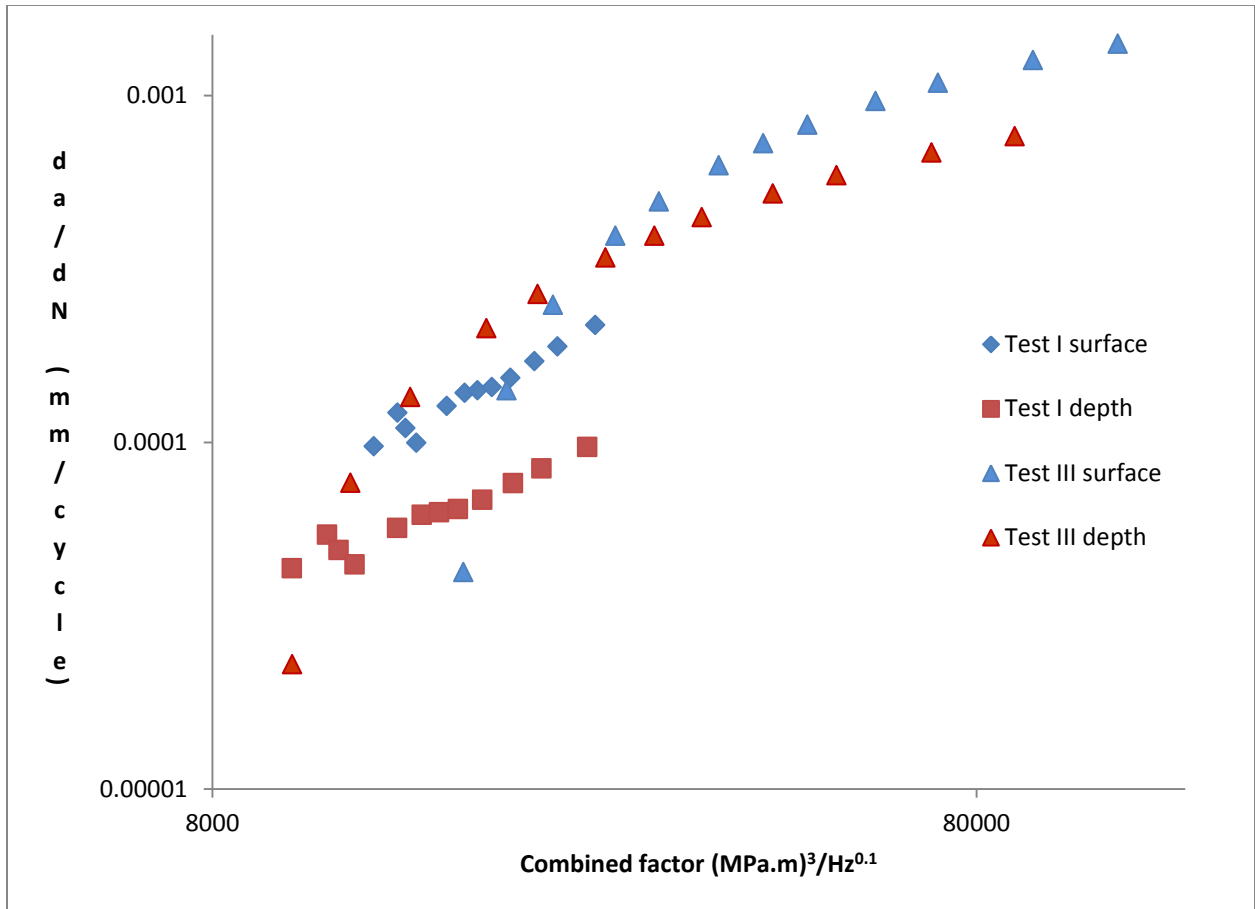


Figure 6-21: Combined crack growth factor plot for tests I and III

However, it is worthy of note that even when cracks are initiated under the increased environmental aggressiveness resulting from the applied cathodic potential, the growth rate of surface flaws is lower than those of through-thickness cracks under OCP conditions (Figure 6-22). This is contrary to the popular opinion that short surface cracks might propagate faster than through-thickness cracks.

Finally, the possibility of the simultaneous occurrence of enhanced deformation and significantly enhanced crack propagation at the OM in test III raises one important issue – the mechanism by which hydrogen rich systems promote SCC crack propagation might involve enhanced localized plastic deformation. Sobotka *et al.* [33], have suggested that hydrogen promotes a tensile strength softening in fcc systems such as steels. Sofronis *et al.* showed that hydrogen induces necking instability under tensile loading at much lower loads than in the absence of hydrogen by causing shear localization [9]. Liang *et al.* [8] also came to similar conclusions. At non-propagating conditions, such softening might result in the crack walls moving apart much more than in the absence of hydrogen, resulting in a wider crack as observed in this study and increasing the extent of crack tip blunting. However, under propagating conditions such localized yielding may enhance crack propagation as necking instability is easier to achieve at/near the tip of the propagating crack. Thus, in steel systems similar to the one observed here, the presence of hydrogen may both promote crack blunting under conditions that are too benign for crack initiation, but may cause crack propagation under conditions that are severe enough to cause crack propagation.

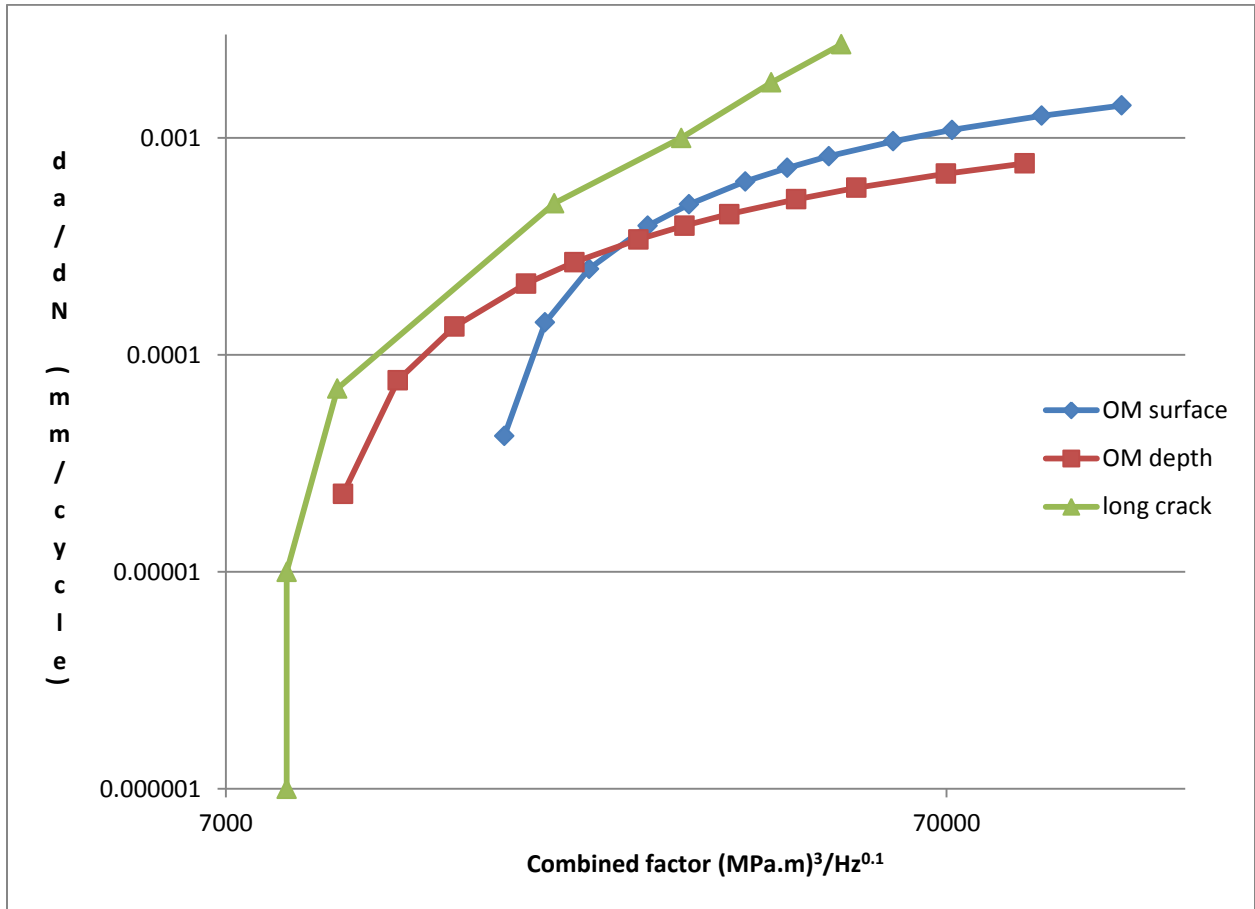


Figure 6-22: Comparison of the growth rates in test III with those of a through-thickness crack

6.6 Conclusions

1. Localized hydrogen concentration could significantly influence crack behavior in NNPHSCC environments. Depending on the operating conditions (stress levels), hydrogen may produce two effects:
 - a. at low to moderate stresses where the combined environmental-mechanical crack driving forces are low, hydrogen may promote enhanced localized plasticity and enhance low temperature creep deformation. These result in crack tip blunting.
 - b. At higher stresses and/or higher lattice hydrogen concentration, enhanced localized plasticity and enhanced low temperature creep deformation may promote more brittle type fracture by aiding transgranular cleavage type crack propagation.
2. The application of moderate cathodic potentials could set up localized hydrogen rich environments that promote higher growth rates by the mechanisms identified above (point 1).

References

- [1] Benbelaid, S., Belouchrani, M. A., Assoul, Y., 2011, "Modeling Damage of the Hydrogen Enhanced Localized Plasticity in Stress Corrosion Cracking," *International Journal of Damage Mechanics*, 20(6) pp. 831-844.
- [2] Birnbaum, H., and Sofronis, P., 1994, "Hydrogen-Enhanced Localized Plasticity - a Mechanism for Hydrogen-Related Fracture," *Materials Science and Engineering A-Structural Materials Properties Microstructure and Processing*, 176(1-2) pp. 191-202.
- [3] Sofronis, P., Liang, Y. M., and Aravas, N., 2001, "Numerical modeling of hydrogen induced shear localization," *Chemistry and Electrochemistry of Stress Corrosion Cracking: A Symposium Honoring the Contributions of R. W. Staehle*, edited by R. H. Jones, TMS (The Minerals, Metals and Materials Society), pp. 251-261.
- [4] Sofronis, P., Liang, Y., and Aravas, N., 2001, "Hydrogen Induced Shear Localization of the Plastic Flow in Metals and Alloys," *European Journal of Mechanics A: Solids (France)*, 20(6) pp. 857-872.
- [5] Sofronis, P., Robertson, I. M., Liang, Y., 2002. "Recent advances in the study of hydrogen embrittlement at the University of Illinois," Invited paper, *Hydrogen-Corrosion Deformation Interactions*, Jackson Lake Lodge, Wyo..
- [6] Delafosse, D., and Magnin, T., 2001, "Hydrogen Induced Plasticity in Stress Corrosion Cracking of Engineering Systems," *Engineering Fracture Mechanics (UK)*, 68(6) pp. 693-729.
- [7] Li, X. C., Eadie, R. L., and Luo, J. L., 2008, "Influence of Plasticity on Corrosion and Stress Corrosion Cracking Behaviour in Near Neutral pH Environment," *Corrosion Engineering Science and Technology*, 43(4) pp. 297-303.
- [8] Liang, Y., Sofronis, P., and Aravas, N., 2003, "On the Effect of Hydrogen on Plastic Instabilities in Metals," *Acta Materialia*, 51(9) pp. 2717-2730.
- [9] Liang, Y., Sofronis, P., and Dodds, R. H., 2004, "Interaction of Hydrogen with Crack-Tip Plasticity: Effects of Constraint on Void Growth," *Materials Science and Engineering A*, 366(2) pp. 397-411.
- [10] Gerland, M., Lefranc, P., Doquet, V., 2009, "Deformation and Damage Mechanisms in an alpha/beta 6242 Ti Alloy in Fatigue, Dwell-Fatigue and Creep at Room Temperature. Influence of Internal Hydrogen," *Materials Science and Engineering A*, 507(1-2) pp. 132-143.

- [11] Tien, C. W., 1994, "Hydrogen-Enhanced Transient Creep of 310S and AL 29-4-2 Stainless Steel,". Phd Dissertation, University of Illinois at Urbana-Champaign.
- [12] Oehlert, A., and Atrens, A., 1994, "Room Temperature Creep of High Strength Steels," *Acta Metall. Mater.*, 42(5) pp. 1493-1508.
- [13] Chen, W., Boven, G. V., and Rogge, R., 2007, "The Role of Residual Stress in Neutral pH Stress Corrosion Cracking of Pipeline Steels - Part II: Crack Dormancy," *Acta Materialia*, 55(1) pp. 43-53.
- [14] Liang, Y., and Sofronis, P., 2004, "On Hydrogen-Induced Void Nucleation and Grain Boundary Decohesion in Nickel-Base Alloys," *Journal of Engineering Materials and Technology (Transactions of the ASME)*, 126(4) pp. 368-377.
- [15] Liang, Y. "Micromechanics of the Hydrogen Effect on Plasticity and Interfacial Decohesion,". PhD dissertation, University of Illinois at Urbana-Champaign, 2003.
- [16] Altstetter, C., and Abraham, D. "Model for plasticity-enhanced decohesion fracture", *Proceedings of the Fifth International Conference on the Effect of Hydrogen on the Behavior of Materials sponsored by the Structural Materials Division (SMD) Mechanical Metallurgy and Corrosion & Environmental Effects Committees of The Minerals, Metals & Materials Society*, 1994, 599-610.
- [17] McMullen, T., Stott, M. J., and Zaremba, E., 1987, "Bond Weakening by Hydrogen in Transition Metals," *Phys. Rev. B, Condens. Matter*, 35(3) pp. 1076-1081.
- [18] Duquette, D.J., 1981, "Mechanisms of Corrosion Fatigue of Aluminum Alloys," AGARD Report No AGARD-CP-316.
- [19] Grinberg, N. M., 1982, "The Effect of Vacuum on Fatigue Crack Growth," *International Journal of Fatigue*, 4(2) pp. 83-95.
- [20] Sudarshan, T. S., and Louthan, M. R., 1987, "Gaseous Environment Effects on Fatigue Behavior of Metals," *International Materials Reviews*, 32(3) pp. 121-151.
- [21] Chen, W., and Sutherby, R. L., 2007, "Crack Growth Behavior of Pipeline Steel in Near-Neutral pH Soil Environments," *Metallurgical and Materials Transactions A*, 38A(6) pp. 1260-1268.

- [22] Egbewande, A. T., Eslami, A. M., Chen, W., 2010, "Growth of surface-type stress corrosion cracks in near-neutral pH environments under disbonded coatings" In: International Pipeline Conference 2010, Paper no. IPC2010-31436, pp. 653-662.
- [23] Egbewande, A. T., Chen, W., Eadie, R., 2013, "Transgranular Crack Growth in the Pipeline Steels Exposed to Near-Neutral pH Soil Aqueous Solutions: Discontinuous Crack Growth Mechanism," *Acta Materialia*, pp. Submitted for publication.
- [24] Egbewande, A. T., Chen, W., Eadie, R., (2013), "Surface Crack Growth Behavior of Pipeline Steel Under Disbonded Coating at Free Corrosion Potential in Near-Neutral pH Soil Environments," *Metallurgical and Materials Transactions*, Submitted for publication.
- [25] Egbewande, A. T., Chen, W., Eadie, R. L. " Growth of Near-Neutral pH Stress Corrosion Cracks at Open Circuit Potential After Hydrostatic Testing," . Manuscript under preparation, 2013.
- [26] Neumann, P. "Embrittlement due to gaseous and liquid environments," *Materials Science and Engineering A*, 176, pp. 9-18, 1994.
- [27] Hinton, B. R. W., and Procter, R. P. M., 1983, "The Effect of Strain-Rate and Cathodic Potential on the Tensile Ductility of X-65 Pipeline Steel," *Corros. Sci.*, 23(2) pp. 101-123.
- [28] Ulmer, D. G., and Altstetter, C. J., 1991, "Hydrogen-Induced Strain Localization and Failure of Austenitic Stainless Steels at High Hydrogen Concentrations," *Acta Metallurgica Et Materialia*, 39(6) pp. 1237-1248.
- [30] Meletis, E. I., and Lian, K., 1996, "Deformation Evolution during Initiation of Transgranular Stress Corrosion Cracking," *International Journal of Fracture (Netherlands)*, 79(2) pp. 165-178.
- [31] Paraventi, D. J., Angeliu, T. M., and Was, G. S., 2002, "The Effect of Hydrogen on Creep in High Purity Ni-16Cr-9Fe Alloys at 360DGC," *International Conference on Hydrogen Effects on Materials Behavior and Corrosion Deformation Interactions*; Moran, WY; USA; 22-26 Sept. 2002, 58(8) pp. 675-686.
- [32] Beavers, J. A., and Harle, B. A., 2001, "Mechanisms of High-pH and Near-Neutral-pH SCC of Underground Pipelines," *Journal of Offshore Mechanics and Arctic Engineering*, 123, pp. 147-151.

[33] Sobotka, J. C., Dodds, R. H., and Sofronis, P., 2009, "Effects of Hydrogen on Steady, Ductile Crack Growth: Computational Studies," *International Journal of Solids and Structures*, 46(22-23) pp. 4095-4106.

CHAPTER SEVEN

**EFFECT OF CATHODE POTENTIALS ON THE DISTRIBUTION OF STRESS
CORROSION CRACK GROWTH RATES IN NEAR-NEUTRAL
ENVIRONMENTS UNDER A DISBONDED COATING AFTER
HYDROSTATIC TESTING**

7.0 Introduction

Stress corrosion cracking of pipeline steels in near-neutral pH environment remains a major pipeline integrity issue to pipeline operators in Canada and elsewhere around the world. To the engineers and integrity managers in the field, the rate of SCC propagation in near-neutral pH environment is very important data to have. Several approaches have been developed, based on laboratory studies, field data and simulations, to tackle this problem. However, most of these approaches have fallen short in terms of accuracy.

Although the industry has developed means of determining where flaws exist, such as by using crack detection tools, pigging *etc.*, the reliability of these techniques are often called into question. Some of the issues that commonly arise center on unsatisfactory probability of detection, probability of identification and probability of sizing. Other issues include miscalls, false negatives, false positives, undercalls *etc.* In addition to the fact that these tools are very expensive to run, issues such as those identified above tend to necessitate the use of other methods for determining safety of operations.

An alternative to these tools is the use of hydrostatic testing. Hydrostatic testing is a qualitative method employed to determine the fitness for service of pressure piping systems. During this process, the pipe is filled with water and loaded to a pressure higher than the design pressure. If the pipe survives without bursting or leaking, then it could be assumed that all existing cracks are below a pre-determined maximum size that is dependent on the pressure used. This information is then used to determine a safe re-inspection interval, assuming a pre-determined constant crack growth rate.

Harle *et al.* [1] found that hydrostatic testing inhibits crack propagation by blunting the crack tip, making it harder for such cracks to re-initiate in service. However, it has also been

contended that substantial crack propagation may occur during the process [2-7]. Chen [6] concluded that the extent of crack propagation during hydrostatic testing is environmentally dependent and that hydrostatic testing can reactivate small dormant cracks, reversing any gains in crack growth retardation by crack tip blunting [7].

Chen *et al.* [8] recently determined that the application of various levels of cathodic protection in a near-neutral pH environment can have a significant effect on the electrochemistry of the solution, including the amount of hydrogen available within the system. The effect of this variation in local environment due to variation in cathodic potential reaching various locations under the disbonded coating on the rate of propagation of stress corrosion cracks has not been investigated. Also, in a recent study, the current authors studied the re-initiation conditions and variation in growth rate of SCC cracks in near-neutral pH environments with distance from the open mouth after hydrostatic testing at open circuit potentials (Chapter 5). The study also revealed the effects of dissolution and low temperature creep on the growth of SCC cracks in near neutral pH environments. In that study the effect of cathodic protection, which is a mandatory practice in the field, was not accounted for. This study will examine the effect of cathodic protection on the variation of the rate of propagation of SCC cracks with distance from the open mouth of the coating disbondment in a near natural pH environment. Such a study will help shed more light on variations in the rate of propagation of SCC cracks in near-neutral pH environment with seasonal changes in soil resistivity. This study reports the influence of such local variations in the environment developed under a disbonded coating on the growth rate of stress corrosion cracks.

7.1 Experimental

Flat tensile specimens (Figure 7-1) with three reduced gauge sections were machined from the longitudinal direction of a sectioned pipe. Samples were machined from a section of X-65 pipeline steel removed from service, but only sections unaffected by mechanical deformation were used. The alloy composition is shown in Table 7-1, while a typical alloy microstructure is shown in Figure 7-2. The dimension of the reduced sections were 23 mm X 45 mm X 9.2 mm and identical semi-circular shallow notches with major and minor axis dimension of 5mm and 2.5mm were EDM machined in the middle of each gauge section. The cracking direction for these flaws is identical to that for the most common cracks in the pipeline.

The corrosion cell, Figure 7-3, consists of two chambers: the inner chamber, called the shielding, was designed to simulate the solution trapped in the disbonded coating crevice while the outer chamber was designed to simulate the bulk surrounding soil solution. The width of this inner tube was made adjustable so that coating disbondment of various sizes can be studied. The bulk solution in the outer tube was sparged with a 5%CO₂ balance nitrogen mix, fed in through openings at the bottom of the cell, so that CO₂ can only diffuse into the simulated disbondment from the open mouth. The bottom of the disbondment was O-ring sealed from the bulk chamber so that the sparging gas could only diffuse into the disbondment from the open mouth. Also ion exchange between the bulk chamber and the simulated disbondment could only occur through the open mouth. The specimen was always mounted in the center of the disbondment.

A reference (saturated calomel electrode) and counter electrode (platinum mesh) arrangement was used to apply cathodic protection to the sample. Test I was carried out at open circuit potential while cathodic protection was applied in tests II and III. Cathodic protection was applied at the open mouth just above the topmost crack. An EG&G potentiostat operating in

constant voltage mode was used to apply cathodic protection voltage of -1.2V and -0.9V for two of the tests reported here, test II and test III respectively. All potentials were measured vs. the Standard Calomel Electrode (SCE). In both tests, all cracks were pre-fatigued to give a surface half crack length of 3.3mm.

Prior to each test, each gauge section was ground to grit 600 and separately pre-fatigue cracked in air to produce the required pre-test surface crack length. The pre-fatigue cracked samples were then exposed to the corrosion media in a sealed test cell and filled with C2 solution (0.0035 KCl, 0.0195 NaHCO₃, 0.0255 CaCl₂.H₂O, 0.0274 MgSO₄.7H₂O, 0.0606CaCO₃ g/l). Cyclic stresses with a maximum stress of 100% specified minimum yield strength and varying stress ratios were applied during the test. This higher stress simulates the combination of operating plus residual stress that is commonly associated with cracking in the field [9]. The sides and back surface of each specimen (the one without the surface cracks) were coated with epoxy in order to isolate these surfaces from the corrosion media. Crack growth rates were monitored by measuring the potential drop across each crack through leads connected to opposite sides of each crack. A constant current of 20A was applied by the potential drop system in order to measure the potential drop across each crack. Other tests conditions are shown in Table 7-2. After each test, the fracture face was examined and post-test crack lengths determined in order to validate potential drop measurements with actual crack growth measured on the surface of fractured specimens. Detailed examination of fracture faces was carried out using a Hitachi scanning electron microscope equipped with energy dispersive x-ray spectrometer for chemical compositional analysis.

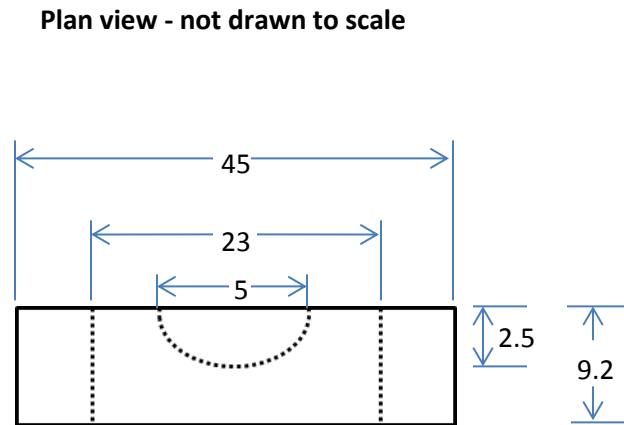
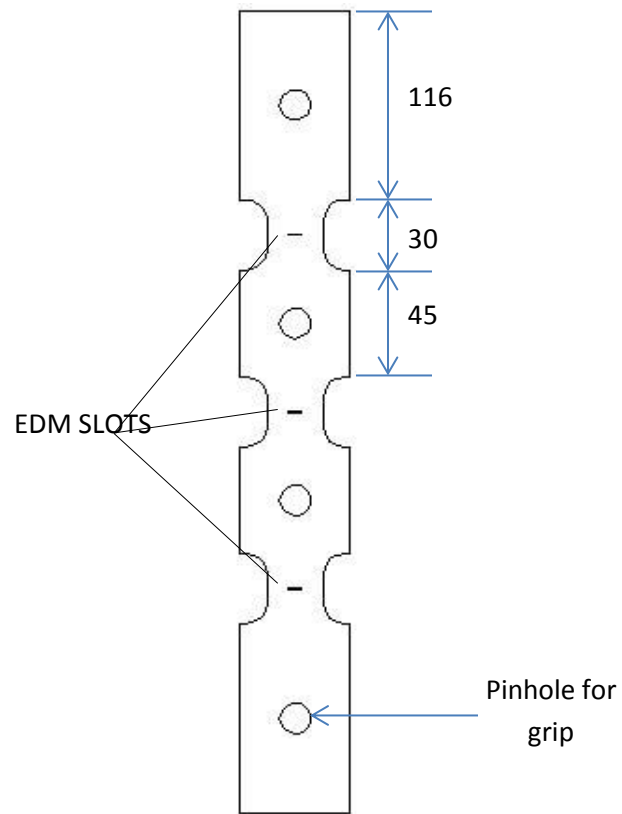


FIGURE 7-1: Test sample designed for this study. All units in mm.

Table 7-5: Alloy (X65) composition

| Element | Composition (wt %) |
|------------|--------------------|
| Carbon | 0.13 |
| Manganese | 1.55 |
| Copper | 0.05 |
| Niobium | 0.05 |
| Chromium | 0.08 |
| Molybdenum | 0.01 |
| Vanadium | 0.002 |
| Nickel | 0.05 |
| Aluminum | 0.042 |
| Titanium | 0.002 |
| Nitrogen | 0.009 |
| Iron | Balance |

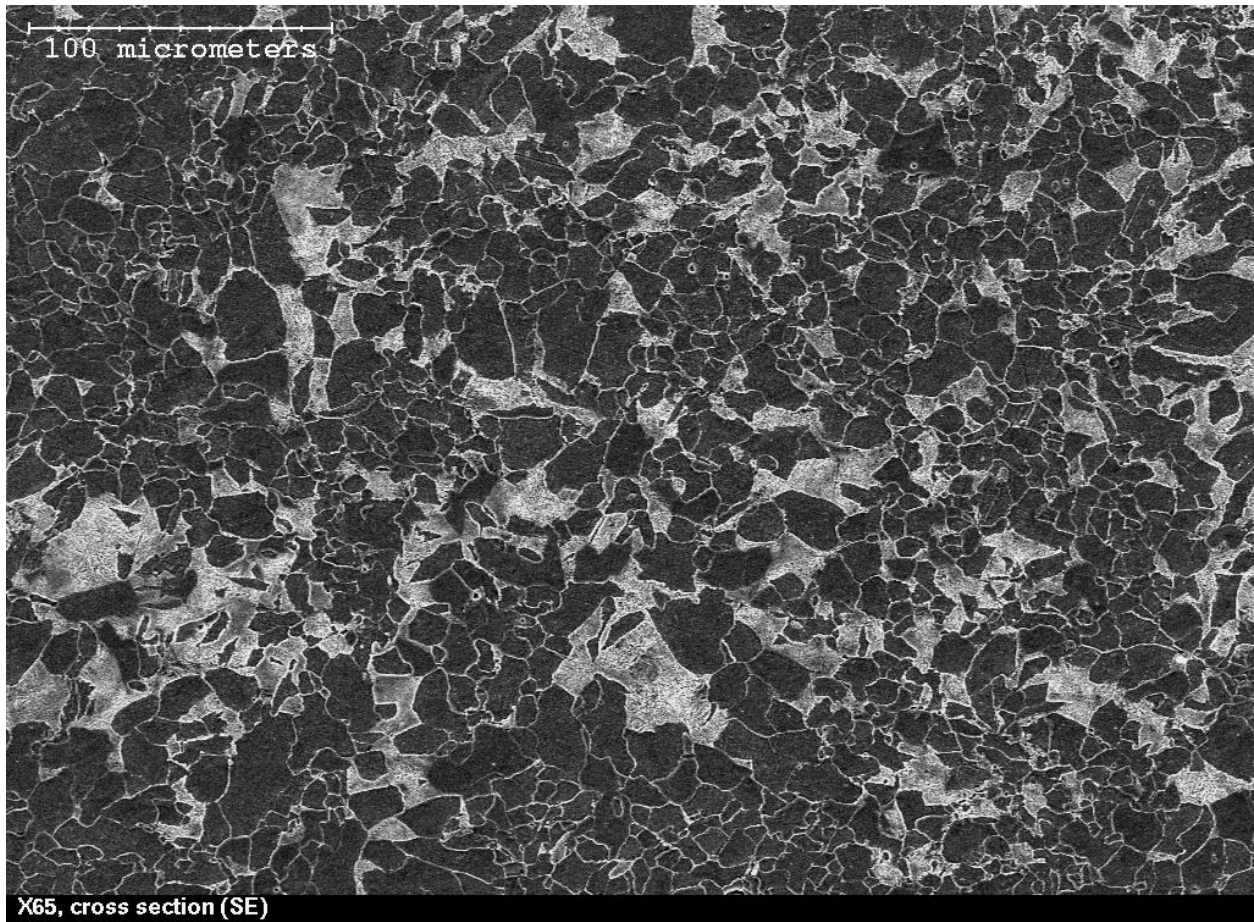


Figure 7-2: Typical microstructure of the alloy X65 used in this study

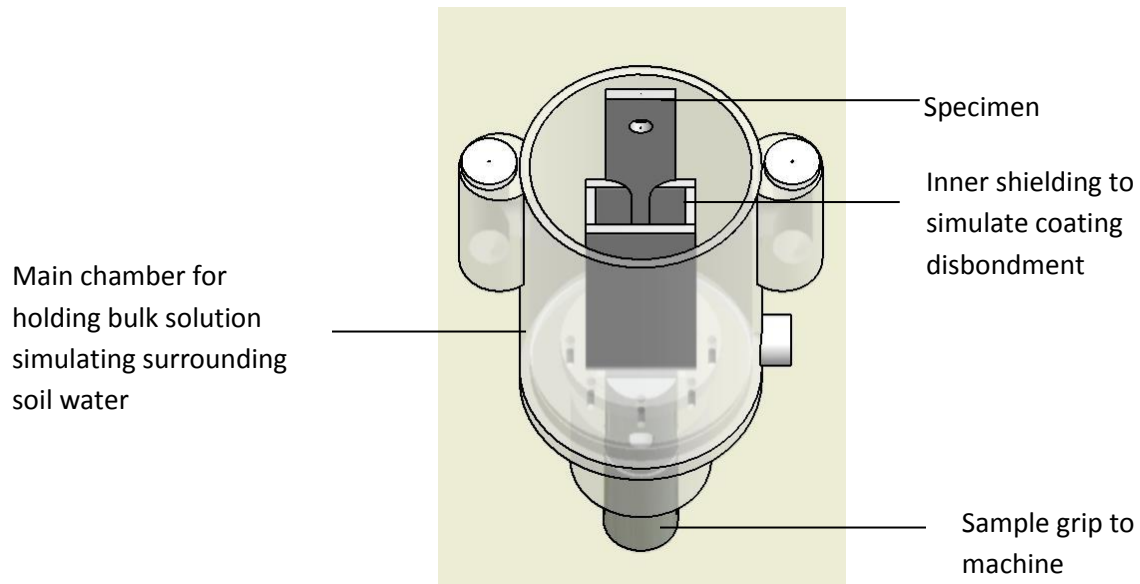


Figure 7-3: Schematic Drawing of the corrosion test cell used for the study

Table 7-2: Summary of test conditions

| | Test I | Test II | Test III |
|------------------------|---|----------------------------------|---------------------------------|
| Stress ratio, duration | 0.65 / 15days 0.60/15days 0.58 / 9.4 days | 0.65, 15days 0.60, 14days | 0.65, 15days 0.60, 7days |
| Stress applied (MPa) | 100% SMYS | | |
| Purging gas | 5% CO ₂ | 5% CO ₂ | 5% CO ₂ |
| Potential (V) | OCP | -0.9 | -1.2 |
| Frequency (Hz) | 0.005 | 0.005 | 0.005 |

7.1.1 Justification of sample geometry and crack size/geometry used

A cursory look at micrographs of SCC obtained from the field show that these cracks are surface type flaws rather than through-thickness flaws. It is well recognized in fracture mechanics that surface type flaws could propagate differently from through-thickness type flaws; hence, the choice of a surface type flaw for this test. In choosing this type of flaw, care was also taken to ensure that the crack size chosen is representative of those in the field and that the mechanical driving forces for crack propagation, maximum stress intensity (K_{\max}) and stress intensity ranges (ΔK) are similar to those that could be obtained in the field. For instance for a semicircular flaw that is 3.3 mm deep as chosen in this study, at 100% SMYS, a K_{\max} of $31.97 \text{ MPa}\cdot\text{m}^{1/2}$ at the depth tip of the crack and a stress intensity range of $12.79 \text{ MPa}\cdot\text{m}^{1/2}$ is obtained at a stress ratio of 0.6. This mechanical condition will be similar to those experienced by 32mm long crack with an aspect ratio of 0.1 on a 9.88 mm thick 36" outside diameter pipeline. This translates to a surface crack measuring 3.2 mm deep in X65 plate with a half width of 2873.28 mm being subjected to a maximum stress of 100% SMYS. In this case, a K_{\max} of $31.97 \text{ MPa}\cdot\text{m}^{1/2}$ and a stress intensity range of $12.8 \text{ MPa}\cdot\text{m}^{1/2}$ is obtained at a stress ratio of 0.6. Thus the crack dimensions chosen could be easily obtained in the field, especially on a liquid line. Although it might be argued that individual cracks in the field may not be 32 mm long, pipeline operators typically rely on industry standards for fitness for service assessments. These standards, recommend a minimum prescribed spacing between adjacent flaws below which such cracks must not be treated as isolated (or single) flaws. For instance ASME B31G (or BS7910) recommends that cracks that are closer than three times the wall thickness be regarded as interacting flaws. At the lowest level of assessment, these cracks will usually be taken as just one flaw by adding the lengths of all the interacting flaws. However, there are higher levels of analysis that employ a

more complex analysis to determine the effective length of cracks. Whichever level of analysis is used, it is typical to have effective cracks lengths that are longer than 32 mm.

7.2 Results

7.2.1 Mechanical deformation of crack tip in air (Test P1)

The reasoning behind this experiment design is as follows. Assume a pipeline contains a crack field (colony) which had been hydrotested before without failure. Since hydrotesting involves stresses up to 110% SMYS, the tips of the existing cracks will likely be deformed. The crack tip morphology after pre-fatigue cracking is shown in Figure 7-4. The figure shows that very fine cracks were initiated at the notch tip during pre-fatigue cracking. The crack morphology after the one minute loading is shown in Figure 7-5. Figure 7-5 clearly shows how intensely deformed the crack tip region could be after loading to 100% SMYS. This intense deformation resulted in the crack walls moving apart inelastically and causing severe crack tip blunting. No crack propagation was observed during this test suggesting hydrostatic testing may not necessarily cause crack propagation.

This type of blunting is generally regarded as mechanical blunting. It was shown in an earlier communication [10] (Chapter 4) that environmental factors can also result in a similar blunting. It is instructive to know that in the field, after a hydrostatic testing is complete, environmental factors can exert their independent effect until the next scheduled hydrostatic testing and this effect can also influence crack propagation during subsequent hydrostatic testing.

Based on this verification test, the remaining tests were designed to study the effect of variations in the local environment under the disbondment in combination with the effect of localized crack tip deformation during hydrostatic testing under cathodic protection conditions. The rest of this study will examine the combined influence of localized deformation and environmental factor on the rate of crack propagation during hydrostatic testing.

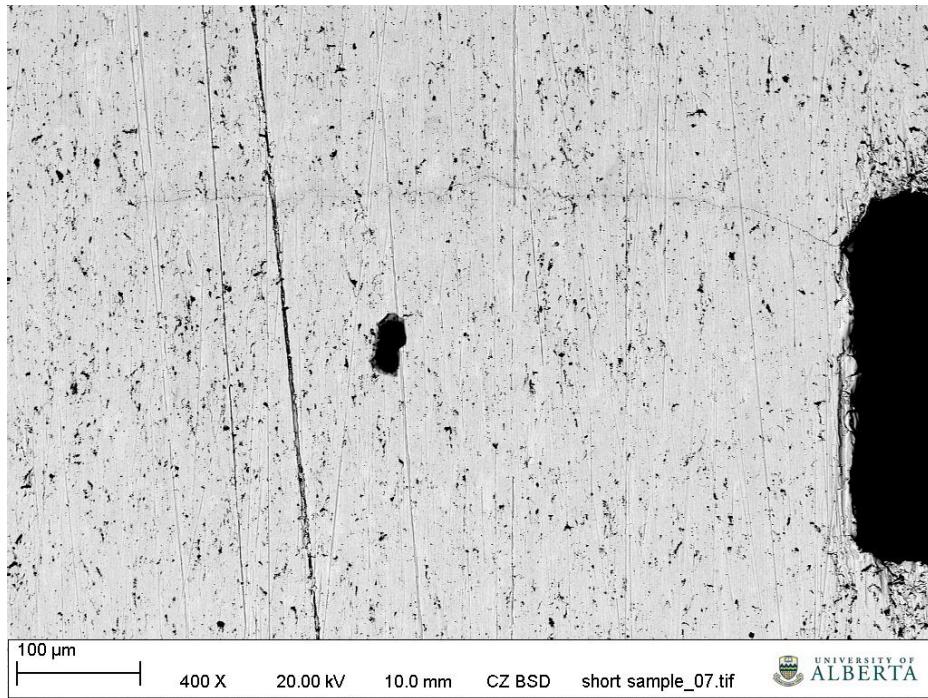


Figure 7-4: Pre-crack morphology of verification test

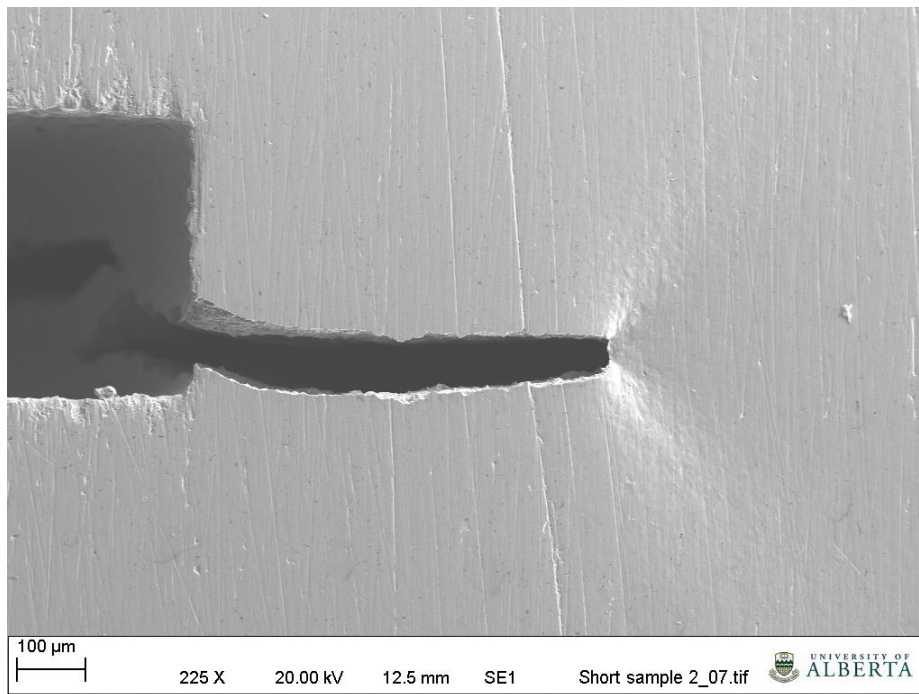


Figure 7-5: Crack tip morphology after 1min hold at 100% SMYS

7.2.2 Open circuit potential test results

7.2.2.1 Corrosion behavior at sample surface at OCP

Typical sample surface features after testing are shown in Figure 7-6. Post-test examination of the corroded sample surfaces revealed a thin layer of corrosion products at the sample surface at all three locations in test I. The corrosion products were analyzed and found to be FeCO_3 , Fe_2O_3 and FeOOH by powder mode x-ray diffraction technique. Severe pitting corresponding to intense localized dissolution, coupled with general corrosion was observed at the open mouth. Less severe pitting was observed at 75 mm from the open mouth while only general corrosion occurred at the bottom of the disbondment – 150 mm from the open mouth (Figure 7-7).

7.2.2.2 Crack re-initiation following loading at OCP

Chen and Sutherby [11] developed a corrosion-fatigue model that accounts for NNPHSCC as a synergistic interaction of fatigue and corrosion. The general form of the model was given as $\frac{da}{dN} = \frac{\Delta K^2 K_{max}}{f^\gamma}$ where ΔK is the change in stress intensity at the crack tip due to cyclic loading, K_{max} is the maximum stress intensity at the crack tip, and γ is found to be around 0.1, a factor representing the influence of the corrosion environment on the crack growth rate. ΔK and K_{max} are strongly dependent on the geometry of the specimen, while γ is dependent on the severity of the corrosion environment. This relationship was used to determine the crack re-initiation conditions for all the tests in this study. In test I, no crack propagation was observed at a stress ratio of 0.6. Growth reinitiated at a stress ratio of 0.58 which corresponded to a combined factor of approximately $11100 (\text{MPa}\cdot\sqrt{\text{m}})^3/\text{Hz}^{0.1}$ in the depth direction and $14400 (\text{MPa}\cdot\sqrt{\text{m}})^3/\text{Hz}^{0.1}$ at the sample surface.

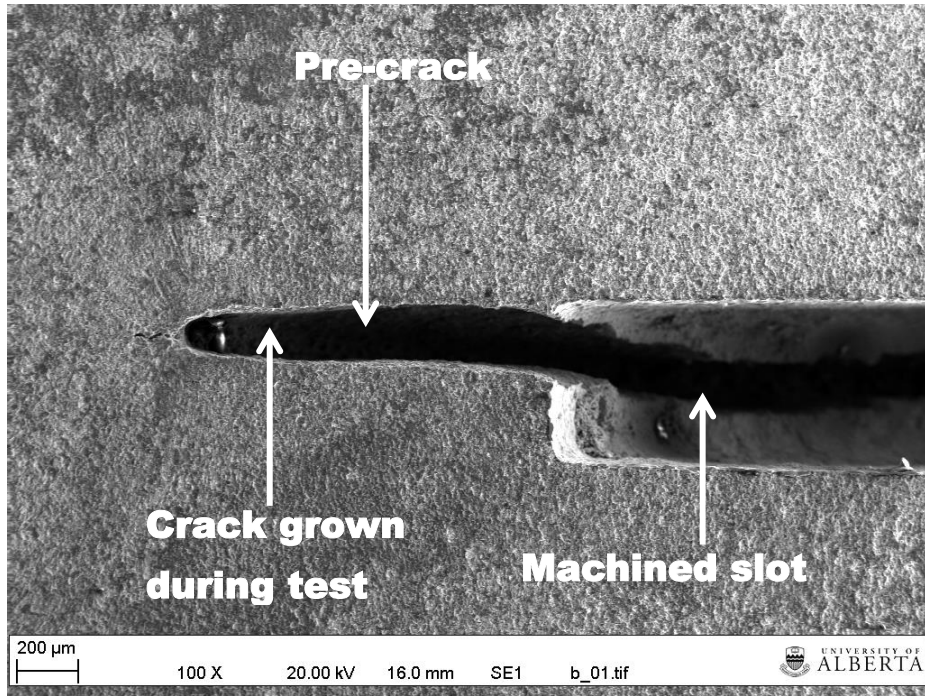


Figure 7-6: Post-test surface features before cleaning in test I

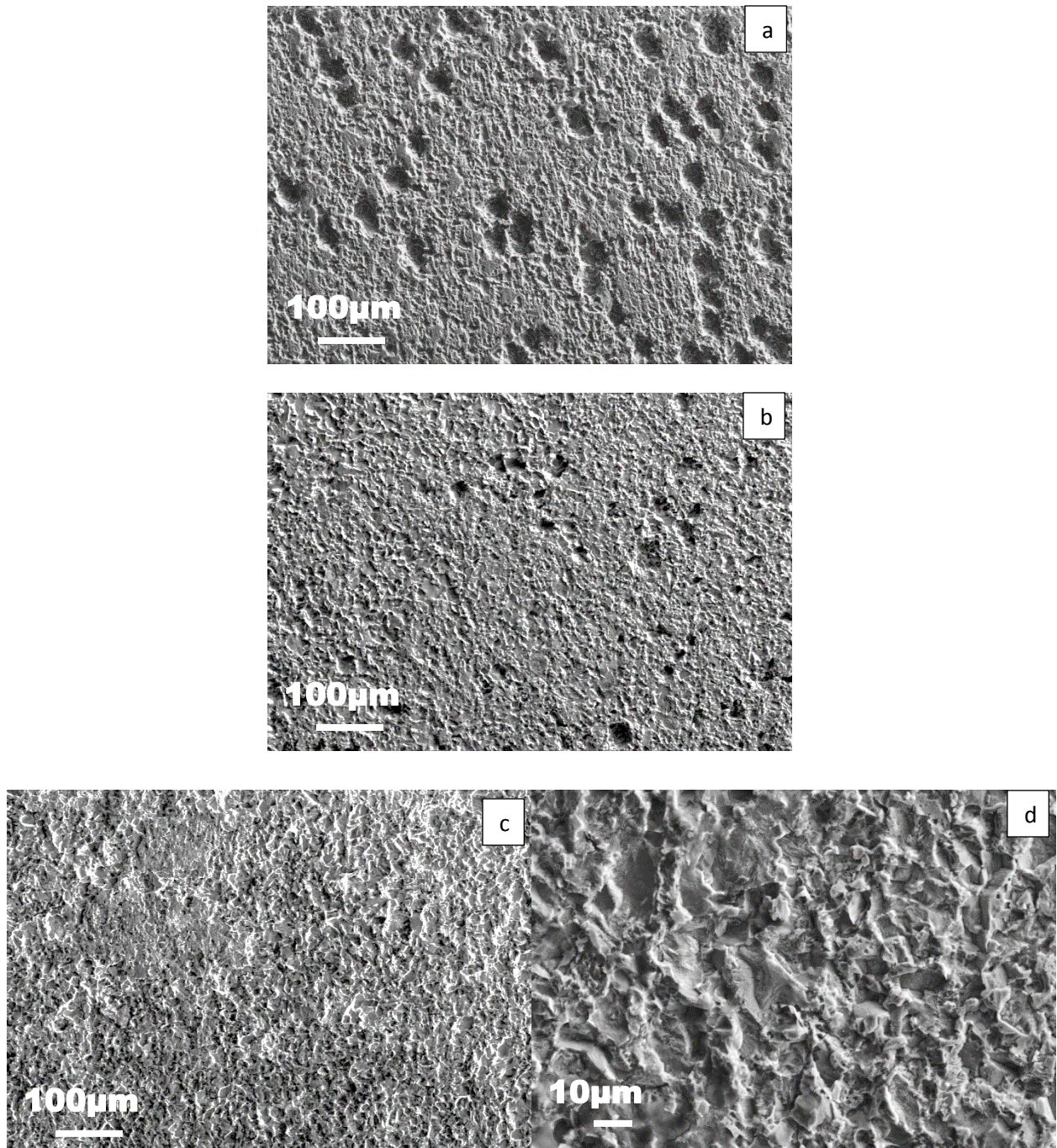


Figure 7-7: Corroded surface at (a) open mouth (b) 75 mm and (c) 150 mm from the open mouth (d) Higher magnification image of 150 mm from OM.

7.2.2.3 Crack propagation behavior at OCP

Post-test crack propagation rates were determined and a summary is shown in Figure 7-8. In test I, average crack growth rate was highest at the open mouth and lowest at 75mm from the open mouth of the disbondment. However, average growth rate at 75 mm and 150 mm from the open mouth are quite comparable.

The initial and final crack sizes are shown in Tables 7-3 and 7-4 while the initial and final aspect ratios are shown in Figure 7-9. These figures indicate that while crack propagation occurred at all locations during the test, variations in the local environment with distance from the open mouth could change the character of growth significantly. In test I, aspect ratios generally decreased at all locations during the test. The largest reduction in aspect ratios occurred at the open mouth while the smallest reduction in aspect ratio occurred at the far end of the disbondment.

7.2.3 Test results at an applied potential of -0.9V

7.2.3.1 Surface features observed at -0.9V

Examination of the sample surface after the test reveals that for the test carried out at a cathodic potential of -0.9V, severe pitting corrosion/pitting occurred at the bottom of the simulated disbondment, at and around 150 mm from the open mouth (Figure 7-10c&d). At the open mouth of the disbondment, no evidence of corrosion was observed (Figure 7-10a). Pre-test scratches were completely preserved during the test and neither pitting nor general corrosion was observed. Complete surface protection evidenced by absence of dissolution also occurred at 75 mm from the open mouth (Figure 7-10b).

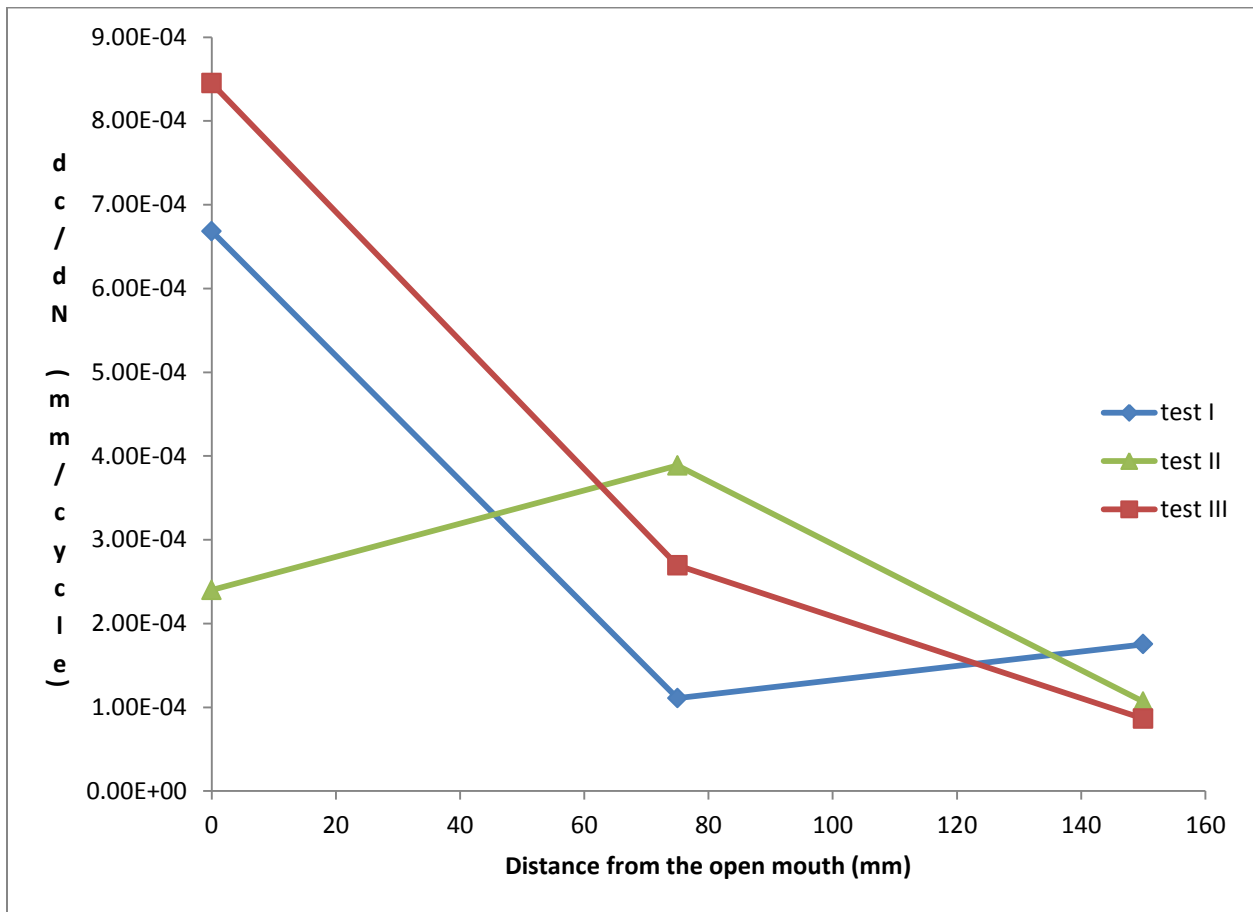


Figure 7-8: Average growth rates; growth initiated at R=0.58 in test I, but at R=0.6 in tests II and III.

Table 7-3: Characteristics of crack growth for cracks on the specimen surface

| | | Initial crack length(mm) | Final Crack length(mm) | Net crack growth(mm) | Average crack growth rate(mm/cycle) |
|----------|----|--------------------------|------------------------|----------------------|-------------------------------------|
| Test I | OM | 3.54E+00 | 6.25E+00 | 2.71E+00 | 8.97E-04 |
| | MP | 3.52E+00 | 3.97E+00 | 4.49E-01 | 1.49E-04 |
| | BP | 3.55E+00 | 4.26E+00 | 7.10E-01 | 2.35E-04 |
| Test II | OM | 3.31E+00 | 4.76E+00 | 1.45E+00 | 2.40E-04 |
| | MP | 3.32E+00 | 5.66E+00 | 2.34E+00 | 3.89E-04 |
| | BP | 3.32E+00 | 3.96E+00 | 6.43E-01 | 1.07E-04 |
| Test III | OM | 3.55E+00 | 6.10E+00 | 2.55E+00 | 8.45E-04 |
| | MP | 3.63E+00 | 4.44E+00 | 8.13E-01 | 2.69E-04 |
| | BP | 3.50E+00 | 3.76E+00 | 2.61E-01 | 8.64E-05 |

Table 7-4: Characteristics of crack growth for cracks in the depth direction

| | | Initial crack length(mm) | Final Crack length(mm) | Net crack growth(mm) | Average crack growth rate(mm/cycle) |
|----------|----|--------------------------|------------------------|----------------------|-------------------------------------|
| Test I | OM | 3.15E+00 | 4.74E+00 | 1.598 | 5.29E-04 |
| | MP | 3.14E+00 | 3.44E+00 | 0.307277 | 1.02E-04 |
| | BP | 3.41E+00 | 4.05E+00 | 0.64 | 2.12E-04 |
| Test II | OM | 3.03E+00 | 3.88E+00 | 0.850275 | 2.24E-04 |
| | MP | 2.97E+00 | 4.81E+00 | 1.84233 | 3.88E-04 |
| | BP | 3.04E+00 | 3.39E+00 | 0.357143 | 1.18E-04 |
| Test III | OM | 3.00E+00 | 5.39E+00 | 2.38612 | 7.91E-04 |
| | MP | 3.07E+00 | 4.24E+00 | 1.17504 | 3.89E-04 |
| | BP | 2.85E+00 | 3.03E+00 | 0.18 | 5.96E-05 |

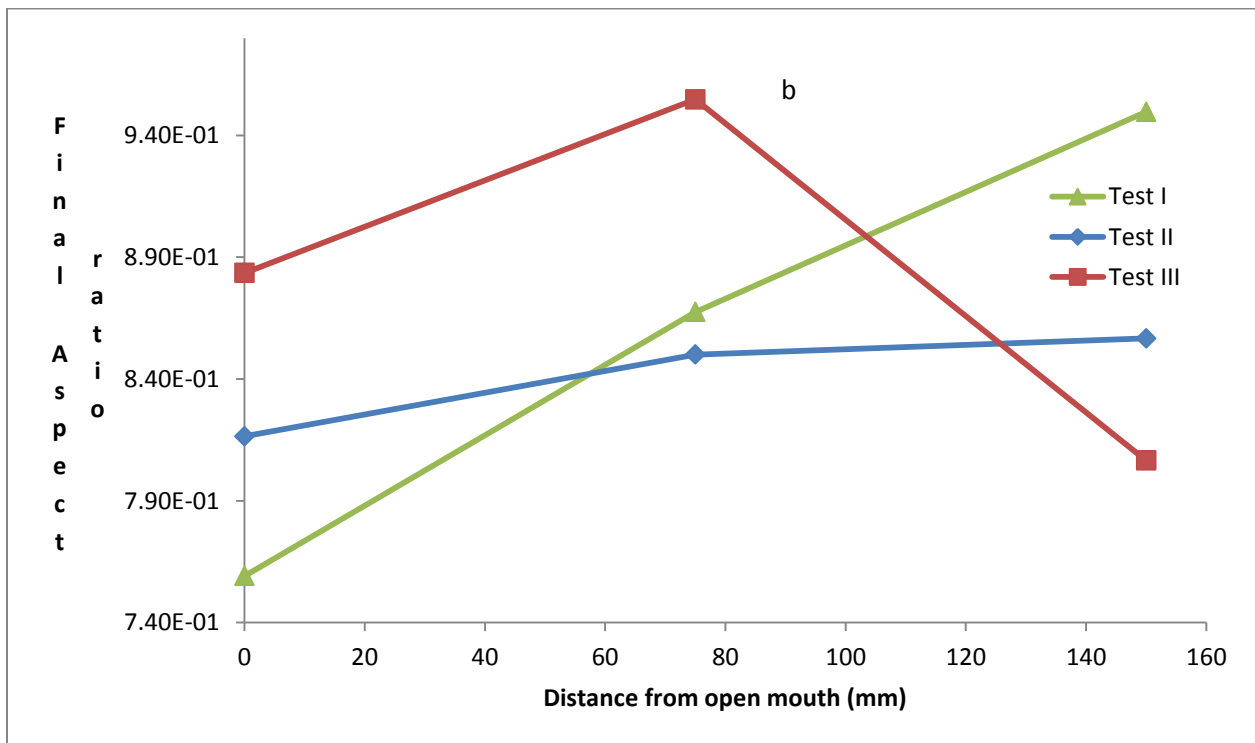
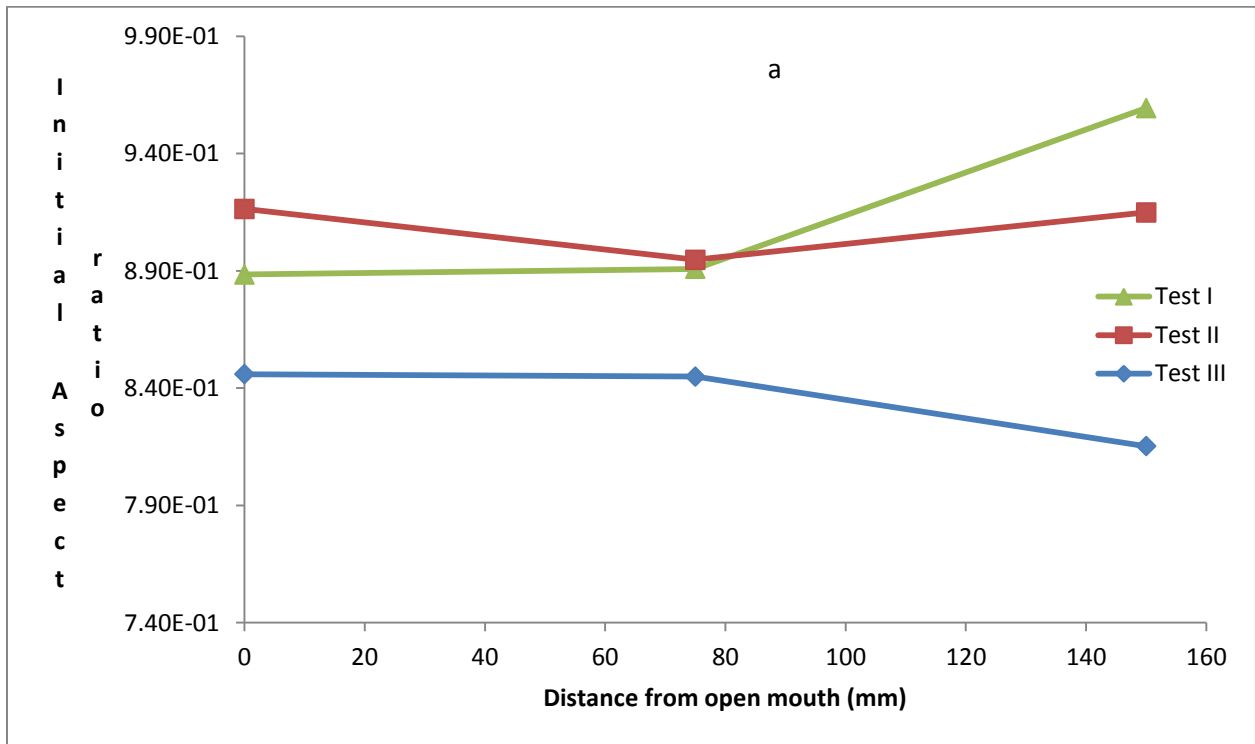


Figure 7-9: (a) Initial aspect ratio (b) Final aspect ratio

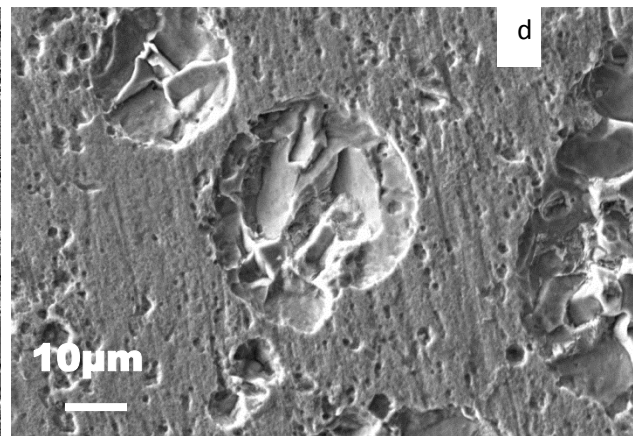
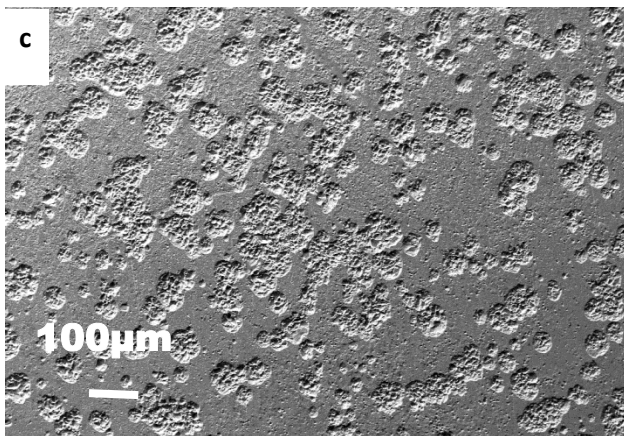
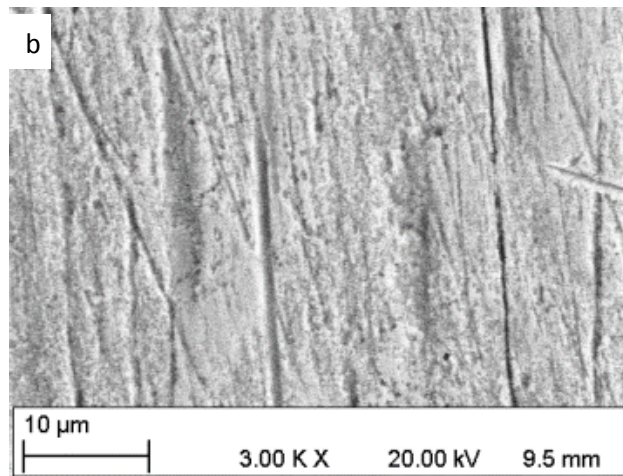
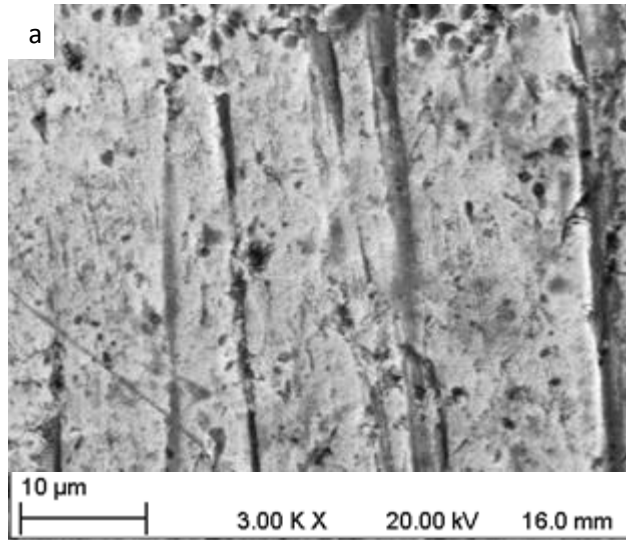


Figure 7-10: Corroded surface of the test sample at (a) open mouth (b) 75 mm from open mouth (c) 150 mm from open mouth (d) 150 mm from open mouth after sample has been rotated at 45° relative to secondary detector to confirm the features seen are pits not deposits on sample surface. Sample was tested at -0.9V cathodic potential

7.2.3.2 Crack re-initiation following loading at -0.9V

In test II, growth reinitiated at a stress ratio of 0.60 which corresponded to a combined factor of between 9100-9165 in the depth direction and 11400-11800 $(\text{MPa}\cdot\sqrt{\text{m}})^3/\text{Hz}^{0.1}$ at the sample surface.

7.2.3.3 Crack propagation behavior at -0.9V

Post-test crack length measurements revealed that different extents of crack growth, hence different crack propagation rates, occurred during the tests (Figure 7-8). The rate of crack propagation varied with distance of the cracks from the open mouth (and point of application of cathodic potential). A careful examination of the growth rate data reveals there is a correlation between the observed growth rates and local potential at different locations.

However, when a cathodic potential of -0.9V is applied, a notable deviation from the above observation occurs – namely, the highest growth rate is recorded in the middle of the cell. Repeat tests also produced the same trends suggesting that the observed rates are real and not artefacts of the procedure. This behaviour is counter intuitive as most researchers believe that since hydrogen concentration is highest at the open mouth and the open mouth is subjected to a higher cathodic potential, crack propagation should be most rapid at the open mouth.

7.2.4 Test results at an applied cathodic potential of -1.2V

7.2.4.1 Surface features observed at -1.2V

Visual examination of the sample tested at cathodic potential of -1.2V revealed that a white powdery substance, calcium carbonate, was deposited at the open mouth early in the test. This powder eventually turned into a dark substance during the test. The dark substance quickly oxidized into the well-known dark brown color of Fe_3O_4 on removal of the sample from the cell after the test. Examination of the corroded surface of this sample revealed that whereas the sample surface is fairly protected at the open mouth of the disbondment, localized pitting

occurred during the test (Figure 7-11a). Localized pitting also occurred near 75 mm from the open mouth as shown in Figure 7-11b. However, only general corrosion occurred at the bottom of the cell (150 mm from the open mouth) as shown in Figure 7-11c. Upon careful examination of the ruptured sample (Figure 7-12), microcracks oriented at 45° to the direction of applied stress were found at the open mouth in an array around the final crack tip position just before rupture (Figure 7-13). The microcracks are shown at a higher magnification in Figure 7-13(b). These cracks were arrayed along a 45° angle away from the crack tip itself. This feature was not observed at 75 mm or 150 mm from the open mouth. Rather only a dense colony of pits was found clustered together stretching away from the crack tip at a 45° angle at 75 mm from the open mouth (Figure 7-14).

7.2.4.2 Crack re-initiation following loading at -1.2V

In test III, growth reinitiated at a stress ratio of 0.60 which corresponded to a combined factor of between 10100 – 10800 (MPa·√m)³/Hz^{0.1} in the depth direction and 10800-12400 (MPa·√m)³/Hz^{0.1} at the sample surface.

7.2.4.3 Crack propagation behavior at -1.2V

At a cathodic potential of -1.2V, there was a sharp distinction between the growth rates recorded at all three locations (Figure 7-8). The highest growth rate occurs at the open mouth where the CP is -1.2V, while the lowest growth rate was recorded at the bottom of the cell. This correlated very strongly with the actual potentials measured at these three locations. The measured potentials at the open mouth, middle and bottom of the cell (0mm, 75 mm and 150 mm from the open mouth respectively) were -1.2V, -0.912V and -0.838V respectively (Figure 7-15).

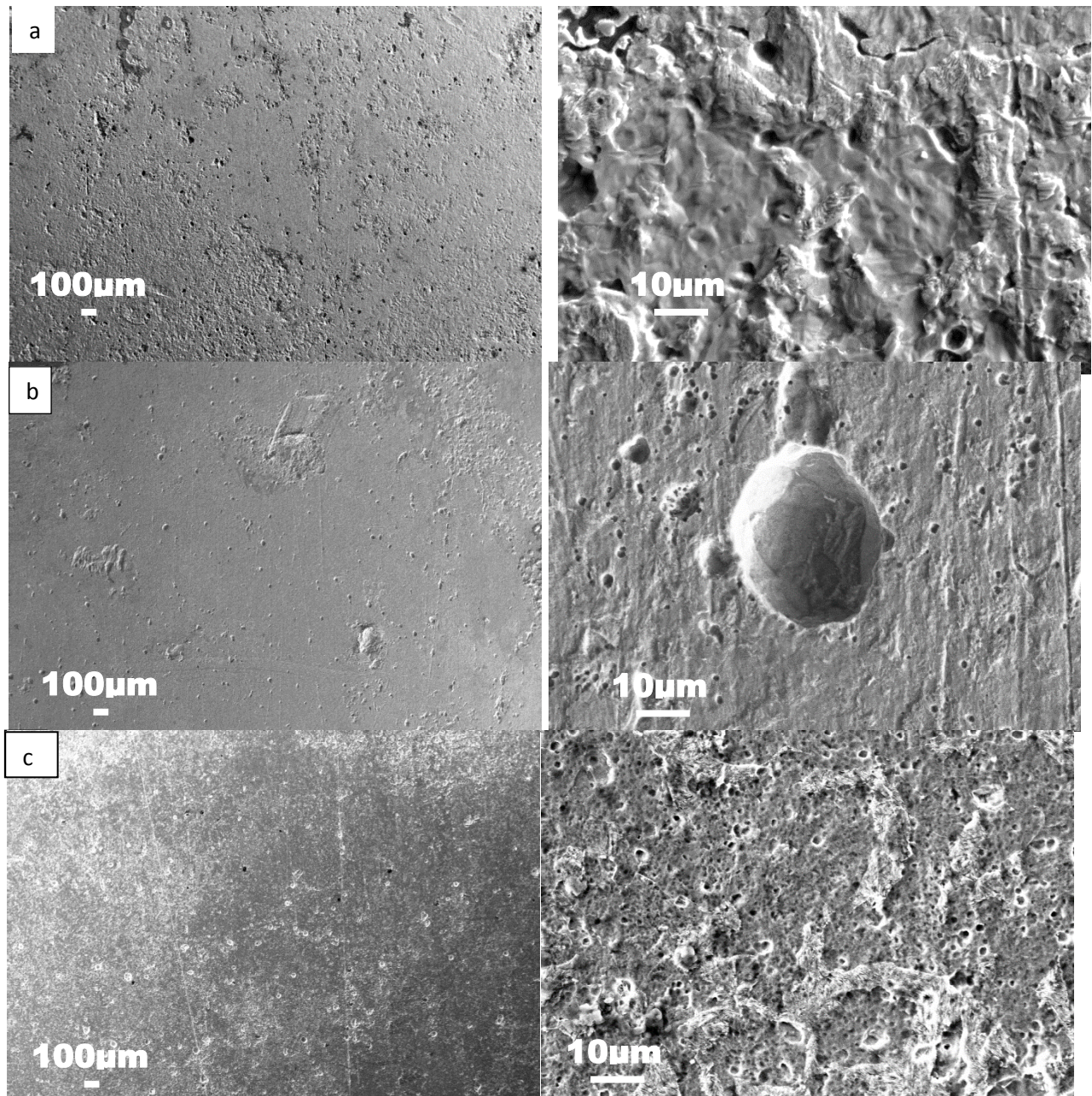


Figure 7-11: Corroded surface of the test sample at (a) open mouth (b) 75 mm from open mouth (c) 150 mm from open mouth. Sample was tested at -1.2V cathodic potential.

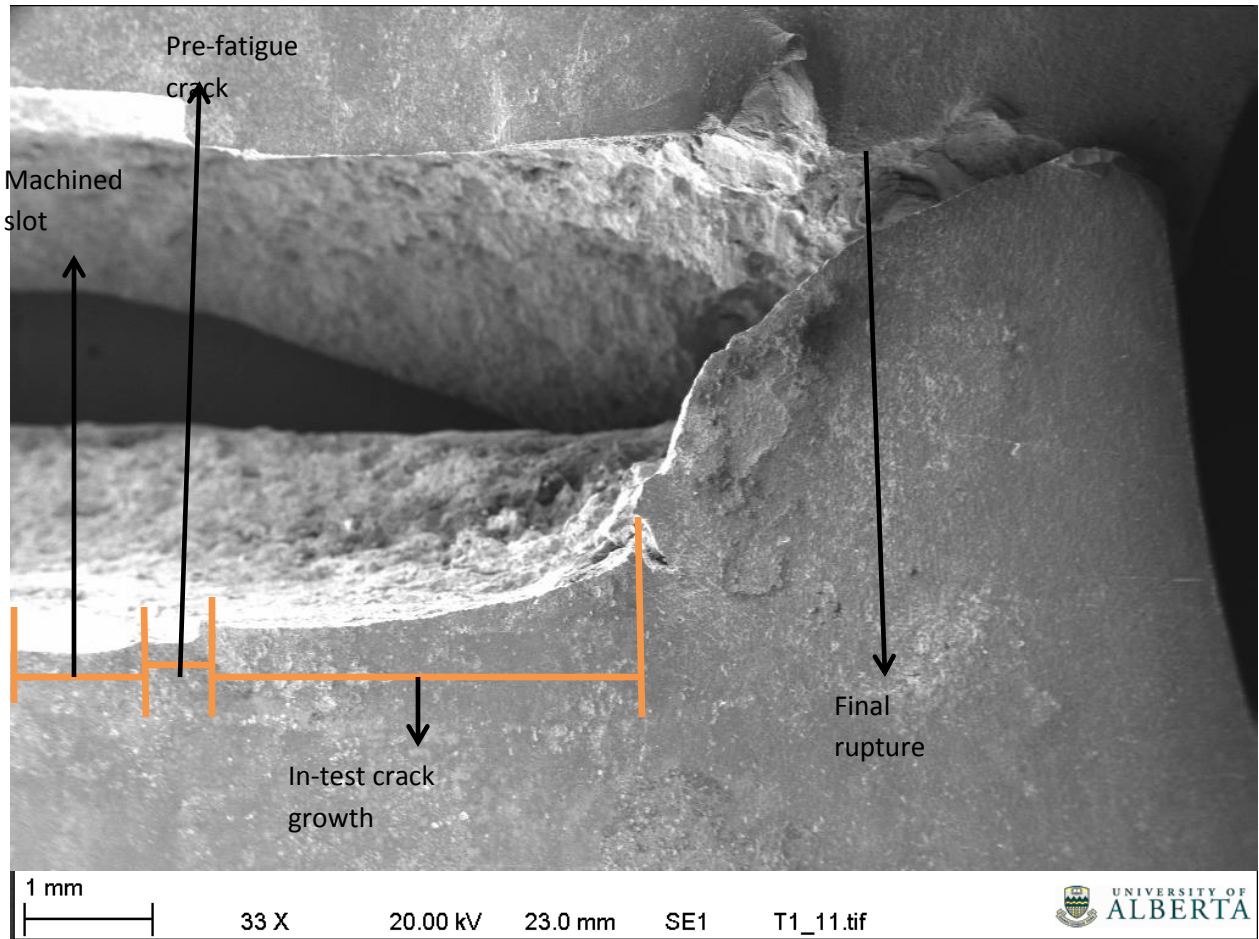


Figure 7-12: Half section of ruptured sample. Sample ruptured during test and was manually held together for photo. Micro-crack colony was found oriented along a 45° line from shear lip.

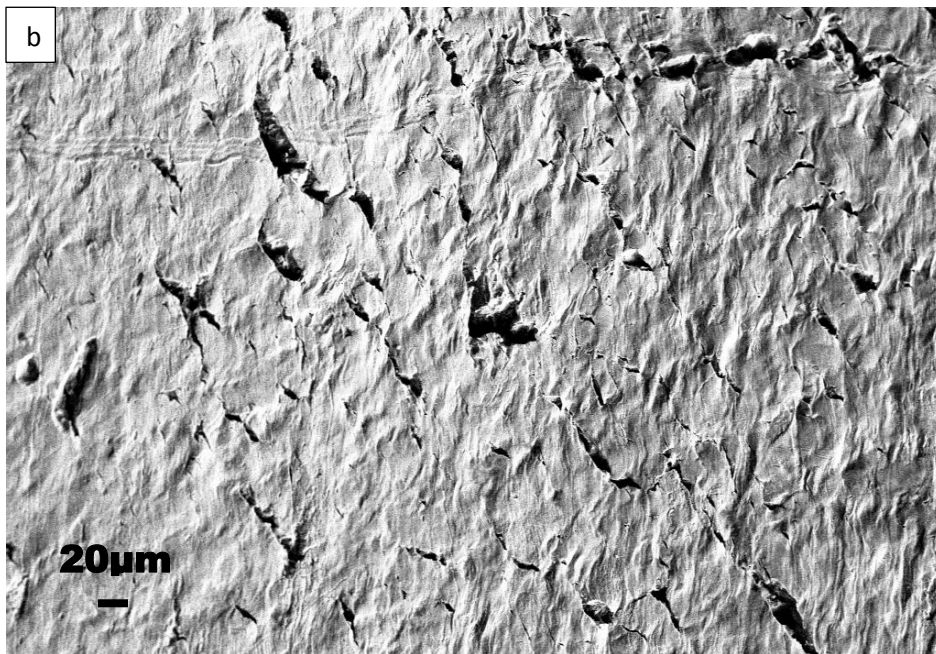
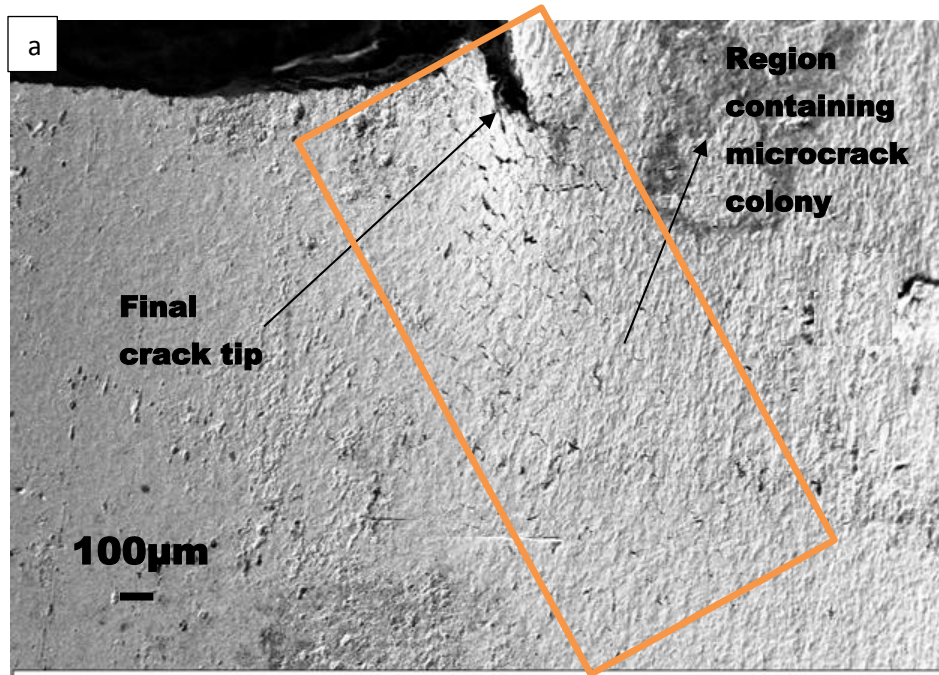


Figure 7-13: a) Array of tiny secondary cracks at crack tip next to shear lip, b) higher magnification image of crack array.

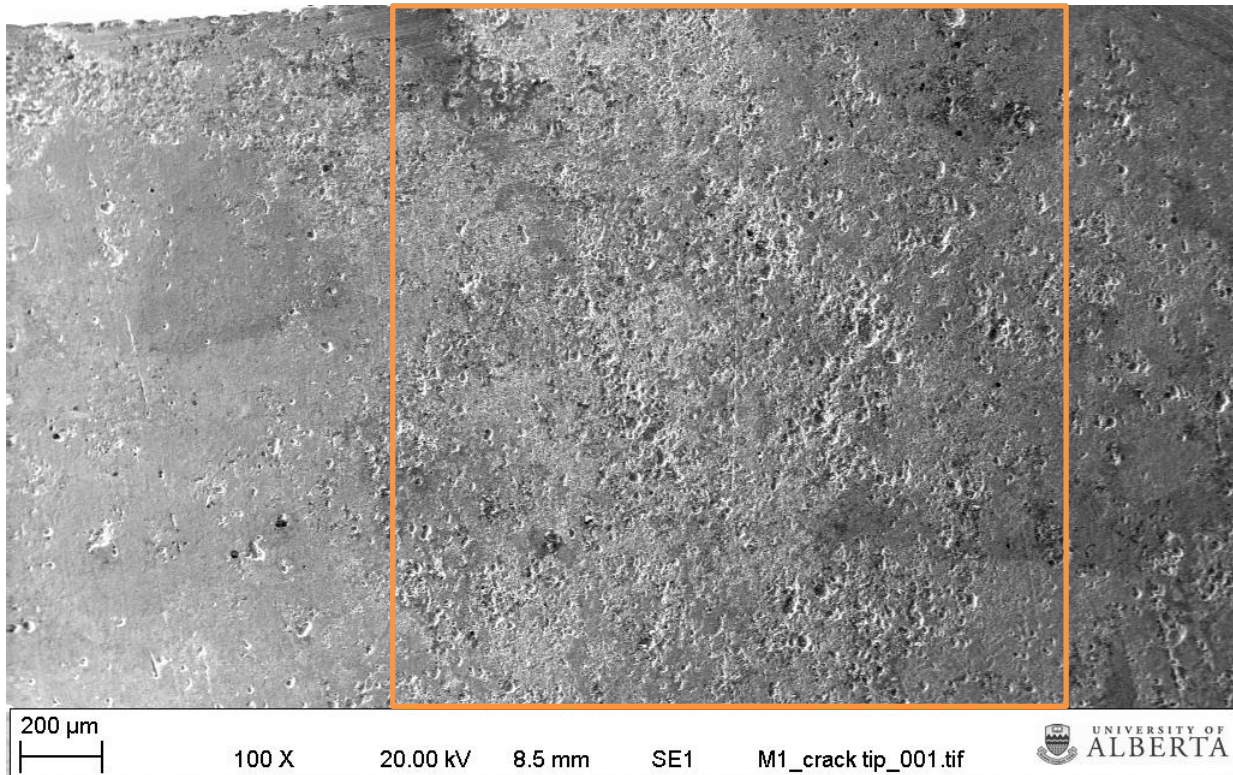


Figure 7-14: Cluster of pits at crack tip (75 mm from open mouth). Highlighted area shows dense pit clusters around the final crack tip

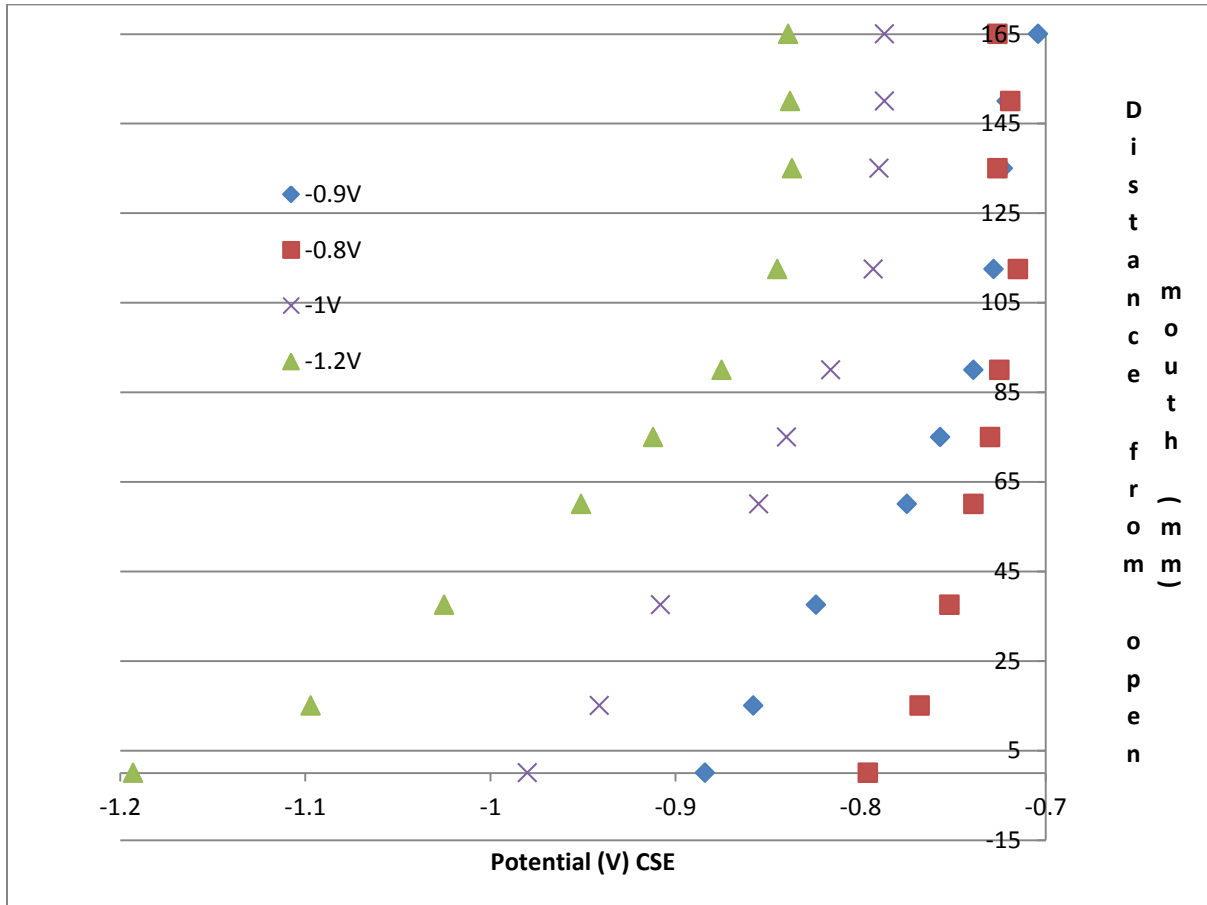


Figure 7-15: Variation of potential with distance from the open mouth of a disbondment

7.3 Discussion

7.3.1 Crack growth mechanism at applied cathodic potential of -1.2V

It has been suggested that microcracks like those found at the open mouth (Figure 7-13) are usually associated with hydrogen induced cracking [12]. The presence of this feature therefore suggests that hydrogen is involved in propagation of cracks in this study. As mentioned above, there is a potential gradient from the open mouth (point of potential application) to the bottom of the disbondment due to ohmic resistance. The open mouth should experience the highest cathodic potential while ohmic resistance should cause a drop in potential to near open circuit potential towards the bottom of the disbondment. Under the influence of a sufficiently high cathodic potential, hydrogen ions being positively charged will preferentially migrate to the more cathodic portions of the specimen [13]. Hence, a hydrogen ion concentration gradient will develop within the disbondment. This potential induced distribution of hydrogen ions inside the disbondment may cause a higher than expected concentration of hydrogen ions at the open mouth. It is also likely that additional hydrogen was produced at the open mouth by the dissociation/reduction of water due to the fairly high cathodic potential applied, further increasing the concentration of hydrogen ion in this region. Under such conditions, a higher amount of hydrogen may diffuse into the metal lattice at the open mouth compared to the other locations resulting in a significantly higher crack propagation rate at this location. The least amount of hydrogen will be available at the bottom of the cell where the least growth rate was also determined. The fact that hydrogen induced microcracks could not be found at 75 mm or 150 mm from the open mouth lends credence to the fact that a hydrogen concentration gradient developed inside the disbondment. The resulting hydrogen concentration gradient at a cathodic potential of -1.2V is schematically illustrated in Figure 7-16.

Some may argue that the presence of microcracks at the open mouth of the disbondment where -1.2V CP was applied indicates that the dominant mechanism is hydrogen induced cracking. However, the following points need to be carefully considered:

1. The microcracks were only formed in the region where final rupture occurred and highest plastic deformation existed (considering the high stress concentration ahead of the crack tip, due to a very small remaining ligament, just before rupture). The absence of such microcracks earlier in the test suggests that the combined environmental and mechanical factors at the start of test and until very close to the final rupture could not cause the initiation of such microcracks. This suggests that even in the presence of a high hydrogen concentration such as existed at the open mouth at an applied potential of -1.2V, severe plastic deformation was still necessary for the formation of these microcracks.
2. Microcracks were not found at the crack tip at 75 mm nor 150 mm from the open mouth. In both of these cases, lesser crack propagation had occurred by the time the crack at the open mouth ruptured, therefore less plastic deformation at the crack tip would have occurred compared to the final stages of cracking at the open mouth. This speaks to the fact that at these locations, hydrogen concentration was not sufficiently high to cause cracking all by itself and a certain combination of hydrogen effect and plastic strain may be necessary to induce such micro-cracking.

It is therefore our firm belief that most of the crack propagation observed in this case is NNPHSCC, a hydrogen enhanced crack propagation, rather than a hydrogen embrittlement/hydrogen damage mechanism.

To determine whether the formation of these microcracks was just a one-time incidence, the remaining samples on which tests were conducted at -1.2V were carefully examined (these tests are not reported here). In all cases microcracks were found on the shear ligament, similar to what was observed in test III. However, these arrays of microcracks were not found in any tests conducted at -0.9V or at OCP.

It must however be pointed out that the two tests conducted at -0.9V did not experience sufficient crack growth to result in final fracture before the tests were stopped due to power failure (as these two tests were performed at a time when the building was undergoing vast re-modeling).

It is often argued that SCC cracks are not likely to be initiated at the open mouth where there is adequate cathodic protection. While this could be true, on careful consideration of the results presented in this study as well as careful consideration of industry reported SCC events it is not difficult to find situations where these results may be relevant. The NEB enquiry [14] reported that “*In almost all pipeline failures associated with SCC, local stress intensifiers such as corrosion, gouges or stress concentrations at the toe of the weld seam have been present.*” Similar observations have been made in other studies.

Situations where gouges or combinations of dents and gouges occur are cases where local stresses could be significantly high, and localized plastic deformation could be severe, similar to the situation at the later stages of crack propagation in test III. It is instructive that the absence of microcracks at -0.9V suggests that even with severe plastic deformation, higher hydrogen concentration at such regions with high stress concentration, such as at high cathodic potentials, could be necessary for the initiation of SCC cracks at or near the open mouth of a disbondment. The formation of a cluster of pits near the crack tip at -0.9V cathodic potential rather than the formation of microcracks could also be a very important piece of information. It is often noted that SCC regions are bordered by pit clusters.

The results presented in this study could therefore suggest that SCC cracks are only initiated in the most severely deformed region in the presence of a high enough hydrogen concentration, whereas localized pitting would occur in areas with borderline combination of local stresses and/or hydrogen concentration, but where the combination of both environmental enhancement due to hydrogen and mechanical loading is not high enough to cause crack initiation. Although it might be argued that SCC develops only in cases where such severe plastic deformation exists, perhaps what is most important is not the severe plastic deformation but the exhaustion of available ductility. For instance, eutectic clusters or hard (brittle) second phase clusters or hard spots developed from arc strikes *etc.* are regions where

ductility could be quickly exhausted locally, without any significant gross plastic deformation. These are all regions where SCC is known to preferentially be formed.

For instance it is well known that rolled alloys with a banded structure are often more susceptible to NNPHSCC than those that are not banded. Perhaps the main reason such structures are more susceptible is not only because of preferential corrosion or strain incompatibility at the ferrite/pearlite interface but because of the exhaustion of ductility in the more brittle pearlite band and subsequent deflection of deformation to the weakest regions within the alloy structure – the ferrite-pearlite interfaces, leading to the formation of micro-cracks and subsequently SCC in such regions. The carbide precipitates being harder than the ferrite matrix are able to resist plastic deformation and shearing by dislocations, so that a much higher stress is required to fill the carbide phase with dislocations. This should lead to the deposition of edge dislocations at the carbide ferrite interfaces as well as the pearlite ferrite interfaces. Since the presence of interfacial dislocations provide a much more efficient diffusion path for hydrogen, the presence of dislocations provide a faster diffusion route which leads to a segregation of atomic hydrogen to the ferrite-pearlite interface. The presence of hydrogen at such regions could then cause a reduction in ductility, aiding quicker exhaustion of ductility at such regions and aiding the formation of microcracks.

The fact that these micro cracks only developed in the final ligament, close to the end of cyclic loading, where very few load cycles are experienced prior to failure, suggests that only very few load cycles are required to cause SCC initiation at locations where very high stresses and high plastic deformation exist. Theoretically, SCC could initiate under static or near static loading, although this has generally not been observed in the laboratory. The current results seem to confirm that if SCC initiation only occurs in regions with severe plastic deformation due to secondary stresses – due to residual, soil sliding, mechanical damage *etc.* – then very few stress cycles or near static loading may very well cause SCC cracking.

Soil resistivity is known to vary with moisture content, salinity and temperature. Generally, an increase in moisture and salt content as sometimes happens in summer can significantly lower soil resistivity allowing more cathodic potential to reach the open mouth of the disbondment. Also more rapid transient variations in soil water composition and moisture content as could occur in the high rain season could induce significant variation in soil resistivity. This could allow cathodic potentials to temporarily or extensively rise to higher values than anticipated and could cause significant cyclic increases in crack propagation rates. However, it can be argued that there are not likely to be any cracks at the open mouth of the disbondment if the cathodic protection system is working properly. The truth is that seasonal variations in soil water levels can move the position of the open mouth around significantly such that there may indeed be a crack present at the open mouth even if the cathodic protection is working properly. If a high cathodic potential reaches the open mouth in such an instance, crack propagation rates may significantly increase at the open mouth with an attendant general increase in propagation rates at other locations in the interior of the disbondment. This could be a very important mechanism when considering crack re-initiation from dormancy. Even if cracks do not initiate at the open mouth, but further inside the coating disbondment, seasonal variations in soil water level or further coating degeneration may cause locations with existing dormant cracks to experience high potentials which could then lead to the reactivation of such cracks under normally benign conditions.

7.3.2 Crack growth mechanism at applied cathodic potential of -0.9V

Usually the distribution of hydrogen within the disbondment is explained in terms of the distribution/amount of hydrogen available in the local environment surrounding the crack tip; the assumption being that the more the hydrogen ions present at a given location within the aqueous solution, the more the hydrogen atoms being generated from reduction on the steel surface at the location and therefore the more lattice concentration of hydrogen at the crack tip at the location. Based on this argument alone, one will expect more hydrogen to be present at the open mouth of the crevice. If this

were the case, a high growth rate should have resulted at the open mouth when a potential of -0.9V is applied. However, the experimental results suggest otherwise. Another possible factor that could play a significant role in hydrogen ingress into pipeline steel – the local availability of electrons for the hydrogen reduction reaction – is often ignored. Figure 7-15 shows that at an applied potential of -0.9V, the potential quickly drops to near OCP values such that the potential at both 75 mm and 150 mm from the open mouth are quite similar. This is similar to results already reported in a few previous studies [8, 15, 16].

Under this condition, more and more metal dissolution could occur towards the bottom of the disbondment, giving up electrons. These electrons may not necessarily be (fully) consumed by the hydrogen reduction reaction at the same site where they were produced, depending on the amount of hydrogen ions present at that site. Since an unbound electron is unstable the availability of unreduced hydrogen ions at other sites may provide a driving force for the migration of unbound electrons that are unused at the site of production to other locations and a corresponding migration of hydrogen ions from other sites in search of free electrons. Under this scenario, the balance of these three processes – water reduction, carbonic acid dissociation, and availability of electrons – will determine the location with the highest concentration of hydrogen ions. At CP=-1.2 V, CP may be high enough to attract larger quantities of hydrogen to the open mouth while suppressing general corrosion at the open mouth and further down the cell. Chen *et al.* [8] concluded that the general increase in pH in a simulated crevice when no CO₂ is being purged in simulated soil solution at an applied potential of -1.2V is a result of water dissociation rather than the accumulation of hydroxyl ions in the crevice as postulated previously. Song *et al.* [17] also arrived at a similar conclusion in a study of chemical evolution under a disbonded coating with cathodic protection. Although water reduction to hydrogen may also be possible at an applied potential of -0.9 V, the kinetics of the process may not support the production of any significant amount of hydrogen. Also, at -0.9 V, the potential may not exert such a strong attraction on hydrogen ions, while still offering enough protection at the open mouth. However, increased dissolution toward the cell bottom, resulting from insufficient cathodic protection, may furnish electrons necessary for hydrogen reduction

and the balance of all forces may drive a higher flux of hydrogen ions to the neighborhood of 75 mm from the open mouth. This may explain the observed high growth rate at -75 mm from the open mouth at an applied potential of -0.9mV.

Evidence of this is seen when one compares the extent of corrosion/pitting that occurred during the test at these three locations within the disbondment (Figure 7-10). Figure 7-10b shows that there is almost perfect protection of the sample surface around 75 mm from the open mouth whereas there was significant pitting at 150 mm from the open mouth. This indicates that whereas there was no need for iron dissolution at 75 mm from the open mouth to support hydrogen reduction at this site, anodic dissolution resulting in localized pitting occurred at the far end of the cell. This suggests that electrons produced from the open mouth and the far end of the disbondment simply fed the process occurring at 75 mm from the open mouth. A depiction of the distribution of hydrogen within the disbondment at an applied potential of -0.9V is shown in Figure 7-17.

The condition simulated in this section could be more representative of conditions at the open mouth of a coating disbondment on a pipeline surface under high soil resistivity conditions such as may obtain in winter for instance. Under such conditions, the cathodic potential at the open mouth of the disbondment can significantly weaken, driving potentials nearer to open circuit potentials. The implication of the above is that more adequate cathodic protection derived from a more balanced equilibrium between the amount of hydrogen resident at the open mouth and cathodic potential can result in a significant decrease in the rate of propagation of any cracks at the open mouth (if one is present). However, crack propagation can be almost double at locations that are a little remote from the open mouth.

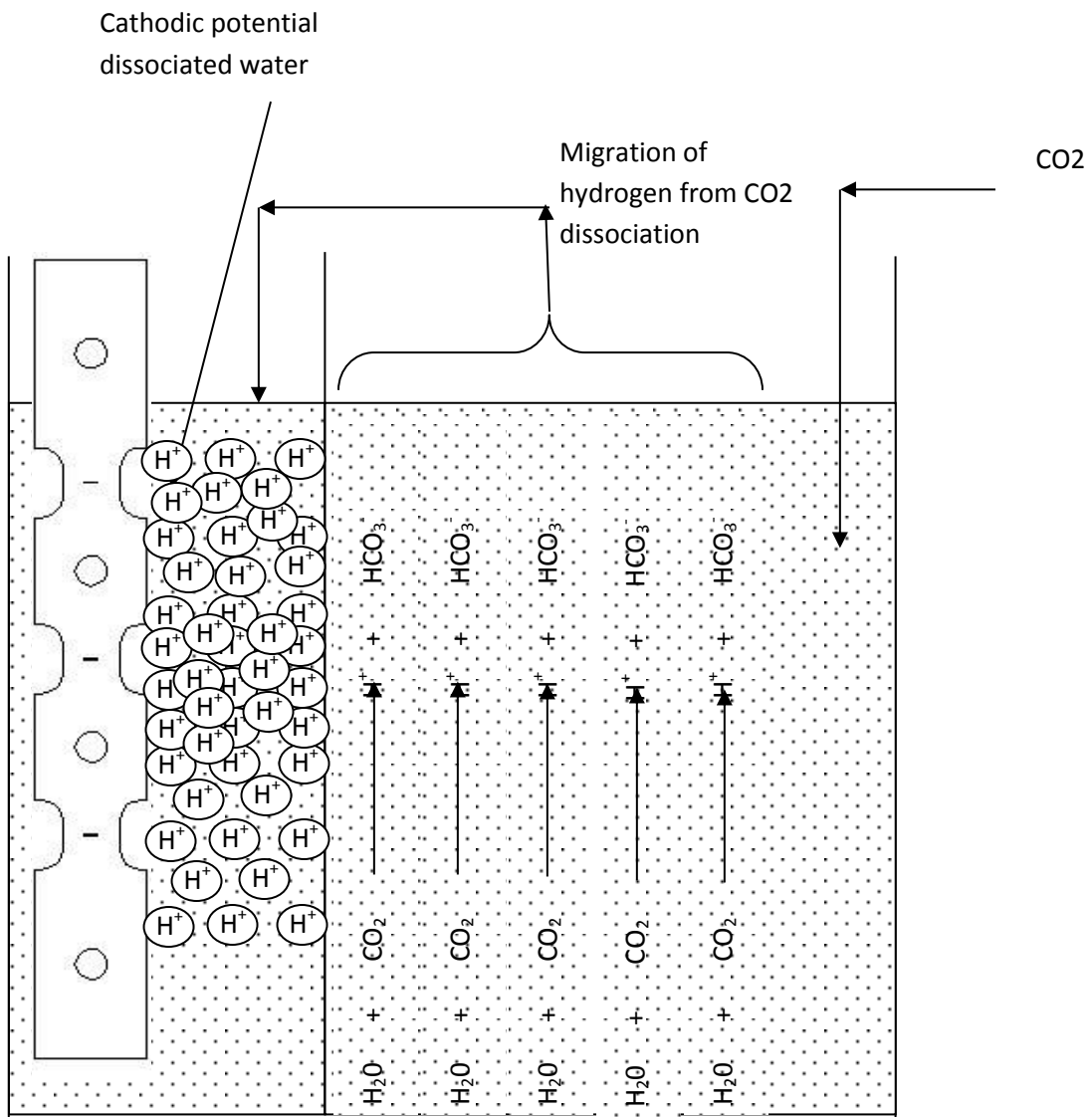


Figure 7-17: Schematic depiction of hydrogen ion distribution inside a disbondment at an applied potential of -0.9V

7.3.3 Crack growth behaviour

7.3.3.1 Crack re-initiation

In earlier communications (Chapters 4 and 5), the role of dissolution in crack re-initiation and subsequent crack propagation was discussed. It was observed that at low maximum operating stresses, such as up to 75% SMYS, which is typical of oil and gas pipelines, crack tip/crack wall dissolution could play a very important role in crack propagation. This could significantly delay crack re-initiation/crack propagation. However, this effect was found to be minimal at higher operating stresses (Chapter 5). The application of cathodic potentials at the open mouth in the current tests should help eliminate the dissolution effect, at least at the open mouth and/or up to 75 mm from the open mouth. Thus growth under these conditions should simulate mechanical propagation and/or hydrogen effects in their purest form without interference from dissolution.

Since mechanical loadings are similar in tests I, II and III, the inability to re-initiate cracks at $R=0.6$ at OCP in test I, whereas re-initiation occurred at $R=0.6$ in tests II and III, speaks to the role of crack tip dissolution. Recall that crack re-initiation not only occurred at the open mouth in tests II and III but also at the far end of the disbondment where local potentials are very close to OCP values. Also note that up till $R=0.6$ loading, the same extent of creep could be assumed to have occurred in all three tests. Hence, the only factor that could possibly explain delayed re-initiation at OCP are 1) crack tip dissolution and/or 2) hydrogen assisted crack re-initiation under the applied cathodic potentials. One would expect hydrogen assisted crack re-initiation to be far less significant at the far end of the disbondment in test II, where near OCP conditions were attained at -150 mm from the open mouth (figure 7-16), yet crack re-initiation occurred even at this location. The application of a cathodic potential modifies the chemistry of the solution such that less hydrogen is resident at the far end of the disbondment under an applied potential, reducing the amount of hydrogen ions available for reduction to hydrogen gas at this location. This reduces the amount of iron that has to be dissolved to furnish electrons required for hydrogen reduction. Hence, more dissolution could occur at the far end of the disbondment under OCP conditions

than under an applied cathodic potential, resulting in a blunter crack tip at OCP than at an applied cathodic potential.

7.3.3.2 Crack propagation

7.3.3.2.1 Crack propagation – Average growth rates

Comparing the average growth rates at the open mouth in both tests II and III reveals that average growth rate at the open mouth is about three times faster at -1.2V than at -0.9V. Since initial mechanical conditions are similar, this disparity in growth rates suggests more environmental enhancement in test III than in test II. In an earlier publication [13], the current authors explained that a moderately high cathodic potential could result in significantly higher hydrogen concentration at the open mouth because (1) hydrogen ions being positively charged could prefer to reside at locations with more cathodic potentials than lower potentials 2) such high cathodic potentials could cause water dissociation generating more hydrogen at the open mouth. The combination of these two factors favours more hydrogen ion concentration at the open mouth in test III than in test II. Thus more hydrogen ions will diffuse into the metal lattice under the influence of a higher concentration gradient between the exposed surface and the completely masked opposite surface. Consequently, more hydrogen will be present ahead of the crack tip to enhance crack propagation in test III than in test II.

In previous communications we explained how variations in the local chemistry could cause a change in the environmental factor $1/f^{\gamma}$ in the corrosion fatigue model ($\Delta K^2 \cdot K_{\max} / f^{\gamma}$). At the commencement of each test, prior to the application of a cathodic potential, the combined factor at the open mouth in the two tests would have been similar. However, when the cathodic potential is applied, cathodic potential induced changes in the solution chemistry, particularly hydrogen concentration, soon causes a marked change in the environmental factor in the two tests. Since da/dN is proportional to $\Delta K^2 \cdot K_{\max} / f^{\gamma}$, a growth rate difference by a factor of three suggests that $\frac{1}{f^{\gamma_{II}}} = \frac{3}{f^{\gamma_{III}}}$. This implies that $\gamma_{II} = 0.2074 + \gamma_{III}$. Since, $\gamma=0.1$ at the open mouth at OCP, the above implies that applying a CP of -1.2V could increase hydrogen concentration at the open mouth to the point that γ is at least three

times that at the open mouth under open circuit potential. Since γ at an applied potential of -0.9V will be closer to that at OCP, it is perhaps safe to assume that γ at -1.2V is at least twice that at an applied potential of -0.9V at the open mouth.

As explained in the earlier publication, γ values will decrease with distance from the open mouth towards the far end of the disbondment. Thus γ at 75 mm from the open mouth should be higher in test III than in test II. Under this condition one would expect a higher growth rate at 75 mm from the OM in test III than in test II. However, the contrary was observed in test III. Reasons for this are provide in the next section.

Comparison of growth rate at the open mouth under OCP conditions with those at -1.2V and -0.9V also reveals an important piece of information. Recall that no growth re-initiation was observed at R=0.6 at OCP conditions unlike at -0.9 and -1.2V. However, once growth was initiated at a slightly more severe mechanical loading condition, the growth rate observed at the open mouth was very similar to that at the open mouth at an applied potential of -1.2V. Comparing the growth rate at the open mouth at OCP to that at -0.9V reveals that growth rate at OCP under slightly more severe mechanical loading is more than three times that at -0.9V. This shows clearly that although higher hydrogen concentration induced by an applied cathodic potential is higher at -0.9V, the combined environmental-mechanical driving force for crack propagation is lower at -0.9V than at OCP but more severe mechanical loading. This suggests that although an applied cathodic potential could aid crack re-initiation at less severe mechanical loading, causing crack re-initiation and sustained growth at conditions where mechanical forces are insufficient to cause re-initiation, crack propagation is a lot more sensitive to changes in mechanical factors than changes in environmental factors. Small changes in mechanical factors could have very remarkable effect on crack propagation.

This observation could explain why many of the cracks observed in the field are dormant. It is well known that SCC cracks are usually formed as very fine cracks by a combination of loading

and environmental conditions. Most of them remain as such while only very few grow into longer cracks. It has also been well documented that residual stresses play a very important role in SCC formation and growth. It could very well be that rare spikes in operational stresses combined with secondary stresses cause an initial growth of suitably located cracks to a critical size. Once loading is restored to normal benign operating conditions, the growth of these cracks stop being mechanically driven. However, if the right environmental factors are locally set up, possibly by the applied cathodic protection or any other factors that may lower potentials locally, such cracks may experience growth re-activation by environmental factors. In such cases, only cracks that were propagated by mechanical factors to the critical size during transient loading would be reactivated and continue to grow. Others will remain dormant.

7.3.3.2.2 *Crack propagation – Corrosion fatigue behaviour*

Combined corrosion fatigue analysis of the crack growth data in test III revealed a trend not observed hitherto in our studies. At both the open mouth and 75 mm from the open mouth, growth curves in the depth direction are shifted to the left relative to growth curves at the sample surface (Figure 7-18). This suggests that growth thresholds may be different along the curved crack front. Also in these tests, growth rates are higher in the depth direction than at the sample surface (Figure 7-18). This behaviour was not observed in any of the previously reported tests conducted at open circuit potential. Also it is quite surprising that although total growth at 75 mm from the open mouth is significantly smaller than at the open mouth, growth rate in the depth direction at 75 mm from the open mouth was significantly higher than surface growth rate at the OM and slightly higher than the depth growth rate at the open mouth.

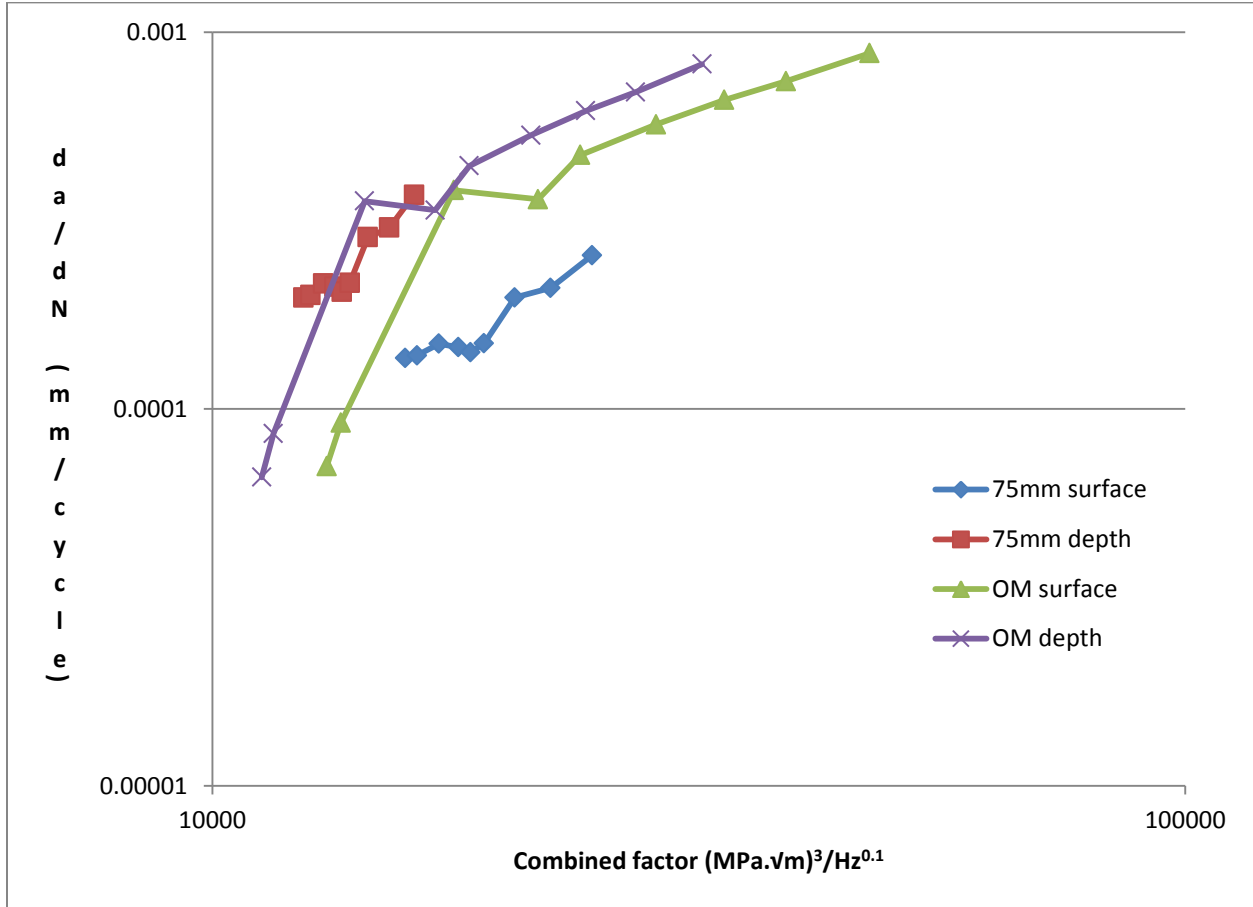


Figure 7-18: Growth curves in test III

This behaviour is consistent with the change in aspect ratios during the test (Figure 7-19). In test III, aspect ratios increased at both the open mouth and 75 mm from the open mouth during the test, contrary to observations in the previously reported studies. Also aspect ratios increased significantly more at 75 mm from the open mouth than at the open mouth. This is consistent with growth rates presented above. Unfortunately, no growth curves were recorded at -0.9V the two times the test was conducted because of damaged potential sensing connections. So it is not clear if this same behaviour occurred at -0.9V. However, aspect ratio data clearly shows that aspect ratio decreased during the test rather than increased as in the -1.2V test. The question then is, what is responsible for this behaviour?

As earlier noted, in test III, initial deposition of an appreciable quantity of a white product which turned black after a few days was observed at the open mouth. However, only white products were observed to have formed at 75 mm from the open mouth through the test. Deposition of these products was not observed in the other tests. It is therefore possible that the deposition of these products was responsible for the preferential crack growth in the depth direction in test III. It is well reported that both carbonates and black magnetite films were present at NNPHSCC sites in field studies [14, 18, 19]. Also, laboratory simulations have revealed similar occurrence. He [20] observed that uniform corrosion occurred while carrying out hydrogen charging in NS4 solution at OCP. However, at -0.9V, the original sample surface was preserved because of adequate protection. Below -0.9V, white particles were deposited on the specimen surface. The size and population of these particles increased with decreasing potential. Particle size and surface coverage peaked at -1.2V and decreased with decreasing potentials after -1.2V. After just 67 hours of charging the deposit layer was so thick it started spalling off in the NS4 environment. This was consistent with our observation in this study. He [20] confirmed by EDX analysis that the white particles were $\text{Ca}(\text{HCO}_3)_2$ and CaCO_3 . He's study occurred for a much shorter period of time than the current study, so it is possible that his test duration was too short to observe the precipitation of the black products, presumably magnetite.

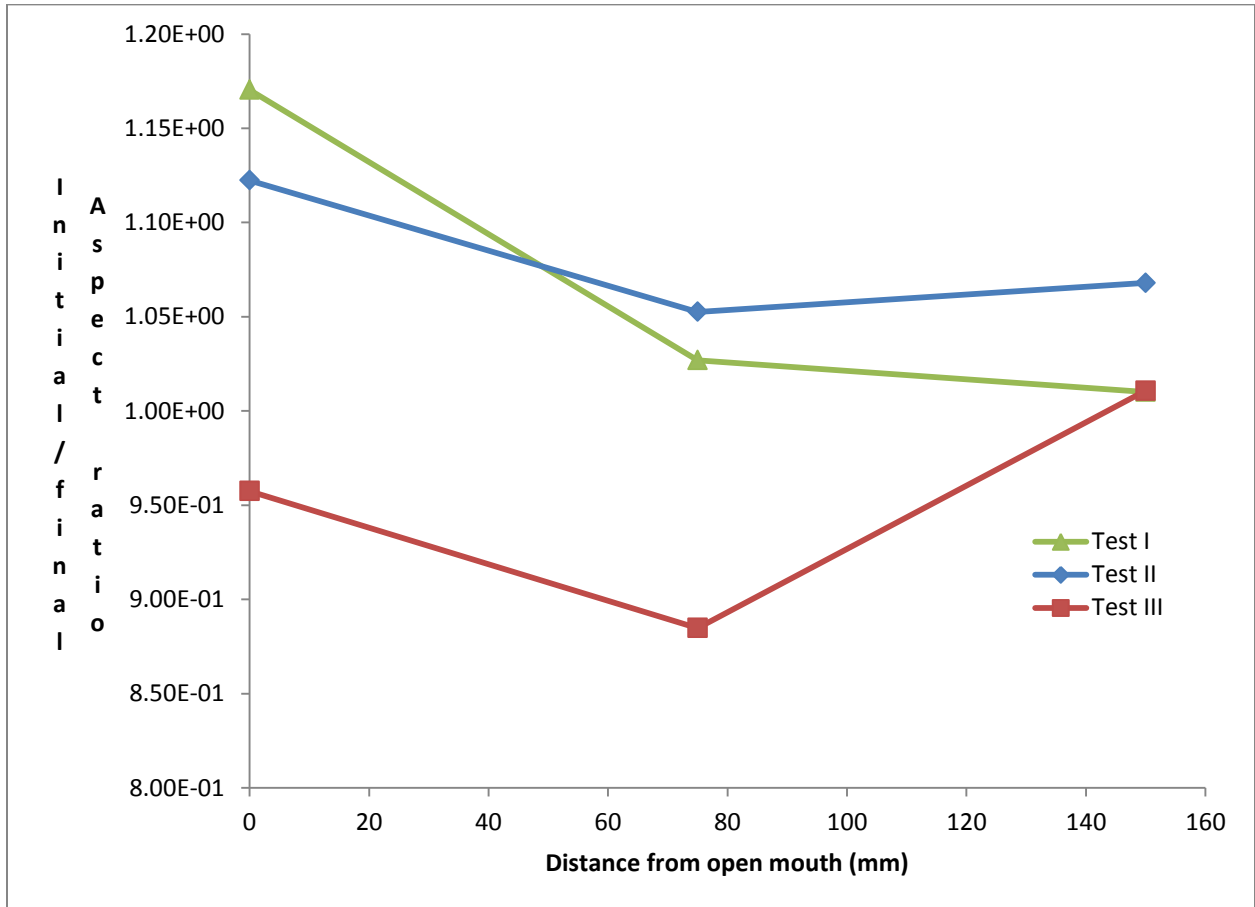


Figure 7-19: Ratio of initial aspect ratio to final aspect ratio

The deposition of these products on the sample surface at lower potentials was found to significantly reduce the hydrogen permeation rate [20]. This could have a significant effect on the growth of cracks in such environments. At the open mouth in test III, the crack tip area at the surface is well covered with these deposits. Although there would also have been deposition inside the slot itself, the slot gap is much wider than the surface crack tip crevice. So, deposit coverage of the crack front in the depth direction could be more limited compared to the crack tip at the sample surface. Thus, the local solution is able to permeate the crack crevice more in the depth direction than at the sample surface. Under this condition, more sample surface is exposed to hydrogen in the depth direction than at the sample surface. Thus the sample could experience more hydrogen enhanced crack propagation in the depth direction than at the sample surface. This could result in the observed higher growth rates in the depth direction as well as an increase in aspect ratios in the depth direction.

It is also interesting to note that growth curves at the open mouth in both tests I and II were very similar despite the fact that growth only initiated under more severe mechanical loading in test I (Figure 7-20). In previous studies (Chapter 5) at open circuit potentials, growth under different loading conditions such as R-ratios and loading frequencies resulted in distinctly different growth curves. The similarity of growth behaviour in the current study suggests that although mechanical forces were more severe in test I, higher environmental driving force in test III, with γ probably three times higher at the open mouth in test III, was able to compensate for the lower mechanical factors. The same trend was observed at 75 mm from the open mouth. This result points to the importance of environmental enhancement in the growth of SCC cracks. Actual pipelines often experience very mild mechanical loading for extensive periods. Crack propagation under such very mild mechanical loadings, very high R-ratios, would have been impossible without environmental enhancement. This study points to the fact that although cathodic protection is great at precluding general corrosion, moderate to high cathodic potentials could set up electrochemical conditions that could be favourable to the re-initiation and subsequent continuous propagation of cracks that would otherwise have remained dormant.

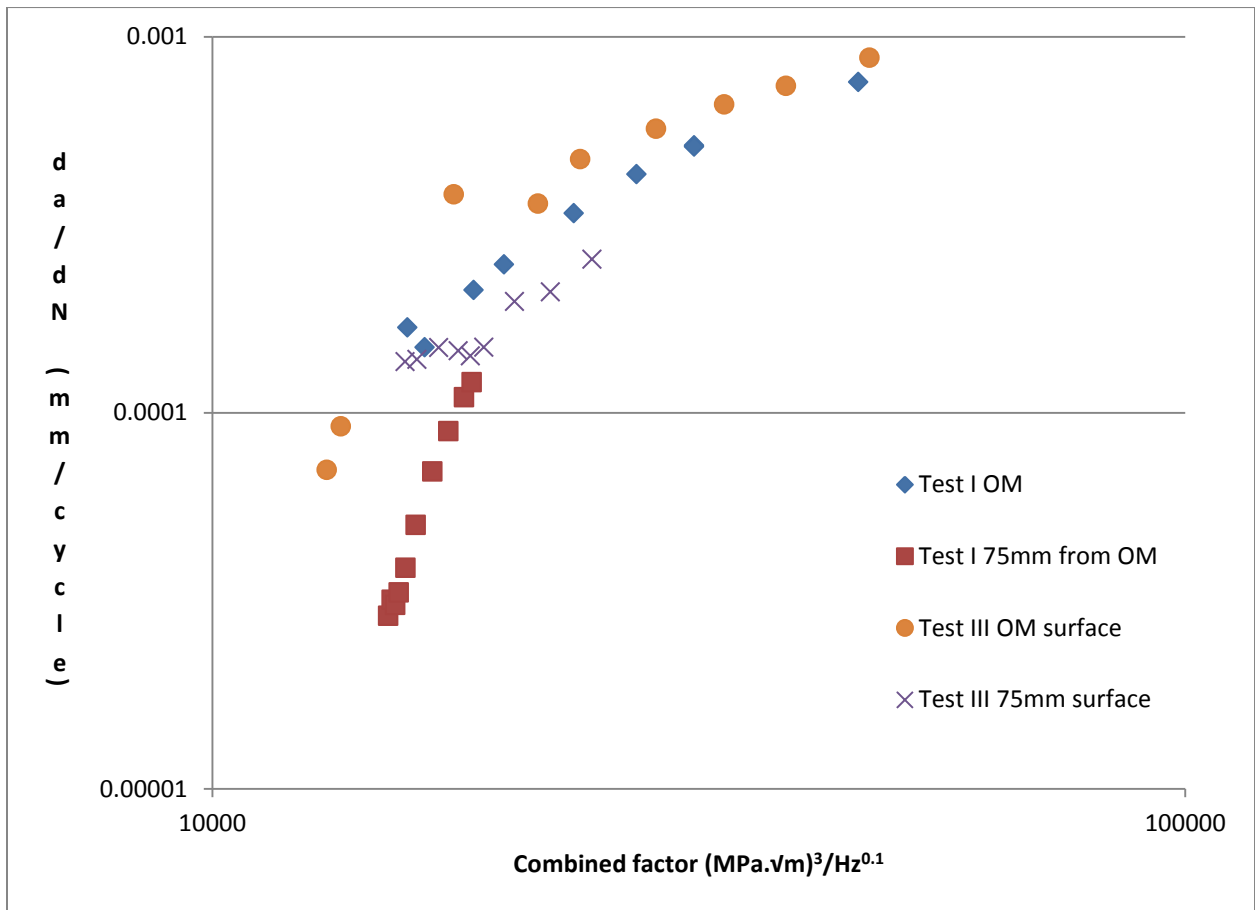


Figure 7-20: Growth curves in tests at OCP and -1.2V

7.4 Conclusion

This study shows that variations in the local environment under a disbonded coating can induce sufficient disparity in the amount of hydrogen available at different locations relative to the open mouth to significantly influence observed crack propagation rates in a near-neutral pH environment.

1. High stresses involved in hydrostatic testing causes a mechanical deformation of the crack tip making it harder to initiate cracks at moderate loading conditions.
2. Crack tip dissolution at open circuit potential could delay crack re-initiation compared to cases where a cathodic potential was applied.
3. The application of cathodic protection following a hydrostatic testing could suppress dissolution controlled growth thereby eliminating dissolution induced retardation of crack propagation.
4. The application of moderate to high cathodic protection could increase the environmental driving force for crack propagation by up to a factor of three. This could aid crack re-initiation at more benign loading conditions where crack re-initiation would otherwise not have occurred.
5. Such increased environmental driving force for crack propagation could also help to sustain continued crack propagation at loading conditions where crack propagation would otherwise not have occurred.
6. Whereas crack growth was faster at and near open circuit potentials, high cathodic enhanced growth in the depth direction relative to that at the sample surface resulted in higher aspect ratios.
7. Contrary to expectations that the highest crack growth rate would always occur at the location with the highest applied cathodic potential, due to higher hydrogen segregation, the highest growth rate was found at 75 mm from the open mouth with a cathodic potential of -0.9 V although it was highest at the OM for -1.2 V applied CP. This was related to the balance between the availability of electrons and hydrogen ion migration within the solution. This observation is consistent with the often observed close proximity between stress corrosion crack colonies and pit

colonies in field excavations of SCC sites. This would suggest that the electrons used in the reduction of hydrogen in crack colonies might have been furnished at nearby pitting sites; hence both features are necessary for sustaining the growth of the other. This conclusion is only a hypothesis at this stage; further studies are being carried out to explore this hypothesis and will be reported in a future study.

From the pipeline operator's perspective, the implications of the results presented in this study are:

1. Soil types or seasonal variations in soil conditions that result in lower soil resistivity may set up a localized chain of electrochemical events that may lead to a rapid propagation of cracks that would otherwise have remained dormant or almost-dormant.
2. If a crack exists at the open mouth of a coating disbondment after hydrostatic testing and cathodic protection is applied, although one expects higher crack propagation rate at the open mouth because of high CO₂ concentration and higher hydrogen concentration at the open mouth, soil types or seasonal variations in soil conditions that result in very high soil resistivity may increase crack propagation rates to higher levels further inside a coating disbondment.
3. At high cathodic potentials such $-1.2V_{SCE}$ crack propagation is most rapid at the open mouth where hydrogen concentration is highest. However at more moderate potentials such as $-0.9V_{SCE}$, the location where highest growth rate was observed shifted to 75 mm from the open mouth.
4. Although these effects may be seasonal (cyclic) the cumulative effect determines the rate of propagation of existing cracks in a near-neutral pH environment.

References

- [1] Harle, B. A., Beavers, J. A., and Jaske, E., 1995, "Mechanical and metallurgical effects on low-pH stress corrosion cracking of natural gas pipelines," Corrosion '95, NACE, Paper #. 646.
- [2] Brongers, M. P. H., Beavers, J. A., Jaske, C. E., 2000, "Effect of Hydrostatic Testing on Ductile Tearing of X-65 Line Pipe Steel with Stress Corrosion Cracks," Corrosion (USA), **56**(10) pp. 1050-1058.
- [3] Beavers, J. A., and Jaske, C. E., 1998, "Near-neutral pH SCC in pipelines: effects of pressure fluctuations on crack propagation," Corrosion '98, NACE, paper # 98257.
- [4] Leis, B. N., and Brust, F. W., 1990, "Hydrotesting Effects. I. Model Predicts Crack Growth and Material Behavior," Oil Gas J., **88**(7) pp. 45-48.
- [5] Leis, B.N., and Brust, F.W., 1992, " Hydrostest strategies for gas transmission pipelines based on ductile-flaw-growth considerations," NG-18 Report No. 194.
- [6] Chen, W., and Sutherby, R.L., 2006, "Laboratory simulation of hydrostatic test in near-neutral pH soil environments", International Pipeline Conference 2006, Calgary, Canada, pp. 25-29.
- [7] Kang, Y., Chen, W., Kania, R., 2011, "Simulation of Crack Growth during Hydrostatic Testing of Pipeline Steel in Near-Neutral pH Environment," Corrosion Science, **53**(3) pp. 968-975.
- [8] Chen, X., Li, X. G., Du, C. W., 2009, "Effect of Cathodic Protection on Corrosion of Pipeline Steel Under Disbonded Coating," Corrosion Science, **51**(9) pp. 2242-2245.
- [9] Beavers, J. A., Johnson, J. T., and Sutherby, R. L., 2000, "Materials factors influencing the initiation of Near-Neutral pH SCC on underground pipelines," International Pipeline Conference, ASME, New York, **2**, pp. 979-988.
- [10] Egbewande, A. T., Chen, W., Eadie, R., 2013, "Transgranular Crack Growth in the Pipeline Steels Exposed to Near-Neutral pH Soil Aqueous Solutions: Discontinuous Crack Growth Mechanism," Acta Materialia, pp. Submitted for publication.

- [11] Chen, W., and Sutherby, R. L., 2007, "Crack Growth Behavior of Pipeline Steel in Near-Neutral pH Soil Environments," *Metallurgical and Materials Transactions A*, **38A**(6) pp. 1260-1268.
- [12] Parkins, R. N., Blanchard, W. K. J., and Delanty, B. S., 1994, "Transgranular Stress Corrosion Cracking of High-Pressure Pipelines in Contact with Solutions of Near Neutral pH," *Corrosion (USA)*, **50**(5) pp. 394-408.
- [13] Egbewande, A. T., Eslami, A. M., Chen, W., 2010, "Growth of surface-type stress corrosion cracks in near-neutral pH environments under disbonded coatings," In: *International Pipeline Conference 2010*, Calgary, paper # IPC2010-31436, pp. 653-662.
- [14] National Energy Board, 1996, "Public Enquiry Concerning Stress Corrosion Cracking on Canadian Oil and Gas Pipelines," Report # MH-2-95.
- [15] Eslami, A., Fang, B., Kania, R., 2010, "Stress Corrosion Cracking Initiation Under the Disbonded Coating of Pipeline Steel in Near-Neutral pH Environment," *Corrosion Science*, **52**(11) pp. 3750-3756.
- [16] Chen, X., Du, C., Li, X., 2009, "Effects of Cathodic Potential on the Local Electrochemical Environment Under a Disbonded Coating," *Journal of Applied Electrochemistry*. Vol.39, **39**(5) pp. 697-704.
- [17] Song, F., and Sridhar, N., 2008, "Predicting Pipeline Corrosion Under Disbonded Coatings with the Influence of Slow Flow Underneath," *Corrosion 2008, NACE*, Paper # 08145.
- [18] Beavers, J. A., and Harle, B. A., 2001, "Mechanisms of High-pH and Near-Neutral-pH SCC of Underground Pipelines," *Journal of Offshore Mechanics and Arctic Engineering*, **123**, pp. 147-151.
- [19] Parkins, R.N., 1999, "A review of stress corrosion cracking of pipelines in contact with near-neutral (low) pH solutions," PRCI, Report for the Line Pipe Research Supervisory Committee of PRC International.

[20] He, D. X., Chen, W., and Luo, J. L., 2004, "Effect of Cathodic Potential on Hydrogen Content in a Pipeline Steel Exposed to NS4 Near-Neutral pH Soil Solution," *Corrosion*, **60**(8) pp. 778-786.

CHAPTER 8

CONCLUSIONS

8.1 Summary and Conclusions

1. A large disbondment on a pipeline may set up a CO₂ concentration gradient that induces electrochemical processes that significantly affect crack growth behavior. This variation in CO₂ concentration induces a hydrogen concentration gradient from the open mouth to the far end of the disbondment
2. Such hydrogen concentration gradient in the solution in contact with the sample surface induces an atomic hydrogen concentration gradient within the metal lattice from the open mouth to the far end of the disbondment. The highest atomic hydrogen concentration at open circuit potential occurs at the open mouth of the disbondment while the least concentration occurs at the far end of the disbondment
3. It is this atomic hydrogen concentration gradient that can significantly influence crack growth behavior under the disbondment. However, the effect produced by the hydrogen induced gradient may vary with the amount of CO₂ present within the groundwater trapped under the disbondment
4. With 5% CO₂ in the bulk solution surrounding the disbonded site, highest growth rate was obtained at the open mouth while growth rates were lower but similar at 75 mm and 150 mm from the open mouth. However, with high CO₂ concentration, 20% CO₂, crack growth rates were very similar at all locations under the disbondment
5. Analysis of crack growth rates suggests that at open circuit potentials and moderate CO₂ concentrations, environmental factors could be three times more severe at the open mouth than at locations further down the disbondment. However, at very high CO₂ concentrations, the environment is so severe at all locations that no variations in environmental severity factor with distance from the open mouth of the disbondment could be deduced from the growth rate
6. Careful analysis of the growth rate pattern and crack morphologies *vis a-vis* testing environment revealed that depending on environmental factors (mainly the amount of CO₂, hence the amount of hydrogen) present within the system, several different factors may

significantly affect growth behavior. These factors include: dissolution, low temperature creep, hydrogen-enhanced crack propagation and hydrogen enhanced plasticity

7. Under benign loading conditions, determined to be at combined environmental-fatigue factors lower than the threshold required for crack propagation, a sharp crack tip may be blunted by either or both of two factors;
 - a. Environmental crack tip blunting. The extent of blunting depends on the amount of CO₂ present within the system. High CO₂ concentration produces severe blunting while blunting is more moderate at lower CO₂ levels
 - b. Mechanical blunting through low temperature creep. It was also determined that local hydrogen concentration can significantly influence the amount of low temperature creep that occurs through the hydrogen enhanced localized plasticity mechanism. Areas with higher local hydrogen concentration such as the open mouth of the disbondment experience more HELP assisted creep blunting
8. Mechanical crack tip blunting may also occur by severe mechanical loading such as those imposed on a pipeline during hydrostatic testing or by pressure spikes during regular pipe operation. Such severe blunting may prevent the mechanical re-initiation of crack propagation at benign loading conditions. Crack re-initiation may require very severe loading conditions, such as high K_{max} and moderate ΔK or low K_{max} and high ΔK , or a high number of stress cycles
9. Careful analysis of test results revealed that crack re-initiation conditions at a blunted tip may be independent of whether blunting was environmentally or mechanically induced. The conditions at which re-initiation occurred were independent of the CO₂ concentration in the groundwater and was also independent of the loading frequency
10. Depending on the operating mechanical loading and/or environmental conditions, crack re-initiation from a dormant state may occur by either
 - a. A dissolution controlled mechanism if mechanical loading is benign and an aggressive environment is present

- b. Purely mechanically driven crack growth if ΔK or R-ratio are severe enough
 - c. By a synergistic effect of environmental and mechanical factors, particularly by hydrogen enhanced crack propagation and mechanical (cyclic) loading. Such synergy results in crack re-initiation at mechanical loading conditions that would have otherwise been below the threshold required for crack propagation
11. Generally, on crack re-initiation, a discontinuous type of crack propagation occurs, moving in discontinuous steps that correlate well with the average grain size. Each step in crack propagation required between 500-1000 stress cycles at a stress ratio of 0.22
 12. Generally the dissolution mechanism contributes significantly to crack tip blunting but has a negligible effect on actual crack propagation. In high CO₂ environments, unless severe mechanical loading is applied, crack propagation may occur by a predominantly dissolution controlled mechanism. However, even with high CO₂ concentrations, the associated growth rates are very low
 13. In the normal pipeline operating stress range (up to 75% SMYS), although increasing CO₂ concentration in the simulated groundwater generates a more aggressive (acidic) solution with more hydrogen ions, it may not necessarily result in a higher crack propagation rate as the increased hydrogen ion concentration may cause increased crack tip blunting by a dissolution mechanism as well as increased hydrogen enhanced localized plasticity which intensifies crack tip blunting. However, the opposite trend was observed at higher stresses. This deviation is probably due to the fact that higher stresses cause fresh metal surface to be exposed to the solution so rapidly that the dissolution rate significantly lagged the rate of crack propagation
 14. The application of moderate to high cathodic protection could increase the environmental driving force for crack propagation by up to a factor of three. This could aid crack re-initiation at more benign loading conditions where crack re-initiation would otherwise not have occurred. Such increased environmental driving force for crack propagation could also help to sustain continued crack propagation at loading conditions where crack propagation would otherwise not have occurred

15. Contrary to expectations that the highest crack growth rate would always occur at the location with the highest applied cathodic potential, due to higher hydrogen segregation, the highest growth rate was found at 75 mm from the open mouth with a cathodic potential of -0.9 V although it was highest at the OM for -1.2 V applied CP. This was related to the balance between the availability of electrons and hydrogen ion migration within the solution. This observation is consistent with the often observed close proximity between stress corrosion crack colonies and pit colonies in field excavations of SCC sites. This would suggest that the electrons used in the reduction of hydrogen in crack colonies might have been furnished at nearby pitting sites, hence both features are necessary for sustaining the growth of the other. This conclusion is only a hypothesis at this stage; further studies are being carried out to explore this hypothesis and will be reported in a future study
16. Generally, surface (semi-elliptical) flaws grew at a slower rate than through-thickness flaws in a near-neutral pH SCC environment. For a CT specimen normally used to simulate through-thickness cracks, the hydrogen concentration in the solution in contact with the crack front is fairly uniform. Hence, atomic hydrogen concentration at the sample surface along the crack path is fairly uniform. However, for surface flaws, there is a concentration gradient between the concentration of hydrogen at the sample surface and the tip of the crack in the depth direction. Therefore growth enhancement is not uniform along the crack path. This and other effects such as the tunneling effect could lead to a slower rate of crack propagation for surface type flaws

8.2 Recommendations for future work

1. The results reported in this thesis provide new information on the role of hydrogen in stress corrosion cracking. However, no study was carried out to quantify the influence of testing conditions and distance from the open mouth on the amount of hydrogen present within the metal lattice. The quantification of hydrogen concentration within the metal lattice under the conditions used in this study will help to properly determine possible variations in the value of α , the environmental factor, used in the corrosion-fatigue equation. This could help to determine more accurate crack growth curves than those determined in this study
2. Although SCC initiation was not part of the objectives of this study, the discovery of microcrack colonies close to the final rupture point suggests that it might indeed be possible to initiate SCC cracks under static or near static loading conditions. It has been well reported that NNPHSCC has not been successfully initiated under static loading conditions in laboratory studies. Perhaps, local plastic deformation is the missing factor in the studies that have attempted to initiate NNPHSCC cracks under static loading in the laboratory. Further work should be carried out to verify the possibility of SCC initiation in locally deformed specimens under static or near static loading in near-neutral pH environments
3. In actual coating disbondment in the field, the weight of the top soil on top of the pipeline squeezes the coating against the actual metal surface. Therefore except for regions with wrinkles and puffs, the gap size between the disbonded coating and the pipe could be very small. Previous studies have well established the fact that the gap size can have a significant effect on the nature and concentration of the species trapped under the disbondment. This could have a significant effect on the crack growth behavior. It is therefore very important to study the effect of variations in gap sizes on the variation in crack growth behavior under a long disbondment using a slightly modified version of the test set up used in this study
4. Actual pipelines do not typically experience symmetric loading spectra such as the ones used in this study. Rather, actual loading rates are variable in the field. Loading spikes are known to have a significant effect on crack growth behavior. It is therefore important to

study the effect of pressure spikes and/or under-loadings on the variation in crack propagation rates with distance from the open mouth of a disbondment, using the setup designed for this study

APPENDIX A

A short paper on the variation in hydrogen permeation behavior with distance from the open mouth of a coating disbondment

A1.0 Introduction

Oil and gas pipelines are very crucial in the delivery of oil and gas components to the end users. However, the protective coating usually applied to the surface of the pipelines at installation sometimes fails either due to imperfections during application or mechanical/chemical damage over time [1]. When this happens ground water is able to gain access to the holiday and the adjoining disbonded surface under the coating . In such situations where the coating is compromised, a near-neutral pH environment enriched with carbonate and bicarbonate species may develop [2]. This environment has been found to support the development of near-neutral pH stress corrosion cracking (NNPHSCC) [3] .

It has been shown that the presence of CO₂ generated from microbial activity and by decaying organic matter is crucial to the process [1, 4-16]. The dissociation of CO₂ leads to the generation of carbonic species and hydrogen [5, 6]. The hydrogen generated from this reaction has been shown to play a crucial role in the development and propagation of NNPHSCC [17, 18]. Although there is no consensus on the exact mechanism by which hydrogen influences crack propagation, it is well established that hydrogen enhances crack propagation by helping to maintain a sharp crack tip which is crucial for rapid crack propagation [4, 17, 19, 20, 20-23].

Although several studies have been conducted on the role of hydrogen in the development and propagation of SCC cracks, most studies have been unable to explain why some cracks propagate while most cracks remain dormant in the field. Most studies have focused on the effect of microstructure or chemical species in the solution on the crack initiation or propagation. Others studied the effect of hydrogen using slow strain rate tests or compact tension specimens,

often neglecting the effect of spatial separation of cracks combined with the effect of variation in local environments with distance from the open mouth of the disbondment on crack initiation and propagation. Also, there has been no systematic study to look at the effect of variations in the concentration of CO₂ in soil solution on hydrogen assimilation into pipeline materials, particularly one that considers the effect of spatial separation from the open mouth on hydrogen enhancement effect.

This study aims to provide additional information on the influence of hydrogen in the propagation of NNPHSCC cracks in a near-neutral pH environment using the hydrogen permeation method. Specifically, the effect of the spatial separation of cracks from the open mouth and the resulting variations in the local environment under the disbondment on the contribution of hydrogen to crack propagation in a near-neutral pH environment was studied.

A2.0 Experimental method

Samples were machined from a section of X-65 pipeline steel removed from service, but only sections unaffected by mechanical deformation were used. Test samples were milled into rectangular plates measuring 257 mm X 63 mm X 2 mm (LxWxT).

A test cell was made out of acrylic to form a modified version of the Devanathan permeation test setup, Figure A-1. The charging side of the test cell consists of two chambers: the inner chamber, called the shielding, was designed to simulate the solution trapped in the disbonded coating crevice while the outer chamber was designed to simulate the bulk surrounding soil solution. The inner tube was selected to represent a 10 mm wide coating disbondment. The bulk solution in the outer tube was sparged with a CO₂/nitrogen mix, fed in through openings at the bottom of the cell, so that CO₂ can only diffuse into the simulated disbondment from the open mouth.

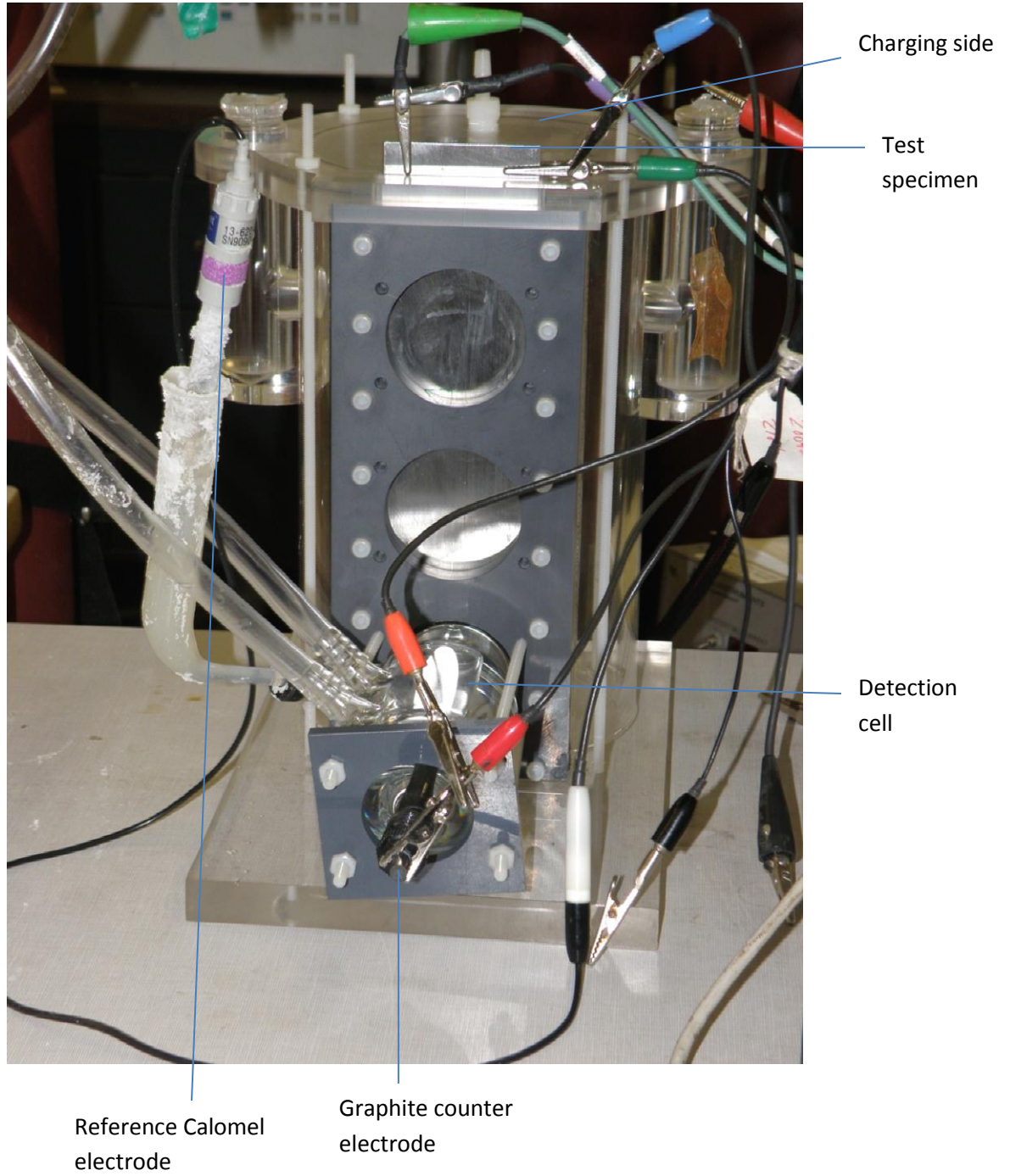


Figure A-1: Test setup

The detection side consisted of a round glass cell that exposes just a 3 cm diameter of the sample surface on the detection side to the oxidizing solution such that hydrogen permeation was measured over this area alone. The glass cell was filled with de-aerated 0.2M NaOH solution to oxidize hydrogen exiting the sample surface on the detection side. A 100% N₂ gas was continuously bubbled through the NaOH solution to ensure continued de-aeration of the oxidizing solution. An anodic potential of 100mV was applied on the detection side using a counter-reference electrode arrangement. Usually, the glass cell was filled with the solution for 30 min. to ensure that a protective film is formed, then the anodic potential is applied to stabilize the protective film for 24 h before the charging side is filled with the test solution.

During test cell assembly, the flat specimen is secured against the inner shielding with screws, so that the X65 plate is in direct contact with the solution trapped inside the simulated disbondment. However the charging side was initially kept empty. The detection side is then set up. After, the detection side is filled with NaOH and conditioned for 24hrs, and a very low steady current is obtained, the flat samples were then exposed to the corrosion media on the charging side by filling with C2 solution (0.0035 KCl, 0.0195 NaHCO₃, 0.0255 CaCl₂.H₂O, 0.0274 MgSO₄.7H₂O, 0.0606CaCO₃ g/l). Prior to each test, both sides of the sample were cleaned in acetone to de-grease them and then cleaned in ethanol several times before the setup is assembled. This procedure is repeated three times to obtain permeation currents from three locations corresponding to the open mouth, 75 mm from the open mouth and 150 mm from the open mouth. A fresh solution was always used for the test at each location. While the test is being carried out at one location the surface of the sample at the other locations are masked off with a double sided tape while a metal sleeve is glued over the surface of the tape to ensure a conductive path for the applied cathodic potential. A photograph of a test set up is shown in Figure A-1.

A reference (saturated calomel electrode) and counter electrode (platinum mesh) arrangement was used to apply cathodic protection to the sample. Cathodic protection was applied at the open mouth just above the topmost crack. An EG&G potentiostat operating in constant voltage mode was used to

apply cathodic protection voltage of -1.2V and -0.9V. Cathodic protection was applied only on the charging side of the test sample.

A matrix of test conditions used in this study is shown in Table A-1. The hydrogen flux measured during the test was used to determine the effective diffusivity of hydrogen through the metal lattice using the breakthrough time method using the relationship:

$$D_{eff} = \frac{L^2}{15.3t_b} \dots\dots\dots A.1$$

where L is the plate thickness, and t_b is the breakthrough time.

Table A-1: Test Matrix

| Test | Gas | Potential (V) vs SCE |
|----------|---------------------|----------------------|
| Test I | 5% CO ₂ | OCP |
| Test II | 5% CO ₂ | -1.2V |
| Test III | 5% CO ₂ | -0.9V |
| Test IV | 20% CO ₂ | OCP |

A3.0 Results and discussion

The permeation curve at open circuit potential for the 5% CO₂ environment (Test I) is shown in Figure A-2. The figure shows only a minor difference in the peak permeation current at all three locations under the disbondment. It is obvious that even with the minor difference in the peak permeation current, there is still a peak current trend suggesting that highest peak current occurs at the open mouth while the lowest peak current occurs at the far end of the disbondment. However, the curves shows a slightly longer breakthrough time at 75 mm from the open mouth compared to the other two locations. The effective diffusion coefficients were determined using the breakthrough time procedure. Comparison of the effective diffusion coefficient shows that the highest flux is obtained at the open mouth while there is a general decrease towards the far end of the disbondment. However, the lowest diffusion coefficient was obtained at 75 mm from the open mouth (midway inside the simulated disbondment). This is probably due to more rapid film formation at the 75 mm location which probably interfered with the extent of surface coverage by hydrogen atoms at that location. It is also obvious from Figure A-2 that there is a continuous rapid drop in the permeation current once the peak current has been reached at all three locations. However, the most rapid drop in permeation current occurred at the far end of the disbondment while the slowest drop occurs at the open mouth of the disbondment.

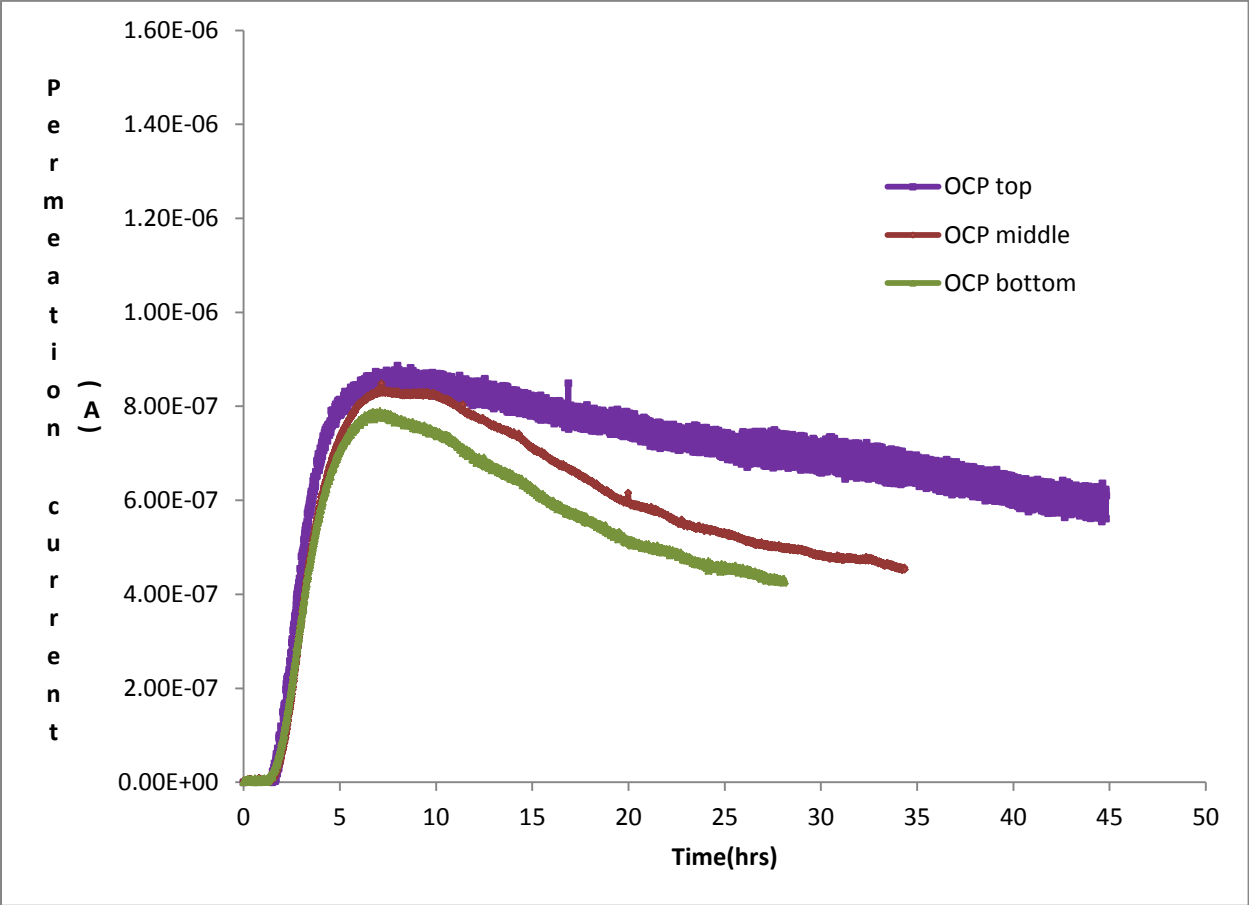


Figure A-2: Variation in permeation behavior with distance from open mouth at OCP in test I

Figure A-3 shows the permeation curve when a cathodic protection potential of -1.2V is applied in a 5% CO₂ environment (Test II). It is clear that the highest peak permeation current is obtained at the open mouth while the lowest peak permeation current was obtained at 75 mm from the open mouth. This test was repeated with a slightly thinner sample (1.5 mm thick) and the confirmation curves are shown in Figure A-4. The repeat test confirms the trend from the earlier test. Again, the highest breakthrough time was obtained at 75 mm from the open mouth while the lowest breakthrough time was obtained at 150 mm from the open mouth. Comparison of the effective diffusion coefficient (Table A-2) shows that the highest diffusion coefficient is at the far end of the disbondment while the lowest is at 75 mm from the open mouth. The diffusion coefficient at the far end of the disbondment is higher than that at the open mouth. Once the peak current is reached, it is obvious that there is only a small drop in the permeation current at all three locations, after which the permeation current tends to remain high, unlike what was observed at open circuit potential. This could have a significant effect on the growth of stress corrosion cracks in a near neutral pH environment. The fact that the permeation current remained high after the peak current is reached suggests that at -1.2V, a rather high hydrogen assimilation rate could be maintained for an extensive period when samples are loaded in a near neutral pH environment at high cathodic potentials. This means that if a crack exists in a region experiencing such a high cathodic potential on an actual pipeline, then the material locally experiences a high hydrogen enhanced crack propagation compared to a crack located in a region at open circuit potential. Since the potential at the open mouth remained substantially higher than those at 75 mm and 150 mm from the open mouth, the most intense hydrogen effect will be felt at the open mouth. Thus, should a crack exist there, the crack may experience a high rate of crack propagation.

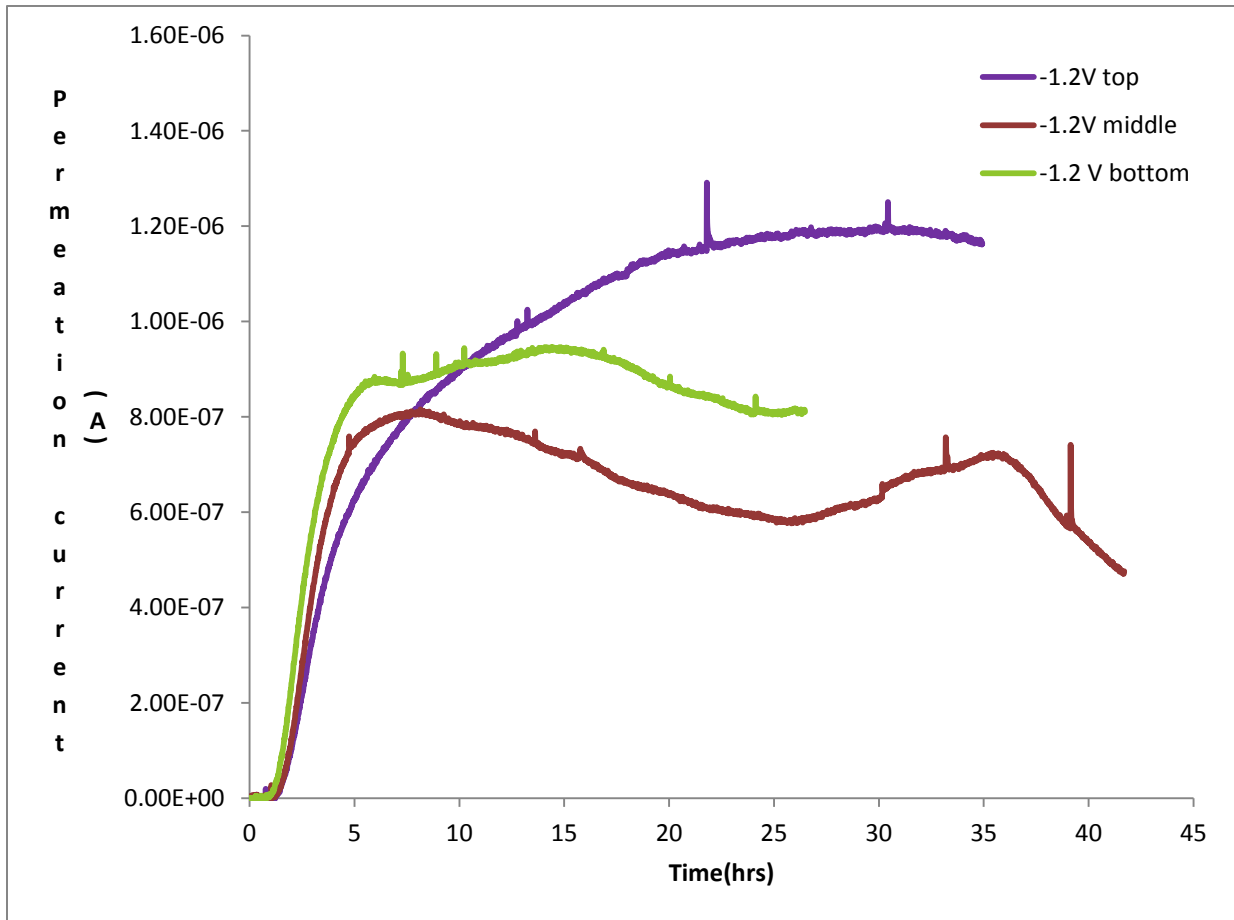


Figure A-3: Variation in permeation behavior with distance from open mouth at -1.2V (Test II)

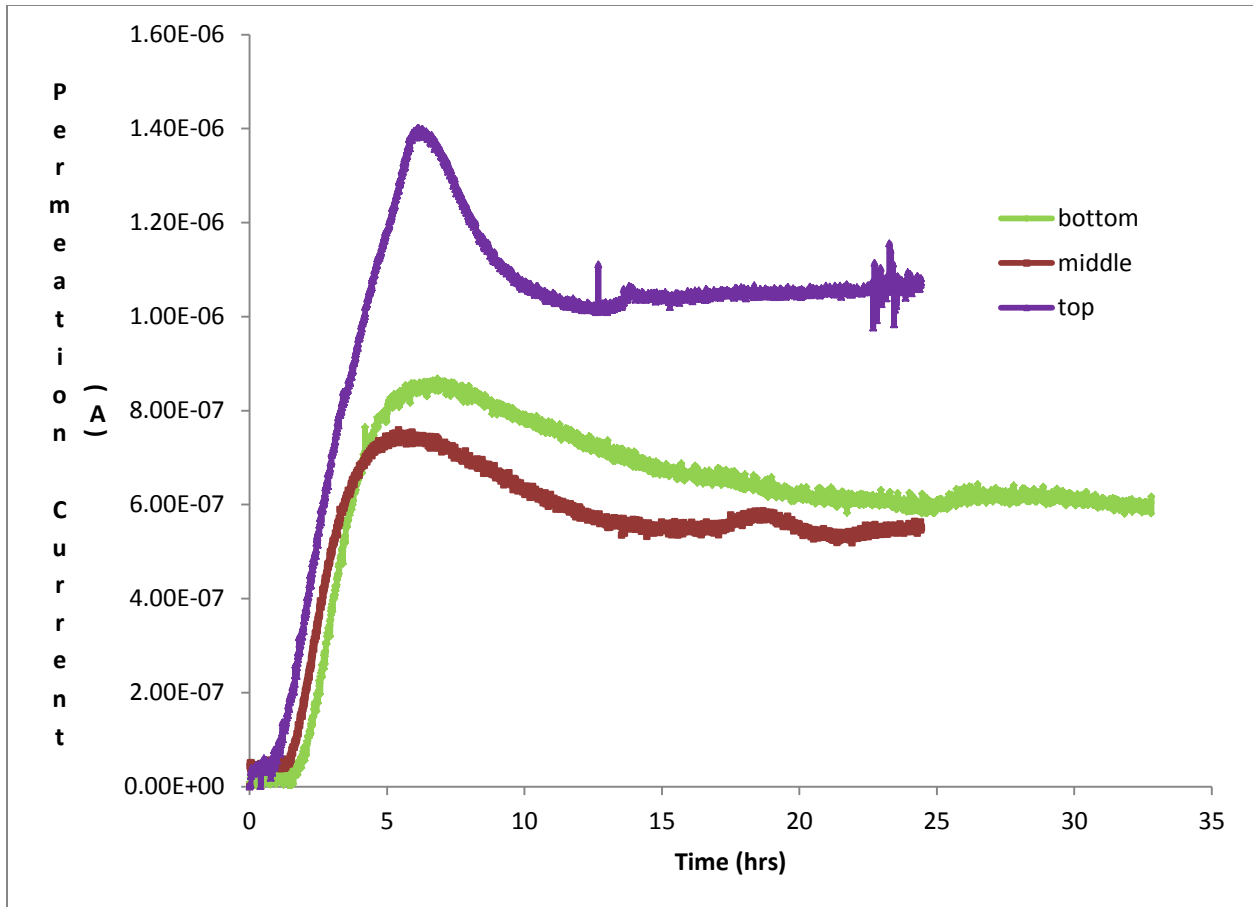


Figure A-4: Repeat test of permeation behavior at -1.2V

Table A-2: Summary of diffusion coefficients

| Distance from open mouth (mm) | 5% CO ₂ | | | 20% CO ₂ |
|-------------------------------|--------------------|------------|------------|---------------------|
| | OCP | -1.2V | 0.9V | OCP |
| 0 | 3.9314E-07 | 4.6685E-07 | 3.9314E-07 | 5.3905E-07 |
| 75 | 4.2167E-07 | 4.5467E-07 | 4.2167E-07 | 4.9328E-07 |
| 150 | 3.6060E-07 | 5.4466E-07 | 3.6060E-07 | 4.8414E-07 |

The results at an applied potential of -0.9V (Test III) are shown in Figure A-5. The calculated diffusion coefficients suggest that the highest diffusion rate occurs at 75 mm from the open mouth while the lowest diffusion rate occurs at 150 mm from the open mouth. Figure A-5 shows that the highest permeation peak occurs at the open mouth while the lowest permeation peak occurs at the far end of the disbondment. Similar to the case where a potential of -1.2V was applied the curves at both the open mouth and 150 mm from the open mouth suggest that no drop in the permeation current occurred once the peak permeation current is attained. Rather, once the peak permeation current is reached at these two locations, the curve seemed to remain at or very near the peak values. Only the curve obtained at 75 mm from the open mouth showed a deviation from this behavior. At this location, once the peak current is reached there is a rapid drop in permeation current similar to those observed at OCP in the 5% CO_2 environment.

Figure A-6 shows the permeation curves for tests carried out in the 20% CO_2 sparging gas environment (Test IV). The peak permeation current reached in this test is almost double the peak current reached at OCP in the 5% CO_2 environment. Similar to the previous OCP test at 5% CO_2 , the permeation current drops rapidly, once the peak current is attained, and seems to drop to a lower plateau close to the peak current in the 5% CO_2 OCP test. The effective diffusion coefficient also decreases consistently from the open mouth to the far end of the disbondment. The diffusion coefficients in the 20% CO_2 environment are generally higher than those obtained in the 5% CO_2 environment, including when a cathodic potential of -1.2V is applied. This suggests that the hydrogen generated from increased CO_2 dissociation is higher than the extra amount of hydrogen generated from water dissociation at the open mouth when a cathodic potential of -1.2V is applied.

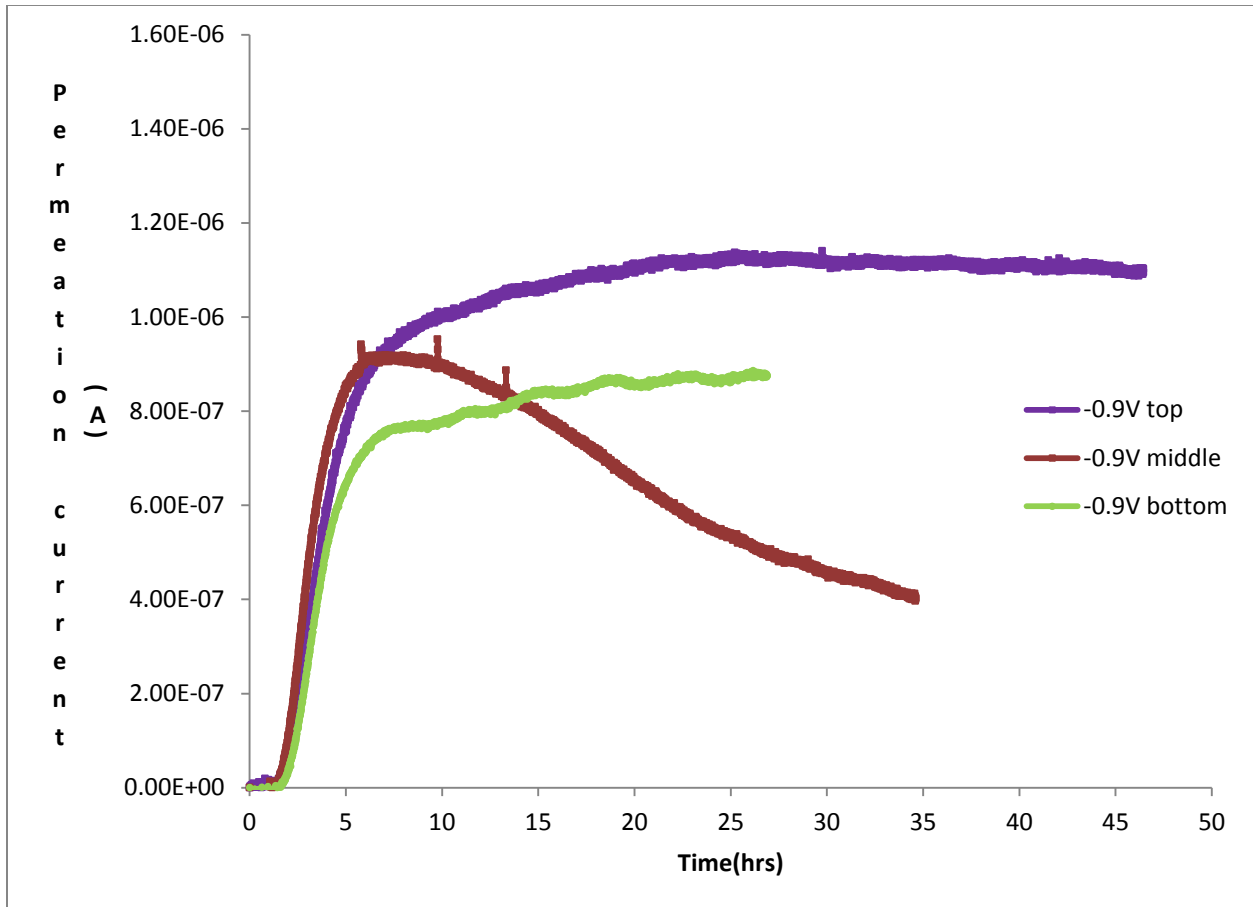


Figure A-5: Variation in permeation behavior with distance from open mouth at -0.9V (test II)

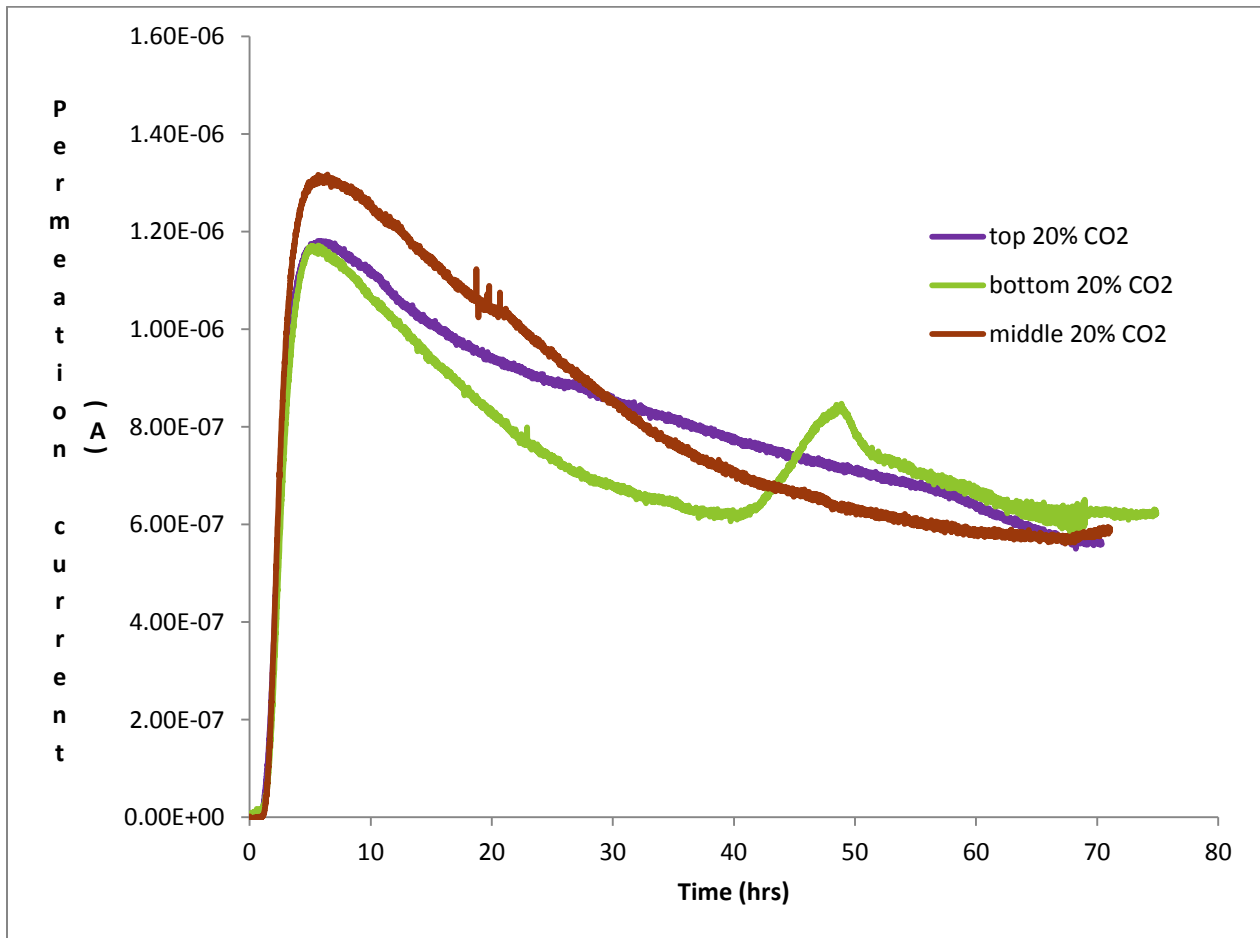


Figure A-6: Variation of permeation behavior with distance from the open mouth at OCP in 20% CO₂ environment.

Park *et al.* [24] observed in their hydrogen permeation tests, carried out in a hydrogen sulphide environment, that permeation curves showing rapid drop in permeation currents after the peak current is attained, similar to those obtained at OCP and at 75 mm from the open mouth at -0.9V in this study, represent situations where unstable behavior occurred at the sample surface due to the formation of sulphide scales. If it is assumed that similar reasons are responsible for this type of behavior in the present study, then the results suggest that the observed drop in permeation current at OCP and midway inside the disbondment at an applied potential of -0.9V may be due to the formation of protective films or corrosion products on the surface of the sample.

Since the sparging gas is always purged inside the outer chamber, hydrogen from the hydrolysis of CO₂ can only migrate into the disbondment through the open mouth. Therefore there should be a higher hydrogen concentration at the open mouth and the concentration should drop progressively towards the bottom of the disbondment. At an applied potential of -1.2V and -0.9V, hydrogen ions should preferably migrate to the open mouth because hydrogen ions being positively charged are attracted towards more cathodic potentials. However, it has been shown in previous studies that higher cathodic potentials intensify the formation of carbonates. He *et al.* [25] showed that the presence of carbonate films on the surface of a pipeline steel specimen reduces the flux of hydrogen through the material. Meng *et al.* [22] also determined that the presence of corrosion deposits on steel surface has the tendency to reduce the absorption and permeation of hydrogen atoms due to the increased spatial separation of cathodic and anodic reaction sites. Visual examination revealed the presence of white particles which are known to be calcium carbonates on the sample surface at the open mouth when both cathodic potentials

were applied. At -1.2V carbonate deposition was also observed at 75 mm from open mouth but none was observed at the same location at -0.9V.

The formation of carbonates could reduce the hydrogen coverage on the surface of the test specimen. This would reduce the rate of adsorption. If these carbonates tend to break down periodically or the carbonate formed is porous, then it is possible that equilibrium may be reached between the rate of hydrogen permeation and carbonate formation resulting in a steady rate of permeation with time as observed with -1.2V cathodic protection. However, if a stable non porous film is formed on the sample surface, then the buildup of such film could cause a drastic continuous reduction in the permeation current as seen as OCP and at 75 mm from open mouth in the -0.9V test. The lower effective diffusivity coefficient at the open mouth in -1.2V compared to that at the far end under the same potential probably confirms the fact that carbonates formed at the open mouth tend to increase the breakthrough time. However, the fact that the peak current and the final current plateau observed at the open mouth are significantly higher at -1.2V probably points to the fact that the breakthrough effect is only a short time event. Once an equilibrium is reached between the rate of carbonate formation/deposition, the total hydrogen contribution to SCC could be quite significant.

A4.0 Relevance of hydrogen permeation study to crack growth study

Although the data presented in this study may appear inconsistent at first, careful consideration of the results reveal some important relevance to the previous studies present in previous chapters:

1. Comparing the data at OCP, both the 5% CO₂ and the 20% CO₂ data confirms that:

- a. Increased CO_2 concentration could significantly increase the hydrogen flux through the steel lattice as assumed in Chapters 4 and 5. However, as explained in chapter 4, this could be accompanied by increased crack wall/ crack tip dissolution and enhanced room temperature creep. Both of these factors could result in significant crack tip blunting. This may retard crack propagation and may drive a crack towards dormancy under benign loading conditions.
- b. In both the 20% CO_2 and 5% CO_2 tests, the permeation current falls rapidly from its peak value to much lower values such that once the lattice and the hydrogen trap sites are filled, the rate of flux through the lattice in the long run are quite similar. However, this does not necessarily mean that for a growing crack , both the 20% and the 5% CO_2 environments always produce the same level of enhancement.

As far as crack growth is concerned, it is the amount of hydrogen that segregates to the hydrogen process zone ahead of the crack tip that determines the extent of crack growth enhancement. For a moving crack, the effectiveness of hydrogen delivery to the moving process zone can significantly determine the extent of growth enhancement. The result in chapter 5 confirms that when loading conditions are aggressive enough, such that there is insufficient time for dissolution and low temperature creep to cause significant blunting at the tip of the moving crack, a higher CO_2 concentration may result in a more significant crack growth enhancement than a lower CO_2 concentration. However, at more benign loading conditions, the opposite trend could be observed since there is

more time for crack tip dissolution and low temperature creep to cause more crack tip blunting.

2. Contrary to OCP results, when a cathodic potential of -1.2V is applied, the permeation current only drops slightly after the peak current is reached. Thus the application of an applied cathodic potential may cause the permeation current, hence hydrogen flux rate through the lattice to remain high. This is consistent with the higher crack growth rates at the open mouth obtained in the studies where a cathodic potential of -1.2V was applied. Also, at 75 mm and 150 mm from the open mouth, the peak currents are significantly lower than at the open mouth. The levels to which the permeation current drops at these two locations are also significantly lower than at the open mouth. This explains the lower growth rate at the two locations compared to the open mouth. The similarity in the values to which the permeation current settles after the peak value also explains the similarity in the growth rates observed at these two locations.
3. Comparison of the permeation curves at an applied cathodic potential of -0.9V and -1.2V reveals that the peak current at the open mouth is lower at -0.9V than at -1.2V . This explains the lower growth rates at -0.9V compared to -1.2V . Also, it is evident that at both the OM and the far end of the disbondment, at an applied potential of -0.9V , the permeation currents also remain high once the peak value is reached. This also explains the higher crack growth rate at an applied cathodic potential of -0.9V compared to the OCP crack growth rates.

A5.0 Conclusion

The main findings of this study include:

1. Although the highest hydrogen concentration should exist at the open mouth of the disbondment, the highest permeation current and diffusion coefficients may not necessarily occur at the open mouth.
2. Surface conditions, which are strongly influenced by local potential, could significantly modify the local hydrogen diffusion into the sample.
3. At OCP, in the 5% CO₂ environment, the lowest permeation current and diffusion coefficients are obtained at 75 mm from the open mouth rather than at 150 mm from the open mouth. However, in the 20% CO₂ environment, the lowest diffusion coefficient was obtained at 150 mm from the open mouth.
4. Permeation currents and diffusion coefficients in 20% CO₂ environment are significantly higher than in the 5% CO₂ environment at open circuit
5. Permeation currents tend to remain high when a cathodic potential is applied compared to OCP results. This suggests that cathodic protection aids hydrogen permeation over an extensive period.
6. At -0.9V, the highest diffusion rate occurred at 75 mm from the open mouth. This was related to the formation of stable films at the surface of the sample at this location.

References

- [1] National Energy Board, 1996, "Public Enquiry Concerning Stress Corrosion Cracking on Canadian Oil and Gas Pipelines," Report # MH-2-95.
- [2] Canadian Energy Pipeline Association, 1996, "Submission to the National Energy Board," Proceeding MH-2-95, .
- [3] Parkins, R. N., 2000, "A review of stress corrosion cracking of high pressure gas pipelines," NACE International, Corrosion 2000; Paper no. 00363.
- [4] Parkins, R. N., Blanchard, W. K. J., and Delanty, B. S., 1994, "Transgranular Stress Corrosion Cracking of High-Pressure Pipelines in Contact with Solutions of Near Neutral pH," Corrosion (USA), **50**(5) pp. 394-408.
- [5] Beavers, J. A., and Harle, B. A., 2001, "Mechanisms of High-pH and Near-Neutral-pH SCC of Underground Pipelines," Journal of Offshore Mechanics and Arctic Engineering, **123**pp. 147-151.
- [6] Asher, S., . Singh, P., Colwell, J., 2005, "Crack Initiation of Line Pipe Steels in Near-Neutral pH Environments," *16th International Corrosion Congress*. 2005. Beijing, China .
- [7] Fang, B. Y., Atrens, A., Wang, J. Q., 2003, "Review of Stress Corrosion Cracking of Pipeline Steels in 'Low' and 'High' pH Solutions," Journal of Materials Science, **38**(1) pp. 127-132.
- [8] Beavers, J. A., and Worthingham, R., 2002, "The influence of soil chemistry on SCC of underground pipelines," 2002 International Pipeline Conference, Calgary, ASME, Paper no. IPC2002-27146.

- [9] Zheng, W., Revie, R.W., MacLeod, F.A., Dinardo, O., 1998, "Low pH SCC: Environmental effects on crack propagation", Catalogue no. L51791e, PRCI, Arlington, VA, USA.
- [10] Parkins, R.N., 1999, "A review of stress corrosion cracking of pipelines in contact with near-neutral (low) pH solutions," PRCI, Report for the Line Pipe Research Supervisory Committee of PRC International, Arlington, VA, USA.
- [11] Chen, W., and Zheng, W., 2005, "Progress in understanding of pipeline SCC: Initiation and propagation," Symposium on Pipelines for the 21st century, W. Chen, ed. pp. 419-416.
- [12] Beavers, J. A., Durr, C. L., Delanty, B. S., 2001, "Near-neutral pH SCC: crack propagation in susceptible soil environments," corrosion/2001, NACE, Houston, Paper No. 01217.
- [13] Wang, Y. Z., Revie, R. W., and Parkins, R. N., 1999, "Mechanistic aspects of stress corrosion crack initiation and early propagation," Corrosion '99, NACE, Houston, Paper no. 99143 .
- [14] Johnson, J. T., Durr, C. L., Beavers, J. A., 2000, "Effects of O₂ and CO₂ on near-neutral-pH stress corrosion crack propagation," High strength low alloy steels (SAHLS), Corrosion 2000, NACE International, Paper no. 00356.
- [15] Chen, W., King, F., Jack, T. R., 2002, "Environmental Aspects of Near-Neutral pH Stress Corrosion Cracking of Pipeline Steel," Metallurgical and Materials Transactions A, **33A**(5) pp. 1429-1436A.
- [16] Burstein, G. T., and Linter, B. R., 1999, "Reactions of Pipeline Steels in Carbon Dioxide Solutions," Corrosion Science (USA), **41**(1) pp. 117-139.

- [17] Cheng, Y. F., 2007, "Thermodynamically Modeling the Interactions of Hydrogen, Stress and Anodic Dissolution at Crack-Tip during Near-Neutral pH SCC in Pipelines," *Journal of Materials Science*, **42**(8) pp. 2701-2705.
- [18] Qiao, L. J., Luo, J. L., and Mao, X., 1998, "Hydrogen Evolution and Enrichment Around Stress Corrosion Crack Tips of Pipeline Steels in Dilute Bicarbonate Solution," *Corrosion*, **54**(2) pp. 115-120.
- [19] Gu, B., Yu, W. Z., Luo, J. L., 1999, "Transgranular Stress Corrosion Cracking of X-80 and X-52 Pipeline Steels in Dilute Aqueous Solution with Near-Neutral pH," *Corrosion (USA)*, **55**(3) pp. 312-318.
- [20] Cheng, Y. F., and Niu, L., 2007, "Mechanism for Hydrogen Evolution Reaction on Pipeline Steel in Near-Neutral pH Solution," *Electrochemistry Communications*, **9**(4) pp. 558-562.
- [21] Cheng, Y. F., 2007, "Analysis of Electrochemical Hydrogen Permeation through X-65 Pipeline Steel and its Implications on Pipeline Stress Corrosion Cracking," *International Journal of Hydrogen Energy*, **32**(9) pp. 1269-1276.
- [22] Meng, G. Z., Zhang, C., and Cheng, Y. F., 2008, "Effects of Corrosion Product Deposit on the Subsequent Cathodic and Anodic Reactions of X-70 Steel in Near-Neutral pH Solution," *Corrosion Science*, **50**(11) pp. 3116-3122.
- [23] Zhang, G. A., and Cheng, Y. F., 2009, "Micro-Electrochemical Characterization of Corrosion of Welded X70 Pipeline Steel in Near-Neutral pH Solution," *Corrosion Science*, **51**(8) pp. 1714-1724.

[24] Park, G. T., Koh, S. U., Jung, H. G., 2008, "Effect of Microstructure on the Hydrogen Trapping Efficiency and Hydrogen Induced Cracking of Linepipe Steel," *Corrosion Science*, **50**(7) pp. 1865-1871.

[25] He, D. X., Chen, W., and Luo, J. L., 2004, "Effect of Cathodic Potential on Hydrogen Content in a Pipeline Steel Exposed to NS4 Near-Neutral pH Soil Solution," *Corrosion*, **60**(8) pp. 778-786.

Appendix B

EXPERIMENTAL METHODOLOGY

B.1 Materials

For this study, X-65 pipeline steel received from Spectra Energy Transmission was used. This particular pipeline steel was chosen because it is one of the most common pipeline materials in service and has been identified with NNPHSCC in the field. The X-65 pipeline steel had a yield strength and tensile strength of 522.8 and 607.8 MPa, respectively. A section of this pipeline removed from service is being used for this study. Only sections that were unaffected by mechanical damage or corrosion damage were selected for test specimen fabrication. Alloy composition is given in Table B-1. A typical microstructure of the alloy is shown in Figure B-1.

B.2 Metallography

In order to reveal sample microstructure, representative samples were taken from the bulk alloy and standard metallographic preparations were carried out. All samples were mounted in bakelite and ground down to 1200 sand paper grit and polished on an emery cloth using 0.05 diamond paste. Polished samples were then etched using 2% Nital. Initial microstructure examination was carried out on an optical microscope. More detailed analysis was done by electron microscopy, using a EVO ZEISS electron microscope.

B.3 Sample preparation

B.3.1 Sample machining

Tensile specimens (Figure B-2) bearing three reduced sections were machined from the longitudinal direction of an X65 pipe section that had failed in service. Only pipe sections unaffected by NNPHSCC and other forms of corrosion, and external damage were used. Gauge sections were 23mm X 45mm X 9.2mm in dimension and identical semi-circular shallow notches, 0.2032mm wide, with dimensions $c=5\text{mm}$ and $a=2.5\text{mm}$ were made by electrical discharge machining (EDM) in the middle of each gauge section. Samples were taken from the circumferential direction of the pipe as shown in Figure

B-3. Prior to pre-fatigue cracking each sample is ground by hand to grit 1200 so pre-fatigue cracks can be easily examined under the light microscope.

Table B- 6: Alloy (X65) composition

| Element | Composition (wt %) |
|------------|--------------------|
| Carbon | 0.13 |
| Manganese | 1.55 |
| Copper | 0.05 |
| Niobium | 0.05 |
| Chromium | 0.08 |
| Molybdenum | 0.01 |
| Vanadium | 0.002 |
| Nickel | 0.05 |
| Aluminum | 0.042 |
| Titanium | 0.002 |
| Nitrogen | 0.009 |
| Iron | Balance |

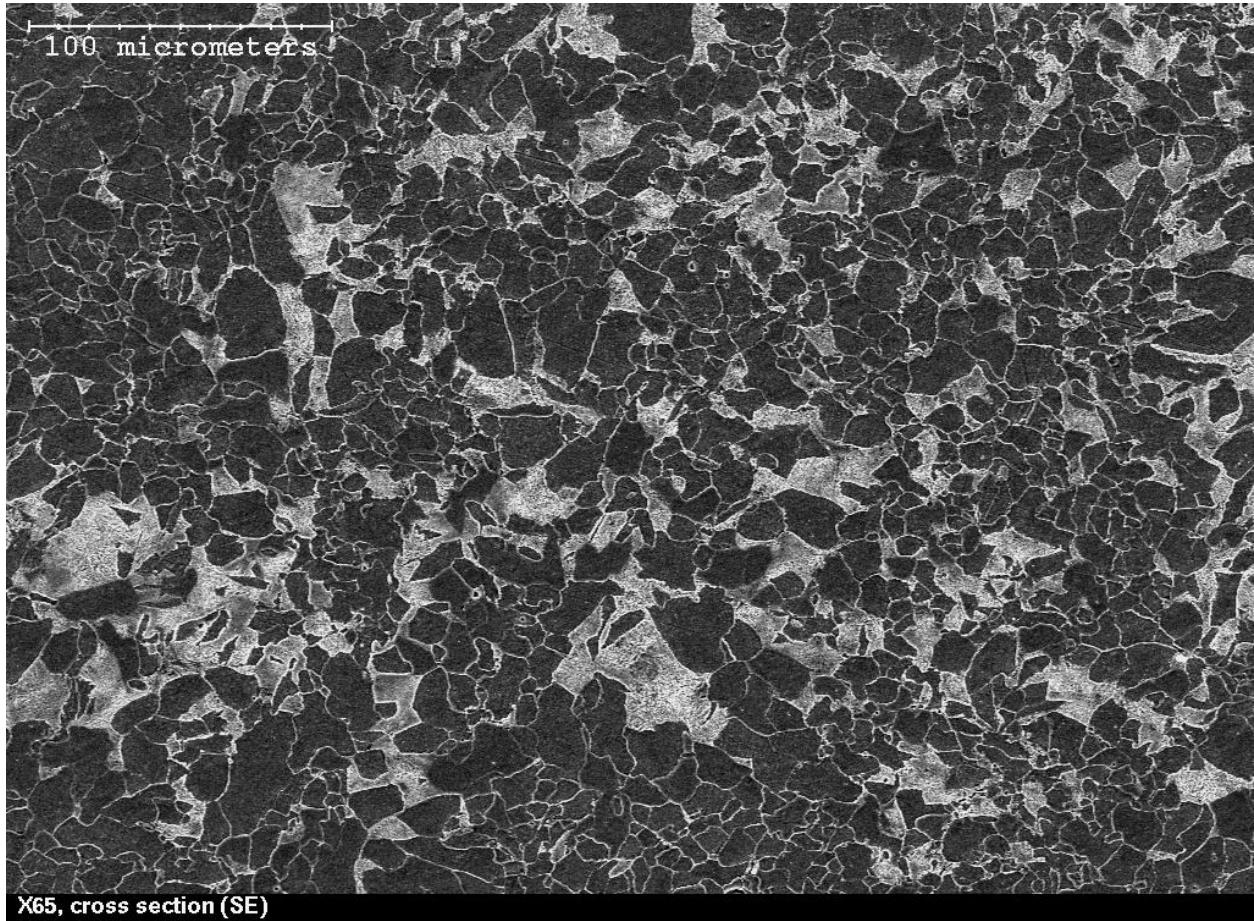


Figure B-1: Typical microstructure of the alloy X65 used in this study

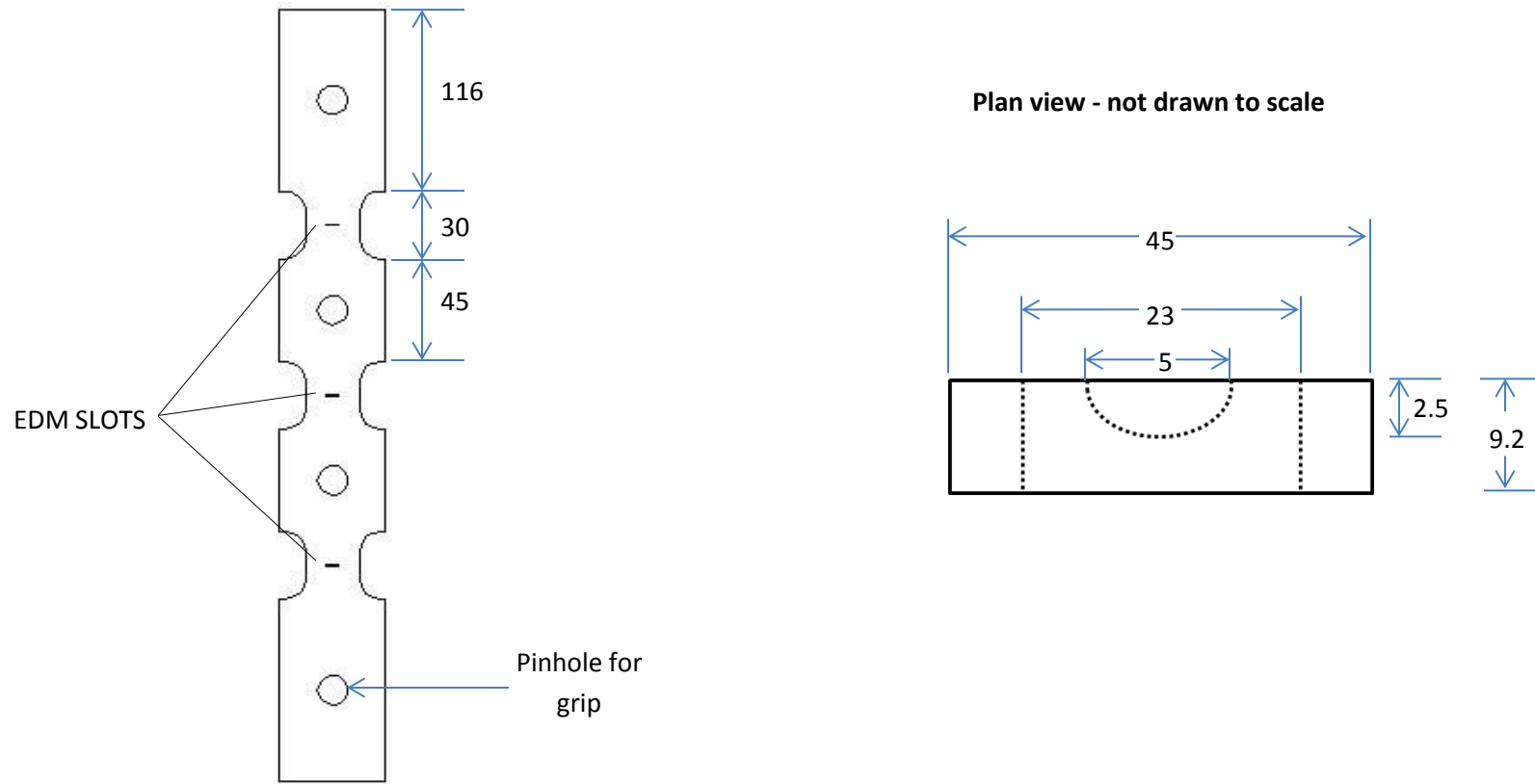


Figure B-2: Test sample designed for this stud

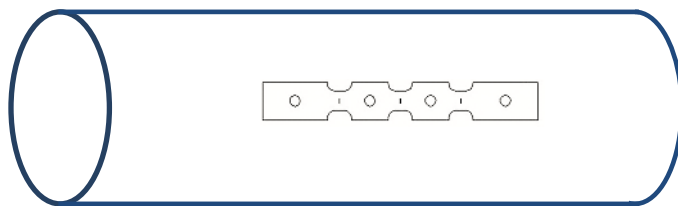


Figure B-3: Test sample orientation on pipe section

B.3.2 Sample Pre-fatigue cracking

Test samples were pre-cracked on a MTS machine frame before each test. Samples were all pre-cracked using a triangular wave with a maximum stress of 0.45SMYS and a stress ratio of 0.4. An optical microscope was used to monitor the pre-crack length by periodically removing the sample from the machine and examining under the microscope until the desired crack length is obtained.

B.3.3 Wire attachment

Before each test, thin strips of stainless steel films were spot welded to the on either side of the backside of each machine slot at a distance of 3mm from each slot. A copper crimp connector is then used to crimp wires to the backside of each wire for signal feedback to the potential drop system. A small 1mm steel plate tab is welded to the inner side of the lower and upper gauge area as shown in Figure B-4. A 0.5mm gauge single wire is then soldered to the small steel tabs. These are the current wires to supply the necessary constant current and potentials to the sample for potential drop measurements.

B.4 Test solution

To determine the growth behavior of the pipeline steel in a near neutral pH environment, the pre-fatigue cracked samples were exposed to the corrosion media in a sealed test cell and filled with C2 solution. C2 solution is a synthetic soil solution with the pH in the near-neutral pH range (5.5-7.5). Chemical composition of the solution is presented in Table B-2. The solution was purged for 48 hours with the N₂/CO₂ gas mixture to obtain the pH value of 6.29 before prior to testing.

B.5 Chemical analysis of test solution

Pre- and post- test chemical analysis of the test solution was contracted out to a commercial analytic company – Maxxam Analytics. Both the Edmonton and the Burnaby offices were used at different times.

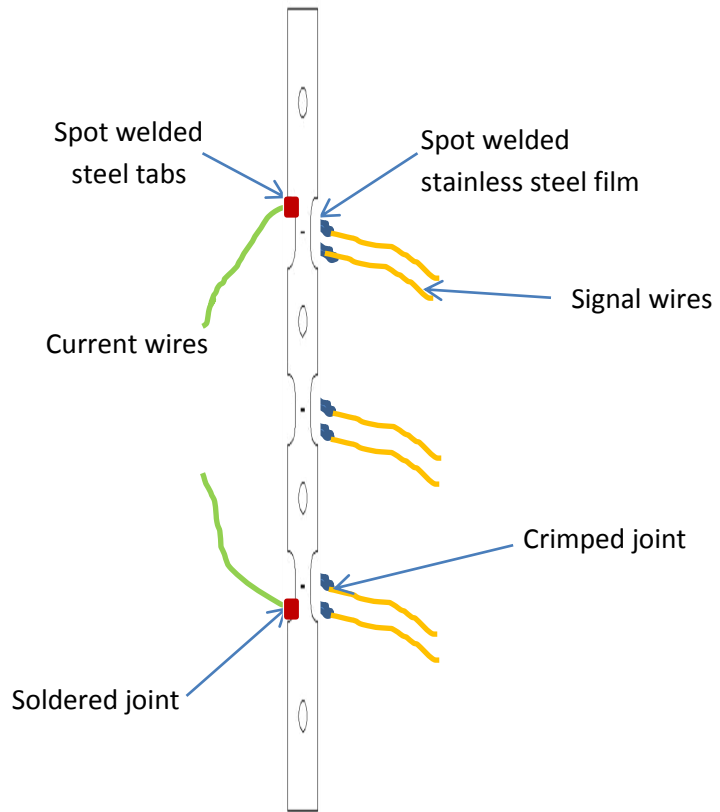


Figure B-4: Wire connections for test setup

Table B- 7: C2 solution composition (pH=6.29)

| Chemicals | Composition (g/L) |
|--------------------------------------|--------------------------|
| MgSO ₄ .7H ₂ O | 0.0274 |
| CaCl ₂ | 0.0255 |
| KCl | 0.0035 |
| NaHCO ₃ | 0.0195 |
| CaCO ₃ | 0.0606 |

B.6 Test Cell

After careful consideration of the details of actual coating disbondment on real pipelines, a revolutionary test setup was designed. A corrosion test cell consisting of two chambers was designed and fabricated from acrylate (Figure B-5). The inner tube, named the shielding, was designed to simulate coating disbondment at the surface of a pipe. The width of this inner tube was made adjustable so that coating disbondment of various sizes can be studied. The outer tube holds the bulk solution which simulates the surrounding soil around a pipe in the field while the solution contained in the inner shielding simulates the solution trapped between the coating and the pipe surface on an actual pipeline. The bulk solution in the outer tube was purged by a mixture CO_2 and N_2 bearing the required concentration of CO_2 and N_2 to balance. The gas mix was fed in through openings at the bottom of the cell, so that CO_2 can only diffuse into the simulated disbondment from the open mouth. The test solution could also be refreshed through these openings if necessary. The corrosion cell design allows for easy assembly and dis-assembly of the cell both pre- and post- test. All joints were O-ring sealed in order to ensure a hermetically sealed chamber. This also precludes the need for chemical sealants in assembling the cell.

B.7 Test assembly

The test specimen was carefully degreased and mounted in the metal grip jaw connector at the bottom of the cell using a dowel pin. The rest of the cell including the O-ring sealed cell bottom and the shielding were then carefully assembled. The O-ring sealing the disbondment from the main chamber is tested for leaks to ensure that the shielding is completely isolated from the main chamber at the bottom of the cell. The O-ring sealed top lid was then mounted in place and all tubing leading into the cell are sealed tight with silicone. All electrical connections for potential drop measurement were then completed. The cell is then filled with C2 solution and the sparging gas in then passed into the cell and the specimen is cyclically loaded.

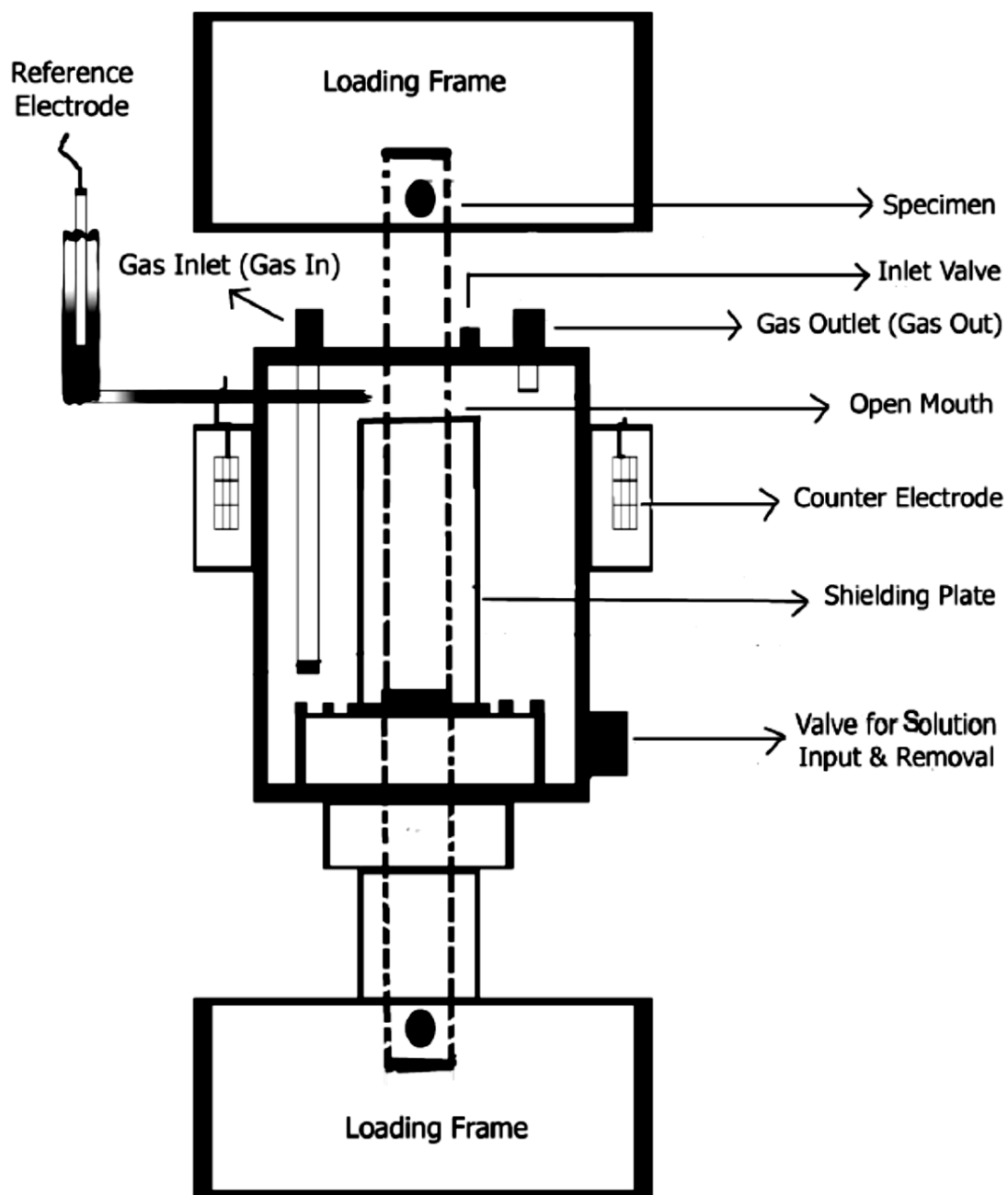


Figure B-5: Corrosion test cell used for this study

The original concept behind this cell design was originally conceived by Eslami^{***}. However slight modifications to the original design were deemed necessary. First, to accommodate the sample dimensions, especially with regards to the crack positions, the cell had to be made longer. Second, the length of the internal shielding had to be reduced in order to allow the positioning of the sample such that the application of cathodic potential right at the location of the open mouth crack was possible. Third, the specimens used in this study were thicker than those used in the Eslami study. To ensure a gap size of 10mm, the width of the internal shielding had to be modified. Lastly, the sample grips were redesigned as the original design led to very high shear stresses on the pin joints which caused pin rupture shortly after the commencement of cyclic loading.

B.8 Cathodic protection

A reference (saturated calomel electrode) and counter electrode (platinum mesh) arrangement was used to apply cathodic protection to the sample using a three electrode configuration. In all cases, cathodic protection was applied just above the open mouth of the inner shielding. An EG&G potentiostat operating in constant voltage mode was used to apply cathodic protection voltage for tests requiring cathodic protection. The specimen is the working electrode, two platinum gauzes are used as counter electrodes, and a saturated calomel electrode (SCE) is used as the reference electrode (Figure B-5). The platinum gauzes are separated from the main chamber of the corrosion cell in order to minimize contamination of solution by oxygen produced on the counter electrodes. To apply the cathodic protection voltage, a salt bridge comprised of Agar-agar saturated with KCl was used. Since only the potential at the open mouth is

^{***} Eslami, A., Chen, W., Worthingham, R.G., 2011, "Effect of CO₂ on Near-Neutral pH Stress Corrosion Cracking Initiation of Pipeline Steel," *Corrosion Science*, 53, pp. 2318–2327

controlled to the set potential, a long very narrow salt bridge was fabricated, so that it could be easily passed into the cell and used to determine the potential at other locations inside the disbondment.

B.9 Crack growth measurement

Crack growth rates were monitored using a self-assembled potential drop system through copper wire leads spot welded across the back of the EDM slots in each gauge section. As mentioned earlier, the thick wires were connected to the galvanostat supplying the current while the wires spot welded across the back of each slot was connected to the terminals of a volt meter with resolution in the millivolt range for measuring the voltage drop across the crack. A constant current of 20A was applied by the potential drop system in order to measure the potential drop across each crack. With crack propagation, the resistivity across the slot increases and higher potentials have to be applied to maintain the set constant current. This change in potential is read by the voltage meters connected to the leads across each slot.

B.10 Post-test Sample analysis

At the end of each test, the test cell is disassembled and the specimen is carefully removed.

1. The sample is dried thoroughly using a hand held blow dryer.
2. Samples cut into three smaller pieces using an hacksaw, taking care not to remove corrosion products around the test sections
3. Each test section is then examined using a SEM to determine the corrosion behaviour of at the sample surface. EDS analysis of corrosion products is carried out where necessary.
4. Prior to fracture surface examination, iron oxide-type corrosion products were removed using a rust remover solution composed of water (100ml), HCl (3ml), and cis-2-but-1-4-diol (4ml) (4ml). The surface of the each test section is then separately cleaned using the rust remover and each section is thoroughly dried.

5. The rust remover solution is preserved and filtered to separate out the corrosion products. The corrosion products are then dried by vacuum suction. The dried corrosion products are then examined using a XRD machine operating in the powder mode.
6. Initial fracture face examination was done using an optical microscope. More detailed examination of fracture surfaces was carried out using a Hitachi scanning electron microscope equipped with an energy dispersive x-ray spectrometer for chemical compositional analysis.
7. Crack morphology at the unpolished sample surface was carefully examined using the SEM.
8. The sample was then carefully grinded using standard procedures, without using water rather using methanol. The decision to use methanol instead of water was taken to prevent any dissolution or modification of the crack tip during grinding.
9. Polishing was then done using oil based diamond polishing fluid.
10. The crack morphology at the polished surface was then carefully examined using the SEM.
11. Each specimen section was then sectioned using electrical discharge machining (EDM), in order to be able to examine crack morphology in the depth (thickness) direction.
12. The transverse section of each specimen section was then polished using standard metallography procedures.
13. SEM microscopy was used to evaluate crack morphology in the transverse direction.
14. Once crack analysis using SEM is complete, the specimen was then quenched in liquid nitrogen and broken open by striking with a hammer, in order to expose the fracture surface so the fracture face can be studied by SEM microscopy.

15. Actual crack sizes, major and minor semi-axis dimensions of the semi-elliptical flaw, were determined by SEM microscopy. The SEM microscopy was also used to verify the initial flaw sizes.
16. SEM microscopy was used for complete fractographic analysis.
17. The crack dimensions obtained were then used to convert the potential drop data, obtained during the test, into actual crack sizes vs number of stress cycles.
18. This data was then converted into a crack growth, da/dN vs combined factors, plots.

B.11 Potential Drop Data analysis

Conversion of the potential drop readings to actual crack sizes was very tricky. None of the methods listed in literature was found to work due to the unique geometry of the cracks. A curve fitting method was therefore used for converting the potentials to actual crack sizes. The method used is summarized below. A typical potential drop curve is shown in Figure B-6.

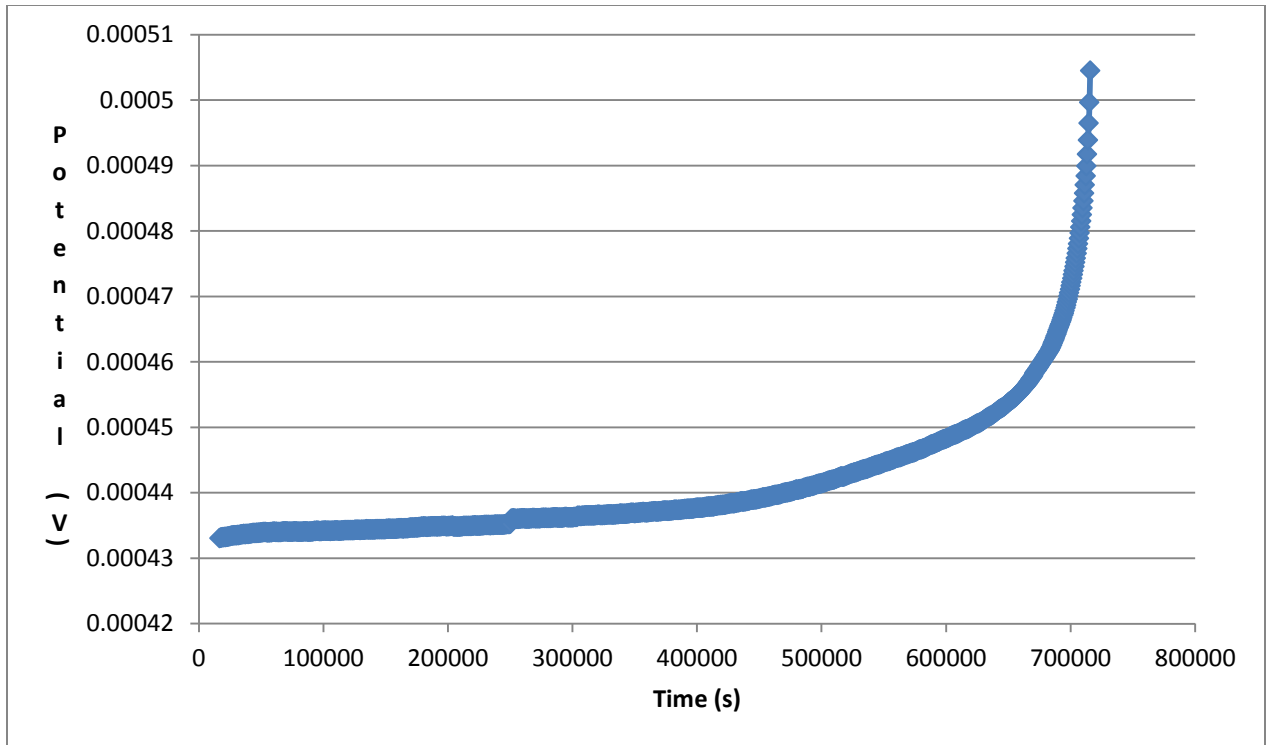


Figure B-6: Typical potential drop data

It is known that the potential drop is related to the crack area through the resistivity of the material through

$$\rho = \frac{RA^*}{l} \dots\dots\dots B.1$$

$$\rho = \frac{VA^*}{Il} \dots\dots\dots B.2$$

where R=material resistance, A* = area of the un-cracked ligament, l=length between the signal wires, I=applied current and V is the potential drop value.

$$V \propto \frac{Il\rho}{A^*} \dots\dots\dots B.3$$

But $A^* = A - A_c \dots\dots\dots B.4$

where A= cross sectional area of gauge area, A_c = the instantaneous crack area. Therefore

$$V \propto \frac{Il\rho}{A - A_c} \dots\dots\dots B.5$$

The initial and final crack sizes are known measurable values. Therefore the measured potential drop could be related to the point to point crack area. Since ρ is a finite value at every point on the curve, the numerator in equation B.5 could be treated as a constant so that

$$V = \frac{k}{A - A_c} \dots\dots\dots B.6$$

To convert the full potential drop data to actual cracks sizes, the following steps could be followed:

1. On the original potential vs time plot, select a few points (up to twelve was used)
2. Record the potentials and times at these points. Convert the times to number of stress cycles (N) that elapsed up to that point during the test.
3. Make a plot of the inverse of the initial and final remaining crack ligaments to the corresponding potential drop values to obtain a linear relationship between V and A*.
4. Use the relationship obtained in step 3 to determine an approximate value for A* for each of the points selected in step 2.
5. From each value of A* determine the value of A_c, the crack area.

6. A_c could then be related to the area of an semi-ellipse:

$$A_c = \frac{\pi ac}{2} \dots\dots\dots B.7$$

where a=crack depth and c= crack size measure along the major semi-axis at the sample surface.

7. Plot the initial and final values of 'c' against the initial and final values of 'a' to obtain a linear relationship between 'c' and 'a'.
8. The relationship obtained could then be used to substitute for c in B.7.
9. The resulting equation could then be solved for 'a' to obtain the crack depth at all the points selected in step 1.
10. Finally the values of 'c' could then be obtained using the relationship obtained in step 7.

The crack growth data obtained by the potential drop method were used to obtain crack growth rates per cycle da/dN, where the da/dN is the slope of the crack size vs number of cycle plot. Also corrosion fatigue analysis was carried out using Chen's corrosion fatigue model to calculate the so called combined factor $(\Delta K)^2 K_{max}/f^\alpha$. All data were finally presented as a da/dN vs. combined factor plot. K_{max} was calculated using the relevant fracture mechanics relationship for surface type flaws (Figure B-7). To calculate the K_{max} at the bottom of the pit a value of 90° is used for ϕ while a value of 0° is used to calculate K_{max} at the sample surface. A value of 0.1 was assigned to α as deduced by Chen and Sutherby.

B.11 Hydrogen permeation testing

A test cell was made out of acrylic to form a modified version of the Devanathan permeation test setup, Figure B- 8. The charging side of the test cell consists of two chambers: the inner chamber, called the shielding, was designed to simulate the solution trapped in the disbonded coating crevice while the outer chamber was designed to simulate the bulk surrounding soil solution. The inner tube was selected to represent a 10mm wide coating disbondment. The bulk solution in the outer tube was sparged with a

CO₂/nitrogen mix, fed in through openings at the bottom of the cell, so that CO₂ can only diffuse into the simulated disbondment from the open mouth.

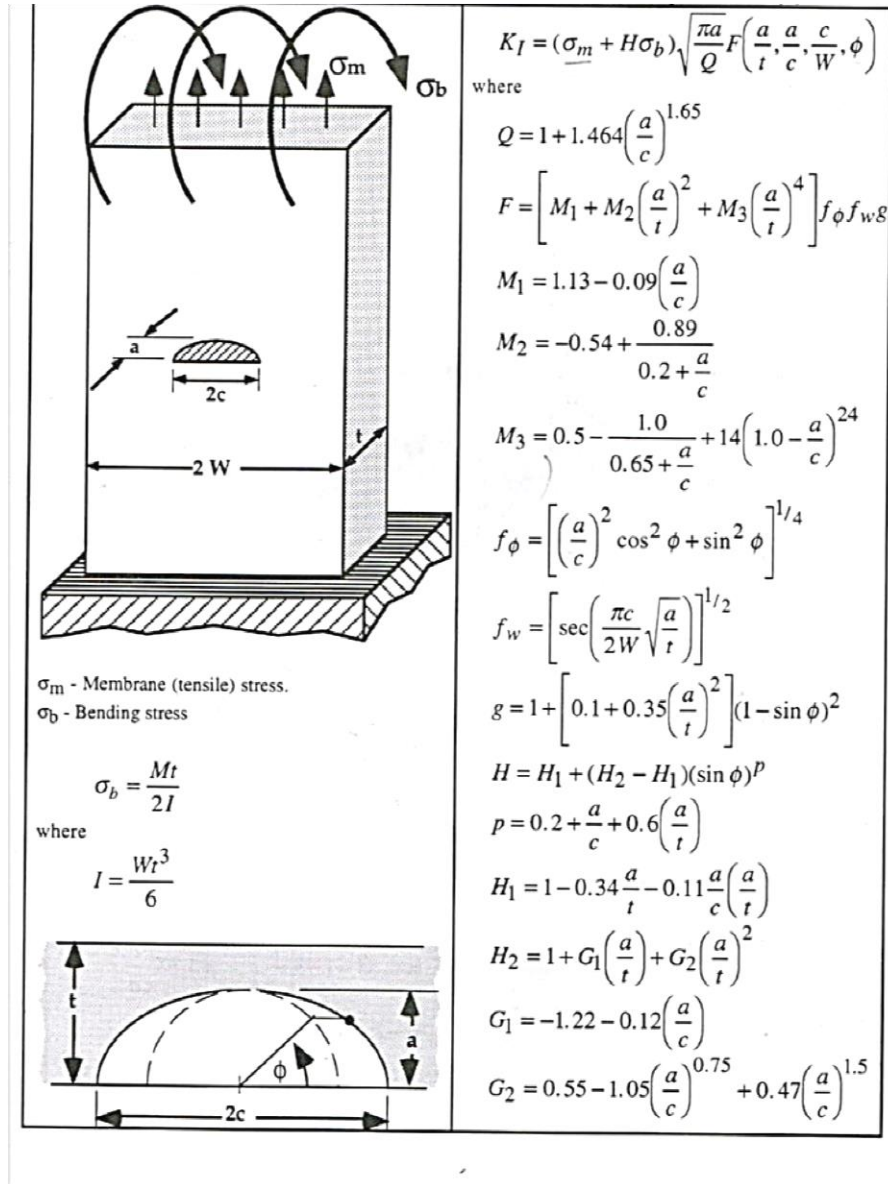


Figure B-7: Stress intensity factor equation for a semi-elliptical crack

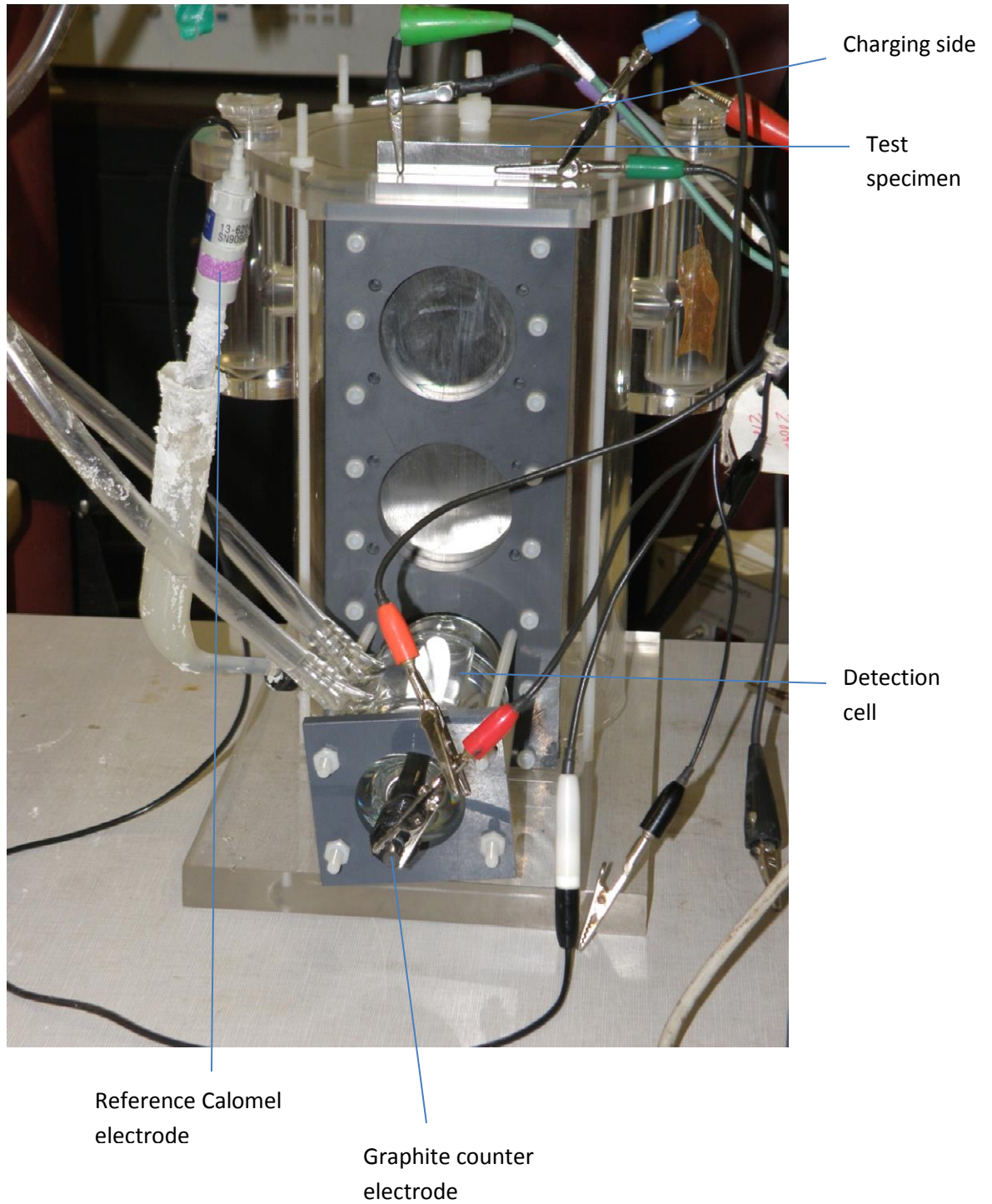


Figure B- 8: Test setup

The detection side consisted of a round glass cell that exposes just a 3cm diameter of the sample surface on the detection side to the oxidizing solution such that hydrogen permeation was measured over this area alone. The glass cell was filled with de-aerated 0.2M NaOH solution to oxidize hydrogen exiting the sample surface on the detection side. A 100% N₂ gas was continuously bubbled through the NaOH solution to ensure continued de-aeration of the oxidizing solution. An anodic potential of 100mV was applied on the detection side using a counter-reference electrode arrangement. Usually, the glass cell was filled with the solution for 30mins to ensure that a protective film is formed, then the anodic potential is applied to stabilize the protective film for 24hrs before the charging side is filled with the test solution.

Flat specimens measuring 257 mm X 63 mm X 1.5mm fabricated from X65 plates were used for the hydrogen permeation tests. The samples were long enough to allow tests to be carried at depths 0, 75 and 150 mm from the open mouth of the disbondment similar to the tensile samples. Three tests were conducted on each sample to determine the hydrogen permeation characteristics at 0, 75, and 150 mm from the open mouth. Only one test was conducted at a time. While one test is being conducted, only the surface of the area to be tested is exposed to the testing solution on the charging side; the rest of the sample is completely masked off to prevent hydrogen entry into the rest of the specimen.

During tests cell assembly, the flat specimens were secured against the inner shielding with screws, so that the X65 plate is in direct contact with the solution trapped inside the simulated disbondment. However, the charging side was initially kept empty. The detection side is then set up. After, the detection side is filled with NaOH and conditioned for 24hrs, and a very low steady current is obtained, the flat samples were then exposed to the corrosion media on the charging side by filling with C2 solution.

Prior to each test, both sides of the sample were cleaned in acetone to de-grease them and then cleaned in ethanol several times before the setup is assembled. This procedure is repeated three times to obtain permeation currents from three locations corresponding to the open mouth, 75 mm from the open

mouth and 150 mm from the open mouth each. A fresh solution was always used for the test at each location. While the test is being carried out at one location the surface of the sample at the other locations are masked off with a double sided tape while a metal sleeve is glued over the surface of the tape to ensure a conductive path for the applied cathodic potential. A photograph of a test set up is shown in Figure B-8.

A reference (saturated calomel electrode) and counter electrode (platinum mesh) arrangement was used to apply cathodic protection to the sample. Cathodic protection was applied at the open mouth just above the topmost crack as earlier described in section B.8. Cathodic protection was applied only on the charging side of the test sample.

The hydrogen flux measured during the test was used to determine the effective diffusivity of hydrogen through the metal lattice using the breakthrough time method using the relationship:

$$D_{eff} = \frac{L^2}{15.3t_b} \dots\dots\dots B.7$$

where L is the plate thickness, and t_b is the breakthrough time.